# STRENGTH OF MATERIALS

## PART II

### Advanced Theory and Problems

BY

## S. TIMOSHENKO
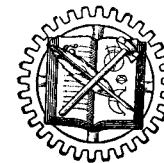
*Professor of Theoretical and Engineering Mechanics*
*Stanford University*

*SECOND EDITION—NINTH PRINTING*

# PREFACE TO THE SECOND EDITION

In the preparation of the new edition of this volume, the general character of the book has remained unchanged; the only effort being to make it more complete and up-to-date by including new theoretical and experimental material representing recent developments in the fields of stress analysis and experimental investigation of mechanical properties of structural materials.

The most important additions to the first edition include:

1. A more complete discussion of problems dealing with bending, compression, and torsion of slender and thin-walled structures. This kind of structure finds at present a wide application in airplane constructions, and it was considered desirable to include in the new edition more problems from that field.

2. A chapter on plastic deformations dealing with bending and torsion of beams and shafts beyond the elastic limit and also with plastic flow of material in thick-walled cylinders subjected to high internal pressures.

3. A considerable amount of new material of an experimental character pertaining to the behavior of structural materials at high temperatures and to the fatigue of metals under reversal of stresses, especially in those cases where fatigue is combined with high stress concentration.

4. Important additions to be found in the portion of the book dealing with beams on elastic foundations; in the chapters on the theory of curved bars and theory of plates and shells; and in the chapter on stress concentration, in which some recent results of photoelastic tests have been included.

Since the appearance of the first edition of this book, the author's three volumes of a more advanced character, "Theory of Elasticity," "Theory of Elastic Stability," and "Theory of Plates and Shells" have been published. Reference to these

books are made in various places in this volume, especially in those cases where only final results are given without a complete mathematical derivation.

It is hoped that with the additions mentioned above the book will give an up-to-date presentation of the subject of strength of materials which may be useful both to graduate students interested in engineering mechanics and to design engineers dealing with complicated problems of stress analysis.

STEPHEN P. TIMOSHENKO

PALO ALTO, CALIFORNIA
   June 12, 1941

# PREFACE TO THE FIRST EDITION

The second volume of THE STRENGTH OF MATERIALS is written principally for advanced students, research engineers, and designers. The writer has endeavored to prepare a book which contains the new developments that are of practical importance in the fields of strength of materials and theory of elasticity. Complete derivations of problems of practical interest are given in most cases. In only a comparatively few cases of the more complicated problems, for which solutions cannot be derived without going beyond the limit of the usual standard in engineering mathematics, the final results only are given. In such cases, the practical applications of the results are discussed, and, at the same time, references are given to the literature in which the complete derivation of the solution can be found.

In the first chapter, more complicated problems of bending of prismatical bars are considered. The important problems of bending of bars on an elastic foundation are discussed in detail and applications of the theory in investigating stresses in rails and stresses in tubes are given. The application of trigonometric series in investigating problems of bending is also discussed, and important approximate formulas for combined direct and transverse loading are derived.

In the second chapter, the theory of curved bars is developed in detail. The application of this theory to machine design is illustrated by an analysis of the stresses, for instance, in hooks, fly wheels, links of chains, piston rings, and curved pipes.

The third chapter contains the theory of bending of plates. The cases of deflection of plates to a cylindrical shape and the symmetrical bending of circular plates are discussed in detail and practical applications are given. Some data regarding the bending of rectangular plates under uniform load are also given.

In the fourth chapter are discussed problems of stress distribution in parts having the form of a generated body and symmetrically loaded. These problems are especially important for designers of vessels submitted to internal pressure and of rotating machinery. Tensile and bending stresses in thin-walled vessels, stresses in thick-walled cylinders, shrink-fit stresses, and also dynamic stresses produced in rotors and rotating discs by inertia forces and the stresses due to non-uniform heating are given attention.

The fifth chapter contains the theory of sidewise buckling of compressed members and thin plates due to elastic instability. These problems are of utmost importance in many modern structures where the cross sectional dimensions are being reduced to a minimum due to the use of stronger materials and the desire to decrease weight. In many cases, failure of an engineering structure is to be attributed to elastic instability and not to lack of strength on the part of the material.

In the sixth chapter, the irregularities in stress distribution produced by sharp variations in cross sections of bars caused by holes and grooves are considered, and the practical significance of stress concentration is discussed. The photoelastic method, which has proved very useful in investigating stress concentration, is also described. The membrane analogy in torsional problems and its application in investigating stress concentration at reentrant corners, as in rolled sections and in tubular sections, is explained. Circular shafts of variable diameter are also discussed, and an electrical analogy is used in explaining local stresses at the fillets in such shafts.

In the last chapter, the mechanical properties of materials are discussed. Attention is directed to the general principles rather than to a description of established, standardized methods of testing materials and manipulating apparatus. The results of modern investigations of the mechanical properties of single crystals and the practical significance of this information are described. Such subjects as the fatigue of metals and the strength of metals at high temperature are

of decided practical interest in modern machine design. These problems are treated more particularly with reference to new developments in these fields.

In concluding, various strength theories are considered. The important subject of the relation of the theories to the method of establishing working stresses under various stress conditions is developed.

It was mentioned that the book was written partially for teaching purposes, and that it is intended also to be used for advanced courses. The writer has, in his experience, usually divided the content of the book into three courses as follows: (1) A course embodying chapters 1, 3, and 5 principally for advanced students interested in structural engineering. (2) A course covering chapters 2, 3, 4, and 6 for students whose chief interest is in machine design. (3) A course using chapter 7 as a basis and accompanied by demonstrations in the material testing laboratory. The author feels that such a course, which treats the fundamentals of mechanical properties of materials and which establishes the relation between these properties and the working stresses used under various conditions in design, is of practical importance, and more attention should be given this sort of study in our engineering curricula.

The author takes this opportunity of thanking his friends who have assisted him by suggestions, reading of manuscript and proofs, particularly Messrs. W. M. Coates and L. H. Donnell, teachers of mathematics and mechanics in the Engineering College of the University of Michigan, and Mr. F. L. Everett of the Department of Engineering Research of the University of Michigan. He is indebted also to Mr. F. C. Wilharm for the preparation of drawings, to Mrs. E. D. Webster for the typing of the manuscript, and to the D. Van Nostrand Company for their care in the publication of the book.

S. Timoshenko

Ann Arbor, Michigan
    May 1, 1930

# NOTATIONS

$\sigma_x,\ \sigma_y,\ \sigma_z$....Normal stresses on planes perpendicular to $x$, $y$ and $z$ axes.

$\sigma_n$.........Normal stress on plane perpendicular to direction $n$.

$\sigma_{Y.P.}$.......Normal stress at yield point.

$\sigma_w$.........Normal working stress

$\tau$.........Shearing stress

$\tau_{xy},\ \tau_{yz},\ \tau_{zx}$..Shearing stresses parallel to $x$, $y$ and $z$ axes on the planes perpendicular to $y$, $z$ and $x$ axes.

$\tau_w$.........Working stress in shear

$\delta$.........Total elongation, total deflection

$\epsilon$.........Unit elongation

$\epsilon_x,\ \epsilon_y,\ \epsilon_z$.....Unit elongations in $x$, $y$ and $z$ directions

$\gamma$.........Unit shear, weight per unit volume

$E$.........Modulus of elasticity in tension and compression

$G$.........Modulus of elasticity in shear

$\mu$.........Poisson's ratio

$\Delta$.........Volume expansion

$K$.........Modulus of elasticity of volume

$M_t$.........Torque

$M$.........Bending moment in a beam

$V$.........Shearing force in a beam

$A$.........Cross sectional area

$I_y,\ I_z$......Moments of inertia of a plane figure with respect to $y$ and $z$ axes

$k_y,\ k_z$......Radii of gyration corresponding to $I_y,\ I_z$

$I_p$.........Polar moment of inertia

$Z$.........Section modulus

$C$.........Torsional rigidity

$l$.........Length of a bar, span of a beam

$P,\ Q$.......Concentrated forces

$t$.........Temperature, thickness

$U$ . . . . . . . . Strain Energy
$s$ . . . . . . . . Distance, arc length
$q$ . . . . . . . . Load per unit length

# CONTENTS

# CHAPTER I

## SPECIAL PROBLEMS IN BENDING OF BEAMS

**1. Beams on Elastic Foundation.**—Let us consider a prismatical beam supported along its entire length by a continuous elastic foundation, such that when the beam is deflected, the intensity of the continuously distributed reaction at every section is proportional to the deflection at that section.[1] Under such conditions the reaction per unit length of the bar can be represented by the expression $ky$, in which $y$ is the deflection and $k$ is a constant usually called the *modulus of the foundation*. This constant denotes the reaction per unit length, when the deflection is equal to unity. The simple assumption that the continuous reaction of the foundation is proportional to the deflection is a satisfactory approximation in many practical cases. For instance, in the case of railway tracks, the solution obtained on this assumption is in good agreement with actual measurements.[2] In studying the deflection curve of the beam we use the differential equation:[3]

$$EI_z\frac{d^4y}{dx^4} = q, \tag{a}$$

in which $q$ denotes the intensity of the load acting on the beam.

---

[1] The beam is inbedded in a material capable of exerting downward as well as upward forces on it.

[2] See S. Timoshenko and B. F. Langer, Trans. A. S. M. E., Vol. 54, p. 277, 1932. The theory of bending of a bar on elastic foundation has been developed by E. Winkler, Die Lehre v. d. Elastizität u. Festigkeit, Prag, 1867, p. 182. See also A. Zimmermann, Die Berechnung des Eisenbahn-Oberbaues, Berlin, 1888. Further development of the theory will be found in the following publications: Hayashi, Theorie des Trägers auf elastischer Unterlage, Berlin, 1921; Wieghardt, Zeitschrift für angewandte Math. u. Mech., Vol. 2 (1922); K. v. Sanden and Schleicher, Beton und Eisen, 1926, Heft 5; Pasternak, Beton u. Eisen, 1926, Heft 9 and 10; W. Prager, Zeitschrift f. angewandte Math. u. Mech., Vol. 7, 1927, p. 354; M. A. Biot, Journal Appl. Mech., Vol. 4, p. 1A, 1937.

[3] See "Strength of Materials," Part I, p. 137.

For an unloaded portion the only force on the beam is the continuously distributed reaction from the side of the foundation of intensity $ky$. Hence $q = - ky$ and equation $(a)$ becomes

$$EI_z \frac{d^4y}{dx^4} = - ky. \qquad (1)$$

Using the notation

$$\sqrt[4]{\frac{k}{4EI_z}} = \beta, \qquad (2)$$

the general solution of eq. $(1)$ can be represented as follows:

$$y = e^{\beta x}(A \cos \beta x + B \sin \beta x)$$
$$+ e^{-\beta x}(C \cos \beta x + D \sin \beta x). \qquad (b)$$

This can easily be verified by substituting $(b)$ in eq. $(1)$. In particular cases the arbitrary constants $A$, $B$, $C$, and $D$ of the solution must be determined from the known conditions at certain points.

Let us consider, as an example, the case of a single concentrated load acting on an infinitely long beam (Fig. 1), taking the origin of coordinates at the point of application of the force. From the condition of symmetry, only that part of the beam to the right of the load need be considered (Fig. 1, $b$). In applying the general solution $(b)$ to this case, the arbitrary constants must first be found. It is reasonable to assume that at points infinitely distant from the force $P$ the deflection and the curvature are equal to zero. This condition can be fulfilled only if the constants $A$ and $B$ in eq. $(b)$ are taken equal to zero. Hence the deflection curve for the right portion of the beam becomes
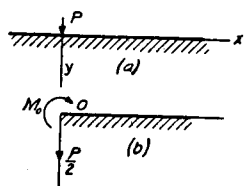
$$y = e^{-\beta x}(C \cos \beta x + D \sin \beta x). \qquad (c)$$

The two remaining constants of integration $C$ and $D$ must be found from the conditions at the origin, $x = 0$. At this point,

FIG. 1.

the deflection curve must have a horizontal tangent; therefore

$$\left(\frac{dy}{dx}\right)_{x=0} = 0,$$

or substituting expression $(c)$ for $y$

$$e^{-\beta x}(C \cos \beta x + D \sin \beta x + C \sin \beta x - D \cos \beta x)_{x=0} = 0$$

from which

$$C = D.$$

Equation $(c)$ therefore becomes

$$y = Ce^{-\beta x}(\cos \beta x + \sin \beta x). \qquad (d)$$

The consecutive derivatives of this equation are

$$\frac{dy}{dx} = - 2\beta Ce^{-\beta x} \sin \beta x,$$

$$\frac{d^2y}{dx^2} = 2\beta^2 Ce^{-\beta x}(\sin \beta x - \cos \beta x), \qquad (e)$$

$$\frac{d^3y}{dx^3} = 4\beta^3 Ce^{-\beta x} \cos \beta x. \qquad (f)$$

The constant $C$ can now be determined from the fact that at $x = 0$ the shearing force for the right part of the beam (Fig. 1, $b$) is equal to $- (P/2)$. The minus sign follows from our convention for signs of shearing forces (see p. 72, Part I). Then

$$(V)_{x=0} = \left(\frac{dM}{dx}\right)_{x=0} = - EI_z\left(\frac{d^3y}{dx^3}\right)_{x=0} = - \frac{P}{2},$$

or using eq. $(f)$

$$EI_z \cdot 4\beta^3 C = \frac{P}{2},$$

from which

$$C = \frac{P}{8\beta^3 EI_z}.$$

Substituting this in eqs. $(d)$ and $(e)$, we obtain the following

equations for the deflection and bending moment curves:

$$y = \frac{P}{8\beta^3 EI_z} e^{-\beta x}(\cos \beta x + \sin \beta x)$$

$$= \frac{P\beta}{2k} e^{-\beta x}(\cos \beta x + \sin \beta x), \quad (3)$$

$$M = - EI_z \frac{d^2 y}{dx^2} = - \frac{P}{4\beta} e^{-\beta x}(\sin \beta x - \cos \beta x). \quad (4)$$

Both expressions (3) and (4) have, when plotted, a wave form with gradually diminishing amplitudes. The length $a$ of these waves is given by the period of the functions $\cos \beta x$ and $\sin \beta x$, i.e.,

$$a = \frac{2\pi}{\beta} = 2\pi \sqrt[4]{\frac{4EI_z}{k}}. \quad (5)$$

To simplify the determination of the deflection, the bending moment, and the shearing force the numerical table below is given, in which the following notations are used:

$$\left.\begin{array}{l} \varphi = e^{-\beta x}(\cos \beta x + \sin \beta x); \\ \psi = - e^{-\beta x}(\sin \beta x - \cos \beta x); \\ \theta = e^{-\beta x}\cos \beta x; \quad \zeta = e^{-\beta x}\sin \beta x \end{array}\right\} \quad (6)$$

In Fig. 2 the functions $\varphi$ and $\psi$ are shown graphically.
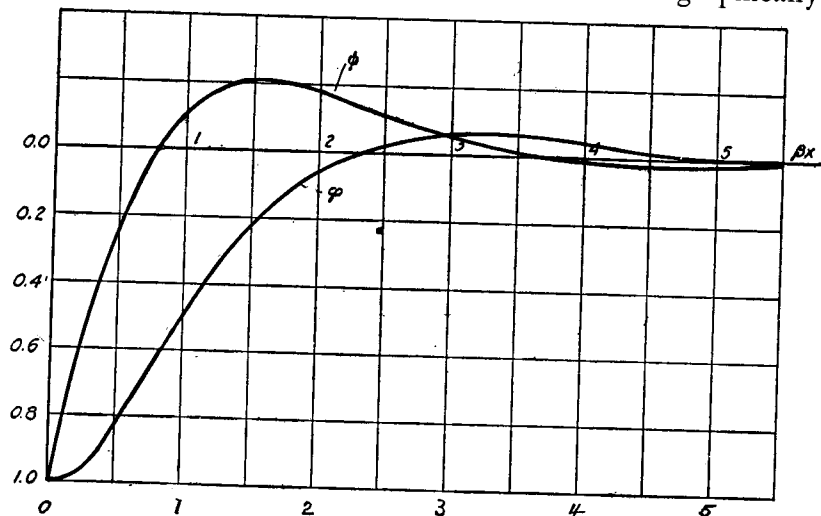


FIG. 2.

TABLE I. FUNCTIONS $\varphi$, $\psi$, $\theta$ AND $\zeta$

| $\beta x$ | $\varphi$ | $\psi$ | $\theta$ | $\zeta$ | $\beta x$ | $\varphi$ | $\psi$ | $\theta$ | $\zeta$ |
|---|---|---|---|---|---|---|---|---|---|
| 0 | 1.0000 | 1.0000 | 1.0000 | 0 | 3.6 | −0.0366 | −0.0124 | −0.0245 | −0.0121 |
| 0.1 | 0.9907 | 0.8100 | 0.9003 | 0.0903 | 3.7 | −0.0341 | −0.0079 | −0.0210 | −0.0131 |
| 0.2 | 0.9651 | 0.6398 | 0.8024 | 0.1627 | 3.8 | −0.0314 | −0.0040 | −0.0177 | −0.0137 |
| 0.3 | 0.9267 | 0.4888 | 0.7077 | 0.2189 | 3.9 | −0.0286 | −0.0008 | −0.0147 | −0.0140 |
| 0.4 | 0.8784 | 0.3564 | 0.6174 | 0.2610 | 4.0 | −0.0258 | 0.0019 | −0.0120 | −0.0139 |
| 0.5 | 0.8231 | 0.2415 | 0.5323 | 0.2908 | 4.1 | −0.0231 | 0.0040 | −0.0095 | −0.0136 |
| 0.6 | 0.7628 | 0.1431 | 0.4530 | 0.3099 | 4.2 | −0.0204 | 0.0057 | −0.0074 | −0.0131 |
| 0.7 | 0.6997 | 0.0599 | 0.3798 | 0.3199 | 4.3 | −0.0179 | 0.0070 | −0.0054 | −0.0125 |
| 0.8 | 0.6354 | −0.0093 | 0.3131 | 0.3223 | 4.4 | −0.0155 | 0.0079 | −0.0038 | −0.0117 |
| 0.9 | 0.5712 | −0.0657 | 0.2527 | 0.3185 | 4.5 | −0.0132 | 0.0085 | −0.0023 | −0.0108 |
| 1.0 | 0.5083 | −0.1108 | 0.1988 | 0.3096 | 4.6 | −0.0111 | 0.0089 | −0.0011 | −0.0100 |
| 1.1 | 0.4476 | −0.1457 | 0.1510 | 0.2967 | 4.7 | −0.0092 | 0.0090 | 0.0001 | −0.0091 |
| 1.2 | 0.3899 | −0.1716 | 0.1091 | 0.2807 | 4.8 | −0.0075 | 0.0089 | 0.0007 | −0.0082 |
| 1.3 | 0.3355 | −0.1897 | 0.0729 | 0.2626 | 4.9 | −0.0059 | 0.0087 | 0.0014 | −0.0073 |
| 1.4 | 0.2849 | −0.2011 | 0.0419 | 0.2430 | 5.0 | −0.0046 | 0.0084 | 0.0019 | −0.0065 |
| 1.5 | 0.2384 | −0.2068 | 0.0158 | 0.2226 | 5.1 | −0.0033 | 0.0080 | 0.0023 | −0.0057 |
| 1.6 | 0.1959 | −0.2077 | −0.0059 | 0.2018 | 5.2 | −0.0023 | 0.0075 | 0.0026 | −0.0049 |
| 1.7 | 0.1576 | −0.2047 | −0.0235 | 0.1812 | 5.3 | −0.0014 | 0.0069 | 0.0028 | −0.0042 |
| 1.8 | 0.1234 | −0.1985 | −0.0376 | 0.1610 | 5.4 | −0.0006 | 0.0064 | 0.0029 | −0.0035 |
| 1.9 | 0.0932 | −0.1899 | −0.0484 | 0.1415 | 5.5 | 0.0000 | 0.0058 | 0.0029 | −0.0029 |
| 2.0 | 0.0667 | −0.1794 | −0.0563 | 0.1230 | 5.6 | 0.0005 | 0.0052 | 0.0029 | −0.0023 |
| 2.1 | 0.0439 | −0.1675 | −0.0618 | 0.1057 | 5.7 | 0.0010 | 0.0046 | 0.0028 | −0.0018 |
| 2.2 | 0.0244 | −0.1548 | −0.0652 | 0.0895 | 5.8 | 0.0013 | 0.0041 | 0.0027 | −0.0014 |
| 2.3 | 0.0080 | −0.1416 | −0.0668 | 0.0748 | 5.9 | 0.0015 | 0.0036 | 0.0026 | −0.0010 |
| 2.4 | −0.0056 | −0.1282 | −0.0669 | 0.0613 | 6.0 | 0.0017 | 0.0031 | 0.0024 | −0.0007 |
| 2.5 | −0.0166 | −0.1149 | −0.0658 | 0.0492 | 6.1 | 0.0018 | 0.0026 | 0.0022 | −0.0004 |
| 2.6 | −0.0254 | −0.1019 | −0.0636 | 0.0383 | 6.2 | 0.0019 | 0.0022 | 0.0020 | −0.0002 |
| 2.7 | −0.0320 | −0.0895 | −0.0608 | 0.0287 | 6.3 | 0.0019 | 0.0018 | 0.0018 | +0.0001 |
| 2.8 | −0.0369 | −0.0777 | −0.0573 | 0.0204 | 6.4 | 0.0018 | 0.0015 | 0.0017 | 0.0003 |
| 2.9 | −0.0403 | −0.0666 | −0.0534 | 0.0132 | 6.5 | 0.0018 | 0.0012 | 0.0015 | 0.0004 |
| 3.0 | −0.0423 | −0.0563 | −0.0493 | 0.0070 | 6.6 | 0.0017 | 0.0009 | 0.0013 | 0.0005 |
| 3.1 | −0.0431 | −0.0469 | −0.0450 | 0.0019 | 6.7 | 0.0016 | 0.0006 | 0.0011 | 0.0006 |
| 3.2 | −0.0431 | −0.0383 | −0.0407 | −0.0024 | 6.8 | 0.0015 | 0.0004 | 0.0010 | 0.0006 |
| 3.3 | −0.0422 | −0.0306 | −0.0364 | −0.0058 | 6.9 | 0.0014 | 0.0002 | 0.0008 | 0.0006 |
| 3.4 | −0.0408 | −0.0237 | −0.0323 | −0.0085 | 7.0 | 0.0013 | 0.0001 | 0.0007 | 0.0006 |
| 3.5 | −0.0389 | −0.0177 | −0.0283 | −0.0106 | | | | | |

Using the notation (6) and equations $(d)$–$(f)$ we obtain

$$y = \frac{P\beta}{2k}\,\varphi(\beta x), \qquad \frac{dy}{dx} = -\frac{P\beta^2}{k}\,\zeta(\beta x),$$

$$M = -EI_z\frac{d^2y}{dx^2} = \frac{P}{4\beta}\,\psi(\beta x),$$

$$V = -EI_z\frac{d^3y}{dx^3} = -\frac{P}{2}\,\theta(\beta x). \qquad (7)$$

By using these equations together with table I, the deflection, the slope, the bending moment, and the shearing force for any cross section of the beam can be readily calculated. The maximum deflection and maximum bending moment occur at the origin and are, respectively,

$$\delta = (y)_{x=0} = \frac{P\beta}{2k}, \qquad (8)$$

$$M_0 = (M)_{x=0} = \frac{P}{4\beta}. \qquad (9)$$

Using the expression (3) for a single load and the principle of superposition, the deflection produced in an infinitely long beam on an elastic foundation by any other type of loading can be readily obtained.
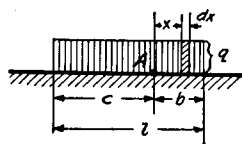
FIG. 3.

As an example let us consider the case of a uniform load distributed over a length $l$ of an infinitely long beam (Fig. 3). Consider any point $A$, and let $c$ and $b$ represent the distances from this point to the ends of the loaded part of the beam. The deflection at $A$, produced by an element $qdx$ of the load, is obtained by substituting $qdx$ for $P$ in eq. (3), which gives

$$\frac{qdx}{8\beta^3 EI_z}e^{-\beta x}(\cos\beta x + \sin\beta x).$$

The deflection produced at $A$ by the loading distributed over the

length $l$ then becomes

$$y = \int_0^b \frac{qdx}{8\beta^3 EI_z}e^{-\beta x}(\cos\beta x + \sin\beta x) + \int_0^c \frac{qdx}{8\beta^3 EI_z}e^{-\beta x}(\cos\beta x + \sin\beta x)$$

$$= \frac{q}{2k}(2 - e^{-\beta b}\cos\beta b - e^{-\beta c}\cos\beta c). \qquad (g)$$

If $c$ and $b$ are large, the values $e^{-\beta b}$ and $e^{-\beta c}$ will be small and the deflection $(g)$ will be equal approximately to $q/k$, i.e., at points remote from the ends of the loaded part of the bar the bending of the bar can be neglected and it can be assumed that the uniform loading $q$ is directly transmitted to the elastic foundation. Taking the point $A$ at the end of the loaded part of the bar, we have $c = 0$, $b = l$, $e^{-\beta c}\cos\beta c = 1$. Assuming that $l$ is large, we have also $e^{-\beta b}\cos\beta b = 0$. Then $y = q/2k$; i.e., the deflection now has only one half of the value obtained above.

In a similar manner, by using equation (4), the expression for bending moment at $A$ can be derived. If the point $A$ is taken outside of the loaded portion of the beam and if the quantities $b$ and $c$ represent, respectively, the larger and the smaller distances from this point to the ends of the loaded part of the beam, the deflection at $A$ is

$$y = \int_0^b \frac{qdx}{8\beta^3 EI_z}e^{-\beta x}(\cos\beta x + \sin\beta x)$$

$$\quad - \int_0^c \frac{qdx}{8\beta^3 EI_z}e^{-\beta x}(\cos\beta x + \sin\beta x)$$

$$= \frac{q}{2k}(e^{-\beta c}\cos\beta c - e^{-\beta b}\cos\beta b). \qquad (h)$$

When $c = 0$ and $b = l$ is a large quantity, we obtain for the deflection the value $q/2k$, which coincides with our previous conclusion. As the distances $b$ and $c$ increase, the deflection $(h)$ decreases, approaching zero as $b$ and $c$ grow larger.

The case of a couple acting on an infinitely long beam, Fig. 4a, can also be analyzed by using the solution (3) for a single load. The action of the couple is equivalent to that of the two forces $P$ shown in Fig. 4b, if $Pe$ approaches $M_0$ while $e$ approaches zero.
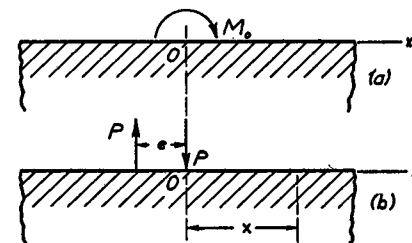
FIG. 4.

Using the first of equations (7), we find the deflection at a distance $x$ from the origin:

$$y = \frac{P\beta}{2k}\{\varphi(\beta x) - \varphi[\beta(x + e)]\}$$
$$= \frac{M_0\beta}{2k} \cdot \frac{\varphi(\beta x) - \varphi[\beta(x + e)]}{e} = -\frac{M_0\beta}{2k}\frac{d\varphi}{dx}.$$

Since, from equations (7),

$$\frac{d\varphi}{dx} = -2\beta\zeta,$$

we obtain for the deflection curve produced by the couple $M_0$ the following equation:

$$y = \frac{M_0\beta^2}{k}\zeta(\beta x). \qquad (10)$$

By differentiating this equation, we obtain

$$\frac{dy}{dx} = \frac{M_0\beta^3}{k}\psi(\beta x),$$

$$M = -EI_z\frac{d^2y}{dx^2} = \frac{M_0}{2}\theta(\beta x), \qquad (10')$$

$$V = -EI_z\frac{d^3y}{dx^3} = -\frac{M_0\beta}{2}\varphi(\beta x).$$

Using these equations together with Table 1, one can readily calculate the deflection, the slope, the bending moment, and the shearing force for any cross section of the beam.

We shall now consider the case of several loads acting on a beam. As an example bending of a rail produced by wheel-pressures of a locomotive will be discussed. The following method of analyzing stresses in rails is based upon the assumption that there is a continuous elastic support under the rail. This assumption is a good approximation,[4] since the distance between the ties is small in comparison to the wave length $a$ of the deflection curve, given by eq. (5). In order to obtain the magnitude $k$ of the modulus of foundation, the load required to depress one tie unit distance must be divided by the tie spacing. It is assumed that the tie is symmetrically loaded by two loads corresponding to the rail pressures. Suppose, for instance, that the tie is depressed 0.3 inch under each of the two loads of 10,000 pounds and that the tie

spacing is 22 inches; then

$$k = \frac{10,000}{0.3 \times 22} = 1,500 \text{ lbs. per square inch.}$$

For the case of a single wheel load $P$, eqs. (8) and (9) are used for the maximum deflection and maximum bending moment. The maximum stress due to the bending of the rail will be

$$\sigma_{max} = \frac{M_{max}}{Z} = \frac{P}{4\beta Z} = \frac{P}{4Z}\sqrt[4]{\frac{4EI_z}{k}}, \qquad (i)$$

where $Z$ denotes the section modulus of the rail.[5]

In order to compare stresses in rails the cross sections of which are geometrically similar, eq. ($i$) may be put in the following form:

$$\sigma_{max} = \frac{P}{A} \cdot \frac{A\sqrt[4]{I_z}}{4Z}\sqrt[4]{\frac{4E}{k}}, \qquad (j)$$

in which $A$ is the area of the cross section of the rail. Since the second factor on the right side of eq. ($j$) remains constant for geometrically similar cross sections and since the third factor does not depend on the dimensions of the rail, the maximum stress is inversely proportional to the area of the cross section, i.e., inversely proportional to the weight of the rail per unit length.

An approximate value of the maximum pressure $R_{max}$ on a tie is obtained by multiplying the maximum depression by the tie spacing $l$ and by the modulus of the foundation. From eq. (8)

$$R_{max} = \frac{P\beta}{2k}lk = \frac{P\beta l}{2} = \frac{P}{2}\sqrt[4]{\frac{kl^4}{4EI_z}}. \qquad (k)$$

It may be seen from this that the pressure on the tie depends principally on the tie spacing $l$. It should be noted also that $k$ occurs in both eqs. ($j$) and ($k$) as a fourth root. Hence an error in the determination of $k$ will introduce a much smaller error in the magnitude of $\sigma_{max}$ and $R_{max}$.

---

[4] See author's paper on "Strength of Rails," Transactions of the Institute of Way of Communications, St. Petersburg, Russia (1915), and author's paper in Proc. of the Second International Congress for Applied Mechanics, Zürich, 1926. See also reference 2.

[5] In writing eq. ($i$) it was assumed that the elementary beam formula can be used at the cross section where the load $P$ is applied. More detailed investigations show that, due to local stresses, considerable deviation from the elementary eq. ($i$) should be expected.

When several loads are acting on the rail, the method of super-position must be used. To illustrate the method of calculation we shall discuss a numerical example. Consider a 100-lb. rail section with $I_z = 44$ in.$^4$ and with a tie spacing such that $k = 1,500$ lbs. per sq. in.; then from eq. (2)

$$\beta = \sqrt[4]{\frac{k}{4EI_z}} = \sqrt[4]{\frac{1,500}{4 \times 30 \times 10^6 \times 44}} = \frac{1}{43.3} \text{ in.}^{-1},$$

and from eq. (5)

$$a = \frac{2\pi}{\beta} = 272 \text{ in.}$$

We take, as an example, a system of four equal wheel loads, 66 inches apart. If we fix the origin of coordinates at the point of contact of the first wheel, the values of $\beta x$ for other wheels will be those in the table 2 below. The corresponding values of functions $\varphi$ and $\psi$ taken from the numerical table on p. 5 are also given.

TABLE 2

| Loads | 1 | 2 | 3 | 4 |
|---|---|---|---|---|
| $\beta x$ | 0 | 1.52 | 3.05 | 4.57 |
| $\psi$ | 1 | −0.207 | −0.051 | 0.008 |
| $\varphi$ | 1 | 0.230 | −0.042 | −0.012 |

Now, after superposing the effects of all the four loads acting on the rail, the bending moment under the first wheel is, from eq. (4),

$$M_1 = \frac{P}{4\beta}(1 - 0.207 - 0.051 + 0.008) = 0.75\frac{P}{4\beta},$$

i.e., the bending moment is 25 per cent less than that produced by a single load $P$.

Proceeding in the same manner for the point of contact of the second wheel we obtain

$$M_2 = \frac{P}{4\beta}(1 - 2 \times 0.207 - 0.051) = 0.535\frac{P}{4\beta}.$$

It may be seen that due to the action of adjacent wheels the bending moment under the second wheel is much smaller than under the first. This fact was proved by numerous experimental measurements of track stresses. Using eq. (3) and the values in the last

line of the numerical table 2, we find the following deflection under the first wheel:

$$\delta_1 = \frac{P\beta}{2k}(1 + 0.230 - 0.042 - 0.012) = 1.18\frac{P\beta}{2k}.$$

The deflections at other points can be obtained in a similar manner.

It will be seen that the method of superposition is easily applied to determine the effect of a combination of loads having any arrangement and any spacing.

The analysis is based on the assumption that the rail support is capable of developing negative reactions. Since there is play between the rail and the spikes, there is little resistance to the upward movement of the rail and this tends to increase the bending moment in the rail under the first and the last wheels. Other elements enter into the problem and these may affect the accuracy of the analysis. Nevertheless, in general, the above theory for the bending of the rail, caused by static loading, is in satisfactory agreement with the experiments which have been made.

## Problems

1. Using the information given in Table 2, construct the bending moment diagram for the rail assuming that the wheel pressures are equal to 40,000 lbs. Such a diagram should show that the moments are negative in sections midway between the wheels, which indicates that during locomotive motion the rail is submitted to the action of reversal of bending stresses which may finally result in fatigue cracks.

2. Find the bending moment at the middle of the loaded portion of the beam shown in Fig. 3 and the slope of the deflection curve at the left end of the same portion.

3. Find the deflection at any point $A$ under the triangular load acting on an infinitely long beam on elastic foundation, Fig. 5.

*Answer.* Proceeding as in the derivation of equation (g), p. 7, we obtain
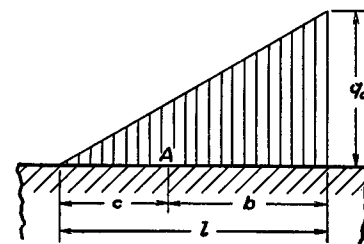


FIG. 5.

$$y = \frac{q_0}{4\beta k}\frac{1}{l}[\psi(\beta c) - \psi(\beta b) - 2\beta l\,\theta(\beta b) + 4\beta c].$$

**2. The Semi-infinite Beam on an Elastic Foundation.**—If a long beam on an elastic foundation is bent by a force $P$ and a moment $M_0$ applied at the end as shown in Fig. 6, we again can use the general solution $(b)$ of the preceding article. Since the deflection and the bending moment approach zero as the distance $x$ from the loaded end increases, we must take $A = B = 0$ in that solution and we obtain
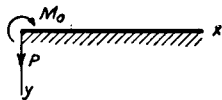


Fig. 6.

$$y = e^{-\beta x}(C \cos \beta x + D \sin \beta x). \qquad (a)$$

For determining the constants of integration $C$ and $D$ we have the conditions at the origin, i.e., under the load $P$:

$$EI_z \left(\frac{d^2y}{dx^2}\right)_{x=0} = -M_0,$$

$$EI_z \left(\frac{d^3y}{dx^3}\right)_{x=0} = -V = P.$$

Substituting expression $(a)$ in these equations, we obtain two linear equations in $C$ and $D$, from which

$$C = \frac{1}{2\beta^3 EI_z}(P - \beta M_0); \qquad D = \frac{M_0}{2\beta^2 EI_z}.$$

Substituting in equation $(a)$, we obtain

$$y = \frac{e^{-\beta x}}{2\beta^3 EI_z}\left[P \cos \beta x - \beta M_0(\cos \beta x - \sin \beta x)\right]$$

$$= \frac{2\beta}{k}\{P\theta(\beta x) - \beta M_0[\theta(\beta x) - \zeta(\beta x)]\}. \quad (11)$$

To get the deflection under the load we must substitute in $(11)$ $x = 0$. Then

$$\delta = (y)_{x=0} = \frac{1}{2\beta^3 EI_z}(P - \beta M_0). \qquad (11')$$

The expression for the slope is obtained by differentiating eq. $(11)$. At the end $(x = 0)$ this becomes

$$\left(\frac{dy}{dx}\right)_{x=0} = -\frac{1}{2\beta^2 EI_z}(P - 2\beta M_0). \qquad (12)$$

Using these equations in conjunction with the principle of super-position, more complicated problems can be solved.

If a uniformly loaded long beam on an elastic foundation has a

simply supported end, Fig. 7a, the reaction $R$ is found from the condition that the deflection at the support is zero. Observing that at a large distance from the support bending of the beam is negligible and that its depression into the foundation can be taken equal to $q/k$, we calculate the value of $R$ by substituting $M_0 = 0$ and $\delta = q/k$ into equation $(11')$. This yields the result:



Fig. 7.

$$R = 2\beta^3 EI_z \cdot \frac{q}{k} = \frac{q}{2\beta}. \qquad (13)$$

The deflection curve is now obtained by subtracting deflections given by equation $(11)$ for $P = R$, $M_0 = 0$ from the uniform depression $q/k$ of the beam, which gives

$$y = \frac{q}{k} - \frac{e^{-\beta x}}{2\beta^3 EI_z}R \cos \beta x = \frac{q}{k}(1 - e^{-\beta x} \cos \beta x). \qquad (14)$$

In the case of a built-in end, Fig. 7b, the magnitudes of the reaction $R$ and of the moment $M_0$ are obtained from the conditions that at the support the deflection and the slope are zero. Observing that at a large distance from the support the deflection is equal to $q/k$ and using equations $(11')$ and $(12)$, we obtain the following equations for calculating $R$ and $M_0$:[6]

$$-\frac{q}{k} = -\frac{1}{2\beta^3 EI_z}(R + \beta M_0)$$

and

$$0 = \frac{1}{2\beta^2 EI_z}(R + 2\beta M_0),$$

from which

$$M_0 = -2\beta^2 EI_z\frac{q}{k}, \qquad R = 4\beta^3 EI_z\frac{q}{k} = \frac{q}{\beta}. \qquad (15)$$

The minus sign of $M_0$ indicates that the moment has the direction shown by the arrow in Fig. 7b.

[6] In equations $(11')$ and $(12)$, $P = -R$ is substituted, since the positive direction for the reaction is taken upwards.

## Problems

1. Find the deflection curve for a semi-infinite beam on an elastic foundation hinged at the end and acted upon by a couple $M_0$, Fig. 8.
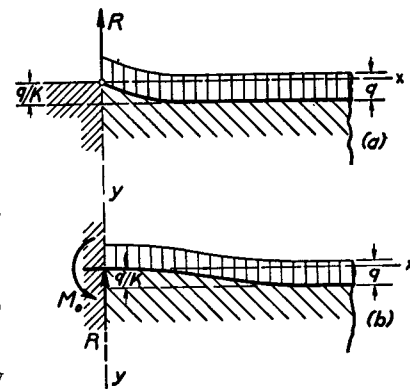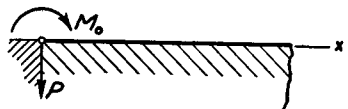
*Solution.* The reaction at the hinge is obtained from equation (11') substituting $\delta = 0$, which gives

$$P = \beta M_0.$$

FIG. 8.

Substituting this value of $P$ in equation (11) we obtain

$$y = \frac{M_0}{2\beta^2 EI_z} e^{-\beta x} \sin \beta x = \frac{M_0}{2\beta^2 EI_z} \zeta(\beta x). \qquad (16)$$

By subsequent differentiation, we find

$$\left.\begin{aligned}
\frac{dy}{dx} &= \frac{2\beta^3 M_0}{k} \cdot \psi(\beta x), \\[2mm]
M &= -EI_z \frac{d^2y}{dx^2} = M_0 \cdot \theta(\beta x), \\[2mm]
V &= -EI_z \frac{d^3y}{dx^3} = -\beta M_0 \cdot \varphi(\beta x).
\end{aligned}\right\} \qquad (b)$$

2. Find the bending moment $M_0$ and the force $P$ acting on the end of a semi-infinite beam on an elastic foundation, Fig. 9, if the deflection $\delta$ and the slope $i$ at the end are given.
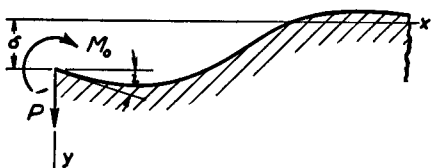
FIG. 9.

*Solution.* The values $M_0$ and $P$ are obtained from equations (11') and (12) by substituting the given quantities for $\delta$ and $(dy/dx)_{x=0} = i$.

3. Find the deflection curve for a semi-infinite beam on an elastic foundation produced by a load $P$ applied at a distance $c$ from the free end $A$ of the beam, Fig. 10.

*Solution.* Assume that the beam is extended to the left of the end $A$ as shown by the dotted line. In such a case equation (3) gives the deflection curve for $x > 0$ and at the cross section $A$ of the fictitious infinite beam we have, from equations (7), using the condition of symmetry:
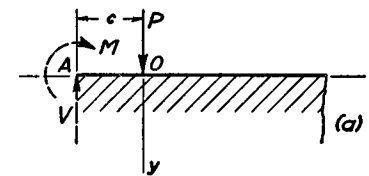
$$M = \frac{P}{4\beta} \psi(\beta c), \quad V = \frac{P}{2} \theta(\beta c). \quad (c)$$

To obtain the required deflection curve for the semi-infinite beam, free at the end $A$, we evidently must superpose the deflection of the semi-infinite beam produced by forces shown in Fig. 10$b$ on the deflection of the fictitious infinite beam. By using equations (3), (11) and (c) in this way we obtain for $x > 0$:
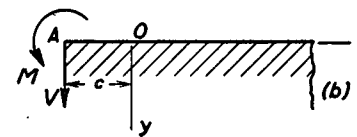
FIG. 10.

$$y = \frac{P\beta}{2k} \varphi(\beta x) + \frac{2\beta}{k} \{ V\theta[\beta(x+c)]$$
$$+ \beta M\theta[\beta(x+c)] - \beta M\zeta[\beta(x+c)]\} \quad (d)$$
$$= \frac{P\beta}{2k} \varphi(\beta x) + \frac{\beta P}{k} \{ \theta(\beta c)\theta[\beta(x+c)]$$
$$+ \tfrac{1}{2}\psi(\beta c)\theta[\beta(x+c)] - \tfrac{1}{2}\psi(\beta c)\zeta[\beta(x+c)]\}.$$

This expression can also be used for $-c < x < 0$; in this case we have only to substitute the absolute value of $x$, instead of $x$, in $\varphi(\beta x)$.

**3. Beams of Finite Length on Elastic Foundations.**—Bending of a beam of finite length on an elastic foundation can also be investigated by using solution (3) for an infinitely long beam together with the method of superposition.[7] To illustrate the method let us consider the case of a beam of finite length with free ends which is loaded by two symmetrically applied forces $P$, Fig. 11$a$. A similar condition exists in the case of a tie under the action of rail pressures  To each of the three portions of the beam the general

[7] This method of analysis was developed by M. Hetényi, Final Report of the Second Congress of the International Assoc. f. Bridge and Structural Engineering, Berlin, 1938.

solution (b) of article 1 can be applied, and the constants of integration can be calculated from the conditions at the ends and at the points of application of the loads. The required solution can, however, be obtained much more easily by superposing the solutions for the two kinds of loading of an infinitely long beam shown in Figs. 11b and 11c. In Fig. 11b the two forces P are acting on
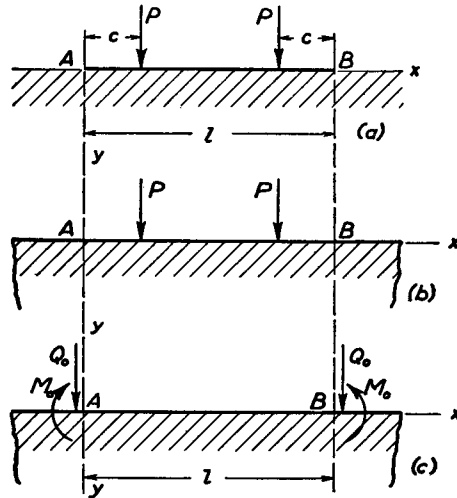


FIG. 11.

the infinitely long beam. In Fig. 11c the infinitely long beam is loaded by forces $Q_0$ and moments $M_0$, both applied outside of the portion $AB$ of the beam and infinitely close to points $A$ and $B$ corresponding to the free ends of the given beam, Fig. 11a. It is easy to see that by a proper selection of the forces $Q_0$ and the moments $M_0$, the bending moment and the shearing force produced by the forces $P$ at the cross sections $A$ and $B$ of the infinite beam (shown in Fig. 11b) can be made to equal zero. Then the middle portion of the infinite beam will be evidently in the same condition as the finite beam represented in Fig. 11a, and all necessary information regarding bending of the latter beam will be obtained by superposing the cases shown in Figs. 11b and 11c. To establish the equations for determining the proper values of $M_0$ and $Q_0$, let us consider the cross section $A$ of the infinitely long beam. Taking the origin of the coordinates at this point and using equations (7), the bending moment $M'$ and the shearing force $V'$ produced at this

point by the two forces $P$, Fig. 11b, are

$$M' = \frac{P}{4\beta} \{\psi[\beta(l-c)] + \psi[\beta c]\},$$

$$V' = \frac{P}{2} \{\theta[\beta(l-c)] + \theta[\beta c]\}. \qquad (a)$$

The moment $M''$ and the shearing force $V''$ produced at the same point by the forces shown in Fig. 11c are obtained by using equations (7) together with equations (10'), which give

$$M'' = \frac{Q_0}{4\beta} [1 + \psi(\beta l)] + \frac{M_0}{2} [1 + \theta(\beta l)],$$

$$V'' = -\frac{Q_0}{2} [1 - \theta(\beta l)] - \frac{M_0\beta}{2} [1 - \varphi(\beta l)]. \qquad (b)$$

The proper values of $M_0$ and $Q_0$ are now obtained from the equations

$$\left. \begin{array}{l} M' + M'' = 0, \\ V' + V'' = 0, \end{array} \right\} \qquad (c)$$

which can be readily solved in each particular case by using Table 1.

Once $M_0$ and $Q_0$ are known, the deflection and the bending moment at any cross section of the actual beam, Fig. 11a, can be obtained by using equations (7), (10) and (10') together with the method of superposition. The particular case shown in Fig. 12 is obtained from our previous discussion by taking $c = 0$.
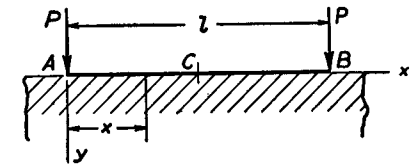


FIG. 12.

Proceeding as previously explained we obtain for the deflections at the ends and at the middle the following expressions:

$$y_a = y_b = \frac{2P\beta}{k} \frac{\cosh \beta l + \cos \beta l}{\sinh \beta l + \sin \beta l}, \qquad (d)$$

$$y_c = \frac{4P\beta}{k} \frac{\cosh \frac{\beta l}{2} \cos \frac{\beta l}{2}}{\sinh \beta l + \sin \beta l}. \qquad (e)$$

The bending moment at the middle is

$$M_c = -\frac{2P}{\beta} \frac{\sinh \frac{\beta l}{2} \sin \frac{\beta l}{2}}{\sinh \beta l + \sin \beta l}. \qquad (f)$$
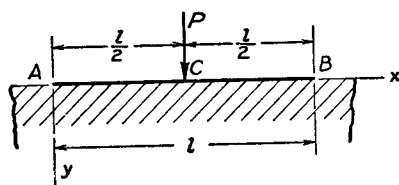
FIG. 13.

The case of a single load at the middle, Fig. 13, can also be obtained from our previous case, shown in Fig. 11a. It is only necessary to take $c = l/2$ and to substitute $P$ for $2P$. In this way we obtain for the deflections at the middle and at the ends the following expressions:

$$y_a = y_b = \frac{2P\beta}{k} \frac{\cosh \frac{\beta l}{2} \cos \frac{\beta l}{2}}{\sinh \beta l + \sin \beta l}, \qquad (g)$$

$$y_c = \frac{P\beta}{2k} \frac{\cosh \beta l + \cos \beta l + 2}{\sinh \beta l + \sin \beta l}. \qquad (h)$$

For the bending moment under the load we find

$$M_c = \frac{P}{4\beta} \frac{\cosh \beta l - \cos \beta l}{\sinh \beta l + \sin \beta l}. \qquad (i)$$
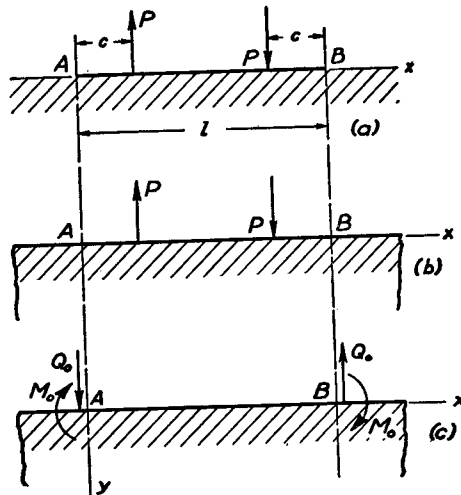


FIG. 14.

The method used for the symmetrical case shown in Fig. 11a can be applied also in the anti-symmetrical case shown in Fig. 14a. $Q_0$ and $M_0$ in this case will also represent an anti-symmetrical system as shown in Fig. 14c. For the determination of the proper

values of $Q_0$ and $M_0$, the system of equations similar to equations (a), (b) and (c) can be readily written. As soon as $Q_0$ and $M_0$ are calculated, all necessary information regarding the bending of the beam shown in Fig. 14a can be obtained by superposing the cases shown in Figures 14b and 14c.

Having the solutions for the symmetrical and for the anti-symmetrical loading of a beam, we can readily obtain the solution for any kind of loading by using the principle of superposition. For example, the solution of the unsymmetrical case shown in Fig. 15a is obtained by superposing the solutions of the symmetrical and the anti-symmetrical cases shown in Figs. 15b and 15c. The
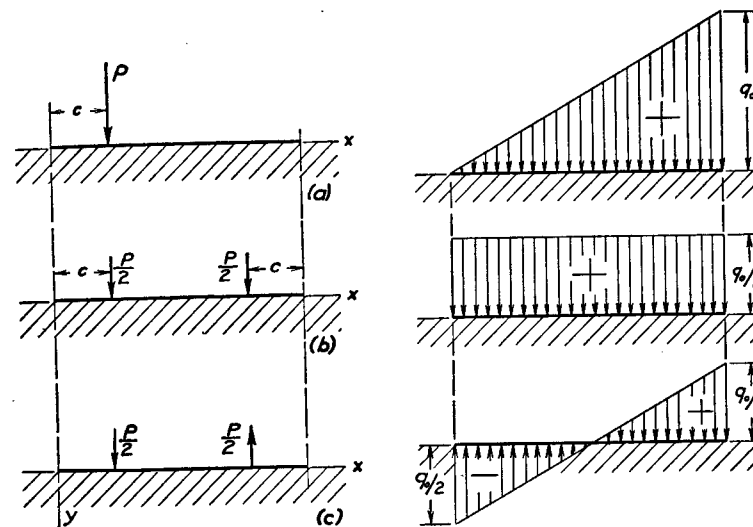


FIG. 15.
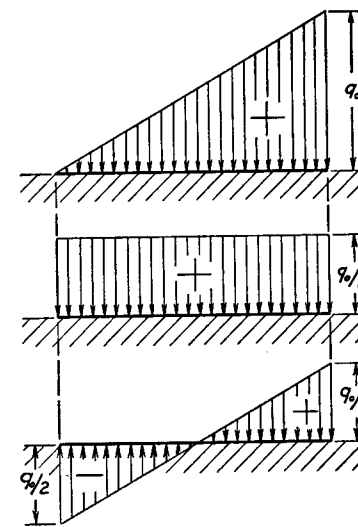


FIG. 16.

problem shown in Fig. 16 can be treated in the same manner. In each case the problem is reduced to the determination of the proper values of the forces $Q_0$ and moments $M_0$ from the two equations (c).

In discussing the bending of beams of finite length we note that the action of forces applied at one end of the beam on the deflection at the other end depends on the magnitude of the quantity $\beta l$. This quantity increases with the increase of the length of the beam. At the same time, as may be seen from Table 1, the functions $\varphi$, $\psi$ and $\theta$ are rapidly decreasing, and beyond a certain value of $\beta l$ we can assume that the force acting at one end of the beam has only a negligible effect at the other end. This justifies our considering the beam as an infinitely long one. In such a case the quantities

$\varphi(\beta l)$, $\psi(\beta l)$ and $\theta(\beta l)$ can be neglected in comparison with unity in equations (b); by so doing equations (c) are considerably simplified.

In general, a discussion of the bending of beams of a finite length falls naturally into the three groups:

      I. Short beams, $\beta l < 0.60$.
     II. Beams of medium length, $0.60 < \beta l < 5$.
    III. Long beams, $\beta l > 5$.

In discussing beams of the first group we can entirely neglect bending and consider these beams as absolutely rigid, since the deflection due to bending is usually negligibly small in comparison with the deflection of the foundation. Taking, for example, the case of a load at the middle, Fig. 13, and assuming $\beta l = 0.60$, we find from the formulas given above for $y_a$ and $y_c$ that the difference between the deflection at the middle and the deflection at the end is only about one-half of one per cent of the total deflection. This indicates that the deflection of the foundation is obtained with a very good accuracy by treating the beam as infinitely rigid and by using for the deflection the formula

$$y = \frac{P}{kl}.$$

The characteristic of beams of the second group is that a force acting on one end of the beam produces a considerable effect at the other end. Thus such beams must be treated as beams of finite length.

In the case of beams of the third group we can assume, in investigating one end of the beam, that the other end is infinitely far away. Hence the beam can be considered as infinitely long.

In our previous discussion it was always assumed that the beam was supported by a continuous elastic foundation but the results obtained can also be applied when the beam is supported by a large number of equidistant elastic supports. As an example of this kind, let us consider a horizontal beam $AB$, Fig. 17, supporting a system of equidistant vertical beams which are carrying a uniformly distributed load $q$.[8] All beams are simply supported at the ends. Denoting by $EI_1$ and $l_1$ the flexural rigidity and the length of vertical beams, we find the deflection at their middle to be

$$y = \frac{5}{384}\frac{ql_1^4}{EI_1} - \frac{Rl_1^3}{48EI_1},\qquad(j)$$

---

[8] Various problems of this kind are encountered in ship structures. A very complete discussion of such problems is given by I. G. Boobnov in his "Theory of Structure of Ships," vol. 2, 1914, S. Petersburg.

where $R$ is the pressure on the horizontal beam $AB$ of the vertical beam under consideration. Solving equation (j) for $R$ we find that the horizontal beam $AB$ is under the action of a concentrated force, Fig. 17c, the magnitude of which is

$$R = \frac{5}{8}ql_1 - \frac{48EI_1}{l_1^3}y.\qquad(k)$$

Assuming that the distance $a$ between the vertical beams is small in comparison with the length $l$ of the horizontal beam and replacing the concentrated forces by the equivalent uniform load, as shown in Fig. 17c, we also replace the stepwise load distribution, indicated
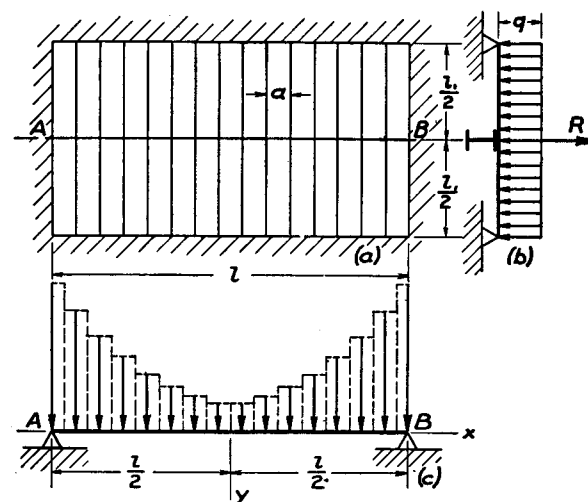


FIG. 17.

in the figure by the dotted lines, by a continuous load distribution of the intensity

$$q_1 - ky$$

where

$$q_1 = \frac{5}{8}\frac{ql_1}{a}; \qquad k = \frac{48EI_1}{al_1^3}.\qquad(l)$$

The differential equation of the deflection curve for the beam $AB$ then is

$$EI\frac{d^4y}{dx^4} = q_1 - ky.\qquad(m)$$

It is seen that the horizontal beam is in the condition of a uniformly

loaded beam on an elastic foundation. The intensity of the load and the modulus of foundation are given by the expressions $(l)$. In discussing the deflection of the beam we can use the method of superposition previously explained or we can directly integrate equation $(m)$. Using the latter method, we may write the general integral of the equation $(m)$ in the following form:

$$y = \frac{q_1}{k} + C_1 \sin \beta x \sinh \beta x + C_2 \sin \beta x \cosh \beta x \atop + C_3 \cos \beta x \sinh \beta x + C_4 \cos \beta x \cosh \beta x. \qquad (n)$$

Taking the origin of the coordinates at the middle, Fig. 17c, we conclude from the condition of symmetry that

$$C_2 = C_3 = 0.$$

Substituting this in the solution $(n)$ and using the conditions at the simply supported ends:

$$(y)_{x=l/2} = 0, \qquad \left(\frac{d^2y}{dx^2}\right)_{x=l/2} = 0,$$

we find

$$C_1 = -\frac{q_1}{k}\frac{2\sin\dfrac{\beta l}{2}\sinh\dfrac{\beta l}{2}}{\cos\beta l + \cosh\beta l},$$

$$C_4 = -\frac{q_1}{k}\frac{2\cos\dfrac{\beta l}{2}\cosh\dfrac{\beta l}{2}}{\cos\beta l + \cosh\beta l}.$$

The deflection curve then is

$$y = \frac{q_1}{k}\left[ 1 - \frac{2\sin\dfrac{\beta l}{2}\sinh\dfrac{\beta l}{2}}{\cos\beta l + \cosh\beta l}\sin\beta x \sinh\beta x \right.$$
$$\left. - \frac{2\cos\dfrac{\beta l}{2}\cosh\dfrac{\beta l}{2}}{\cos\beta l + \cosh\beta l}\cos\beta x \cosh\beta x \right]. \quad (o)$$

The deflection at the middle is obtained by taking $x = 0$ which gives

$$(y)_{x=0} = \frac{q_1}{k}\left(1 - \frac{2\cos\dfrac{\beta l}{2}\cosh\dfrac{\beta l}{2}}{\cos\beta l + \cosh\beta l}\right). \qquad (p)$$

Substituting this value in equation $(k)$, we find the reaction at the middle support of the vertical beam, which intersects the beam $AB$ at its mid-point. It is interesting to note that this reaction may become negative, which indicates that the horizontal beam actually supports the vertical beams only if it is sufficiently rigid; otherwise it may actually increase the bending of some of the vertical beams.

### Problems

1. Find a general expression for the deflection curve for the case illustrated in Fig. 12.

*Answer.*

$$y = \frac{2P\beta}{k}\frac{\cosh\beta x \cos\beta(l-x) + \cosh\beta(l-x)\cos\beta x}{\sinh\beta l + \sin\beta l}.$$

2. Find the deflections at the ends and the bending moment at the middle of the beam bent by two equal and opposite couples $M_0$, Fig. 18.
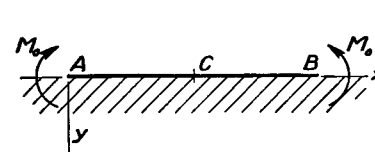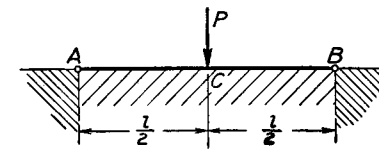


FIG. 18.                    FIG. 19.

*Answer.*

$$y_a = y_b = -\frac{2M_0\beta^2}{k}\frac{\sinh\beta l - \sin\beta l}{\sinh\beta l + \sin\beta l},$$

$$M_c = 2M_0\frac{\sinh\dfrac{\beta l}{2}\cos\dfrac{\beta l}{2} + \cosh\dfrac{\beta l}{2}\sin\dfrac{\beta l}{2}}{\sinh\beta l + \sin\beta l}.$$

3. Find the deflection and the bending moment at the middle of the beam with hinged ends and on an elastic foundation, the load being applied at the middle of the beam, Fig. 19.

*Answer.*

$$y_c = \frac{P\beta}{2k}\frac{\sinh\beta l - \sin\beta l}{\cosh\beta l + \cos\beta l},$$

$$M_c = \frac{P}{4\beta}\frac{\sinh\beta l + \sin\beta l}{\cosh\beta l + \cos\beta l}.$$

4. Find the deflection and the bending moment at the middle of the uniformly loaded beam with hinged ends on an elastic foundation, Fig. 20.
*Answer.*

$$y_c = \frac{q}{k}\left\{1 - \frac{2\cosh\frac{\beta l}{2}\cos\frac{\beta l}{2}}{\cosh\beta l + \cos\beta l}\right\},$$

$$M_c = \frac{q}{2\beta^2}\frac{\sinh\frac{\beta l}{2}\sin\frac{\beta l}{2}}{\cosh\beta l + \cos\beta l}.$$

5. Find the bending moments at the ends of the beam with built-in ends and on an elastic foundation. The beam is carrying a uniform load and a load at the middle, Fig. 21.
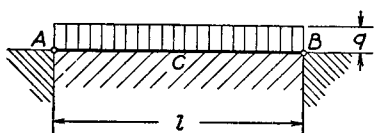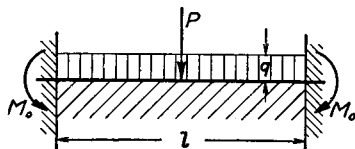


FIG. 20.          FIG. 21.

*Answer.*

$$M_0 = -\frac{P}{\beta}\frac{\sinh\frac{\beta l}{2}\sin\frac{\beta l}{2}}{\sinh\beta l + \sin\beta l} - \frac{q}{2\beta^2}\frac{\sinh\beta l - \sin\beta l}{\sinh\beta l + \sin\beta l}.$$

6. Find the deflection curve for the beam on an elastic foundation with the load applied at one end, Fig. 22.
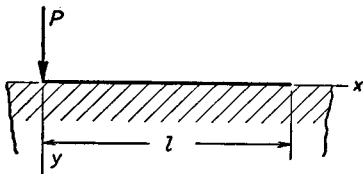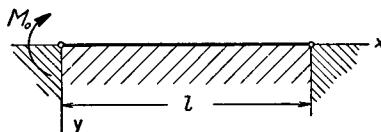


FIG. 22.          FIG. 23.

*Answer.*

$$y = \frac{2P\beta}{k(\sinh^2\beta l - \sin^2\beta l)}[\sinh\beta l \cos\beta x \cosh\beta(l - x)$$
$$- \sin\beta l \cosh\beta x \cos\beta(l - x)].$$

7. A beam on an elastic foundation and with hinged ends is bent by a couple $M_0$ applied at the end, Fig. 23. Find the deflection curve of the beam.
*Answer.*

$$y = \frac{2M_0\beta^2}{k(\cosh^2\beta l - \cos^2\beta l)}[\cosh\beta l \sin\beta x \sinh\beta(l - x)$$
$$- \cos\beta l \sinh\beta x \sin\beta(l - x)].$$

**4. Combined Direct Compression and Lateral Load.—** Let us begin with the simple problem of a strut with hinged ends, loaded by a single force $P$, and centrally compressed by two equal and opposite forces $S$, Fig. 24. Assuming that the
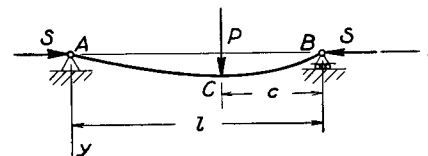


FIG. 24.

force $P$ acts in one of the principal planes of the strut, we see that the bending proceeds in the same plane. The differential equations of the deflection curve for the two portions of the strut are:

$$EI\frac{d^2y}{dx^2} = -Sy - \frac{Pc}{l}x, \qquad (a)$$

$$EI\frac{d^2y}{dx^2} = -Sy - \frac{P(l-c)}{l}(l-x). \qquad (b)$$

Using the notation

$$\frac{S}{EI} = p^2, \qquad (17)$$

we represent the solutions of the equations $(a)$ and $(b)$ in the following form:

$$y = C_1\cos px + C_2\sin px - \frac{Pc}{Sl}x, \qquad (c)$$

$$y = C_3\cos px + C_4\sin px - \frac{P(l-c)}{Sl}(l-x). \qquad (d)$$

Since the deflections vanish at the ends of the strut, we conclude that

$$C_1 = 0,$$
$$C_3 = -C_4 \tan pl.$$

The remaining two constants of integration we find from the conditions of continuity at the point of application of the load $P$, which require that equations $(c)$ and $(d)$ give the same deflection and the same slope for $x = l - c$; we obtain:

$$C_2 \sin p(l - c) = C_4[\sin p(l - c) - \tan pl \cos p(l - c)],$$
$$C_2 p \cos p(l - c)$$
$$= C_4 p[\cos p(l - c) + \tan pl \sin p(l - c)] + \frac{P}{S},$$

from which

$$C_2 = \frac{P \sin pc}{Sp \sin pl}, \qquad C_4 = -\frac{P \sin p(l - c)}{Sp \tan pl}.$$

Substituting in equation $(c)$ we obtain for the left portion of the strut:

$$y = \frac{P \sin pc}{Sp \sin pl} \sin px - \frac{Pc}{Sl} x. \tag{18}$$

From this, by differentiation, we find:

$$\left.\begin{aligned}
\frac{dy}{dx} &= \frac{P \sin pc}{S \sin pl} \cos px - \frac{Pc}{Sl}, \\
\frac{d^2y}{dx^2} &= -\frac{Pp \sin pc}{S \sin pl} \sin px.
\end{aligned}\right\} \tag{19}$$

The corresponding expressions for the right portion of the strut are obtained by substituting $(l - x)$ instead of $x$, and $(l - c)$ instead of $c$, and by changing the sign of $dy/dx$ in equations (18) and (19). These substitutions give:

$$y = \frac{P \sin p(l - c)}{Sp \sin pl} \sin p(l - x) - \frac{P(l - c)}{Sl} (l - x), \tag{20}$$

$$\frac{dy}{dx} = -\frac{P \sin p(l - c)}{S \sin pl} \cos p(l - x) + \frac{P(l - c)}{Sl}, \tag{21}$$

$$\frac{d^2y}{dx^2} = -\frac{Pp \sin p(l - c)}{S \sin pl} \sin p(l - x). \tag{22}$$

In a particular case, when the load $P$ is applied at the middle, we have $c = l/2$, and, by introducing the notation

$$\frac{Sl^2}{4EI} = \frac{p^2l^2}{4} = u^2, \tag{23}$$

we obtain from equation (18)

$$(y)_{max} = (y)_{x=l/2} = \frac{P}{2Sp}\left(\tan\frac{pl}{2} - \frac{pl}{2}\right)$$
$$= \frac{Pl^3}{48EI} \cdot \frac{\tan u - u}{\frac{1}{3}u^3}. \tag{24}$$

The first factor in expression (24) represents the deflection produced by the lateral load $P$ acting alone. The second factor indicates in what proportion the deflection produced by $P$ is magnified by the axial compressive force $S$. When $S$ is small in comparison with Euler load $(S_e = EI\pi^2/l^2)$, the quantity $u$ is small and the second factor in equation (24) approaches unity, which indicates that under this condition the effect on the deflection of the axial compressive force is negligible. When $S$ approaches the Euler value, the quantity $u$ approaches the value $\pi/2$ (see eq. 23) and the second factor in expression (24) increases indefinitely, as should be expected from our previous discussion of critical load (see p. 244, Part I).

The maximum value of the bending moment is under the load and its value is obtained from the second of equations (19), and

$$M_{max} = -EI\left(\frac{d^2y}{dx^2}\right)_{x=l/2} = EI\frac{Pp}{2S}\tan\frac{pl}{2} = \frac{Pl}{4} \cdot \frac{\tan u}{u}. \tag{25}$$

Again we see that the first factor in expression (25) represents

the bending moment produced by the load $P$ acting alone, while the second factor is the *magnification factor* representing the action of the axial force $S$ on the maximum bending moment.

Having solved the problem for one lateral load $P$, Fig. 24, we can readily obtain the solution for the case of a strut bend by a couple applied at the end, Fig. 25. It is only necessary



FIG. 25.

to assume that in our previous discussion the distance $c$ is indefinitely diminishing approaching zero, while $Pc$ remains a constant equal to $M_0$. Substituting $Pc = M_0$ and $\sin kc = kc$ in equation (18), we obtain the deflection curve:

$$y = \frac{M_0}{S}\left(\frac{\sin px}{\sin pl} - \frac{x}{l}\right), \tag{26}$$

from which

$$\frac{dy}{dx} = \frac{M_0}{S}\left(\frac{p \cos px}{\sin pl} - \frac{1}{l}\right).$$

The slopes of the beam at the ends are

$$\left(\frac{dy}{dx}\right)_{x=0} = \frac{M_0}{S}\left(\frac{p}{\sin pl} - \frac{1}{l}\right)$$
$$= \frac{M_0 l}{6EI} \cdot 6\left(\frac{1}{2u \sin 2u} - \frac{1}{(2u)^2}\right), \tag{27}$$

$$\left(\frac{dy}{dx}\right)_{x=l} = \frac{M_0}{S}\left(\frac{p}{\tan pl} - \frac{1}{l}\right)$$
$$= \frac{M_0 l}{3EI} \cdot 3\left(\frac{1}{2u \tan 2u} - \frac{1}{(2u)^2}\right). \tag{28}$$

Again the first factors in expressions (27) and (28) taken with proper signs represent the slopes produced by the couple

$M_0$ acting alone (see p. 158, Part I), and the second factors represent the effect of the axial force $S$.

Considering equations (18) and (26), we see that the lateral force $P$ and the couple $M_0$ occur in these expressions linearly, while the axial force $S$ occurs in the same expressions in a more complicated manner, since $p$ also contains $S$ (see eq. 17). From this we conclude that if at point $C$, Fig. 24, two forces $P$ and $Q$ are applied, the deflection at any point may be obtained by superposing the deflections produced by the load $Q$ and the axial forces $S$ on the deflection produced by the load $P$ and the same axial forces. A similar conclusion can be reached regarding couples applied to one end of the beam.

The conclusion regarding superposition can be readily generalized and extended to cover the case of several loads, Fig. 26. For each portion of the strut an equation similar to
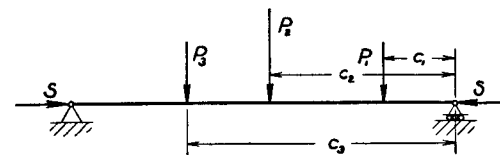


FIG. 26.

equations (*a*) and (*b*) can be written, and a solution similar to those in (*c*) and (*d*) can be obtained. The constants of integration can be found from the conditions of continuity at the points of load application and from the conditions at the ends of the strut. In this way it can be shown that the deflection at any point of the strut is a linear function of the loads $P_1$, $P_2$, $\cdots$ and that the deflection at any point can be obtained by superposing the deflections produced at that point by each of the lateral loads acting together with the axial force $S$. Let us consider a general case when $n$ forces are acting and $m$ of these forces are applied to the right of the cross section for which we are calculating the deflection. The expression for this deflection is obtained by using equation (18) for the forces $P_1$, $P_2$, $\cdots P_m$ and equation (20) for the

forces $P_{m+1}, P_{m+2}, \cdots P_n$. In this way we obtain the required deflection:

$$y = \frac{\sin px}{Sp \sin pl} \sum_{i=1}^{i=m} P_i \sin pc_i - \frac{x}{Sl} \sum_{i=1}^{i=m} P_i c_i$$

$$+ \frac{\sin p(l-x)}{Sp \sin pl} \sum_{i=m+1}^{i=n} P_i \sin p(l-c_i)$$

$$- \frac{l-x}{Sl} \sum_{i=m+1}^{i=n} P_i(l-c_i). \quad (29)$$

If, instead of concentrated forces, there is a uniform load of intensity $q$ acting on the strut, each element $qdc$ of this load, taken at a distance $c$ from the right end, can be considered as a concentrated force. Substituting it, instead of $P_i$, in equation (29) and replacing summation signs by integration, we obtain the following expression for the deflection curve:

$$y = \frac{\sin px}{Sp \sin pl} \int_0^{l-x} q \sin pc \, dc - \frac{x}{Sl} \int_0^{l-x} qc \, dc$$

$$+ \frac{\sin p(l-x)}{Sp \sin pl} \int_{l-x}^{l} q \sin p(l-c) \, dc - \frac{l-x}{Sl} \int_{l-x}^{l} q(l-c) \, dc.$$

Integrating the above gives

$$y = \frac{q}{Sp^2}\left[\frac{\cos\left(\frac{pl}{2} - px\right)}{\cos \frac{pl}{2}} - 1\right] - \frac{q}{2S} x(l-x) \quad (30)$$

and

$$y_{max} = (y)_{x=l/2} = \frac{q}{Sp^2}\left(\frac{1}{\cos u} - 1 - \frac{u^2}{2}\right)$$

$$= \frac{5}{384}\frac{ql^2}{EI} \cdot \frac{\frac{1}{\cos u} - 1 - \frac{u^2}{2}}{(5/24)u^4}. \quad (31)$$

By differentiating equation (30), we readily obtain the expressions for the slope and for the bending moment. The slope at the left end of the strut is

$$\left(\frac{dy}{dx}\right)_{x=0} = \frac{ql}{2S}\left[\frac{\tan \frac{pl}{2}}{\frac{pl}{2}} - 1\right] = \frac{ql^3}{24EI}\frac{\tan u - u}{\frac{1}{3}u^3}. \quad (32)$$

The maximum bending moment is at the middle where

$$M_{max} = -EI\left(\frac{d^2y}{dx^2}\right)_{x=l/2}$$

$$= EI\frac{q\left(1 - \cos \frac{pl}{2}\right)}{S \cos \frac{pl}{2}} = \frac{ql^2}{8} \cdot \frac{2(1 - \cos u)}{u^2 \cos u}. \quad (33)$$

By using solution (26) for the case of a couple together with solution (29) for lateral loads, and applying the method of superposition, various statically indeterminate cases of bending of struts can be readily solved. Taking as an example the case of a uniformly loaded strut built in at one end, Fig. 27, we find the bending moment $M_0$ at the built-in end from the condition that this end does not rotate during bending. By using equations (28) and (32) this condition is found to be
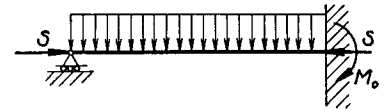


FIG. 27.

$$-\frac{ql^3}{24EI}\frac{\tan u - u}{\frac{1}{3}u^3} + \frac{M_0 l}{3EI} \cdot \left(\frac{3}{2u \tan 2u} - \frac{3}{(2u)^2}\right) = 0$$

from which

$$M_0 = -\frac{ql^2}{8} \cdot \frac{4 \tan 2u(\tan u - u)}{u(\tan 2u - 2u)}. \quad (34)$$

In the case of a uniformly loaded strut with both ends built-in the moments $M_0$ at the ends are obtained from the

equation:

$$-\frac{ql^3}{24EI}\frac{\tan u - u}{\frac{1}{3}u^3} + \frac{M_0 l}{3EI}\left[\frac{3}{2u \tan 2u} - \frac{3}{(2u)^2}\right]$$
$$-\frac{M_0 l}{6EI}\left(\frac{6}{2u \sin 2u} - \frac{6}{(2u)^2}\right) = 0,$$

from which

$$M_0 = -\frac{ql^2}{12} \cdot \frac{\tan u - u}{\frac{1}{3}u^2 \tan u} \cdot \qquad (35)$$

It is seen from expressions (34) and (35) that the values of the statically indeterminate moments in the case of struts are obtained by multiplying the corresponding moments calculated from the beam formulas by certain magnification factors. All necessary calculations can be greatly simplified by using the prepared numerical tables for determining magnification factors.[9]

When the maximum bending moment for a strut is found, the numerical stress maximum is obtained by combining the direct stress with the maximum bending stress, which gives

$$|\sigma|_{max} = \frac{S}{A} + \frac{M_{max}}{Z} \qquad (e)$$

where $A$ and $Z$ are, respectively, the cross-sectional area and the section modulus for the strut. Taking, as an example, the case of a uniformly loaded strut with hinged ends, we obtain from equation (33):

$$|\sigma|_{max} = \frac{S}{A} + \frac{ql^2}{8Z} \cdot \frac{2(1 - \cos u)}{u^2 \cos u} \cdot \qquad (f)$$

In selecting the proper cross-sectional dimensions of the strut it is necessary to consider that the right side of the equation (f) is not linear in $S$ since the quantity $u$ also depends on $S$, as may be seen from expression (23). Owing to this fact the maximum stress increases at a greater rate than

---

[9] Various particular cases of laterally loaded struts have been discussed by A. P. Van der Fleet, Bull. Soc. of Engineers of Ways of Communication, 1900–1903, St. Petersburg. Numerous tables of magnification factors are given in that work.

the force $S$. Thus the usual method for determining the proper dimensions by taking [10]

$$|\sigma_{max}| = \frac{\sigma_{yp}}{n}, \qquad (g)$$

where $n$ is the factor of safety, fails in this case.

If the strut must be designed so that it will begin to yield when the forces $S$ and $q$ increase $n$ times, the cross section must be selected so that $|\sigma|_{max}$ will be somewhat smaller than $\sigma_{yp}/n$ in order to satisfy the equation:

$$\frac{\sigma_{yp}}{n} = \frac{S}{A} + \frac{ql^2}{8Z} \cdot \frac{2(1 - \cos u_1)}{u_1^2 \cos u_1}, \qquad (h)$$

in which $u_1 = nu$.

It is apparent that if we proceed in this manner we satisfy the requirement regarding the beginning of yielding; by multiplying both sides of the equation (h) by $n$ we find

$$\sigma_{yp} = \frac{nS}{A} + \frac{nql^2}{8Z} \cdot \frac{2(1 - \cos u_1)}{u_1^2 \cos u_1}, \qquad (i)$$

which indicates that the maximum stress reaches the yield point stress when $S$ and $q$ have been increased $n$ times. Similar procedure in the design of struts can be applied in other cases of loading. We can conclude from the above discussion that to ascertain a factor of safety $n$ in the design of struts,[11] we must use instead of equation (g) a modified equation similar to equation (h), in which the parameter $u$ is replaced by $u_1 = nu$.

### Problems

1. Find the slope at the left end of a strut with hinged ends which is loaded at the middle by the load $P$.

---

[10] It is assumed that material of the strut has a pronounced yield point.

[11] This method of design of struts was developed by K. S. Zavriev, see Memoirs of the Institute of Engineers of Ways of Communication, 1913, S. Petersburg.

*Answer.*

$$\left(\frac{dy}{dx}\right)_{x=0} = \frac{P}{2S}\frac{1 - \cos u}{\cos u} = \frac{Pl^2}{16EI}\frac{1 - \cos u}{\frac{1}{2}u^2 \cos u}.$$

2. Find the slopes at the ends of a strut carrying a triangular load, Fig. 28.
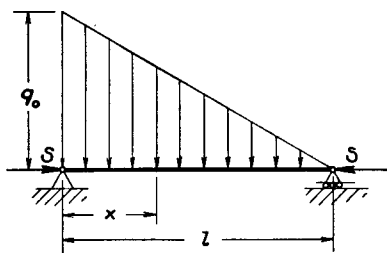


FIG. 28.

*Solution.* Substituting in equation (29) $q_0 c\,dc/l$, instead of $P_i$, and replacing summation by integration we find:

$$y = \frac{\sin px}{Sp \sin pl}\int_0^{l-x} \frac{q_0 c}{l}\sin pc\,dc - \frac{x}{Sl}\int_0^{l-x}\frac{q_0 c^2}{l}\,dc$$

$$+ \frac{\sin p(l-x)}{Sp \sin pl}\int_{l-x}^l \frac{q_0 c}{l}\sin p(l-c)\,dc - \frac{l-x}{Sl}\int_{l-x}^l \frac{q_0 c}{l}(l-c)\,dc.$$

Differentiating this with respect to $x$, we find that

$$\left(\frac{dy}{dx}\right)_{x=0} = \frac{2q_0 l}{6p^2 EI}(\beta - 1)$$

and

$$\left(\frac{dy}{dx}\right)_{x=l} = -\frac{q_0 l}{6p^2 EI}(\alpha - 1),$$

where $\alpha$ and $\beta$ are functions given by expressions (36) (see p. 36).

3. Find the slopes at the ends of a strut symmetrically loaded by two loads $P$, as shown in Fig. 29.

*Answer.*

$$\left(\frac{dy}{dx}\right)_{x=0} = -\left(\frac{dy}{dx}\right)_{x=l} = \frac{P}{S}\left(\frac{\cos pb}{\cos \frac{pl}{2}} - 1\right).$$

4. A strut with built-in ends is loaded as shown in Fig. 29. Find the bending moments, $M_0$, at the ends.

*Solution.* The moments $M_0$ are found from the conditions that the ends of the strut do not rotate. By using the answer of the
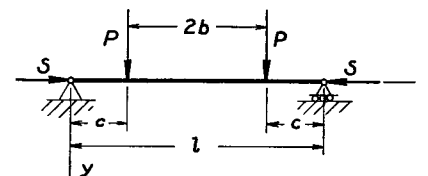


FIG. 29.

preceding problem and also equations (27) and (28), the following equation for calculating $M_0$ is obtained:

$$\frac{M_0 l}{6EI}\alpha + \frac{M_0 l}{3EI}\beta + \frac{P}{S}\left(\frac{\cos pb}{\cos \frac{pl}{2}} - 1\right) = 0,$$

from which

$$M_0 = -\frac{2PEI}{Sl}\frac{u}{\tan u}\left(\frac{\cos pb}{\cos u} - 1\right).$$

If $b = 0$, we obtain the case of a load $2P$ concentrated at the middle.
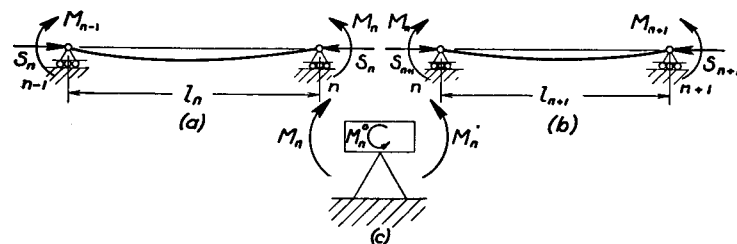


FIG. 30.

**5. Continuous Struts.**—In the case of a continuous strut we proceed as in the case of continuous beams (see p. 201, Part I) and consider two adjacent spans, Fig. 30.[12] Using equations (23), (27), and (28) and introducing notations for the $n$th span:

$$u_n = \frac{S_n l_n^2}{4EI_n},$$

---

[12] The theory is due to H. Zimmermann, Sitzungsb., Akad. Wiss., Berlin, 1907 and 1909.

$$\alpha_n = 6 \left[ \frac{1}{2u_n \sin 2u_n} - \frac{1}{(2u_n)^2} \right],$$
$$\beta_n = 3 \left[ \frac{1}{(2u_n)^2} - \frac{1}{2u_n \tan 2u_n} \right],$$
(36)

$$\gamma_n = \frac{\tan u_n - u_n}{\frac{1}{3} u_n^3}.$$
(37)

We conclude that the slope at the right end of the $n$th span, Fig. 30$a$, produced by the end moments $M_{n-1}$ and $M_n$, is

$$- \beta_n \frac{M_n l_n}{3EI_n} - \alpha_n \frac{M_{n-1} l_n}{6EI_n}.$$
(a)

The slope produced at the left end of the $n + 1$ span by the moments $M_n$ and $M_{n+1}$ is

$$\alpha_{n+1} \frac{M_{n+1} l_{n+1}}{6EI_{n+1}} + \beta_{n+1} \frac{M_n l_{n+1}}{3EI_{n+1}}.$$
(b)

If there is no lateral load acting on the two spans under consideration, the expressions (a) and (b) must be equal, and we obtain:

$$\frac{\alpha_n l_n}{I_n} M_{n-1} + 2 \left( \beta_n \frac{l_n}{I_n} + \beta_{n+1} \frac{l_{n+1}}{I_{n+1}} \right) M_n + \alpha_{n+1} \frac{l_{n+1}}{I_{n+1}} M_{n+1} = 0.$$ (38)

This is the three moment equation for a continuous strut if there is no lateral load on the two spans under consideration.

If there is lateral load acting, the corresponding slopes produced by this load must be added to expressions (a) and (b). Taking, for example, the case of uniform load $q_n$ and $q_{n+1}$ acting on the spans $n$ and $n + 1$ in a downward direction, we obtain the corresponding slopes from equation (32) and, instead of expressions (a) and (b), we obtain:

$$- \beta_n \frac{M_n l_n}{3EI_n} - \alpha_n \frac{M_{n-1} l_n}{6EI_n} - \gamma_n \frac{q_n l_n^3}{24EI_n},$$
(c)

$$\alpha_{n+1} \frac{M_{n+1} l_{n+1}}{6EI_{n+1}} + \beta_{n+1} \frac{M_n l_{n+1}}{3EI_{n+1}} + \gamma_{n+1} \frac{q_{n+1} l_{n+1}^3}{24EI_{n+1}}.$$
(d)

Equating these two expressions we obtain:

$$\frac{\alpha_n l_n}{I_n} M_{n-1} + 2 \left( \beta_n \frac{l_n}{I_n} + \beta_{n+1} \frac{l_{n+1}}{I_{n+1}} \right) M_n + \alpha_{n+1} \frac{l_{n+1}}{I_{n+1}} M_{n+1} \cdot$$
$$= - \gamma_n \frac{q_n l_n^3}{4I_n} - \gamma_{n+1} \frac{q_{n+1} l_{n+1}^3}{4I_{n+1}}.$$ (39)

This is the three moment equation for a strut with a uniform load in each span. It is similar to the three moment equation for a continuous beam and coincides with it when $S = 0$ and all functions $\alpha$, $\beta$, $\gamma$ become equal to unity.

For any other kind of lateral load we have to change only the right side of the equation (39), which depends on the rotation of the adjacent ends of the two spans produced by lateral loading. Taking, for example, the case of a trapezoidal load shown in Fig. 31 and dividing the load into two parts, uniform loads and triangular loads, we use for the uniform loads the terms which we already have on the right side of equation (39). To these terms we must add the terms corresponding to the triangular loads. Using the expressions for the slopes in problem 2 of the preceding article, we find that the two terms which we have to add to the right side of equation (39) in the case of the load shown in Fig. 31 are:
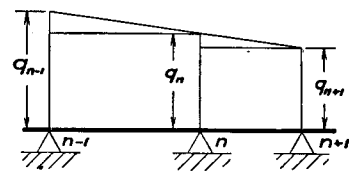


FIG. 31.

$$- \frac{(q_{n-1} - q_n) l_n}{p^2 I_n} (\alpha_n - 1) - \frac{2(q_n - q_{n+1}) l_{n+1}}{p^2 I_{n+1}} (\beta_{n+1} - 1),$$ (e)

in which $\alpha_n$ and $\beta_{n+1}$ are defined by expressions (36). If concentrated forces are acting on the spans under consideration the required expressions for the rotations are readily obtainable from the general expression for the deflection curve (29).

The calculation of moments from the three moment equations (39) can be considerably simplified by using numerical tables of functions $\alpha$, $\beta$ and $\gamma$.[13]

In the derivation of equation (39) it was assumed that the moment $M_n$ at the $n$th support had the same value for both adjacent spans. There are cases, however, in which an external moment $M_n^0$ is applied at the support as shown in Fig. 30$c$; in such cases we must distinguish between the value of the bending moment to the left and to the right of the support. The relation between these two moments is given by the equation of statics:[14]

$$M_n - M_n^0 - M_n' = 0,$$

---

[13] Such tables can be found in the book by A. S. Niles and J. S. Newell, "Airplane Structures," Vol. 2, 1938, see also writer's book, "Theory of Elastic Stability," 1936.

[14] The direction of $M_n^0$ indicated in the Fig. 30$c$ is taken as positive direction for an external moment.

from which

$$M_n' = M_n - M_n^0. \qquad (f)$$

Equation (39) in such a case is replaced by the following equation:

$$\frac{\alpha_n l_n}{I_n} M_{n-1} + 2\beta_n \frac{l_n}{I_n} M_n + 2\beta_{n+1} \frac{l_{n+1}}{I_{n+1}} M_n' + \alpha_{n+1} \frac{l_{n+1}}{I_{n+1}} M_{n+1}$$

$$= -\gamma_n \frac{q_n l_n^3}{4 I_n} - \gamma_{n+1} \frac{q_{n+1} l_{n+1}^3}{4 I_{n+1}}. \qquad (40)$$

If the supports of a continuous strut are not on a straight line, the additional terms, depending on the differences in the levels of the three consecutive supports, must be put on the right side of equation (39) or (40). These terms are not affected by the presence of the axial forces, and are the same as in the case of a beam (see p. 204, Part I).

### Problems

1. Write the right side of the three moment equation if there is a concentrated force $P$ in the span $n + 1$ at a distance $c_{n+1}$ from the support $n + 1$.
*Answer.*

$$-\frac{6PE}{S_{n+1}} \left( \frac{\sin p_{n+1}c_{n+1}}{\sin p_{n+1}l_{n+1}} - \frac{c_{n+1}}{l_{n+1}} \right) = -\frac{6P}{p^2_{n+1}I_{n+1}} \left( \frac{\sin p_{n+1}c_{n+1}}{\sin p_{n+1}l_{n+1}} - \frac{c_{n+1}}{l_{n+1}} \right).$$

2. Write the right side of the three moment equation if the $n$th span is loaded as shown in Fig. 29, p. 35, and if there is no load on span $n + 1$.
*Answer.* Using the solution of problem 3, p. 34, we obtain the following expression:

$$-\frac{6PE}{S_n} \left( \frac{\cos p_n b_n}{\cos \frac{p_n l_n}{2}} - 1 \right) = -\frac{6P}{p_n^2 I_n} \left( \frac{\cos p_n b_n}{\cos \frac{p_n l_n}{2}} - 1 \right).$$
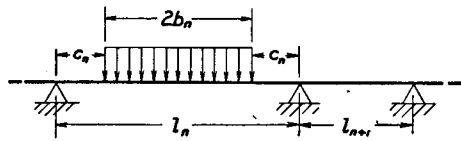


FIG. 32.

3. Find the right side of the three moment equation if the load is as shown in Fig. 32.
*Answer.*

$$-\frac{6q_n}{p_n^2 I_n} \left( \frac{\cos p_n b_n}{p_n \cos \frac{p_n l_n}{2}} - b_n \right).$$

**6. Tie-Rod with Lateral Loading.**—If a tie-rod is submitted to the action of tensile forces $S$ and a lateral load $P$, Fig. 33, we can write the differential equation of the deflection
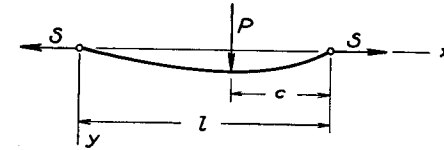


FIG. 33.

curve for each portion of the rod in exactly the same manner as we did for a strut, Art. 4. It is only necessary to change the sign of $S$. In such a case instead of quantities $p^2$ and $u^2$ defined by expressions (17) and (23), respectively, we shall have $-p^2$ and $-u^2$, and instead of $p$ and $u$ we shall have $p\sqrt{-1} = pi$ and $u\sqrt{-1} = ui$. Substituting $-S$, $pi$, and $ui$ in the place of $S$, $p$ and $u$ in the formulas obtained for the strut in Fig. 24, we obtain necessary formulas for the tie-rod in Fig. 33. In making this substitution we use the known relations:

$$\sin ui = i \sinh u, \quad \cos ui = \cosh u, \quad \tan ui = i \tanh u.$$

In this way we obtain for the left portion of the tie-rod in Fig. 33, from equations (18) and (19):

$$y = -\frac{P \sinh pc}{Sp \sinh pl} \sinh px + \frac{Pc}{Sl} x, \qquad (41)$$

$$\frac{dy}{dx} = -\frac{P \sinh pc}{S \sinh pl} \cosh px + \frac{Pc}{Sl},$$

$$\frac{d^2y}{dx^2} = -\frac{Pp \sinh pc}{S \sinh pl} \sinh px. \qquad (42)$$

Similar formulas can also be obtained for the right-hand portion of the tie-rod by using equations (20)–(22). Having the deflection curve for the case of one load $P$ acting on the tie-rod, we can readily obtain the deflection curve for any other kind of loading by using the method of superposition.

Considering, for example, a uniformly loaded tie-rod and using equations (30) and (31) for a strut, we obtain:

$$y = \frac{q}{Sp^2}\left[\frac{\cosh\left(\frac{pl}{2} - px\right)}{\cosh\frac{pl}{2}} - 1\right] + \frac{q}{2S}x(l - x),$$

and the maximum deflection is

$$y_{max} = (y)_{x=l/2}$$

$$= \frac{5}{384}\frac{ql^4}{EI}\cdot\frac{\frac{1}{\cosh u} - 1 + \frac{u^2}{2}}{(5/24)u^4} = \frac{5}{384}\frac{ql^4}{EI}\cdot\varphi_1(u), \quad (43)$$

where

$$\varphi_1(u) = \frac{\frac{1}{\cosh u} - 1 + \frac{u^2}{2}}{(5/24)u^4}.$$

The slope of the deflection curve at the left-hand end, from equation (32), is

$$\left(\frac{dy}{dx}\right)_{x=0} = \frac{ql^3}{24EI}\frac{u - \tanh u}{\frac{1}{3}u^3}. \quad (44)$$

The maximum bending moment, which in this case is at the middle of the span, is obtained from expression (33):

$$M_{max} = \frac{ql^2}{8}\cdot\frac{2(\cosh u - 1)}{u^2\cosh u} = \frac{ql^2}{8}\psi_1(u) \quad (45)$$

where

$$\psi_1(u) = \frac{2(\cosh u - 1)}{u^2\cosh u}.$$

The deflection and the maximum bending moment are obtained by multiplying the corresponding expressions for a

simple beam by factors $\varphi_1(u)$ and $\psi_1(u)$, depending on the magnitude of the axial tensile force $S$. The numerical values of these factors are given in Table 3.[15]

In the case of bending of a tie-rod by a couple applied at the right-hand end, the deflection curve is obtained from equation (26), from which

$$y = \frac{M_0}{S}\left(\frac{x}{l} - \frac{\sinh px}{\sinh pl}\right). \quad (46)$$

If there are two equal and opposite couples applied at the ends of a tie-rod, the deflection curve is obtained by the method of superposition:

$$y = \frac{M_0}{S}\left(\frac{x}{l} - \frac{\sinh px}{\sinh pl}\right) + \frac{M_0}{S}\left[\frac{l - x}{l} - \frac{\sinh p(l - x)}{\sinh pl}\right]$$

$$= \frac{M_0}{S}\left[1 - \frac{\cosh p\left(\frac{l}{2} - x\right)}{\cosh\frac{pl}{2}}\right]. \quad (47)$$

From this equation we find the deflection at the middle and the slope at the left-hand end of the tie-rod:

$$(y)_{x=l/2} = \frac{M_0}{S}\cdot\frac{\cosh u - 1}{\cosh u} = \frac{M_0 l^2}{8EI}\cdot\frac{\cosh u - 1}{\frac{1}{2}u^2\cosh u},$$

$$\left(\frac{dy}{dx}\right)_{x=0} = \frac{M_0}{S}p\tanh u = \frac{M_0 l}{2EI}\cdot\frac{\tanh u}{u}. \quad (48)$$

The bending moment at the middle is

$$(M)_{x=l/2} = -EI\left(\frac{d^2y}{dx^2}\right)_{x=l/2} = M_0\cdot\frac{1}{\cosh u}. \quad (49)$$

Having the deflection curves for a tie-rod with hinged ends bent by transerve loading and by couples at the ends, we can readily obtain various statically indeterminate cases of

[15] Various cases of bending of tie-rods are investigated in the papers by A. P. Van der Fleet previously mentioned (see p. 32) and also in the book by I. G. Boobnov, "Theory of Structure of Ships," vol. 2, 1914, S. Petersburg. From the later book the Table 3 is taken.

bending of tie-rods by the method of superposition. Taking, for example, the case of a uniformly loaded tie-rod with built-in ends and using expressions (44) and (48), we obtain the bending moments $M_0$ at the ends from the equation:

$$\frac{ql^3}{24EI} \cdot \frac{u - \tanh u}{\frac{1}{3}u^3} + \frac{M_0 l}{2EI} \cdot \frac{\tanh u}{u} = 0,$$

from which

$$M_0 = -\frac{ql^2}{12} \cdot \frac{u - \tanh u}{\frac{1}{3}u^2 \tanh u} = -\frac{ql^2}{12}\psi_2(u), \qquad (50)$$

where

$$\psi_2(u) = \frac{u - \tanh u}{\frac{1}{3}u^2 \tanh u}.$$

The numerical values of the function $\psi_2(u)$ are given in Table 3. By using expressions (45) and (49) the bending moment at the middle, $M_1$, is obtained:

$$M_1 = \frac{ql^2}{8} \cdot \frac{2(\cosh u - 1)}{u^2 \cosh u} - \frac{ql^2}{12} \cdot \frac{u - \tanh u}{\frac{1}{3}u^2 \sinh u}$$

$$= \frac{ql^2}{24} \cdot \frac{6(\sinh u - u)}{u^2 \sinh u} = \frac{ql^2}{24}\psi_3(u). \quad (51)$$

The deflection at the middle is obtained by using equations (43) and (48) which give

$$y_{\max} = (y)_{x=l/2} = \frac{5}{384}\frac{ql^4}{EI} \cdot \frac{\frac{1}{\cosh u} - 1 + \frac{u^2}{2}}{(5/24)u^4}$$

$$- \frac{ql^4}{16EI}\frac{(u - \tanh u)(\cosh u - 1)}{u^4 \sinh u} = \frac{ql^4}{384EI} \cdot \varphi_2(u) \quad (52)$$

where

$$\varphi_2(u) = \frac{24}{u^4}\left(\frac{u^2}{2} - \frac{u \cosh u - u}{\sinh u}\right).$$

TABLE 3. DEFLECTIONS AND MAXIMUM BENDING MOMENT CONSTANTS IN LATERALLY LOADED TIE-RODS

| $u$ | $\varphi_1$ | $\varphi_2$ | $\psi_1$ | $\psi_2$ | $\psi_3$ | $u$ | $\varphi_1$ | $\varphi_2$ | $\psi_1$ | $\psi_2$ | $\psi_3$ |
|---|---|---|---|---|---|---|---|---|---|---|---|
| 0 | 1.000 | 1.000 | 1.000 | 1.000 | 1.000 | 6.5 | 0.054 | 0.197 | 0.047 | 0.391 | 0.139 |
| 0.5 | 0.908 | 0.976 | 0.905 | 0.984 | 0.972 | 7.0 | 0.047 | 0.175 | 0.041 | 0.367 | 0.121 |
| 1.0 | 0.711 | 0.909 | 0.704 | 0.939 | 0.894 | 7.5 | 0.041 | 0.156 | 0.036 | 0.347 | 0.106 |
| 1.5 | 0.523 | 0.817 | 0.511 | 0.876 | 0.788 | 8.0 | 0.036 | 0.141 | 0.031 | 0.328 | 0.093 |
| 2.0 | 0.380 | 0.715 | 0.367 | 0.806 | 0.673 | 8.5 | 0.032 | 0.127 | 0.028 | 0.311 | 0.083 |
| 2.5 | 0.281 | 0.617 | 0.268 | 0.736 | 0.563 | 9.0 | 0.029 | 0.115 | 0.025 | 0.296 | 0.074 |
| 3.0 | 0.213 | 0.529 | 0.200 | 0.672 | 0.467 | 9.5 | 0.026 | 0.105 | 0.022 | 0.283 | 0.066 |
| 3.5 | 0.166 | 0.453 | 0.153 | 0.614 | 0.386 | 10.0 | 0.024 | 0.096 | 0.020 | 0.270 | 0.060 |
| 4.0 | 0.132 | 0.388 | 0.120 | 0.563 | 0.320 | 10.5 | 0.021 | 0.088 | 0.018 | 0.259 | 0.054 |
| 4.5 | 0.107 | 0.335 | 0.097 | 0.519 | 0.267 | 11.0 | 0.020 | 0.081 | 0.017 | 0.248 | 0.050 |
| 5.0 | 0.088 | 0.291 | 0.079 | 0.480 | 0.224 | 11.5 | 0.018 | 0.075 | 0.015 | 0.238 | 0.045 |
| 5.5 | 0.074 | 0.254 | 0.066 | 0.446 | 0.189 | 12.0 | 0.016 | 0.069 | 0.014 | 0.229 | 0.042 |
| 6.0 | 0.063 | 0.223 | 0.055 | 0.417 | 0.162 | | | | | | |

All these functions are equal to unity at $u = 0$, i.e., when only a transverse load is acting. As the longitudinal tensile force increases, each function decreases, i.e., the longitudinal tensile forces diminish the deflections and the bending moments in laterally loaded tie-rods. Some applications of the above table will be given later in discussing the bending of thin plates (see p. 122).

### Problems

1. Find the maximum deflection and the maximum bending moment for a tie-rod loaded at the middle.
   *Answer.*

$$(y)_{\max} = \frac{Pl^3}{48EI} \cdot \frac{u - \tanh u}{\frac{1}{3}u^3},$$

$$M_{\max} = \frac{Pl}{4} \cdot \frac{\tanh u}{u}.$$

2. Find the bending moments $M_0$ at the ends of a tie-rod with built-in ends symmetrically loaded by two forces $P$ as shown in Fig. 29.
   *Solution.* The bending moments at the ends are obtained from the equation:

$$\frac{P}{S}\left(1 - \frac{\cosh pb}{\cosh \frac{pl}{2}}\right) + \frac{M_0 l}{2EI} \cdot \frac{\tanh u}{u} = 0.$$

3. Find the bending moments at the ends of a tie-rod with built-in ends loaded by a triangular load as shown in Fig. 28.
   *Hint.* Use solution of problem 2 on p. 34 together with equation (46).

## 7. Representation of the Deflection Curve by a Trigonometrical Series.

—In discussing the deflection of beams, it is sometimes very useful to represent the deflection curve in the form of a trigonometrical series.[16] This has the advantage that a single mathematical expression for the curve holds for the entire length of the span. Taking the c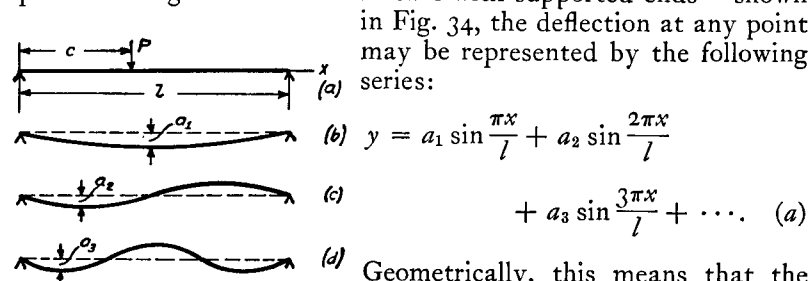ase of the beam with supported ends [17] shown in Fig. 34, the deflection at any point may be represented by the following series:



FIG. 34.

$$y = a_1 \sin \frac{\pi x}{l} + a_2 \sin \frac{2\pi x}{l}$$
$$+ a_3 \sin \frac{3\pi x}{l} + \cdots. \quad (a)$$

Geometrically, this means that the deflection curve may be obtained by superposing simple sinusoidal curves such as shown in Fig. 34 (b), (c), (d), etc. The first term in series (a) represents the first curve, the second term, the second curve, etc. The coefficients $a_1$, $a_2$, $a_3$ of the series give the maximum ordinates of these sine curves and the numbers 1, 2, 3, $\cdots$ the number of waves. By properly determining the coefficients $a_1$, $a_2$, $\cdots$, the series (a) can be made to represent any deflection curve [18] with a degree of accuracy which depends upon the number of terms taken. We will make this determination of the coefficients by a consideration of the strain energy of the beam (eq. 188, p. 297, Part I) as given by the equation

$$U = \frac{EI}{2} \int_0^l \left( \frac{d^2 y}{dx^2} \right)^2 dx. \quad (b)$$

The second derivative of $y$, from (a), is

$$\frac{d^2 y}{dx^2} = - a_1 \frac{\pi^2}{l^2} \sin \frac{\pi x}{l} - a_2 2^2 \frac{\pi^2}{l^2} \sin \frac{2\pi x}{l} - a_3 3^2 \frac{\pi^2}{l^2} \sin \frac{3\pi x}{l} \cdots.$$

Equation (b) involves the square of this derivative, which contains

[16] See the author's paper, "Application of General Coordinates in Solution of Problems on Bending of Bars and Plates," Bulletin of the Polytechnic Institute in Kiev, 1909 (Russian); see also H. M. Westergaard, Proc. Amer. Soc. Civ. Eng., Vol. 47, pp. 455–533.

[17] For other cases analysis becomes too complicated for most practical purposes.

[18] See Byerly, "Fourier Series and Spherical Harmonics," §§ 19–24. See also Osgood, "Advanced Calculus," 1928, p. 391.

terms of two kinds:

$$a_n^2 \frac{n^4 \pi^4}{l^4} \sin^2 \frac{n\pi x}{l} \quad \text{and} \quad 2 a_n a_m \frac{n^2 m^2 \pi^4}{l^4} \sin \frac{n\pi x}{l} \cdot \sin \frac{m\pi x}{l}.$$

By direct integration it may be shown that

$$\int_0^l \sin^2 \frac{n\pi x}{l} dx = \frac{l}{2} \quad \text{and} \quad \int_0^l \sin \frac{n\pi x}{l} \sin \frac{m\pi x}{l} dx = 0,$$

where

$$n \neq m.$$

Hence, in integral (b), all terms containing products of coefficients such as $a_n a_m$ disappear and only the terms with squares of those coefficients remain. Then

$$U = \frac{EI \pi^4}{4 l^3} (1 \cdot a_1^2 + 2^4 \cdot a_2^2 + 3^4 \cdot a_3^2 + \cdots) = \frac{EI \pi^4}{4 l^3} \sum_{n=1}^{n=\infty} n^4 a_n^2. \quad (53)$$

In a previous discussion (see eq. a, p. 339, Part I) it was shown that if an elastic system undergoes a small displacement from its position of equilibrium, the corresponding increase in the potential energy of the system is equal to the work done by the external forces during such a displacement. When the deflection curve is given by series (a), small displacements can be obtained by small variations of the coefficients $a_1$, $a_2$, $a_3$, $\cdots$. If any coefficient $a_n$ is given an increase $da_n$, we have the term $(a_n + da_n) \sin (n\pi x/l)$ in series (a) instead of the term $a_n \sin (n\pi x/l)$, the other members remaining unchanged. This increase $da_n$ in the coefficient $a_n$ represents an additional small deflection given by the sine curve $da_n \sin (n\pi x/l)$, superposed upon the original deflection curve. During this additional deflection the external loads do work. In the case of a single load $P$, applied at a distance $c$ from the left support, the point of application of the load undergoes a vertical displacement $da_n \sin (n\pi c/l)$ and the load does the work:

$$da_n \left( \sin \frac{n\pi c}{l} \right) P. \quad (c)$$

Let us consider now the increase in the strain energy, given by eq. (53), due to the increase $da_n$ in $a_n$,

$$dU = \frac{\partial U}{\partial a_n} da_n = \frac{EI \pi^4}{2 l^3} n^4 a_n da_n. \quad (d)$$

Equating this to the work done ($c$),

$$\frac{EI\pi^4}{2l^3} n^4 a_n = P \sin \frac{n\pi c}{l},$$

from which

$$a_n = \frac{2Pl^3}{EI\pi^4} \cdot \frac{1}{n^4} \sin \frac{n\pi c}{l}.$$

From this we can determine each of the coefficients in the series ($a$) and the deflection curve becomes

$$y = \frac{2Pl^3}{EI\pi^4}\left( \sin \frac{\pi c}{l} \sin \frac{\pi x}{l} + \frac{1}{2^4} \cdot \sin \frac{2\pi c}{l} \sin \frac{2\pi x}{l} + \cdots \right)$$

$$= \frac{2Pl^3}{EI\pi^4} \sum_{n=1}^{\infty} \frac{1}{n^4} \sin \frac{n\pi c}{l} \sin \frac{n\pi x}{l}. \quad (54)$$

From this the deflection may be calculated for any value of $x$. For example, the deflection at the middle when the load is at the middle, $c = x = l/2$, will be

$$\delta = (y)_{x=l/2} = \frac{2Pl^3}{EI\pi^4}\left( 1 + \frac{1}{3^4} + \frac{1}{5^4} + \cdots \right).$$

By taking only the first term of this series, we obtain

$$\delta = \frac{2Pl^3}{EI\pi^4} = \frac{Pl^3}{48.7EI}.$$

Comparison with eq. (90), p. 143, Part I, shows that we obtained 48.7 where the exact value was 48, so that the error made in using only the first term instead of the whole series is about $1\frac{1}{2}$ per cent. Such accuracy is sufficient in many practical cases and we shall have other examples where a satisfactory accuracy is obtained by using only one term in the series ($a$).

From the solution for a single load (eq. 54), more complicated problems can be studied by using the method of superposition. For example, take a beam carrying a uniformly distributed load, of intensity $q$. Each elemental load $qdc$ at distance $c$ from the left support produces a deflection obtained from eq. (54), with $P = qdc$,

$$dy = \frac{2qdcl^3}{EI\pi^4} \sum_{n=1}^{\infty} \frac{\sin \frac{n\pi c}{l} \sin \frac{n\pi x}{l}}{n^4}.$$

Integrating this with respect to $c$ between the limits $c = 0$ and

$c = l$ gives the deflection produced by the entire load

$$y = \frac{4ql^4}{EI\pi^5} \sum_{n=1,3,5,\ldots}^{\infty} \frac{1}{n^5} \sin \frac{n\pi x}{l}. \quad (55)$$

Taking the first term only, the deflection at the middle of a uniformly loaded beam is

$$\delta = \frac{4ql^4}{EI\pi^5} = \frac{ql^4}{76.5EI}.$$

Comparing this with the exact solution

$$\delta = \frac{5}{384} \frac{ql^4}{EI} = \frac{ql^4}{76.8EI},$$

we find that the error in taking only the first term was less than $\frac{1}{2}$ per cent in this case.

The trigonometric series ($a$) is especially useful when the beam is submitted to the action of a longitudinal compressive or tensile force in addition to lateral loading. In the problem shown in Fig. 35, the hinge $B$ approaches the fixed hinge $A$ during deflection
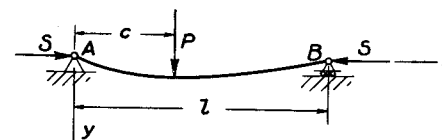


FIG. 35.

by an amount equal to the difference between the length of the deflection curve and the length of the cord $AB$.[19] For a flat curve this difference is (see p. 177, Part I)

$$\lambda = \frac{1}{2} \int_0^l \left( \frac{dy}{dx} \right)^2 dx. \quad (56)$$

With $y$ as given by series ($a$), the square of its derivative contains terms of the two forms:

$$a_n^2 \frac{n^2\pi^2}{l^2} \cos^2 \frac{n\pi x}{l} \quad \text{and} \quad 2a_n a_m \frac{nm\pi^2}{l^2} \cos \frac{n\pi x}{l} \cos \frac{m\pi x}{l}.$$

By integration it can be shown that

$$\int_0^l \cos^2 \frac{n\pi x}{l} dx = \frac{l}{2}; \quad \int_0^l \cos \frac{n\pi x}{l} \cos \frac{m\pi x}{l} dx = 0, \quad n \neq m.$$

[19] Longidutinal contraction due to the axial force can be considered as constant for small deflections.

The equation for $\lambda$ then becomes

$$\lambda = \frac{\pi^2}{4l} \sum_{n=1}^{\infty} n^2 a_n^2. \qquad (57)$$

To calculate the coefficients $a_1$, $a_2$, $a_3$, $\cdots$ in the series ($a$) we consider the work done by the external forces during a small displacement $da_n \sin(n\pi x/l)$ from the position of equilibrium. In the case represented in Fig. 35 both the force $P$ and the longitudinal force $S$ do work during such a displacement. The displacement $\lambda$, due to the increase $da_n$ in the coefficient $a_n$, increases by an amount

$$d\lambda = \frac{\partial \lambda}{\partial a_n} da_n = \frac{\pi^2}{2l} n^2 a_n da_n.$$

Then the work done by the force $S$ is

$$S \frac{\pi^2}{2l} n^2 a_n da_n.$$

This is added to the work ($c$) done by the lateral force and the sum is equated to the increase in the potential energy (eq. $d$). This gives us the following equation for determining any coefficient $a_n$:

$$P \sin\frac{n\pi c}{l} da_n + S \frac{\pi^2}{2l} n^2 a_n da_n = \frac{EI\pi^4}{2l^3} n^4 a_n da_n,$$

from which

$$a_n = \frac{2Pl^3}{EI\pi^4} \frac{1}{n^2 \left( n^2 - \dfrac{Sl^2}{EI\pi^2} \right)} \sin\frac{n\pi c}{l}.$$

If the ratio of the longitudinal force to the critical value of this load (see p. 27) be denoted by $\alpha = Sl^2/EI\pi^2$, we obtain

$$a_n = \frac{2Pl^3}{EI\pi^4} \frac{1}{n^2(n^2 - \alpha)} \sin\frac{n\pi c}{l}.$$

Substituting in the series ($a$), the deflection curve is

$$y = \frac{2Pl^3}{EI\pi^4} \left( \frac{1}{1-\alpha} \sin\frac{\pi c}{l} \sin\frac{\pi x}{l} + \frac{1}{2^2(2^2-\alpha)} \sin\frac{2\pi c}{l} \sin\frac{2\pi x}{l} + \cdots \right)$$

$$= \frac{2Pl^3}{EI\pi^4} \sum_{n=1}^{\infty} \frac{1}{n^2(n^2-\alpha)} \sin\frac{n\pi c}{l} \sin\frac{n\pi x}{l}. \qquad (58)$$

Comparing this with eq. (54) for the case of a lateral force $P$ only, we see that the deflection of the bar increases due to the action of the longitudinal compressive force $S$. We have seen that the first

term in series ($a$) represents a good approximation for the deflection; hence the increase of the deflection produced by the longitudinal force will be approximately in the ratio $1 : (1 - \alpha)$.

This conclusion holds also if there are several transverse loads of the same direction or if there is a continuous load acting on the beam. Denoting by $\delta_0$ the maximum deflection produced by lateral load acting alone we can assume with satisfactory accuracy that under the combined action of compressive forces $S$ and lateral load the maximum deflection is

$$\delta = \frac{\delta_0}{1 - \alpha}. \qquad (59)$$

This expression for the maximum deflection can be used also for an approximate calculation of bending moments in a strut. For example, in the case of a uniformly loaded strut with hinged ends the maximum bending moment can be calculated from the following approximate formula:

$$M_{max} = \frac{ql^2}{8} + \frac{S\delta_0}{1 - \alpha}. \qquad (60)$$

If the longitudinal force is tensile instead of compressive, the method discussed above still holds, with $-\alpha$ instead of $\alpha$ in the expressions for the deflection curve (58). Taking only the first term in this expression, the approximate formula for the deflection at the middle becomes

$$\delta = \frac{\delta_0}{1 + \alpha}, \qquad (61)$$

where $\delta_0$ denotes the deflection produced by lateral loads only. It must be noted that in the case of longitudinal tensile forces $\alpha$ can be larger than unity, and the accuracy of the approximate equation (61) decreases with increase of $\alpha$. Taking, for instance, a uniformly distributed lateral load, the error in eq. (61) at $\alpha = 1$ is about 0.3 per cent. At $\alpha = 2$ the error is 0.7 per cent and at $\alpha = 10$ the error is 1.7 per cent.

In the case of a bar with built-in ends an approximate equation, analogous to eq. (61), may be derived for calculating the deflection at the middle, which gives

$$\delta = \frac{\delta_0}{1 + \dfrac{\alpha}{4}}, \qquad (62)$$

in which $\delta_0$ is the deflection at the middle produced by lateral loads acting alone and $\alpha$ has the same meaning as before.

The applications of these approximate equations will be shown later in considering the deflection of thin rectangular plates. The method of trigonometric series can be extended also in analyzing beams of variable cross section.[20]

## 8. Bending of Beams in a Principal Plane which is not a Plane of Symmetry. Center of Twist.

—In the discussion of pure bending (see p. 93, Part I) it was shown that the plane of the deflection curve coincides with the plane of the bending couples provided these couples act in one of the two *principal planes of bending*. This does not hold however in the case of bending of a beam by a coplanar system of transverse forces. If the plane in which the forces are acting is 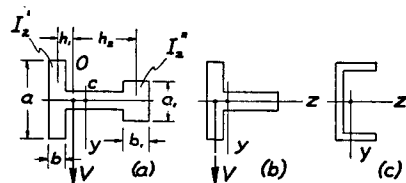not a plane of symmetry of the beam, such bending is usually accompanied by torsion of the beam. The following discussion will show how this torsion can be eliminated and a *simple bending* established by a proper displacement of the plane of the acting forces parallel to itself.



FIG. 36.

We begin with simple examples in which the cross section of the beam has one axis of symmetry ($z$ axis), and the forces are acting in a plane perpendicular to this axis, Fig. 36. Let us consider the case shown in Fig. 36a and determine the position of the vertical plane in which the transverse loads should act to produce *simple bending* of the beam in a vertical plane. From our previous discussion of distribution of vertical shearing stresses $\tau_{yx}$, see p. 109, Part I, we may conclude that practically the whole of the shearing force $V$ will be taken by the flanges alone. If we consider the flanges as two separate beams whose cross sections have moments of inertia $I_z'$ and $I_z''$ respectively, then their curvatures and their deflections in bending will be equal if the loads are distributed

[20] See paper by M. Hetényi, Journal of Applied Mechanics, 1937, vol. 42 A–49.

between them in the ratio $I_z' : I_z''$.[21] The shearing forces in these flanges also will be in the same ratio. This condition will be satisfied if the transverse loads act in the vertical plane through the point $O$ (Fig. 36, $a$), such that

$$\frac{h_1}{h_2} = \frac{I_z''}{I_z'},$$

where $h_1$ and $h_2$ are the distances of $O$ from the centroids of the cross sections of the flanges. In this manner we find that for the case of flanges of small thickness the point $O$ is displaced from the centroid $C$ of the cross section towards the flange whose cross section has the larger moment of inertia. In the limiting case, shown in Fig. 36, $b$, in which one of the flanges disappears, it can be assumed with sufficient accuracy that the point $O$ coincides with the centroid of the flange and that the transverse loads should act in the vertical plane through this point in order to have simple bending. The point $O$, through which the plane of loading must pass to eliminate torsion, is called *center of twist*.

Let us now consider the channel section (Fig. 36, $c$) and determine the position of the plane in which vertical loads must act to produce simple bending with the $z$ axis as the neutral axis. For this purpose it is necessary to consider the distribution of the shearing stresses over the cross section in simple bending. To calculate the vertical shearing stresses $\tau_{yx}$ for the cross section of the web, the same method is used as in the case of an I beam (page 109, Part I) and it can be assumed with sufficient accuracy that the vertical shearing force $V$ is taken by the web only. In the flanges there will be horizontal shearing stresses which we shall denote by $\tau_{zx}$. To find the magnitude of these stresses let us consider an element cut from the flange by two adjacent cross sections $dx$ apart and by a vertical plane $mnm_1n_1$ parallel to the web (Fig. 37). If the beam is bent convex downward, the upper flange will be

[21] The effect of shearing force on deflection of flanges is neglected in this consideration.

in compression and the compressive forces $N$ and $N + dN$ acting on the above element will be numerically equal to

$$N = -\frac{M}{I_z}\int y\,dA$$

and $\quad N + dN = -\frac{\left(M + \dfrac{dM}{dx}\,dx\right)}{I_z}\int y\,dA,$

where the integration must be extended over the shaded portion of the cross section of the flange. The integral repre-

FIG. 37.

sents the moment of the shaded area with respect to the $z$ axis. The difference of the compressive forces $N$ and $N + dN$ must be equal to the sum of the shearing stresses $\tau_{xz}$ acting over the side $mnm_1n_1$ of the element. Assuming that these stresses are uniformly distributed over this side and denoting by $t$ the thickness of the flange, we obtain the following equation for calculating $\tau_{xz}$:
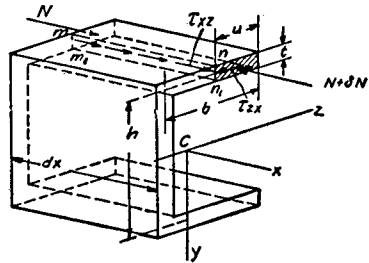
$$\tau_{xz}t\,dx = dN = -\frac{dM}{dx}\cdot\frac{dx}{I_z}\int y\,dA,$$

from which

$$\tau_{xz} = -\frac{V}{tI_z}\int y\,dA. \tag{a}$$

The moment of the shaded area is proportional to the distance $u$ from the edge of the flange; hence $\tau_{xz}$ is proportional to $u$. As we have shown before (see p. 111, Part I), shearing stresses $\tau_{zx}$, equal to $\tau_{xz}$, must act horizontally at points along the line $nn_1$ in the cross section of the flange. Hence the stresses $\tau_{zx}$ are distributed non-uniformly over the cross section of the flange but are proportional to the distance $u$. At the junction of flange and web the distribution of shearing stresses is complicated. In our approximate calculation we shall assume that eq. $(a)$ holds from $u = 0$ to $u = b$. Then denoting

by $h$ the distance between the centroids of the flanges and observing that the moment of the cross section $bt$ of the flange with respect to the axis $z$ numerically is $bt(h/2)$, we obtain, from eq. $(a)$,

$$(\tau_{xz})_{\max} = (\tau_{zx})_{\max} = \frac{Vbh}{2I_z}. \tag{b}$$

The resultant $R$ of the shearing stresses $\tau_{zx}$ distributed over the cross sectional area $bt$ of the flange is

$$R = \frac{Vbh}{2I_z}\cdot\frac{bt}{2} = \frac{Vb^2ht}{4I_z}. \tag{c}$$

The sum of the shearing stresses $\tau_{zx}$ over the cross section of the lower flange will evidently be an equal and opposite force. Thus the shearing stresses over a channel section reduce to the forces shown in Fig. 38. This system of forces is statically equivalent to a force $V$ applied at a point $O$ at a distance from the center of the web:

$$e = \frac{Rh}{V} = \frac{b^2h^2t}{4I_z}.$$

From this it is seen that, in order to obtain simple bending with $z$ the neutral axis, the vertical plane in which the transverse loads act should pass through the point $O$, which is called the *center of twist*. At any other position of this plane, bending of the beam will be accompanied by twist, and the stresses will no longer follow the simple law in which $\sigma_x$ is proportional to $y$ and hence does not depend entirely upon the coordinate $z$.

FIG. 38.

In the case of an angle section (Fig. 39) the shearing stress $\tau$ at points along $mn$ will be in the direction shown, and will be equal to [22]

[22] The same method of calculating these stresses as in the case of channel sections is used.

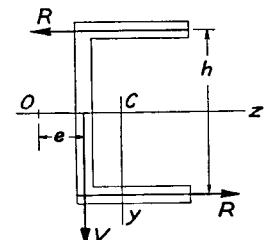$$\tau = -\frac{V}{tI_z} \int y\, dA,$$

in which the integral represents the moment of the shaded area with respect to the $z$ axis. These shearing stresses yield a resultant force in the direction shown in Fig. 39, $b$ equal to

$$R = \frac{Vb^3 t}{3I_z\sqrt{2}}.$$

A force of the same magnitude will also be obtained for the lower flange. The resultant of these two forces is equal to $V$ and passes through the point of intersection of the middle lines of the flanges $O$, which is therefore the *center of twist* in this case.
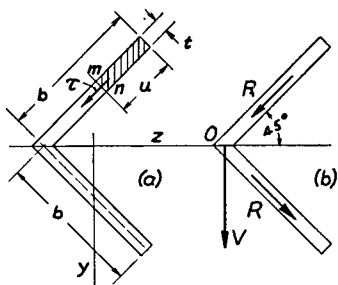


FIG. 39.

FIG. 40.

In the case of a ⌐ section, Fig. 40, assuming *simple bending* in a vertical plane and proceeding as in the case of an ⌐⌐ section, we find that the shearing forces $R$ in both flanges have the same direction. Their resultant goes through the centroid $C$. By geometrically adding this resultant to the vertical shearing force $V$, we obtained the direction of the inclined plane in which the transverse forces must be applied to produce simple bending of the beam in the vertical plane. Point $C$ is the center of twist in this case.

Assuming that the cross sections which were discussed above belong to cantilever beams fixed at one end and loaded by a concentrated force $P$ at the other end, we may conclude that if the load $P$ is applied at the center of twist, it produces
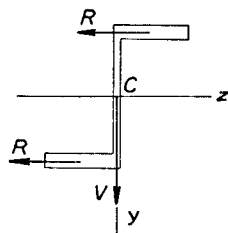
only bending of the cantilever without any twist. By using the *reciprocal theorem* (see p. 330, Part I) it can at once be concluded that a torque applied at the same end in the plane perpendicular to the axis of the cantilever and producing torsion of the cantilever will not produce any deflection of the center of twist. Hence during such torsion each cross section of the cantilever is rotating with respect to the axis passing through the center of twist and parallel to the axis of the beam.

The method of determining the position of the center of twist shown above on several simple examples can be generalized and extended to embrace cases of non-symmetrical cross sections of thin-walled members, provided the thickness of the material is so small that the distribution of shearing stresses over the thickness can be taken with sufficient accuracy to be uniform.[23] A further discussion of this problem is given in Art. 53 (p. 292).

When all the dimensions of a cross section are of the same order, the problem of determining the center of twist becomes more complicated; exact solutions of this problem exist in only a few cases.[24]

**9. Effective Width of Thin Flanges.**—The simple bending formula (see Eq. 55, p. 90, Part I) shows that bending stresses in a beam are proportional to the distance from the neutral axis. This conclusion is correct so long as we are dealing with beams, the cross-sectional dimensions of which

[23] The problem of determining the center of twist has been discussed by several authors. See, for example, A. A. Griffith and G. I. Taylor, Technical Reports of the Advisory Committee for Aeronautics, England, Volume 3, p. 950, 1917, R. Maillart, Schweiz. Bauz., vol. 77, p. 197; vol. 79, p. 254 and vol. 83, p. 111 and p. 176. C. Weber, Zeitschr. f. angew. Math. u. Mech., vol. 4, 1924, p. 334. A. Eggenschwyler, Proc. of the Second Internat. Congress for Appl. Mech. Zürich, 1926, p. 434. In recent time the problem became of importance in airplane design. The review of the corresponding literature is given in a paper by P. Kuhn, Techn. Notes, Nat. Adv. Comm., no. 691.

[24] See paper by M. Seegar and K. Pearson, London, Roy. Soc. Proc. (ser. A), vol. 96, 1920, p. 211, and the writer's paper, London Math. Soc. Proc. (ser. 2), vol. 20, 1922, p. 398. See also "Theory of Elasticity," 1934, p. 301.

are small in comparison with their length and so long as we are considering points at a considerable distance from the ends. In practical applications we sometimes use beams with

(b)

Fig. 41.

(c)

wide flanges, to which the elementary beam formula cannot be applied with sufficient accuracy. Take, as an example, the case of a beam consist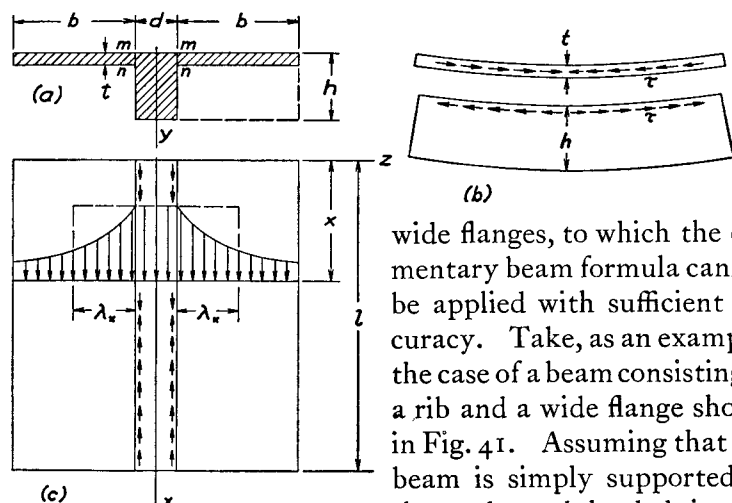ing of a rib and a wide flange shown in Fig. 41. Assuming that the beam is simply supported at the ends and loaded in the middle plane $xy$, we observe that there are shearing stresses acting between the flanges and the rib at the surfaces of contingency $mn$, Fig. 41$a$, and directed as shown in Fig. 41$b$. It is seen that these stresses tend to reduce the deflection of the rib, to make it stiffer. At the same time they produce compression of the flanges. Considering a flange at one side of the rib as a rectangular plate submitted to the action of shearing forces along one edge, Fig. 41$c$, we see that the compressive stresses will not be uniformly distributed along the width of the flange, and a rigorous analysis shows [25] that the distribution will be such as is indicated by the shaded area, the maximum stress in the flange being the same as in the utmost fibers of the rib. From

---

[25] The discussion of the rigorous solution, obtained by Th. von Karman, is given in the "Theory of Elasticity," p. 156, 1934. See also W. Metzer, Luftfahrtforschung, vol. 4, p. 1, 1929. K. Girkmann, der Stahlbau, vol. 6, 1933, p. 98; H. Reissner, Z. angew. Math. Mech., vol. 14, 1934, p. 312; E. Reissner, Der Stahlbau, vol. 7, 1934, p. 206; E. Chwalla, Der Stahlbau, vol. 9, 1936, p. 73.

---

this non-uniformity of stress distribution it can be concluded that in applying to the beam in Fig. 41$a$ the simple beam formula for maximum bending stress we must use a somewhat *reduced width* $2\lambda_x$ instead of the actual width $2b$ of the two flanges, in order to obtain the correct value of the maximum stress. This reduced width, usually called the *effective width*, can be calculated if the compressive stress distribution, shown by the shaded area in Fig. 41$c$, is known. It is only necessary to make the area of the rectangle, indicated in the figure by the dotted lines, equal to the shaded area. Its magnitude, $2\lambda_x$, usually varies along the span of the beam, for it depends on the proportions of the beam and also on the shape of the bending moment diagram.

In the particular case when the width of the flange is very large, say $2b \gtreqqless l$, and the bending moment diagram is given by the sine curve:

$$M = M_1 \sin \frac{\pi x}{l}, \qquad (a)$$

the reduced width becomes constant and equal to

$$2\lambda_x = \frac{4l}{\pi(1 + \mu)(3 - \mu)},$$

where $\mu$ is Poisson ratio. For $\mu = 0.3$ we obtain

$$2\lambda_x = 0.363l. \qquad (63)$$

Hence, in this particular case the actual beam can be replaced by an *equivalent T beam* of a constant cross section and with the width of the two flanges equal to $0.363l$. Applying to this beam the simple beam formulas, we obtain the same maximum stress and the same flexural rigidity as the actual beam has.

In a general case of transverse loading, the bending moment diagram can be represented by a sine series:

$$M_x = \Sigma M_n \sin \frac{n\pi x}{l}, \qquad (b)$$

in which the coefficients $M_n$ can be calculated, in each particular case, from the known formula: [26]

---

[26] See Article 7.

$$M_n = \frac{2}{l} \int_0^l M_x \sin \frac{n\pi x}{l} \, dx. \qquad (c)$$

In the case of a uniform load, for example, we have

$$M_x = \frac{qx(l-x)}{2}$$

and formula $(c)$ gives

$$M_n = \frac{4ql^2}{n^3\pi^3}, \qquad (d)$$

where $n = 1, 3, 5, \cdots$.

Having the coefficients $M_n$ in the series $(b)$, we obtain the effective width from the rigorous solution, which, in the case of a large width of the flanges, gives

$$\frac{l}{2\lambda_x} = \beta \left[ \frac{M_x}{\displaystyle\sum_{n=1,3,5,\ldots} \frac{M_n \sin \dfrac{n\pi x}{l}}{4 + \dfrac{k}{\beta} n\pi}} - 4 \right], \qquad (64)$$

in which $\beta = tl/dh$ is the ratio of the area $tl$ to the cross-sectional area of the rib, and

$$k = \frac{(1+\mu)(3-\mu)}{4} = 0.878 \text{ for } \mu = 0.3.$$

Taking, for example, the case of a uniformly distributed load and substituting the expression $(d)$ for $M_n$ in formula $(64)$, we find that for various values of the ratio $\beta$ the variation of the effective width
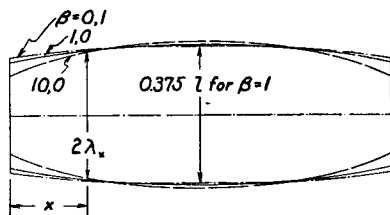


FIG. 42.

along the length of the beam is as shown in Fig. 42. It is seen that in the middle portion of the span the effective width varies very little and is approximately the same as for a sinusoidal bending moment diagram (see eq. 63). When the effective width is found from formula $(64)$, the maximum stress and maximum deflection are found by applying simple beam formulas to the equivalent beam.

We discussed the case in which the flanges of the beam have a very large width. There are also rigorous solutions for the case in which the flanges are not so very wide and for the case of a long

rectangular slab, reinforced by a system of identical and equidistant ribs. In all these cases the problem is reduced to that of calculating stresses and deflections in an equivalent beam.[27]

**10. Limitations of the Method of Superposition.**—In discussing the bending of beams (see p. 146, Part I) it was shown that the calculation of the deflections can be greatly simplified by using the method of superposition. This method can always be used if the bending of the beam does not introduce changes in the action of the external forces. For instance, small deflections of beams by lateral loads do not change the bending moment diagrams for these loads, and superposition can be successfully used. But if we have bending combined with axial tension or compression, the deflection produced by the lateral loads changes the action of the axial forces, and the latter produce not only axial tension or compression but also some additional bending. In such cases, as we have seen (see Art. 4), there are some limitations of the method of superposition; we can use this method only with regard to the lateral loads, assuming that the axial force always remains constant. There are other cases in which small deflections of beams may introduce considerable changes in the action of forces. In such cases the method of superposition fails. Some examples of this kind will now be discussed.

As a first example let us consider the bending of the cantilever $AB$, Fig. 43, if during bending it comes gradually into contact with a rigid cylindrical supporting surface $AC$ having a constant curvature $1/R$ and a horizontal tangent at $A$. It is seen that as long as the curvature of the beam at the end $A$, as given by the formula

$$\frac{1}{r} = \frac{M}{EI_z} = \frac{Pl}{EI_z}, \qquad (a)$$

[27] These rigorous solutions found some application in specifications for concrete slabs reinforced by ribs. In airplane design the fact of non-uniform stress distribution in wide flanges is taken care of by using an approximate theory, the discussion of which can be found in papers by P. Kuhn, National Adv. Committee for Aeronautics, Reports No. 608, 1937, No. 636, 1938. See also H. Ebner, Luftfahrt-Forschung, vol. 14, 1937, p. 93 and vol. 15, 1938, p. 527.

is less than the curvature of the support $1/R$, the cantilever will touch the surface $AC$ only at the point $A$, and the deflection $\delta$ at the end $B$ will be given by the known formula:

$$\delta = \frac{Pl^3}{3EI_z}. \qquad (b)$$

From the equation

$$\frac{1}{r} = \frac{Pl}{EI_z} = \frac{1}{R} \qquad (c)$$

we can obtain the limiting value of the load $P$, for which the beam begins to come into contact with the cylindrical supporting surface beyond the point $A$. Let $P_1 = EI_z/lR$ be this limit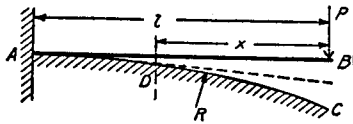ing value of the load; then for $P > P_1$ a part $AD$ of the beam will be supported as indicated in Fig. 43 by the dotted line. The length $x$ of the unsupported portion of the cantilever is obtained from the condition that at $D$ the curvature,



FIG. 43.

$1/r$, of the beam is equal to the curvature of the supporting surface; hence

$$\frac{Px}{EI_z} = \frac{1}{R},$$

and we obtain

$$x = \frac{EI_z}{PR}. \qquad (d)$$

The total deflection at the end $B$ of the cantilever consists of three parts: (1) deflection of the portion $DB$ of the beam as a simple cantilever, which is

$$\delta_1 = \frac{Px^3}{3EI_z} = \frac{(EI_z)^2}{3P^2R^3}, \qquad (e)$$

(2) deflection owing to the slope at $D$,

$$\delta_2 = \frac{x(l-x)}{R} = \frac{EI_z}{PR^2}\left(l - \frac{EI_z}{PR}\right), \qquad (f)$$

and (3) deflection representing the distance of the point $D$ from the horizontal tangent at $A$, which is

$$\delta_3 \approx \frac{(l-x)^2}{2R} = \left(l - \frac{EI_z}{PR}\right)^2 \frac{1}{2R}. \qquad (g)$$

Summing up these three parts, we obtain the total deflection:

$$\delta = \delta_1 + \delta_2 + \delta_3 = \frac{l^2}{2R} - \frac{1}{6}\frac{(EI_z)^2}{P^2R^3}. \qquad (h)$$

This expression for the deflection must be used instead of equation $(b)$, if $P$ is larger than the limiting value $P_1 = EI_z/lR$. Note that the deflection is no longer proportional to $P$. If, in addition to $P$, there is a load $Q$ applied at the end $B$ of the cantilever, the total deflection will not be equal to the sum of the deflections produced by $P$ and produced by $Q$ if both are considered to be acting alone. Hence the method of superposition does not hold in this case.
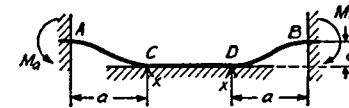


FIG. 44.

As a second example let us consider the case of a uniformly loaded beam with built-in ends, as shown in Fig. 44. It is assumed that during bending the middle portion of the beam is supported by a rigid horizontal foundation so that along this portion the deflection is constant and equal to $\delta$. It is seen that if the deflection at the middle is less than $\delta$, we have an ordinary case of bending of a beam with built-in ends. The limiting value $q_1$ of the load is obtained from the known equation:

$$\frac{1}{384}\frac{q_1 l^4}{EI_z} = \delta. \qquad (i)$$

For an intensity of the load larger than $q_1$, a portion of the

beam will be supported by the foundation as shown in the figure. This part remains straight; there is no bending moment acting in the portion $\overline{CD}$ of the beam, and the load is balanced by the uniformly distributed reaction. At the ends $C$ and $D$, however, concentrated reactions $X$ may act on the unsupported portions of the beam. The length $a$ of the unsupported portions of the beam and the magnitude $X$ of the concentrated reactions can be obtained by considering the portion $AC$ of the beam as a cantilever with a uniform load $q$ and with a concentrated load $X$ at the end. Observing that the cross section at $C$ does not rotate during bending and using equations (94) and (100) from Part I (see p. 147 and p. 149), we obtain

$$\frac{qa^3}{6EI_z} = \frac{Xa^2}{2EI_z},$$

from which

$$X = \frac{qa}{3}. \tag{j}$$

Another equation is obtained from the condition that the deflection at $C$ is equal to $\delta$. Using the known formulas for the deflection of the cantilever, we obtain

$$\frac{qa^4}{8EI_z} - \frac{Xa^3}{3EI_z} = \delta. \tag{k}$$

Solving equations $(j)$ and $(k)$ we find

$$a = \sqrt[4]{\frac{72\delta EI_z}{q}}, \qquad X = \sqrt[4]{8/9\delta EI_z q^3}. \tag{l}$$

It is immediately apparent that the reaction $X$ is not proportional to the load. The numerical maximum of the bending moment, which is at the built-in ends, is obtained from the equation:

$$|M_a| = |M_b| = \frac{qa^2}{2} - Xa,$$

which gives

$$M_a = \frac{qa^2}{6} = \sqrt{2\delta EI_z q}. \tag{m}$$

Again we see that the bending moment does not increase in the same proportion as the load. Hence the method of superposition cannot be used.

### Problems

1. Find the deflection of the cantilever shown in Fig. 43 if, instead of force $P$, there is a uniformly distributed load $q$.

2. Find an expression for the deflection at the middle of a beam, supported by two identical cylindrical surfaces of the radius $R$ and loaded at the middle, Fig. 45.
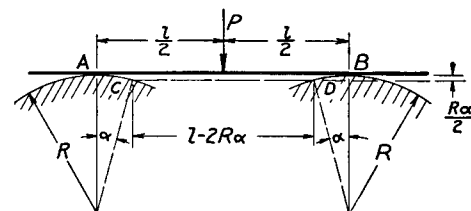


FIG. 45.

*Solution.* As the load $P$ increases, the points of contact of the beam with the supporting surfaces move inwards and the span diminishes; hence the deflection increases in a smaller proportion than does the load $P$. The angle $\alpha$, defining the positions of the points of contact, is found from the condition that at these points the deflection curve is tangent to the supporting surfaces; hence, for small values of $\alpha$,

$$\alpha = \frac{P(l - 2R\alpha)^2}{16EI_z}.$$

Having $\alpha$, we obtain the deflection at the middle from equation:

$$\delta = \frac{P(l - 2R\alpha)^3}{48EI_z} + \frac{R\alpha^2}{2}.$$

3. Solve the preceding problem assuming that the beam is built-in at the points $A$ and $B$.

4. Solve problem 2 if the load is not at the middle of the span *AB*.
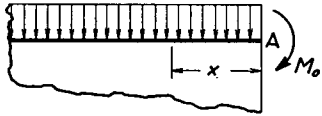


FIG. 46.

5. A long, uniformly loaded beam is supported by a horizontal, rigid foundation, Fig. 46. Find the angle $\alpha$ of rotation of the end $A$ and the length $x$ which will be bent by the moment $M_0$ applied at the end.

*Solution.* The length $x$ is found from the equation:

$$\frac{qx^3}{24EI} = \frac{M_0 x}{6EI}.$$

The angle of rotation at the end $A$ is

$$\alpha = \frac{M_0 x}{3EI} - \frac{qx^3}{24EI}$$

# CHAPTER II

## CURVED BARS

**11. Bending Stresses in Curved Bars.**—In the following discussion it is assumed that the *center line* [1] of the bar is a plane curve and that the cross sections have an axis of symmetry in this plane. The bar is submitted to the action of forces lying in this plane of symmetry. Let us consider first the case of a bar of constant cross section in pure bending, produced by couples applied at the ends (Fig. 47). The stress distribution
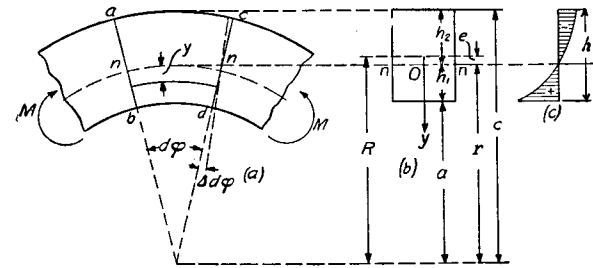


FIG. 47.

for this case is obtained by using the same assumption as in the case of straight bars, namely, that transverse cross sections of the bar originally plane and normal to the center line of the bar remain so after bending.[2] Let *ab* and *cd*

[1] The center line is the line joining the centroids of the cross sections of the bar.

[2] This approximate theory was developed by H. Résal, Annales des Mines, 1862, p. 617, and by E. Winkler, Der Civilingenieur, Vol. 4, 1858, p. 232; see also his book, "Die Lehre von der Elastizität und Festigkeit," Prag, 1867, Chapter 15. Further development of the theory was made by F. Grashof, "Elastizität und Festigkeit," 1878, p. 251, and by K. Pearson, "History of the Theory of Elasticity," Vol. 2, part I, 1893, p. 422. The exact solution of the same problem was given by H. Golovin, Bulletin of the Institute of Technology at St. Petersburg, 1881. See also C. Ribière, C. R., Vol. 108, 1889, and Vol. 132, 1901, and L. Prandtl in the paper by A. Timpe, Zeitschr. f. Math. u. Phys., Vol. 52, 1905, p. 348. The above approximate theory is in good agreement with the exact solution. See "Theory of Elasticity," p. 58, 1934.

denote two neighboring cross sections of the bar and let $d\varphi$ denote the small angle between them before bending. As a result of bending, the cross section $cd$ rotates with respect to $ab$. Let $\Delta d\varphi$ denote the small angle of rotation. Due to this rotation the longitudinal fibers on the convex side of the bar are compressed and the fibers on the concave side are extended. If $n$–$n$ denotes the neutral surface, the extension of any fiber a distance [3] $y$ from this surface is $y\Delta d\varphi$ and the corresponding unit elongation is

$$\epsilon = \frac{y\Delta d\varphi}{(r-y)d\varphi}, \qquad (a)$$

where $r$ denotes the radius of the neutral surface and the denominator in eq. $(a)$ is the length of the fiber between the adjacent cross sections before bending. Assuming that there is no lateral pressure between the longitudinal fibers,[4] the bending stress at a distance $y$ from the neutral axis is

$$\sigma_x = \frac{Ey\Delta d\varphi}{(r-y)d\varphi}. \qquad (b)$$

It will be seen that the stress distribution is no longer linear as in the case of straight bars, but that it follows a hyperbolic law as shown in Fig. 47 $(c)$. From the condition that the sum of the normal forces distributed over the cross section is zero, it can be concluded that the neutral axis is displaced from the centroid of the cross section towards the center of curvature of the bar. In the case of a rectangular cross section, the shaded area (Fig. 47, $c$) in tension must equal that in compression; hence the greatest bending stress acts on the concave side. In order to make the stresses in the most remote fibers in tension and in compression equal, it is necessary to use sectional shapes which have the centroid nearer the concave side of the bar.

---

[3] $y$ is taken positive in the direction towards the center of curvature of the bar.

[4] The exact theory shows that there is a certain radial pressure but that it has no substantial effect on the stress $\sigma_x$ and can be neglected. The lateral pressures in direction perpendicular to the plane of curvature may be of importance in the case of bending of thin shells (see art. 20).

Equation $(b)$ contains two unknowns, the radius $r$ of the neutral surface and the angle $\Delta d\varphi$ which represents the angular displacement due to bending. To determine them we must use the two equations of statics. The first equation is based on the condition that the sum of the normal forces distributed over a cross section is equal to zero. The second equation is based on the condition that the moment of these normal forces is equal to the bending moment $M$. These equations are:

$$\int \sigma_x dA = \frac{E\Delta d\varphi}{d\varphi}\int \frac{ydA}{r-y} = 0, \qquad (c)$$

$$\int \sigma_x ydA = \frac{E\Delta d\varphi}{d\varphi}\int \frac{y^2 dA}{r-y} = M. \qquad (d)$$

The integration in both equations is extended over the total area of the cross section. The integral in eq. $(d)$ may be simplified as follows:

$$\int \frac{y^2 dA}{r-y} = -\int \left(y - \frac{ry}{r-y}\right)dA$$

$$= -\int ydA + r\int \frac{ydA}{r-y}. \qquad (e)$$

The first integral on the right side of eq. $(e)$ represents the moment of the cross sectional area with respect to the neutral axis and the second, as is seen from eq. $(c)$, is equal to zero. Hence

$$\int \frac{y^2 dA}{r-y} = Ae, \qquad (f)$$

in which $e$ denotes the distance of the neutral axis from the centroid of the cross section. Equation $(d)$ then becomes

$$\frac{E\Delta d\varphi}{d\varphi} = \frac{M}{Ae} \qquad (65)$$

and eq. $(b)$ gives

$$\sigma_x = \frac{My}{Ae(r-y)}. \qquad (g)$$

The stresses in the most remote fibers, which are the largest

stresses in the bar are

$$(\sigma_x)_{max} = \frac{Mh_1}{Aea} \quad \text{and} \quad (\sigma_x)_{min} = -\frac{Mh_2}{Aec}, \quad (66)$$

in which $h_1$ and $h_2$ are the distances from the neutral axis to the most remote fibers and $a$ and $c$ are the inner and outer radii of the bar. The radius $r$ is determined from eq. $(c)$. Several examples of such calculations are shown in the next article.

If the depth of the cross section is small in comparison with the radius $R$ of the center line of the bar, $y$ may be neglected in comparison with $r$ in eqs. $(c)$ and $(d)$. Then, from $(c)$, we obtain

$$\int y\,dA = 0,$$

i.e., the neutral axis passes through the centroid of the cross section. From eq. $(d)$

$$\frac{E\Delta d\varphi}{d\varphi}\frac{I_z}{R} = M. \quad (h)$$

Substituting this into eq. $(b)$,

$$\sigma_x = \frac{My}{I_z}.$$

Hence, in the case of a relatively small depth $h$, the distribution of the bending stresses $\sigma_x$ approaches a linear one, and the same equation as used for straight bars can be used to calculate them.

From eq. $(h)$ we obtain for a thin bar

$$\Delta d\varphi = \frac{MR\,d\varphi}{EI_z} = \frac{M\,ds}{EI_z}, \quad (67)$$

in which $ds$ denotes the element of the center line between two adjacent cross sections. This equation is analogous to eq. $(a)$, p. 145, Part I, for the straight bars, and is often used in calculating the deflections of thin curved bars.

In a more general case when a curved bar is submitted to the action of any coplanar system of forces in the plane of

symmetry of the curved bar, the forces acting upon the portion of the bar to one side of any cross section may be reduced to a couple and a force applied at the centroid of the cross section. The stresses produced by the couple are obtained as explained above. The force is resolved into two components, a longitudinal force $N$ in the direction of the tangent to the center line of the bar and a shearing force $V$ in the plane of the cross section. The longitudinal force produces tensile or compressive stresses uniformly distributed over the cross section and equal to $N/A$. Due to these stresses the center line of the bar undergoes extension or contraction and the angle $d\varphi$ between the two adjacent cross sections changes by the amount

$$\Delta_1 d\varphi = \frac{N\,ds}{AE} \cdot \frac{1}{R}. \quad (68)$$

The transverse force $V$ produces shearing stresses and the distribution of these stresses over the cross section can be taken the same as for a straight bar.[5]

**12. Particular Cases of Curved Bars.**—It was shown in the previous article (eq. 66) that bending stresses in curved bars are readily calculated provided the position of the neutral axis is known. In the following examples the calculation of the distance $e$ of the neutral axis from the centroid of the cross section is given for several particular cases.

*Rectangular Cross Section.*—The magnitude of the radius $r$ of the neutral surface is determined from eq. $(c)$ of the previous article, from which

$$\int \frac{y\,dA}{r - y} = 0. \quad (a)$$

If we denote by $v$ (Fig. 48) the radius of a shaded element $dA$, then

$$v = r - y \quad \text{or} \quad y = r - v.$$

---

[5] This assumption is in a good agreement with the exact solution for a narrow rectangular cross section; see "Theory of Elasticity," p. 73, 1934.

Substituting into eq. (a),

$$\int \frac{(r-v)dA}{v} = 0,$$

from which

$$r = \frac{A}{\int \frac{dA}{v}}. \qquad (69)$$



FIG. 48.

In the case represented in Fig. 48, $A = bh$, $dA = bdv$ and integration is extended from $v = a$ to $v = c$, where $a$ and $c$ are the inner and the outer radii of the curved bar. Substituting in equation (69), we obtain

$$r = \frac{bh}{\int_a^c \frac{bdv}{v}} = \frac{h}{\log_n \frac{c}{a}}. \qquad (70)$$
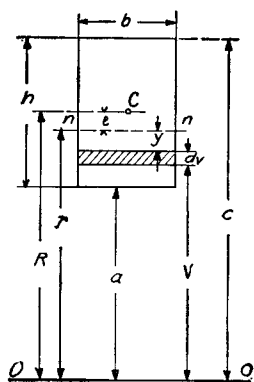
Using the known series

$$\log_n \frac{c}{a} = \log_n \frac{R + \frac{1}{2}h}{R - \frac{1}{2}h} = \log_n \frac{1 + \frac{1}{2}h/R}{1 - \frac{1}{2}h/R}$$

$$= \frac{h}{R}\left[ 1 + \frac{1}{3}\left(\frac{h}{2R}\right)^2 + \frac{1}{5}\left(\frac{h}{2R}\right)^4 + \cdots \right], \quad (b)$$

we obtain

$$e = R - r = R - \frac{R}{1 + \frac{1}{3}\left(\frac{h}{2R}\right)^2 + \frac{1}{5}\left(\frac{h}{2R}\right)^4 + \cdots}.$$

A first approximation for $e$ is obtained by taking only the two first terms in the denominator on the right side. Then

$$e = R\left[ 1 - \frac{1}{1 + \frac{1}{3}\left(\frac{h}{2R}\right)^2} \right] \approx \frac{h^2}{12R}. \qquad (71)$$

By using three terms of the series (b), a second approximation is obtained:

$$e = \frac{h^2}{12R}\left[ 1 + \frac{4}{15}\left(\frac{h}{2R}\right)^2 \right]. \qquad (72)$$

It can be seen that the distance $e$ of the neutral axis from the centroid decreases as the ratio $h/R$ decreases. For small values of this ratio the distance $e$ is small and a linear stress distribution, instead of a hyperbolic one, may be assumed with good accuracy. In the table below, the values of the maximum stress obtained by assuming a linear stress distribution are compared with those obtained on the basis of a hyperbolic distribution (eq. 66).

TABLE 4. COMPARISON OF HYPERBOLIC AND LINEAR STRESS DISTRIBUTIONS

| | Hyperbolic stress distribution | | Linear stress distribution | | Error in $\sigma_{max}$ due to assuming linear law |
|---|---|---|---|---|---|
| $R/h$ | $\dfrac{\sigma_{max}}{M/AR}$ | $\dfrac{\sigma_{min}}{M/AR}$ | $\dfrac{\sigma_{max}}{M/AR}$ | $\dfrac{\sigma_{min}}{M/AR}$ | % |
| 1 | 9.2 | − 4.4 | 6 | − 6 | 35 |
| 2 | 14.4 | −10.3 | 12 | −12 | 17 |
| 3 | 20.2 | −16.1 | 18 | −18 | 10.9 |
| 4 | 26.2 | −22.2 | 24 | −24 | 9.2 |
| 10 | 62.0 | −58.0 | 60 | −60 | 3.2 |

This indicates that for $R/h > 10$ a linear stress distribution can be assumed and the straight beam formula for maximum bending stress may be used with sufficient accuracy.

*Trapezoidal Cross Section.* The length of an elemental strip at distance $v$ from the axis $O$–$O$ (Fig. 49) is
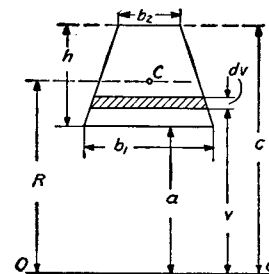
$$b = b_2 + (b_1 - b_2)\frac{c - v}{c - a}.$$



FIG. 49.

Substituting into eq. (69), we obtain

$$r = \frac{A}{\int \frac{bdv}{v}} = \frac{A}{\frac{b_1 c - b_2 a}{h}\log_n \frac{c}{a} - (b_1 - b_2)}. \qquad (73)$$

When $b_1 = b_2 = b$, the above equation coincides with eq. (70) for a rectangle. When $b_2 = 0$, the case of a triangular cross section is obtained.

$\perp$ *Cross Section.* In this case eq. (69) gives (Fig. 50)

$$r = \frac{b_1 f_1 + b_2 f_2}{b_1 \int_a^d \frac{dv}{v} + b_2 \int_d^c \frac{dv}{v}} = \frac{b_1 f_1 + b_2 f_2}{b_1 \log_n \frac{d}{a} + b_2 \log_n \frac{c}{d}}. \qquad (74)$$
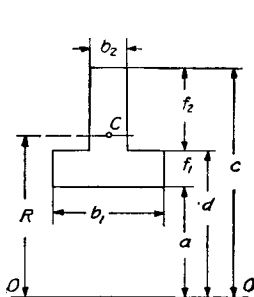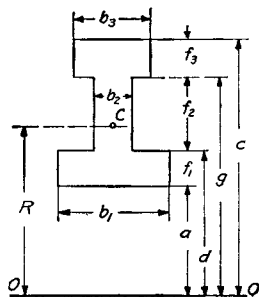


FIG. 50.          FIG. 51.

I *Cross Section.* From eq. (69) (Fig. 51)

$$r = \frac{b_1 f_1 + b_2 f_2 + b_3 f_3}{b_1 \log_n \frac{d}{a} + b_2 \log_n \frac{g}{d} + b_3 \log_n \frac{c}{g}}. \qquad (75)$$

It may be seen that a suitable choice of proportions in the cases of $\perp$ and I sections will so locate the centroid that eqs. (66) will give the same numerical values for $\sigma_{max}$ and $\sigma_{min}$. Such proportions are desirable if the material is equally strong in tension and compression, as, for instance, structural steel.

In the previous discussion the distance $e$ from the neutral axis to the centroid of the cross section was determined as the difference $R - r$. As $h/R$ decreases, this difference becomes small. To determine it with sufficient accuracy, $r$ must be calculated very accurately. In order to avoid this difficulty and to obtain $e$ directly, the following method may be used. If we let $y_1$ denote the distance of any point in the cross section from the axis through the centroid parallel to the neutral axis, then $y_1 = y + e$ and eq. (a) for determining the position of the neutral axes becomes

$$\int \frac{(y_1 - e)dA}{R - y_1} = \int \frac{y_1 dA}{R - y_1} - e \int \frac{dA}{R - y_1} = 0. \qquad (c)$$

The first integral on the right side represents a *modified area* of the cross section and can be represented as follows:

$$\int \frac{y_1 dA}{R - y_1} = mA, \qquad (d)$$

where $m$ denotes a number to be determined in each particular case. The second integral on the right side of eq. (c) can be transformed as follows:

$$\int \frac{dA}{R - y_1} = \frac{1}{R} \int \left( 1 + \frac{y_1}{R - y_1} \right) dA = \frac{A}{R} (1 + m). \qquad (e)$$

Substituting (d) and (e) in eq. (c), we obtain

$$mA - \frac{e(1 + m)A}{R} = 0,$$

from which

$$e = R \frac{m}{1 + m}. \qquad (76)$$

In calculating $m$ from eq. (d) the factor $1/(R - y_1)$ can be expanded in the series

$$\frac{1}{R - y_1} = \frac{1}{R} \left( 1 + \frac{y_1}{R} + \frac{y_1^2}{R^2} + \cdots \right).$$

Then

$$\int \frac{y_1 dA}{R - y_1} = \frac{1}{R} \int \left( 1 + \frac{y_1}{R} + \frac{y_1^2}{R^2} + \cdots \right) y_1 dA$$

and

$$m = \frac{1}{AR} \int \left( 1 + \frac{y_1}{R} + \frac{y_1^2}{R^2} + \cdots \right) y_1 dA. \qquad (77)$$

As an example, for a rectangular cross section $A = bh$, $dA = bdy_1$, and substituting in (77),

$$m = \frac{1}{hR} \int_{-h/2}^{+h/2} \left( 1 + \frac{y_1}{R} + \frac{y_1^2}{R^2} + \cdots \right) y_1 dy_1$$

$$= \frac{1}{3} \left( \frac{h}{2R} \right)^2 + \frac{1}{5} \left( \frac{h}{2R} \right)^4 + \frac{1}{7} \left( \frac{h}{2R} \right)^6 + \cdots.$$



FIG. 52.

This series converges very quickly and $m$ can be calculated very accurately. Substituting $m$ in eq. (76), the distance $e$ is obtained.

For a *circular cross section* (Fig. 52),

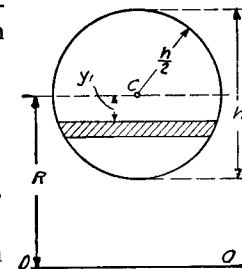$$dA = 2\sqrt{\tfrac{1}{4}h^2 - y_1^2}\, dy_1. \qquad (f)$$

Substituting into eq. (e),

$$\frac{A}{R}(1 + m) = 2\int_{-h/2}^{+h/2} \frac{\sqrt{\frac{1}{4}h^2 - y_1^2}\,dy_1}{R - y_1} = 2\pi\left(R - \sqrt{R^2 - \frac{h^2}{4}}\right), \quad (g)$$

from which, using the series

$$\sqrt{R^2 - \frac{h^2}{4}} = R\left[1 - \frac{1}{2}\frac{h^2}{4R^2} - \frac{1}{8}\left(\frac{h^2}{4R^2}\right)^2\right.$$
$$\left. - \frac{1}{16}\left(\frac{h^2}{4R^2}\right)^3 - \frac{5}{128}\left(\frac{h^2}{4R^2}\right)^4 - \cdots\right],$$

we obtain

$$m = \frac{1}{4}\left(\frac{h}{2R}\right)^2 + \frac{1}{8}\left(\frac{h}{2R}\right)^4 + \frac{5}{64}\left(\frac{h}{2R}\right)^6 + \cdots. \quad (78)$$

This is a rapidly converging series, from which $m$ may easily be calculated. Substitution of $m$ into eq. (76) gives the position of the neutral axis.

It can be seen that in calculating $m$ from equation (e) the magnitude of $m$ does not change if all elements $dA$ are multiplied by some constant, since in this way the integral on the left side of equation (e) and the area $A$ on the right side of the same equation will be increased in the same proportion. From this it follows that the value (78) of $m$ obtained for a circular cross section can be used also for an ellipse with the axes $h$ and $h_1$, since in this case each elemental area (f) obtained for a circle is to be multiplied by the constant ratio $h_1/h$.

The calculation of the integral on the left side of equation (e) can sometimes be simplified by dividing the cross section into several parts, integrating for each part, and adding the results of these integrations. Taking, for example, a circular ring cross section with outer diameter $h$ and inner diameter $h_1$, and using equation (g) for the outer and inner circles, we find for the ring cross section:

$$m = \frac{1}{h^2 - h_1^2}\left\{h^2\left[\frac{1}{4}\left(\frac{h}{2R}\right)^2 + \frac{1}{8}\left(\frac{h}{2R}\right)^4 + \cdots\right]\right.$$
$$\left. - h_1^2\left[\frac{1}{4}\left(\frac{h_1}{2R}\right)^2 + \frac{1}{8}\left(\frac{h_1}{2R}\right)^4 + \cdots\right]\right\}. \quad (79)$$

In a similar manner we can develop formulas for the cross sections shown in Figs. 50 and 51.

When $m$ is calculated, we find $e$ from equation (76) and the

maximum stress from equation (66). But we can also proceed in a somewhat different way and continue to use distance $y_1$ from the centroidal axis instead of distance $y$ from the neutral axis. Substituting $y_1 - e$ instead of $y$ into equation (g) (p. 67), we obtain

$$\sigma_x = \frac{M(y_1 - e)}{Ae(R - y_1)} = \frac{M}{AR}\left(\frac{y_1}{mv} - 1\right), \quad (80)$$

where $v$ is the distance of the point from the axis through the center of curvature of the axis of the bar, Fig. 48.

Equation (d) is the basis of a graphical determination of the quantity $m$ for cases in which the shape of the cross section cannot be simply expressed analytically. It is seen that in calculating the modified area from eq. (d) every elemental area must be diminished in the ratio $y_1/(R - y_1)$. This can be done by retaining the width of the elemental strips but diminishing their lengths in the above ratio (Fig. 53). In this manner the shaded area in the figure is obtained.
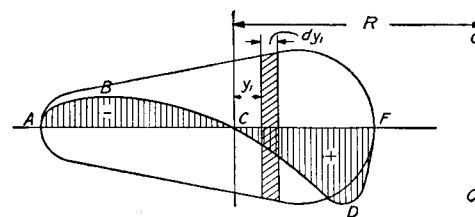


FIG. 53.

The difference between the areas $CDF$ and $ABC$ gives the modified area $mA$. Knowing this, the quantities $m$ and $e$ can readily be calculated.

The theory of curved bars developed above is applied in designing crane hooks.[6] In Fig. 54 is represented the working portion of a hook of a constant circular cross section. It is

[6] A theoretical and experimental investigation of crane hooks was recently made by the National Physical Laboratory in England. See the paper by H. J. Gough, H. L. Cox and D. G. Sopwith, Proc. Inst. Mech. Engrs., December 1934. The comparison of the theoretical stresses in hooks of a rectangular cross section with experimental results is given in the paper by K. Böttcher, Forschungsarbeiten, Heft 337, Berlin, 1931.

assumed that the vertical force $P$ is passing through the center of curvature $O$ of the axis of the hook. The maximum bending stress occurs in the cross section perpendicular to the load $P$. Then, proceeding as explained in the preceding article, we find that on the horizontal cross section of the hook the tensile force $P$, applied at the center $C$ of the cross section, and the bending moment $M = PR$ are acting. Combining direct and bending stresses and using equation (80) for the latter, we obtain



FIG. 54.

$$\sigma_x = \frac{P}{A} + \frac{M}{AR}\left(\frac{y_1}{mv} - 1\right) = \frac{Py_1}{Amv}.$$

Applying this formula to the most remote points, for which $y_1 = \pm\dfrac{h}{2}$, we find that

$$(\sigma_x)_{max} = \frac{P}{A} \cdot \frac{h}{2m(R - h/2)};$$
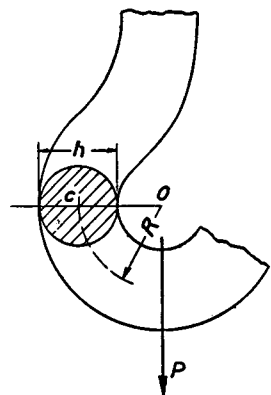
$$(\sigma_x)_{min} = -\frac{P}{A} \cdot \frac{h}{2m(R + h/2)}. \quad (81)$$

It is seen that the numerically largest stress is the tensile stress at the intrados, which is obtained by multiplying the stress $P/A$ by the *stress factor*:

$$k = \frac{h}{2m(R - h/2)} \quad (82)$$

the magnitude of which depends on the ratio $h/2R$. Using expression (78) for $m$, we find that $k$ varies from 13.5 to 15.4 as the ratio $h/2R$ changes from 0.6 to 0.4.[7]

---

[7] At $h/2R = 0.6$ the factor $k$ has its minimum value.

### Problems

1. Determine the ratio of the numerical values of $\sigma_{max}$ and $\sigma_{min}$ for a curved bar of rectangular cross section in pure bending if $R = 5$ in. and $h = 4$ in.

*Solution.* From eq. (66) the ratio is $h_1c/h_2a$. The distance of the neutral axis from the centroid, from eq. (72), is

$$e = 4\frac{4}{12 \times 5}\left[1 + \frac{4}{15}\left(\frac{4}{10}\right)^2\right] = 0.278 \text{ in.}$$

Then $h_1 = 2 - 0.278 = 1.722$ in.; $h_2 = 2 + 0.278 = 2.278$. The above ratio is

$$\frac{1.722 \times 7}{2.278 \times 3} = 1.75.$$

2. Solve the previous problem, assuming a circular cross section. *Answer.*

$$e = 0.208 \text{ in.;} \qquad \frac{\sigma_{max}}{\sigma_{min}} = \frac{1.792}{2.208} \cdot \frac{7}{3} = 1.89.$$

3. Determine the dimensions $b_1$ and $b_3$ of an I cross section (Fig. 51) to make $\sigma_{max}$ and $\sigma_{min}$ numerically equal, in pure bending. Given $f_1 = 1$ in., $f_2 = 2$ in., $f_3 = 1$ in., $a = 3$ in., $b_2 = 1$ in., $b_1 + b_3 = 5$ in.

*Solution.* From eqs. (66),

$$\frac{h_1}{a} = \frac{h_2}{c} \qquad \text{or} \qquad \frac{r - a}{a} = \frac{c - r}{c},$$

from which

$$r = \frac{2ac}{a + c} = \frac{2 \times 3 \times 7}{3 + 7} = 4.20 \text{ in.}$$

Substituting into eq. (75),

$$4.20 = \frac{7}{b_1 \log_n 4/3 + 1 \cdot \log_n 6/4 + (5 - b_1)\log_n 7/6},$$

from which

$$b_1 \log_n 4/3 + (5 - b_1)\log_n 7/6 = \frac{7}{4.20} - 1 \cdot \log_n 6/4,$$

$$0.288b_1 + 0.154(5 - b_1) = 1.667 - 0.406 = 1.261 \text{ in.,}$$

$$b_1 = 3.67 \text{ in.;} \qquad b_3 = 5 - 3.67 = 1.33 \text{ in.}$$

4. Determine the dimension $b_1$ of the $\perp$ section (Fig. 50) to make $\sigma_{max}$ and $\sigma_{min}$ numerically equal in pure bending. Given $f_1 = 1$ in., $f_2 = 3$ in., $b_2 = 1$ in., $a = 3$ in.
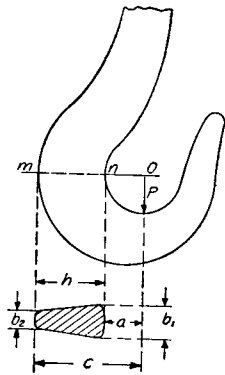
*Answer.* $b_1 = 3.09$ in.

5. Determine $\sigma_{max}$ and $\sigma_{min}$ for the trapezoidal cross section $mn$ of the hook represented in Fig. 55 if $P = 4,500$ lbs., $b_1 = 1\frac{5}{8}$ in., $b_2 = \frac{3}{8}$ in., $a = 1\frac{1}{4}$ in., $c = 5$ in.

*Solution.* From eq. (73),

$$r = \frac{3.750}{\dfrac{1\frac{5}{8} \times 5 - \frac{3}{8} \times 1\frac{1}{4}}{3\frac{3}{4}} \log_n 5/1\frac{1}{4} - (1\frac{5}{8} - \frac{3}{8})}$$

$$= \frac{3.750}{1.580} = 2.373 \text{ in.}$$

The radius of the center line

$$R = a + \frac{b_1 + 2b_2}{b_1 + b_2} \cdot \frac{h}{3} = 2.734 \text{ in.}$$

Therefore, $e = R - r = 0.361$ in.; $h_1 = r - a = 2.373 - 1.250 = 1.123$ in.; $h_2 = c - r = 5 - 2.373 = 2.627$ in.; $Ae = 3.75 \times 0.361 = 1.35$; $M = PR = 12,300$ lbs. ins. The bending stresses, from eqs. (66), are

$$(\sigma_x)_{max} = \frac{12,300 \times 1.123}{1.35 \times 1.25} = 8,200 \text{ lbs. per sq. in.}$$

$$(\sigma_x)_{min} = - \frac{12,300 \times 2.627}{1.35 \times 5} = - 4,800 \text{ lbs. per sq. in.}$$

On these bending stresses, a uniformly distributed tensile stress $P/A = 4,500/3.75 = 1,200$ lbs. per sq. in. must be superposed. The total stresses are

$$\sigma_{max} = 8,200 + 1,200 = 9,400 \text{ lbs. per sq. in.,}$$

$$\sigma_{min} = - 4,800 + 1,200 = - 3,600 \text{ lbs. per sq. in.}$$

6. Find the maximum stress in a hook of circular cross section if the diameter of the cross section is $h = 1$ in., radius of the central axis $R = 1$ in., and $P = 1,000$ lbs.

Fig. 55.

*Answer.* $k = 13.9$, $\sigma_{max} = 13.9 \dfrac{1000}{0.785} = 17,700$ lbs. per sq. in.

7. Find $\sigma_{max}$ and $\sigma_{min}$ for the curved bar of a circular cross section, loaded as shown in Fig. 56, if $h = 4$ in., $R = 4$ in., $e = 4$ in., and $P = 5,000$ lbs.

*Answer.* $\sigma_{max} = 10,650$ lbs. per sq. in., $\sigma_{min} = - 4,080$ lbs. per sq. in.

8. Solve the preceding problem assuming that the cross section $mn$ has the form shown in Fig. 50 with the following dimensions $a = 2$ in., $d = 3$ in., $c = 9$ in., $b_1 = 4$ in., $b_2 = 1$ in., $e = 4$ in., and $P = 4,000$ lbs.

*Answer.* $\sigma_{max} = 3,510$ lbs. per sq. in.; $\sigma_{min} = - 1,800$ lbs. per sq. in.

9. Solve problem 7 assuming that the cross section $mn$ is trapezoidal, as in Fig. 49, with the dimensions $a = 2$ in., $c = 4$-$1/4$ in., $b_1 = 2$ in., $b_2 = 1$ in., $e = 0$, and $P = 1.25$ tons.

*Answer.* $\sigma_{max} = 3.97$ tons per sq. in.; $\sigma_{min} = - 2.33$ tons per sq. in.
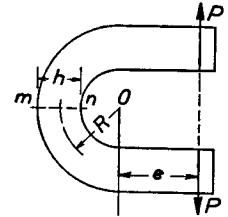
Fig. 56.

**13. Deflection of Curved Bars.**—The deflections of curved bars are usually calculated by the Castigliano theorem.[8] The simplest case is when the cross-sectional dimensions of the bar are small in comparison with the radius of curvature of its center line.[9] Then the change in the angle between two adjacent cross sections is given by eq. (67), analogous to eq. (a), p. 150, Part I, for straight bars, and the strain energy of bending is given by the equation

$$U = \int_0^s \frac{M^2 ds}{2EI_z}, \qquad (83)$$

in which the integration is extended along the total length $s$ of the bar. Equation (83) is analogous to that (187)
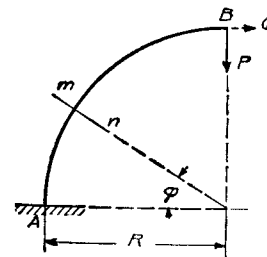
Fig 57.

---

[8] See p. 308, Part I.

[9] The case in which the cross-sectional dimensions are not small is discussed in problem 6, p. 87.

(see Part I) for straight beams,[10] and the deflection of the point of application of any load $P$ acting on the bar in the direction of the load is

$$\delta = \frac{\partial U}{\partial P}.$$

As an example, take a curved bar of uniform cross section whose center line is a quarter of a circle (Fig. 57), built in at the lower end $A$ with a vertical tangent and loaded at the other end by a vertical load $P$. The bending moment at any cross section $mn$ is $M = PR \cos \varphi$. Substituting in eq. (83), the vertical deflection of the end $B$ is

$$\delta = \frac{d}{dP} \int_0^{\pi/2} \frac{M^2 R d\varphi}{2EI_z} = \frac{1}{EI_z} \int_0^{\pi/2} M \frac{dM}{dP} R d\varphi$$

$$= \frac{1}{EI_z} \int_0^{\pi/2} PR^3 \cos^2 \varphi d\varphi = \frac{\pi}{4} \frac{PR^3}{EI_z}.$$

If the horizontal displacement of the end $B$ is needed, a horizontal imaginary load $Q$ must be added as shown in the figure by the dotted line. Then

$$M = PR \cos \varphi + QR(1 - \sin \varphi)$$

and

$$\frac{\partial M}{\partial Q} = R(1 - \sin \varphi).$$

The horizontal deflection is

$$\delta_1 = \left( \frac{\partial U}{\partial Q} \right)_{Q=0} = \frac{\partial}{\partial Q} \int_0^{\pi/2} \frac{M^2 R d\varphi}{2EI_z} = \frac{1}{EI_z} \int_0^{\pi/2} M \frac{\partial M}{\partial Q} R d\varphi.$$

$Q = 0$ must be substituted in the expression for $M$, giving

$$\delta_1 = \frac{1}{EI_z} \int_0^{\pi/2} PR^3 \cos \varphi (1 - \sin \varphi) d\varphi = \frac{PR^3}{2EI_z}.$$

*Thin Ring.*—As a second example consider the case of a thin circular ring submitted to the action of two equal and

[10] The strain energy due to longitudinal and shearing forces can be neglected in the case of thin curved bars. See p. 84.

opposite forces $P$ acting along the vertical diameter (Fig. 58). Due to symmetry only one quadrant of the ring (Fig. 58, $b$) need be considered, and we can also conclude that there are no shearing stresses over the cross section $mn$, and that the tensile force on this cross section is equal to $P/2$. The magnitude of the bending moment $M_0$ acting on this cross section is statically indeterminate, and we shall use the Castigliano theorem to find it.



FIG. 58.

It may be seen from the condition of symmetry that the cross section $mn$ does not rotate during the bending of the ring. Hence the displacement corresponding to $M_0$ is zero and

$$\frac{dU}{dM_0} = 0, \qquad (a)$$

in which $U$ is the strain energy of the quadrant of the ring which we are considering. For any cross section $m_1 n_1$ at an angle $\varphi$ with the horizontal the bending moment is [11]

$$M = M_0 - \frac{P}{2} R(1 - \cos \varphi) \qquad (b)$$

and

$$\frac{dM}{dM_0} = 1.$$

Substituting this into expression (83) for the potential energy and using eq. ($a$), we find

$$0 = \frac{d}{dM_0} \int_0^{\pi/2} \frac{M^2 R d\varphi}{2EI_z} = \frac{1}{EI_z} \int_0^{\pi/2} M \frac{dM}{dM_0} R d\varphi$$

$$= \frac{1}{EI_z} \int_0^{\pi/2} \left[ M_0 - \frac{P}{2} R(1 - \cos \varphi) \right] R d\varphi,$$

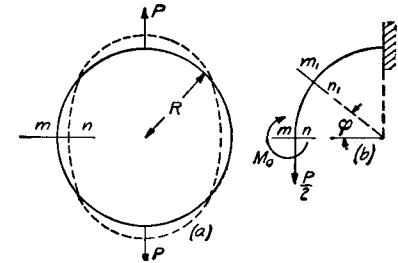[11] Moments which tend to decrease the initial curvature of the bar are taken as positive.

from which

$$M_0 = \frac{PR}{2}\left(1 - \frac{2}{\pi}\right) = 0.182PR. \qquad (84)$$

Substituting into eq. ($b$),

$$M = \frac{PR}{2}\left(\cos\varphi - \frac{2}{\pi}\right). \qquad (c)$$

The bending moment at any cross section of the ring may be calculated from this expression. The greatest bending moment is at the points of application of the forces $P$. Substituting $\varphi = \pi/2$ in eq. ($c$), we find

$$M = -\frac{PR}{\pi} = -0.318PR. \qquad (85)$$

The minus sign indicates that the bending moments at the points of application of the forces $P$ tend to increase the curvature while the moment $M_0$ at the cross section $mn$ tends to decrease the curvature of the ring, and the shape of the ring after bending is that indicated in the figure by the dotted line.

The increase in the vertical diameter of the ring may be calculated by the Castigliano theorem. The total strain energy stored in the ring is

$$U = 4\int_0^{\pi/2} \frac{M^2 R\,d\varphi}{2EI_z},$$

in which $M$ is given by eq. ($c$). Then the increase in the vertical diameter is

$$\begin{aligned}
\delta = \frac{dU}{dP} &= \frac{4}{EI_z}\int_0^{\pi/2} M\frac{dM}{dP}R\,d\varphi \\
&= \frac{PR^3}{EI_z}\int_0^{\pi/2}\left(\cos\varphi - \frac{2}{\pi}\right)^2 d\varphi \\
&= \left(\frac{\pi}{4} - \frac{2}{\pi}\right)\frac{PR^3}{EI_z} = 0.149\frac{PR^3}{EI_z}. \qquad (86)
\end{aligned}$$

For calculating the decrease of the horizontal diameter of the ring in Fig. 58, two oppositely directed imaginary forces $Q$ are applied at the ends of the horizontal diameter. Then by calculating $(\partial U/\partial Q)_{Q=0}$ we find that the decrease in the horizontal diameter is

$$\delta_1 = \left(\frac{2}{\pi} - \frac{1}{2}\right)\frac{PR^3}{EI_z} = 0.137\frac{PR^3}{EI_z}. \qquad (87)$$

*Thick Ring.*—When the cross sectional dimensions of a curved bar are not small in comparison with the radius of the center line, not only the strain energy due to bending moment but also that due to longitudinal and shearing forces must be taken into account. The change in the angle between two adjacent cross sections (Fig. 59) in this case, from eq. (65), is

$$\Delta d\varphi = \frac{M\,d\varphi}{AEe} = \frac{M\,ds}{AEeR}$$
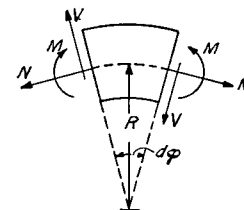


FIG. 59.

and the energy due to bending for the element between the two adjacent cross sections is

$$dU_1 = \tfrac{1}{2}M\Delta d\varphi = \frac{M^2\,ds}{2AEeR}. \qquad (d)$$

The longitudinal force $N$ produces an elongation of the element between the two adjacent cross sections in the direction of the center line of the bar equal to $N\,ds/AE$ and increases the angle $d\varphi$ by $N\,ds/AER$ (eq. 68). The work done by the forces $N$ during their application is $N^2\,ds/2AE$. During the application of the forces $N$ the couples $M$ do the negative work $-MN\,ds/AER$. Hence the total energy stored in an element of the bar during the application of the forces $N$ is

$$dU_2 = \frac{N^2\,ds}{2AE} - \frac{MN\,ds}{AER}. \qquad (e)$$

The shearing force $V$ produces sliding of one cross section with respect to another, of the amount $\alpha V\,ds/AG$, where $\alpha$ is a numerical factor depending upon the shape of the cross section (see p. 170, Part I). The corresponding amount of strain energy is

$$dU_3 = \frac{\alpha V^2\,ds}{2AG}. \qquad (f)$$

Adding (d), (e) and (f) and integrating along the length of the bar, the total energy of strain of a curved bar becomes

$$U = \int_0^s \left( \frac{M^2}{2AEeR} + \frac{N^2}{2AE} - \frac{MN}{AER} + \frac{\alpha V^2}{2AG} \right) ds. \quad (88)$$

Let us use this equation to solve the problem represented in Fig. 57. Taking as positive the directions shown in Fig. 59, we have

$$M = -PR \cos \varphi; \quad N = -P \cos \varphi; \quad V = P \sin \varphi,$$

where $R$ is the radius of the center line. Substituting in equation (88) and using the Castigliano theorem, we find the vertical deflection of the point $B$ to be

$$\delta = \frac{dU}{dP} = \frac{PR}{AE} \int_0^{\pi/2} \left( \frac{R \cos^2 \varphi}{e} - \cos^2 \varphi + \frac{\alpha E}{G} \sin^2 \varphi \right) d\varphi$$

$$= \frac{\pi PR}{4AE} \left( \frac{R}{e} + \frac{\alpha E}{G} - 1 \right).$$

If the cross section of the bar is a rectangle of the width $b$ and depth $h$, using for $e$ the approximate value (71) and taking $\alpha = 1.2$, $E/G = 2.6$,

$$\delta = \frac{\pi PR}{4AE} \left( \frac{12R^2}{h^2} + 2.12 \right).$$

When $h$ is small in comparison with $R$, the second term in the parenthesis representing the influence on the deflection of $N$ and $V$ can be neglected and we arrive at the equation obtained before (see p. 80).

The above theory of curved bars is often applied in calculating stresses in such machine elements as links and eye-shaped ends of bars (Fig. 60). In such cases a difficulty arises in determining the load distribution over the surface of the curved bar. This distribution depends on the amount of clearance between the bolt and the curved bar. A satisfactory solution of the problem may be expected only by
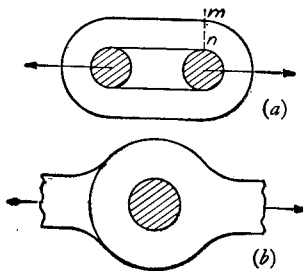


FIG. 60.

combining analytical and experimental methods of investigation.[12]

In a recent paper[13] the particular case of an eye-shaped end of rectangular cross section, Fig. 60b, was investigated. In this discussion it was assumed that there are no clearances and that the bolt is absolutely rigid. The maximum tensile stress occurs at the intrados in the cross sections perpendicular to the axis of the bar, and its magnitude can be represented by the formula:

$$\sigma_{\max} = \alpha \cdot \frac{8P}{\pi^2 r_a t}, \quad (g)$$

in which $P$ is the total tensile force transmitted by the bar, $\alpha$ is the numerical factor depending on the ratio $r_a/r_i$ between the outer and the inner radii of the eye, and $t$ is the thickness of the eye perpendicular to the plane of the figure. For $r_a/r_i$ equal to 2 and 4 the values of $\alpha$ are respectively 4.30 and 4.39. The values obtained from formula (g) are in satisfactory agreement with experiments.[14]

### Problems

1. Determine the vertical deflection of the end $B$ of the thin curved bar of uniform cross section and semicircular center line (Fig. 61).

---

[12] For a theoretical investigation of the problem, see H. Reissner, Jahrbuch der wissenschaftlichen Gesellschaft für Luftfahrt, 1928; also J. Beke, Der Eisenbau, 1921, p. 233; Fr. Bleich, Theorie und Berechnung der eis. Brücken, 1924, p. 256; Blumenfeld, V. D. I., 1907, and Baumann, V. D. I., 1908, p. 397. Experiments have been made by Dr. Mathar, Forschungsarbeiten nr. 306, 1928; see also D. Rühl, Dissertation, Danzig, 1920; Preuss, V. D. I., Vol. 55, 1911, p. 2173; M. Voropaeff, Bulletin of Polytechnical Institute, Kiew, 1910; E. G. Coker, "Photoelasticity," Journal of the Franklin Inst., 1925.

[13] H. Reissner und Fr. Strauch, Ingenieur Archiv, vol. 4, 1933, p. 481.

[14] See G. Bierett, Mitt. d. deutsch. Mat.-Prüf.-Amtes, 1931, sonderheft 15. The photo-elastic investigation of the eye-shaped end was made by K. Takemura and Y. Hosokawa, Rep. Aero. Inst., Tokyo, vol. 18, 1926, p. 128. See also M. M. Frocht and H. N. Hill, Journal of Applied Mechanics, vol. 7, p. 5. In the latter paper the effect of clearance between the bolt and the hole is investigated.

*Solution.* The strain energy of bending is

$$U = \int_0^\pi \frac{M^2 R d\varphi}{2EI_z} = \int_0^\pi \frac{P^2 R^2 (1 - \cos\varphi)^2 R d\varphi}{2EI_z}.$$

The deflection at the end is

$$\delta = \frac{dU}{dP} = \frac{PR^3}{EI_z} \int_0^\pi (1 - \cos\varphi)^2 d\varphi = \frac{3\pi}{2} \frac{PR^3}{EI_z}.$$
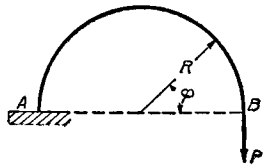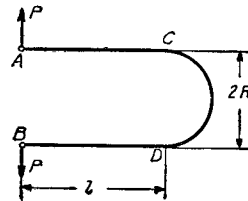


FIG. 61.          FIG. 62.

2. Determine the horizontal displacement of the end $B$ in the previous problem.

*Answer.*

$$\delta = \frac{2PR^3}{EI_z}.$$

3. Determine the increase in the distance between the ends $A$ and $B$ of a thin bar of uniform cross section consisting of a semicircular portion $CD$ and two straight portions $AC$ and $BD$ (Fig 62).

*Answer.*

$$\delta = \frac{2P}{EI_z} \left[ \frac{l^3}{3} + R\left( \frac{\pi}{2} l^2 + \frac{\pi}{4} R^2 + 2lR \right) \right].$$
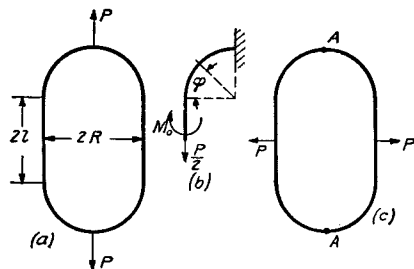


FIG. 63.

4. A link consisting of two semicircles and of two straight portions is submitted to the action of two equal and opposite forces acting along the vertical axis of symmetry (Fig. 63). Determine the maximum bending moment, assuming that the cross sectional dimensions of the link are small in comparison with the radius $R$.

*Solution.* Considering only one quarter of the link (Fig. 63, $b$), we find the statically indeterminate moment $M_0$ from the condition that the cross section, on which this moment acts, does not rotate. Then

$$\frac{dU}{dM_0} = 0.$$

Noting that for the straight portion $M = M_0$ and that for a curved portion $M = M_0 - (P/2)R(1 - \cos\varphi)$ and taking into consideration the strain energy of bending only, we find

$$\frac{dU}{dM_0} = \frac{d}{dM_0} \left\{ \frac{1}{2EI_z} \int_0^l M_0^2 dx \right.$$
$$\left. + \frac{1}{2EI_z} \int_0^{\pi/2} \left[ M_0 - \frac{PR}{2}(1 - \cos\varphi) \right]^2 R d\varphi \right\} = 0,$$

from which

$$M_0 = \frac{PR^2}{2} \frac{\pi - 2}{2l + \pi R}.$$

For $l = 0$, this coincides with eq. (84) obtained before for a circular ring. The largest moment is at the points of application of forces $P$ and is equal to

$$M_1 = M_0 - \frac{PR}{2}.$$

5. Solve the previous problem, assuming that forces $P$ are applied as shown in Fig. 63 $(c)$.

*Answer.* The bending moment at points $A$ is

$$M_1 = \frac{P}{2} \frac{R^2(\pi - 2) + 2Rl + l^2}{\pi R + 2l}.$$

For $l = 0$, the equation coincides with that for a circular ring. For $R = 0$, $M_1 = Pl/4$ as for a bar with built-in ends.

6. Determine the bending moment $M_0$ and the increase in the vertical diameter of the circular ring shown in Fig. 58, assuming that the cross section of the ring is a rectangle of width $b$ and

depth $h$, which dimensions are not small in comparison with the radius $R$ of the center line.

*Solution.* If we use eq. (88) for the potential energy and eq. (b) for the bending moment, the equation for determining $M_0$ is

$$\frac{dU}{dM_0} = \int_0^{\pi/2} \left( \frac{M}{AEe} - \frac{N}{AE} \right) d\varphi = 0,$$

from which

$$M_0 = \frac{PR}{2} \left( 1 - \frac{2}{\pi} + \frac{2e}{\pi R} \right).$$

Comparing this with eq. (84) we see that the third term in the parenthesis represents the effect of the longitudinal force and of the non-linear stress distribution. The magnitudes of the errors in using the approximate eq. (84) instead of the above accurate equation are given in the table below.

| $R/h =$ | 1 | 1.5 | 2 | 3 |
|---|---|---|---|---|
| $e/R =$ | 0.090 | 0.038 | 0.021 | 0.009 |
| Error in % = | 15.8 | 6.7 | 3.7 | 1.6 |

It can be seen that in the majority of cases the approximate eq. (84) can be used for calculating $M_0$ and that the error is substantial only when $h$ approaches $R$ or becomes larger than $R$.

The increase in the vertical diameter of the ring is obtained from equation

$$\delta = \frac{dU}{dP}.$$

Using eq. (88) for $U$ and substituting in this equation

$$M = M_0 - \frac{PR}{2}(1 - \cos\varphi); \qquad N = \frac{P}{2}\cos\varphi; \qquad V = -\frac{P}{2}\sin\varphi,$$

we find

$$\delta = \frac{PR^2}{AEe} \left\{ \frac{\pi}{4} - \frac{2}{\pi}\left(1 - \frac{e^2}{R^2}\right) + \frac{2e}{R}\left[\frac{2}{\pi}\left(1 - \frac{e}{R}\right) - \frac{\pi}{8}\right] + \frac{\pi\alpha}{4}\frac{E}{G}\frac{e}{R} \right\}.$$

Comparison with eq. (86) shows that the effect of the longitudinal and of the shearing forces on the magnitude of $\delta$ is usually very small.[15]

---

[15] A more accurate solution of the problem shown in Fig. 58 is given by the author; see Bulletin of the Polytechnical Institute in Kiew, 1910; see also Phil. Mag., Vol. 44, 1922, p. 1014, and "Theory of Elasticity," p. 119, 1934. This solution shows that the above theory, based on the assumption that cross sections remain plane during bending, gives very satisfactory results.

7. Determine the bending moments in a thin ring with two axes of symmetry submitted to the action of a uniform internal pressure $p$.

*Solution.* Consider one quadrant of the ring (Fig. 64), with semi-axes $a$ and $b$. If $M_0$ represents the statically indeterminate moment at $A$, the bending moment at any cross section $C$ with coordinates $x$ and $y$ is
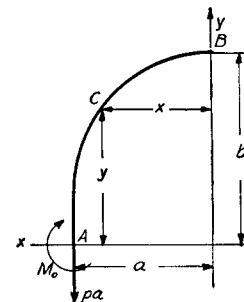


FIG. 64.

$$M = M_0 - pa(a-x) + \frac{p(a-x)^2}{2} + \frac{py^2}{2}$$

$$= M_0 - \frac{pa^2}{2} + \frac{px^2}{2} + \frac{py^2}{2}. \quad (g)$$

Substituting into equation $dU/dM_0 = 0$, we find

$$\left(M_0 - \frac{pa^2}{2}\right)s + \frac{p}{2}(I_x + I_y) = 0,$$

in which $s$ denotes the length of the quadrant of the ring,

$$I_x = \int_0^s y^2 ds \qquad \text{and} \qquad I_y = \int_0^s x^2 ds.$$

Then

$$M_0 = \frac{pa^2}{2} - \frac{p}{2s}(I_x + I_y). \quad (h)$$

If the ring has the shape of the link shown in Fig. 63, with $a = R$ and $b = l + R$, we obtain

$$s = b - a + \frac{\pi a}{2};$$

$$I_x = \frac{1}{3}(b-a)^3 + \frac{\pi a}{2}(b-a)^2 + \frac{\pi}{4}a^3 + 2a^2(b-a);$$

$$I_y = (b-a)a^2 + \frac{\pi a^3}{4}.$$

Substituting into eq (h),

$$M_0 = \frac{pa^2}{2} - \frac{p}{2b + (\pi-2)a}\left[\frac{1}{3}(b-a)^3 + \frac{\pi}{2}a^3 + 3a^2(b-a) + \frac{\pi}{2}a(b-a)^2\right].$$

The bending moment at any other cross section may now be obtained from eq. (g).

For an elliptical ring the calculations are more complicated.[16] Using the notations $I_x + I_y = \alpha a^2 b$, $M_0 = -\beta pa^2$, the moment at $B$ (Fig. 64) $= M_1 = \gamma pa^2$, and the values of the numerical factors $\alpha$, $\beta$ and $\gamma$, for different values of the ratio $a/b$, are as given in the table 5 below:

TABLE 5. CONSTANTS FOR CALCULATING ELLIPTICAL RINGS

| $a/b =$ | I | 0.9 | 0.8 | 0.7 | 0.6 | 0.5 | 0.4 | 0.3 |
|---|---|---|---|---|---|---|---|---|
| $\alpha$........ | 1.571 | 1.663 | 1.795 | 1.982 | 2.273 | 2.736 | 3.559 | 5.327 |
| $\beta$........ | 0 | 0.057 | 0.133 | 0.237 | 0.391 | 0.629 | 1.049 | 1.927 |
| $\gamma$........ | 0 | 0.060 | 0.148 | 0.283 | 0.498 | 0.870 | 1.576 | 3.128 |

8. A flat *spiral spring* (Fig. 65) is attached at the center to a spindle $C$. A couple $M_0$ is applied to this spindle to wind up the spring. It is balanced by a horizontal force $P$ at the outer end of the spring $A$ and by the reaction at the axis of the spindle. Establish the relation between $M_0$ and the angle of rotation of the spindle if all the dimensions of the spring are given. It is assumed that the angle of twist is not large enough to cause adjacent coils to touch each other.

*Solution.* Taking the origin of coordinates at $A$, the bending moment at any point of the spring at distance $y$ from the force $P$ is $M = Py$. The change in the angle between two adjacent cross sections at the point taken, from eq. (67), is

$$\Delta d\varphi = \frac{Mds}{EI_z} = \frac{Pyds}{EI_z}.$$



FIG. 65.

The total angle of rotation of one end of the spring with respect to the other during winding is

$$\varphi = \int_0^s \frac{Pyds}{EI_z} = \frac{P}{EI_z}\int_0^s yds. \qquad (k)$$

[16] See J. A. C. H. Bresse, Cours de Méchanique appliquée, 3d ed., Paris, 1880, p. 493. See, also, H. Résal, Journal de Math. (Liouville) (3), Vol. 3, 1877; M. Marbec, Bulletin de l'Association Technique Maritime, Vol. 19, 1908; M. Goupil, Annales des Ponts et Chaussées, Vol. 2, 1912, p. 386, and Mayer Mita, V. D. I., Vol. 58, 1914, p. 649. W. F. Burke, Nat. Adv. Com. Aeron., Techn. Notes, 444, 1933.

The integral on the right side of this equation represents the moment of the center line of the spring with respect to the $x$ axis. This moment is obtained by multiplying the total length $s$ of the spiral by the distance of its center of gravity from the $x$ axis. In the usual case, it is sufficiently accurate to take this distance equal to $r$, the distance from the center of the spindle to the force $P$. Then, from eq. ($k$),

$$\varphi = \frac{Prs}{EI_z} = \frac{M_0 s}{EI_z}. \qquad (l)$$

If the end $A$ is pin-connected, the turning moment $M_0$ applied at $c$ produces a reactive force $P$ at fixed end $A$ of the spring. As long as the thickness of the spring is very small and the number of windings of the spiral is large and the coils do not touch, the above assumption that the force $P$ remains horizontal can be considered as sufficiently accurate; hence eq. ($l$) holds.[17]

9. Assuming that the spring represented in Fig. 65 is in an unstressed condition and pin-connected at $A$, determine the maximum stress produced and the amount of energy stored in the spring by three complete turns of the spindle. Take the spring to be of steel, $\frac{1}{2}$ inch wide, $\frac{1}{40}$ inch thick and 120 inches long.

*Solution.* Substituting the above figures into eq. ($l$),

$$6\pi = M_0 \frac{120 \times 40^3 \times 12}{30 \times 10^6 \times \frac{1}{2}},$$

from which $M_0 = 3.07$ lbs. ins.

The amount of energy stored is

$$U = \int_0^s \frac{M^2 ds}{2EI} = \frac{P^2}{2EI}\int_0^s y^2 ds = \frac{P^2}{2EI}\left(sr^2 + \frac{sr^2}{4}\right)$$

$$= \frac{5}{8}\frac{M_0^2 s}{EI} = 36.1 \text{ lbs. in.}$$

The maximum bending stress is at point $B$, where the bending moment can be taken equal to $2Pr = 2M_0$, then

$$\sigma_{max} = 3.07 \times 2 \times 40^2 \times 6 \times 2 = 118,000 \text{ lbs. per sq. in.}$$

[17] A more complete discussion of the problem is given in the book by A. Castigliano, "Theorie d. Biegungs-u. Torsions Federn," Wien, 1888. See also E. C. Wadlow, "Engineer," Vol. 150, p. 474, 1930, and J. A. Van den Broek, Trans. A. S. M. E., Vol. 53, p. 247, 1931.
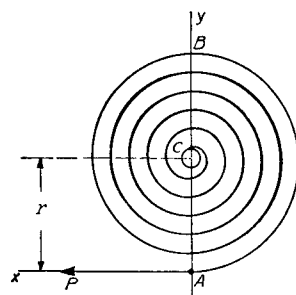
10. A *piston ring* of a circular outer boundary has a rectangular cross section of constant width $b$ and of a variable depth $h$ (Fig. 66). Determine the law of variation of the depth $h$ to obtain a ring which, when assembled with the piston in the cylinder, produces a uniformly distributed pressure on the cylinder wall.
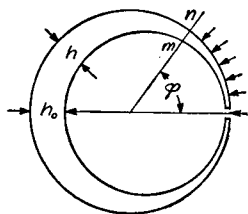


FIG. 66.

*Solution.* Let $r$ denote the radius of the cylinder, and $r + \delta$ the outer radius of the ring in the unstrained state. An approximate solution of the problem is obtained by using the outer radius of the ring instead of the variable radius of curvature of its center line. Then, by using eq. (67), the change in curvature due to bending is

$$\frac{\Delta d\varphi}{ds} = \frac{1}{r} - \frac{1}{r+\delta} = -\frac{M}{EI}. \tag{a}$$

The bending moment $M$ produced at any cross section $mn$ of the ring by the pressure $p$ uniformly distributed over the outer surface of the ring is

$$M = -2pbr^2 \sin^2 \frac{\varphi}{2}. \tag{b}$$

If we substitute this into (a) and take $bh^3/12$ for $I$ and use $\delta/r^2$ instead of $(1/r) - 1/(r+\delta)$ (for a small $\delta$), then the following equation for calculating $h$ is obtained:

$$\frac{\delta}{r^2} = \frac{p}{E} \frac{24r^2}{h^3} \sin^2 \frac{\varphi}{2}, \tag{c}$$

from which

$$h^3 = \frac{p}{E} \frac{24r^4}{\delta} \sin^2 \frac{\varphi}{2}. \tag{d}$$

Letting $\varphi = \pi$, the maximum value of $h^3$, denoted by $h_0^3$, is

$$h_0^3 = \frac{p}{E} \frac{24r^4}{\delta}. \tag{e}$$

The maximum bending stress at any cross section $mn$ is

$$\sigma = \frac{M}{Z} = \frac{12pr^2 \sin^2 (\varphi/2)}{h^2}. \tag{f}$$

From (f) and (d) it may be seen that the maximum bending stress occurs at $\varphi = \pi$, i.e., at the cross section opposite to the slot of the

ring. Substituting $h = h_0$ and $\varphi = \pi$ in eq. (f),

$$\sigma_{\max} = \frac{12pr^2}{h_0^2}, \tag{g}$$

from which $h_0$ can be calculated if the working stress for the ring and the pressure $p$ are given. The value of $\delta$ is found by substituting $h_0$ into eq. (e).

It may be noted that if two equal and opposite tensile forces $P$ be applied tangentially to the ends of the ring at the slot they produce at any cross section $mn$, the bending moment

$$-Pr(1 - \cos \varphi) = -2Pr \sin^2 \varphi/2,$$

i.e., the bending moment varies with $\varphi$ exactly in the same manner as that given by eq. (b). Therefore, if the ends of the open ring be pulled together, and in this condition it be machined to the outer radius $r$, such a ring will, when assembled, produce a uniform pressure against the wall of the cylinder.[18]

Determine, for example, $\delta$ and $h_0$ for a cast iron piston ring if $r = 10$ in., $\sigma_w = 4,200$ lbs. per sq. in., $p = 1.4$ lbs. per sq. in., and $E = 12 \times 10^6$ lbs. per sq. in. Substituting in eq. (g), we find $h_0 = 0.632$ in. From eq. (e), $\delta = 0.111$ in.

11. Derive formula (87), given on p. 83.

12. Experience shows that the insertion of a stud in a chain link considerably increases its strength. Find the bending moment $M_1$ at the points of application of the loads $P$ and the axial compressive force $2H$ in the stud for the link shown in Fig. 63.

*Solution.* Since in the case of a stud the horizontal cross section, Fig. 63b, does not move horizontally and does not rotate, the statically indeterminate quantities $M_0$ and $H$ are found from the equations:

$$\frac{\partial U}{\partial M_0} = 0 \quad \text{and} \quad \frac{\partial U}{\partial H} = 0,$$

from which

$$M_0 = \frac{PR}{2}(1 - \alpha) \quad \text{and} \quad H = \frac{P}{2} \cdot \beta,$$

---

[18] This theory was developed by H. Résal, Annales des mines, Vol. 5, p. 38, 1874; Comptes Rendus, Vol. 73, p. 542, 1871. See also E. Reinhardt, V. D. I., Vol. 45, p. 232, 1901; H. Friedmann, Zeitschr. d. Österreich. Ing. u. Arch. Verein, Vol. 60, p. 632, 1908, and V. D. I., Vol. 68, p. 254, 1924.

where [19]

$$\alpha = \frac{(m + 2)[m^3 + 6m^2 + 12(4 - \pi)m + 48(\pi - 3)]}{m^4 + 4\pi m^3 + 48m^2 + 24\pi m + 24(\pi^2 - 8)},$$

$$\beta = \frac{12(m + 2)[(\pi - 2)m + 2(4 - \pi)]}{m^4 + 4\pi m^3 + 48m^2 + 24\pi m + 24(\pi^2 - 8)},$$

$$m = \frac{l}{R}.$$
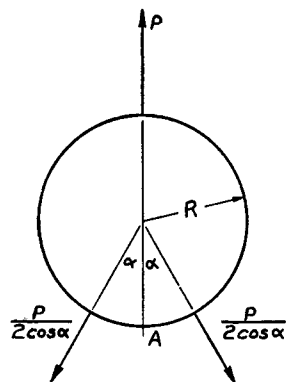
13. Find bending moment $M_0$ and tensile force $H$ in the cross section $A$ of the symmetrically loaded circular ring shown in Fig. 67.
*Answer.*

$$H = P \cdot \frac{\pi - \alpha}{2\pi} \tan \alpha,$$

$$M_0 = -\frac{PR}{2\pi}[1 + \sec \alpha$$
$$- (\pi - \alpha) \tan \alpha].$$



Fig. 67.

14. **Arch Hinged at the Ends.**—Figure 68 shows an arch with hinged ends at the same level carrying a vertical load. The vertical components of the reactions at $A$ and $B$ may be determined from equations of equilibrium in the same manner as for a simply supported beam, and the horizontal com-
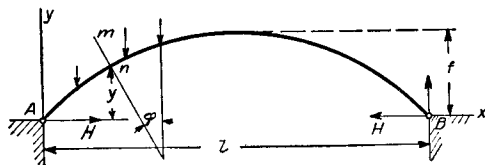


Fig. 68.

ponents must be equal and opposite in direction. The magnitude $H$ of these components is called the *thrust of the arch*. It cannot be obtained statically, but may be de-

[19] See paper by H. J. Gough, H. L. Cox and D. G. Sopwith, loc. cit. p. 75.

termined by use of the theorem of Castigliano. In the case of a flat arch, the two last terms in the general expression (88) for the strain energy can be neglected and for usual proportions of arches the product $AeR$ can be replaced by the moment of inertia $I_z$ of the cross section. The equation for calculating $H$ is then

$$\frac{dU}{dH} = \frac{d}{dH} \int_0^s \left( \frac{M^2}{2EI_z} + \frac{N^2}{2AE} \right) ds = 0. \qquad (a)$$

The bending moment at any cross section $mn$ of the arch can be represented by

$$M = M_0 - Hy, \qquad (b)$$

in which $M_0$ is the bending moment calculated for the corresponding section of a simply supported beam having the same load and the same span as the arch. The second term under the integral sign of eq. ($a$) represents the strain energy due to compression in the tangential direction and is of secondary importance. A satisfactory approximation for flat arches is obtained by assuming this compression equal to the thrust $H$. Substituting expression ($b$) and $N = H$ in eq. ($a$) we obtain

$$- \int_0^s \frac{(M_0 - Hy)y\,ds}{EI_z} + \int_0^s \frac{H\,ds}{AE} = 0,$$

from which

$$H = \frac{\int_0^s \frac{M_0 y\,ds}{EI_z}}{\int_0^s \frac{y^2 ds}{EI_z} + \int_0^s \frac{ds}{AE}}. \qquad (89)$$

For an arch of constant cross section, using the notation $k^2 = I_z/A$, eq. (89) becomes

$$H = \frac{\int_0^s M_0 y\,ds}{\int_0^s y^2 ds + k^2 \int_0^s ds}. \qquad (90)$$

The second term in the denominator represents the effect of

the shortening of the center line of the arch due to the longitudinal compression. In many cases it is small and can be neglected. Then

$$H = \frac{\int_0^s M_0 y \, ds}{\int_0^s y^2 \, ds}.$$  (91)

Take, for example, the case of a parabolic arch carrying a continuous load uniformly distributed along the length of the span with a center line given by the equation:

$$y = \frac{4fx(l - x)}{l^2}.$$  (c)

Then

$$M_0 = \frac{q}{2}x(l - x).$$  (d)

Substituting (c) and (d) into eq. (91), we obtain

$$H = \frac{ql^2}{8f}.$$  (e)

The actual thrust, $H$, will be less than that obtained from eq. (e). To give some idea of the possible error $\Delta H$, the ratios $(\Delta H)/H$ for various proportions of arches are given in the Table 6 below.[20] In calculating this table the whole expres-

TABLE 6

| $\frac{f}{l} =$ | $\frac{1}{12}$ | | | $\frac{1}{8}$ | | | $\frac{1}{4}$ | | |
|---|---|---|---|---|---|---|---|---|---|
| $\frac{h}{l} =$ | $\frac{1}{10}$ | $\frac{1}{20}$ | $\frac{1}{30}$ | $\frac{1}{10}$ | $\frac{1}{20}$ | $\frac{1}{30}$ | $\frac{1}{10}$ | $\frac{1}{20}$ | $\frac{1}{30}$ |
| $\frac{\Delta H}{H} =$ | 0.1771 | 0.0513 | 0.0235 | 0.0837 | 0.0224 | 0.0101 | 0.0175 | 0.00444 | 0.00198 |

[20] See author's paper, "Calcul des Arcs Élastiques," Paris, 1922. Béranger, Ed.

sion (88) for strain energy was used and it was assumed that for any cross section of the arch

$$A = \frac{A_0}{\cos \varphi}; \qquad EI_z = \frac{EI_0}{\cos \varphi},$$

where $A_0$ and $EI_0$ are respectively the cross sectional area and the flexural rigidity of the arch at the top, $\varphi$ is the angle between the cross section and the $y$ axis and $h$ is the depth of the cross section at the top. Equation (e) was used in calculating the value of $H$ in the ratio $\Delta H/H$.

This shows that the error of equation (e) has perceptible magnitude only for flat arches of considerable thickness.

As the supports of the arch are a fixed distance apart, a change in the temperature may produce appreciable stresses in the structure. To calculate the thrust due to an increase in temperature of $t$ degrees, we assume that one of the supports is movable. Then, thermal expansion would increase the span of the arch by $l\alpha t$, where $\alpha$ is the coefficient of thermal expansion of the material of the arch. The thrust is then found from the condition that it prevents such an expansion by producing a decrease in the span equal to $\alpha l t$. Using the Castigliano theorem, we obtain

$$\frac{dU}{dH} = \frac{d}{dH}\int_0^s \left( \frac{M^2}{2EI_z} + \frac{N^2}{2AE} \right) ds = \alpha l t.$$  (f)

Taking only the thermal effect and putting $M_0 = 0$ and $N = H$, we obtain from (f)

$$H = \frac{\alpha l t}{\int_0^s \frac{y^2 ds}{EI_z} + \int_0^s \frac{ds}{AE}}.$$  (92)

A more detailed study of stresses in arches may be found in books on the theory of structure.[21]

[21] Johnson, Bryan and Turneare, "Modern Framed Structures," Part II. See also Weyrauch, "Theorie d. Elastischen Bogenträger"; E. Mörsch, "Schweizerische Bauzeitung," Vol. 47.

**15. Stresses in a Flywheel.**—Due to the effect of the spokes, the rim of a rotating flywheel undergoes not only extension but also bending. We take as the free body a portion of the rim (Fig.
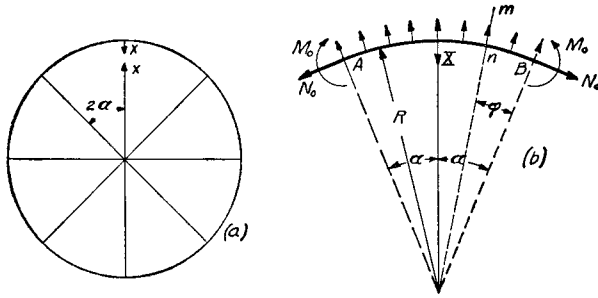


Fig. 69.

69, b) between two cross sections which bisect the angles between the spokes. Let

$R$ = the radius of the center line of the rim
$A$ = the cross sectional area of the rim
$A_1$ = the cross sectional area of a spoke
$I$ = moment of inertia of the cross section of the rim
$2\alpha$ = the angle between two consecutive spokes
$q$ = the weight of the rim per unit length of the center line
$q_1$ = the weight of a spoke per unit length
$\omega$ = the angular velocity of the wheel.

From the condition of symmetry there can be no shearing stresses over the cross sections $A$ and $B$ and the forces acting on these cross sections are reducible to the longitudinal force $N_0$ and the bending moment $M_0$. If $X$ denotes the force exerted by the spoke on the rim, the equation of equilibrium of the portion $AB$ of the rim is

$$2N_0 \sin \alpha + X - 2R^2 \sin \alpha \frac{q}{g} \omega^2 = 0,$$

from which

$$N_0 = \frac{q}{g} \omega^2 R^2 - \frac{X}{2 \sin \alpha}. \qquad (a)$$

The longitudinal force $N$ at any cross section $mn$ is

$$N = N_0 \cos \varphi + \frac{q\omega^2 R}{g} 2R \sin^2 \frac{\varphi}{2} = \frac{q\omega^2 R^2}{g} - \frac{X \cos \varphi}{2 \sin \alpha}. \qquad (b)$$

The bending moment for the same cross section is

$$M = M_0 - N_0 R(1 - \cos \varphi) + \frac{q\omega^2 R^3}{g} 2 \sin^2 \frac{\varphi}{2} = M_0 + \frac{XR}{\sin \alpha} \sin^2 \frac{\varphi}{2}. \qquad (c)$$

The force $X$ and the moment $M_0$ cannot be determined from the equations of statics but are calculated by use of the theorem of least work. The strain energy of the portion $AB$ of the rim is [22]

$$U_1 = 2 \int_0^\alpha \frac{M^2 R d\varphi}{2EI} + 2 \int_0^\alpha \frac{N^2 R d\varphi}{2EA}. \qquad (d)$$

The tensile force $N_1$ at any cross section of the spoke at distance $r$ from the center of the wheel is [23]

$$N_1 = X + \frac{q_1 \omega^2}{2g} (R^2 - r^2);$$

hence the strain energy of the spoke is

$$U_2 = \int_0^R \frac{N_1^2 dr}{2A_1 E}. \qquad (e)$$

The equations for calculating $M_0$ and $X$ are

$$\frac{\partial}{\partial M_0} (U_1 + U_2) = 0, \qquad (f)$$

$$\frac{\partial}{\partial X} (U_1 + U_2) = 0. \qquad (g)$$

Substituting $(d)$ and $(e)$, we obtain, from eqs. $(f)$ and $(g)$,

$$M_0 = -\frac{XR}{2} \left( \frac{1}{\sin \alpha} - \frac{1}{\alpha} \right), \qquad (93)$$

$$X = \frac{2}{3} \frac{q\omega^2 R^2}{g} \cdot \frac{1}{\dfrac{AR^2}{I} f_2(\alpha) + f_1(\alpha) + \dfrac{A}{A_1}}, \qquad (94)$$

in which

$$f_1(\alpha) = \frac{1}{2 \sin^2 \alpha} \left( \frac{\sin 2\alpha}{4} + \frac{\alpha}{2} \right),$$

$$f_2(\alpha) = \frac{1}{2 \sin^2 \alpha} \left( \frac{\sin 2\alpha}{4} + \frac{\alpha}{2} \right) - \frac{1}{2\alpha};$$

[22] It is assumed that the thickness of the rim is small in comparison with $R$ and only the energy of the bending and tension is taken into account.

[23] The length of the spoke is taken equal to $R$. In practice it will be somewhat less than $R$.

several values of the functions $f_1$ and $f_2$, for various numbers of spokes, are given in the table 7 below.

TABLE 7

| $n =$ | 4 | 6 | 8 |
|---|---|---|---|
| $f_1(\alpha)$ | 0.643 | 0.957 | 1.274 |
| $f_2(\alpha)$ | 0.00608 | 0.00169 | 0.00076 |

From this table the force $X$ in the spoke is determined from eq. (94) and the bending moment $M_0$ from eq. (93). Then the longitudinal force and bending moment for any cross section $mn$ of the rim may be found from eqs. (a), (b) and (c).[24]

Take, as an example, a steel flywheel making 600 r.p.m., with radius $R = 60$ in., cross section of the rim a square $12 \times 12$ sq. in., and with six spokes of cross sectional area $A_1 = 24$ sq. in. The rim is considered as a rotating ring which can expand freely; then the tensile stress due to centrifugal force is, from eq. (15), Part I,

$$\sigma_0 = 0.106 \times \omega^2 \times R^2 = 0.106 \times 62.8^2 \times 5^2 = 10,450 \text{ lbs. per sq. in.}$$

In the case of six spokes, $\alpha = 30°$, $f_1(\alpha) = 0.957$, $f_2(\alpha) = 0.00169$. Then the force in each spoke is, from eq. (94),

$$X = \frac{2}{3}\frac{q\omega^2 R^2}{g} \cdot \frac{1}{300 \times 0.00169 + 0.957 + 6} = 0.0893 \frac{q\omega^2 R^2}{g}.$$

The longitudinal force for the cross section bisecting the angle between the spokes is, from eq. (a),

$$N_0 = \frac{q\omega^2 R^2}{g} - 0.0893 \frac{q\omega^2 R^2}{g} = 0.911 \frac{q\omega^2 R^2}{g}.$$

The bending moment for the same cross section, from eq. (93), is

$$M_0 = -0.242 \frac{q\omega^2 R^2}{g}.$$

[24] The above theory was developed by R. Bredt, V. D. I., Vol. 45 (1901), p. 267, and H. Brauer, Dinglers Polytechn. Journ., 1908, p. 353, see also J. G. Longbottom, Inst. Mech. Eng. Proc., London, 1924, p. 43; and K. Reinhardt, Forschungsarbeiten, nr. 226, 1920. A similar problem arises when calculating stresses in retaining rings of large turbo-generators, see E. Schwerin, Electrotechn. Ztschr. 1931, p. 40.

The maximum stress at this cross section is

$$\sigma_{max} = \frac{N_0}{A} - \frac{M_0}{Z} = 10,780 \text{ lbs. per sq. in.}$$

For the cross section of the rim at the axis of the spoke, eqs. (b) and (c) give

$$(N)_{\varphi=\alpha} = 0.923 \frac{q\omega^2 R^2}{g}; \qquad (M)_{\varphi=\alpha} = 0.476 \frac{q\omega^2 R^2}{g}.$$

The maximum stress at this cross section is

$$\sigma_{max} = 12,100 \text{ lbs. per sq. in.}$$

In this case the effect of the bending of the rim on the maximum stress is small and the calculation of the stresses in the rim, as in a free rotating ring, gives a satisfactory result.

**16. Deflection Curve for a Bar with a Circular Center Line.**—In the case of a thin curved bar with a circular center line the differential equation for the deflection curve is analogous to that for a straight bar (eq. 141, p. 182, Part I). Let $ABCD$ (Fig. 70) represent the center line of a circular ring after deformation and let $u$ denote the small radial displacements during this deformation. The variation in the curvature of the center line during bending can be studied by considering one element $mn$ of the ring and the corresponding element $m_1n_1$ of the deformed ring included between the same radii (Fig. 70, b). The initial length of the element $mn$ and its initial curvature are

$$ds = Rd\varphi; \qquad \frac{d\varphi}{ds} = \frac{d\varphi}{Rd\varphi} = \frac{1}{R}. \qquad (a)$$

For small deflections the curvature of the same element after deformation can be taken equal to the curvature of the element $m_1n_1$. This latter is given by equation:

$$\frac{1}{R_1} = \frac{d\varphi + \Delta d\varphi}{ds + \Delta ds}, \qquad (b)$$

in which $d\varphi + \Delta d\varphi$ denotes the angle between the normal cross sections $m_1$ and $n_1$ of the deformed bar and $ds + \Delta ds$ the
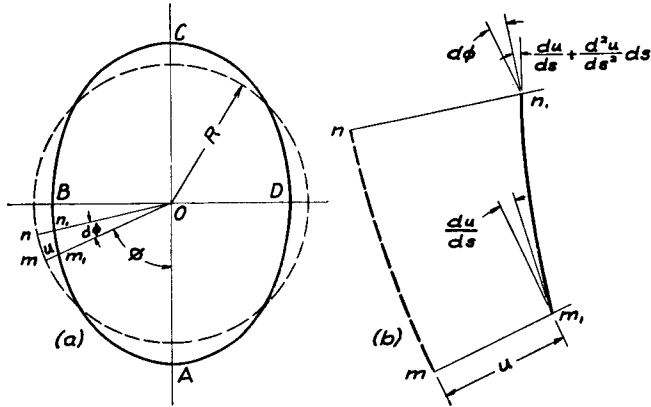


FIG. 70.

length of the element $m_1n_1$. The displacement $u$ is considered positive if towards the center of the ring and is assumed to be very small in comparison with the radius of the ring. Then the angle between the tangent at $m_1$ to the center line and the normal to the radius $m_1o$ is $du/ds$. The corresponding angle at the cross section $n_1$ is

$$\frac{du}{ds} + \frac{d^2u}{ds^2}\, ds.$$

Then

$$\Delta d\varphi = \frac{d^2u}{ds^2}\, ds. \qquad (c)$$

In comparing the length of the element $m_1n_1$ with that of the element $mn$, the small angle $du/ds$ is neglected and the length $m_1n_1$ is taken equal to $(R - u)d\varphi$. Then

$$\Delta ds = -\, ud\varphi = -\,\frac{uds}{R}. \qquad (d)$$

Substituting $(c)$ and $(d)$ into eq. $(b)$, we obtain

$$\frac{1}{R_1} = \frac{d\varphi + \dfrac{d^2u}{ds^2}\, ds}{ds\left(1 - \dfrac{u}{R}\right)},$$

or neglecting the small quantities of higher order,

$$\frac{1}{R_1} = \frac{d\varphi}{ds}\left(1 + \frac{u}{R}\right) + \frac{d^2u}{ds^2} = \frac{1}{R}\left(1 + \frac{u}{R}\right) + \frac{d^2u}{ds^2},$$

from which

$$\frac{1}{R_1} - \frac{1}{R} = \frac{u}{R^2} + \frac{d^2u}{ds^2}. \qquad (e)$$

The relationship between the change in curvature and the magnitude of bending moment, from eq. (67), for thin bars is

$$\frac{1}{R_1} - \frac{1}{R} = -\frac{M}{EI}. \qquad (f)$$

The minus sign on the right side of the equation follows from the sign of the bending moment which is taken to be positive when it produces a decrease in the initial curvature of the bar (Fig. 47). From $(e)$ and $(f)$ it follows that

$$\frac{d^2u}{ds^2} + \frac{u}{R^2} = -\frac{M}{EI}. \qquad (95)$$

This is the differential equation for the deflection curve of a thin bar with circular center line. For an infinitely large $R$ this equation coincides with eq. (79), Part I, for straight bars.

As an example of the application of eq. (95) let us consider the problem represented in Fig. 58. The bending moment at any cross section $m_1n_1$ is, from eq. $(c)$, p. 82,

$$M = \frac{PR}{2}\left(\cos\varphi - \frac{2}{\pi}\right),$$

and eq. (95) becomes

$$\frac{d^2u}{ds^2} + \frac{u}{R^2} = \frac{PR}{2EI}\left(\frac{2}{\pi} - \cos\varphi\right)$$

or

$$\frac{d^2u}{d\varphi^2} + u = \frac{PR^3}{2EI}\left(\frac{2}{\pi} - \cos\varphi\right).$$

The general solution of this equation is

$$u = A\cos\varphi + B\sin\varphi + \frac{PR^3}{EI\pi} - \frac{PR^3}{4EI}\varphi\sin\varphi.$$

The constants of integration $A$ and $B$ here are determined from the condition of symmetry

$$\frac{du}{d\varphi} = 0, \quad \text{for} \quad \varphi = 0 \quad \text{and for} \quad \varphi = \frac{\pi}{2};$$

which are satisfied by taking

$$B = 0; \quad A = -\frac{PR^3}{4EI}.$$

Then

$$u = \frac{PR^3}{EI\pi} - \frac{PR^3}{4EI}\varphi\sin\varphi - \frac{PR^3}{4EI}\cos\varphi.$$

For $\varphi = 0$ and $\varphi = \pi/2$, we obtain

$$(u)_{\varphi=0} = \frac{PR^3}{EI}\left(\frac{1}{\pi} - \frac{1}{4}\right); \quad (u)_{\varphi=\pi/2} = \frac{PR^3}{EI}\left(\frac{1}{\pi} - \frac{\pi}{8}\right).$$

These results are in complete agreement with eqs. (86) and (87) obtained before by using the Castigliano theorem.[25]

**17. Deflection of Bars with a Small Initial Curvature.**—If a bar with a small initial curvature is bent by transverse forces only, the deflections may be calculated by the method used for a straight bar. The conditions are quite different, however, if there are longitudinal forces in addition to the transverse forces. A small initial curvature makes a great change in the effect of these longitudinal forces on the deflection. The solution of this involved problem may be greatly simplified by using trigonometric series for representing the initial shape of the curve and the deflection due to

[25] Differential eq. (95) for the deflection of a circular ring was established by J. Boussinesq; see Comptes Rendus, Vol. 97, p. 843, 1883. See also H. Lamb, London Math. Soc. Proc., Vol. 19, p. 365, 1888. Various examples of applications of this equation are given in a paper by R. Mayer in Zeitschr. f. Math. u. Phys., Vol. 61, p. 246, 1913.

bending.[26] It is assumed, as before, that the curved bar has a plane of symmetry in which the external forces act and the bar is taken as simply supported at the ends. Let $y_0$ denote the initial ordinates of the center line of the bar, measured from the chord joining the centroids of the ends, and $y_1$ the deflections produced by the external forces, so that the total ordinates after bending are

$$y = y_0 + y_1. \tag{a}$$

Let the initial deflection curve be represented by the series

$$y_0 = b_1\sin\frac{\pi x}{l} + b_2\sin\frac{2\pi x}{l} + \cdots \tag{b}$$

and the deflection produced by the load be

$$y_1 = a_1\sin\frac{\pi x}{l} + a_2\sin\frac{2\pi x}{l} + \cdots. \tag{c}$$

In this case the same expression (53) for strain energy can be used as for straight bars. Taking the loading shown in Fig. 35, it is necessary in calculating the work done by the longitudinal forces $S$ to replace the quantity $\lambda$ (see eq. 56) by

$$\lambda_1 - \lambda_0 = \frac{1}{2}\int_0^l\left[\frac{d(y_1 + y_0)}{dx}\right]^2 dx - \frac{1}{2}\int_0^l\left(\frac{dy_0}{dx}\right)^2 dx$$
$$= \frac{\pi^2}{4l}\left(2\sum_{n=1}^{\infty} n^2 a_n b_n + \sum_{n=1}^{\infty} n^2 a_n^2\right). \tag{96}$$

This represents the longitudinal displacement of one end of the curved bar with respect to the other during deflection.

We proceed as in the case of straight bars (p. 48) and give to the bar an infinitely small additional deflection $da_n\sin(n\pi x/l)$. The work done by the longitudinal forces $S$ during this deflection is

$$S\frac{\partial(\lambda_1 - \lambda_0)}{\partial a_n}da_n = S\frac{n^2\pi^2}{2l}(a_n + b_n)da_n.$$

The work done by the load $P$ is

$$P\sin\frac{n\pi c}{l}da_n$$

and the increase in strain energy, from eq. (53), is

$$\frac{EI\pi^4}{2l^3}n^4 a_n da_n.$$

[26] See author's paper, Festschrift zum siebzigsten Geburtstage A. Föppl, p. 74.

The equation for calculating $a_n$ is

$$\frac{EI\pi^4}{2l^3} n^4 a_n da_n = P \sin \frac{n\pi c}{l} da_n + S \frac{n^2\pi^2}{2l} (a_n + b_n)da_n,$$

from which

$$a_n = \frac{2Pl^3 \sin \frac{n\pi c}{l} + Sn^2\pi^2 l^2 b_n}{EI\pi^4 n^4 - Sn^2\pi^2 l^2}.$$

Substituting into expression (c) and using the notation,

$$\frac{Sl^2}{EI\pi^2} = \alpha,$$

$$y_1 = \frac{2Pl^3}{EI\pi^4}\left( \frac{\sin\frac{\pi c}{l}\sin\frac{\pi x}{l}}{1 - \alpha} + \frac{\sin\frac{2\pi c}{l}\sin\frac{2\pi x}{l}}{2^4 - 2^2\alpha} + \cdots \right.$$
$$\left. + \alpha\left( \frac{b_1 \sin\frac{\pi x}{l}}{1 - \alpha} + \frac{b_2 \sin\frac{2\pi x}{l}}{2^2 - \alpha} + \cdots \right) \right). \quad (97)$$

The first member of the right side of eq. (97) represents the deflection of a straight bar (see eq. 58), while the second gives the additional deflection due to the initial curvature.

Take, for example, a bar which has an initial deflection $y_0 = b \sin (\pi x/l)$. The maximum deflection is at the middle of the span and is equal to $b$. If only the longitudinal forces $S$ act on the bar ($P = 0$), the deflection at the middle produced by these forces is obtained from eq. (97) by substituting $P = 0$; $b_1 = b$; $b_2 = b_3 = \cdots = 0$. Then

$$y_1 = \frac{\alpha b \sin\frac{\pi x}{l}}{1 - \alpha}. \quad (d)$$

The total ordinates of the center line after bending are

$$y = y_1 + y_0 = \frac{\alpha b \sin\frac{\pi x}{l}}{1 - \alpha} + b \sin\frac{\pi x}{l} = \frac{b}{1 - \alpha} \sin\frac{\pi x}{l} \cdots. \quad (98)$$

Due to longitudinal compressive forces $S$ the ordinates of the center line increase in the ratio $1/(1 - \alpha)$, i.e., the increase of ordinates depends upon the quantity $\alpha$, which is the ratio of the longitudinal force to the critical force. If, instead of compressive forces, longi-

tudinal tensile forces act on the bar, it is only necessary to substitute $-\alpha$ instead of $\alpha$ in the previous equations. In the particular case in which $y_0 = b \sin (\pi x/l)$ the ordinates of the center line after deformation become

$$y = \frac{b}{1 + \alpha} \sin\frac{\pi x}{l}. \quad (99)$$

It is seen that the longitudinal tensile force diminishes the initial ordinates. Taking, for instance, $\alpha = 1$, i.e., taking the longitudinal force equal to its critical value, we find

$$y = \tfrac{1}{2}b \sin\frac{\pi x}{l},$$

i.e., such a longitudinal force reduces the initial ordinates of the bar by half.

**18. Bending of Curved Tubes.**—In discussing the distribution of bending stresses in curved bars (art. 11) it was assumed that the shape of the cross section remains unchanged. Such an assumption is justifiable as long as we have a solid bar, because the very small displacements in the plane of the cross section due to lateral contraction and expansion have no substantial effect on the stress distribution. The condition is very different, however, in the case of a thin curved tube in bending. It is well known that curved tubes with comparatively thin walls prove to be more flexible during bending than would be expected from the usual theory of curved bars.[27] A consideration of the distortion of the cross section during bending is necessary in such cases.[28]

Consider an element between two adjacent cross sections of a curved round pipe (Fig. 71) which is bent by couples in the direction indicated. Since both the tensile forces at the

[27] Extensive experimental work on the flexibility of pipe bends was done by A. Bantlin, V. D. I., Vol. 54, 1910, p. 45, and Forschungsarbeiten, nr. 96. See also W. Hovgaard, Journal of Math. and Phys., Mass. Institute of Technology, Vol. 7, 1928, and A. M. Wahl, Trans. Amer. Soc. Mech. Eng., Vol. 49, 1927.

[28] This problem for the pipe of circular section was discussed by Th. v. Kármán, V. D. I., Vol. 55, p. 1889, 1911. The case of curved pipes of rectangular cross section was considered by the author; see Amer. Soc. Mech. Eng., Vol. 45, p. 135, 1923.

convex side of the tube and the compressive forces at the concave side have resultants towards the neutral axis, the previously circular cross sections are flattened and become elliptical. This flattening of the cross section affects the strain of longitudinal fibers of the tube. The outer fiber $ab$ takes some position $a_1b_1$ after bending; denote its displacement towards the neutral axis by $\delta$. The total elongation of the fiber is

$$a_1b_1 - ab = a_1b_1 - a_1e_1 - (ab - a_1e_1). \qquad (a)$$

The angle between the adjacent cross sections $ac$ and $bd$ is denoted by $d\varphi$, its variation during bending by $\Delta d\varphi$, the radius of the center line by $R$, and the radius of the middle surface of the tube by $a$. It is assumed that the ratio $a/R$ is small enough that the neutral axis can be taken through the centroid of the cross section. Then, from the figure we obtain

$$a_1b_1 - a_1e_1 = (a - \delta)\Delta d\varphi \approx a\Delta d\varphi.^{29}$$

The total elongation of the fiber $ab$ as given by eq. $(a)$ is

$$a\Delta d\varphi - \delta d\varphi$$

and the unit elongation is

$$\epsilon = \frac{a\Delta d\varphi - \delta d\varphi}{(R + a)d\varphi} = \frac{a}{R + a}\frac{\Delta d\varphi}{d\varphi} - \frac{\delta}{R + a}. \qquad (b)$$

The first term on the right side of this equation represents the strain in the fiber due to the rotation of the cross section $bd$ with respect to the cross section $ac$. This is the elongation which is considered in the bending of solid bars. The second term on the right side of eq. $(b)$ represents the effect of the flattening of the cross section. It is evident that this effect may be of considerable inportance. Take, for instance, $R + a = 60$ in. and $\delta = 0.02$ in. Then $\delta/(R + a) = 1/3,000$ and the corresponding stress for a steel tube is 10,000 lbs. per sq. in.

---

[29] The displacement $\delta$ is considered as very small in comparison with the radius $a$.

Hence a very small flattening of the cross section produces a substantial decrease in the stress at the outermost fiber $ab$. A similar conclusion may be drawn for the fiber $cd$ on the concave side of the bend. A change in the direction of the bending
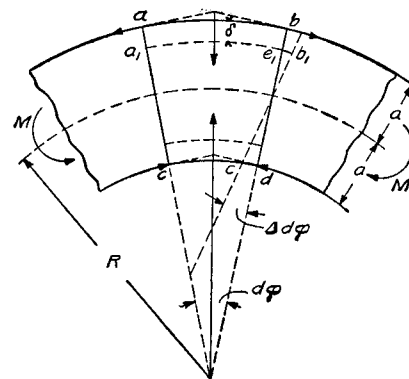


FIG. 71.

moment causes a change of sign of the normal stresses and as a result, instead of a flattening of the tube in the radial direction, there is a flattening in the direction perpendicular to the plane of Fig. 71 and the fiber $ab$, due to this flattening, is displaced outward. From the same reasoning as above it may be shown that here again the flattening of the cross section produces a decrease in the stress at the most remote fibers. It may therefore be concluded that the fibers of the tube farthest from the neutral axis do not take the share in the stresses which the ordinary theory of bending indicates. This affects the bending of the tube in the same way as a decrease in its moment of inertia. Instead of eq. (67) which was derived for solid curved bars, the following equation must be used in calculating the deflections of thin tubes:

$$\Delta d\varphi = \frac{MRd\varphi}{kEI_z}, \qquad (100)$$

in which $k$ is a numerical factor, less than unity, which takes care of the flattening. This factor depends upon the proportions of the bend and can be calculated from the following

approximate formula[30]

$$k = 1 - \frac{9}{10 + 12\left(\dfrac{tR}{a^2}\right)^2}, \qquad (101)$$

in which $t$ is the thickness of the tube. This indicates that the effect of the flattening depends only upon the magnitude of the ratio $tR/a^2$.

As for the effect of the flattening on the stress distribution, Kármán showed that, instead of the simple equation for normal bending stresses [31] $\sigma = My/I_z$ in which $y$ denotes the distance from the neutral axis, the following more complicated equation must be used:

$$\sigma = \frac{My}{kI_z}\left(1 - \beta\frac{y^2}{a^2}\right), \qquad (c)$$

in which

$$\beta = \frac{6}{5 + 6\left(\dfrac{tR}{a^2}\right)^2}.$$

The maximum stress, obtained from $(c)$, is

$$\sigma_{max} = k_1\frac{Md}{2I_z}, \qquad (102)$$

in which $d$ is the outer diameter of the tube and

$$k_1 = \frac{2}{3k\sqrt{3\beta}}$$

is a numerical factor which depends upon the proportions of the bend. Several values of $k_1$ are given below:

TABLE 8

| $\dfrac{tR}{a^2} = 0.3$ | 0.5 | 1.0 |
|---|---|---|
| $k_1 = 1.98$ | 1.30 | 0.88 |

[30] See paper by Th. Kármán, loc. cit., p. 107.
[31] It is assumed that $R$ is large in comparison with $a$ and that a linear stress distribution is a sufficiently accurate assumption.

It is seen that when $tR/a^2$ is small, the actual maximum stress is considerably greater than that given by the usual theory which neglects the flattening of the cross section.

A theory analogous to the above may also be developed in the case of a tube of rectangular cross section.[32] For example, in the case of a thin tube of square cross section, the coefficient $k$ in eq. (100) is found to depend upon the magnitude of the ratio

$$n = \frac{b^4}{R^2t^2},$$

in which $t$ is the thickness of the wall, $R$ the radius of the center line of the bend and $b$ the length of the side of the cross section. Then

$$k = \frac{1 + 0.0270n}{1 + 0.0656n}. \qquad (103)$$

For instance, if $b/R = 0.1$ and $b/t = 50$, we obtain $n = 25$ and, from (103), $k = 0.63$. The maximum stress in tubes of rectangular section increases in the same proportion as the flexibility, i.e., in the above example the distortion of the cross section increases the maximum stress approximately, by 60 per cent.

If a cross section of a curved bar has flanges of a considerable width, again the question of distortion of the cross section becomes of practical importance. Such a problem we have, for example, when investigating bending stresses at a corner of a rigid frame of an $I$ section, Fig. 72a. Considering an element of the frame between the two consecutive cross sections $mn$ and $m_1n_1$, we see that the longitudinal bending stresses $\sigma$ in the flanges give the components in a radial direction which tend to produce bending of the flanges, Fig. 72b. This bending results in some diminishing of longitudinal
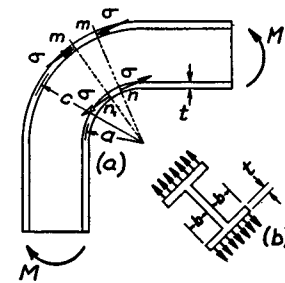


Fig. 72.

[32] Such a problem occurs, for instance, in the design of a Fairbairn crane. See reference 28.

bending stress $\sigma$ in portions of the flanges at a considerable distance from the web. To take into account this fact, an *effective width* $\alpha b$ of a flange must be used in using formula (75) for an $I$ section. Naturally the magnitude of the factor $\alpha$, defining the effective width of the flange, depends on the flexibility of the flanges, which is expressed by the quantity:

$$\beta = 1.32 \frac{b}{\sqrt{tr}}, \qquad (d)$$

in which $t$ is the thickness of the flange and $r$ its radius of curvature. For the flange at the intrados $r = a$, and for the outer flange $r = c$. The calculations show that if $\beta < 0.65$, the bending of the flanges can be neglected and we can directly apply the theory developed in Art. 11. For larger values of $\beta$ the formula

$$\alpha b = \left( \frac{1}{\beta} - \frac{1}{2\pi\beta^3} \right) b \qquad (e)$$

can be used [33] for calculating the *effective width* of a flange. Assume, for example, that we have the width of the flange $b = 6$ in., the corresponding radius $r = 8$ in., and the thickness $t = 1$ in. Then, from formula $(d)$, we obtain $\beta = 2.80$ and the effective width of the flange is $0.35 \times 6 = 2.1$ in.

## 19. Bending of a Curved Bar out of its Plane of Initial Curvature.

—In our previous discussion we have dealt with the bending of curved bars in the plane of their initial curvature. There are cases, however, in which the forces acting on a curved bar do not lie in the plane of the center line of the bar.[34]

[33] For derivation of this formula see Dr. Dissertation by Otto Steinhardt, Darmstadt, 1938. The experiments made by Steinhardt are in satisfactory agreement with the formula.

[34] Several problems of this kind have been discussed by I. Stutz, Zeitschr. d. Österr. Arch.- u. Ing.-Ver., 1904, p. 682; H. Müller-Breslau, Die neueren Methoden der Festigkeitslehre, 2 ed., 1913, p. 258, and 4th ed., p. 265; and B. G. Kannenberg, Der Eisenbau, 1913, p. 329. The case of a circular ring supported at several points and loaded by forces perpendicular to the plane of the ring was discussed by F. Düsterbehn, Der Eisenbau, 1920, p. 73, and by G. Unold, Forschungsarbeiten, nr. 255, Berlin, 1922. The same problem was discussed by C. B. Biezeno

Then it is necessary to consider the deflection of the bar in two perpendicular planes and the twist of the bar. A simple problem of this kind is shown in Fig. 73a in which a portion of a horizontal circular ring, built in at $A$, is loaded by a vertical load $P$ applied at the end $B$.[35] Considering a cross section $D$ of the bar and taking the coordinate axes as shown in Figures 73$b$ and 73$c$ [36] we find that the moments of the external load $P$ with respect to these axes are
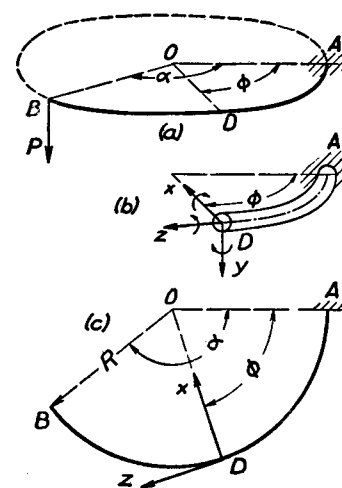


FIG. 73.

$$M_x = -PR \sin(\alpha - \varphi), \qquad M_y = 0,$$
$$M_z = PR[1 - \cos(\alpha - \varphi)]. \qquad (a)$$

By using these expressions the bending and torsion stresses can be calculated in any cross section of the bar. In calculating deflection at the end $B$ the Castigliano theorem will be used, for which purpose we need the expression for the strain energy of the bar. Assuming that the cross sectional dimensions of the bar are small in comparison with radius $R$,

by using the principle of least work, "De Ingenieur," 1927, and Zeitschr. f. angew. Math. u. Mech., Vol. 8, 1928, p. 237. The application of trigonometric series in the same problem is shown by C. B. Biezeno and J. J. Koch, Zeitschr. f. angew. Math. Mech., vol. 16, 1936, p. 321. The problem is of a practical importance in design of steam piping. The corresponding bibliography is given in the paper by H. E. Mayrose, Journal of Applied Mechanics, Trans. A. S. M. E., vol. 4, 1937, p. 89. See also the book by A. H. Gibson and E. G. Ritchie, "A Study of the Circular-Arc Bow-Girder," London, 1914.

[35] This problem has been discussed by Saint Venant; see his papers in Comptes Rendus, vol. 17, 1843, Paris.

[36] It is assumed that the horizontal axis $x$ and the vertical axis $y$ are the axes of symmetry of the cross section and that the $z$ axis is tangent to the center line of the ring at $D$.

we apply the same formulas as we already had for a straight bar (see pp. 294 and 297, part I). Thus the expression for the strain energy of our bar is

$$U = \int_0^\alpha \left( \frac{M_x^2}{2EI_x} + \frac{M_z^2}{2C} \right) R\, d\varphi, \qquad (b)$$

where $C$ denotes the torsional rigidity of the bar.[37] The required deflection $\delta$ is then obtained from the equation:

$$\delta = \frac{\partial U}{\partial P}.$$

Substituting for $U$ expression (b), and observing that

$$\frac{\partial M_x}{\partial P} = -R \sin(\alpha - \varphi) \quad \text{and} \quad \frac{\partial M_z}{\partial P} = R[1 - \cos(\alpha - \varphi)],$$

we obtain

$$\delta = \frac{PR^3}{EI_x} \int_0^\alpha \left\{ \sin^2(\alpha - \varphi) \right. \\ \left. + \frac{EI_x}{C}[1 - \cos(\alpha - \varphi)]^2 \right\} d\varphi. \quad (104)$$

In the particular case, when $\alpha = \pi/2$,

$$\delta = \frac{PR^3}{EI_x} \left[ \frac{\pi}{4} + \frac{EI_x}{C} \left( \frac{3\pi}{4} - 2 \right) \right]. \qquad (c)$$

If the cross section of the ring is circular, $C = G I_p = 2 G I_x$; taking $E = 2.6G$, we obtain

$$\delta = \frac{PR^3}{EI_x} \left[ \frac{\pi}{4} + 1.3 \left( \frac{3\pi}{4} - 2 \right) \right] = 1.248 \frac{PR^3}{EI_x}. \quad (105)$$

As an example of statically indeterminate problems, let us consider a horizontal semi-circular bar with built-in ends, loaded at the middle, Fig. 74a. Considering only small vertical deflections of the bar, we can entirely neglect any displacements in the horizontal plane as small quantities of a

[37] The calculation of $C$ for various shapes of the cross section is discussed in Chapter VI.

higher order. Hence there will be no bending of the ring in its plane and no forces or moments in that plane at the ends $A$ and $B$. Considering the built-in end $B$, we conclude from the equilibrium conditions that there will act a vertical reaction $P/2$ and the moment $M_{x_0} = PR/2$. The moment $M_{z_0}$ will also act, preventing the end section $B$ from rotation with respect to $z_0$ axis. The magnitude of this moment cannot be determined from statics; we shall find it by using the principle of least work, which requires that



FIG. 74.

$$\frac{\partial U}{\partial M_{z_0}} = 0. \qquad (d)$$

In deriving the strain energy of the bar we represent the moments applied at the end $B$ by the vectors $PR/2$ and $M_{z_0}$, as shown in Fig. 74b. Then the moments $M_x$ and $M_z$ at any cross section $D$ are

$$M_x = \frac{PR}{2} \cos \varphi - M_{z_0} \sin \varphi - \frac{PR}{2} \sin \varphi, \qquad (e)$$

$$M_z = \frac{PR}{2} \sin \varphi + M_{z_0} \cos \varphi - \frac{PR}{2} (1 - \cos \varphi), \qquad (f)$$

and the expression for strain energy is

$$U = 2 \int_0^{\pi/2} \left( \frac{M_x^2}{2EI_x} + \frac{M_z^2}{2C} \right) R\, d\varphi. \qquad (g)$$

Substituting this in equation (d) and observing that

$$\frac{\partial M_x}{\partial M_{z_0}} = -\sin \varphi, \qquad \frac{\partial M_z}{\partial M_{z_0}} = \cos \varphi,$$
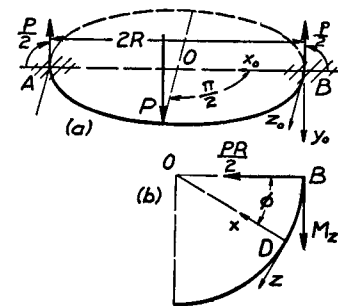
we obtain

$$\frac{1}{EI_x}\int_0^{\pi/2}\left(\frac{PR}{2}\sin^2\varphi + M_{z_0}\sin^2\varphi\right.$$
$$\left. - \frac{PR}{2}\sin\varphi\cos\varphi\right)d\varphi + \frac{1}{C}\int_0^{\pi/2}\left[\frac{PR}{2}\sin\varphi\cos\varphi\right.$$
$$\left. + M_{z_0}\cos^2\varphi - \frac{PR}{2}(1-\cos\varphi)\cos\varphi\right]d\varphi = 0,$$

from which

$$M_{z_0} = \frac{PR}{2}\left(\frac{2}{\pi} - 1\right) = -0.182PR. \qquad (106)$$

The minus sign indicates that the direction of $M_{z_0}$ is opposite to that shown in Fig. 74a. Knowing $M_{z_0}$ we obtain the bending and the twisting moments at any cross section from the expressions (e) and (f).

The maximum deflection is evidently under the load and we readily obtain it from Castigliano's equation:

$$\delta = \frac{\partial U}{\partial P}. \qquad (h)$$

Substituting expression (g) for $U$ and observing that

$$\frac{\partial M_x}{\partial P} = \frac{R}{2}(\cos\varphi - \sin\varphi),$$
$$\frac{\partial M_z}{\partial P} = \frac{R}{2}(\sin\varphi + \cos\varphi - 1), \qquad (i)$$

we obtain

$$\delta = \frac{PR^3}{2EI_x}\left\{(2 - 0.363)\left(\frac{\pi}{4} - \frac{1}{2}\right)\right.$$
$$\left. + \frac{EI_x}{C}\left[(2 - 0.363)\left(\frac{\pi}{4} + \frac{1}{2}\right) + \frac{\pi}{2} - 4 + 0.363\right]\right\}$$
$$= 0.514\frac{PR^3}{2EI_x}. \qquad (107)$$

In the calculation of the partial derivatives (i) we disregarded the fact that the twisting moment $M_{z_0}$ is not an independent quantity but the function of $P$ as defined by expression (106).

If we should take this into consideration, the right-hand side of the equation (h) should be written in the following form:

$$\frac{\partial U}{\partial P} + \frac{\partial U}{\partial M_{z_0}}\cdot\frac{dM_{z_0}}{dP}. \qquad (j)$$

But the second term in this expression vanishes, by virtue of equation (d). Hence our previous procedure of calculating deflection $\delta$ is justified.

### Problems

1. A curved bar with circular axis and with $\alpha = \pi/2$ (Fig. 73) is loaded at end $B$ by a twisting couple $M_z = T$. Find the deflection of the end $B$ in a vertical direction.
   *Answer.* Assuming $EI_x : C = 1.3$,

$$\delta = 0.506\frac{TR^2}{EI_x}.$$

2. Solve the preceding problem assuming that at end $B$ a bending couple, $M_x = M_0$, is applied in the vertical plane tangent to the center line at $B$.
   *Answer.*

$$\delta = 1.150\frac{M_0R^2}{EI_x}.$$

3. A semicircular bar with the center line in a horizontal plane is built in at $A$ and $B$ and loaded symmetrically by two vertical loads $P$ at $C$ and $D$, Fig. 75. Find the twisting moments $M_{z_0}$ at the built-in ends.
   *Answer.*
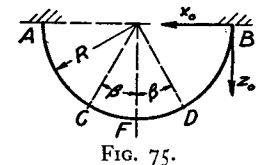

FIG. 75.

$$M_{z_0} = -\frac{2}{\pi}PR\left(\frac{\pi}{2} - \cos\beta - \beta\sin\beta\right).$$

4. Solve the preceding problem for the case of a uniform vertical load of intensity $q$ distributed along the entire length of the bar.
   *Answer.*

$$M_{z_0} = -qR^2\left(\frac{\pi}{2} - \frac{4}{\pi}\right) = -0.32\,qR^2.$$

5. The horizontal semicircular bar, shown in Fig. 75 and uniformly loaded as in the preceding problem, is supported at the middle cross section $F$. Find the vertical reaction $N$ at the support $F$.

*Answer.* $N = 2qR$.

## CHAPTER III

### THIN PLATES AND SHELLS

**20. Bending of a Plate to a Cylindrical Surface.**—Assume that a rectangular plate of uniform thickness $h$ is bent to a cylindrical surface [1] (Fig. 76). In such a case it is sufficient to consider only one strip of unit width, such as $AB$, as a beam of rectangular cross section and of the length $l$. From the condition of continuity it may be concluded that there will be no distortion in the cross section of the strip during bending, such as shown in Fig. 77$b$, p. 89, Part I. Hence a fiber l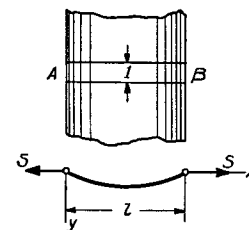engthwise of the strip such as $ss$ (Fig. 77) suffers not only the longitudinal tensile stress $\sigma_x$ but also tensile stress $\sigma_z$ in the lateral direction, which must be such as to prevent lateral contraction of the fiber. We assume, as before (see p. 88, Part I), that cross sections of the strip remain plane during bending. Hence the unit elongations in the $x$ and $z$ directions are
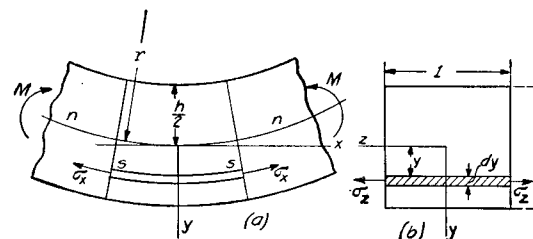
Fig. 76.

Fig. 77.

$$\epsilon_x = \frac{y}{r}; \qquad \epsilon_z = 0.$$

[1] We have such bending in the case of long rectangular plates if the acting forces do not vary along the length of the plate and if only the portion at a sufficient distance from the ends is considered.

The corresponding stresses in $x$ and $z$ directions are then obtained as in the case of tension in two perpendicular directions. By use of eqs. (38) (p. 52, Part I),

$$\sigma_x = \frac{\epsilon_x E}{1 - \mu^2} = \frac{Ey}{(1 - \mu^2)r}; \qquad \sigma_z = \frac{\mu\epsilon_x E}{1 - \mu^2} = \frac{\mu Ey}{(1 - \mu^2)r}.$$

We proceed as in the case of bending of a bar and calculate the bending moment at any cross section of the strip. Then

$$M = \int_{-h/2}^{+h/2} \sigma_x y\, dy = \frac{E}{(1 - \mu^2)r} \int_{-h/2}^{+h/2} y^2 dy = \frac{Eh^3}{12(1 - \mu^2)r},$$

from which

$$\frac{1}{r} = \frac{M}{D}, \tag{108}$$

where

$$D = \frac{Eh^3}{12(1 - \mu^2)}. \tag{109}$$

This quantity is called the *flexural rigidity* of a plate and takes the place of $EI_z$ in discussing bending of beams. 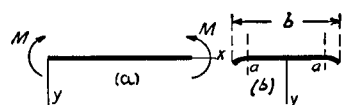Comparison of eq. (108) for the strip with eq. (56), Part I, for a bar shows that the rigidity of the strip in the plate is larger than that of an isolated bar of the same cross section in the ratio $1 : (1 - \mu^2)$.



FIG. 78.

The experiments show that, in the case of bending of an isolated thin strip of considerable width $b$, distortion of the cross section takes place only near the edges (Fig. 78, $b$) and the middle portion $aa$ of the strip is bent into a cylindrical form;[2] hence eq. (108) is applicable in calculating deflections and the strip will prove more rigid than will be expected from the simple beam formula.

For small deflections of the strip $AB$ (Fig. 77) the curva-

[2] Explanation of this phenomenon is given by G. F. C. Searle, Experimental Elasticity, Cambridge, 1908. See also H. Lamb, London Math. Soc. Proc., Vol. 21, 1891, p. 70, and author's paper in Mechanical Engineering, 1923, p. 259.

ture $1/r$ can be replaced by its approximate value $d^2y/dx^2$ and the differential equation for the deflection curve of the strip is

$$D\frac{d^2y}{dx^2} = -M. \tag{110}$$

The discussion of bending of a plate to a cylindrical surface involves the integration of this equation. A particular case in which the bending to a cylindrical surface is done by a uniformly distributed load is discussed in the next article.

**21. Bending of a Long Uniformly Loaded Rectangular Plate.**—If a rectangular plate whose length is large in comparison with the width is uniformly loaded, then it may be assumed that near the center, where the maximum deflection and stresses occur, the deflection surface is nearly a cylindrical one and eq. (110) may be used to calculate these.[3] Let us consider this important problem[4] for two extreme conditions: (1) the edges of the plate are simply supported and can rotate freely during bending and (2) the edges are built-in. In both cases it is assumed that there are no displacements at the edges in the plane of the plate. Then an elemental strip such as $AB$ in Fig. 76 is in the same condition as a tie-rod with uniform lateral loading (see article 6) and the tensile forces $S$. The magnitude of the forces $S$ is found from the condition that the extension of the strip is equal to the difference between the length of the deflection curve and the length $l$ of the chord $AB$ (Fig. 76).

*Simply Supported Edges.* In the case of simply supported edges, a good approximation for $S$ is obtained by assuming that the deflection curve is a sine curve

$$y = \delta \sin\frac{\pi x}{l}, \tag{a}$$

where $\delta$ denotes the deflection at the middle. Then by using eq. (56), p. 47, the extension of the center line of the strip is

$$\lambda = \frac{1}{2}\int_0^l \left(\frac{dy}{dx}\right)^2 dx = \frac{\pi^2\delta^2}{4l}. \tag{b}$$

[3] If the length is three times the width for a supported plate and twice the width for a clamped plate, the solution derived on this assumption is sufficiently accurate.

[4] A solution of the problem was given by J. Boobnov. See his "Theory of Structure of Ships," Vol. 2, p. 545, St. Petersburg, 1914. The discussion of this problem, together with calculation of stresses in the hull of a ship, is given in "Theory of Plates and Shells," 1940.

Taking for the deflection at the middle the approximate equation (59), we have

$$\delta = \frac{\delta_0}{1 + \alpha}, \qquad (c)$$

in which

$$\delta_0 = \frac{5}{384} \frac{q l^4}{D} \qquad \text{and} \qquad \alpha = S : S_{cr} = \frac{S l^2}{D \pi^2}. \qquad (111)$$

Substituting in equation (b), we obtain

$$\lambda = \frac{\pi^2}{4l} \cdot \frac{\delta_0^2}{(1 + \alpha)^2}. \qquad (d)$$

The lateral contraction of the strip in the plane of the plate during bending is assumed to be zero; hence from eqs. (109) and (111) the elongation of the center line of the strip produced by forces $S$ is

$$\lambda = \frac{S l (1 - \mu^2)}{E h} = \frac{\pi^2 \alpha h^2}{12 l}. \qquad (e)$$

Equating (d) and (e), the equation for determining $\alpha$, i.e., for determining the longitudinal force $S$, is obtained in the form:

$$\alpha (1 + \alpha)^2 = \frac{3 \delta_0^2}{h^2}. \qquad (112)$$

If the load $q$ and the dimensions of the plate are given, the right side of eq. (112) can easily be calculated. The solution of eq. (112) can be simplified by letting

$$1 + \alpha = x. \qquad (f)$$

Then this equation becomes

$$x^3 - x^2 = \frac{3 \delta_0^2}{h^2},$$

i.e., the quantity $x$ is such that the difference between its cube and its square has a known value. It can be determined from a slide rule or a suitable table and $\alpha$ found from eq. (f). The deflection and stresses in the strip $AB$ are then calculated by using the table given for tie-rods (see p. 43). In using this table it is necessary to remember that, from eqs. (23) and (111),

$$u = \frac{p l}{2} = \frac{\pi}{2} \sqrt{\alpha}. \qquad (113)$$

Take, for example, a steel plate of dimensions $l = 45$ in. and $h = 3/8$ in. loaded by a uniformly distributed load $q = 10$ lbs. per sq. in.

Then eq. (112) becomes

$$\alpha (1 + \alpha)^2 = 290, \qquad (g)$$

from which

$$\alpha = 5.97 \qquad \text{and} \qquad u = \frac{\pi}{2} \sqrt{\alpha} = 3.83.$$

The tensile stress produced by the longitudinal force $S$ is

$$\sigma_x' = \frac{S}{h} = \frac{\alpha S_{cr}}{h} = \frac{\alpha \pi^2 D}{h l^2} = 11,300 \text{ lbs. per sq. in.}$$

and the maximum bending moment at the middle of the strip, from eq. (45), is

$$M_{max} = \frac{q l^2}{8} \psi_1(u). \qquad (h)$$

By using the table 3, mentioned above, we find by interpolation, for $u = 3.83$, $\psi_1(u) = 0.131$. This shows that, due to the action of the longitudinal force $S$, the bending moment is greatly diminished and is only about 13 per cent of that which is produced by the action of transverse loading alone. Using eq. (h),

$$M_{max} = \frac{10 \times 45^2}{8} \times 0.131 = 332 \text{ lbs. ins.}$$

The corresponding maximum bending stress is

$$\sigma_x'' = \frac{6 M_{max}}{h^2} = \frac{6 \times 332 \times 8^2}{3^2} = 14,200 \text{ lbs. per sq. in.}$$

and, superposing the tensile and bending stresses, the maximum stress is

$$\sigma_{max} = \sigma_x' + \sigma_x'' = 11,300 + 14,200 = 25,500 \text{ lbs. per sq. in.}$$

It may be seen that, due to the action of the longitudinal force, the maximum stress does not increase in the same proportion as the intensity of the load. For instance, in the above numerical example with $q = 20$ lbs. per sq. in., from (g)

$$\alpha (1 + \alpha)^2 = 290 \times 4 = 1,160,$$

from which

$$\alpha = 9.85; \qquad u = 4.93.$$

The tensile stress produced by the longitudinal force $S$ is

$$\sigma_x' = \frac{S}{h} = 18,600 \text{ lbs. per sq. in.}$$

$\psi_1(u)$, for $u = 4.93$, is equal to $0.082$; then

$$\sigma_x'' = \frac{6M_{\max}}{h^2} = \frac{6 \times 20 \times 45^2 \times 8^2}{8 \times 3^2} \times 0.082 = 17,900 \text{ lbs. per sq. in.}$$

The maximum total stress is

$$\sigma_{\max} = \sigma_x' + \sigma_x'' = 18,600 + 17,900 = 36,500 \text{ lbs. per sq. in.}$$

In other words, due to the action of the longitudinal forces $S$, the stresses increase less rapidly than the load. When the load is doubled, the maximum stress is in our case increased only 43 per cent.

*Clamped Edges.* In the case of clamped edges eq. (*a*) is replaced by [5] equation

$$y = \frac{\delta}{2} \left( 1 - \cos \frac{2\pi x}{l} \right), \tag{k}$$

which satisfies conditions at the clamped edges because the deflection $y$ and the slope $dy/dx$ both become zero at $x = 0$ and at $x = l$. Substituting (*k*) into eq. (*b*), the extension of the center line of the strip is

$$\lambda = \frac{1}{2} \int_0^l \left( \frac{dy}{dx} \right)^2 dx = \frac{\pi^2 \delta^2}{4l}. \tag{l}$$

For the deflection at the middle we use the approximate equation (62)

$$\delta = \frac{\delta_0}{1 + \frac{1}{4}\alpha}$$

and find, from (*l*) and (*e*), the following equation for $\alpha$:

$$\alpha \left( 1 + \frac{\alpha}{4} \right)^2 = \frac{3\delta_0^2}{h^2} \tag{114}$$

or, by letting $1 + (\alpha/4) = x$,

$$x^3 - x^2 = \frac{3}{4} \frac{\delta_0^2}{h^2}. \tag{m}$$

In the previous numerical example with $q = 10$ lbs. per sq. in., eq. (*m*) becomes

$$x^3 - x^2 = 2.90,$$

from which $x = 1.849$ and $\alpha = 3.40$. Hence the tensile force is less than in the case of supported edges considered above in the ratio

---

[5] See the author's paper mentioned above, loc. cit., p. 44.

$3.40/5.97$ and we obtain

$$\sigma_x' = \frac{3.40}{5.97} \times 11,300 = 6,430 \text{ lbs. per sq. in.}$$

In calculating the bending stresses the table 3 of page 43 is used. Noting that in our case $u = (\pi/2)\sqrt{\alpha} = 2.89$, we find from the table, by interpolation, $\psi_2 = 0.686$, $\psi_3 = 0.488$. The bending moment at each clamped edge is

$$M = -0.686 \frac{ql^2}{12} = -1.150 \text{ lbs. ins.}$$

The corresponding maximum bending stress is

$$\sigma_x'' = 49,300 \text{ lbs. per sq. in.}$$

The maximum total stress is [6]

$$\sigma_{\max} = \sigma_x' + \sigma_x'' = 6,430 + 49,300 = 55,700 \text{ lbs. per sq. in.}$$

Comparison of this stress with that obtained above for the same plate with simply supported edges shows that clamping the edges increases the maximum stress. This result can be explained as follows: Due to clamping the edges, the deflection of the plate is diminished, and as a result the longitudinal force $S$ and its effect on the bending moment are also diminished. In the case of simply supported edges, the maximum bending moment was only 0.131 of that produced by the transverse load alone. But in the case of clamped edges the bending moment at these edges is 0.686 of that produced by the transverse load alone, i.e., the effect of the longitudinal force is more pronounced in the case of simply supported edges.

This approximate method can be used in the calculation of stresses in the plates of a ship's hull submitted to hydrostatic pressure.

The maximum stress evidently depends on the intensity of the load $q$ and on the ratio $l/h$. The magnitudes of this stress for the case of simply supported edges and for various values of the ratio $l/h$ are represented by curves [7] in Fig. 79. It is seen that because of the presence of tensile forces $S$, which increase with the load,

---

[6] It is assumed that the steel has a proportional limit above the stress calculated.

[7] These curves are taken from the paper by S. Way presented at the meeting of Applied Mechanics, A. S. M. E., New Haven, June, 1932.

the maximum stress is not proportional to the load $q$; for large values of $q$ this stress does not vary much with the thickness of the plate.

In Fig. 80 the curves for maximum stress in the case of plates with built-in edges are given. It is seen that for small values of the intensity of the load $q$, when the effect of the axial force on the deflections of the strip is small, the maximum stress increases approximately in the same ratio as $q$ increases. But for larger values of $q$ the relation between the load and the maximum stress becomes non-linear.
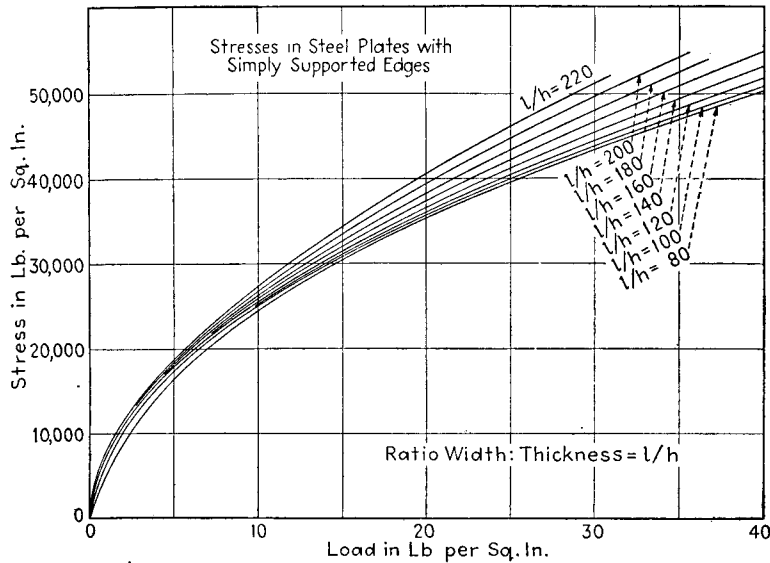


FIG. 79.

**22. Deflection of Long Rectangular Plates Having a Small Initial Cylindrical Curvature.**[8]—In this problem, we may use the results already obtained for the bending of bars with small initial curvature (p. 104). The edges of the plate are assumed to be simply supported and the coordinate axes and an elemental strip are taken as in Fig. 76. Let

$$y_0 = b \sin \frac{\pi x}{l} \qquad (a)$$

represent the small initial deflection of the plate, with the maximum deflection at the middle equal to $b$. If a uniform load $q$ is applied,

an additional deflection is produced, accompanied by an extension of the *middle surface* [9] of the plate. As before, let $S$ denote the tensile force on the strip $AB$ of unit width and $\alpha$ the ratio of this force to the critical force $S_{cr} = \pi^2 D/l^2$. Then the additional deflection produced by the load $q$ is

$$y_1 = \frac{\delta_0}{1 + \alpha} \sin \frac{\pi x}{l} - \frac{\alpha b}{1 + \alpha} \sin \frac{\pi x}{l}. \qquad (b)$$

The first term on the right side represents the approximate expression for the deflection of a straight line strip, which was used
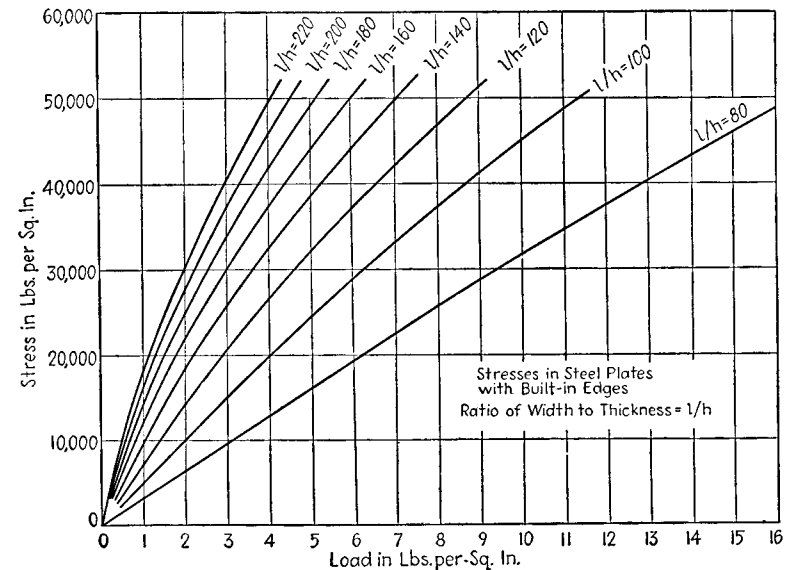


FIG. 80.

before for flat plates; the second member represents the effect of the initial curvature (see eq. (d), p. 106). By adding (a) and (b) we obtain the total deflection

$$y = y_0 + y_1 = b \sin \frac{\pi x}{l} + \frac{\delta_0}{1 + \alpha} \sin \frac{\pi x}{l}$$

$$- \frac{\alpha b}{1 + \alpha} \sin \frac{\pi x}{l} = \frac{b + \delta_0}{1 + \alpha} \sin \frac{\pi x}{l} \cdots. \qquad (c)$$

The magnitude of $\alpha$ is determined from the consideration of extension of the strip $AB$. Using the same reasoning as in the

preceding article we obtain the following expression for this extension

$$\lambda = \frac{1}{2} \int_0^l \left(\frac{dy}{dx}\right)^2 dx - \frac{1}{2} \int_0^l \left(\frac{dy_0}{dx}\right)^2 dx.$$

Substituting ($a$) and ($c$) for $y_0$ and $y$ and integrating, we have

$$\lambda = \frac{\pi^2}{4l} \left[ \left(\frac{b + \delta_0}{1 + \alpha}\right)^2 - b^2 \right].$$

Setting this equal to the extension produced by the longitudinal force $S$ (eq. $e$, p. 122), we obtain

$$\frac{\pi^2}{4l} \left[ \left(\frac{b + \delta_0}{1 + \alpha}\right)^2 - b^2 \right] = \frac{\pi^2 \alpha h^2}{12l}$$

or

$$\alpha(1 + \alpha)^2 = 3 \left(\frac{b + \delta_0}{h}\right)^2 - 3 \frac{b^2}{h^2} (1 + \alpha)^2. \qquad (115)$$

If $b = 0$, this reduces to eq. (112) for a flat plate.

Take as an example a steel plate of the same dimensions as in the previous article:

$$l = 45 \text{ in.}, \qquad h = 3/8 \text{ in.}, \qquad q = 10 \text{ lbs. per sq. in.},$$

and assume $b = 3/8$ in. Then

$$\delta_0 = \frac{5}{384} \frac{ql^4}{D} = 3.686 \text{ in.},$$

and eq. (115) becomes

$$\alpha(1 + \alpha)^2 = 351.6 - 3(1 + \alpha)^2. \qquad (d)$$

As before, let

$$1 + \alpha = x;$$

then

$$x^3 + 2x^2 = 351.6,$$

from which

$$x = 6.45, \qquad \alpha = 5.45.$$

The tensile stress produced by the longitudinal force $S$ is

$$\sigma_x' = \frac{S}{h} = \frac{\alpha \pi^2 D}{hl^2} = 10,200 \text{ lbs. per sq. in.}$$

---

[8] See author's article in the book, Festschrift zum Siebzigsten Geburtstage August Föppl, p. 74, 1923, Berlin.

[9] The middle surface is the surface midway between the faces of the plate.

This stress is somewhat less than the corresponding stress for the flat plate (see p. 123). In calculating bending stresses it should be noted that the deflection given by eq. ($b$) consists of two parts. The first is the same as that for a flat plate and the second,

$$- \frac{\alpha b}{1 + \alpha} \sin \frac{\pi x}{l},$$

represents the effect of the initial curvature. The maximum bending stress corresponding to the first part of the deflection for $\alpha = 5.45$; $u = \frac{\pi}{2} \sqrt{\alpha} = 3.67$ and $\psi_1 = 0.142$, from table 3 on p. 43, is 15,300 lbs. per sq. in. The bending moment corresponding to the second part of the deflection is

$$- D \frac{d^2}{dx^2} \left( - \frac{\alpha b}{1 + \alpha} \sin \frac{\pi x}{l} \right) = - \frac{\alpha \pi^2 b D}{(1 + \alpha) l^2} \sin \frac{\pi x}{l}. \qquad (e)$$

This moment has a negative sign and the corresponding maximum compressive stress, which is to be subtracted from the stress calculated as for a flat plate, is

$$- \frac{6}{h^2} \cdot \frac{\alpha \pi^2 b D}{(1 + \alpha) l^2} = - 9,500 \text{ lbs. per sq. in.}$$

The combination of this with the stress $\sigma_x'$ calculated above and the bending stress 15,300 lbs. per sq. in. obtained as for a flat plate gives the complete stress

$$\sigma_x = 10,200 + 15,300 - 9,500 = 16,000 \text{ lbs. per sq. in.}$$

A comparison of these results with those for flat plates shows that here the tensile forces $S$ are somewhat reduced and that the bending stress at the middle is much less, due to the negative sign of the bending moment ($e$). The effect of the initial curvature is to reduce the resultant stress from 25,500 lbs. per sq. in. to 16,000 lbs. per sq. in. This result is obtained with the initial deflection equal to the thickness of the plate. By increasing the initial deflection, the maximum stress can be reduced still further.

### 23. Combination of Pure Bending in Two Perpendicular Directions.

—Let us consider first a rectangular plate bent by moments uniformly distributed along the edges (Fig. 81). $M_1$ denotes the bending moment per unit length of the edges parallel to the $y$ axis and $M_2$ the moment per unit length

of the edges parallel to the $x$ axis. The plane midway between the faces of the plate, the so-called *middle plane* of the plate, is taken as the $xy$ plane and the $z$ axis is perpendicular to this plane and downward. An element is cut out of the
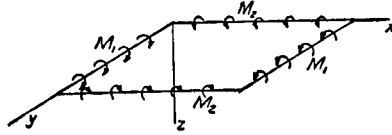


FIG. 81.

plate by two pairs of planes parallel to the $xz$ and $yz$ planes (Fig. 82). The theory of pure bending of the plate is based on the assumption that during bending the lateral sides of this element remain plane and rotate about the neutral axes $n$–$n$. For moments as indicated in Fig. 81 the upper part of the element is under compression and the lower part under tension. The middle plane $nn$ does not undergo any deformation during this bending of the plate and is therefore a *neutral surface*. Let $1/r_1$ and $1/r_2$ denote the curvatures of this neutral surface in sections parallel to the $zx$ and the $zy$ planes respectively; then the unit elongations in the $x$ and $y$ directions of an elemental sheet $abcd$, a distance $z$ from the neutral surface, are found as in the case of a beam (p. 90, Part I) and are equal to
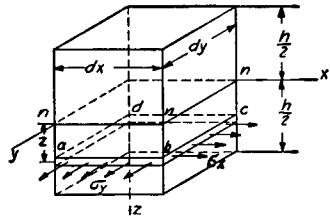


FIG. 82.

$$\epsilon_x = \frac{z}{r_1}; \qquad \epsilon_y = \frac{z}{r_2}. \tag{a}$$

Using eqs. (38) (p. 52, Part I), the corresponding stresses are

$$\sigma_x = \frac{Ez}{1 - \mu^2}\left(\frac{1}{r_1} + \mu\frac{1}{r_2}\right), \tag{b}$$

$$\sigma_y = \frac{Ez}{1 - \mu^2}\left(\frac{1}{r_2} + \mu\frac{1}{r_1}\right). \tag{c}$$

These stresses are proportional to the distance $z$ from neutral surface. The moments of the internal forces acting on the sides of the element are equaled to the moments of external couples, giving the following equations:

$$\int_{-h/2}^{+h/2} \sigma_x z\, dy\, dz = M_1 dy, \tag{d}$$

$$\int_{-h/2}^{+h/2} \sigma_y z\, dx\, dz = M_2 dx. \tag{e}$$

Substituting (b) and (c) for $\sigma_x$ and $\sigma_y$ and noting that

$$\frac{E}{1 - \mu^2}\int_{-h/2}^{+h/2} z^2 dz = \frac{Eh^3}{12(1 - \mu^2)} = D,$$

where $D$ denotes the *flexural rigidity of the plate* (eq. 109), we find

$$D\left(\frac{1}{r_1} + \mu\frac{1}{r_2}\right) = M_1, \tag{116}$$

$$D\left(\frac{1}{r_2} + \mu\frac{1}{r_1}\right) = M_2, \tag{117}$$

which correspond to eq. (56), p. 91, Part I, for the pure bending of a straight bar. Denoting by $w$ small deflections of the plate, the approximate formulas for curvatures are

$$\frac{1}{r_1} = -\frac{\partial^2 w}{\partial x^2} \quad \text{and} \quad \frac{1}{r_2} = -\frac{\partial^2 w}{\partial y^2}.$$

In terms of $w$, eqs. (116) and (117) become

$$-D\left(\frac{\partial^2 w}{\partial x^2} + \mu\frac{\partial^2 w}{\partial y^2}\right) = M_1, \tag{118}$$

$$-D\left(\frac{\partial^2 w}{\partial y^2} + \mu\frac{\partial^2 w}{\partial x^2}\right) = M_2. \tag{119}$$

These correspond to eq. (79) (p. 135, Part I) for the deflection curve of a straight bar. In the particular case in which $M_1 = M_2 = M$, the curvatures of the deflection surface in two perpendicular directions are equal and the surface is

spherical. The curvature of the sphere, from eq. (116), is

$$\frac{1}{r} = \frac{M}{D(1 + \mu)}. \tag{120}$$

Such a spherical deflection surface is obtained for a plate of any shape if the bending moments $M$ are uniformly distributed along its edge.

In the above, it was assumed that there is no change in the length of the fibers of the middle surface, i.e., that this surface is the neutral surface in the bent plate. This condition can be rigorously satisfied only if the surface of the bent plate is a *developable* surface, such for instance as a cylindrical surface discussed in the previous article. For non-developable surfaces the above assumption is sufficiently accurate only if the deflection $w$ of the plate is small in comparison to its thickness $h$. To show this, consider the bending of a circular plate produced by couples $M$ uniformly distributed along the edge. It follows from the previous theory that the deflection surface is a sphere with the radius given by eq. (120). Let $AOB$ (Fig. 83) represent the diametral section of the bent circular plate, $a$ its outer radius, and $\delta$ the deflection at the middle. We assume first that there is no stretching of the middle plane of the plate in its meridional direction; then arc $OB = a$, $\varphi = a/r$, and $\overline{CB} = a_1 = r \sin \varphi$. In such a case the deflection of the plate is obviously accompanied by a compressive strain in the circumferential direction. The magnitude of this strain for the edge of the plate is



Fig. 83.

$$\epsilon = \frac{a - a_1}{a} = \frac{r\varphi - r \sin \varphi}{r\varphi}.$$

For a small deflection $\delta$, the angle $\varphi$ is small and $\sin \varphi = \varphi - \varphi^3/6$ approximately, giving

$$\epsilon = \frac{\varphi^2}{6}, \tag{f}$$

or, noting that

$$\delta = r(1 - \cos \varphi) = \frac{r\varphi^2}{2} \text{ approximately,}$$

we obtain

$$\epsilon = \frac{\delta}{3r}. \tag{k}$$

This represents the upper limit of circumferential strain at the edge. It was obtained by assuming that the meridional strain is zero. Under actual conditions there will be a certain amount of strain in the meridional direction and the true circumferential compression will be smaller than that given by eq. (k).[10]

The approximate theory of the bending of plates neglects entirely the strain in the middle plane and considers only strains such as given by eqs. (a), the maximum value of which in the above example is $h/2r$. Hence a strain such as that given by (k) can be neglected and the middle surface can be considered as unstrained if $\delta/3r$ is small in comparison with $h/2r$, i.e., if the deflection $\delta$ is small in comparison with the thickness of the plate $h$. Only in this assumption can the results given later for some special cases of bending of plates be used with sufficient accuracy.

**24. Thermal Stresses in Plates.**—Equation (120) of the previous article, for deflection to a spherical shape, is very useful in calculating thermal stresses produced in a plate by non-uniform heating. Let $t$ denote the difference in temperature of the upper and lower faces of the plate and $\alpha$ the coefficient of linear expansion of the material. Assuming that the variation of the temperature through the thickness of the

[10] If the deflections are not small and the strain in the middle surface is taken into consideration, it has been shown that in the case of pure bending of a circular plate, of radius $a = 23h$, the circumferential compressive stress in the middle surface at the edge is about 18 per cent of the maximum bending stress when the deflection at the middle is equal to six tenths the thickness of the plate. See author's paper in Memoirs of the Institute of Ways of Communication, St. Petersburg, 1915. See also "Theory of Plates and Shells," 1940.

plate follows a linear law, the corresponding expansions follow the same law, and if the edge of the plate is free, the deflection produced by these expansions will be a spherical one.[11] The difference between the maximum expansion and the expansion at the middle surface is $\alpha t/2$, and the curvature resulting from this non-uniform expansion is given by the equation

$$\frac{\alpha t}{2} = \frac{h}{2r},$$

from which

$$\frac{1}{r} = \frac{\alpha t}{h}. \tag{121}$$

This bending of the plate does not produce any stresses, provided the edges are free and the deflection is small as compared with the thickness.

If, however, the edge of the plate be clamped, heating will produce bending moments along the edge. The magnitude of these moments is such as to eliminate the curvature produced by the non-uniform heating and given by eq. (121), as only in this manner can the condition at the clamped edge be satisfied. From eqs. (121) and (120) we obtain the following equation for the bending moment per unit length of the clamped edge:

$$M = \frac{\alpha t(1 + \mu)D}{h}.$$

Noting that $M$ is acting on a rectangular area of unit width and of depth $h$ the corresponding maximum bending stress is

$$\sigma_{\max} = \frac{6M}{h^2} = \frac{6\alpha t(1 + \mu)D}{h^3} = \frac{\alpha t}{2}\frac{E}{1 - \mu}. \tag{122}$$

This stress is proportional to the coefficient of thermal expansion $\alpha$, to the difference in temperature $t$ [12] at the two faces

[11] It is assumed that deflections are small in comparison with the thickness $h$ of the plate.

[12] It must be noted that $t$ denotes the difference in temperature between the two faces of the plate and not that between liquids or gases in contact with the plate. The latter, due to abrupt change in temperature at the plate surface, may be much greater than $t$.

of the plate, and to the modulus of elasticity. The difference in temperature $t$ is likely to increase with the thickness of the plate; therefore greater thermal stress can be expected in thick plates than in thin ones. It is interesting to note that eq. (122), developed for flat plates, can also be used with sufficient accuracy in cases of spherical and cylindrical shells (see p. 262).

**25. Bending of Circular Plates Loaded Symmetrically with Respect to the Center.**[13]—The deflection surface in this case is symmetrical about the axis perpendicular to the plate through its center and the consideration of a diametral section through this axis is sufficient for calculating deflections and stresses. Figure 84 represents such a diametral section, with the axis of symmetry $oz$. Let $w$ denote the deflection of the plate at any point $A$ a distance $x$ from the axis, and restrict it to small values. Let

$$\varphi \approx -\frac{dw}{dx}$$

represent the slope of the deflection surface at the same point. The curvature of the plate in the diametral section $xz$ is

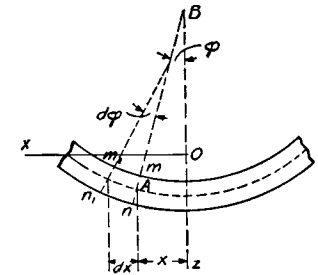$$\frac{1}{r_1} = -\frac{d^2w}{dx^2} = \frac{d\varphi}{dx}. \tag{a}$$



FIG. 84.

In determining the radius of curvature $r_2$ in the direction perpendicular to the $xz$ plane it is necessary to note that after deflection of the plate sections such as $nm$ form a conical surface whose apex $B$ is the point of intersection of $nm$ with the axis $oz$. Then $AB$ represents the radius $r_2$ and, from the figure,

$$\frac{1}{r_2} = \frac{\varphi}{x}. \tag{b}$$

[13] This case of bending was developed by Poisson, Paris, Mém. de l'Acad., Vol. 8, 1829.

We proceed in the same manner as in the bending of a bar and assume that there is always the same relation between the bending moments and the curvatures as in the case of pure bending of a plate (art. 23). Equations (116) and (117) can therefore be used here also. Substituting (a) and (b) into these equations we find

$$M_1 = D\left(\frac{d\varphi}{dx} + \mu\,\frac{\varphi}{x}\right),\qquad(123)$$

$$M_2 = D\left(\frac{\varphi}{x} + \mu\,\frac{d\varphi}{dx}\right).\qquad(124)$$

Here, as before, $M_1$ and $M_2$ denote bending moments per unit length, $M_1$ along circumferential sections of the plate such as $mn$, and $M_2$ along diametral sections $xz$. Equations (123) and (124) contain only one variable $\varphi$, which is determined from the equilibrium of an element $abcd$ (Fig. 85) cut out from the plate by two cylindrical sections $ab$ and $cd$ and by two diametral sections $ao$ and $bo$. The couple acting on the side $cd$ of the element is
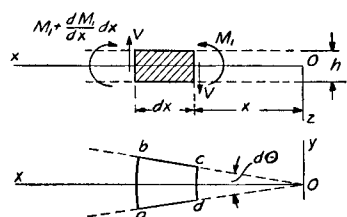
$$M_1 x\,d\theta.\qquad(c)$$

The corresponding couple on side $ab$ is

$$\left(M_1 + \frac{dM_1}{dx}\,dx\right)(x + dx)d\theta.\qquad(d)$$



Fig. 85.

The couples on the sides $ad$ and $bc$ are each $M_2 dx$, and they have a resultant in the plane $xz$ equal to

$$M_2 dx\,d\theta.\qquad(e)$$

In addition to these couples there are shearing forces $V$ on the sides $ab$ and $cd$.[14] If $V$ represents the shearing force per unit length, the total shearing force acting on the side $cd$ of the element is $Vx\,d\theta$. Neglecting small quantities of

[14] It follows from symmetry that there are no shearing forces on the sides $bc$ and $ad$ of the element.

higher order, a shearing force of the same magnitude acts on the side $ab$. These two forces give a couple in the plane $xz$ equal to

$$Vx\,d\theta\,dx.\qquad(f)$$

Summing up moments (c), (d), (e) and (f) with proper signs, the equation of equilibrium of the element $abcd$ is

$$\left(M_1 + \frac{dM_1}{dx}\,dx\right)(x + dx)d\theta - M_1 x\,d\theta - M_2\,dx\,d\theta + Vx\,dx\,d\theta = 0,$$

from which we find, by neglecting small quantities of higher order,

$$M_1 + \frac{dM_1}{dx}\,x - M_2 + Vx = 0.\qquad(g)$$

Substituting expressions (123) and (124) for $M_1$ and $M_2$, eq. (g) becomes

$$\frac{d^2\varphi}{dx^2} + \frac{1}{x}\frac{d\varphi}{dx} - \frac{\varphi}{x^2} = -\frac{V}{D}.\qquad(125)$$

In any particular case of a symmetrically loaded circular plate, the shearing force $V$ may be determined from statics; then eq. (125) can be used for determining the slope $\varphi$ and the deflection $w$ of the plate. Take, for example, a circular plate loaded by a uniformly distributed load of intensity $q$ and a concentrated load $P$ applied at the center. Taking a section of the plate by a cylindrical surface with axis $oz$ and radius $x$, the shearing force $V$ per unit length of this section is found from the statement of the equilibrium of the inner part of the plate cut out by the cylindrical surface. The load acting on this part of the plate is $P + \pi x^2 q$. This load must be equal to the resultant of the shearing forces distributed over the cylindrical section; hence

$$2\pi x V = P + \pi x^2 q$$

and

$$V = \frac{qx}{2} + \frac{P}{2\pi x}.\qquad(126)$$

Substituting into eq. (125),

$$\frac{d^2\varphi}{dx^2} + \frac{1}{x}\frac{d\varphi}{dx} - \frac{\varphi}{x^2} = -\frac{1}{D}\left(\frac{qx}{2} + \frac{P}{2\pi x}\right)$$

or

$$\frac{d}{dx}\left[\frac{1}{x}\frac{d}{dx}(x\varphi)\right] = -\frac{1}{D}\left(\frac{qx}{2} + \frac{P}{2\pi x}\right),$$

from which, by simple integration,

$$\frac{1}{x}\frac{d}{dx}(x\varphi) = -\frac{1}{D}\left(\frac{qx^2}{4} + \frac{P}{2\pi}\log_n x\right) + C_1, \qquad (h)$$

where $C_1$ is a constant of integration. The integration of $(h)$ gives

$$x\varphi = -\frac{qx^4}{16D} - \frac{P}{2\pi D}\left(\frac{x^2\log_n x}{2} - \frac{x^2}{4}\right) + C_1\frac{x^2}{2} + C_2$$

or

$$\varphi = -\frac{qx^3}{16D} - \frac{Px}{8\pi D}(2\log_n x - 1) + \frac{C_1 x}{2} + \frac{C_2}{x}, \quad (127)$$

where $C_2$ is the second constant of integration. For small deflections (Fig. 84),

$$\varphi = -\frac{dw}{dx},$$

giving us the following equation for deflections:

$$\frac{dw}{dx} = \frac{qx^3}{16D} + \frac{Px}{8\pi D}(2\log_n x - 1) - \frac{C_1 x}{2} - \frac{C_2}{x},$$

from which, by integration,

$$w = \frac{qx^4}{64D} + \frac{Px^2}{8\pi D}(\log_n x - 1) - \frac{C_1 x^2}{4} - C_2\log_n x + C_3. \quad (128)$$

The constants of integration $C_1$, $C_2$ and $C_3$ must be determined in each particular case from the conditions at the edge of the plate.

In the above discussion it was assumed that the middle surface of the plate is a neutral surface, i.e., that there is no strain in this plane. This assumption is justified only if the edges of the plate are free from stresses in the middle plane of the plate and the deflections are small in comparison with the thickness of the plate.

**26. Uniformly Loaded Circular Plate.**—*Clamped Edges.* The slope and the deflection are given by eqs. (127) and (128) by putting $P = 0$ in these equations. In the case of clamped edges, $\varphi = 0$ for $x = a$ and for $x = 0$, where $a$ is the outer radius of the plate. The following equations for calculating the arbitrary constants $C_1$ and $C_2$ are then obtained from eq. (127):

$$\left(\frac{qx^3}{16D} - \frac{C_1 x}{2} - \frac{C_2}{x}\right)_{x=a} = 0,$$

$$\left(\frac{qx^3}{16D} - \frac{C_1 x}{2} - \frac{C_2}{x}\right)_{x=0} = 0,$$

from which

$$C_2 = 0 \qquad \text{and} \qquad C_1 = \frac{qa^2}{8D}, \qquad (a)$$

and these, put in eq. (127), give

$$\varphi = \frac{qx}{16D}(a^2 - x^2). \qquad (129)$$

The deflections are calculated from eq. (128). In this equation set $P = 0$ and the arbitrary constants $C_1$ and $C_2$ as in eqs. (a). Then

$$w = \frac{qx^4}{64D} - \frac{qa^2 x^2}{32D} + C_3. \qquad (b)$$

The constant $C_3$ is found from the condition that at the edge the deflection is zero. Hence

$$\frac{qa^4}{64D} - \frac{qa^4}{32D} + C_3 = 0,$$

from which

$$C_3 = \frac{qa^4}{64D}.$$

Substituting in equation $(b)$, we obtain

$$w = \frac{q}{64D}(a^2 - x^2)^2. \qquad (130)$$

The maximum deflection is at the center of the plate and is

$$\delta = \frac{qa^4}{64D}. \tag{131}$$

This deflection is equal to $\frac{5}{8}$ of the deflection of a strip (Fig. 76) clamped at the ends and of length equal to the diameter of the plate. The bending moments are obtained from eqs. (123) and (124); expression (129) for ($\varphi$) is substituted into these equations, which gives

$$M_1 = \frac{q}{16}\left[a^2(1+\mu) - x^2(3+\mu)\right], \tag{c}$$

$$M_2 = \frac{q}{16}\left[a^2(1+\mu) - x^2(1+3\mu)\right]. \tag{d}$$

At the edge ($x = a$) these equations give

$$M_1 = -\frac{qa^2}{8}; \qquad M_2 = -\frac{\mu qa^2}{8}. \tag{e}$$

At the center ($x = 0$),

$$M_1 = M_2 = \frac{1+\mu}{16}qa^2. \tag{f}$$

The maximum stress is at the edge and is equal to

$$(\sigma_x)_{\max} = \frac{6}{h^2}\frac{qa^2}{8} = \frac{3}{4}\frac{qa^2}{h^2}. \tag{132}$$

*Simply Supported at the Edge.* The method of superposition is used in calculating deflections of a plate simply supported at the edge. It was shown (eqs. *e*) that in the case of clamped edges there are negative bending moments $M_1 = -(qa^2/8)$ acting along the edge, Fig. 86 (*a*). If this case is combined with that of pure bending shown in Fig. 86 (*b*), so as to eliminate the bending moment at the edge, we get the bending of a plate simply supported at the edge. The deflection
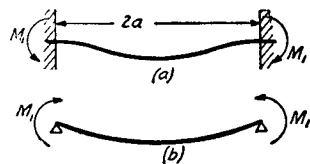
Fig. 86.

due to pure bending is obtained from eq. (120). Substituting in this equation $M = qa^2/8$, we find

$$\frac{1}{r} = \frac{qa^2}{8D(1+\mu)}.$$

The corresponding deflection at the middle for a spherical surface is (see p. 94, Part I)

$$\delta_1 = \frac{a^2}{2r} = \frac{qa^4}{16D(1+\mu)}.$$

This is added to the deflection (131) to get the deflection of a plate supported at the edge,

$$\delta = \frac{qa^4}{64D} + \frac{qa^4}{16D(1+\mu)} = \frac{5+\mu}{64(1+\mu)D}qa^4. \tag{133}$$

For $\mu = 0.3$, this deflection is about four times as great as it is when the edges are clamped.

In calculating bending moments, the constant bending moment $qa^2/8$ must be superposed on the moments (*c*) and (*d*) found above for the case of clamped edges. Hence

$$M_1 = \frac{q}{16}(3+\mu)(a^2 - x^2),$$

$$M_2 = \frac{q}{16}\left[a^2(3+\mu) - x^2(1+3\mu)\right].$$

The maximum bending moment is at the center, where

$$M_1 = M_2 = \frac{3+\mu}{16}qa^2.$$

The corresponding maximum stress is

$$(\sigma_x)_{\max} = (\sigma_y)_{\max} = \frac{6M_1}{h^2} = \frac{3(3+\mu)}{8}\cdot\frac{qa^2}{h^2}. \tag{134}$$

For comparison of the bending stresses $\sigma_x$ and $\sigma_y$ at the lower sides of the plates with clamped and simply supported edges, the variation in these stresses along the radius of the plates is graphically represented in Fig. 87. Measuring the ordi-

nates from the horizontal axis passing through the point $O$, we obtain the stresses for the plate with the clamped edges. Adding to these stresses the constant value $3qa^2/4h^2$, i.e., measuring the ordinates from the horizontal axis passing through the point $O_1$ in Fig. 87, we obtain the stresses for the
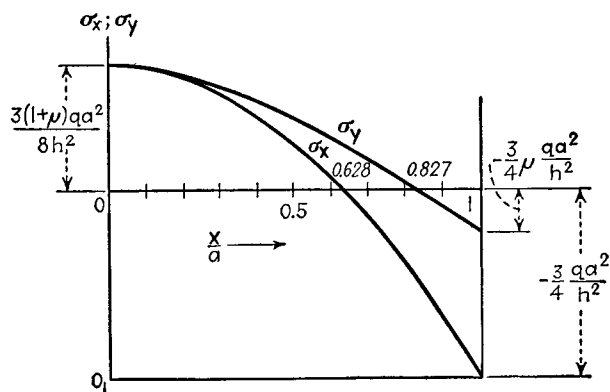


FIG. 87.

simply supported plate. It may be seen that a more favorable stress condition is obtained by clamping the edge.

In the previous discussion the effect of shearing strain on the deflection was neglected. When the thickness of the plate is fairly large in comparison with its radius, this effect may be considerable and must be taken into account.[15] The additional deflection due to shear is found by the same method as in the case of beams (art. 39, Part I). In the case of uniform loading the shearing force, from eq. (126), is

$$V = \frac{qx}{2}.$$

If we assume the same distribution of shearing stresses over the thickness of the plate, as in the case of a bar of rectangular cross section, the maximum shearing stress is at the middle

[15] The increase in deflection due to shear was demonstrated by experiments made by G. M. Russell, Engineering, Vol. 123, 1927, p. 343. See also paper by H. Carrington, Engineering, Vol. 125, 1928, p. 31.

surface and its magnitude at a distance $x$ from the center of the plate is

$$\tau = \frac{3}{2}\frac{V}{h} = \frac{3}{4}\frac{qx}{h}.$$

The corresponding shearing strain at the middle surface of the plate is

$$\gamma = \frac{\tau}{G} = \frac{3}{4}\frac{qx}{Gh},$$

and the additional deflection due to distortion of such an element as $abcd$ in Fig. 85 is

$$\gamma dx = \frac{3}{4}\frac{qx dx}{Gh}.$$

Summing up these deflections along the length of the radius of the plate and noting that at the edge the deflection is zero, we find

$$w_1 = \frac{3}{4}\frac{q}{Gh}\int_x^a x dx = \frac{3}{8}\frac{q}{Gh}(a^2 - x^2).$$

This is added to the deflection (130) due to bending moments to get the total deflection,

$$w = \frac{q}{64D}(a^2 - x^2)^2 + \frac{3}{8}\frac{q}{Gh}(a^2 - x^2),$$

or, using eq. (109),

$$w = \frac{q}{64D}\left[(a^2 - x^2)^2 + \frac{4}{1-\mu}h^2(a^2 - x^2)\right]. \quad (135)$$

The deflection at the center is

$$\delta = \frac{qa^4}{64D}\left(1 + \frac{4}{1-\mu}\frac{h^2}{a^2}\right). \quad (136)$$

In the case of thick plates the second term in the parenthesis, which represents the effect of shearing stresses, may be of practical importance.

The above theory of bending of circular plates is based on the assumption that deflections are small in comparison

with the thickness. For larger deflections the stretching of the middle surface of the plate must be considered. If this is done it can be shown that at larger deflections the plate becomes stiffer than the above theory [16] indicates and the deflections are no longer proportional to the load.

In the case of a uniformly loaded circular plate clamped at the edge the deflection can be calculated from the following equation: [17]

$$\delta + 0.58\frac{\delta^3}{h^2} = \frac{qa^4}{64D},\qquad(137)$$

which is in good agreement with experiments.

In practical applications, very thin uniformly loaded plates are sometimes used. In such cases the bending stresses may be small in comparison with the stresses due to the stretching of the middle surface and the plate can be considered as a thin membrane which has no flexural rigidity at
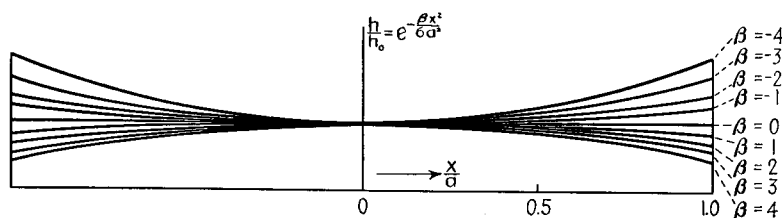


FIG. 88.

all.[18] The deflection at the middle of a uniformly loaded circular membrane is given by the equation

$$\delta = 0.662a\sqrt[3]{\frac{qa}{Eh}}.\qquad(138)$$

We obtain an analogous equation by neglecting $\delta$ in comparison with the term containing $\delta^3$ in eq. (137). Experiments

---

[16] See author's paper, loc. cit., p. 133. See also "Theory of Plates and Shells," 1940.

[17] See "Theory of Plates and Shells," p. 336, 1940.

[18] See H. Hencky, Zeitschr. f. Math. u. Physik, Vol. 63 (1915), p. 311.

---

made on thin membranes are in good agreement with eq. (138).[19]

In the case of a uniformly loaded circular plate of variable thickness the variation of the thickness with the radial distance can be expressed with sufficient accuracy by the equation:

$$\frac{h}{h_0} = e^{-\beta x^2/6a^2},$$

in which $h/h_0$ is the ratio of the thickness at the radial distance $x$ to the thickness $h_0$ at the center, and $\beta$ is a constant. The
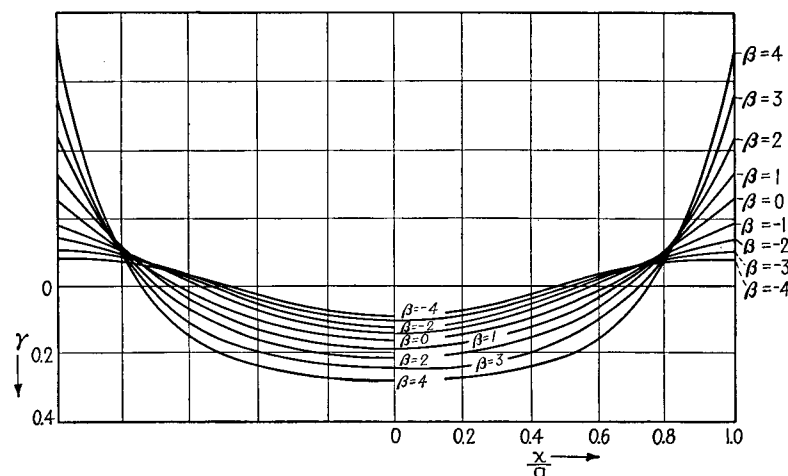


FIG. 89.

shapes of the diametrical sections of plates for various values of the constant $\beta$ are shown in Fig. 88. The maximum bending stress $\sigma_x$ in radial direction at a radial distance $x$ from the center can be expressed by the equation:

$$\sigma_x = \gamma\frac{3qa^2}{h_0^2},$$

in which $\gamma$ is a factor varying with the radial distance $x$.

---

[19] Bruno Eck, Zeitschr. f. angew. Math. und Mech., Vol. 7, 1927, p. 498. Information on corrugated diaphragms see in "Techn. Notes" 738, 1939, Nat. Adv. Comm. Aeron.

The values of this factor [20] for a plate with clamped edges are given by the curves in Fig. 89. For a simply supported plate these values are given in Fig. 90.
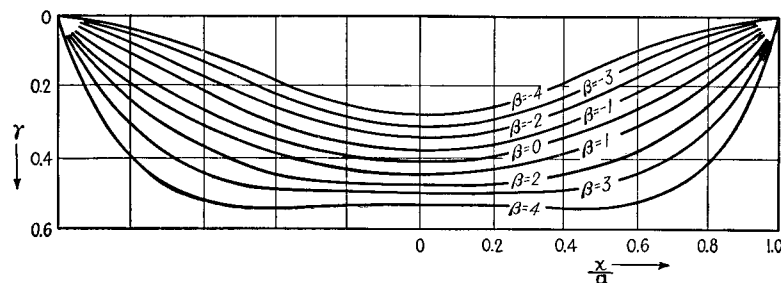


FIG. 90.

## 27. Circular Plate Loaded at the Center.—*Clamped Edge.*

For this case $q = 0$ is substituted in eq. (127), which gives

$$\varphi = -\frac{Px}{8\pi D}(2 \log_n x - 1) + \frac{C_1 x}{2} + \frac{C_2}{x}. \tag{a}$$

The constants of integration $C_1$ and $C_2$ are found from the conditions that $\varphi$ is equal to zero at the clamped edge and at the center of the plate; hence

$$\left[ -\frac{Px}{8\pi D}(2 \log_n x - 1) + \frac{C_1 x}{2} + \frac{C_2}{x} \right]_{x=0} = 0,$$

$$\left[ -\frac{Px}{8\pi D}(2 \log_n x - 1) + \frac{C_1 x}{2} + \frac{C_2}{x} \right]_{x=a} = 0. \tag{b}$$

As $(x \log_n x)_{x=0} = 0$, the following values of arbitrary constants are obtained from $(b)$:

$$C_1 = \frac{P}{4\pi D}(2 \log_n a - 1); \qquad C_2 = 0, \tag{c}$$

and eq. $(a)$ becomes

$$\varphi = \frac{Px}{4\pi D} \log_n \frac{a}{x}. \tag{d}$$

[20] These values are given in the dissertation by O. Pichler, "Die Biegung Kreissymmetrischer Platten von Veränderlicher Dicke," Berlin, 1928.

The equation for the deflection surface is obtained by substituting $q = 0$ and the values $(c)$ of the arbitrary constants into eq. (128), which gives

$$w = \frac{Px^2}{8\pi D}\left( \log_n \frac{x}{a} - \frac{1}{2} \right) + C_3. \tag{e}$$

The constant $C_3$ is obtained from the condition that at the clamped edge the deflection is zero, giving $C_3 = Pa^2/16\pi D$. Substituting this into eq. $(e)$ we obtain

$$w = \frac{Px^2}{8\pi D} \log_n \frac{x}{a} + \frac{P}{16\pi D}(a^2 - x^2). \tag{f}$$

The deflection at the middle is

$$\delta = \frac{Pa^2}{16\pi D}. \tag{139}$$

This deflection is four times as great as that produced by a uniformly distributed load of the same magnitude (eq. 131).

Bending moments are calculated from eqs. (123) and (124), using expression $(d)$,

$$M_1 = \frac{P}{4\pi}\left[ (1 + \mu) \log_n \frac{a}{x} - 1 \right], \tag{g}$$

$$M_2 = \frac{P}{4\pi}\left[ (1 + \mu) \log_n \frac{a}{x} - \mu \right]. \tag{h}$$

At the edge $(x = a)$ these moments become

$$M_1 = -\frac{P}{4\pi}; \qquad M_2 = -\mu\frac{P}{4\pi}, \tag{140}$$

and the corresponding maximum stresses are

$$\sigma_x = \frac{3}{2}\frac{P}{\pi h^2}, \qquad \sigma_y = \frac{3\mu}{2}\frac{P}{\pi h^2}. \tag{141}$$

Comparison with eq. (132) for a uniform load shows that the concentrated load at the center produces stresses at the clamped edge of the plate which are twice as great as the stresses produced by a load of the same magnitude but uniformly distributed over the plate.

At the center of the plate, eqs. (g) and (h) give infinitely large values for the bending moments and the stresses. This result is due to the assumption made that the load is concentrated at the point.[21] If the distribution of the load is taken over a small circle, the stresses become finite (see p. 151).

In determining the safe dimensions of a circular plate loaded at the center we can limit our investigation to the calculation of the maximum tensile bending stresses at the bottom of the plate. It was already mentioned that expressions (g) and (h) are not suitable for this purpose, and the more detailed investigation indicates [22] that the proper formula for calculating the above mentioned tensile stress is

$$(\sigma_x)_{max} = \frac{P}{h^2}(1 + \mu)\left(0.485 \log \frac{a}{h} + 0.52\right). \quad (142)$$

Although the compressive stresses at the top of the plate may be many times as large as the tensile stresses at the bottom in the case of a strong concentration of the load, they do not represent a direct danger because of their highly localized character. The local yielding in the case of a ductile material will not affect the deformation of the plate in general if the tensile stresses at the bottom of the plate remain within safe limits. The compressive strength of a brittle material is usually many times greater than its tensile strength, so that a plate of such a material will also be safe if the tensile stress at the bottom is within the limit of safety.

*Simply Supported Edge.* The deflection of a plate simply supported at the edge is obtained by the method of superposition. On the deflections (f) found above for the case of a clamped edge, we superpose the deflection produced in the

---

[21] Local stresses at the point of application of a concentrated load are discussed in the paper by H. Hencky, Der Spannungszustand in rechteckigen Platten, Darmstadt, 1913, p. 54. See also A. Nadai, "Elastische Platten," p. 97, 1925.

[22] This question is discussed in "Theory of Plates and Shells," p. 75.

plate by moments $M_1 = P/4\pi$ uniformly distributed along the edge and thus obtain the case of a simply supported plate. The curvature produced by the moments $M_1 = P/4\pi$ is, from eq. (120),

$$\frac{1}{r} = \frac{P}{4\pi(1 + \mu)D},$$

and the corresponding deflection at the middle is

$$\delta_1 = \frac{a^2}{2r} = \frac{Pa^2}{8\pi(1 + \mu)D}.$$

This is added to the deflection (139), and the deflection at the middle of a simply supported plate becomes

$$\delta = \frac{Pa^2}{16\pi D} + \frac{Pa^2}{8\pi(1 + \mu)D} = \frac{Pa^2}{16\pi D} \cdot \frac{3 + \mu}{1 + \mu}. \quad (143)$$

This deflection is about 2.5 times as great as that for the case of a clamped plate.

The expressions for bending moments are found by adding $P/4\pi$ to the moments (g) and (h) obtained above for a clamped plate. The maximum tensile stress is obtained by adding $6/h^2 \cdot P/4\pi$ to the stress calculated from formula (142).

**28. Circular Plate Concentrically Loaded.**—We begin with the case in which the load is uniformly distributed along a circle of radius $b$ (Fig. 91). In this case we consider separately the portion of the plate inside this circle and the portion outside. For each portion the general eq. (128) is used, with $q = 0$ for both portions and $P = 0$ for the inner portion. The arbitrary constants are determined in such a manner as to satisfy the conditions of continuity at the circle $x = b$.[23] Denoting by $P$ the total load, the following results are obtained: [24]
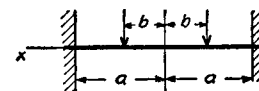


Fig. 91.

---

[23] The effect of shearing stress which produces discontinuity in the slope at the circle $x = b$ is neglected in this case; see paper by G. A. Garabedian, J. de l'École Polytechnique, 2e Ser., C. no. 26, 1927.

[24] See note of article 45 of St. Venant's translation of the book by Clebsch, "Theorie der Elasticität fester Körper," Paris.

*Clamped Edge.* For inner portion $(x < b)$,

$$w = \frac{P}{8\pi D}\left[ -(x^2 + b^2)\log_n\frac{a}{b} + (x^2 - b^2)\right.$$
$$\left. + \frac{1}{2}\left(1 + \frac{b^2}{a^2}\right)(a^2 - x^2)\right]. \quad (a)$$

For outer portion $(x > b)$,

$$w = \frac{P}{8\pi D}\left[ -(x^2 + b^2)\log_n\frac{a}{x} + \frac{1}{2}\left(1 + \frac{b^2}{a^2}\right)(a^2 - x^2)\right]. \quad (b)$$

*Simply Supported Edge.* For inner portion $(x < b)$,

$$w = \frac{P}{8\pi D}\left[ -(x^2 + b^2)\log_n\frac{a}{b} + (x^2 - b^2)\right.$$
$$\left. + \frac{(3 + \mu)a^2 - (1 - \mu)b^2}{2(1 + \mu)a^2}(a^2 - x^2)\right]. \quad (c)$$

For outer portion $(x > b)$,

$$w = \frac{P}{8\pi D}\left[ -(x^2 + b^2)\log_n\frac{a}{x}\right.$$
$$\left. + \frac{(3 + \mu)a^2 - (1 - \mu)b^2}{2(1 + \mu)a^2}(a^2 - x^2)\right]. \quad (d)$$

Any case of bending of a circular plate loaded symmetrically with respect to the center can be solved by use of these equations together with the method of superposition. Consider, for instance, the case shown in Fig. 92, in which the load is uniformly distributed over the inner part of the plate bounded by a circle of radius $c$. Substitute



FIG. 92.

in eq. (a) $P = 2\pi bqdb$, and the deflection produced at the center of the plate by the elemental ring loading shown in the figure is

$$dw = \frac{q}{4D}\left[ -b^2\log_n\frac{a}{b} - b^2 + \frac{1}{2}(a^2 + b^2)\right]bdb. \quad (e)$$

The deflection produced by the entire load is

$$\delta = \int_0^c dw = \frac{q}{4D}\int_0^c\left[ -b^2\log_n\frac{a}{b} - b^2 + \frac{1}{2}(a^2 + b^2)\right]bdb$$
$$= \frac{q}{4D}\left[ -\frac{c^4}{4}\log_n\frac{a}{c} - \frac{3}{16}c^4 + \frac{a^2c^2}{4}\right]. \quad (144)$$
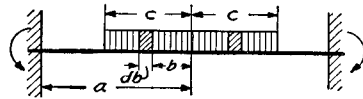
If $c = a$, this equation coincides with eq. (131) for a uniformly loaded plate. By substituting in eq. (144) $c = 0$ and $\pi c^2 q = P$, eq. (139) for deflection by a concentrated load is obtained. To determine bending moments and stresses at the center of the plate, we calculate the second derivative with respect to $x$ of the expression (a). Setting $x = 0$ and $P = 2\pi bqdb$ in this derivative, the curvature at the center, produced by the elemental ring loading (Fig. 92), is

$$\frac{q}{4D}\left( -2\log_n\frac{a}{b} + 1 - \frac{b^2}{a^2}\right)bdb.$$

The curvature at the center produced by the entire load is then

$$\left(\frac{d^2w}{dx^2}\right)_{x=0} = \frac{q}{4D}\int_0^c\left( -2\log_n\frac{a}{b} + 1 - \frac{b^2}{a^2}\right)bdb$$
$$= -\frac{qc^2}{4D}\left(\log_n\frac{a}{c} + \frac{c^2}{4a^2}\right). \quad (145)$$

The corresponding bending moment at the center from eqs. (118) and (119) is

$$M_1 = M_2 = -D(1 + \mu)\frac{d^2w}{dx^2} = \frac{1 + \mu}{4}qc^2\left(\log_n\frac{a}{c} + \frac{c^2}{4a^2}\right) \quad (146)$$

and the maximum bending stresses at the center are

$$(\sigma_x)_{max} = (\sigma_y)_{max} = \frac{3}{2}(1 + \mu)\frac{qc^2}{h^2}\left(\log_n\frac{a}{c} + \frac{c^2}{4a^2}\right). \quad (147)$$

Using the notation $P$ for the entire load $\pi c^2 q$, this becomes

$$(\sigma_x)_{max} = (\sigma_y)_{max} = \frac{3}{2}(1 + \mu)\frac{P}{\pi h^2}\left(\log_n\frac{a}{c} + \frac{c^2}{4a^2}\right). \quad (148)$$

By diminishing the radius $c$ of the circle over which the load is distributed, we approach the condition of a concentrated load. The stresses at the center increase as $c$ decreases, but remain finite as long as $c$ is finite.

**29. Deflection of a Symmetrically Loaded Circular Plate with a Circular Hole at the Center.—** *Bending by Couples.* Denote by $M_{1a}$ and $M_{1b}$ the bending moments per unit length on the outer and inner edges respectively (Fig. 93, a). For this case let $P = q = 0$
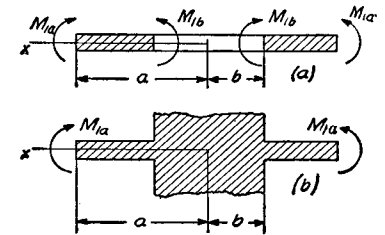


FIG. 93.

in eqs. (127) and (128) and we find

$$\varphi = \frac{C_1 x}{2} + \frac{C_2}{x}, \tag{a}$$

$$w = -\frac{C_1 x^2}{4} - C_2 \log_n \frac{x}{a} + C_3. \tag{b}$$

The arbitrary constants are now to be determined from the conditions at the edges. Substituting (a) into eq. (123) we obtain

$$M_1 = D\left[ \frac{C_1}{2} - \frac{C_2}{x^2} + \mu\left( \frac{C_1}{2} + \frac{C_2}{x^2} \right) \right]. \tag{c}$$

By putting $x = a$ and afterwards $x = b$ we get the following equations for determining $C_1$ and $C_2$:

$$D\left[ \frac{C_1}{2}(1 + \mu) - \frac{C_2}{a^2}(1 - \mu) \right] = M_{1a},$$

$$D\left[ \frac{C_1}{2}(1 + \mu) - \frac{C_2}{b^2}(1 - \mu) \right] = M_{1b},$$

from which

$$C_1 = \frac{2(a^2 M_{1a} - b^2 M_{1b})}{(1 + \mu)D(a^2 - b^2)}; \qquad C_2 = \frac{a^2 b^2 (M_{1a} - M_{1b})}{(1 - \mu)D(a^2 - b^2)}. \tag{d}$$

The constant $C_3$ is determined from a consideration of the deflection of the plate. Assume, for instance, that the plate is supported at the outer edge; then the deflection at this edge is zero and $C_3$ is calculated from (b), which becomes

$$-\frac{C_1 a^2}{4} + C_3 = 0.$$

The deflection surface of the plate is obtained by substituting $C_1$, $C_2$ and $C_3$ into eq. (b).

As a second example let us consider the case of bending of the plate by the couples $M_{1a}$ when the inner edge is built in (Fig. 93, b). The arbitrary constants $C_1$ and $C_2$ in eq. (a) are determined from the conditions $\varphi = 0$ for $x = b$ and $M_1 = M_{1a}$ for $x = a$. Then from eqs. (a) and (c)

$$\frac{C_1 b}{2} + \frac{C_2}{b} = 0,$$

$$\frac{C_1}{2}(1 + \mu) - \frac{C_2}{a^2}(1 - \mu) = \frac{M_{1a}}{D},$$

from which

$$C_1 = \frac{2a^2 M_{1a}}{D[a^2(1 + \mu) + b^2(1 - \mu)]},$$

$$C_2 = -\frac{a^2 b^2 M_{1a}}{D[a^2(1 + \mu) + b^2(1 - \mu)]}.$$

Substituting into (a) and (c),

$$\varphi = \frac{a^2 M_{1a}}{D[a^2(1 + \mu) + b^2(1 - \mu)]}\left( x - \frac{b^2}{x} \right), \tag{e}$$

$$M_1 = \frac{a^2 M_{1a}}{a^2(1 + \mu) + b^2(1 - \mu)}\left[ 1 + \mu + (1 - \mu)\frac{b^2}{x^2} \right]. \tag{f}$$

*Bending by Load Uniformly Distributed along Inner and Outer Edges.* If bending is produced by a loading uniformly distributed along the edges (Fig. 94, a), $q = 0$ and $P$ is equal to the entire load on the inner edge. These values are substituted into eqs. (127) and (128). Then, from eq. (127),

$$\varphi = -\frac{Px}{8\pi D}(2 \log_n x - 1) + \frac{C_1 x}{2} + \frac{C_2}{x}. \tag{g}$$

The arbitrary constants $C_1$ and $C_2$ are to be determined from the conditions at the edges. For example, if the plate is clamped at the edges (Fig. 94, b), the arbitrary constants are determined from the conditions $\varphi = 0$ for $x = a$ and $x = b$. Then, from eq. (g),

$$-\frac{Pa}{8\pi D}(2 \log_n a - 1) + \frac{C_1 a}{2} + \frac{C_2}{a} = 0,$$

$$-\frac{Pb}{8\pi D}(2 \log_n b - 1) + \frac{C_1 b}{2} + \frac{C_2}{b} = 0.$$
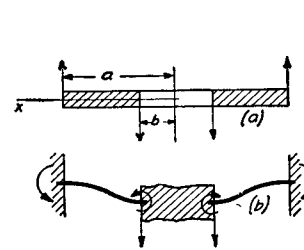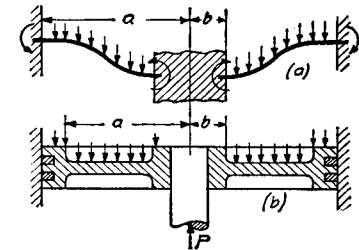


FIG. 94.          FIG. 95.

The expression for $\varphi$ is obtained after $C_1$ and $C_2$ are calculated and

substituted into eq. (g). The bending moments may then be calculated from eqs. (123) and (124).

In the case of a uniformly distributed load (Fig. 95, a) the shearing force $V$ at any point a distance $x$ from the center is

$$V = \frac{1}{2\pi x} \pi q(x^2 - b^2) = \frac{qx}{2} - \frac{qb^2}{2x} .$$

This quantity must be substituted into eq. (125), and eqs. (127) and (128) become

$$\varphi = -\frac{qx^3}{16D} + \frac{qb^2x}{8D}(2\log_n x - 1) + \frac{C_1 x}{2} + \frac{C_2}{x},$$

$$w = \frac{qx^4}{64D} - \frac{b^2 q x^2}{8D}(\log_n x - 1) - \frac{C_1 x^2}{4} - C_2 \log_n x + C_3.$$

For determining arbitrary constants the conditions at the edges are used. For instance, if the plate is clamped at the edges, the equations for determining $C_1$ and $C_2$ are

$$-\frac{qa^3}{16D} + \frac{qab^2}{8D}(2\log_n a - 1) + \frac{C_1 a}{2} + \frac{C_2}{a} = 0,$$

$$-\frac{qb^3}{16D} + \frac{qb^3}{8D}(2\log_n b - 1) + \frac{C_1 b}{2} + \frac{C_2}{b} = 0.$$

Solutions of such problems as the bending of pistons of steam engines and the bending of flanges[25] of cylinders and tubes may be obtained by combining the solutions discussed in this article. For example, by combining the cases shown in Figs. 94 (b) and 95 (a), an approximate solution of the problem of the bending of a piston (Fig. 95, b) by steam pressure may be obtained.[26]

Several cases of practical importance are represented in Fig. 96.[27] In all these cases the maximum stress is given by a formula

[25] See paper by Everett O. Waters and J. Hall Taylor, Trans. Amer. Soc. Mech. Engrs., 1927.

[26] Several problems of this kind are considered in the paper by M. Ensslin, Dinglers Polytech. Journal, 1903 and 1904. See also Pfleiderer, Forschungsarbeiten, n. 97, 1911. Experiments with pistons are described in the paper by C. Codron, Revue de Mécanique, Vol. 13 (1903), p. 340. Circular plates reinforced by ribs are discussed by M. Schilhansl; see Zeitschr. f. Angew. Mathem. und Mech., Vol. 6 (1926), p. 484, and V. D. I., Vol. 71 (1927), p. 1154. A further discussion of circular plates see in "Theory of Plates and Shells," 1940.

[27] See paper by A. M. Wahl and G. Lobo, Trans. A. S. M. E. Vol. 52, 1929.

of the type:

$$\sigma_{max} = k\frac{qa^2}{h^2} \quad \text{or} \quad \sigma_{max} = \frac{kP}{h^2}, \tag{149}$$

depending on whether the applied load is uniformly distributed over the surface or concentrated along the edge. The numerical values
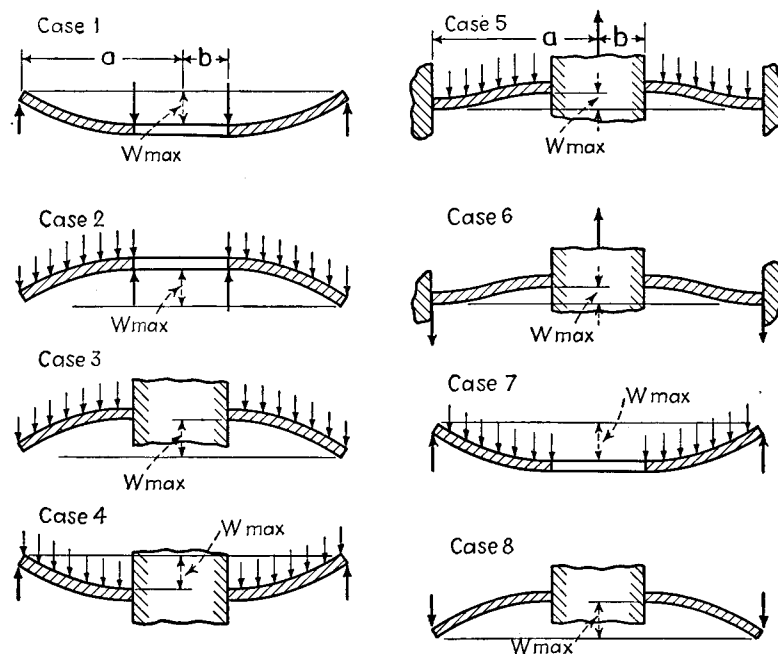


FIG. 96.

of the factor $k$, calculated for several values of the ratio $a/b$ and for Poisson's ratio $\mu = 0.3$, are given in Table 9.

The maximum deflections in the same cases are given by formulas of the type:

$$w_{max} = k_1 \cdot \frac{qa^4}{Eh^3} \quad \text{or} \quad w_{max} = k_1 \cdot \frac{Pa^2}{Eh^3}. \tag{150}$$

The coefficients $k_1$ are also given in Table 9.

**30. Bending of Rectangular Plates.**—The theory of bending of rectangular plates is more complicated than that for circular plates and only some final results for the bending moments and deflections

are given below.[28]  In deriving these results, it is assumed that deflections are small in comparison with the thickness of the plate, and that during bending the edges can freely displace in the plane of

TABLE 9.—COEFFICIENTS $k$ AND $k_1$ IN EQS. (149) AND (150) FOR THE EIGHT CASES SHOWN IN FIG. 96

| $a/b =$ | 1.25 | | 1.5 | | 2 | | 3 | | 4 | | 5 | |
|---|---|---|---|---|---|---|---|---|---|---|---|---|
| Case | $k$ | $k_1$ | $k$ | $k_1$ | $k$ | $k_1$ | $k$ | $k_1$ | $k$ | $k_1$ | $k$ | $k_1$ |
| 1 | 1.10 | 0.341 | 1.26 | 0.519 | 1.48 | 0.672 | 1.88 | 0.734 | 2.17 | 0.724 | 2.34 | 0.704 |
| 2 | 0.66 | 0.202 | 1.19 | 0.491 | 2.04 | 0.902 | 3.34 | 1.220 | 4.30 | 1.300 | 5.10 | 1.310 |
| 3 | 0.135 | 0.00231 | 0.410 | 0.0183 | 1.04 | 0.0938 | 2.15 | 0.293 | 2.99 | 0.448 | 3.69 | 0.564 |
| 4 | 0.122 | 0.00343 | 0.336 | 0.0313 | 0.74 | 0.1250 | 1.21 | 0.291 | 1.45 | 0.417 | 1.59 | 0.492 |
| 5 | 0.090 | 0.00077 | 0.273 | 0.0062 | 0.71 | 0.0329 | 1.54 | 0.110 | 2.23 | 0.179 | 2.80 | 0.234 |
| 6 | 0.115 | 0.00129 | 0.220 | 0.0064 | 0.405 | 0.0237 | 0.703 | 0.062 | 0.933 | 0.092 | 1.13 | 0.114 |
| 7 | 0.592 | 0.184 | 0.976 | 0.414 | 1.440 | 0.664 | 1.880 | 0.824 | 2.08 | 0.830 | 2.19 | 0.813 |
| 8 | 0.227 | 0.00510 | 0.428 | 0.0249 | 0.753 | 0.0877 | 1.205 | 0.209 | 1.514 | 0.293 | 1.745 | 0.350 |

the plate, i.e., there are no stresses acting on the middle plane of the plate.

*Plate Supported at the Edges.*  In the case of a uniformly distributed load $q$ the maximum deflection occurs at the center of the plate (Fig. 97) and is given by the equation:

$$\delta = \alpha \frac{qa^4}{Eh^3},\qquad (151)$$

in which $a$ is the shorter side of the plate, $h$ the thickness of the plate and $\alpha$ is a numerical factor depending on the magnitude of the ratio $b/a$.  As before, we use the notations $M_1$ and $M_2$ for the bending moments per unit length on the sections parallel to the $y$ and $x$ axes respectively.  The maximum bending moments occur at the center of the plate and are


FIG. 97.

$$(M_1)_{max} = \beta_1 qa^2;\quad (M_2)_{max} = \beta_2 qa^2,\quad (152)$$

in which $\beta_1$ and $\beta_2$ denote numerical factors depending upon the ratio $b/a$.  Several values of the coefficients $\alpha$, $\beta_1$ and $\beta_2$ are given in Table 10.  These values are calculated on the assumption that Poisson's ratio is equal to 0.3.

---

[28] The complete discussion of bending of rectangular plates is given in "Theory of Plates and Shells," 1940.

TABLE 10.—CONSTANTS FOR CALCULATING UNIFORMLY LOADED RECTANGULAR PLATES WITH SIMPLY SUPPORTED EDGES

| $b/a =$ | 1.0 | 1.1 | 1.2 | 1.3 | 1.4 | 1.5 | 1.6 | 1.7 |
|---|---|---|---|---|---|---|---|---|
| $\alpha =$ | 0.0443 | 0.0530 | 0.0616 | 0.0697 | 0.0770 | 0.0843 | 0.0906 | 0.0964 |
| $\beta_1 =$ | 0.0479 | 0.0553 | 0.0626 | 0.0693 | 0.0753 | 0.0812 | 0.0862 | 0.0908 |
| $\beta_2 =$ | 0.0479 | 0.0494 | 0.0501 | 0.0504 | 0.0506 | 0.0500 | 0.0493 | 0.0486 |
| $b/a =$ | 1.8 | 1.9 | 2.0 | 3.0 | 4.0 | 5.0 | $\infty$ | |
| $\alpha =$ | 0.1017 | 0.1064 | 0.1106 | 0.1336 | 0.1400 | 0.1416 | 0.1422 | |
| $\beta_1 =$ | 0.0948 | 0.0985 | 0.1017 | 0.1189 | 0.1235 | 0.1246 | 0.1250 | |
| $\beta_2 =$ | 0.0479 | 0.0471 | 0.0464 | 0.0404 | 0.0384 | 0.0375 | 0.0375 | |

It may be seen from the above table that for $b/a > 3$ the maximum deflection and the maximum bending moment do not differ substantially from those calculated for $b/a = \infty$.  This means that for long rectangular plates ($b/a > 3$) the effect of the short sides can be neglected and the formulas derived in arts. 20, 21, 22 for bending to a cylindrical surface can be used with sufficient accuracy.

*Plate Built-In at the Edges.*  The maximum deflection takes place at the center of the plate and can be expressed by the same equation (151) as was used for the plate with supported edges.  The numerical maximum bending moment occurs at the middle of the longer sides and is given by the equation:

$$(M_1)_{max} = \beta qa^2.\qquad (153)$$

Several values of the coefficients $\alpha$ and $\beta$ are given in Table 11 below.

TABLE 11.—CONSTANTS FOR UNIFORMLY LOADED RECTANGULAR PLATES WITH CLAMPED EDGES

| $b/a =$ | 1.00 | 1.25 | 1.50 | 1.75 | 2.00 | $\infty$ |
|---|---|---|---|---|---|---|
| $\alpha =$ | 0.0138 | 0.0199 | 0.0240 | 0.0264 | 0.0277 | 0.0284 |
| $\beta =$ | 0.0513 | 0.0665 | 0.0757 | 0.0806 | 0.0829 | 0.0833 |

This indicates that clamping the edges of the plate diminishes considerably its maximum deflection.  The effect of clamping on the magnitude of the maximum bending stress is not so large.  Also in the case of clamped edges the maximum deflection and the maximum bending moment for $b/a = 2$ nearly coincide with those obtained for $b/a = \infty$.  This justifies the use of the results obtained in art. 21 for bending to a cylinder, when we make calculations for comparatively long rectangular plates ($b/a \geq 2$) with clamped edges.
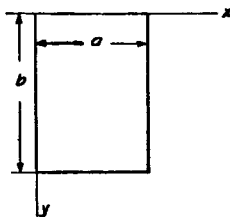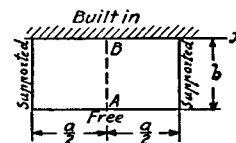

FIG. 98.

*Plate with Two Opposite Sides Supported, Third Side Built-In and the Fourth Side Free (Fig. 98).* In the case of a uniformly distributed load, the maximum deflection is at the middle of the free side at the point $A$. This deflection can be represented by the equation:

$$\delta = \alpha \frac{qb^4}{Eh^3}. \qquad (154)$$

The values of the numerical factor $\alpha$ in this equation are given in the table below. The maximum bending moment $M_1$ also occurs at the point $A$, and its magnitude is given by the equation:

$$(M_1)_{max} = \beta_1 q a^2. \qquad (155)$$

The maximum bending moment $M_2$ occurs at the point $B$, at the middle of the built-in side, and is given by the equation:

$$(M_2)_{max} = -\beta_2 q b^2. \qquad (156)$$

Several values of the coefficients $\beta_1$ and $\beta_2$ are given in the table below.

TABLE 12.—CONSTANTS FOR UNIFORMLY LOADED RECTANGULAR PLATE SHOWN IN FIG. 98

| $b/a =$ | 0 | 1/3 | 1/2 | 2/3 | 1 |
|---|---|---|---|---|---|
| $\alpha =$ | 1.37 | 1.03 | 0.635 | 0.366 | 0.123 |
| $\beta_1 =$ | 0 | 0.0078 | 0.0293 | 0.0558 | 0.0972 |
| $\beta_2 =$ | 0.500 | 0.428 | 0.319 | 0.227 | 0.119 |
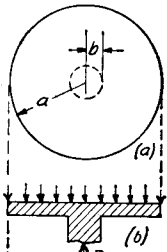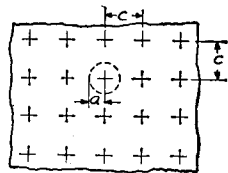


FIG. 99.

It can be seen from the table that when $a$ is large compared to $b$ the middle strip $AB$ approaches the condition of a cantilever built-in at $B$ and uniformly loaded.

*Uniformly Loaded Plate Supported at Many Equidistant Points (Fig. 99).* In this case we can obtain a good approximation to the maximum stress and to the stress distribution near a support as follows. A part of the plate near the support, bounded by a circle of radius $a = 0.22c$ (where $c$ is the distance between supports), is considered as a circular plate simply supported at the outer edge loaded at the inner edge by the load, $P = qc^2$ acting upward and uniformly loaded by a load of intensity $q$ acting downward. This loading is

shown in Fig. 99 (b).[29] The problem may be solved by using the methods developed in art. 29.

The bending of rectangular plates on an elastic foundation in connection with the stress analysis in concrete roads was discussed by H. M. Westergaard.[30]

**31. Thin-walled Vessels Submitted to Internal Pressure.** —This consideration will be confined to vessels having the form of a surface of revolution, which are subjected to a continuous internal pressure of intensity $p$, not necessarily uniform but symmetrically distributed with reference to the axis of revolution $O$–$O$ (Fig. 100). If the thickness of the
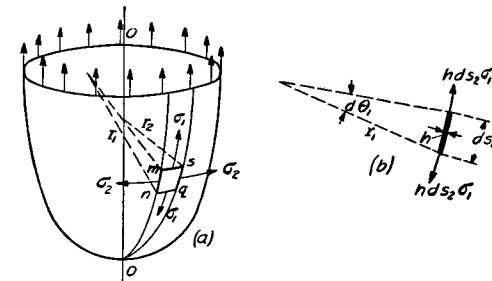


FIG. 100.

wall is small in comparison with the radii of curvature and there are no discontinuities such as sharp bends in the meridional curves, the stresses can be calculated with sufficient accuracy by neglecting the bending of the wall of the vessel, i.e., by assuming that the tensile stresses in the wall are uniformly distributed through the thickness.[31] The magnitudes of the stresses may then be easily calculated from the equations of statics.

Let us consider an element $mnsq$, cut from the wall of the vessel by two meridional sections such as $mn$ and $sq$ and two sections $ms$ and $nq$ normal to the meridians. From the

[29] See paper by H. M. Westergaard and A. Slater, Proceedings of the Amer. Concrete Inst., Vol. 17, 1921. See also V. Lewe, "Die strenge Lösung des Pilzdeckenproblems," Berlin, 1922.

[30] See his paper in "Ingenioren," Copenhagen, Denmark, 1923, p. 513, and also in "Public Roads," Vol. 7, 1926, p. 25.

[31] Shells which do not resist bending are sometimes called "membranes" and the stresses calculated by neglecting bending are called "membrane stresses." It is assumed that the external forces, uniformly distributed along the edge of the shell, are tangent to meridians.

condition of symmetry it is seen that only normal stresses act on the sides of this element. Let

$\sigma_1$ be the tensile stress in the meridional direction, i.e., *the meridional stress,*

$\sigma_2$, the tensile stress along the parallel circle, i.e., the *hoop stress,*

$h$, the uniform thickness of the shell,

$ds_1$, the dimension of the element in the meridional direction,

$ds_2$, the dimension of the element in the direction of the parallel circle,

$r_1$, the meridional radius of curvature,

$r_2$, the radius of curvature of the section perpendicular to the meridian.

Then the total tensile forces acting on the sides of element are $h\sigma_1 ds_2$ and $h\sigma_2 ds_1$. The tensile forces $h ds_2 \sigma_1$ acting on the sides *ms* and *nq* of the element have a component in the direction normal to the element equal to (see Fig. 100, *b*)

$$h ds_2 \sigma_1 d\theta_1 = \frac{h\sigma_1 ds_1 ds_2}{r_1}. \qquad (a)$$

In the same manner the tensile forces acting on the sides *mn* and *sq* have a normal component,

$$h ds_1 \sigma_2 d\theta_2 = \frac{h\sigma_2 ds_1 ds_2}{r_2}. \qquad (b)$$

The sum of these normal components is in equilibrium with the normal pressure on the element; hence

$$\frac{h\sigma_1 ds_1 ds_2}{r_1} + \frac{h\sigma_2 ds_1 ds_2}{r_2} = p ds_1 ds_2 \qquad (c)$$

or

$$\frac{\sigma_1}{r_1} + \frac{\sigma_2}{r_2} = \frac{p}{h}. \qquad (157)$$

Some applications of this equation will now be discussed.

*Spherical Vessel.* In this case $r_1 = r_2 = r$ and $\sigma_1 = \sigma_2 = \sigma$. Equation (157) becomes

$$\sigma = \frac{pr}{2h}.$$

*Conical Tank.* Let us consider an open conical tank filled with a liquid (Fig. 101). In this case, the curvature of the meridian $1/r_1 = 0$ and the hoop stress $\sigma_2$ due to the liquid pressure can be calculated from eq. (157). The internal pressure at points *m–n* a distance $d - y$ from the surface of the liquid is

$$p = \gamma(d - y),$$



Fig. 101.

where $\gamma$ is the weight per unit volume of the liquid. The radius of curvature $r_2$ at these points is

$$r_2 = \frac{y \tan \alpha}{\cos \alpha}.$$

Equation (157) then becomes

$$\sigma_2 \frac{\cos \alpha}{y \tan \alpha} = \frac{\gamma(d - y)}{h},$$

from which

$$\sigma_2 = \frac{\gamma(d - y)}{h} \frac{y \tan \alpha}{\cos \alpha}. \qquad (d)$$

The maximum value of this stress occurs at points where the product $(d - y)y$ is a maximum. If we set the derivative of $(d - y)y$ equal to zero, we find $y = d/2$ and the stress at this point is

$$(\sigma_2)_{max} = \frac{\gamma d^2}{4h} \frac{\tan \alpha}{\cos \alpha}. \qquad (e)$$

The stress $\sigma_1$ at the level *m–n* is found from the condition that the vertical components of the meridional tensile forces in the shell support the weight of the volume *tmons* of the liquid (Fig. 101); hence

$$2\pi y \tan \alpha \, h\sigma_1 \cos \alpha = \pi y^2 \tan^2 \alpha (d - y + \tfrac{1}{3}y)\gamma,$$

from which

$$\sigma_1 = \frac{y \tan \alpha (d - \tfrac{2}{3}y)\gamma}{2h \cos \alpha}. \qquad (f)$$

This stress is maximum when $y = \frac{3}{4}d$. Substituting in eq. ($f$), we find

$$(\sigma_1)_{max} = \frac{3}{16}\frac{d^2\gamma}{h}\frac{\tan\alpha}{\cos\alpha}. \qquad (g)$$

Equations ($d$) and ($f$) represent the complete solution of the problem as long as the bending stresses in the wall of the tank may be neglected.

In the case of a *cylindrical shell* of diameter $d$, submitted to uniform pressure $p$, we found before (see p. 42, Part I)

$$\sigma_1 = \frac{pd}{4h}; \qquad \sigma_2 = \frac{pd}{2h}.$$

### Problems

1. The tank of Fig. 102 contains liquid at the level shown.
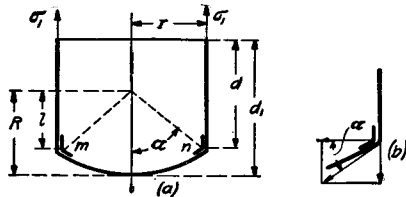


FIG. 102.

Determine the maximum stresses $\sigma_1$ and $\sigma_2$ in the cylindrical and the spherical portions and also the compressive force in the reinforcing ring $mn$.

*Solution.* The weight of the liquid in the container is

$$Q = \left[\pi dr^2 + \pi\left(\frac{2}{3}R^3 - R^2 l + \frac{l^3}{3}\right)\right]\gamma.$$

For the cylindrical portion of the tank,

$$\sigma_1 = \frac{Q}{2\pi rh} = \text{const.} \quad \text{and} \quad (\sigma_2)_{max} = \frac{d\gamma r}{h}.$$

For the spherical portion of the tank the maximum stress is at the bottom, where the liquid pressure is $\gamma d_1$ and $\sigma_1 = \sigma_2 = \gamma d_1 R/2h$. The tensile force in the spherical portion of the tank per unit length of the ring $mn$ is $Q/(2\pi r \sin\alpha)$. The radial component of this force, producing compression of the ring (Fig. 102, $b$), is $(Q/2\pi r)\cot\alpha$, and

the compressive force in the ring is $(Q/2\pi)\cot\alpha$. This is only an approximation obtained on the assumption that the cylindrical and spherical portions are membranes, resisting only to tension. In calculating compressive stress in the ring adjacent portions of cylindrical and spherical shells must be added to the cross section of the ring $mn$ itself.

2. Determine the stresses at the points $mn$ of a cylindrical tank with a hemispherical bottom, which contains liquid at the level indicated (Fig. 103).

*Solution.* From eq. (157) for any point of the spherical portion at a distance $x$ from the surface of the liquid we have

$$\frac{\sigma_1 + \sigma_2}{R} = \frac{\gamma x}{h}. \qquad (a)$$
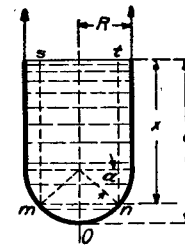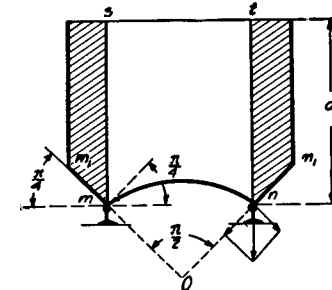


FIG. 103.    FIG. 104.

Since the meridional forces along the section $mn$ support the weight of the volume *smont* of the liquid, the second equation is

$$\sigma_1 = \frac{\gamma R}{h}\left(\frac{d-R}{2} + \frac{R}{3}\frac{1-\sin^3\alpha}{\cos^2\alpha}\right) \qquad (b)$$

and eq. ($a$) becomes

$$\sigma_2 = \frac{\gamma R}{h}\left(\frac{d-R}{2} + \frac{R}{3}\frac{\sin^3\alpha + 3\sin\alpha\cos^2\alpha - 1}{\cos^2\alpha}\right).$$

3. In Fig. 104 determine the relation between the outer diameter of the tank, the diameter of the supporting ring $mn$ and the depth $d$ of the liquid for which the ring $mn$ is submitted to vertical pressure only. The middle portion of the bottom of the tank is a *spherical surface* of central angle $\pi/2$. The same angle has also the conical portion $mm_1nn_1$.

*Hint.* The necessary relation may be obtained from the con-

dition that the pressures on the ring from the side of the spherical bottom and from the conical lateral surface both inclined $45°$ give no horizontal component. From this it follows that the volume of the liquid indicated in the figure by the shaded areas is equal to the volume *mnst*.

4. Determine the maximum stress in the tank represented in Fig. 102 if $R = 10$ feet, $r = 8$ feet, $d = 20$ feet, $\gamma = 62.5$ lbs. per cubic foot and $h = \frac{1}{4}$ in.

5. Determine stresses $\sigma_1$ and $\sigma_2$ in the wall of a torus submitted to uniform inner pressure $p$ (Fig. 105).
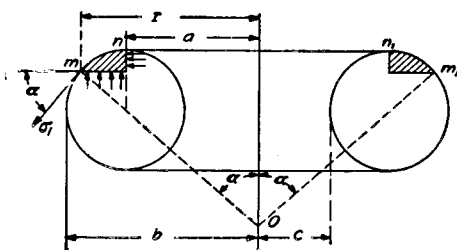


FIG. 105.

*Solution.* The condition of equilibrium with respect to vertical forces of the portion $mnm_1n_1$ cut from the vessel by a vertical cylindrical surface of radius $a$ and conical surface $mom_1$ gives

$$\pi(r^2 - a^2)p - \sigma_1 h 2\pi r \sin \alpha = 0,$$

from which

$$\sigma_1 = \frac{p(r^2 - a^2)}{2rh \sin \alpha}.$$

The stress $\sigma_2$ can now be calculated from eq. (157).
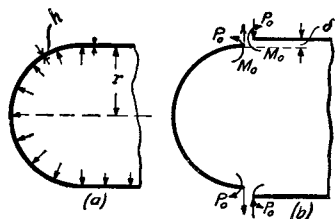


FIG. 106.

6. Determine the maximum stress in the wall of the vessel represented in Fig. 105 if $a = 10'$, $b = 12'$, $h = \frac{1}{4}''$ and $p = 50$ lbs. per sq. in.

**32. Local Bending Stresses in Thin Vessels.**—In the previous article, bending of the wall of the vessel was neglected and only tensile stresses, so-called *membrane stresses*, were considered. The displacements due to membrane stresses cause bending of the wall and the resulting bending stresses

may be of practical importance. This is especially so at the places of discontinuity in the meridian. If the meridian consists of curves which are not tangent, a reinforcing ring as shown in Fig. 102 is necessary in order to prevent large bending of the wall of the vessel. The stresses may be high also at the junctions in a meridian consisting of several curves tangent to one another. The additional stresses set up at such points will be called *discontinuity stresses*.

The method of calculating them will now be shown for the simple case of a cylindrical vessel with hemispherical ends submitted to the action of uniform internal pressure (Fig. 106). We consider first the membrane stresses only, and find for the cylindrical portion

$$\sigma_1 = \frac{pr}{2h}; \qquad \sigma_2 = \frac{pr}{h}, \qquad (a)$$

where $r$ is the radius of cylinder and hemisphere and $h$ the thickness of the wall. For the spherical portion,

$$\sigma_1 = \sigma_2 = \sigma = \frac{pr}{2h}.$$

The corresponding radial displacements for the cylindrical and spherical portions are

$$\frac{r}{E}(\sigma_2 - \mu\sigma_1) = \frac{pr^2}{2hE}(2 - \mu) \qquad \text{and} \qquad \frac{pr^2}{2hE}(1 - \mu)$$

respectively.

If the spherical and cylindrical parts of the vessel were disjointed (Fig. 106, $b$), the difference in radii due to membrane stresses would be

$$\delta = \frac{pr^2}{2hE}. \qquad (b)$$

In the actual vessel, the head and the cylinder are kept together at the joint by shearing forces $P_0$ and bending moments $M_0$ (Fig. 106, $b$) per unit length of the circumference of the middle surface of the vessel. These forces produce bending of the adjacent parts of the vessel. In discussing bending in the cylinder, since the deformation is symmetrical with respect to the axis, it is sufficient to consider the bending of an elemental strip (Fig. 107), and the deflection of this strip will be radial. For simplicity it is assumed the strip is of unit

width.  If $y$ denotes the radial displacement at any cross section of the strip, then the radius of the cylinder shortens at this section by $y$ and as a result of this there is a compressive strain in the circumferential direction of the magnitude $y/r$.  The corresponding compressive stress is $Ey/r$.  Hence when the strip deflects towards the axis of the cylinder, lateral compressive forces $T$ (Fig. 107, $c$) are produced whose magnitude per unit length of the strip is
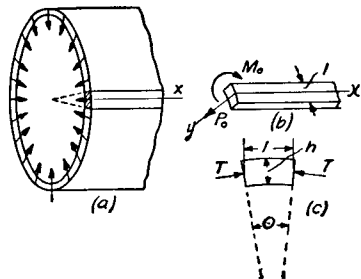


FIG. 107.

$$T = \frac{Ey}{r} h. \qquad (c)$$

Since the angle $\theta$ is equal to $1/r$, these forces give a radial resultant [32]

$$\frac{Eyh}{r} \theta = \frac{Eyh}{r^2}, \qquad (d)$$

which opposes the deflection of the strip.  These reactive forces are distributed along the strip in proportion to the deflections $y$ so that the strip is in the same condition with respect to bending as a beam on an elastic foundation (art. 1) with $k = Eh/r^2$.  Since any change in the shape of the cross section of the strip is prevented by the adjacent strips in a manner similar to that in plates (see p. 119), $D = Eh^3/12(1 - \mu^2)$ is to be used for its flexural rigidity.  The differential equation of the deflection curve of the strip is then (see eq. 1)

$$D \frac{d^4 y}{dx^4} = - \frac{Eh}{r^2} y.$$

Introducing, as before, the notation

$$\beta = \sqrt[4]{\frac{Eh}{4Dr^2}} = \sqrt[4]{\frac{3(1 - \mu^2)}{r^2 h^2}}, \qquad (158)$$

the deflection curve of the strip becomes (see eq. 11, p. 12)

$$y = \frac{e^{-\beta x}}{2\beta^3 D} [P_0 \cos \beta x - \beta M_0 (\cos \beta x - \sin \beta x)]. \qquad (e)$$

This is a rapidly damped oscillatory curve of wave length

$$l = \frac{2\pi}{\beta} = 2\pi \sqrt[4]{\frac{r^2 h^2}{3(1 - \mu^2)}}, \qquad (f)$$

[32] It is assumed that $\theta$ is a small angle.

which is small in comparison with $r$ if $h$ is small.  From this it can be shown that bending at the joint of cylinder and head is of *local character* and has an appreciable effect on the stresses only in a narrow zone in the vicinity of the joint.  This narrow zone at the edge of the head is nearly cylindrical in shape and hence eq. ($e$) can be used for calculating deflections and stresses in the head also.[33]

In the simplest case, in which cylindrical wall and spherical head are of the same thickness, the deflections and the slopes produced at the edges of the spherical and cylindrical parts by the forces $P_0$ are equal.  The conditions of continuity at the joint are satisfied if $M_0 = 0$ and $P_0$ has such a magnitude as to produce a deflection at the edge of the cylinder equal to $\delta/2$.  Putting $M_0 = 0$, $x = 0$ in eq. ($e$), the equation for calculating $P_0$ is

$$\frac{P_0}{2\beta^3 D} = \frac{\delta}{2},$$

from which

$$P_0 = \delta \beta^3 D = \frac{pr^2}{2hE} \frac{Eh}{4\beta r^2} = \frac{p}{8\beta}. \qquad (159)$$

With $P_0$ known the deflection and the bending moment at any cross section of the strip may be calculated from eq. ($e$).  The corresponding discontinuity stresses must be added to the membrane stresses given by eqs. ($a$).  If the head and the cylindrical portion of the vessel have different thicknesses, there will be both a shearing force $P_0$ and a moment $M_0$ at the joint.  These two quantities are calculated from the conditions: (1) the sum of edge deflections in the spherical and in the cylindrical parts must be equal to $\delta$ (Fig. 106, $b$); (2) the angles of rotations of the two edges must be equal.

The above method can be used also in the cases of heads which are not of hemispherical shape.[34]  If the thickness of the wall of

[33] The proof that this is a sufficiently accurate assumption was given by E. Meissner, Schweiz. Bauzeitung, Vol. 86, 1925, p. 1.

[34] This method was used in investigating stress distribution in various shapes of steam boiler heads.  See E. Höhn and A. Huggenberger, Über die Festigkeit der gewölbten Boden und der Zylinderschale, Zürich, 1927.  See also W. M. Coates, "The State of Stress in Full Heads of Pressure Vessels," Transactions, A. S. M. E., Applied Mech. Div., 1929.  It was used also in investigating local bending in tanks containing liquid.  See T. Pöschl and K. Terzaghi, Berechnung von Behältern, Berlin, 1926; H. Reissner, Beton und Eisen, Vol. 7, 1908, and C. Runge, Zeitschr. f. Math. u. Phys., Vol. 51, 1904, p. 254.  Cylindrical shells with flat ends were discussed by E. O. Holmberg and K. Axelson, Trans. A. S. M. E. Vol. 54, p. 13, 1932.  A further discussion of cylindrical shells see in "Theory of Plates and Shells," 1940.

pressure vessels is not small, the bending stresses in the wall may become of primary importance and a more detailed investigation of the stress distribution becomes necessary.[35]

## Problems

1. Determine the discontinuity stresses in the vessel represented in Fig. 106 if $p = 150$ lbs. per sq. in., $r = 25$ in., $h = \frac{1}{2}$ in., $\mu = 0.3$.
*Solution.* From eq. (158) $\beta = 0.364$ and from eq. (159)

$$P_0 = \frac{150}{8 \times 0.364} = 51.5 \text{ lbs. per in.}$$

The bending moment in the elemental strip is

$$M = -D\frac{d^2y}{dx^2}$$

and, by using eq. (e) and substituting

$$y = \frac{P_0}{2\beta^3 D}e^{-\beta x}\cos\beta x,$$

we obtain

$$M = -\frac{P_0}{\beta}e^{-\beta x}\sin\beta x.$$

The numerical maximum of this moment is at $\beta x = \pi/4$, when $M_{max} = 45.4$ lbs. ins. The corresponding maximum bending stress in the strip is $6M_{max}/h^2 = 1,090$ lbs. per sq. in. This stress must be added to the membrane stress

$$\sigma_1 = \frac{pr}{2h} = 150 \times 25 = 3,750 \text{ lbs. per sq. in.}$$

The bending of the strip produces also hoop stresses. These are made up of two parts: (1) stresses preventing cross sections of the strip from distortion (see p. 120) (the maximum value of these stresses at any cross section of the strip is $\pm 6\mu M/h^2$) and (2) stresses $-(yE/r)$ due to shortening of the circumference. Substituting the above expressions for $y$ and $M$, the discontinuity stress, which must be added to the membrane stress $\sigma_2$, is

$$-\frac{P_0 E}{2\beta^3 Dr}e^{-\beta x}\cos\beta x + \frac{6\mu P_0}{\beta h^2}e^{-\beta x}\sin\beta x$$

$$= \frac{6\mu P_0}{\beta h^2}e^{-\beta x}(\sin\beta x - 1.83\cos\beta x).$$

[35] See "Theory of Plates and Shells," 1940.

The maximum value of this stress can easily be found by the usual method. It will be small in comparison with the membrane hoop stress $pr/h = 7,500$ lbs. per sq. in., so that discontinuity stresses in this case do not materially affect the maximum stress.

2. A thin cylindrical drum attached to two solid discs rotates about the axis $O$–$O$ (Fig. 108) with a peripheral velocity $v$. Determine the local bending stresses in the drum if it is built in along the edges $mn$ and $m_1n_1$.
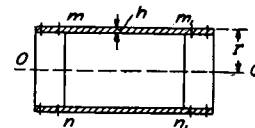


FIG. 108.

*Solution.* If the drum were separated from the discs the increase in the radius of the drum, due to centrifugal force, would be (see eq. 15, Part I) $\gamma v^2 r/gE$. The increase in the radius of the solid discs is (see eq. 223)

$$\frac{1 - \mu}{4}\frac{\gamma v^2 r}{gE}.$$

The difference of these two quantities is

$$\delta = \frac{3 + \mu}{4}\frac{\gamma v^2 r}{gE}.$$

Applying the same method as in the previous problem and considering a strip of unit width, the magnitude of the shearing force $P_0$ and the bending moment $M_0$ at the edge $mn$ is found by using eqs. (11) and (12). Consider the discs as very rigid in comparison with the drum and neglect the deformations produced in them by the forces $P_0$ and couples $M_0$. The equations for calculating $P_0$ and $M_0$ are

$$\frac{1}{2\beta^3 D}(P_0 - \beta M_0) = \delta,$$

$$\frac{1}{2\beta^2 D}(P_0 - 2\beta M_0) = 0,$$

from which

$$P_0 = 4\delta\beta^3 D; \qquad M_0 = 2\delta\beta^2 D.$$

Having these quantities, the deflections and the bending stresses are found from an equation analogous to eq. (11).

3. Determine the maximum bending stress in the drum of the previous problem if $r = 25$ in., $h = \frac{1}{2}$ in., $v = 500$ feet per sec. and the material is steel.

4. Determine the bending stresses produced in a pipe by a narrow ring shrunk onto it (Fig. 109).

*Solution.* Consider a longitudinal strip of unit width and denote by $P$ the pressure between the ring and the pipe, per unit length of the circumference of the pipe. The bending of the strip is the same as that of a long bar on an elastic foundation, which carries a single load $P$ (art. 1). The decrease in the radius of the pipe due to $P$, from (eq. 8), is $P/8\beta^3 D$. The increase in the radius of the ring is [36] $Pr^2/AE$, where $A$ is the cross-sectional area of the ring. If $\delta$ is the initial difference in the inner radius of the ring and the outer radius of the pipe, the equation for calculating $P$ is

$$\frac{P}{8\beta^3 D} + \frac{Pr^2}{AE} = \delta$$

or, by using eq. (158) and taking $\mu = 0.3$,

$$0.643 \frac{P}{E}\left(\frac{r}{h}\right)^{3/2} + \frac{Pr^2}{AE} = \delta. \qquad (g)$$

$P$ is determined from this equation, and the maximum bending moment in the strip is found from eq. (9).[37] The maximum bending stress in the strip is

$$\sigma = \frac{3}{2}\frac{P}{h^2}\sqrt[4]{\frac{r^2 h^2}{3(1-\mu^2)}}.$$

The same method is applicable also to cases in which a cylindrical tube with reinforcing rings is submitted to either a uniform internal or a uniform external pressure. If the distance between the rings is so large that the effect of each on the deflections produced by the others may be neglected, $P$ can be obtained from eq. ($g$) by substituting $\delta = pr^2/Eh$. This represents the change in the radius of the pipe due to the uniform pressure.[38]

5. Solve the preceding problem assuming that the length $l$ of the pipe is not large and that the ring is at the middle of the length.

---

[36] The dimension of the ring in the radial direction is assumed to be small in comparison with $r$.

[37] An example of such calculations is given in the paper by G. Cook, Engineering, Vol. 116, 1923, p. 479. See also R. Lorenz, V. D. I., Vol. 52, 1908, p. 1706; M. Westphal, V. D. I., Vol. 41, 1897, p. 1036.

[38] The application of this method to the calculation of hull stresses in a submarine having a circular cross section is given in the paper by K. v. Sanden in the periodical, Werft und Reederei, 1920, p. 189.
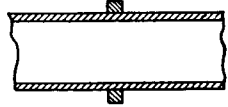
*Hint.* In calculating the pressure $P$ per unit length of the ring we use the results obtained for the problem shown in Fig. 13, p. 18. Then the deflection produced in the pipe by the forces $P$ is

$$\frac{P\beta}{2k}\cdot\frac{\cosh\beta l + \cos\beta l + 2}{\sinh\beta l + \sin\beta l} = \frac{P}{8\beta^3 D}\cdot\frac{\cosh\beta l + \cos\beta l + 2}{\sinh\beta l + \sin\beta l}.$$

The equation for calculating $P$ then is

$$\frac{P}{8\beta^3 D}\cdot\frac{\cosh\beta l + \cos\beta l + 2}{\sinh\beta l + \sin\beta l} + \frac{Pr^2}{AE} = \delta.$$

Find $P$ for steel pipe if $r = 25$ in., $h = \frac{1}{2}$ in., $l = 50$ in., $A = 4$ sq. in., and $\delta = 0.05$ in.

6. A cylindrical pipe with simply supported edges is submitted to a uniform internal pressure $p$. Find the longitudinal bending stress and the deflection at the middle of the pipe, Fig. 110. The dimensions of the pipe are the same as in the preceding problem.
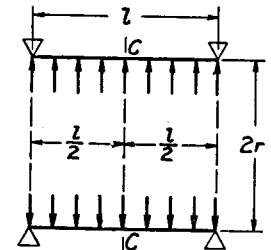
*Hint.* From the results of the problem shown in Fig. 20, p. 24, the deflection and the bending moment per unit length of the circumference at the middle cross section $c$–$c$ are

$$y_c = \frac{pr^2}{Eh}\left(1 - \frac{2\cosh\dfrac{\beta l}{2}\cos\dfrac{\beta l}{2}}{\cosh\beta l + \cos\beta l}\right),$$

$$M = \frac{p}{2\beta^2}\cdot\frac{\sinh\dfrac{\beta l}{2}\sin\dfrac{\beta l}{2}}{\cosh\beta l + \cos\beta l}.$$



FIG. 110.

7. Solve the preceding problem assuming that the edges of the pipe are absolutely built-in.

*Hint.* Use the results of the problem shown in Fig. 21, p. 24.

8. A circular steel pipe is reinforced by rings, a distance $l$ apart, Fig. 111a, and submitted to internal pressure $p$. Find the pressure $P$ produced per unit length of the inner circumference of a ring. Find the maximum bending stresses in the pipe.

*Solution.* Let us begin with a consideration of the portion of the pipe between the two rings [39] under the action of shearing forces

---

[39] The width of the ring is assumed to be negligible in comparison with the distance $l$ between the rings.

$V_0$ (Fig. 111$b$) and bending moments $M_0$ (Fig. 111$c$) per unit length of the circumference of the pipe. Considering a longitudinal strip of unit width as a beam on an elastic foundation and using the
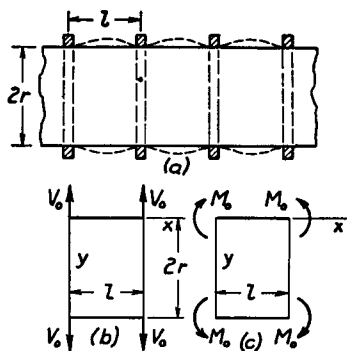


FIG. 111.

results of the problems in Fig. 12, p. 17, and in Fig. 18, p. 23, we find for the deflection and the slope at the left end of the strip in Fig. 111$b$:

$$(w_1)_{x=0} = -\frac{2V_0\beta r^2}{Eh}\cdot\frac{\cosh\beta l + \cos\beta l}{\sinh\beta l + \sin\beta l}, \qquad (h)$$

$$\left(\frac{dw_1}{dx}\right)_{x=0} = \frac{2V_0\beta^2 r^2}{Eh}\cdot\frac{\sinh\beta l - \sin\beta l}{\sinh\beta l + \sin\beta l}. \qquad (i)$$

For the left end in Fig. 111$c$ we obtain

$$(w_2)_{x=0} = -\frac{2M_0\beta^2 r^2}{Eh}\cdot\frac{\sinh\beta l - \sin\beta l}{\sinh\beta l + \sin\beta l}, \qquad (j)$$

$$\left(\frac{dw_2}{dx}\right)_{x=0} = \frac{4M_0\beta^3 r^2}{Eh}\frac{\cosh\beta l - \cos\beta l}{\sinh\beta l + \sin\beta l}. \qquad (k)$$

From our definition of $P$ it follows that

$$V_0 = -\frac{P}{2}.$$

Substituting this in equation ($i$) and observing that in the pipe (Fig. 111$a$) the tangent to the strip must be parallel to the axis of the pipe, we obtain

$$\left(\frac{dw_1}{dx}\right)_{x=0} + \left(\frac{dw_2}{dx}\right)_{x=0} = 0,$$

from which

$$M_0 = \frac{P}{4\beta}\cdot\frac{\sinh\beta l - \sin\beta l}{\cosh\beta l - \cos\beta l}. \qquad (l)$$

In calculating $P$ we assume first that the rings are absolutely rigid. In such a case the deflection in the pipe produced by forces $P$ under the rings must be equal to the radial expansion $pr^2/Eh$ which the pipe would have in the absence of the reinforcing rings. Hence the equation for calculating $P$ is

$$(w_1)_{x=0} + (w_2)_{x=0} = \frac{pr^2}{Eh}$$

or

$$\frac{P\beta r^2}{Eh}\cdot\frac{\cosh\beta l + \cos\beta l}{\sinh\beta l + \sin\beta l} - \frac{P\beta r^2}{2Eh}$$
$$\times\frac{(\sinh\beta l - \sin\beta l)^2}{(\sinh\beta l + \sin\beta l)(\cosh\beta l - \cos\beta l)} = \frac{pr^2}{Eh}. \qquad (m)$$

In each particular case this equation can be readily solved for $P$. Substituting the value of $P$ in expression ($l$), we obtain the required value of the bending moment $M_0$.

To take into account the expansion of the reinforcing rings, we observe that the forces $P$ produce an extension of the inner radius of the ring equal to $Pr^2/AE$, where $A$ is the cross-sectional area of the ring. By the same amount the deflection of the pipe is diminished. Hence to obtain the force $P$ in this case we have only to substitute

$$\frac{pr^2}{Eh} - \frac{Pr^2}{AE}$$

instead of $pr^2/Eh$ into equation ($m$).

9. Find the bending moment $M_0$ and the shearing force $V_0$ per unit length of circumference at the bottom of the cylindrical tank filled with liquid, Fig. 112, if $r = 30$ ft., $d = 26$ ft., $h = 14$ in., $\gamma = 0.03613$ lb. per cu. in., and $\mu = 0.25$.

*Answer.* $M_0 = 13,960$ in. lb. per in., $V_0 = 563.6$ lb. per in.



FIG. 112.

10. Solve problem 5 assuming that the ring is fitted at the left end of the pipe. The resistance of the ring to torsion should be neglected.

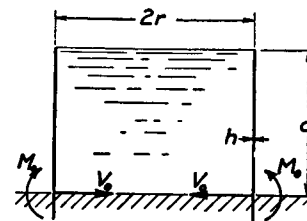*Hint.* Use the result obtained for the problem shown in Fig. 22, p. 24.

**33. Thermal Stresses in Cylindrical Shells.**—If a cylindrical shell with free edges undergoes a uniform temperature change, no thermal stresses will be produced. But if the edges are supported or clamped, free expansion of the shell is prevented, and local bending stresses are set up at the edges. Assume, for example, that the edges of a long cylindrical pipe are built-in; then the shearing forces and the bending moments at the edges are obtained as in problem 2 of the preceding article. It is only necessary to substitute in the equation of that problem $\delta = r\alpha t$, which represents the increase in the radius of the shell due to thermal expansion. If the length of the pipe is not large and both ends have to be considered simultaneously, the bending moments and the shearing forces can be readily obtained by using the results of problem 8 of the preceding article.

Let us now consider the case in which there is a temperature gradient in the radial direction. Assume that $t_1$ and $t_2$ are the uniform temperatures of the cylindrical wall at the inside and the outside surfaces, respectively, and that the variation of the temperature through the thickness is linear. In such a case, at points at a large distance from the ends of the shell, there will be no bending, and the stresses can be calculated by using equation (122), p. 132, derived for a plate with a clamped edge. This gives for the maximum bending stress

$$\sigma_{\max} = \frac{\alpha E(t_1 - t_2)}{2(1 - \mu)}. \qquad (a)$$

It is assumed that $t_1 > t_2$. Then the tensile stress will act at the outer surface of the shell.

Near the ends of the shell there will be some bending of the shell and the total thermal stresses will be obtained by superposing upon stresses (a) the stresses due to that bending. Let us consider, as an example, the stresses at a free end of a long cylindrical pipe. In calculating the stresses in this case we observe that at the edge the stresses represented by expression (a) result in uniformly distributed moments $M_0$,

Fig. 113 $a$, of the magnitude

$$M_0 = \frac{\alpha E(t_1 - t_2)h^2}{12(1 - \mu)}. \qquad (b)$$

To obtain a free edge, the moments of the same magnitude but opposite in direction must be superposed, Fig. 113 $b$. Hence the thermal stresses at the free edge are obtained by superposing upon the stresses (a) the stresses produced by the moments shown in Fig. 113 $b$. These later stresses can be readily obtained by considering the bending of an elemental strip and then using solution (11), p. 12, which gives
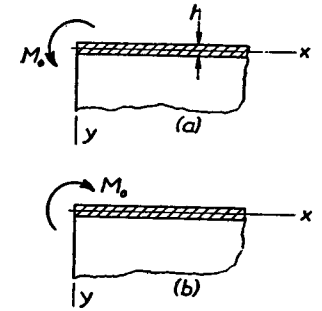


FIG. 113.

$$y = -\frac{M_0}{2\beta^2 D} e^{-\beta x}(\cos \beta x - \sin \beta x), \qquad (c)$$

where $\beta$ is given by equation (158). The largest deflection, obtained at the free edge ($x = 0$), is

$$y_{\max} = -\frac{M_0}{2\beta^2 D} \qquad (d)$$

and the corresponding hoop stresses are

$$\frac{M_0}{2\beta^2 D} \cdot \frac{E}{r} = \frac{E\alpha(t_1 - t_2)}{2\sqrt{3}(1 - \mu)} \sqrt{1 - \mu^2}. \qquad (e)$$

The bending moment acting on the end of the elemental strip is given by expression (b). The bending moments preventing the cross sections of the strip from distortion during bending are

$$\mu M_0 = \mu \frac{\alpha E(t_1 - t_2)h^2}{12(1 - \mu)}. \qquad (f)$$

The maximum thermal stress is acting at the outer surface of

the pipe in the circumferential direction and consists of the three parts: (1) stress $(a)$, (2) stress $(e)$, and (3) stress produced by moments $(f)$. Hence

$$\sigma_{\max} = \frac{\alpha E(t_1 - t_2)}{2(1 - \mu)}\left[ 1 + \frac{\sqrt{1 - \mu^2}}{\sqrt{3}} - \mu \right]. \qquad (160)$$

For $\mu = 0.3$ this stress is about 25 per cent greater than the stress $(a)$ calculated at points at a large distance from the ends. We can therefore conclude that if a crack will occur in a brittle material such as glass due to a temperature difference $t_1 - t_2$, it will start at the edge and will proceed in the axial direction. In a similar manner the stresses can also be calculated in cases in which the edges are clamped or supported.[40]

### Problems

1. Find the thermal stresses produced in a long steel pipe with built-in edges if $r = 25$ in., $h = \frac{1}{2}$ in., $\mu = 0.3$, coefficient of thermal expansion $\alpha = 70.10^{-7}$, and the increase in the uniform temperature of the pipe is $100°$ F.

*Solution.* With the given dimensions we find

$$\beta = 0.364 \text{ in.}^{-1}, \qquad D = 343.10^3 \text{ lb. in.}$$

The free elongation of the radius of the pipe due to temperature rise is $\delta = \alpha r(t - t_0) = 70 \cdot 25 \cdot 100 \cdot 10^{-7} = 175 \cdot 10^{-4}$ in. Substituting in the equations of the problem 2 of the preceding article, we find the shearing force and the bending moment per unit length of the circumference at the built-in edge:

$$P_0 = 4\delta\beta^3 D = 1160 \text{ lbs. per in.}$$
$$M_0 = 2\delta\beta^2 D = 1590 \text{ lb. in. per in.}$$

With these values of $P_0$ and $M_0$ the stresses in axial and circumferential directions at the built-in edge can be readily calculated.

2. Solve the preceding problem assuming that the edges are simply supported.

3. A steel tube of the same dimensions as in problem 1 has the temperatures $t_1$ and $t_2$ at the inside and the outside surfaces re-

---

[40] Several examples of this kind are discussed in the paper by C. H. Kent, Trans. Am. Soc. Mech. Eng. vol. 53, p. 167, 1931. The case of a temperature gradient in the axial direction is discussed in "Theory of Plates and Shells," p. 423.

spectively. Find the maximum stress in the tube if $t_1 - t_2 = 100°$ F. and the edges are free.

*Answer.* $\sigma_{\max} = 18,750$ lbs. per sq. in.

4. Solve the preceding problem assuming that the edges of the tube were built-in when the tube had a uniform temperature equal to $(t_1 + t_2)/2$.

### 34. Twisting of a Circular Ring by Couples Uniformly Distributed along its Center Line.—There are cases in which

a circular ring of uniform cross section is submitted to the action of twisting couples uniformly distributed along its center line.[41] Taking half the ring (Fig. 114, $a$) as a free body, from the condition of equilibrium with respect to moments about the diameter $ox$, there must be a bending moment on each cross section $m$ and $n$,
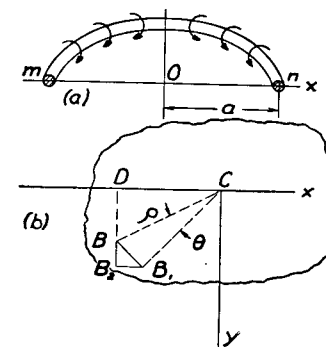


$$M = M_t a, \qquad (a)$$

Fig. 114.

where $a$ is the radius of the center line and $M_t$ is twisting couple per unit length of the center line. Let us consider now the deformation of the ring. From the condition of symmetry it can be concluded that during twist each cross section rotates in its own plane through the same angle $\theta$, which is assumed to be small in the following discussion.[42] Let $C$ be the center of rotation (Fig. 114, $b$) and $B$ a point in the cross section at distance $\rho$ from $C$. Due to rotation of the cross section the point $B$ describes a small arc $\overline{BB_1} = \rho\theta$. Due to this displacement the annular fiber of the ring, which is perpendicular to the section at the point $B$, increases its radius by $\overline{B_2B_1}$. If the coordinate axes are taken as indicated, we have,

---

[41] An instance of such a problem is the calculation of stresses in the retaining rings of commutators of electric machines. Another is the stress analysis of pipe flanges.

[42] A general discussion of the problem, when $\theta$ is not small, is given by R. Grammel, Zeitschr. f. Angew. Math. u. Mech., Vol. 3, 1923, p. 429, and Vol. 7, 1927, p. 198.

from the similarity of the triangles $BB_1B_2$ and $BDC$,

$$\overline{B_1B_2} = \overline{BB_1}\frac{\overline{DB}}{\overline{BC}} = \rho\theta\frac{y}{\rho} = \theta y. \qquad (b)$$

Let us consider first the case in which the cross sectional dimensions of the ring are small in comparison with the radius $a$ of the center line. Then the radii of all ring fibers may be taken equal to $a$ without great error and the unit elongation of the fiber $B$, due to the displacement given by eq. ($b$), is

$$\epsilon = \frac{\theta y}{a}. \qquad (c)$$

If there is no lateral pressure between the ring fibers, the fiber stress, due to elongation $\epsilon$, is

$$\sigma = \frac{E\theta y}{a}. \qquad (d)$$

Now, from the equilibrium of the half ring, the sum of all the normal forces acting on the cross section of the ring must be equal to zero and the moment of these forces about the $x$ axis must be equal to $M$ (see eq. $a$). If $dA$ denotes an elemental area of the cross section, these equations of equilibrium become

$$\int_A \frac{E\theta y}{a}\,dA = 0; \qquad \int_A \frac{E\theta y^2}{a}\,dA = M, \qquad (e)$$

where the integration is extended over the cross sectional area $A$. The first of these equations shows that the centroid of the cross section must be on the $x$ axis; from the second, we find

$$\theta = \frac{Ma}{EI_x} = \frac{M_t a^2}{EI_x}, \qquad (161)$$

where $I_x$ is the moment of inertia of the cross section of the ring with respect to the $x$ axis. Substituting in eq. ($d$), we find

$$\sigma = \frac{M_t a y}{I_x}, \qquad (162)$$

i.e., the distribution of the normal stresses over the cross section of the ring is the same as in the case of bending of straight bars; the stress is proportional to the distance from the neutral axis $x$ and the maximum stress occurs at the points most remote from this axis.

As a second example let us consider a ring of rectangular cross section (Fig. 115) whose width $b$ is not small in comparison with the radius $a$ of the center line. Let $c$ and $d$ denote the inner and outer radii of the ring respectively, and $r$ the radius of any fiber of the ring, and assume as before that the deformation of the ring consists of a rotation of its cross section [43] through an angle $\theta$. The elongation of the fiber at a radius $r$ and the corresponding stress are
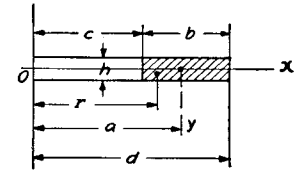


Fig. 115.

$$\epsilon = \frac{\theta y}{r}; \qquad \sigma = \frac{E\theta y}{r}. \qquad (f)$$

The equation of equilibrium analogous to the second of eqs. ($e$) becomes

$$\int_{-h/2}^{+h/2}\int_c^d \frac{E\theta y^2\,dr\,dy}{r} = M$$

and, by performing the integration,

$$\frac{E\theta h^3}{12}\log_e\frac{d}{c} = M,$$

from which

$$\theta = \frac{12M}{Eh^3\log_e\dfrac{d}{c}} = \frac{12M_t a}{Eh^3\log_e\dfrac{d}{c}}. \qquad (163)$$

Substitute into the second of eqs. ($f$), and

$$\sigma = \frac{12My}{h^3 r\log_e\dfrac{d}{c}}.$$

[43] The possibility of distortion of the cross section is neglected in this consideration. The corresponding error is small, provided $d/c < 1.5$. See A. M. Wahl, Trans. Amer. Soc. Mech. Engrs., 1929.

The maximum stress is found at the inner corners of the ring, where $r = c$ and $y = h/2$:

$$\sigma_{\max} = \frac{6M}{h^2 c \log_e \dfrac{d}{c}} = \frac{6M_t a}{h^2 c \log_e \dfrac{d}{c}} . \tag{164}$$

If $b$ is small, eq. (163) can easily be changed to the form (161). Put

$$d = a + \frac{b}{2} \quad \text{and} \quad c = a - \frac{b}{2};$$

then

$$\log_e \frac{d}{c} = \log_e \frac{a + \dfrac{b}{2}}{a - \dfrac{b}{2}} \cong \log_e \left( 1 + \frac{b}{a} \right) .$$

For small values of the ratio $b/a$ the above logarithm is approximately equal to $b/a$. Substitution of this into eq. (163) gives eq. (161).

These results can be used in calculating the stresses produced at the joint of a pipe and a flange [44] by forces $R$ (Fig. 116). $R$ is the force per unit length of the inner circumference of the pipe. The force per unit length of the outer circumference of the flange is $R(c/d)$. Under the action of these forces the cross section of the flange rotates through the angle $\theta$, and the wall of the pipe bends as shown in Fig. 116 (b) by the dotted lines. Let $M_0$ and $P_0$ be the bending moment and the shearing force at the joint per unit length of the inner circumference of the pipe. The magnitude of these quantities can be found from the condition of continuity at the junction of pipe and flange. As ordinarily the flange is very rigid in the plane perpendicular to the axis of the pipe, the radial displacement produced in the flange by forces $P_0$ is negligible, and the deflection at the edge of the pipe can be considered zero. The angle of rotation of the edge of the pipe is equal to $\theta$, the angle of rotation of cross sections of the flange. Then eqs. (11) and (12)



Fig. 116.

[44] Another method of calculating these stresses is given by E. O. Waters, Journal Appl. Mech., Vol. 59, 1937, p. 161. See also J. D. Mattimore, N. O. Smith-Petersen and H. C. Bell, Trans. A. S. M. E., Vol. 60, 1938, p. 297.
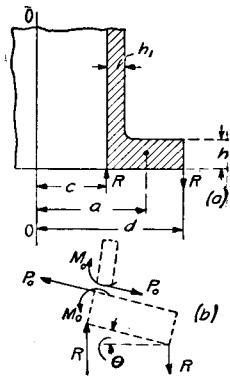
give the following equations for calculating $M_0$ and $P_0$:

$$\frac{1}{2\beta^3 D} (P_0 - \beta M_0) = 0,$$

$$-\frac{1}{2\beta^2 D} (P_0 - 2\beta M_0) = \theta.$$

From the first of these equations

$$P_0 = \beta M_0. \tag{g}$$

Then

$$M_0 = 2\beta D\theta \quad \text{and} \quad P_0 = 2\beta^2 D\theta. \tag{h}$$

For a pipe of thickness $h_1$ and inner radius $c, \beta$ is [45] given by eq. (158),

$$\beta = \sqrt[4]{\frac{3(1 - \mu^2)}{c^2 h_1^2}} . \tag{k}$$

The torque per unit length of the center line of the flange, produced by the forces shown in the figure, is

$$M_t = \frac{c}{a} \left[ R(d - c) - M_0 - P_0 \frac{h}{2} \right]$$

$$= \frac{c}{a} \left[ R(d - c) - M_0 - M_0 \frac{h}{2} \beta \right]. \tag{l}$$

The substitution of this into eq. (163) gives the angle $\theta$ and from the first of eqs. (h)

$$M_0 = 2\beta D \cdot \frac{12c}{Eh^3 \log_e \dfrac{d}{c}} \left[ R(d - c) - M_0 - M_0 \frac{h}{2} \beta \right].$$

Replace $D$ by its magnitude $Eh_1^3/12(1 - \mu^2)$, and

$$M_0 = R(d - c) \frac{1}{1 + \dfrac{\beta h}{2} + \dfrac{1 - \mu^2}{2\beta c} \left( \dfrac{h}{h_1} \right)^3 \log_e \dfrac{d}{c}} . \tag{165}$$

From eqs. (165) and (g) the quantities $M_0$ and $P_0$ can be calculated if we are given the dimensions of the pipe, Poisson's ratio and the forces $R$. Then the bending stresses in the pipe may be found as in article 32.

[45] For small thickness of the pipe the difference between the inner radius and the radius of the middle surface can be neglected.

### Problems

1. Determine the bending moment $M_0$ and the shearing force $P_0$ in the pipe shown in Fig. 116 if $d = 6\frac{1}{4}''$, $c = 3\frac{5}{16}''$, $h = 1\frac{7}{16}''$, $h_1 = 13/16''$, $\mu = 0.3$.

*Solution.* From eq. (k)

$$\beta = \frac{\sqrt[4]{2.73}}{\sqrt{ch_1}} = 0.784 \text{ in.}^{-1},$$

$$\log_e \frac{d}{c} = 0.635; \qquad \frac{\beta h}{2} = 0.564.$$

Substituting in eq. (165), we have

$$M_0 = 0.459 R(d - c); \qquad P_0 = \beta M_0 = 0.360 R(d - c).$$

The maximum bending stress in the pipe is given by

$$\sigma = \frac{6 M_0}{h_1^2}.$$

2. Find the expression for the small deflection of the conical ring, shown in Fig. 117, which represents an element of a Belleville
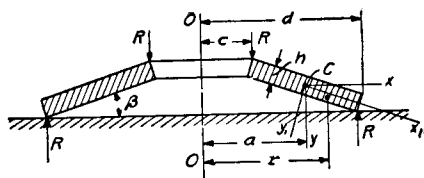


FIG. 117.

spring. $R$ is the load per unit length of the inner edge of the ring.

*Solution.* Take, as before, the coordinates $x$ and $y$ with the origin at the center of rotation $C$. The unit elongation and the stress for any fiber with the radius $r$ are given by eqs. (f). From the equilibrium of the half ring, we obtain

$$\int_A \frac{E\theta y}{r} dA = 0; \qquad \int_A \frac{E\theta y^2}{r} dA = M = Rc(d - c). \qquad (m)$$

The position of the center of rotation $C$ can be determined from the first of these two equations. Let $a$ be the radius at the point $C$ and assume the angle $\beta$ of the cone to be so small that we can take $\sin \beta = \beta$; $\cos \beta = 1$. Then by taking the axes $x_1$ and $y_1$ parallel to the sides of the rectangular cross section and noting that $y = y_1$

$+ \beta x_1 = y_1 + \beta(r - a)$ the first of eqs. (m) becomes

$$\int_{-h/2}^{+h/2} \int_c^d \frac{E\theta}{r} [y_1 + \beta(r - a)] dr dy_1 = E\theta\beta h \left| r - a \log_e r \right|_c^d$$

$$= E\theta\beta h \left( d - c - a \log_e \frac{d}{c} \right) = 0,$$

from which

$$a = \frac{d - c}{\log_e \dfrac{d}{c}}. \qquad (n)$$

The second of eqs. (m) becomes

$$\int_{-h/2}^{+h/2} \int_c^d \frac{E\theta}{r} [y_1 + \beta(r - a)]^2 dr dy_1$$

$$= E\theta \left[ \frac{h^3}{12} \log_e \frac{d}{c} + \beta^2 h \left( \frac{d^2 - c^2}{2} \right.\right.$$

$$\left.\left. - 2a(d - c) + a^2 \log_e \frac{d}{c} \right) \right] = Rc(d - c),$$

and by substituting eq. (n) for $a$ we obtain for the vertical deflection of the upper edge of the cone with respect to the lower

$$\delta = \theta(d - c) = \frac{Rc(d - c)}{E\left[ \dfrac{h^3}{12(d-c)} \log_e \dfrac{d}{c} + \beta^2 h \left( \dfrac{d+c}{2} - \dfrac{d-c}{\log_e \dfrac{d}{c}} \right) \right]} \cdot \qquad (p)$$

This gives $\delta$ if we know the dimensions of the ring, the modulus of elasticity of the material and the load $R$. This derivation neglects the effect of the change in the angle $\beta$ due to the rotation $\theta$.[46]

---

[46] For larger deflections the change in the angle $\beta$ must be considered. In such cases the deflection is no longer proportional to the load. See paper by W. A. Brecht and A. M. Wahl, Journal Appl. Mech. Trans. A. S. M. E. Vol. 52, 1930, p. 52. See also papers by J. O. Almen and A. Laszlo, Trans. Am. Soc. Mech. Engrs. Vol. 58, p. 305, 1936, and Siegfried Gross, V. D. I. Vol. 79, p. 865, 1935.

## CHAPTER IV

### BUCKLING OF BARS, PLATES, AND SHELLS [1]

**35. Lateral Buckling of Bars Compressed within the Elastic Limit.**—The discussion of simultaneous bending and compression of struts (p. 244, Part I) showed that there is a certain *critical value* of the compressive force at which large lateral deflection may be produced by the slightest lateral load. For a prismatical bar with hinged ends this *critical compressive force* is

$$P_{cr} = \frac{\pi^2 EI}{l^2}. \qquad (a)$$

Experiments show that when the compressive force in a slender [2] strut approaches this value, lateral deflection begins and increases so rapidly with increase of the compressive force that a load equal to the critical value is usually sufficient to produce complete failure of the structure. Consequently this *critical load* must be considered as the criterion of strength for slender columns and struts.

From the equation above it will be seen that this critical load does not depend upon the strength of the *material* but only upon the dimensions of the structure and the modulus of elasticity of the material. Two equal slender struts, one of high strength steel and the other of common structural steel, will buckle at the same compressive force, although the strength of the material in the two cases is very different. Equation (*a*) shows also that the strength of a strut may be raised by increasing *I*. This may be done without changing the cross sectional area by distributing the material as far as possible from the principal axes of the cross section. Hence

tubular sections are more economical than solid for compression members. By diminishing the wall thickness of such sections and increasing the transverse dimensions their stability can be increased. There is a lower limit for the wall thickness however below which the wall itself becomes unstable and, instead of buckling of the strut as a whole, there occurs a buckling of its longitudinal elements, which brings about a corrugation of the wall.

This discussion shows then that the sidewise buckling of compression members, i.e., their *elastic stability*, is of great practical importance. This is especially true in many modern structures where the cross sectional dimensions are being made smaller and smaller due to the use of stronger materials and the desire to save weight. In many cases failure of an engineering structure is to be attributed to elastic instability and not to the lack of strength on the part of the material.

In the previous discussion (p. 239, Part I) the magnitude of the critical load was obtained by considering the simultaneous action of compressive and bending forces. The same result may be obtained by assuming that the bar is only compressed by a centrally applied load.[3] Let us consider the case of a bar in the form of a slender vertical prism built in at the bottom and loaded axially at the top (Fig. 118). If the load *P* is less than its critical value the bar remains straight and undergoes only axial compression. This straight form of elastic equilibrium is *stable*, i.e., if a lateral force be applied and a small deflection produced, this deflection disappears when the lateral force is removed and the bar becomes straight
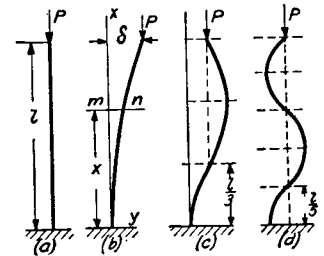


Fig. 118.

---

[1] For more information on buckling problems see, "Theory of Elastic Stability," 1936.

[2] When the strut is not slender enough, lateral buckling occurs at a compressive stress above proportional limit. This case is discussed in "Theory of Elastic Stability," p. 156, 1936.

[3] The values of the critical loads, for various conditions at the ends of a compressed prismatical bar, were obtained first by L. Euler; see Additamentum, "De curvis elasticis," in the "Methodus inveniendi lineas curvas maximi minimive proprietate gaudentes," Lausanne, 1744. See also Histoire de l'Académie, Berlin, Vol. 13, 1757. An English translation of this work is given in "Isis," No. 58, Vol. 201, 1933.

again. By increasing $P$ gradually we may arrive at a condition in which the straight form of equilibrium becomes unstable and a slight lateral force may produce a lateral deflection which does not disappear with the cause which produces it. The critical load is then defined as the axial load, which is sufficient to keep the bar in a slightly bent form (Fig. 118, $b$).

This load is calculated by use of the differential equation of the deflection curve (eq. 79, Part I). The axes are taken as indicated in Fig. 118, $b$. Then the bending moment at any cross section $mn$ is $P(\delta - y)$ and the differential equation of the deflection curve is [4]

$$EI \frac{d^2y}{dx^2} = P(\delta - y). \qquad (b)$$

It is clear that, with the upper end free, buckling of the bar will occur in the plane of *smallest flexural rigidity* which we will call $EI$. Let

$$p^2 = \frac{P}{EI}. \qquad (c)$$

Equation ($b$) then becomes

$$\frac{d^2y}{dx^2} + p^2y = p^2\delta. \qquad (b')$$

The general solution of this equation is

$$y = \delta + C_1 \cos px + C_2 \sin px, \qquad (d)$$

in which $C_1$ and $C_2$ are constants which must be adjusted to satisfy the conditions at the built-in end:

$$(y)_{x=0} = 0; \qquad \left(\frac{dy}{dx}\right)_{x=0} = 0.$$

These conditions are fulfilled if

$$C_1 = -\delta; \qquad C_2 = 0.$$

Then

$$y = \delta(1 - \cos px). \qquad (e)$$

[4] For the deflection shown in Fig. 118 ($b$) $d^2y/dx^2$ is positive, hence the positive sign on the right side of eq. ($b$).

The condition at the upper end is that

$$(y)_{x=l} = \delta.$$

It is satisfied if $\cos pl = 0$, i.e., if

$$pl = (2n + 1)\frac{\pi}{2}, \qquad (f)$$

where $n$ is an integer. The smallest value of $pl$, and therefore of $P$, which satisfies eq. ($f$) is obtained by putting $n = 0$. Then, using eq. ($c$),

$$pl = l\sqrt{\frac{P}{EI}} = \frac{\pi}{2},$$

from which

$$P_{cr} = \frac{\pi^2 EI}{4l^2}. \qquad (166)$$

This is the *critical load* for the bar represented in Fig. 118$a$, i.e., the smallest load which can keep the bar in a slightly bent shape.

With $n = 1$, $n = 2$, $\cdots$, in eq. ($f$) we obtain

$$P = \frac{9EI\pi^2}{4l^2}, \qquad P = \frac{25EI\pi^2}{4l^2}.$$

The corresponding deflection curves are shown in Figs. 118 ($c$) and 118 ($d$). For the shape shown in Fig. 118 ($c$) a force nine times larger than critical is necessary, and for that in part ($d$) twenty-five times larger. These forms of buckling are unstable and have no practical meaning because the structure fails as the load reaches the value (166).

The critical load for some other cases can easily be obtained from the solution for the foregoing case. For example, in the case of a bar with hinged ends (Fig. 119) it is evident from symmetry that each half of the bar is in the same condition as the entire bar of Fig. 118. Hence the critical load for this case

is obtained by using $l/2$, instead of $l$, in eq. (166), which gives

$$P_{cr} = \frac{EI\pi^2}{l^2}.\qquad(167)$$

The case of a bar with hinged ends is very often encountered in practical applications and is called the *fundamental* case of
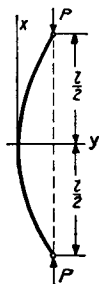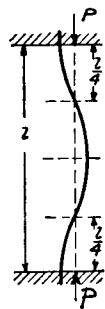


FIG. 119.        FIG. 120.

buckling of a prismatical bar.  In the case of a bar with built-in ends (Fig. 120) there are reactive moments which keep the ends from rotating during buckling.  The combination of the compressive force with these moments is equivalent to the compressive force $P$, Fig. 120, applied eccentrically.  There are inflection points where the line of action of $P$ intersects the deflection curve, because the bending moment at these points is zero.  These points and the mid point of the span divide the bar into four equal portions, each of which is in the same condition as the bar represented in Fig. 118.  Hence the critical load for a bar with built-in ends is found from eq. (166) by using $l/4$ instead of $l$, which gives

$$P_{cr} = \frac{4\pi^2 EI}{l^2}.\qquad(168)$$

It was assumed in the previous discussion that the bar is very slender so that the bending, which occurs during buckling, remains within the proportional limit.  Only with this condition can eq. (*b*) be applied.  To establish the limit of applicability of the above formulas for critical loads let us

consider the *fundamental* case (Fig. 119).   Divide eq. (167) by the cross sectional area $A$ of the bar, and let $k = \sqrt{I/A}$ be the smaller radius of gyration.   Then the critical value of the compressive stress is

$$\sigma_{cr} = \frac{P_{cr}}{A} = \pi^2 E\left(\frac{k}{l}\right)^2.\qquad(169)$$

This equation is applicable as long as the stress $\sigma_{cr}$ remains within the proportional limit.  With this limit and also the modulus $E$ known for a given material, the limiting value of the ratio $l/k$ (which characterizes the *slenderness* of the bar) can easily be obtained from eq. (169) for each particular case.

In the cases represented in Figs. 118 and 120, proceeding as above, we find

$$\sigma_{cr} = \pi^2 E\left(\frac{k}{2l}\right)^2;\quad(170)\qquad \sigma_{cr} = \pi^2 E\left(\frac{k}{\frac{1}{2}l}\right)^2.\quad(171)$$

The equation for the fundamental case (169) may be used for these cases also if we use a *reduced length* $l_1$ instead of the length of the bar.  In the case of a prismatical bar with one end built in and the other free the reduced length is twice as great as the actual length $l_1 = 2l$.  In the case of a prismatical bar with both ends built in the reduced length is half the actual length, $l_1 = \frac{1}{2}l$.  The equation for the critical stress may consequently be represented in the form:

$$\sigma_{cr} = \pi^2 E\left(\frac{k}{\beta l}\right)^2 = \pi^2 E\left(\frac{k}{l_1}\right)^2,\qquad(172)$$

in which $\beta$ depends upon the conditions at the ends of the bar and is sometimes called the *length coefficient*.

In discussing the design of columns (p. 249, Part I) the fundamental case of a column with hinged ends was considered.  The information given there can be applied to columns, with other end conditions, provided the reduced length, $l_1$, instead of the actual length, $l$, is used.  Thus in each particular case the design of a column reduces to the determination of the proper value of the *length coefficient*.

As an example of the calculation of this coefficient, let us consider the case of a centrally compressed strut with the lower end built in and the upper end hinged (Fig. 121). The critical value of the compressive force is that value, $P_{cr}$, which can keep the strut in a slightly buckled shape. It may be seen that in this case, during buckling, a lateral reaction $Q$ will be produced, and the differential equation of the deflection curve becomes:



FIG. 121.

$$EI \frac{d^2y}{dx^2} = - Py + Q(l - x). \qquad (g)$$

The general solution of this equation with notation (c) is

$$y = C_1 \cos px + C_2 \sin px + \frac{Q}{P}(l - x). \qquad (h)$$

For determining the constants $C_1$ and $C_2$ and the unknown reaction $Q$, we have the following conditions at the ends:

$$(y)_{x=0} = 0, \qquad (y)_{x=l} = 0, \qquad \left(\frac{dy}{dx}\right)_{x=0} = 0.$$

Substituting solution (h) for $y$ we obtain

$$C_1 + \frac{Q}{P}l = 0, \quad C_1 \cos pl + C_2 \sin pl = 0, \quad pC_2 - \frac{Q}{P} = 0. \quad (i)$$

Determining the constants $C_1$ and $C_2$ from the first and the third of these equations and substituting in the second equation, we find

$$\tan pl = pl. \qquad (j)$$

The graphical method is useful in solving this trigonometric equation. In Fig. 122 the curves represent $\tan pl$ as a function of $pl$. These curves have the verticals $pl = \pi/2, 3\pi/2,$ $\cdots$ as asymptotes, since for these values of $pl$, $\tan pl$ becomes infinity. The roots of equation (j) are now obtained as the intersection points of the above curves with the straight line

$y = pl$. The smallest root, obtained in this way, is

$$pl = 4.493.$$

Then

$$P_{cr} = p^2 EI = \frac{20.16EI}{l^2} \approx \frac{\pi^2 EI}{(0.7l)^2}. \qquad (173)$$

Thus the critical load is the same as for a strut with hinged ends having a reduced length:

$$l_1 = 0.7l.$$

As a second example let us consider a strut on three supports and centrally compressed by forces $P$, Fig. 123. In calculating the critical value of the compressive force we keep our previous definition and assume that $P_{cr}$ is the force which can keep the strut in a slightly buckled shape. As a result of buckling there will be some bending moment $M_2$ at the middle [5] support, for calculation of which equation (38), derived for continuous struts, can be used. By observing that in our case the ends of the strut are hinged, we obtain $M_1 = M_3 = 0$ and equation (38) becomes



FIG. 122.



FIG. 123.

$$\left(\beta_1 \frac{l_1}{I_1} + \beta_2 \frac{l_2}{I_2}\right) M_2 = 0. \qquad (i)$$

This equation is satisfied and a buckled shape of the strut becomes possible if

$$\beta_1 \frac{l_1}{I_1} + \beta_2 \frac{l_2}{I_2} = 0. \qquad (j)$$

[5] An exception is the trivial case when the two spans are equal and the cross section is constant along the entire length. In this case $M_2 = 0$ at the intermediate support, and each span is in the same condition as a strut with hinged ends.
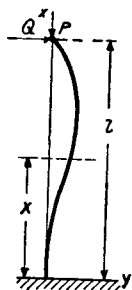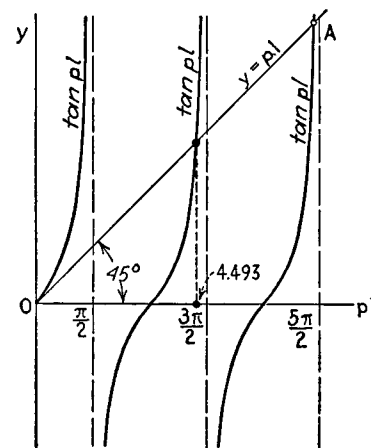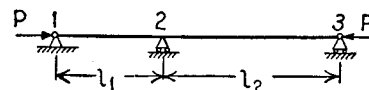
where $\beta_1$ and $\beta_2$ are (see expressions (36) p. 36)

$$\beta_1 = 3\left[\frac{1}{(2u_1)^2} - \frac{1}{2u_1 \tan 2u_1}\right],$$

$$\beta_2 = 3\left[\frac{1}{(2u_2)^2} - \frac{1}{2u_2 \tan 2u_2}\right] \quad (k)$$

and

$$u_1 = \frac{l_1}{2}\sqrt{\frac{P}{EI_1}}, \qquad u_2 = \frac{l_2}{2}\sqrt{\frac{P}{EI_2}}. \quad (l)$$

If the dimensions of the strut are given, the ratio $u_1 : u_2$ is known from the expressions $(l)$ and the ratio $\beta_1 : \beta_2$ from equation $(j)$, which gives

$$\frac{\beta_1}{\beta_2} = -\frac{l_2}{l_1}\frac{I_1}{I_2}. \quad (m)$$

Having the numerical table of functions $\beta$, we can readily solve this equation for the proper values of $u_1$ and $u_2$. Then, from expressions $(l)$, the critical value of $P$ is obtained. Take, for example, $I_1 = I_2 = I$ and $l_2 = 2l_1$. Then $u_2 = 2u_1$ and

$$\frac{\beta_1}{\beta_2} = -2. \quad (n)$$

To solve this equation we have to find such a value $2u_1$ of the argument $2u$ that after doubling it the function $\beta$ changes the sign and reduces to a half of its numerical value at the argument $2u_1$. Using the table of numerical values of $\beta$,[6] we readily find that this condition is satisfied if

$$2u_1 = 1.93.$$

Hence, from equations $(l)$,

$$P_{cr} = \frac{1.93^2 EI}{l_1^2} = \frac{3.72 EI}{l_1^2} = \frac{14.9 EI}{l_2^2}.$$

It is seen that the value of the critical load lies between the two values $\pi^2 EI/l_1^2$ and $\pi^2 EI/l_2^2$, calculated for separate spans as if each were a strut with hinged ends. The stability of the shorter span is reduced, owing to the action of the longer span, while the stability of the longer span is increased.

[6] See such table in "Theory of Elastic Stability."

In the derivation of eq. $(e)$ for the deflection curve after bending, the maximum deflection $\delta$ remained indeterminate, i.e., at the critical load the bar may have any small deflection. The above theory applied only to *small* deflections because only for such deflections may we use the approximate expression $d^2y/dx^2$ for the curvature, in place of the exact expression:

$$\frac{\dfrac{d^2y}{dx^2}}{\left[1 + \left(\dfrac{dy}{dx}\right)^2\right]^{\frac{3}{2}}}.$$

The solution of the exact differential equation for the deflection curve has been found for several cases [7] and shows that there is really no such indeterminateness in the deflection as implied above. For example for a bar with hinged ends the maximum deflection may be represented by the equation: [8]

$$\delta = \frac{l\sqrt{8}}{\pi}\sqrt{\frac{P}{P_{cr}} - 1}\left[1 - \frac{1}{8}\left(\frac{P}{P_{cr}} - 1\right)\right], \quad (174)$$

which shows that the deflection increases very rapidly, with the load above the critical value. Assuming, for instance, a load only 1 per cent larger than $P_{cr}$, we find from eq. (174) a deflection about 9 per cent of the length $l$ of the bar.[9]
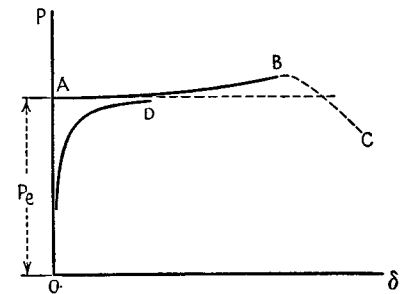
The relation between the load and deflection may be



FIG. 124.

[7] Saalschütz, "Der Belastete Stab," Leipzig, 1880. See also Halphen Traité des Fonctions elliptiques, Vol. 2 (1888), p. 192.

[8] See R. v. Mises, Zeitschr. f. Angew. Math. u. Mech., Vol. 4, 1924, p. 435; see also O. Domke, Die Bautechnik, Vol. 4, 1926, p. 747, and R. W. Burges, Phys. Rev., 1917.

[9] It is assumed that deformation remains within the proportional limit.

represented graphically as shown in Fig. 124 by the curve *OAB*, in which the load is represented by ordinates and the deflections by the abscissas. As long as the load is smaller than $P_{cr}$ the deflection is zero. Beyond this limit the deflection increases rapidly with the load.[10]

In experimental investigations of the lateral buckling of compressed bars, the relation between the deflection and the load depends very much upon the accuracy with which the load is centered and on the straightness and homogeneity of the bar. The load deflection curve is usually like curve *OD* in Fig. 124. Due to inaccuracies of one sort or another deflection begins at small loads, but progresses very slowly as long as the load is far below critical but very rapidly when the load approaches the critical value. The more accurately the bar is made and loaded the more nearly the curve approaches the theoretical curve *OAB*.[11]

### Problems

1. A steel bar of rectangular cross section $1 \times 2$ in. with hinged ends is axially compressed. Determine the minimum length at which eq. (167) can be applied if $E = 30 \times 10^6$ lbs. per sq. in. and the limit of proportionality is 30,000 lbs. per sq. in. Determine the magnitude of the critical stress if the length is 5 feet.

*Solution.* The smaller radius of gyration is $k = 1/2\sqrt{3}$ in.; the minimum length from eq. (169) is

$$l = 100k = \frac{100}{2\sqrt{3}} = 28.9 \text{ in.}$$

---

[10] When yielding begins the curve *AB* is no longer applicable and the further buckling is going as indicated by dotted line *BC*, Fig. 124.

[11] A very close coincidence of experimental and calculated values of critical loads was obtained by Th. v. Karman, Forschungsarbeiten, nr. 81, 1910, Berlin; see also K. Memmler, Proceedings of the 2d Internat. Congress of Applied Mech., Zürich, 1926, p. 357.

The critical stress for $l = 5'$, from eq. (169), is

$$\sigma_{cr} = \pi^2 \times 30 \times 10^6 \frac{1}{12 \times 60^2} = 6,850 \text{ lbs. per sq. in.}$$

2. Solve the above problem, assuming a bar of circular cross section 1 in. in diameter and built-in ends.

*Answer.* Minimum length $= 50$ in. For $l = 5'$, $\sigma_{cr} = 20,800$ lbs. per sq. in.

3. Determine the critical compressive load for a standard I section 6' long, 6" depth, weight 12.5 lbs. per foot, and with hinged ends.

*Answer.*

$$P_{cr} = \frac{\pi^2 EI}{l^2} = \frac{9.87 \times 30 \times 10^6 \times 1.8}{72^2} = 103,000 \text{ lbs.}$$

4. Solve problem 1 assuming that one end of the bar is hinged and the other built-in as in Fig. 121.

5. Determine the critical value of the forces $P$ which compress the vertical members of the rectangular frame shown in Fig. 125.

*Solution.* Buckling produces reactive bending moments $M_0$ which resist free rotation of the ends of the vertical members. The differential equation for the deflection curve of the vertical member is



FIG. 125.

$$EI \frac{d^2y}{dx^2} = -Py + M_0.$$

The general solution of this equation is

$$y = C_1 \cos px + C_2 \sin px + \frac{M_0}{P}.$$

The constants of integration and $M_0$ are to be determined from the following conditions based on the symmetrical form of the buckled frame (Fig. 125):

$$(y)_{x=0} = 0; \quad \left(\frac{dy}{dx}\right)_{x=l/2} = 0; \quad \left(\frac{dy}{dx}\right)_{x=0} = \theta = \frac{M_0 l_1}{2EI_1}.$$
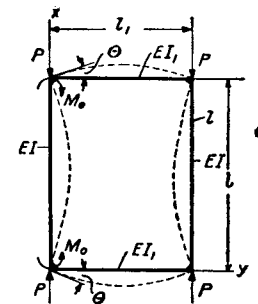
From the above solution for $y$,

$$C_1 + \frac{M_0}{P} = 0; \quad -C_1 p \sin \frac{pl}{2} + C_2 p \cos \frac{pl}{2} = 0; \quad C_2 p = \frac{M_0 l_1}{2EI_1}.$$

These give the following transcendental equation for determining $p$ and the critical load:

$$\tan \frac{pl}{2} + \frac{Pl_1}{2pEI_1} = 0,$$

or, using notation $(c)$,

$$\tan \frac{pl}{2} + \frac{I}{I_1} \frac{l_1}{l} \frac{pl}{2} = 0. \tag{o}$$

When $(I/I_1)(l_1/l)$ is large, i.e., when the resistance of the horizontal members of the frame to buckling of the vertical members is small, $\tan (pl/2)$ is a large negative number and $pl/2$ approaches $\pi/2$. The critical load then approaches the value $\pi^2 EI/l^2$ obtained before for a bar with hinged ends (eq. 167).

When $(I/I_1)(l_1/l)$ is small, i.e., when the resistance of the horizontal members of the frame to buckling of the vertical members is very great, $\tan (pl/2)$ is a small negative number and $pl/2$ approaches $\pi$. Then the critical load approaches the value $4\pi^2 EI/l^2$ obtained before (eq. 168) for a bar with built-in ends.

In the case of a square frame with all members of the same cross section $l = l_1$, $I = I_1$, and the equation for determining the critical load becomes

$$\tan \frac{pl}{2} + \frac{pl}{2} = 0,$$

from which [12]

$$\frac{pl}{2} = 2.029,$$

$$P_{cr} = \frac{16.47 EI}{l^2} = \frac{\pi^2 EI}{(0.774l)^2}. \tag{p}$$

The reduced length in this case is therefore $l_1 = 0.774l$.

6. Solve the preceding problem assuming that in addition to vertical forces $P$ there are two pairs of horizontal forces $Q$ which are producing a compression of the horizontal members of the frame.

*Hint.* Since the horizontal bars are compressed, the angle of

---

[12] Curves similar to those in Fig. 122 can be used also in this case.

rotation $\theta$, indicated in Fig. 125, is [13]

$$\theta = \frac{M_0 l_1}{2EI_1} \frac{\tan u}{u},$$

where

$$u^2 = \frac{Ql_1^2}{4EI_1}.$$

The equation for calculating the critical value of $P$ is obtained by substituting $I_1 u/\tan u$ instead of $I_1$ in equation $(o)$ of the preceding problem.

7. A strut with hinged ends $AB$, Fig. 126, is compressed by forces $P_1$ and $P_2$. Find the critical value of the force $P_1 + P_2$ if $(P_1 + P_2) : P_1 = m$, $I_2 : I_1 = n$, $l_2/l_1 = r$.

*Solution.* Assuming that the buckled shape of the strut is as shown in Fig. 126 by the dotted line, there will be horizontal reactions $Q = \delta P_2/l$ produced during buckling. The differential equations of the upper and the lower portions of the deflection curve are



FIG. 126.

$$\left. \begin{aligned} EI_1 \frac{d^2 y_1}{dx^2} &= -P_1 y_1 - \frac{\delta P_2}{l}(l - x), \\ EI_2 \frac{d^2 y_2}{dx^2} &= -P_1 y_2 - \frac{\delta P_2}{l}(l - x) + P_2(\delta - y_2). \end{aligned} \right\} \tag{r}$$
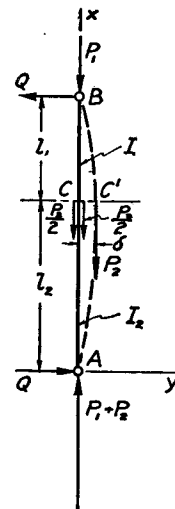
Using notations

$$\frac{P_1}{EI_1} = p_1^2, \quad \frac{P_2}{EI_2} = p_2^2, \quad \frac{P_1 + P_2}{EI_2} = p_3^2, \quad \frac{P_2}{EI_1} = p_4^2, \tag{s}$$

we obtain the solutions of equations $(r)$:

$$y_1 = C_1 \sin p_1 x + C_2 \cos p_1 x - \frac{\delta}{l} \frac{p_4^2}{p_1^2}(l - x)$$

$$y_2 = C_3 \sin p_3 x + C_4 \cos p_3 x + \frac{\delta}{l} \frac{p_2^2}{p_3^2} x.$$

The constants of integration are obtained from the end conditions

---

[13] It is obtained from equation (48) by substituting $ui$ for $u$.

of the two portions of the buckled bar:

$$(y_1)_{x=l} = 0, \qquad (y_1)_{x=l_2} = \delta, \qquad (y_2)_{x=l_2} = \delta, \qquad (y_2)_{x=0} = 0.$$

From these,

$$C_1 = \frac{\delta(p_1{}^2 l + p_4{}^2 l_1)}{p_1{}^2 l(\sin p_1 l_2 - \tan p_1 l \cos p_1 l_2)}, \qquad C_2 = -C_1 \tan p_1 l$$

$$C_3 = \frac{\delta(p_3{}^2 l - p_2{}^2 l_2)}{p_3{}^2 l \sin p_3 l_2}, \qquad C_4 = 0.$$

Substituting these in the continuity condition

$$\left(\frac{dy_1}{dx}\right)_{x=l_2} = \left(\frac{dy_2}{dx}\right)_{x=l_2}$$

we obtain the following transcendental equation for calculating critical loads:

$$\frac{p_4{}^2}{p_1{}^2} - \frac{p_1{}^2 l + p_4{}^2 l_1}{p_1 \tan p_1 l_1} = \frac{p_2{}^2}{p_3{}^2} + \frac{p_3{}^2 l - p_2{}^2 l_2}{p_3 \tan p_3 l_2} \qquad (t)$$

which can be solved in each particular case by trial and error or by plotting both sides of the equation and determining the intersection point of the two curves. Taking, as an example, $l_1 = l_2$, $I_1 = I_2 = I$ and $P_1 = P_2$, we obtain

$$(P_1 + P_2)_{cr} = \frac{\pi^2 EI}{(0.87l)^2}.$$
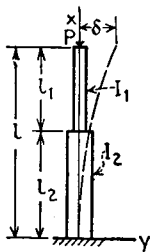


FIG. 127.

8. Find the critical load for the column built-in at the bottom and free at the top and consisting of the two prismatical portions with moments of inertia $I_1$ and $I_2$, Fig. 127.

*Solution.* If $\delta$ is the deflection at the top during buckling the differential equations for the two portions of the deflection curve are

$$EI_1 \frac{d^2 y_1}{dx^2} = P(\delta - y_1),$$

$$EI_2 \frac{d^2 y_2}{dx^2} = P(\delta - y_2).$$

By making use of our previous notations $(s)$ the solutions of these

equations are reached:

$$y_1 = \delta + C \cos p_1 x + D \sin p_1 x,$$
$$y_2 = \delta(1 - \cos p_2 x).$$

The constants of integration are obtained from the conditions:

$$(y_1)_{x=l} = \delta, \qquad (y_1)_{x=l_2} = (y_2)_{x=l_2},$$

which give

$$\delta + C \cos p_1 l + D \sin p_1 l = \delta,$$
$$\delta + C \cos p_1 l_2 + D \sin p_1 l_2 = \delta(1 - \cos p_2 l_2),$$

from which

$$C = -D \tan p_1 l, \qquad D = \frac{\delta \cos p_2 l_2 \cos p_1 l}{\sin p_1 l_1}.$$

Since the two portions of the deflection curve have the same tangent at $x = l_2$ we have the equation:

$$\delta p_2 \sin p_2 l_2 = -C p_1 \sin p_1 l_2 + D p_1 \cos p_1 l_2.$$

Substituting for $C$ and $D$ the above values, we finally obtain the following equation for calculating $P_{cr}$:

$$\tan p_1 l_1 \tan p_2 l_2 = \frac{p_1}{p_2}.$$

In the particular case when

$$p_1 l_1 = p_2 l_2 = \frac{l}{2}\sqrt{\frac{P}{EI}},$$

we obtain

$$\tan^2\left(\frac{l}{2}\sqrt{\frac{P}{EI}}\right) = 1,$$

$$\frac{l}{2}\sqrt{\frac{P}{EI}} = \frac{\pi}{4}$$

and

$$P_{cr} = \frac{\pi^2 EI}{4l^2}.$$

This is the critical load for a column of constant cross section.

### 36. Energy Method of Calculating Critical Compressive Loads.[14]—Euler's formulas, given in article 35, were derived

---

[14] See writer's papers in Bulletins of the Polytechnical Institute in Kiev, 1910, and Annales des Ponts et Chaussées, 1913, Paris.

by solving the differential equation of the deflection curve for a compression member with certain end conditions. There are cases in which this equation is complicated and exact solution becomes difficult. We may then use an approximate method, based on consideration of the energy of the system. As a simple example consider a column built in at the bottom and carrying a load at the top (Fig. 118 (a) and (b)). The straight form of equilibrium of the compressed bar is *stable* if the compressive force $P$ is small, but *unstable* after $P$ reaches its critical value, at which lateral buckling begins. This critical value of $P$ may be found by comparing the energy of the system in the two cases: (1) when the bar is simply *compressed*, and (2) when it is *compressed and bent*. The strain energy in the bent bar is larger than that in the straight compressed form, because the energy of bending must be added to the energy of compression, which may be considered constant for small deflections. The potential energy of the load $P$ must also be considered; the deflection of the bar is accompanied by a lowering of the point of application of the load $P$ so that the potential energy of the load diminishes. Let $U$ be the potential energy of bending and $U_1$ the decrease in the potential energy of the load. Then, if $U_1$ is less than $U$, deflection of the bar is accompanied by an increase in the potential energy of the system; this means that it would be necessary to apply some additional lateral force to produce bending. In such a case the straight form of equilibrium is *stable*. On the other hand, when $U_1 > U$, the deflection of the bar is accompanied by a decrease in the potential energy of the system and the bending will proceed without the application of any lateral force, i.e., the straight form of equilibrium is *unstable*. The critical value of the compressive force is therefore obtained when

$$U = U_1. \tag{175}$$

To calculate the magnitude of the critical load from this equation we must obtain expressions for $U$ and $U_1$. From eq. (e) (p. 186), the deflection curve of the bar, when under the

action of a compressive load equal to the critical load ($pl = \pi/2$), is

$$y = \delta\left(1 - \cos\frac{\pi x}{2l}\right). \tag{a}$$

With this value for $y$, expression for the strain energy of bending becomes

$$U = \frac{1}{2} EI \int_0^l \left(\frac{d^2y}{dx^2}\right)^2 dx = \frac{\delta^2\pi^4}{64l^3} EI. \tag{b}$$

The lowering of the point of application of the load during bending is (see p. 47)

$$\lambda = \frac{1}{2} \int_0^l \left(\frac{dy}{dx}\right)^2 dx = \frac{\delta^2\pi^2}{16l}. \tag{c}$$

Therefore,

$$U_1 = P\lambda = \frac{\delta^2\pi^2 P}{16l}. \tag{d}$$

Substituting (b) and (d) into the fundamental eq. (175), we have

$$P_{cr} = \frac{EI\pi^2}{4l^2},$$

which coincides with eq. (166) obtained previously.

In this case the deflection curve (a) was known and the exact solution for the critical load was obtained from eq. (175). In cases where the deflection curve is unknown an approximation to the critical load may be obtained by assuming a *suitable curve* (that is, one satisfying the conditions at the ends of the bar) for the deflection curve and proceeding in exactly the same manner as above.

In order to show what accuracy can be obtained by using this method, the previous problem will be considered again. Assume, for instance, that in the case shown in Fig. 118 (b) the deflection curve is the same as for a cantilever loaded at the end by a transverse force $Q$. Then, from eq. (97) Part I, $y = [Qx^2/6EI](3l - x)$. This is substituted into the expression (b) for the strain energy $U$ of bending, and into the

expression (d) for $U_1$:

$$U = \frac{EI}{2} \int_0^l \left(\frac{d^2y}{dx^2}\right)^2 dx = \frac{Q^2 l^3}{6EI},$$

$$U_1 = P\lambda = \frac{P}{2} \int_0^l \left(\frac{dy}{dx}\right)^2 dx = \frac{P}{15} \frac{Q^2 l^5}{(EI)^2}.$$

Substituting into eq. (175), $P_{cr} = 2.5 EI/l^2$. Comparing this result with the exact formula (166) above, we see that the error arising from this approximation is only about 1 per cent·

This error can be considerably reduced and a better approximation obtained if we take for the strain energy of bending the expression:

$$U = \frac{1}{2EI} \int_0^l M^2 dx. \qquad (e)$$

Substituting in this expression

$$M = P(\delta - y) = P\left[\delta - \frac{Qx^2}{6EI}(3l - x)\right]$$

$$= P\delta\left[1 - \frac{x^2}{2l^3}(3l - x)\right], \quad (f)$$

we find

$$U = \frac{P^2\delta^2}{2EI} \frac{17l}{35}.$$

The diminishing of the potential energy of the load $P$ is

$$U_1 = \frac{P}{15} \cdot \frac{Q^2 l^5}{(EI)^2} = \frac{3P}{5} \cdot \frac{\delta^2}{l}.$$

Substituting into eq. (175), we obtain

$$\frac{P^2\delta^2}{2EI} \frac{17l}{35} = \frac{3P}{5} \frac{\delta^2}{l},$$

from which

$$P_{cr} = \frac{42}{17} \cdot \frac{EI}{l^2} = 2.4706 \frac{EI}{l^2}.$$

The correct value is

$$P_{cr} = \frac{\pi^2}{4} \frac{EI}{l^2} = 2.4674 \frac{EI}{l^2}.$$

Hence the error of the approximate solution is only 0.13 per cent. In using expression (e), instead of expression (b), for strain energy we introduce in our calculations the deflection $y$ of the assumed curve, instead of the derivative $d^2y/dx^2$. Since $y$ is represented with a much better accuracy than $d^2y/dx^2$ by the assumed curve, the second method of calculation actually results in a better approximation for $P_{cr}$.

The energy method usually gives a very satisfactory approximation provided the assumed curve is properly chosen. Sometimes we can make a very rough assumption for the shape of the curve and still obtain a satisfactory result. For example, we might assume the deflection curve in the above example to be a parabola given by the equation

$$y = \frac{\delta x^2}{l^2}.$$

Then

$$U = \int_0^l \frac{M^2 dx}{2EI} = \frac{P^2\delta^2}{2EI} \int_0^l \left(1 - \frac{x^2}{l^2}\right)^2 dx = \frac{P^2\delta^2}{2EI} \frac{8}{15} l,$$

$$U_1 = \frac{P}{2} \int_0^l \left(\frac{dy}{dx}\right)^2 dx = \frac{2}{3} \frac{\delta^2}{l} P.$$

By substituting into equation (175),

$$\frac{P^2\delta^2}{2EI} \frac{8}{15} l = \frac{2}{3} \frac{\delta^2}{l} P$$

and

$$P_{cr} = 2.5 \frac{EI}{l^2}.$$

A satisfactory approximation is thus obtained although the parabolic curve, which we assumed, cannot be considered as a very satisfactory one. It has an approximately constant curvature along the length while in the actual curve the

curvature is proportional to the bending moment. It is zero at the top of the bar and a maximum at the bottom.

Applying the energy method with an assumed curve satisfying the end conditions, we always obtain a value for the critical load which is higher than the true value. This follows from the fact that the actual deflection curve of a buckled bar is always the one that corresponds to the least resistance of the bar. Only by the merest chance will an assumed curve be the true curve of the least resistance. In almost every case the assumed curve will be different from this curve of least resistance, thus giving values too high for the critical loads.

### Problems

1. Solve the problem shown in Fig. 121 assuming the deflection curve is the same as for a uniformly loaded beam with one end built-in and the other hinged.

2. Solve by the energy method problem 7 of the preceding article (p. 197) assuming $l_1 = l_2 = l/2$.

*Solution.* Assuming that the deflection curve is a sine curve,

$$y = \delta \sin \frac{\pi x}{l},$$

the bending moments for the two portions of the curve are

$$M_1 = P_1 y + \frac{\delta P_2}{l}(l - x),$$

$$M_2 = (P_1 + P_2)y - \frac{\delta P_2 x}{l}.$$

The strain energy of bending is

$$U = \int_{l/2}^{l} \frac{M_1{}^2 dx}{2EI_1} + \int_{0}^{l/2} \frac{M_2{}^2 dx}{2EI_2}$$

$$= \frac{\delta^2}{2EI_1}\left(P_1{}^2 \frac{l}{4} + P_2{}^2 \frac{l}{24} + P_1 P_2 \frac{2l}{\pi^2}\right)$$

$$+ \frac{\delta^2}{2EI_2}\left[(P_1 + P_2)^2 \frac{l}{4} + P_2{}^2 \frac{l}{24} - P_2(P_1 + P_2)\frac{2l}{P^2}\right].$$

The diminishing of the potential energy due to lowering of the

points of application of the loads $P_1$ and $P_2$ is

$$U_1 = \frac{P_1}{2}\int_0^l \left(\frac{dy}{dx}\right)^2 dx + \frac{P_2}{2}\int_0^{l/2}\left(\frac{dy}{dx}\right)^2 dx = \frac{\delta^2 \pi^2}{4l}(P_1 + \tfrac{1}{2}P_2).$$

Substituting in equation (175) and using our previous notations, we obtain

$$(P_1 + P_2)_{cr} =$$

$$\frac{(\pi^2 EI_2/l^2)(m + 1)}{m + \frac{m}{6}\left(\frac{m-1}{m}\right)^2 - \frac{8}{\pi^2}(m-1) + n\left[\frac{1}{m} + \frac{m}{6}\left(\frac{m-1}{m}\right)^2 + \frac{8}{\pi^2}\frac{m-1}{m}\right]}. \quad (176)$$

3. Solve problem 8 of the preceding article by using the energy method.

*Answer.* Assuming the deflection curve

$$y = \delta\left(1 - \cos\frac{\pi x}{2l}\right)$$

we obtain

$$P_{cr} = \pi^2 \frac{EI_2}{4l^2} \cdot \frac{1}{\frac{l_2}{l} + \frac{l_1}{l}\frac{I_2}{I_1} - \frac{1}{\pi}\left(\frac{I_2}{I_1} - 1\right)\sin\frac{\pi l_2}{l}}. \quad (177)$$

**37. Buckling of Prismatical Bars under the Action of Uniformly Distributed Axial Forces.**—Assuming that under the action of uniform axial load a slight lateral buckling occurred, Fig. 128, we can obtain the critical value of the load by integrating the differential equation of the deflection curve. The equation in this case is not as simple as we had before and its solution requires the use of Bessel's function.[15] An approximate solution can be readily obtained by using the energy method. As an approximate expression for the deflection curve let us take



FIG. 128.

$$y = \delta\left(1 - \cos\frac{\pi x}{2l}\right) \quad (a)$$

which is the true curve for the case where buckling occurs under the action of a compressive load applied at the end. The bending moment resulting from that portion of the load above a cross section

---
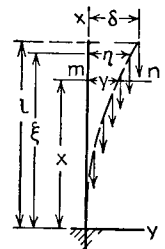
[15] See "Theory of Elastic Stability," p. 115.

$mn$ at that cross section is

$$M = \int_x^l q(\eta - y)d\xi.$$

Substituting equation (a) for $y$ and setting

$$\eta = \delta\left(1 - \cos\frac{\pi\xi}{2l}\right),$$

we obtain after integration with respect to $\xi$:

$$M = \delta q\left[(l - x)\cos\frac{\pi x}{2l} - \frac{2l}{\pi}\left(1 - \sin\frac{\pi x}{2l}\right)\right].$$

Substituting this in the expression for the strain energy of bending, we obtain

$$U = \int_0^l \frac{M^2 dx}{2EI} = \frac{\delta^2 q^2 l^3}{2EI}\left(\frac{1}{6} + \frac{9}{\pi^2} - \frac{32}{\pi^3}\right). \tag{b}$$

In calculating the decrease of the potential energy of the distributed load during lateral buckling, we note that, owing to the inclination of an element $ds$ of the deflection curve at the cross section $mn$, the upper part of the load undergoes a downward displacement equal to

$$ds - dx \approx \frac{1}{2}\left(\frac{dy}{dx}\right)^2 dx,$$

and the corresponding reduction in the potential energy is

$$\frac{1}{2}\left(\frac{dy}{dx}\right)^2 q(l - x)dx.$$

The total decrease of the potential energy of the load during buckling then is

$$U_1 = \frac{1}{2}q\int_0^l \left(\frac{dy}{dx}\right)^2 (l - x)dx = \frac{\pi^2 \delta^2 q}{8}\left(\frac{1}{4} - \frac{1}{\pi^2}\right). \tag{c}$$

Substituting expressions (b) and (c) into equation (175), we obtain

$$\frac{\delta^2 q^2 l^3}{2EI}\left(\frac{1}{6} + \frac{9}{\pi^2} - \frac{32}{\pi^3}\right) = \frac{\pi^2 \delta^2 q}{8}\left(\frac{1}{4} - \frac{1}{\pi^2}\right),$$

from which

$$(ql)_{cr} = \frac{7 89EI}{l^2}.$$

The exact solution for this case is

$$(ql)_{cr} = \frac{7.83EI}{l^2} = \frac{\pi^2 EI}{(1.122l)^2}. \tag{178}$$

Thus the error of our approximate solution is less than 1 per cent.

### Problems

1. A prismatical bar with hinged ends, Fig. 129, is submitted to the action of a uniformly distributed load of intensity $q$ and of a central compressive force $P$. Find the critical value of $P$ by assuming for the deflection curve the equation:

$$y = \delta \sin\frac{\pi x}{l}.$$

*Answer.*

$$P_{cr} = \frac{\pi^2 EI}{l^2} - \frac{ql}{2}.$$
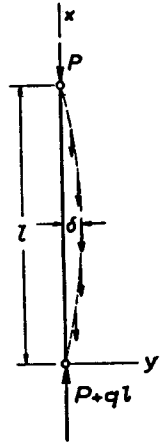
FIG. 129.

### 38. Buckling of Bars of Variable Cross Section.

—A bar of variable cross section symmetrical with respect to the middle and having two axial planes of symmetry is shown in Fig. 130. The middle portion is of uniform cross section with a smaller moment of inertia $I_0$. At the ends the cross section varies and the smaller moments of inertia follow the law:

$$I = I_0\left(\frac{x}{a}\right)^m, \tag{a}$$
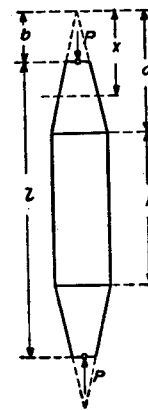
FIG. 130.

in which $x$ and $a$ are distances from a certain fixed point (Fig. 130) and $m$ is a number depending upon the type of column. When the middle portion is a solid cylinder and the ends are solid cones, $I$ varies as the fourth power of $x$ and $m = 4$ in eq. (a). When the column has a constant thickness in the direction perpendicular to the plane of Fig. 130, the moments of inertia $I$ with respect to axes parallel to the plane of the figure are proportional to $x$ and $m = 1$ in eq. (a). When the column consists of four angles connected by lattices, as in Fig. 131, the cross sectional area remains constant and $I$ can be taken proportional to

$x^2$. Then $m = 2$ in eq. (a). Calculations made for $m = 1, 2, 3, 4$, show [16] that the critical load within the elastic limit can be represented by the equation:

$$P_{cr} = \alpha \frac{EI_0}{l^2}, \qquad (179)$$

in which $\alpha$ is a numerical factor depending upon the ratios $h/l$ and $I_1/I_0$, where $I_1 = I_0(b/a)^m$ is the moment of inertia of the end cross sections. Assuming the ends of the column hinged, the magnitudes of $\alpha$ for various proportions are given in the table. It can be seen that as the ratio $h/l$ or the ratio $I_1/I_0$ approaches unity the factor $\alpha$ approaches $\pi^2$ and eq. (179) approaches eq. (167) for a prismatical bar.

TABLE 13.—COEFFICIENT $\alpha$ IN EQ. (179)

| $I_1/I_0$ | $h/l =$ | 0 | 0.2 | 0.4 | 0.6 | 0.8 | 1 |
|---|---|---|---|---|---|---|---|
| 0.1 | $m = 1$ | 6.48 | 7.58 | 8.68 | 9.46 | 9.82 | $\pi^2$ |
| | $m = 2$ | 5.40 | 6.67 | 8.08 | 9.25 | 9.79 | " |
| | $m = 3$ | 5.01 | 6.32 | 7.84 | 9.14 | 9.77 | " |
| | $m = 4$ | 4.81 | 6.11 | 7.68 | 9.08 | 9.77 | " |
| 0.2 | $m = 1$ | 7.01 | 7.99 | 8.91 | 9.63 | 9.82 | " |
| | $m = 2$ | 6.37 | 7.49 | 8.61 | 9.44 | 9.81 | " |
| | $m = 3$ | 6.14 | 7.31 | 8.49 | 9.39 | 9.81 | " |
| | $m = 4$ | 6.02 | 7.20 | 8.42 | 9.38 | 9.80 | " |
| 0.4 | $m = 1$ | 7.87 | 8.60 | 9.19 | 9.70 | 9.84 | " |
| | $m = 2$ | 7.61 | 8.42 | 9.15 | 9.63 | 9.84 | " |
| | $m = 3$ | 7.52 | 8.38 | 9.10 | 9.63 | 9.84 | " |
| | $m = 4$ | 7.48 | 8.33 | 9.10 | 9.62 | 9.84 | " |
| 0.6 | $m = 1$ | 8.60 | 9.12 | 9.55 | 9.74 | 9.85 | " |
| | $m = 2$ | 8.51 | 9.03 | 9.48 | 9.74 | 9.85 | " |
| | $m = 3$ | 8.50 | 9.02 | 9.47 | 9.74 | 9.85 | " |
| | $m = 4$ | 8.47 | 9.01 | 9.45 | 9.74 | 9.85 | " |
| 0.8 | $m = 1$ | 9.27 | 9.54 | 9.69 | 9.83 | 9.86 | " |
| | $m = 2$ | 9.24 | 9.50 | 9.69 | 9.82 | 9.86 | " |
| | $m = 3$ | 9.23 | 9.50 | 9.69 | 9.81 | 9.86 | " |
| | $m = 4$ | 9.23 | 9.49 | 9.69 | 9.81 | 9.86 | " |
| 1 | | $\pi^2$ | $\pi^2$ | $\pi^2$ | $\pi^2$ | $\pi^2$ | " |

[16] See A. Dinnik, Bulletins of Engineers (Westnik Ingenerov), 1927 (Russian). The numerical table below is taken from this paper.

As an example in the application of this table consider a wooden strut 6' 6" long of rectangular cross section. The thickness of the strut remains constant and equal to $\frac{3}{4}$ in. The width varies according to a straight-line law and is 4 in. at the middle and 2.4 in. at the ends. Determine $P_{cr}$ if $E = 1.2 \times 10^6$. In this case $h/l = 0$, $m = 1$ and $I_1/I_0 = 2.4/4 = 0.6$. From the above table $\alpha = 8.60$ and the critical load, from eq. (179), is

$$P_{cr} = 8.60 \frac{1.2 \times 10^6 \times 4 \times 3^3}{4^3 \times 12 \times 78^2} = 239 \text{ lbs.}$$

As a second example let us consider a pyramidal column (Fig. 131) whose square cross section consists of four angles $3\frac{1}{2} \times 3\frac{1}{2} \times \frac{3}{8}$ in. The outside width of the column at the ends is 12 in. and at the middle $20\frac{1}{2}$ inches. The length of the column is 65 feet. Determine the critical load for this column, taking for structural steel $E = 30 \times 10^6$ lbs. per sq. in. and assuming that the lattice bars are rigid enough to allow the application of eq. (179), derived for solid bars. The cross sectional area $A = 2.48 \times 4 = 9.92$ in.; $I_1 = 2.9 \times 4 + 2.48 \times 4 \times (6 - 1.01)^2 = 259$ in.[4]; $I_0 = 2.9 \times 4 + 2.48 \times 4 \times (10.25 - 1.01)^2 = 860$ in.[4]. Taking $I_1 : I_0 = 0.3$, $m = 2$ approximately and $h/l = 0$, we find from the above table by interpolation $\alpha = 7$ approximately. Then, from eq. (179),

$$P_{cr} = 7 \times \frac{30 \times 10^6 \times 860}{65^2 \times 12^2} = 297,000 \text{ lbs.}$$

FIG. 131.

### 39. The Effect of Shearing Force on Critical Load.—In the derivation of the critical load, the differential equation used for the deflection curve (see p. 186) neglected the effect of shearing force on the deflection. When buckling occurs, the cross sections of the bar are no longer perpendicular to the compressive force and there will be shearing forces. The effect of these forces may be found by use of the energy method developed in article 36. In using this method the energy of shear must be added to the energy of bending in calculating the strain energy $U$ due to buckling. Let $AB$ (Fig. 132) represent a solid strut with hinged ends, buckled under the action of compressive force $P$. The
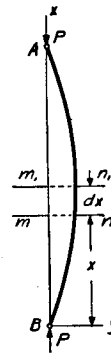
FIG. 132.

magnitudes of the bending moment and the shearing force at any cross section $mn$ are

$$M = Py; \qquad V = P\frac{dy}{dx}. \qquad (a)$$

From previous considerations (see art. 66, Part I) the potential energy stored in an element of the bar is

$$dU = \frac{M^2 dx}{2EI} + \frac{\alpha V^2 dx}{2GA}, \qquad (b)$$

where $A$ is cross sectional area,

$\alpha$ is coefficient depending on the shape of the cross section such that

$\alpha V/GA$ is the magnitude of the shearing strain at the neutral axis (art. 39, Part I).

Accordingly, the displacement of the section $mn$ with respect to $m_1 n_1$, due to this shear, is $(\alpha V/GA)dx$, and the second member on the right side of $(b)$ represents the potential energy of shear stored in the element. By using $(a)$ and $(b)$, the energy stored in the strut during buckling is

$$U = \int_0^l \frac{P^2 y^2 dx}{2EI} + \int_0^l \frac{\alpha P^2}{2GA}\left(\frac{dy}{dx}\right)^2 dx. \qquad (c)$$

The decrease in the potential energy of the load $P$ is

$$U_1 = \frac{P}{2}\int_0^l \left(\frac{dy}{dx}\right)^2 dx. \qquad (d)$$

Assuming that the deflection curve of the buckled strut is a sine curve,

$$y = \delta \sin\frac{\pi x}{l}, \qquad (e)$$

and with this value in $(c)$ and $(d)$

$$U = \delta^2 \frac{P^2 l}{4EI} + \delta^2 \frac{P^2 l}{4GA}\frac{\alpha \pi^2}{l^2}, \qquad (f)$$

$$U_1 = \delta^2 \frac{P\pi^2}{4l}.$$

Substituting in eq. 175 we obtain

$$P_{cr} = \frac{\pi^2 EI}{l^2}\frac{1}{1 + \dfrac{EI}{GA}\dfrac{\alpha\pi^2}{l^2}}. \qquad (g)$$

Comparison with Euler's formula (167) shows that, due to the action of shear, the critical load is diminished in the ratio

$$\frac{1}{1 + \dfrac{EI}{GA}\dfrac{\alpha\pi^2}{l^2}}. \qquad (180)$$

Let

$$\frac{\pi^2 EI}{l^2} = P_e; \qquad \frac{GA}{\alpha} = P_d; \qquad (h)$$

then eq. $(g)$ becomes

$$P_{cr} = P_e \frac{1}{1 + \dfrac{P_e}{P_d}}. \qquad (181)$$

For solid bars, $P_d$ is very large in comparison with $P_e$, and the effect of the shearing force can be neglected. In the case of latticed bars, especially when spacing plates or battens only are used (Fig. 134, $a$), $P_d$ may become of the same order as $P_e$, in which case the effect of shearing force can no longer be neglected. This will now be considered.

**40. Buckling of Latticed Struts.**[17]—Latticed struts are used extensively in steel structures. Their resisting capacities are always less than those of solid columns having the same cross sectional area and the same slenderness ratio $l/k$, and depend greatly on the spacing details such as lattice bars, spacing plates and battens. This lowering of the critical stresses is due principally to the fact that in the case of latticed columns shearing forces produce a much larger effect on deflections than in the case of solid bars. To calculate the

---

[17] See F. Engesser, Zentralblatt d. Bauverw., 1891, p. 483, and 1907, p. 609; L. Prandtl, V. D. I., 1907, and also writer's paper in Bulletin of the Polytechnical Institute at Kiev, 1908. These papers discuss the problem of buckling of latticed struts in connection with the collapse of the Quebec bridge.

effect of shearing force on the critical load, eq. (181), which was derived for solid bars, can be adapted to latticed struts. As before, let $P_e$ be the critical load obtained from eq. (167); $P_d$ in eq. (181) has, in the case of solid struts, a simple physical meaning, namely, that $V/P_d$ represents the additional slope $\gamma$ in the deflection curve produced by shearing forces. $P_d$ has the same meaning also in the case of latticed struts, provided the number of panels is large. To determine $P_d$ in any particular case, therefore, we must investigate the lateral displacements produced by the shearing force.

Consider first one panel of the latticed bar shown in Fig. 133a. The displacement due to shear is that due to the elongation and contraction of the diagonals and battens in each panel (Fig. 133, b). Assuming hinges at the joints, the elongation of the diagonal produced by the shearing force $V$ is $Va/\sin \varphi \cos \varphi E A_d$, in which
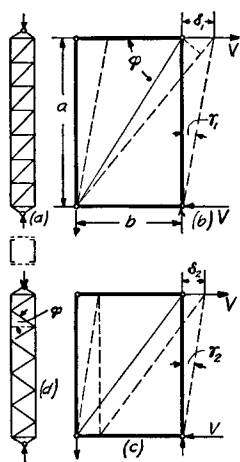
$\varphi$ is the angle between the batten and the diagonal,

$\dfrac{V}{\cos \varphi}$ is the tensile force in the diagonal,

$\dfrac{a}{\sin \varphi}$ is the length of the diagonal,

$A_d$ is the cross sectional area of two diagonals.

Fig. 133.

The corresponding lateral displacement, Fig. 133b, is

$$\delta_1 = \frac{Va}{\sin \varphi \cos^2 \varphi E A_d}. \qquad (a)$$

The shortening of a batten and the corresponding lateral displacement (Fig. 133, c) is

$$\delta_2 = \frac{Vb}{E A_b}, \qquad (b)$$

where

$b$ is the length of the batten,
$A_b$ is the cross sectional area of two battens.

From (a) and (b), the angular displacement produced by the shearing force $V$ is

$$\gamma = \frac{\delta_1 + \delta_2}{a} = \frac{V}{\sin \varphi \cos^2 \varphi E A_b} + \frac{Vb}{a E A_b}.$$

Then using the above definition $V/P_d = \gamma$, we find

$$\frac{1}{P_d} = \frac{1}{\sin \varphi \cos^2 \varphi E A_d} + \frac{b}{a E A_b}.$$

Substituting in eq. (181),

$$P_{cr} = \frac{\pi^2 E I}{l^2} \frac{1}{1 + \dfrac{\pi^2 E I}{l^2} \left( \dfrac{1}{\sin \varphi \cos^2 \varphi E A_d} + \dfrac{b}{a E A_b} \right)}. \qquad (182)$$

If the sectional areas $A_d$ and $A_b$ are very small in comparison with the cross sectional area of the channels (Fig. 133, a), the critical load (182) may be considerably lower than that obtained from Euler's formula (167).

Equation (182) can be used also in the case represented in Fig. 133 (d) if the angle $\varphi$ is measured as shown in the figure and the member due to the deformation of the battens is omitted.

In the case of a strut made with battens alone as in Fig. 134a, to obtain the lateral displacement produced by the shearing force $V$, we must consider the deformation of an element of the strut cut out by the sections $mn$ and $m_1 n_1$. Assuming that the deflection curves of the channels have points of inflection at these sections, the condition of bending will be as shown in Fig. 134 (b).[18] The deflection consists of
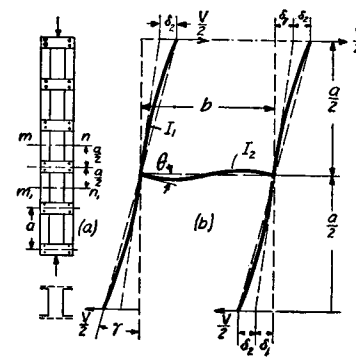
Fig. 134.

[18] The tension and compression forces acting on the cords are not shown in the figure.

two parts: the displacement $\delta_1$ due to bending of the batten, and the displacement $\delta_2$ due to bending of the channels. There are couples $Va/2$ at the ends of the batten and the angle $\theta$ of rotation of these ends of the batten is (see eqs. 103, 104, Part I)

$$\theta = \frac{Va}{2}\frac{b}{3EI_2} - \frac{Va}{2}\frac{b}{6EI_2} = \frac{Vab}{12EI_2},$$

where $b$ is the length of the battens and $EI_2$ is their flexural rigidity. The lateral displacement $\delta_1$ produced by this bending of the battens is

$$\delta_1 = \theta\frac{a}{2} = \frac{Va^2b}{24EI_2}. \qquad (e)$$

The displacement $\delta_2$ can be calculated from the cantilever formula:

$$\delta_2 = \frac{V\left(\frac{a}{2}\right)^3}{2\ 3EI_1} = \frac{Va^3}{48EI_1}. \qquad (d)$$

The total angular displacement produced by the shearing force $V$ is

$$\gamma = \frac{\delta_1 + \delta_2}{\frac{a}{2}} = \frac{Vab}{12EI_2} + \frac{Va^2}{24EI_1};$$

then, since $V/P_d = \gamma$, we obtain

$$\frac{1}{P_d} = \frac{ab}{12EI_2} + \frac{a^2}{24EI_1},$$

and eq. (181) for determining the critical load becomes

$$P_{cr} = \frac{EI\pi^2}{l^2}\frac{1}{1 + \frac{\pi^2EI}{l^2}\left(\frac{ab}{12EI_2} + \frac{a^2}{24EI_1}\right)}, \qquad (183)$$

where, as before, $EI\pi^2/l^2$ represents the critical load calculated from Euler's formula. It may be seen that when the flexural rigidity of the battens is small the actual critical load is much lower than that given by Euler's formula.

From equations (182) and (183) we note that in calculating critical loads for built-up columns the actual length of a column is replaced by *a reduced length* which is to be determined in the case of a latticed column as shown in Fig. 133, from the equation:

$$l_1 = l\sqrt{1 + \frac{\pi^2EI}{l^2}\left(\frac{1}{\sin\varphi\cos^2\varphi\ EA_d} + \frac{b}{aEA_b}\right)}$$

and, in the case of a batten-plate column as shown in Fig. 134, from the equation:

$$l_1 = l\sqrt{1 + \frac{\pi^2EI}{l^2}\left(\frac{ab}{12EI_2} + \frac{a^2}{24EI_1}\right)}.$$

When the reduced length of a built-up column is determined, the allowable stress is obtained as for a solid column with the slenderness ratio equal to $l_1/k$. If the design is made on the basis of the assumed inaccuracies (see art. 56, Part I), the proposed procedure results in a slightly higher factor of safety for built-up columns, which seems completely satisfactory.

In the design of built-up columns the proper dimensioning of the lattice bars and batten plates is of great practical importance. As a basis for determining stresses in these details, an eccentricity in application of compressive forces should be assumed in the design of shorter columns.[19] If the eccentricities at the two ends are equal to $e$ and are in opposite directions, the compressive forces $P$ form a couple of the magnitude $2Pe$ which produces at the ends of the strut the shearing forces:

$$V = \frac{2Pe}{l}. \qquad (184)$$

[19] This question is discussed in more detail in the paper by D. H. Young, Proc. Am. Soc. Civil Eng., December, 1934, and another paper by the same author in Pub. Intern. Assoc. Bridge and Structural Eng., Zürich, vol. 2, 1934, p. 480. See also "Theory of Elastic Stability," p. 197.

The maximum value of $V$ is obtained by substituting in this equation for $P$ the maximum load which the column can carry. The eccentricity $e$ is usually taken as a certain portion of the core radius $r$, say $e/r = 0.3$. The details should then be designed in such a way that the maximum stresses produced in them by $V_{max}$ does not exceed the yield point stress.

In the case of a compressed latticed member of a truss with rigid joints, some bending moments at the ends of the member are produced during loading of the truss. If the magnitudes $M_1$ and $M_2$ of these moments are calculated from the *secondary stresses* analysis, the corresponding eccentricities $e_1 = M_1/P$ and $e_2 = M_2/P$ in application of the compressive force $P$ are known, and the magnitude of their algebraic sum must be substituted in equation (184) instead of $2e$.

**41. Buckling of Circular Rings and Tubes under External Pressure.**—*Buckling of a Circular Ring.* It is well known that a circular ring or tube can collapse due to external pressure alone; and if the flexural rigidity of the ring is insufficient, such a failure can occur at stresses far below the
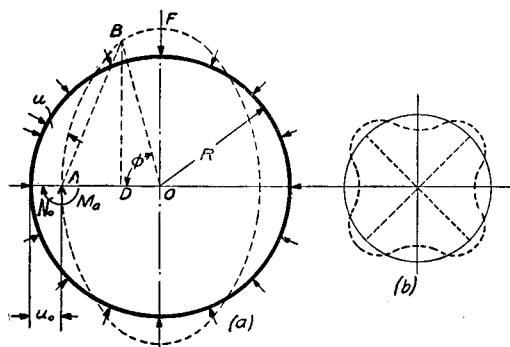


FIG. 135.

elastic limit of the material. This phenomenon must be taken into consideration in such problems as the design of boiler tubes submitted to external pressure and reinforcing rings for submarines.

The pressure at which the circular form becomes unstable

and buckling occurs is known as the critical pressure. Its value will be obtained by use of the general equation (95, p. 103) for the deflection curve.

Assume that under external pressure the ring (Fig. 135) is buckled into an elliptical form as shown by the dotted line. Suppose that

$q$ is external pressure per unit length, of the center line,
$R$ is the radius of the center line of the ring,
$u$ is radial displacements during buckling,
$u_0$ is radial displacement for the cross section $A$,
$M_0$ is bending moment at the cross section $A$,
$N_0 = q(R - u_0)$ is longitudinal compressive force at the cross section $A$.

The bending moment at any cross section $B$ of the buckled ring is

$$M = M_0 + q\overline{AO}\,\overline{AD} - \frac{q}{2}\,\overline{AB}^2. \qquad (a)$$

Now, in the triangle $AOB$,

$$\overline{OB}^2 = \overline{AB}^2 + \overline{AO}^2 - 2\overline{AO}\,\overline{AD}$$

or

$$\tfrac{1}{2}\overline{AB}^2 - \overline{AO}\,\overline{AD} = \tfrac{1}{2}(\overline{OB}^2 - \overline{AO}^2)$$
$$= \tfrac{1}{2}[(R - u)^2 - (R - u_0)^2].$$

Since $u$ is small in comparison to $R$, terms in $u^2$ or $u_0^2$ can be neglected, whence

$$\tfrac{1}{2}\overline{AB}^2 - \overline{AO}\,\overline{AD} = R(u_0 - u).$$

Substituting this value in equation $(a)$, we obtain

$$M = M_0 - qR(u_0 - u).$$

Equation (95), page 103, becomes

$$\frac{d^2u}{d\varphi^2} + u = -\frac{R^2}{EI}[M_0 - qR(u_0 - u)]$$

or

$$\frac{d^2u}{d\varphi^2} + u\left(1 + \frac{qR^3}{EI}\right) = \frac{-M_0R^2 + qR^3u_0}{EI}. \qquad (b)$$

The general solution of this equation is

$$u = C_1 \sin p\varphi + C_2 \cos p\varphi + \frac{- M_0 R^2 + q R^3 u_0}{EI + qR^3}, \quad (c)$$

in which $C_1$ and $C_2$ are constants to be determined from the conditions at the cross sections $A$ and $F$ of the buckled ring, and

$$p^2 = 1 + \frac{qR^3}{EI}. \quad (d)$$

From symmetry, it follows that

$$\left(\frac{du}{d\varphi}\right)_{\varphi=0} = 0; \qquad \left(\frac{du}{d\varphi}\right)_{\varphi=\pi/2} = 0. \quad (e)$$

From the first of these conditions $C_1 = 0$ and from the second,

$$\sin \frac{p\pi}{2} = 0. \quad (f)$$

The smallest root of this equation is

$$\frac{p\pi}{2} = \pi$$

or

$$p = 2.$$
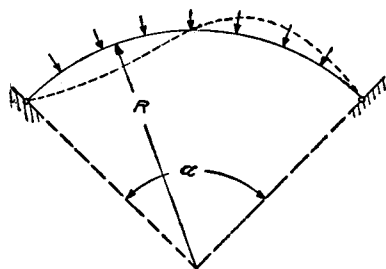


Substituting this in $(d)$, we obtain the value for the critical pressure [20]

$$q_{cr} = \frac{3EI}{R^3}. \quad (185)$$

Other roots of the eq. $(f)$ such as $p\pi/2 = 2\pi$, $p\pi/2 = 3\pi$, etc., correspond to a larger number of waves in the buck-

FIG. 136.

led ring and give greater values for the pressure $q$. Figure 135 $(b)$ shows, for instance, the buckled form for $p\pi/2 = 2\pi$.

[20] This problem was solved by M. Bresse, "Cours de Mécanique Appliquée," Part I, p. 334. Paris, 1866.

These higher forms of buckling are of interest in studying the stability of short cylindrical tubes with fastened ends.

*Buckling of a Circular Arch.*—If a circular arch having hinged ends be submitted to uniform pressure, it can buckle as indicated by the dotted line in Fig. 136. The critical value of the pressure depends upon the magnitude of the angle $\alpha$ and may be calculated from the equation: [21]

$$q_{cr} = \frac{EI}{R^3}\left(\frac{4\pi^2}{\alpha^2} - 1\right). \quad (186)$$

The problem of the buckling of a ring in the direction perpendicular to its plane has also been solved.[22]

*Buckling of Circular Tubes.*—The theory of buckling developed above for a circular ring can also be used in the case of a long circular tube submitted to uniform external pressure. Consider an elementary ring cut out of the tube by two cross sections unit distance apart. The moment of inertia of the cross section of this ring is

$$I = \frac{1 \cdot h^3}{12},$$

where $h$ denotes the thickness of the wall of the tube. Since the cross section of the ring will not be distorted during bending,

$$\frac{E}{1 - \mu^2}$$

must be used instead of $E$. Equation (185), for calculating the critical pressure, becomes

$$p_{cr} = \frac{Eh^3}{4(1 - \mu^2)R^3}. \quad (187)$$

[21] See author's paper on the stability of elastic systems, Bulletin of the Polytechnical Institute in Kiev, 1910. French translation, Annales des Ponts et Chaussées, 1913. See also E. Hurlbrink, Schiffbau, Vol. 9, p. 640, 1907–1908; E. Chwalla and C. F. Kollbrunner, "Der Stahlbau," 1937 and 1938; and the recent book by A. N. Dinnik, "Buckling of Bars," Moscow, 1939.

[22] See E. L. Nicolai, Zeitschr. f. Angew. Math. u. Mech., Vol. 3, p. 227, 1923. See also author's paper, Zeitschr. f. Angew. Math. u. Mech., Vol. 3, p. 358, 1923.

This equation may be used as long as the corresponding compressive stress in the tube is less than the proportional limit of the material. Beyond the elastic limit the true critical pressure will be less than that obtained from (187) and the following equation may be used: [23]

$$p_{cr} = \frac{h}{R} \frac{\sigma_{Y.P.}}{1 + 4\frac{\sigma_{Y.P.}}{E}\frac{R^2}{h^2}},\qquad (188)$$

in which $\sigma_{Y.P.}$ denotes the yield point of the material in compression. As the thickness reduces, the critical pressure approaches the limiting value $Eh^3/4R^3$, which is slightly less than that given by eq. (187) and in all cases its value is less than $h\sigma_{Y.P.}/R$, i.e., less than the pressure corresponding to the yield point.[24]

The failure of tubes under uniform external pressure depends very much upon the various kinds of imperfections in them. The most important imperfection is an initial ellipticity, the limiting value of which in each type of tube is usually well-known from numerous inspection measurements. Hence it seems desirable to have a design formula in which this initial ellipticity appears explicitly. To derive such a formula [25] let us assume that the initial deviation of the shape of the tube from the perfect circular form, indicated by the dotted line in Fig. 137, is given by the equation:

$$u_1 = u_0 \cos 2\varphi,\qquad (a)$$

in which $u_0$ is the maximum initial radial deviation, which is considered small in comparison with $R$, and $\varphi$ is the central angle measured as shown in the figure. The initial shape of

[23] See R. V. Southwell, Phil. Mag., Vol. 29, p. 67, 1915.

[24] Experiments on the collapse of short tubes by external pressure are described by G. Cook, Phil. Mag., p. 51, 1914. For bibliography on the subject by the same author see Brit. Assoc. Rep. (Birmingham), 1913.

[25] See writer's paper, Trans. A. S. M. E., Journal of Applied Mechanics, vol. 1, 1933, p. 173.

the tube is then represented by the full line in Fig. 137. If on such a non-circular tube an external pressure $p$ is applied, a further flattening of the tube occurs. Denoting the radial displacements corresponding to the later flattening by $u_2$ and considering an elemental ring of unit width, we obtain from equation (95):

$$\frac{d^2u_2}{d\varphi^2} + u_2 = -\frac{1}{D}MR^2\qquad (b)$$

where

$$D = \frac{Eh^3}{12(1-\mu^2)}$$

is the flexural rigidity of the elemental ring. Regarding the bending moment $M$, we see that owing to pressure $p$, the decrease in curvature occurs in the portions $AB$ and $CD$ of the elemental ring, hence $M$ is positive there, while in the remaining portions of the ring the moment is negative. At points $A$, $B$, $C$ and $D$ the bending moment is zero, and the interaction between the parts of the elemental ring is given by forces $S$ tangential to the dotted circle representing the ideal shape of the tube.[26] This circle can be considered as a funicular curve for the external uniform pressure $p$. The compressive force along this curve remains constant and equal to $S = pR$. Thus the bending moment at any cross section is obtained by multiplying $S$ by the total radial deviation $u_1 + u_2$ at this cross section. Then



Fig. 137.

$$M = pR(u_2 + u_0 \cos 2\varphi),\qquad (c)$$

and equation (b) becomes

$$\frac{d^2u_2}{d\varphi^2} + u_2 = -\frac{1}{D}pR^3(u_2 + u_0 \cos 2\varphi)$$
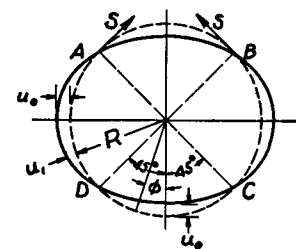
[26] The action of forces $S$ on the portion $AB$ of the ring is shown in the figure.

or

$$\frac{d^2u_2}{d\varphi^2} + u_2\left(1 + p\frac{R^3}{D}\right) = -\frac{1}{D}pR^3u_0\cos 2\varphi.$$

The solution of this equation satisfying the conditions of continuity at the points $A$, $B$, $C$, and $D$ is

$$u_2 = \frac{u_0p}{p_{cr} - p}\cos 2\varphi,\qquad(189)$$

in which $p_{cr}$ is given by formula (187). It is seen that at the points $A$, $B$, $C$ and $D$ the displacement $u_2$ and its second derivative vanish. Hence the bending moments at these points are zero, as was previously assumed. The maximum bending moment occurs at $\varphi = 0$ and $\varphi = \pi$ where

$$M_{max} = pR\left(u_0 + \frac{u_0p}{p_{cr} - p}\right) = \frac{pu_0R}{1 - \dfrac{p}{p_{cr}}}.\qquad(190)$$

It is seen that for small values of the ratio $p/p_{cr}$ the change in the ellipticity of the tube due to pressure $p$ can be neglected, and that the maximum bending moment is obtained by multiplying the compressive force $S = pR$ by the initial deviation $u_0$. If the ratio $p/p_{cr}$ is not small, the change in the initial ellipticity of the tube must be considered, and equation (190) must be used in calculating $M_{max}$.

The maximum compressive stress is now obtained by adding the maximum compressive stress due to bending moment $M_{max}$ to the stress produced by the compressive force $pR$. Thus we find:

$$\sigma_{max} = \frac{pR}{h} + \frac{6pRu_0}{h^2}\cdot\frac{1}{1 - \dfrac{p}{p_{cr}}}.\qquad(d)$$

The dangerous value of the pressure $p$ is that value at which the yielding of the material begins. Denoting this value by

$p_{Y.P.}$ and substituting $\sigma_{Y.P.}$ for $\sigma_{max}$, we obtain

$$\sigma_{Y.P.} = \frac{p_{Y.P.}R}{h} + \frac{6p_{Y.P.}Ru_0}{h^2}\cdot\frac{1}{1 - \dfrac{p_{Y.P.}}{p_{cr}}}\qquad(e)$$

from which the value of the dangerous pressure $p_{Y.P.}$ can be calculated if $\sigma_{Y.P.}$ and initial deviation $u_0$ are known. By using the notations

$$\frac{R}{h} = m\qquad\text{and}\qquad\frac{u_0}{R} = n,\qquad(f)$$

the equation ($e$) for calculating $p_{Y.P.}$ becomes

$$p^2_{Y.P.} - \left[\frac{\sigma_{Y.P.}}{m} + (1 + 6mn)p_{cr}\right]p_{Y.P.} + \frac{\sigma_{Y.P.}p_{cr}}{m} = 0.\qquad(191)$$

From this equation the curves can be plotted giving the average compressive stress $p_{Y.P.}R/h$ as a function of $R/h$ for various values of the ratio $u_0/R$ and for various values of $\sigma_{Y.P.}$. By using such curves, together with a proper factor of safety, the suitable wall thickness of a pipe can be readily calculated. It should be noted that the pressure $p_{Y.P.}$ determined in this manner is smaller than the pressure at which the complete collapsing of the tube occurs; hence by using $p_{Y.P.}$ as the ultimate value of pressure, we are always on the safe side.

In our preceding discussion it was assumed that the length of the tube $l$ is large in comparison with its radius, say $l/R > 20$. For shorter tubes, if the edges are built-in or supported, the value of $p_{cr}$ is larger than that given by equation (187) and depends on the ratio $l/R$. The theory of buckling of such tubes is more complicated,[27] since the tube subdivides during buckling in several waves along the circumference and the number of these waves depends on the ratio $l/R$.[28]

---

[27] For discussion of this problem see writer's "Theory of Elastic Stability," p. 445.

[28] Some curves for calculating critical pressures on short tubes are prepared by the Research Committee on the Strength of Vessels under External Pressure, A. S. M. E., December 1933.

The problem of the buckling of tubes closed at the ends and submitted to uniform pressure on both the ends and the sides [29] has also been solved.[30]
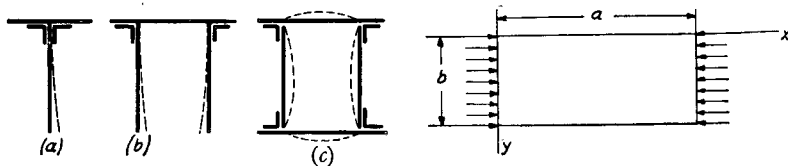


FIG. 138.



FIG. 139.

**42. Buckling of Rectangular Plates.**—The problem of buckling of compressed rectangular plates is of a practical importance in discussing elastic stability of compression members built up of plates such as we often encounter in steel structures, Fig. 138. A failure of such members may be brought about by buckling of the web or of the sides, instead of by buckling of the member as a whole. For example, in the cases shown in Fig. 138 such buckling of the plates as is indicated by the dotted lines may occur if the thickness of the plate is not satisfactorily chosen. Since the length of a compression member is usually large in comparison with the cross-sectional dimensions, the problem reduces to that of buckling of a long compressed plate, Fig. 139. The short sides of the plate can be considered as simply supported; the conditions along the other two sides depend on the shape of the cross section. For example, if a tubular section, shown in Fig. 138c, has a square form, and the side plates are all of the same thickness, they have the tendency to buckle simultaneously, and each side can be considered as a compressed rectangular plate, all four sides of which are simply supported. In the cases shown in Figs. 138a and 138b, the

---

[29] We have such a condition in the investigation of the stability of the hull of a submarine between two reinforcing rings.

[30] See paper by R. v. Mises in Festschrift von Prof. A. Stodola, Zürich, 1929.

lower edges of the vertical webs are free and the upper are elastically built-in.[31]

Rigorous solutions of the buckling problem for various conditions along the longitudinal sides of a plate such as shown in Fig. 139 have been worked out.[32] We give here only the values of the critical stresses obtained from these solutions.

*Rectangular plate supported on four sides* under uniform compression in the direction of the $x$ axis (Fig. 139) buckles by subdividing into squares or rectangles which approximate squares.

The critical value of the compressive stress is given by the equation: [33]

$$\sigma_{cr} = \beta \sigma_e, \tag{192}$$

in which

$$\sigma_e = \frac{\pi^2 E h^2}{12 b^2 (1 - \mu^2)}, \tag{193}$$

$h$ is the thickness of the plate, $b$ its width.

$$\beta = \left( \frac{a}{mb} + \frac{mb}{a} \right)^2 \tag{a}$$

denotes a coefficient depending upon the magnitude of the ratio $a/b$ and the integer $m$, the number of waves into which the plate divides in buckling. This later must be so chosen as to make $\beta$ a minimum.[34] Several values of this coefficient are given in table 14.

---

[31] First experiments in which the question of buckling of the thin-walled structures was discussed were made by William Fairbairn and were described in his book, "Britannia and Conway Tubular Bridges," London, 1849.

[32] See "Theory of Elastic Stability," 1936.

[33] The solution of this problem is due to G. H. Bryan; see London Math. Soc. Proc., Vol. XXII, p. 54, 1891. Other cases of buckling of rectangular plates were considered by the writer. See author's papers: (1) On the stability of compressed plates, Bull. of the Polyt. Inst. in Kiev, 1907; (2) Z. f. Mathematik und Physik, Vol. 58, 1910; (3) Der Eisenbau, Vol. 12, 1921; Proceedings Am. Soc. C. E., Vol. 55, 1929, p. 855. See also H. Reissner, Zentralbl. d. Bauverw. (Berlin), p. 93, 1909.

[34] It may be seen that this minimum is equal to 4 and occurs when $a = mb$, i.e., when the plates subdivide during buckling in squares.

TABLE 14.—CONSTANTS FOR CALCULATING CRITICAL COMPRESSIVE STRESS FOR SIMPLY SUPPORTED RECTANGULAR PLATES

| $a/b =$ | 0.4 | 0.6 | 0.8 | 1.0 | 1.2 | 1.4 | 1.6 |
|---|---|---|---|---|---|---|---|
| $\beta =$ | 8.41 | 5.14 | 4.20 | 4.00 | 4.13 | 4.47 | 4.20 |
| $\sigma_{cr} =$ | 22,800 | 14,000 | 11,400 | 10,900 | 11,200 | 12,100 | 11,400 |

| $a/b =$ | 1.8 | 2.0 | 2.2 | 2.4 | 2.7 | 3 |
|---|---|---|---|---|---|---|
| $\beta =$ | 4.04 | 4.00 | 4.04 | 4.13 | 4.04 | 4.00 |
| $\sigma_{cr} =$ | 11,000 | 10,900 | 11,000 | 11,200 | 11,000 | 10,900 |

For longer plates $(a/b > 3)\beta = 4$ is always a good approximation. The values of $\sigma_{cr}$ given in the above table are calculated on the assumption that $E = 30 \times 10^6$ lbs. per sq. in., $\mu = 0.3$ and $h/b = 0.01$. The critical stress for any other value of the ratio $h/b$ can be obtained by multiplying the tabular values by $10^4(h^2/b^2)$. To illustrate, consider a long steel plate having a yield point stress of 40,000 lbs. per sq. in.; suppose we wish to determine the value of the ratio $b/h$ at which the critical stress is equal to the yield point stress. Assuming $\beta = 4$ and using Table 14,

$$\sigma_{cr} = 10,900 \times 10^4 \times \frac{h^2}{b^2} = 40,000 \text{ lbs. per sq. in.,}$$

from which

$$\frac{b}{h} = 52.2. \tag{b}$$

For larger values of the ratio $b/h$ failure occurs by buckling at a compressive stress smaller than the yield point of the material.

TABLE 15.—CONSTANT $\beta$ FOR CALCULATING CRITICAL COMPRESSIVE STRESS FOR A RECTANGULAR PLATE WITH THREE SUPPORTED EDGES AND THE FOURTH ($y = b$) FREE

| $a/b =$ | 0.5 | 1.0 | 1.2 | 1.4 | 1.6 | 1.8 | 2.0 | 2.5 | 3.0 | 4.0 | 5.0 |
|---|---|---|---|---|---|---|---|---|---|---|---|
| $\beta =$ | 4.40 | 1.440 | 1.135 | 0.952 | 0.835 | 0.755 | 0.698 | 0.610 | 0.564 | 0.516 | 0.506 |

Under such condition the critical stress and not the yield point of the material must be taken as the basis for determining working stress.

*Three Sides of the Plate Supported and the Fourth Free.* If one

of the longitudinal edges such as $y = b$ (see Fig. 139) is free, the previous equation (192) can be used for calculating the critical values of the compressive stress, taking the values of the coefficient $\beta$ from the table 15.

*Two Opposite Sides Simply Supported, the Third Built-In, and the Fourth Free.* The sides $x = 0$, $x = a$ in Fig. 139 are considered as simply supported and side $y = 0$ as built-in. The same equation (192) can be used. The values of the coefficient $\beta$ are given in Table 16.

TABLE 16.—CONSTANT $\beta$ FOR CALCULATING CRITICAL COMPRESSIVE STRESS FOR A RECTANGULAR PLATE WITH TWO OPPOSITE SIDES SIMPLY SUPPORTED, THE THIRD BUILT-IN, AND THE FOURTH ($y = b$) FREE

| $a/b =$ | 1.0 | 1.1 | 1.2 | 1.3 | 1.4 | 1.5 | 1.6 | 1.7 | 1.8 | 1.9 | 2.0 | 2.2 | 2.4 | 2.6 | 2.8 | 3 |
|---|---|---|---|---|---|---|---|---|---|---|---|---|---|---|---|---|
| $\beta =$ | 1.70 | 1.56 | 1.47 | 1.41 | 1.36 | 1.34 | 1.33 | 1.33 | 1.34 | 1.36 | 1.38 | 1.45 | 1.47 | 1.41 | 1.36 | 1.34 |

For larger values of the ratio $a/b$, a good approximation is $\beta = 1.33$.

*Two Opposite Sides Simply Supported and Other Two Built-In.*[35] The sides $x = 0$ and $x = a$ are considered simply supported. The corresponding values of the coefficient $\beta$ in eq. (192) are given in the table below:

TABLE 17.—CONSTANT $\beta$ FOR CALCULATING CRITICAL COMPRESSIVE STRESS FOR A RECTANGULAR PLATE, TWO OPPOSITE SIDES OF WHICH ARE SIMPLY SUPPORTED, AND TWO OTHERS BUILT-IN

| $a/b =$ | 0.4 | 0.5 | 0.6 | 0.7 | 0.8 | 0.9 | 1.0 | 1.2 | 1.4 | 1.6 | 1.8 | 2.1 |
|---|---|---|---|---|---|---|---|---|---|---|---|---|
| $\beta =$ | 9.44 | 7.69 | 7.05 | 7.00 | 7.29 | 7.83 | 7.69 | 7.05 | 7.00 | 7.29 | 7.05 | 7.00 |

*Rectangular Plate Supported on Four Sides and Submitted to the Action of Shearing Stresses Uniformly Distributed along the Sides (Fig. 140).* The critical value of the shearing stress which may produce buckling of the plate is
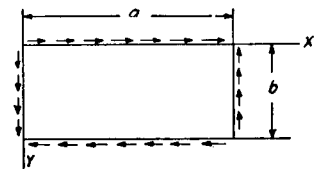


FIG. 140.

$$\tau_{cr} = \beta\sigma_e. \tag{194}$$

[35] Such condition we have when the two opposite sides of the compressed member, shown in Fig. 138c, are very rigid and only the other two may buckle.

The values of the numerical coefficient $\beta$ are given in the table below.

TABLE 18.—CONSTANT $\beta$ FOR CALCULATING CRITICAL STRESS FOR A RECTANGULAR PLATE SUPPORTED ON FOUR SIDES AND SUBMITTED TO THE ACTION OF A UNIFORM SHEAR

| $a/b =$ | 1 | 1.2 | 1.4 | 1.5 | 1.6 | 1.8 | 2.0 | 2.5 | 3 | $\infty$ |
|---|---|---|---|---|---|---|---|---|---|---|
| $\beta =$ | 9.42 | 8.0 | 7.3 | 7.1 | 7.0 | 6.8 | 6.6 | 6.3 | 6.1 | 5.4 |

This table can be used in choosing the thickness of the web of a plate girder. Near the supports the shearing force is the most important factor. Therefore the part of the web between two stiffeners may be considered as a rectangular plate with supported edges, subjected only to the action of shearing stresses. For instance, if the distance between the stiffeners is 5 ft., $E = 30 \times 10^6$ lbs. per sq. in. and $\mu = 0.3$, the following values of critical stress in lbs. per sq. in. are obtained for girders of thickness $h$ and depth $b$ by using the above table: [36]

TABLE 19

| $b$ | $h = 3/8''$ | $h = 7/16''$ | $h = 1/2''$ | $h = 9/16''$ |
|---|---|---|---|---|
| 5' | 9,980 | 13,600 | 17,700 | 22,400 |
| 7' | 7,730 | 10,500 | 13,700 | 17,400 |
| 10' | 6,990 | 9,510 | 12,400 | 15,700 |

The necessary thickness of steel plates to be used in the built-up compression members whose sections are shown in Fig. 138 can be obtained from Tables 14–19. If the sides of the hollow section (Fig. 138, $c$) are considered to be long rectangular plates simply supported, the critical compressive stress is then

$$\sigma_{cr} = 4\sigma_e = \frac{\pi^2 h^2}{3 b^2} \frac{E}{1 - \mu^2}. \qquad (c)$$

[36] More data regarding the buckling of the web and design of stiffeners are given in the writer's papers, Proc. Am. Soc. C. E., Vol. 55 (1929), p. 855, "Engineering," Vol. 138, p. 207, 1934. See also E. Chwalla, Reports Second Congress International Assoc. for Bridge and Structural Eng., Berlin, 1936; "Der Stahlbau," 1936, Heft, 21 and 22.

Taking, for instance, $h/b = 0.01$, we find

$$\sigma_{cr} = 10,900 \text{ lbs. per sq. in.}$$

This stress is far below the proportional limit of structural steel. If the longitudinal edges of the same plate are assumed to be built in, we find

$$\sigma_{cr} = 7\sigma_e = \frac{7}{4} 10,900 = 19,100 \text{ lbs. per sq. in.}$$

In cases ($a$) and ($b$) (Fig. 138) the compressed vertical steel plates may be considered as long plates built-in [37] along the upper edge and free along the lower edge. The critical stress is therefore

$$\sigma_{cr} = 1.33\sigma_e = \frac{1.33\pi^2}{12} \frac{h^2}{b^2} \frac{E}{1 - \mu^2}. \qquad (d)$$

Again the stability of the plate depends on the magnitude of the ratio $b/h$. Assuming that the yield point of structural steel is 30,000 lbs. per sq. in., the value of $b/h$ which makes $\sigma_{cr}$ equal to this stress is, from ($d$),

$$\frac{b}{h} = \sqrt{\frac{1.33\pi^2}{12 \times 30,000} \times \frac{30 \times 10^6}{0.91}} \approx 35.$$

Consequently, if $b/h > 35$, the critical stress becomes less than yield point of the material. This fact must be considered in choosing the magnitude of working stress. The stability of the plate can be increased by reinforcing the free edge of the plate.

In all the above cases it was assumed that the critical stress is below the proportional limit. For stresses beyond the proportional limit our equations give exaggerated values of the critical stresses. [38]

**43. Buckling of Beams without Lateral Supports.**—It is well known that, in the absence of lateral supports, I beams loaded in the plane of the web may prove to be insufficiently stable in a lateral direction. If the load is increased beyond a certain *critical limit*, such beams buckle sidewise, and further loading causes them

[37] This assumption gives an upper limit for the critical stress. The true critical stress will be somewhat lower, due to the fact that the fastening of the upper edge is not absolutely rigid.

[38] This question is discussed in "Theory of Elastic Stability," p. 384, 1936.

to collapse.[39]   The energy method may be used to determine this limit.

As an illustration consider a beam $AB$ (Fig. 141) of narrow rectangular cross section with a central concentrated load $P$ acting in the longitudinal vertical plane of symmetry.  If this force is
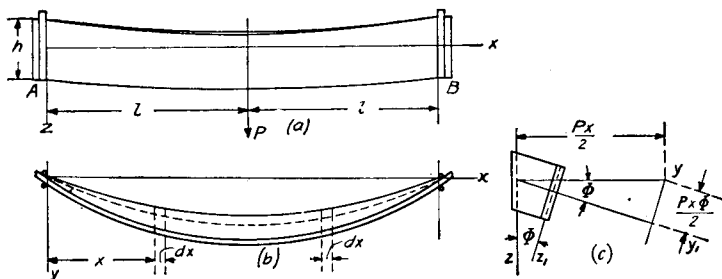


FIG. 141.

small, the deflection of the beam is in the vertical plane only and this plane form of bending is a stable one.  If the beam is deflected sidewise by a lateral force, this deflection disappears with the removal of the force and the beam returns to its initial form.  If $P$ is increased, a limiting value is reached at which the plane form of bending becomes unstable.  The beam then buckles sidewise and large lateral deflections may occur with a very small increase of the load.  This limiting value of $P$ is called the *critical load*.  It is determined by considering the potential energy of the system.  Any lateral deflection of the beam is accompanied by an increase of the strain energy.  Since after a small lateral buckling we have not only the strain energy of bending in the vertical plane, which may be considered unchanged, but also strain energy of bending in the lateral direction and strain energy of twist.  At the same time, the potential energy of the load diminishes, because sidewise buckling

[39] The collapse of girders as a consequence of sidewise buckling is illustrated by the bridge disaster near Tarbes, France.  See La Revue Technique, November 15, 1897.  The lateral buckling of beams of a narrow rectangular cross section was discussed by L. Prandtl, Dissertation, Nürnberg, 1899, and A. G. M. Michell, Phil. Mag., Vol. 48, 1899. Buckling of I beams was discussed by the writer; see Bulletin of the Polytechnical Institute, St. Petersburg, Vols. 4 and 5, 1905, 1906.  See also Annales des Ponts et Chaussées, 1913, and Transactions Amer. Soc. C. E., Vol. 87 (1924), p. 1247.  The practical application of the theory is discussed by E. Chwalla, "Die Kipp-Stabilität gerader Träger mit doppelt-symmetrischem I-Querschnitt," Berlin, 1939.

is accompanied by a lowering of its point of application.  Let $U_1$ denote this decrease in the potential energy of the load, $U$ the strain energy due to bending in the lateral direction, and $U_2$ that due to twist.  Then the critical load is determined by eq. (175) (p. 200), which becomes

$$U + U_2 = U_1. \tag{a}$$

We must now calculate the quantities entering into this equation. The bending moment in the vertical plane at any cross section a distance $x$ from the left support (see Fig. 141) is $Px/2$.  In calculating sidewise buckling, the bending moment with respect to the $z_1$ axis (Fig. 141, c) must be considered.  This moment is equal to $(Px/2)\varphi$, in which $\varphi$ denotes the small angle of twist, variable along the length of the beam.  Then for small lateral deflection [40] we have the following differential equation:

$$EI_z \frac{d^2y}{dx^2} = -\frac{Px}{2}\varphi. \tag{b}$$

The corresponding strain energy of bending is

$$U = EI_z \int_0^l \left(\frac{d^2y}{dx^2}\right)^2 dx = \frac{P^2}{4EI_z}\int_0^l x^2\varphi^2 dx. \tag{c}$$

The strain energy of twist is (see eq. 210, Part I)

$$U_2 = C \int_0^l \left(\frac{d\varphi}{dx}\right)^2 dx, \tag{d}$$

in which the torsional rigidity $C$ for a rectangular cross section is obtained from eq. (156), Part I.

Let us consider now the lowering of the point of application of the load $P$ due to the lateral deflection.  Take two symmetrically situated elements $dx$ of the beam (Fig. 141, b and c) and consider the effect of the bending in the plane $xy_1$ of these two elements only. The angular deflection due to this bending is equal to $-(d^2y/dx^2)dx$. As this bending occurs in the plane $xy_1$ inclined at an angle $\varphi$ to the horizontal (Fig. 141, c), it causes a lowering of the load $P$ equal to $-x\varphi(d^2y/dx^2)dx$.  The total lowering of $P$ due to such bending of all the elements of the beam in buckling is therefore

$$\delta = -\int_0^l x\varphi \frac{d^2y}{dx^2} dx,$$

[40] In this case it is legitimate to take $d^2y/dx^2$ for the curvature instead of $d^2y_1/dx^2$.

or, using eq. (b),

$$\delta = \frac{P}{2EI_z} \int_0^l x^2 \varphi^2 dx.$$

Hence

$$U_1 = P\delta = \frac{P^2}{2EI_z} \int_0^l x^2 \varphi^2 dx. \qquad (e)$$

Substituting (c), (d) and (e) in eq. (a), we find

$$P_{cr}^2 = \frac{4EI_z C \int_0^l \left(\frac{d\varphi}{dx}\right)^2 dx}{\int_0^l x^2 \varphi^2 dx}. \qquad (f)$$

By taking for the angle of twist $\varphi$ a suitably chosen function of $x$ to satisfy the end conditions we obtain an approximate value of the critical load from eq. (f). Assume, for instance, that

$$\varphi = a \sin \frac{\pi x}{2l}. \qquad (g)$$

This function is zero at the ends of the beam, where the angle of twist is zero, and is a maximum at the middle ($x = l$). Substituting (g) in eq. (f), we find [41]

$$P_{cr} = \frac{17.2\sqrt{CEI_z}}{(2l)^2}. \qquad (195)$$

The critical value of the load thus depends upon the product of the torsional and lateral flexural rigidities of the beam.

It was assumed that the load $P$ is applied at the centroid of the middle cross section of the beam. If the point of application is at a distance $a$ above the centroid, the right side of eq. (195) must be multiplied by $[1 - 1.74(a/2l)\sqrt{EI_z/C}]$.[42]

If the load is uniformly distributed along the central axis of the beam (Fig. 141), its critical value is

$$(2ql)_{cr} = \frac{28.3\sqrt{CEI_z}}{(2l)^2}. \qquad (196)$$

For a cantilever of length $l$ loaded at the center of the free end, the

[41] A more detailed investigation shows that the error of this approximate solution is about $1\frac{1}{2}$ per cent. Hence eq. (195) is accurate enough for applications.

[42] See writer's paper in Annales des Ponts et Chaussées, 1913. See also "Theory of Elastic Stability," p. 254, 1936.

critical load is

$$P_{cr} = \frac{4.01\sqrt{CEI_z}}{l^2}. \qquad (197)$$

In the case of an I beam, the equations for the critical loads have the form obtained above for a beam of narrow rectangular cross section except that the numerical factor in the numerator on the right side is not a constant but depends upon the magnitude of the expression: [43]

$$\alpha = \frac{C}{EI_z}\left(\frac{2l}{h}\right)^2. \qquad (h)$$

For instance, if an I beam is supported as shown in Fig. 141 and uniformly loaded along the central axis of the beam, the critical value of the total distributed load is

$$(2ql)_{cr} = \frac{\beta\sqrt{CEI_z}}{(2l)^2}. \qquad (198)$$

The magnitudes of the coefficient $\beta$ for various values of the ratio $\alpha$ are given in the table.

TABLE 20.—CRITICAL STRESSES, IN TERMS OF THE CONSTANT $\alpha$, FOR $\gamma = 0.0001$ AND $E = 30,000,000$ LBS. PER SQ. IN., UNIFORM LOAD (STRESSES IN POUNDS PER SQUARE INCH)

| $\alpha =$ | 0.1 | 1 | 2 | 4 | 6 | 8 | 12 |
|---|---|---|---|---|---|---|---|
| $\beta =$ | 143.0 | 53.0 | 42.6 | 36.3 | 33.8 | 32.6 | 31.5 |
| $\sigma_{cr} =$ | 8,520 | 9,950 | 11,300 | 13,600 | 15,600 | 17,300 | 20,300 |
| $\sigma_{cr}' =$ | 5,510 | 6,810 | 8,070 | 10,300 | 12,200 | 13,800 | 16,800 |
| $\sigma_{cr}'' =$ | 13,200 | 14,500 | 15,800 | 18,000 | 20,000 | 21,500 | 24,500 |
| $\alpha =$ | 16 | 20 | 32 | 50 | 70 | 90 | 100 |
| $\beta =$ | 30.5 | 30.1 | 29.4 | 29.0 | 28.8 | 28.6 | 28.6 |
| $\sigma_{cr} =$ | 23,000 | 25,200 | 31,200 | 38,600 | 45,300 | 51,000 | 53,700 |
| $\sigma_{cr}' =$ | 19,400 | 21,600 | 27,600 | 35,000 | 41,600 | 47,400 | 50,000 |
| $\sigma_{cr}'' =$ | 27,200 | 29,400 | 35,300 | 42,600 | 49,200 | 55,100 | 57,600 |

It will be seen that as $\alpha$ increases the constant $\beta$ approaches the magnitude given before for a beam of rectangular cross section. In the third line of the table the magnitudes of the corresponding

[43] Torsional rigidity $C$ of I-beams is discussed in art. 51, p. 275.

values of the critical bending stresses are given, calculated on the assumption that the quantity

$$\gamma = \frac{I_z}{I_y}\left(\frac{h}{2l}\right)^2 = 0.0001. \tag{k}$$

Here $I_z/I_y$ is the ratio of lateral and vertical flexural rigidities, and $h/2l$ is the ratio of the depth of the beam to its span. For any other proportions of the beam the critical stresses are obtained by multiplying the figures of the third line by the number $10^4\gamma$.

The fourth and the fifth lines of this table give the critical stress when the load is applied to the upper or to the lower flange of the beam respectively. All calculations are made assuming perfect elasticity of the material.[44] Consider as an example a structural beam of the following dimensions:

$$
\begin{aligned}
&\text{Length } 2l = 20 \text{ ft.}\\
&\text{Depth } h = 24 \text{ in.}\\
&\text{Flange width } b = 7 \text{ in.}\\
&\text{Thickness of web } \delta_1 = 0.5 \text{ in.}\\
&\text{Mean thickness of flanges } \delta = \tfrac{1}{2}(0.60 + 1.14) = 0.87 \text{ in.}\\
&\text{Area of section } A = 23.3 \text{ sq. in.}\\
&\text{Principal rigidity } EI_y = 2,087E \text{ lb.} \times \text{sq. in.}\\
&\text{Principal rigidity } EI_z = 42.7E \text{ lb.} \times \text{sq. in.}
\end{aligned}
$$

Using eq. (256), p. 275,

$$C = G(\tfrac{2}{3}b\delta^3 + \tfrac{1}{3}h\delta_1{}^3) = 4.07G.$$

Then, from eq. (h), assuming $E = 2.6G$,

$$\alpha = 3.67,$$

and from eq. (k),

$$\gamma = \frac{42.7}{2,087 \times 100} = 205 \times 10^{-6}.$$

Table 20 gives, by interpolation, for $\alpha = 3.67$,

$$\sigma_{cr} = 11,300 + \tfrac{1}{2}(13,600 - 11,300)1.67 = 13,200 \text{ lbs. per sq. in.}$$

This is the critical stress for $\gamma = 0.0001$. The critical stress in the example considered will be $13,200 \times \gamma \times 10^4 = 26,900$ lbs. per

[44] For more detailed investigation of this subject, see the writer's paper, Trans. Amer. Soc. C. E., Vol. 87, 1924, p. 1247, and "Theory of Elastic Stability," Chapter 5. See also E. Chwalla, "Die Kipp-Stabilität gerader Träger," Berlin, 1939.

sq. in. The load corresponding to this stress must be considered as the ultimate for the beam. This numerical result shows that sidewise buckling may occur at stresses far less than the ultimate stress of the material under direct compression and even less than the elastic limit. This fact must be considered and the critical stress instead of yield point must be taken as the basis for determination of working stresses. For instance, with a factor of safety of 3, the working stress will be equal to $26,900/3 = 8,970$ lbs. per sq. in.

# CHAPTER V

## DEFORMATIONS SYMMETRICAL ABOUT AXIS

**44. Thick Walled Cylinder.**—If a circular cylinder of constant wall thickness is submitted to the action of uniformly distributed internal and external pressures, the deformation produced is symmetrical about the axis of the cylinder and does not change along its length. In the following we consider a ring cut from the cylinder by two planes perpendicular to its axis a unit distance apart (Fig. 142). From the condition of symmetry, there are no shearing stresses on the sides of an element of this ring, such as $mnm_1n_1$ (Fig. 142) which is bounded by two axial planes and two concentric cylindrical surfaces. Let $\sigma_t$ denote the normal hoop stress acting on the sides $mm_1$ and $nn_1$ of the element, and $\sigma_r$ the normal radial stress on the side $mn$. This stress varies with the radius $r$ and changes by an amount $(d\sigma_r/dr)dr$ in the distance $dr$. The normal radial stress on the side $m_1n_1$ is consequently

$$\sigma_r + \frac{d\sigma_r}{dr}\,dr.$$

Summing up the forces on the element in the direction of the bisector of the angle $d\varphi$ gives us the following equation of equilibrium:[1]

$$\sigma_r r\,d\varphi + \sigma_t\,dr\,d\varphi - \left(\sigma_r + \frac{d\sigma_r}{dr}\,dr\right)(r + dr)\,d\varphi = 0, \quad (a)$$

or, neglecting small quantities of higher order,

$$\sigma_t - \sigma_r - r\frac{d\sigma_r}{dr} = 0. \quad (b)$$

This equation contains two unknowns, the stresses $\sigma_t$ and $\sigma_r$. The second equation necessary for the determination of these quantities is obtained from a consideration of the deformation

---

[1] The weight of the element is neglected here.

of the cylinder. The deformation is symmetrical with respect to the axis and consists of a radial displacement of all points in the wall of the cylinder. This displacement is constant in the circumferential direction but varies along the radius, i.e., it is a function of the radius. If $u$ denotes the displacement of a cylindrical surface of radius $r$, then the displacement for a surface of radius $r + dr$ is



$$u + \frac{du}{dr}\,dr.$$
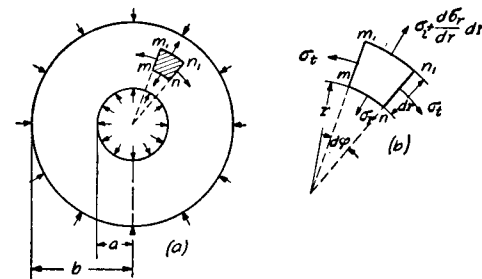
FIG. 142.

Hence an element such as $mnm_1n_1$ undergoes a total elongation in the radial direction of $(du/dr)dr$, and the unit elongation in the radial direction is therefore

$$\epsilon_r = \frac{du}{dr}. \quad (c)$$

The unit elongation of the same element in the tangential direction is equal to the unit elongation of the corresponding radius, i.e.,

$$\epsilon_t = \frac{u}{r}. \quad (d)$$

From eqs. (38), p. 52, Part I, the expressions for the stresses in terms of the strains are

$$\sigma_r = \frac{E}{1 - \mu^2}\left(\frac{du}{dr} + \mu\frac{u}{r}\right),$$

$$\sigma_t = \frac{E}{1 - \mu^2}\left(\frac{u}{r} + \mu\frac{du}{dr}\right). \quad (199)$$

The normal stresses $\sigma_r$ and $\sigma_t$ are evidently not independent, as they can be expressed in terms of one function $u$. By

substituting expressions (199) into eq. (b), we obtain the following equation for determining $u$:

$$\frac{d^2u}{dr^2} + \frac{1}{r}\frac{du}{dr} - \frac{u}{r^2} = 0. \qquad (e)$$

The general solution of this equation is

$$u = C_1 r + \frac{C_2}{r}, \qquad (f)$$

which can be verified by substitution. The constants $C_1$ and $C_2$ are determined from the conditions at the inner and outer surfaces of the cylinder where the pressures, i.e., the normal stresses $\sigma_r$, are known. Substituting (f) into eqs. (199), we obtain

$$\sigma_r = \frac{E}{1-\mu^2}\left[ C_1(1+\mu) - C_2\frac{1-\mu}{r^2} \right], \qquad (h)$$

$$\sigma_t = \frac{E}{1-\mu^2}\left[ C_1(1+\mu) + C_2\frac{1-\mu}{r^2} \right]. \qquad (k)$$

If $p_i$ and $p_0$ denote the internal and external pressures respectively, the conditions at the outer and inner surfaces of the cylinder are

$$(\sigma_r)_{r=b} = -p_0 \quad \text{and} \quad (\sigma_r)_{r=a} = -p_i. \qquad (l)$$

The sign on the right side of each equation is negative because normal stress is taken as positive for tension. Substitution of expression (h) for $\sigma_r$ in eqs. (l) gives two equations for determining the constants $C_1$ and $C_2$, from which

$$C_1 = \frac{1-\mu}{E}\frac{a^2p_i - b^2p_0}{b^2-a^2}; \quad C_2 = \frac{1+\mu}{E}\frac{a^2b^2(p_i-p_0)}{b^2-a^2}. \qquad (m)$$

With these values for the constants in eqs. (h) and (k) the general expressions for the normal stresses $\sigma_r$ and $\sigma_t$ become [2]

---

[2] This solution appeared first in the paper by Lamé and Clapeyron, "Mémoire sur l'équilibre intérieur des corps solides homogènes," Mémoires présentés par divers savans, Vol. 4, 1833.

$$\sigma_r = \frac{a^2p_i - b^2p_0}{b^2-a^2} - \frac{(p_i - p_0)a^2b^2}{r^2(b^2-a^2)},$$

$$\sigma_t = \frac{a^2p_i - b^2p_0}{b^2-a^2} + \frac{(p_i - p_0)a^2b^2}{r^2(b^2-a^2)}. \qquad (200)$$

It is interesting to note that the sum of these two stresses remains constant, so that the deformation of all elements in the direction of the axis of the cylinder is the same, and cross sections of the cylinder remain plane after deformation.

Let us consider the particular case $p_0 = 0$, i.e., the cylinder is submitted to *internal pressure only*. Then eqs. (200) become

$$\sigma_r = \frac{a^2p_i}{b^2-a^2}\left(1 - \frac{b^2}{r^2}\right), \qquad (201)$$

$$\sigma_t = \frac{a^2p_i}{b^2-a^2}\left(1 + \frac{b^2}{r^2}\right). \qquad (202)$$

These equations show that $\sigma_r$ is always a compressive stress and $\sigma_t$ a tensile stress. The latter is maximum at the inner surface of the cylinder, where

$$(\sigma_t)_{max} = \frac{p_i(a^2 + b^2)}{b^2 - a^2}. \qquad (203)$$

$(\sigma_t)_{max}$ is always numerically greater than the internal pressure and approaches this quantity as $b$ increases. The minimum value of $\sigma_t$ is at the outer surface of the cylinder. The ratio

$$\frac{(\sigma_t)_{max}}{(\sigma_t)_{min}} = \frac{a^2 + b^2}{2a^2}$$

increases with increase in the thickness of the wall of the cylinder. For a comparatively small thickness there is not a great difference between the maximum and minimum values of $\sigma_t$. Taking, for instance, $b = 1.1a$, $(\sigma_t)_{max}$ exceeds $(\sigma_t)_{min}$ by only $10\frac{1}{2}$ per cent. We should then make no very great error if we assume the tensile stresses $\sigma_t$ uniformly distributed

over the thickness of the wall and use the equation:

$$\sigma_t = \frac{p_i a}{b - a},$$

which coincides with equation on page 162 given for thin cylinders. The shearing stress is maximum at the inner surface of the cylinder where

$$\tau_{max} = \frac{\sigma_t - \sigma_r}{2} = \frac{1}{2}\left[\frac{p_i(a^2 + b^2)}{b^2 - a^2} + \frac{p_i(b^2 - a^2)}{b^2 - a^2}\right] = \frac{p_i b^2}{b^2 - a^2}. \qquad (n)$$

When only an *external pressure* acts on the cylinder, $p_i = 0$, and eqs. (200) give

$$\sigma_r = -\frac{p_0 b^2}{b^2 - a^2}\left(1 - \frac{a^2}{r^2}\right), \qquad (204)$$

$$\sigma_t = -\frac{p_0 b^2}{b^2 - a^2}\left(1 + \frac{a^2}{r^2}\right). \qquad (205)$$

In this case $\sigma_r$ and $\sigma_t$ are both compressive stresses and $\sigma_t$ is always numerically greater than $\sigma_r$. The maximum compressive stress is at the inner surface of the cylinder, where

$$(\sigma_t)_{r=a} = -\frac{2p_0 b^2}{b^2 - a^2}. \qquad (206)$$

It is interesting to note that as the ratio $b/a$ of the radii of the cylinder is increased, this maximum compressive stress approaches twice the value of the external pressure acting on the cylinder, namely, $-2p_0$.

Let us consider now the *deformation of the cylinder*. Substituting expressions (m) for the arbitrary constants in eq. (f), we find

$$u = \frac{1 - \mu}{E}\frac{a^2 p_i - b^2 p_0}{b^2 - a^2}r + \frac{1 + \mu}{E}\frac{a^2 b^2(p_i - p_0)}{(b^2 - a^2)r}. \qquad (207)$$

This gives the radial displacement of any point in the wall of the cylinder. In the particular case of a cylinder submitted to internal pressure only, $p_0 = 0$, and the radial displacement

at the inner surface, from eq. (207), is

$$(u)_{r=a} = \frac{a p_i}{E}\left(\frac{a^2 + b^2}{b^2 - a^2} + \mu\right). \qquad (208)$$

When the cylinder is submitted to external pressure only, $p_i = 0$, and the radial displacement at the outer surface is

$$(u)_{r=b} = -\frac{b p_0}{E}\left(\frac{a^2 + b^2}{b^2 - a^2} - \mu\right). \qquad (209)$$

The minus sign indicates that the displacement is towards the axis of the cylinder.

**45. Stresses Produced by Shrink Fits.**—If it is necessary to produce contact pressure between a hub and a shaft or between two rings mounted one inside the other, it is usual practice to make the inner radius of the outer part smaller than the outer radius of the inner part and to assemble the structure after a preliminary heating of the outer part. After cooling, a contact pressure between the two parts is produced, which is called the *shrink-fit pressure*. The magnitude of this pressure and the stresses produced by it can easily be calculated with the equations of the previous article. Assume, for instance, that the external radius of the inner cylinder in an unstressed condition is larger than the internal radius of the outer cylinder (Fig. 143) by the amount δ. Then, after assembly, a pressure $p$ is produced between the cylinders; its
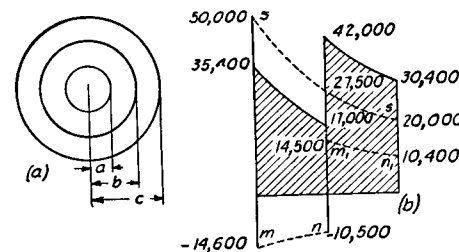


FIG. 143.

magnitude is found from the condition that the increase in the inner radius of the outer cylinder plus the decrease in

the outer radius of the inner cylinder, produced by $p$, must be equal to $\delta$ . Hence, from eqs. (208) and (209),

$$\frac{bp}{E}\left(\frac{b^2 + c^2}{c^2 - b^2} + \mu\right) + \frac{bp}{E}\left(\frac{a^2 + b^2}{b^2 - a^2} - \mu\right) = \delta,$$

from which

$$p = \frac{E\delta}{b}\frac{(b^2 - a^2)(c^2 - b^2)}{2b^2(c^2 - a^2)}. \qquad (210)$$

Equations (201) and (202) then give the stresses in the outer cylinder and eqs. (204) and (205) the stresses in the inner cylinder. Usually the stresses to be considered in design are those at the inner surface of the outer cylinder. These stresses are

$$\sigma_t = \frac{p(b^2 + c^2)}{c^2 - b^2}, \qquad \sigma_r = -p.$$

The maximum shearing stress at this surface is (see eq. $n$, p. 240)

$$\tau_{\max} = \frac{pc^2}{c^2 - b^2}$$

or, substituting expression (210) for $p$,

$$\tau_{\max} = \frac{E\delta c^2(b^2 - a^2)}{2b^3(c^2 - a^2)}. \qquad (211)$$

In the particular case of a solid shaft and a hub we have $a = 0$, from which

$$p = \frac{E\delta}{2bc^2}(c^2 - b^2), \qquad (212)$$

$$\tau_{\max} = \frac{E\delta}{2b}, \qquad (213)$$
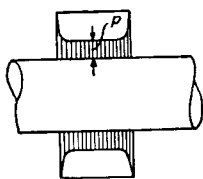


Fig. 144.

i.e., the maximum shearing stress is the same as in a simple tie rod which undergoes a unit elongation equal to $\delta/b$.

The above discussion assumed that both cylinders have the same length. In dealing with a hub and a shaft (Fig. 144) the projecting portions of the shaft resist com-

pression which results in an increased pressure near the faces of the hub as indicated by the shaded areas.[3]

If a built-up cylinder, such as represented in Fig. 143, is subjected to internal pressure, the stresses produced by this pressure are the same as in a cylinder with a solid wall of the thickness $c - a$. These stresses are superposed on the shrink fit stresses. The shrink fit produces a tangential compressive stress at the inner surface of the cylinder which reduces the maximum tangential tensile stress at this point produced by the internal pressure so that a more favorable stress distribution may be obtained than in the case of a solid tube (see problem 2, p. 244). This is one reason why cylinders built up of several tubes are used in cases of very high internal pressures, such as are found in guns.

A distribution of initial stresses analogous to those described above in the case of built-up cylinders can also be obtained in a solid tube by applying a high internal pressure sufficient to produce permanent set in the inner part of the tube. After removing this internal pressure some stresses remain in the tube due to the permanent set, so that the inner part is then in a state of compression, and the outer in a state of tension.[4]

### Problems

1. Determine the tangential stresses at the inner and outer surfaces and at the middle thickness of the wall of a cylinder with inner radius 4 in. and outer radius 8 in. submitted to an internal pressure $p_i = 30,000$ lbs. per sq. in.

   *Answer.* From eq. (202): $(\sigma_t)_{r=4''} = 50,000$ lbs. per sq. in.; $(\sigma_t)_{r=6''} = 27,500$ lbs. per sq. in.; $(\sigma_t)_{r=8''} = 20,000$ lbs. per sq. in.

---

[3] An experimental investigation of shrink fit stresses is given in a paper by A. Huggenberger, Technische Blätter, Schweiz. Lokomotiv. und Maschinenfabrik, Winterthur, 1926. A further discussion of shrink fit stresses see in the paper by W. Janicki, "Schweiz. Bauz.," Vol. 88, p. 93, 1926 and Vol. 90, p. 127, 1927. See also papers by J. W. Baugher, Trans. A. S. M. E., Vol. 52, 1930, and O. J. Horger and C. W. Nelson, "Journal of Appl. Mech.," Vol. 4, p. 183, 1937 and Vol. 5, p. 32, 1938.

[4] A further discussion of this question see in art. 71.

2. Determine the stresses in a built-up steel cylinder (Fig. 143) submitted to an internal pressure $p_i = 30,000$ lbs. per sq. in. if $a = 4$ in.; $b = 6$ in.; $c = 8$ in.; and the shrinkage $\delta = 0.005$ in.

*Solution.* Determine first the initial stresses in the cylinder due to shrinkage. From eq. (210)

$$p = \frac{30 \times 10^6 \times 0.005(6^2 - 4^2)(8^2 - 6^2)}{6 \times 2 \times 6^2(8^2 - 4^2)} = 4,050 \text{ lbs. per sq. in.}$$

The tangential stresses produced by this pressure in the inner, cylinder, from eq. (205), are

$$(\sigma_t)_{r=4''} = -\frac{2pb^2}{b^2 - a^2} = -\frac{2 \times 4,050 \times 6^2}{6^2 - 4^2} = -14,600 \text{ lbs. per sq. in.,}$$

$$(\sigma_t)_{r=6''} = -\frac{p(b^2 + a^2)}{b^2 - a^2} = -10,500 \text{ lbs. per sq. in.}$$

The stresses for the outer cylinder, from eq. (202), are

$$(\sigma_t)_{r=6''} = \frac{p(b^2 + c^2)}{c^2 - b^2} = \frac{4,050(6^2 + 8^2)}{8^2 - 6^2} = 14,500 \text{ lbs. per sq. in.,}$$

$$(\sigma_t)_{r=8''} = \frac{2pb^2}{c^2 - b^2} = \frac{4,050 \times 2 \times 6^2}{8^2 - 6^2} = 10,400 \text{ lbs. per sq. in.;}$$

the distribution of initial stresses $\sigma_t$ over the thickness of the wall is shown in Fig. 143 (b) by the dotted lines $mn$ and $m_1n_1$. The stresses produced by the internal pressure are the same as in the previous problem and are represented in the figure by the dotted line $ss$. Superposition of the two stress distributions gives the distribution represented by the shaded area. It may be seen that, due to assembly stresses, the maximum stress when the cylinder is submitted to internal pressure is reduced from 50,000 to 42,000 lbs. per sq. in.

3. Referring to Fig. 143 find the shrink fit stresses $\sigma_t$ at $r = 6$ in. and $r = 10$ in. if $a = 4$ in., $b = 8$ in., $c = 12$ in. Use a shrinkage factor $\delta/b = 0.001$, and take $E = 30.10^6$ lbs. per sq. in.

*Answer.*

$$(\sigma_t)_{r=6''} = -13,500 \text{ lbs. per sq. in.}$$
$$(\sigma_t)_{r=10''} = 13,750 \text{ lbs. per sq. in.}$$

4. For the hub and shaft in Fig. 144 find the uniform pressure $p$ if the radius of the shaft is 6 in., and the outer radius of the hub is 12 in. The initial difference in diameters between hub and shaft is 0.012 in. Take $E = 30.10^6$ lbs. per sq. in.

**46. Rotating Disc of Uniform Thickness.**—When a circular disc rotates about the axis of symmetry perpendicular to the disc the inertia forces set up stresses which become considerable at high speeds. These stresses are distributed symmetrically with respect to the axis of rotation and may be calculated by the method indicated in article 44. It is assumed that the stresses do not vary over the thickness of the disc and this thickness is taken equal to unity. The equation of equilibrium of an element such as $mnm_1n_1$ in Fig. 142 is derived by adding to the forces which were considered in article 44 the inertia force acting on the element

$$\frac{\gamma\omega^2 r^2}{g} dr d\theta. \tag{a}$$

Here $\gamma$ is the weight per unit volume and $\omega$ the angular velocity of the disc. The remaining notation is the same as in article 44. The equation of equilibrium is now

$$\sigma_t - \sigma_r - r\frac{d\sigma_r}{dr} - \frac{\gamma\omega^2 r^2}{g} = 0. \tag{b}$$

By substituting for the stresses their expressions as functions of the displacement $u$ (eqs. 199, p. 238), we obtain the following equation:

$$\frac{d^2u}{dr^2} + \frac{1}{r}\frac{du}{dr} - \frac{u}{r^2} + (1 - \mu^2)\frac{\gamma\omega^2 r}{gE} = 0. \tag{214}$$

The general solution of this equation is obtained by adding any particular solution of it to the solution of the corresponding homogeneous equation (see eq. $f$, p. 238). Such a particular solution is

$$u = -(1 - \mu^2)\frac{\gamma\omega^2}{gE}\frac{r^3}{8}.$$

Then, using the notation

$$N = (1 - \mu^2)\frac{\gamma\omega^2}{gE}, \tag{c}$$

the general solution of eq. (214) is

$$u = - N\frac{r^3}{8} + C_1 r + \frac{C_2}{r}, \qquad (d)$$

in which, as before, $C_1$ and $C_2$ are constants which must be determined in such a way as to satisfy the conditions at the edges of the disc. For a *disc with a hole at the center* (Fig. 142) and with no forces acting on its edges, these conditions are

$$(\sigma_r)_{r=a} = 0; \qquad (\sigma_r)_{r=b} = 0. \qquad (e)$$

The general expression for $\sigma_r$ is obtained by substituting expression (d) into the first of eqs. (199) (p. 238) which gives

$$\sigma_r = \frac{E}{1 - \mu^2}\left[ -\frac{3 + \mu}{8} N r^2 + (1 + \mu)C_1 - (1 - \mu)C_2 \frac{1}{r^2} \right]. \qquad (f)$$

When $r = a$, $r = b$, this must be zero, as stated in eqs. (e). Making this substitution, we obtain the following equations for calculating $C_1$ and $C_2$:

$$-\frac{3 + \mu}{8} N a^2 + (1 + \mu)C_1 - (1 - \mu)C_2 \frac{1}{a^2} = 0,$$
$$\qquad\qquad (g)$$
$$-\frac{3 + \mu}{8} N b^2 + (1 + \mu)C_1 - (1 - \mu)C_2 \frac{1}{b^2} = 0,$$

from which

$$C_1 = \frac{3 + \mu}{8(1 + \mu)}(a^2 + b^2)N; \qquad C_2 = \frac{3 + \mu}{8(1 - \mu)} a^2 b^2 N. \qquad (h)$$

The general expression for $u$ is obtained when these values are put into eq. (d). Substituting this expression for $u$ into eqs. (199) (p. 238), we find:

$$\sigma_r = \frac{3 + \mu}{8(1 - \mu^2)} EN\left( a^2 + b^2 - r^2 - \frac{a^2 b^2}{r^2} \right), \qquad (215)$$

$$\sigma_t = \frac{3 + \mu}{8(1 - \mu^2)} EN\left( a^2 + b^2 - \frac{1 + 3\mu}{3 + \mu} r^2 + \frac{a^2 b^2}{r^2} \right). \qquad (216)$$

Replace $N$ by its value (eq. c) and let

$$\frac{a}{b} = \alpha; \qquad \frac{r}{b} = x; \qquad b\omega = v. \qquad (k)$$

Equations (215) and (216) then become

$$\sigma_r = \frac{\gamma v^2}{g}\frac{3 + \mu}{8}\left( 1 + \alpha^2 - x^2 - \frac{\alpha^2}{x^2} \right), \qquad (217)$$

$$\sigma_t = \frac{\gamma v^2}{g}\frac{3 + \mu}{8}\left( 1 + \alpha^2 - \frac{1 + 3\mu}{3 + \mu} x^2 + \frac{\alpha^2}{x^2} \right). \qquad (218)$$

It will be seen that the radial stress $\sigma_r$ becomes zero at the edges, where $x = 1$ or $x = \alpha$, and that it is positive for other values of $x$ and becomes maximum at the points

$$x = \sqrt{\alpha} = \sqrt{\frac{a}{b}},$$

i.e., where

$$r = \sqrt{ab}, \qquad (l)$$

with this value for $r$, eq. (217) gives

$$(\sigma_r)_{max} = \frac{\gamma v^2}{g}\frac{3 + \mu}{8}(1 - \alpha)^2. \qquad (219)$$

The tangential stress $\sigma_t$ is maximum at the inner edge of the disc, where $x = \alpha$. From eq. (218) we then obtain

$$(\sigma_t)_{max} = \frac{\gamma v^2}{g}\frac{3 + \mu}{4}\left( 1 + \frac{1 - \mu}{3 + \mu}\alpha^2 \right). \qquad (220)$$

It can be seen that $(\sigma_t)_{max}$ is always larger than $(\sigma_r)_{max}$. In Fig. 145 the values of the parentheses of eqs. (217) and (218) are plotted as ordinates for values of $x$ as abscissas; the full lines represent the case $\alpha = \frac{1}{4}$, i.e., the inner radius is one fourth the outer radius. The dotted lines represent the values of the parenthesis of eq. (218) for other values of $\alpha$. Equation (220) shows that the stress $(\sigma_t)_{max}$ at the inner edge varies with $\alpha$ according to a parabolic law. This is shown by the curve $mn$ in Fig. 145.

It is interesting to note that when the inner radius is very small, i.e., $\alpha$ approaches zero, there is a very sharp change in the stress $\sigma_t$ near the hole. This is shown by the curve $mpq$, for which



FIG. 145.

$$(\sigma_t)_{max} = \frac{\gamma v^2}{g} \frac{3 + \mu}{4}. \quad (221)$$

For the other extreme case, when the inner radius approaches the outer radius of the disc, $\alpha$ approaches unity, and eq. (220) becomes

$$(\sigma_t)_{max} = \frac{\gamma v^2}{g}.$$
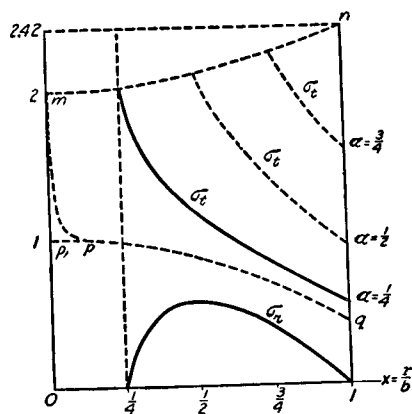
This coincides with eq. (15), Part I, which was obtained for a thin rotating ring. It will be seen that, in the case of the disc with a hole at the center, the maximum stress does not change very much with the radius of the hole; the value for a very thin ring is only about 20 per cent higher than that for a very small hole.

In the case of a *solid disc* $u = 0$ for $r = 0$; hence the constant $C_2$ in the general solution (d) must be taken equal to zero. The constant $C_1$ is found from the condition that $\sigma_r = 0$ at the outer edge of the disc. Then, from the second of eqs. (g),

$$C_1 = \frac{3 + \mu}{8(1 + \mu)} N b^2. \quad (m)$$

This value of $C_1$, and zero for $C_2$, are introduced into the general expression for the displacement $u$ (eq. d) which is then substituted into eqs. (199) (p. 238). In this way we obtain

$$\sigma_r = \frac{\gamma v^2}{g} \frac{3 + \mu}{8} (1 - x^2), \quad (222)$$

$$\sigma_t = \frac{\gamma v^2}{g} \frac{3 + \mu}{8} \left(1 - \frac{1 + 3\mu}{3 + \mu} x^2\right), \quad (223)$$

where, as before, $x = r/b$. Both stresses are always positive and increase with decrease of $x$, i.e., as we approach the center. At the center $x = 0$ and

$$(\sigma_t)_{max} = (\sigma_r)_{max} = \frac{\gamma v^2}{g} \frac{3 + \mu}{8}. \quad (224)$$

Comparing this with eq. (221), we see that, due to stress concentration, the stress at the edge of a small central hole is twice as great as that at the center of a solid disc. The variation of the stress $\sigma_t$ along the radius of a solid disc is represented in Fig. 145 by the dotted line $p_1pq$.

The equations derived above for rotating discs are sometimes used also for comparatively long cylinders,[5] for instance for rotors of electric machines. In large machines the peripheral velocities are very large. The above discussion shows that the stresses produced by inertia forces are proportional to the square of the peripheral velocity and are therefore of primary importance in such cases. Hence, for a material of a given strength and for a given angular velocity of the rotor, there is a definite limit to the diameter of the rotor beyond which it is dangerous to go. In discussing working stresses for such rotors it is important to note that very large forgings are likely to have defects in the material at the center, which is exactly the place of maximum stress produced by inertia forces. To eliminate uncertainties it is a usual practice now to bore a central hole along the axis of the rotor. Although the maximum stress is doubled, due to the presence of the hole, this is compensated for by the possibility of investigating the soundness of the material inside the forging. It is also usual to run the rotor at a certain overspeed [6] during the preliminary tests, so that the stresses around the hole may exceed the yield point. After stopping the rotor, the stresses will not disappear completely, due to a permanent set of the material at the hole. The inner portion of metal, which has

---

[5] Stress distribution in thick discs is discussed in "Theory of Elasticity," p. 319.

[6] In electric machines usually 20 per cent above service speed.

yielded, is compressed by the outer, and the outer is kept in tension by the inner.[7] The conditions are similar to those in a thick cylinder, overstressed by internal pressure (p. 243). The residual stress, produced at the hole by overstressing, is opposite in sign to that produced by inertia forces; hence overstressing produces a favorable effect on the final distribution of stresses in the rotor.[8]

It is important to note also that the equations for stresses obtained above (see eqs. 217, 218) contain besides $v$ only ratios such as $\alpha$ and $x$; hence for a given material and peripheral velocity, the stresses are equal in similarly situated points of geometrically similar rotors. This may simplify the calculations of stresses in geometrically similar discs. It is also used in establishing the strength of large discs from tests on models.

In the previous discussion it was assumed that the edges of the discs are free from external forces. If there are tensile or compressive forces uniformly distributed around the edges of the disc, the stresses due to them are found by using the theory of thick cylinders (article 44). These stresses (see eqs. 200) can be represented in the following form:

$$\sigma_r = k - \frac{n}{r^2},$$

$$\sigma_t = k + \frac{n}{r^2}, \qquad (n)$$

in which $k$ and $n$ are constants depending upon the dimensions of the disc and the magnitude of the external forces acting at the edges. Stresses $(n)$ are to be superposed upon the stresses (217) and (218) and the total stresses may then be represented in the

---

[7] This question is discussed by C. Honegger, Brown Bowery C. Mitteilungen, November, 1919.

[8] Residual stresses in rotating discs due to yielding of metal were investigated by A. Nadai and L. H. Donnell; see Trans. Amer. Soc. Mech. Engrs., Applied Mechanics Division, 1928. See also H. Hencky, Zeitschr. f. Angew. Math. u. Mech., Vol. 4, 1924, p. 331, and F. Laszlo, Zeitschr. f. Angew. Math. u. Mech., Vol. 5, 1925, p. 281.

---

following form:

$$\sigma_r = A + \frac{B}{r^2} - \beta_1 \omega^2 r^2,$$

$$\sigma_t = A - \frac{B}{r^2} - \beta \omega^2 r^2, \qquad (225)$$

in which

$$\beta_1 = \frac{\gamma}{g} \frac{3+\mu}{8}; \qquad \beta = \frac{\gamma}{g} \frac{1+3\mu}{8}, \qquad (226)$$

and $A$ and $B$ are constants of integration which may be calculated in each particular case by using eqs. (200), (217), (218). With the notation:

$$s = \sigma_r + \beta_1 \omega^2 r^2,$$

$$t = \sigma_t + \beta \omega^2 r^2 \qquad (227)$$

and

$$w = \frac{1}{r^2}, \qquad (228)$$

eqs. (225) become

$$s = A + Bw; \qquad t = A - Bw. \qquad (229)$$

If $s$ and $t$ are known for any point of the disc, their magnitudes for any other point can easily be obtained by using the following graphical method.[9] Let $s_1$ and $t_1$ denote the magnitudes of $s$ and $t$ for the point where $w = w_1$ (see Fig. 146). Then the magnitudes $s_2$ and $t_2$ of $s$ and $t$ for any other point where $w = w_2$ are obtained from the intersection of the vertical line through $w_2$ with the straight lines $s_1 s_2$ and $t_1 t_2$, which have their point of intersection on the vertical axis of the coordinates ($w = 0$) and are equally inclined to this axis. These lines represent equations (229) graphically. They have the common ordinate $A$ on the axis $w = 0$, and have equal and opposite slopes ($\pm B$). This graphical construction is very useful in calculating stresses in rotating discs of variable thickness as we shall see later.
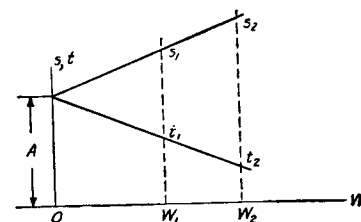


FIG. 146.

---

[9] This method was developed by R. Grammel, Dinglers Polytechnical Journal, Vol. 338, 1923, p. 217.

### Problems

1. Determine the stresses due to centrifugal forces in a rotor with 26″ outer radius and 4″ radius of inner hole. The outer portion of the rotor is cut by slots 10″ deep, which take the windings (Fig. 147). The rotor is of steel and makes 1,800 revolutions per minute. The weight of the windings in the slots is the same as that of the material removed.

*Solution.* Because of the radial slots, the part of rotor between the outer and the 16 inch radii can support no tensile hoop stresses. The centrifugal force due to this rotating ring is transmitted as a radial tensile stress across the surface of the cylinder of 16 inch radius. The magnitude of this stress is
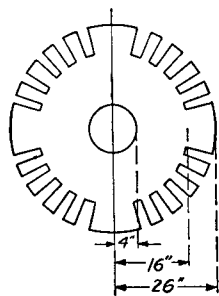
$$p_0 = \frac{1}{2\pi \times 16} \int_{r=16}^{r=26} \frac{\gamma}{g} \omega^2 r dV = \frac{1}{2\pi \times 16} \frac{\gamma \omega^2}{g}$$

$$2\pi \int_{16}^{26} r^2 dr = \frac{\gamma \omega^2}{g} \frac{1685}{6},$$

with $\gamma = 0.284$ lb. per cubic inch, $g = 32.2 \times 12$ inch sec.$^{-2}$; this gives

FIG. 147.                $p_0 = 7,334$ lbs. per sq. in.

The maximum tangential stress at the inner edge produced by the tensile stress $p_0$ is, from eq. (206),

$$\sigma_t' = 7,334 \times \frac{2 \times 16^2}{16^2 - 4^2} = 15,700 \text{ lbs. per sq. in.}$$

The maximum tangential stress at the same edge due to the mass between the 16 inch and 4 inch radii, calculated as for a rotating disc (eq. 220), is $\sigma_t'' = 5,580$ lbs. per sq. in. The total maximum circumferential stress at the inner edge is then $(\sigma_t)_{max} = \sigma_t' + \sigma_t'' = 15,700 + 5,580 \approx 21,300$ lbs. per sq. in.

2. A steel ring is shrunk on a cast iron disc (Fig. 143). Determine the change in the shrink fit pressure produced by inertia forces at 3,600 r.p.m., if $a = 1″$, $b = 5″$, $c = 10″$, $E_s = 30 \times 10^6$ lbs. per sq. in., $E_{c.i.} = 16 \times 10^6$ lbs. per sq. in., $\gamma_s = 0.284$ lb. per cubic in., $\gamma_{c.i.} = 0.260$ lb. per cubic in.

*Solution.* Let $p_0$ be the increase in pressure between the ring and the disc. The arbitrary constants in eq. (*f*) for the outer ring

are determined by the equations:

$$\frac{E}{1 - \mu^2}\left[ -\frac{3 + \mu}{8} Nc^2 + (1 + \mu)C_1 - (1 - \mu)C_2 \frac{1}{c^2} \right] = 0,$$

$$\frac{E}{1 - \mu^2}\left[ -\frac{3 + \mu}{8} Nb^2 + (1 + \mu)C_1 - (1 - \mu)C_2 \frac{1}{b^2} \right] = -p_0. \qquad (p)$$

When we apply eq. (*f*) to the inner disc, for which the arbitrary constants are denoted by $C_1'$ and $C_2'$ and $N'$ is the constant defined by eq. (*c*), we obtain the equations for determining $C_1'$ and $C_2'$:

$$\frac{E}{1 - \mu^2}\left[ -\frac{3 + \mu}{8} N'b^2 + (1 + \mu)C_1' - (1 - \mu)C_2' \frac{1}{b^2} \right] = -p_0,$$

$$\frac{E}{1 - \mu^2}\left[ -\frac{3 + \mu}{8} N'a^2 + (1 + \mu)C_1' - (1 - \mu)C_2' \frac{1}{a^2} \right] = 0. \qquad (r)$$

From equations (*p*) and (*r*), the four constants $C_1$, $C_2$, $C_1'$ and $C_2'$ can be found as functions of $p_0$. The magnitude of $p_0$ is now found from the condition that, at the surface of contact, the radial displacements of the disc and of the ring are equal. Using eq. (*d*), the equation for determining $p_0$ is therefore

$$-N\frac{b^3}{8} + C_1 b + \frac{C_2}{b} = -N'\frac{b^3}{8} + C_1'b + \frac{C_2'}{b}. \qquad (s)$$

The numerical calculations are left to the reader.

3. Find the change in pressure $p$ calculated for problem 4 of the preceding article if the shaft and the hub rotate at 1,800 r.p.m., $\gamma = 0.284$, $E = 30.10^6$ lbs. per sq. in.

### 47. Rotating Disc of Variable Thickness.

—In the case of a disc of variable thickness the problem of determining stresses becomes more involved.[10] We will now discuss an approximate method of solving this problem, based on the replacement of the actual profile by a system of discs of uniform thickness (Fig. 148).[11]

[10] The general equation for this case, together with a consideration of the different methods of its solution, can be found in the well-known book by A. Stodola, "Dampf- und Gasturbinen," 6th ed., pp. 312–340, 1924. A rotating disc of conical profile was considered by H. M. Martin, Engineering, Vol. 115, p. 1, 1923; by B. Hodkinson, Engineering, Vol. 116, p. 274, 1923; and A. Fischer, Zeitschr. d. Oesterr. Ing. u. Arch. Vereines, Vol. 74, 1922, p. 46. See also the book by I. Malkin, "Festigkeitsberechnung rotierender Scheiben," Berlin, 1935.

[11] This method was developed by M. Donath, "Die Berechnung rotierender Scheiben und Ringe," 1912, Berlin. It is described in English

The stresses in the separate discs are calculated by the equations given in art. 46. We must then consider conditions at the boundaries between these discs, that is, at sections such as 2, 3, 4 (Fig. 148), where abrupt changes in the thickness occur. If $y$ and $y + \Delta y$ denote the thickness of the discs on opposite sides of the section under consideration, the corresponding change $\Delta\sigma_r$ in the magnitude of the radial stress $\sigma_r$ is found from the equation:

$$\sigma_r y = (\sigma_r + \Delta\sigma_r)(y + \Delta y),$$

in which it is assumed, as before, that the stresses are uniformly distributed over the thickness of the disc. Then

$$\Delta\sigma_r = -\frac{\Delta y}{y + \Delta y}\,\sigma_r. \qquad (a)$$

The change $\Delta\sigma_t$ in the tangential stress at the same section is found from the condition that the unit circumferential elongation is the same on both sides of the section. Hence

$$\sigma_t - \mu\sigma_r = (\sigma_t + \Delta\sigma_t) - \mu(\sigma_r + \Delta\sigma_r),$$

from which

$$\Delta\sigma_t = \mu\Delta\sigma_r.$$

From eqs. (227),

$$\left.\begin{array}{l} \Delta s = \Delta\sigma_r = -\dfrac{\Delta y}{y + \Delta y}\,\sigma_r, \\[2ex] \Delta t = \Delta\sigma_t = \mu\Delta s. \end{array}\right\} \qquad (230)$$

Equations (226), (227), (228) and (230) together with the graphical solution given in Fig. 146 are sufficient for the calculation of a disc of a variable thickness.

Consider, as an example, the disc represented in Fig. 148, rotating at a speed of 3,000 r.p.m. All the dimensions are given in the table below. Assume that the centrifugal forces applied at the outer edge, for instance centrifugal forces due to the blades in the case of a turbine disc, are such that at the outer edge

$$(\sigma_r)_1 = 1,420 \text{ lbs. per sq. in.}$$

by H. Hearle in Engineering, Vol. 106, 1918, p. 131. Further development of the method was given by R. Grammel, loc. cit., p. 251, and the numerical example given below is taken from this paper. See also the paper by M. G. Driessen, Trans. Amer. Soc. Mech. Eng., 1928, Applied Mechanics Division; R. Grammel, Ing. Arch., Vol. 7, p. 136, 1936; R. G. Olsson, Ing. Arch., Vol. 8, p. 270 and p. 373, 1937; A. Held, Ing. Arch., Vol. 10, p. 339, 1939.

TABLE 21. STRESS CALCULATION IN ROTATING DISCS

| 1 Cross Section | 2 $r$ in. | .3 $r^2$ in.² | 4 $10^3 w$ in.⁻² | 5 $\beta_1\omega^2 r^2$ lbs./in.² | 6 $\beta_0\omega^2 r^2$ lbs./in.² | 7 $y$ in. | 8 $\dfrac{\Delta y}{y+\Delta y}$ | 9 $\sigma_r$ lbs./in.² | 10 $\Delta s$ lbs./in.² | 11 $\Delta t$ lbs./in.² | 12 $\sigma_t$ lbs./in.² | 13 $\sigma_r^0$ lbs./in.² | 14 $\sigma_t^0$ lbs./in.² |
|---|---|---|---|---|---|---|---|---|---|---|---|---|---|
| 1 | 19.7 | 388 | 2.58 | 11,620 | 6,680 | .985 | + 1.50 | 1,420 / 0 | | | 6,360 / 710 | 1,420 | 6,800 |
| 2 | 17.7 | 314 | 3.18 | 9,410 | 5,420 | .394 | − .333 | 3,630 / 80 | − 5,450 / 130 | − 1,640 / 40 | 7,620 / 795 | 6,250 | 8,900 |
| 3 | 13.8 | 190 | 5.26 | 5,700 | 3,290 | .591 | − .400 | 14,000 / 510 | + 4,670 / 170 | + 1,390 / 60 | 10,020 / 1,070 | 11,400 | 10,000 |
| 4 | 9.85 | 97.0 | 10.31 | 2,910 | 1,680 | .985 | − .286 | 13,500 / 1,020 | + 5,400 / 410 | + 1,620 / 130 | 8,900 / 1,820 | 10,300 | 9,300 |
| 5 | 7.87 | 62.0 | 16.1 | 1,860 | 1,070 | 1.38 | − .263 | 9,680 / 1,340 | + 2,740 / 380 | + 825 / 110 | 7,300 / 2,640 | 7,600 | 8,600 |
| 6 | 6.89 | 47.4 | 21.1 | 1,420 | 820 | 1.87 | − .321 | 7,550 / 1,550 | + 1,990 / 410 | + 597 / 130 | 6,530 / 3,300 | 5,700 | 8,400 |
| 7 | 5.91 | 34.9 | 28.6 | 1,050 | 603 | 2.76 | − .300 | 5,970 / 1,990 | + 1,920 / 640 | + 570 / 200 | 6,110 / 4,270 | 3,980 | 8,600 |
| 8 | 4.92 | 24.2 | 41.3 | 726 | 418 | 3.94 | | 4,280 / 2,590 | + 1,250 / 780 | + 370 / 230 | 5,960 / 5,720 | 2,260 | 9,500 |
| 9 | 3.94 | 15.5 | 64.5 | 465 | 268 | | | 2,530 / 4,000 | | | 6,335 / 8,100 | 0 | 11,500 |

and that $\mu = 0.3$; $\gamma = 0.283$ lb. per cubic inch.   Then from eqs. (226)

$$\beta_1\omega^2 = 30.0 \frac{\text{lbs.}}{\text{in.}^4}; \qquad \beta\omega^2 = 17.3 \frac{\text{lbs.}}{\text{in.}^4}.$$

The first eight columns of the table above are filled from these data and from Fig. 148.

We begin the stress calculation from the outer edge of the disc, where $(\sigma_r)_1$ is given.   The magnitude of the tangential stress $(\sigma_t)_1$
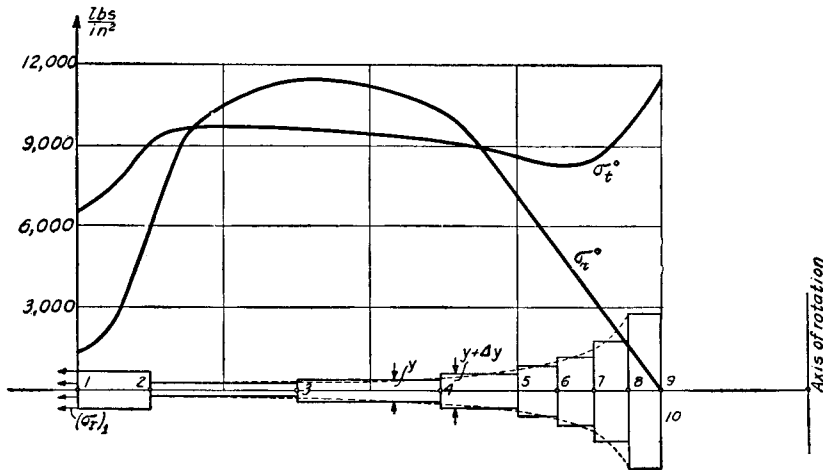


FIG. 148.

at the outer edge is usually unknown and an arbitrary magnitude must be assumed for a beginning.   The simplest assumption is to take $(\sigma_t)_1$ so as to make $s$ and $t$ (see eq. 227) equal, in which case

$$(\sigma_t)_1 = (\sigma_r)_1 + \beta_1\omega^2 r_1^2 - \beta\omega^2 r_1^2,$$

or, by using the figures in the fifth and sixth columns of the table,

$$(\sigma_t)_1 = 1{,}420 + 11{,}620 - 6{,}680 = 6{,}360 \text{ lbs. per sq. in.}$$

Now, from eqs. (227),

$$s_1 = (\sigma_r)_1 + \beta_1\omega^2 r_1^2 = 1{,}420 + 11{,}620 = 13{,}040 \text{ lbs. per sq. in.,}$$
$$t_1 = (\sigma_t)_1 + \beta\omega^2 r_1^2 = 6{,}360 + 6{,}680 = 13{,}040 \text{ lbs. per sq. in.}$$

Since $s_1 = t_1$, the $s$ and $t$ straight lines coincide in the construction explained in Fig. 146.   In Fig. 149 in which $s$ and $t$ are taken as ordinates and $w = 1/r^2$ as abscissa these lines are represented by the line $a$–$a$ parallel to the $w$ axis.   The length of this line, corresponding

to the radial distance 1–2 of the disc (Fig. 149), is determined from the figures in column 4 of the table.   From this we obtain for section 2 (Fig. 148)

$$s_2 = t_2 = 13{,}040 \text{ lbs. per sq. in.;}$$

then by using eqs. (227),

$$(\sigma_r)_2 = s_2 - \beta_1\omega^2 r_2^2 = 13{,}040 - 9{,}410 = 3{,}630 \text{ lbs. per sq. in.,}$$
$$(\sigma_t)_2 = t_2 - \beta\omega^2 r_2^2 = 13{,}040 - 5{,}420 = 7{,}620 \text{ lbs. per sq. in.}$$

At section 2 an abrupt change in the thickness of the disc takes place.   To take this into account, we use eqs. (230) together with the figures in column 8 in the table.   Then

$$(\Delta s)_2 = (\Delta\sigma_r)_2 = \left( -\frac{\Delta y}{y + \Delta y}\,\sigma_r \right)$$
$$= 1.50 \times 3{,}630 = 5{,}450 \text{ lbs. per sq. in.,}$$
$$(\Delta t)_2 = (\Delta\sigma_t)_2 = \mu(\Delta s)_2 = 0.3 \times 5{,}450 = 1{,}640 \text{ lbs. per sq. in.}$$
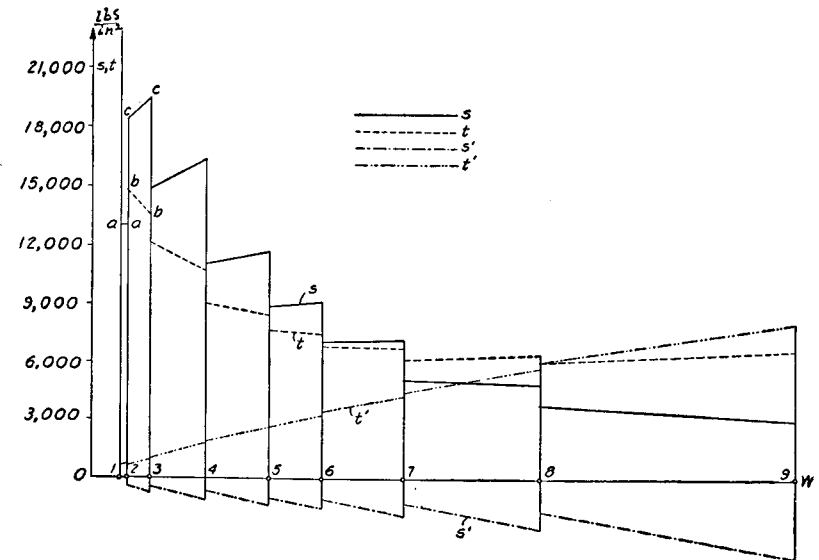


FIG. 149.

These quantities are added to the ordinate of the point $a$ in Fig. 149 which gives points $b$ and $c$; the lines $bb$ and $cc$ are then constructed as explained in Fig. 146.   In this manner $s_3$ and $t_3$ are found for section 3.   By repeating the above process all the data

necessary for the third section are obtained, and so on. By this method we may compute all the values in the upper lines in columns nine to twelve of the above table.

Due to the fact that the stress $(\sigma_t)_1$ at the periphery of the disc was taken arbitrarily, the conditions at the inner edge will usually not be satisfied, and the stress $(\sigma_r)_9$ obtained by the above method will not be the stress which actually exists there. In order to satisfy the condition at the inner edge, an additional calculation is required. We assume $(\sigma_r)_1 = 0$, $\omega = 0$, and take an arbitrary value for $(\sigma_t)_1$ (in the calculations $(\sigma_t)_1$ was taken 710 lbs. per sq. in.) and obtain the corresponding stress distribution in the same manner as before. For this case, from eqs. (227), $s = \sigma_r$ and $t = \sigma_t$. The results of these calculations are given in columns nine to twelve in the lower lines, and the corresponding constructions, in Fig. 149, by the lines $t'$ and $s'$. The solution which satisfies the actual condition at the inner edge of the disc is obtained by combining the above two stress distributions as follows: Let $(\sigma_r)_9$ and $(\sigma_r)_9'$ be the radial stresses at the inner edge of the disc, obtained by the first and the second calculations respectively, and $(\sigma_r)_9^0$ denote the actual stress at the inner edge. Then the solution for the actual condition is obtained by superposing on the first stress distribution the stresses of the second distribution multiplied by

$$n = \frac{(\sigma_r)_9^0 - (\sigma_r)_9}{(\sigma_r)_9'}.$$

The average stresses at the sections at which the thickness changes abruptly may be calculated as follows:

$$(\sigma_r)^0 = \left( \sigma_r + \frac{\Delta s}{2} \right) + n \left( \sigma_r' + \frac{\Delta s'}{2} \right),$$

$$(\sigma_t)^0 = \left( \sigma_t + \frac{\Delta t}{2} \right) + n \left( \sigma_t' + \frac{\Delta t'}{2} \right).$$

The results of such calculations for the case when the radial stress at the inner edge is zero are given in the last two columns of the above table and are represented by the two curves in Fig. 148.

**48. Thermal Stresses in a Long Hollow Cylinder.**—When the wall of a cylinder is non-uniformly heated, its elements do not expand uniformly, and mutual interference sets up thermal stresses. In the following the distribution of the temperature is taken to be symmetrical with respect to the axis of the cylinder, and constant along this axis. The deformation of the cylinder is then symmetrical about the axis and we may use the method developed in

art. 44. A ring is cut from the cylinder by two cross sections perpendicular to the axis, unit distance apart. During deformation such cross sections can be assumed to remain plane if taken sufficiently distant from the ends of the cylinder,[12] hence the unit elongations in the direction of the axis are constant. Let the $z$ axis be the axis of the cylinder, $w$ the displacement in the direction of the $z$ axis, and the other notation the same as in article 44 and Fig. 142. Then the unit elongations in the three perpendicular directions are

$$\epsilon_z = \frac{dw}{dz} = \text{const.},$$

$$\epsilon_r = \frac{du}{dr}, \tag{a}$$

$$\epsilon_t = \frac{u}{r}.$$

These elongations can be represented as functions of the stresses $\sigma_z$, $\sigma_r$, $\sigma_t$, and the thermal expansion. Let $\alpha$ denote the coefficient of linear expansion and $t$ the increase in temperature, which varies with the radial distance $r$. From eqs. (43) (see p. 62, Part I) the elongations are

$$\epsilon_z = \frac{\sigma_z}{E} - \frac{\mu}{E} (\sigma_r + \sigma_t) + \alpha t,$$

$$\epsilon_r = \frac{\sigma_r}{E} - \frac{\mu}{E} (\sigma_z + \sigma_t) + \alpha t \tag{b}$$

$$\epsilon_t = \frac{\sigma_t}{E} - \frac{\mu}{E} (\sigma_z + \sigma_r) + \alpha t,$$

Using the notation $\Delta$ for unit increase in volume,

$$\Delta = \epsilon_z + \epsilon_r + \epsilon_t = \frac{1 - 2\mu}{E} (\sigma_z + \sigma_r + \sigma_t) + 3\alpha t. \tag{c}$$

From this and eqs. (b) we find

$$\sigma_z = \frac{E}{1 + \mu} \left( \epsilon_z + \frac{\mu}{1 - 2\mu} \Delta \right) - \frac{\alpha t E}{1 - 2\mu},$$

$$\sigma_r = \frac{E}{1 + \mu} \left( \epsilon_r + \frac{\mu}{1 - 2\mu} \Delta \right) - \frac{\alpha t E}{1 - 2\mu}, \tag{d}$$

$$\sigma_t = \frac{E}{1 + \mu} \left( \epsilon_t + \frac{\mu}{1 - 2\mu} \Delta \right) - \frac{\alpha t E}{1 - 2\mu}.$$

---

[12] At the ends the stresses in the direction of the axis of the cylinder are zero and the stress distribution is more complicated.

These values are substituted into the equation of equilibrium of the element $mnm_1n_1$ in Fig. 142 (eq. (b), p. 236)

$$\frac{d\sigma_r}{dr} + \frac{\sigma_r - \sigma_t}{r} = 0 \qquad (e)$$

and give, after using eqs. (a),

$$\frac{d^2u}{dr^2} + \frac{1}{r}\frac{du}{dr} - \frac{u}{r^2} = \frac{1+\mu}{1-\mu}\alpha\frac{dt}{dr}. \qquad (231)$$

This equation determines the displacement $u$ for any particular distribution of temperature. It may be written in the form:

$$\frac{d}{dr}\left[\frac{1}{r}\frac{d}{dr}(ru)\right] = \frac{1+\mu}{1-\mu}\alpha\frac{dt}{dr}.$$

Integration with respect to $r$ gives

$$\frac{d}{dr}(ru) = \frac{1+\mu}{1-\mu}\alpha tr + 2C_1 r.$$

A second integration gives the solution:

$$u = \frac{1}{r}\frac{1+\mu}{1-\mu}\int_a^r \alpha tr\,dr + C_1 r + C_2\frac{1}{r}, \qquad (f)$$

in which $C_1$ and $C_2$ are constants of integration which must be determined in such a manner as to satisfy the conditions at the surfaces of the cylinder. If these surfaces are assumed to be free from external forces, $C_1$ and $C_2$ are determined from the conditions

$$(\sigma_r)_{r=a} = 0; \qquad (\sigma_r)_{r=b} = 0. \qquad (g)$$

A general expression for $\sigma_r$ is obtained by substituting $\epsilon_r = du/dr$ and $\epsilon_t = u/r$ into the second of eqs. (d) and taking $u$ from eq. (f), which gives

$$\sigma_r = \frac{E}{1+\mu}\left(-\frac{1+\mu}{1-\mu}\frac{1}{r^2}\int_a^r \alpha tr\,dr + \frac{C_1}{1-2\mu} - \frac{C_2}{r^2} + \frac{\mu}{1-2\mu}\epsilon_z\right). \qquad (h)$$

From eqs. (g) we obtain

$$C_2 = \frac{1+\mu}{1-\mu}\frac{a^2}{b^2-a^2}\int_a^b \alpha tr\,dr,$$

$$C_1 = \frac{(1+\mu)(1-2\mu)}{1-\mu}\frac{1}{b^2-a^2}\int_a^b \alpha tr\,dr - \mu\epsilon_z. \qquad (k)$$

With these values substituted in expression (h) the general expression for $\sigma_r$ becomes

$$\sigma_r = \frac{E}{1-\mu}\left[-\frac{1}{r^2}\int_a^r \alpha tr\,dr + \frac{r^2-a^2}{r^2(b^2-a^2)}\int_a^b \alpha tr\,dr\right]. \qquad (232)$$

The general expression for $\sigma_t$ is obtained from the equation of equilibrium (e) which gives

$$\sigma_t = \sigma_r + r\frac{d\sigma_r}{dr} = \frac{E}{1-\mu}\left[\frac{1}{r^2}\int_a^r \alpha tr\,dr \right.$$
$$\left. + \frac{r^2+a^2}{r^2(b^2-a^2)}\int_a^b \alpha tr\,dr - \alpha t\right]. \qquad (233)$$

When the distribution of the temperature over the thickness of the wall is known, we can evaluate the integrals of eqs. (232) and (233) and obtain $\sigma_r$ and $\sigma_t$.

Let us consider the case of a cylinder with a thin wall at the temperature $t_i$ on the inner surface and zero on the outer.[13] For thin walls the stationary distribution of the temperature over the thickness is practically linear; hence

$$t = t_i\left(1 - \frac{r-a}{b-a}\right). \qquad (234)$$

When this is substituted into eqs. (232) and (233) and the integration is performed, we obtain

$$\sigma_r = \frac{E\alpha t_i}{3(1-\mu)(b-a)}\left[r - \frac{a^3}{r^2} - \left(1 - \frac{a^2}{r^2}\right)\frac{b^3-a^3}{b^2-a^2}\right], \qquad (235)$$

$$\sigma_t = \frac{E\alpha t_i}{3(1-\mu)(b-a)}\left[2r + \frac{a^3}{r^2} - \left(1 + \frac{a^2}{r^2}\right)\frac{b^3-a^3}{b^2-a^2}\right]. \qquad (236)$$

The tangential stresses at the inner and outer surfaces are

$$(\sigma_t)_{r=a} = \frac{E\alpha t_i}{3(1-\mu)(b-a)}\left(3a - 2\frac{b^3-a^3}{b^2-a^2}\right),$$

$$(\sigma_t)_{r=b} = \frac{E\alpha t_i}{3(1-\mu)(b-a)}\left[2b + \frac{a^3}{b^2} - \left(1 + \frac{a^2}{b^2}\right)\frac{b^3-a^3}{b^2-a^2}\right].$$

---

[13] Any temperature condition at the surfaces of the cylinder may be obtained by superposing on this a uniform heating or cooling, which does not produce stresses.

These equations may be represented in a simpler form by using

$$\frac{b}{a} = 1 + m, \qquad (l)$$

where $m$ is small for a thin cylinder. With this notation the above eqs. become

$$(\sigma_t)_{r=a} = -\frac{E\alpha t_i}{2(1-\mu)}\left(1 + \frac{m}{6+3m}\right), \qquad (237)$$

$$(\sigma_t)_{r=b} = \frac{E\alpha t_i}{2(1-\mu)}\left(1 - \frac{m}{6+3m}\right). \qquad (238)$$

In the case of a very thin wall, the second term in the parenthesis of these equations is negligible and the equations coincide with that derived for a non-uniformly heated plate (see eq. 122).

When the thickness of the wall is not small, the stationary temperature distribution is no longer a linear function of $r$ but may be represented by the function

$$t = \frac{t_i}{\log_e \dfrac{b}{a}} \log_e \frac{b}{r}. \qquad (239)$$

With this expression for $t$ eqs. (232) and (233) become

$$\sigma_r = \frac{E\alpha t_i}{2(1-\mu)\log_e \dfrac{b}{a}}\left[-\log_e \frac{b}{r} - \frac{a^2}{b^2-a^2}\left(1 - \frac{b^2}{r^2}\right)\log_e \frac{b}{a}\right], \qquad (240)$$

$$\sigma_t = \frac{E\alpha t_i}{2(1-\mu)\log_e \dfrac{b}{a}}\left[1 - \log_e \frac{b}{r} - \frac{a^2}{b^2-a^2}\left(1 + \frac{b^2}{r^2}\right)\log_e \frac{b}{a}\right]. \qquad (241)$$

The maximum $\sigma_t$ occurs at the inner or outer surface of the cylinder. Substituting in the above equation $r = a$ and $r = b$,

$$(\sigma_t)_{r=a} = \frac{E\alpha t_i}{2(1-\mu)\log_e \dfrac{b}{a}}\left(1 - \frac{2b^2}{b^2-a^2}\log_e \frac{b}{a}\right), \qquad (242)$$

$$(\sigma_t)_{r=b} = \frac{E\alpha t_i}{2(1-\mu)\log_e \dfrac{b}{a}}\left(1 - \frac{2a^2}{b^2-a^2}\log_e \frac{b}{a}\right). \qquad (243)$$

In the above discussion only $\sigma_r$ and $\sigma_t$ were considered and it was shown that these quantities do not depend upon the elongation $\epsilon_z$

in the direction of the cylinder. $\sigma_z$ may be calculated from the first of eqs. $(d)$. Substituting $\epsilon_r = du/dr$, $\epsilon_t = u/r$, and using eq. $(f)$ for $u$ and eqs. $(k)$ for the arbitrary constants, we find the general expression for $\sigma_z$ to contain the constant elongation $\epsilon_z$ in the direction of the axis of the cylinder. If we assume that the cylinder can expand freely, we calculate the magnitude of $\epsilon_z$ from the condition that the sum of the normal forces over the cross section of the cylinder perpendicular to the $z$ axis is equal to zero. As a result of this calculation the following final expression for $\sigma_z$ is obtained:

$$\sigma_z = \frac{E\alpha t_i}{2(1-\mu)\log_e \dfrac{b}{a}}\left(1 - 2\log_e \frac{b}{r} - \frac{2a^2}{b^2-a^2}\log_e \frac{b}{a}\right). \qquad (244)$$

It may be seen that at the inner and outer surfaces of the cylinder the stress $\sigma_z$ is equal to $\sigma_t$. A more detailed discussion of thermal stresses in cylinders has been made by C. H. Lees.[14] Charts for rapid calculation of stresses from eqs. (240), (241) and (244) are given by L. H. Barker.[15]

In the case of a disc without a hole at the center and of a uniform thickness, which is assumed small in comparison with the radius $b$ of the disc, the radial and the tangential stresses are given by the following expressions:

$$\sigma_r = \alpha E\left(\frac{1}{b^2}\int_0^b tr\,dr - \frac{1}{r^2}\int_0^r tr\,dr\right), \qquad (m)$$

$$\sigma_t = \alpha E\left(-t + \frac{1}{b^2}\int_0^b tr\,dr + \frac{1}{r^2}\int_0^r tr\,dr\right). \qquad (n)$$

In each particular case when the temperature $t$ is known as a certain function of $r$, the integrals entering in these expressions can be readily evaluated and the thermal stresses obtained.

Thermal stresses are of great practical importance, especially in the case of large cylinders, such as steam turbine rotors, heavy shafts or large turbine discs. In all these cases the heating or cooling must be made gradual in order to reduce the temperature

---

[14] See C. H. Lees, Proc. Roy. Soc., Ser. A, Vol. 101 (1922).
[15] L. H. Barker, Engineering, Vol. 124 (1927), p. 443. The numerical example given below is taken from this paper.

gradient in a radial direction.[16] Thermal stresses are also important in Diesel engines.[17]

## Problems

1. Determine the thermal stresses in a cylinder having $2a = 3/8$ in., $2b = 1\frac{1}{4}$ in., $E\alpha/(1 - \mu) = 615$, if the inner temperature is $t_i = -1°$ C. and the outer temperature is zero.

*Solution.* From eqs. (242) and (243)

$$(\sigma_t)_{r=a} = (\sigma_z)_{r=a} = 420 \text{ lbs. per sq. in.,}$$
$$(\sigma_t)_{r=b} = (\sigma_z)_{r=b} = -194 \text{ lbs. per sq. in.}$$

$\sigma_r$ maximum, from eq. (240), occurs at $r = 0.3$ in. and is equal to 87 lbs. per sq. in. The distribution of the stresses over the thickness of the wall is shown in Fig. 150.
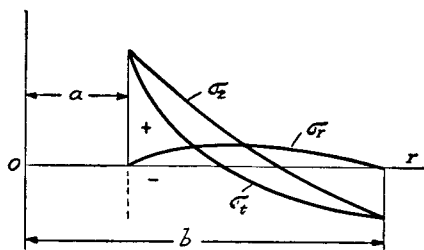


FIG. 150.

[16] A discussion of thermal stresses in cylinders in which the temperature varies along the axis is given by A. Stodola, loc. cit., p. 253, Appendix. See also G. Eichelberg, Forschungsarbeiten, nr. 220, 1923, and nr. 263. For thermal stresses in discs, see H. Quednau, V. D. I., Vol. 72, 1928, p. 522. The same problem is discussed in "Theory of Elasticity," p. 366, 1934.

[17] See R. Zulzer, "Temperature Variation and Heat Stresses in Diesel Engines," Engineering, Vol. 121 (1926), p. 447; A. Nägel, "The Transfer of Heat in Reciprocating Engines," Engineering, Vol. 127 (1929), p. 282, and W. Nusselt, V. D. I., Vol. 70 (1926), p. 468; J. N. Goodier, Journal Appl. Mech., Vol. 4, p. 33A, 1937.

## CHAPTER VI

### TORSION

**49. Shafts of Non-Circular Cross Section.**—In the first part of our book (see p. 261, part I) the problem of torsion of circular shafts was considered. Formulas for maximum stress and for the angle of twist for rectangular shafts also were given. There are several other shapes of cross section of a twisted shaft for which the problems of stress distribution and of the angle of twist are solved. In the following only some final results, which may be of practical interest, are given.
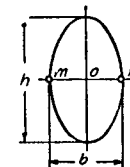


FIG. 151.

*Elliptical Cross Section.*[1]—The maximum shearing stress takes place at the ends of the minor axis, Fig. 151, and is



$$\tau_{\max} = \frac{16M_t}{\pi b^2 h} . \tag{245}$$

The angle of twist per unit length is

$$\theta = \frac{4\pi^2 M_t I_p}{A^4 G} , \tag{246}$$
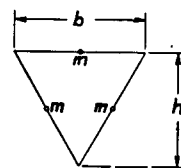
FIG. 152.

where $I_p = (\pi/64)(bh^3 + b^3h)$ is the polar moment of inertia of the cross section (see appendix, Part I, p. 347), and $A = \pi bh/4$ is area of the cross section.

*Equilateral Triangle.*—The maximum shearing stress occurs at the middle of the sides (points $m$ in Fig. 152) and can be calculated from the equation

$$\tau_{\max} = \frac{20M_t}{b^3} . \tag{247}$$

The angle of twist per unit length is

$$\theta = \frac{M_t}{0.6 G I_p} = \frac{46.2 M_t}{b^4 G} . \tag{248}$$

[1] The solution of this problem and of the following is due to Saint Venant, Mém. des Savans étrangers, Vol. 14, 1855. The derivation of the given formulas can be found in "Theory of Elasticity," see p. 234.

*Regular Hexagon.*[2]—For this case

$$\tau_{\max} = \frac{M_t}{0.217Ad}, \qquad (249)$$

$$\theta = \frac{M_t}{0.133Ad^2G}, \qquad (250)$$

where $d$ is the diameter of the inscribed circle and $A$ the cross sectional area.

*Regular Octagon.*[3]—For this case

$$\tau_{\max} = \frac{M_t}{0.223Ad}, \qquad (251)$$

$$\theta = \frac{M_t}{0.130Ad^2G}, \qquad (252)$$

where $A$ and $d$ have the same meaning as in the previous case.

*Trapezoid.*[4]—In the case of an isosceles trapezoid approximate values for the maximum stress and the angle of twist are obtained by replacing the trapezoid by an *equivalent* rectangle, which is obtained as indicated by the dotted lines in Fig. 153. From the centroid $C$ of the trapezoid are drawn perpendiculars, $BC$ and $CD$, to the lateral sides, and then verticals are drawn through $B$ and $D$. Equations (155) and (156) given in Part I (see p. 270), if applied to the rectangular cross section thus obtained, give approximate values



Fig. 153.

of $\tau_{\max}$ and $\theta$ for the trapezoid in Fig. 153.
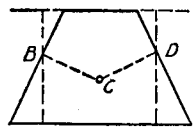
For any solid (non-tubular) shaft an approximate value for the angle of twist is obtained by replacing the cross section by an *equivalent* elliptical one of the same area $A$ and the same polar moment of inertia $I_p$. Then the approximate value for $\theta$ is given by formula (246).

## 50. Membrane Analogy.[5]—This analogy establishes certain relations between the deflection surface of a uniformly

[2] See C. Weber, Die Lehre von der Drehungsfestigkeit, Berlin, 1921.
[3] See C. Weber, ref. 2.
[4] See C. Weber, ref. 2.
[5] This analogy was developed by L. Prandtl; see Phys. Zeitschr.,

loaded membrane and the distribution of stresses in a twisted bar. Imagine a homogeneous membrane with the same outline as that of the cross section of the torsional member subjected to uniform tension at the edges and submitted to a uniform lateral pressure. It can be shown that the differential equation of the deflection surface [6] of this membrane has the same form as the equation which determines the stress distribution over the cross section of the twisted bar. If $S$ is the tensile force per unit length of the boundary line of the membrane, $p$ the lateral pressure per unit area, and $\theta$ the angle of twist per unit length of the bar, then the two above-mentioned equations are identical if

$$\frac{p}{S} = 2G\theta. \qquad (a)$$

If this condition is fulfilled, the following relationships hold between the surface of the membrane and the distribution of shearing stresses in twist: (1) The tangent to a *contour line* at any point of the deflected membrane gives the direction of the shearing stress at the corresponding point in the cross section of the twisted bar. (2) The maximum slope of the membrane at any point is equal to the magnitude of the shearing stress at the corresponding point in the twisted bar. (3) Twice the volume included between the surface of the deflected membrane and the plane of its outline is equal to the torque of the twisted bar.

All these statements can be readily proved in the case of a circular shaft. Let Fig. 154 represent the corresponding circular membrane uniformly stretched by the forces $S$ and loaded by uniform pressure $p$ acting upwards. Considering a concentric portion $mn$ of a radius $r$ of the membrane, Fig.

1903, p. 758; Jahresberichte d. Deutsch. Math. Ver., Vol. 13 (1904), p. 31. For further development see the papers by A. A. Griffith and G. I. Taylor, in Proc. Inst. Mech. Eng., 1917, p. 755, and in Technical Report of the Advisory Committee for Aeronautics, Vol. 3 (1917–1918), pp. 920, 938, 950. See also "Theory of Elasticity," p. 239.
[6] It is assumed that deflections are small.

154a, we observe that the total pressure on that portion is $\pi r^2 p$. This pressure is balanced by the tensile forces $S$ uniformly distributed along a circle of the radius $r$ and having that direction tangent to the deflected membrane. Denoting by $w$ the deflections of the membrane, we obtain

$$\pi r^2 p = -2\pi r S \frac{dw}{dr}$$

and

$$-\frac{dw}{dr} = \frac{pr}{2S} . \tag{b}$$

Substituting in this equation the value of $p/S$ given by the formula $(a)$, we obtain

$$-\frac{dw}{dr} = G\theta r. \tag{c}$$

On the right side of this equation we have the known expression for the torsional stress in a twisted circular shaft (see equation $(b)$, p. 263, Part I). Hence the slope of the deflected
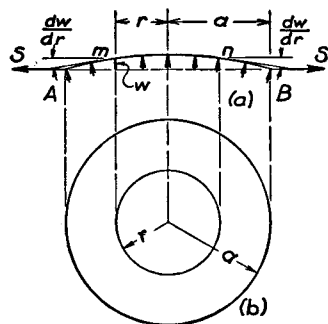


FIG. 154.

membrane gives us the required magnitude of the torsional stress. The maximum slope of the membrane at each point is in the direction of the meridian; hence the torsional stress in the shaft at each point has that direction perpendicular to the radius. This conclusion again agrees with the result of the elementary theory of torsion. To determine the torque which produces the stresses given by the equation $(c)$, let us calculate the volume included between the deflected membrane, Fig. 154a, and the plane of the boundary $AB$. The integration of equation $(c)$ gives the deflection surface of the membrane:

$$w = \frac{G\theta}{2}(a^2 - r^2),$$

and the required volume is

$$V = \int_0^a 2\pi r dr w = G\theta \frac{\pi a^4}{4} = \frac{1}{2} G\theta I_p.$$

Comparing this with the usual formula for torque (see eq. 147, Part I), we conclude that in the membrane analogy the double volume gives the magnitude of the torque. Hence all three statements made above regarding the analogy can be readily proved in the case of a circular shaft.

In other cases the shape of the surface of the deflected membrane is easily visualized for a given cross section of the shaft; consequently qualitative conclusions are readily drawn concerning the stress distribution in torsion. For instance, with a rectangular cross section (Fig. 155a), the corresponding surface of the deflected membrane is as represented by the contour lines. The stress is inversely proportional to the distance between these lines; hence it is larger where the lines are closer to each other. The maximum stress occurs at points $m$–$m$, where the slope of the membrane is largest. At the corners $a$, $b$, $c$, $d$, where the surface of the membrane coincides with the plane of the contour $abcd$, the slope of this surface is zero; hence the shearing stress at these points is zero.
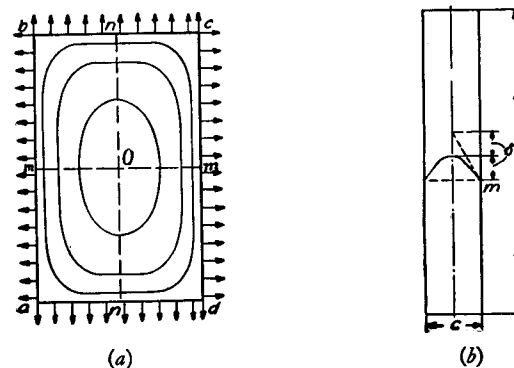


FIG. 155.

Consider now the case of a narrow rectangular cross section (Fig. 155b). The deflection surface of the uniformly loaded membrane at some distance from the short sides of

the rectangle can be considered cylindrical. With this as-sumption, each strip $mm$ of the surface behaves like a uni-formly loaded cord and its maximum deflection is given by equation:

$$\delta = \frac{pc^2}{8S},\qquad (b)$$

or, using eq. $(a)$,

$$\delta = \frac{c^2}{4}G\theta. \qquad (c)$$

The maximum stress is equal to the slope at points $m$–$m$. This slope is $4\delta/c$, for a parabolic curve; hence

$$\tau_{max} = \frac{4\delta}{c} = cG\theta. \qquad (d)$$

The corresponding torque is twice the volume enclosed by the membrane. Neglecting the effect of the short sides of the rectangle on the deflection of the membrane and calculating the volume as for a parabolic cylinder of length $b$, we find

$$M_t = 2 \cdot \frac{2}{3}\delta bc = \frac{1}{3}bc^3 G\theta. \qquad (e)$$
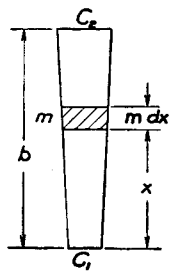
from which

$$\theta = \frac{M_t}{\frac{1}{3}bc^3 G}. \qquad (253)$$

Substituting in equation $(d)$, we obtain

$$\tau_{max} = \frac{M_t}{\frac{1}{3}bc^2}. \qquad (254)$$

Fig. 156.    These formulas coincide with formulas (155) and (156) given in Part I (see p. 270) if the rectangle is assumed to be a very narrow one.

If instead of a narrow rectangle we have a narrow trapezoid, as shown in Fig. 156, an approximate solution is obtained by assuming that the surface of the deflected membrane at a sufficient distance from the narrow sides is a conical one. The double vol-ume corresponding to an element $mm$ of the cross section is obtained

as in equation $(e)$ above and is equal to

$$\frac{1}{3}G\theta c^3 dx, \qquad (f)$$

where $c$ is the variable width of the cross section given by the equation:

$$c = c_1 + \frac{c_2 - c_1}{b}x. \qquad (g)$$

Substituting this in expression $(f)$ and integrating the result, we obtain the torque:

$$M_t = \int_0^b \frac{1}{3}G\theta c^3 dx = \frac{bG\theta}{12}(c_1 + c_2)(c_1^2 + c_2^2).$$

The angle of twist then is

$$\theta = \frac{M_t}{\frac{1}{12}b(c_1 + c_2)(c_1^2 + c_2^2)G}. \qquad (255)$$

When $c_1 = c_2 = c$, this formula coincides with formula (253) ob-tained for the narrow rectangle.

In more complicated cases in which the form of the deflec-tion surface of the membrane cannot easily be obtained analytically, this surface can be investigated experimentally by using soap film for the uniformly stretched membrane and measuring the slope of its surface by optical methods. For this purpose the apparatus shown in Fig. 157 has been used.[7] The aluminum plate with two holes—one circular and the other of the required shape—is clamped between the two halves of the cast-iron box $A$. The lower part of the box, having the form of a shallow tray, is supported on leveling screws. By pumping air into this portion of the box, the deflection of soap films covering the above mentioned holes is produced. The mapping of contour lines of the soap film surfaces is done by using the screw $B$ passing through a hole in a sheet of plate glass sufficiently large to cover the box in any possible position. The lower end of the screw carries a

[7] See the paper by G. I. Taylor and A. A. Griffith, loc. cit., p. 267.

hard steel point, whose distance from the glass plate is adjustable by the screw. The point is made to approach the film by moving the glass plate until the distortion of the image in the film shows that contact has occurred. The record is
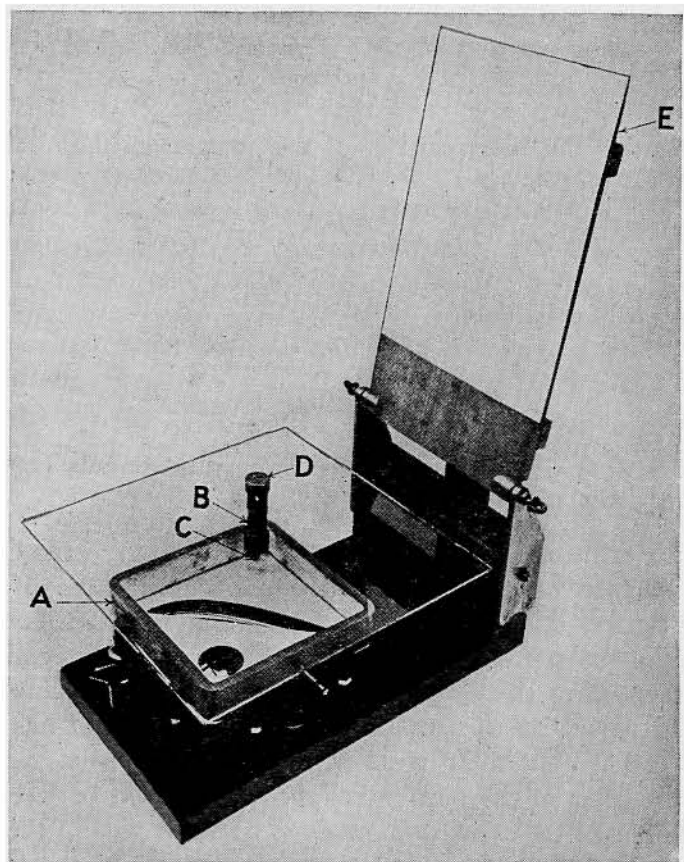


FIG. 157.

made on a sheet of paper attached to the board $E$, which can swing about a horizontal axis at the same height as the steel recording point $D$. To mark any position of the screw it is only necessary to prick a dot on the paper by swinging it down on the recording point. After the point has been made to touch the film at a number of places, the dots recorded on the

paper are used for drawing a contour line. By adjusting the screw $B$, this can be repeated for as many contour lines as may be required. When these lines have been mapped, the volume and the corresponding torque can be obtained by summation. The slopes and the corresponding stresses are obtained by measuring the distances between neighboring contour lines. A better accuracy for measuring slopes can be obtained by projecting a beam of light onto the surface of the film and measuring the angle of the reflected ray. To establish the relation between the measured slope and the stress, the films covering the two holes mentioned before are compared at the same air pressure. Since both films have the same ratio $p/S$, the corresponding two shafts have the same values of $G\theta$ (see equation $(a)$). Hence, by measuring the slopes of the two soap films we can compare the stresses in the shaft of the given cross section with those in a circular shaft of known diameter under the condition that they have the same angle of twist $\theta$ per unit length and the same shearing modulus $G$. The corresponding ratio $n$ of the torques is determined by the ratio of the volumes between the soap films and the plane of the plate. This ratio gives, evidently, the ratio of the torsional rigidities of the two shafts. Regarding stresses for a circular shaft, the stress can be readily calculated at any point for any given torque $M_t$. The stress $\tau$, produced at any point of the noncircular shaft by the torque $nM_t$, is obtained by multiplying the stress $\tau_0$ in a chosen point of the circular shaft by the experimentally determined ratio of the maximum slopes at the two points under consideration. Figure 158 represents an example of contour lines obtained for a portion of the I-beam (wooden wing spar of an airplane). From the close grouping
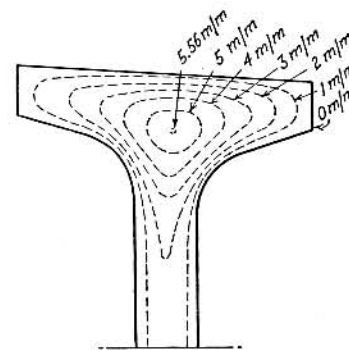


FIG. 158.

of the contour lines at the fillets of the reëntrant corners and at the middle of the upper face, it follows that the shearing stresses are high at these places. The projecting parts of the flange are very lightly stressed. The maximum stress in the middle portion of the web is practically constant along the side of the web and equal to that in a narrow rectangle for the same angle of twist.
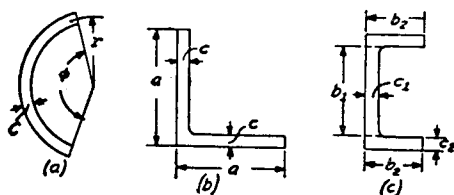


Fig. 159.

**51. Torsion of Rolled Profile Sections.**—Equations (253) and (254), derived for a narrow rectangular cross section, can be used also for approximate solutions in other cases in which the width of the cross section is small. For instance, in the case of the cross sections of equal thickness shown in Fig. 159 (a) and (b) the angle of twist is obtained from equation (253) by putting in this equation for $b$ the developed length of the center line, namely, $b = \varphi r$ in the case of section represented in Fig. 159 (a) and $b = 2a - c$ in the case represented in Fig. 159 (b). The maximum stress for the first of these two sections will be obtained from equation (254). For the angle section (Fig. 159, b) the maximum stress is at the reentrant corner. This maximum stress is obtained by multiplying the stress given by equation (254) by a factor larger than unity; the magnitude of this factor will be discussed later (see article 60, p. 329).

These conclusions follow from the membrane analogy discussed in the preceding article. The reader may have anticipated from that discussion that if the thickness $c$ of the cross section shown in Fig. 159 (a) is small in comparison with

the radius $r$, the parabolic curve shown in Fig. 155 (b) and defining the deflection of the film can still be used with a sufficient accuracy.[8] In such a case the maximum slope of the film and the corresponding maximum stress for the cross section in Fig. 159 (a) will be approximately the same as for a narrow rectangle.

In the case of a channel section (Fig. 159, c) the angle of twist is obtained by subdividing the cross section into the three rectangles shown in the figure and substituting, in equation (253), $b_1 c_1^3 + 2 b_2 c_2^3$ instead of $bc^3$. Then

$$\theta = \frac{3M_t}{(b_1 c_1^3 + 2 b_2 c_2^3)G}. \tag{256}$$

To calculate the stress, which occurs at the middle of the sides $b_2$ of the sections of flanges, it is only necessary, as seen from equations (253) and (254), to multiply $\theta$ by $c_2 G$; then

$$\tau = \frac{3M_t \cdot c_2}{b_1 c_1^3 + 2 b_2 c_2^3}. \tag{257}$$

The same approximate equations can be used also in the case of the twist of I beams [9] with a constant thickness of the flanges (Fig. 160, a).

In the case of an I beam with sloping flanges, Fig. 160 (b), we denote by $c_2$ the thickness of the flange at the edges and by $c_3$ the largest thickness of the flange defined by the equation:

$$c_3 = c_2 + \tfrac{1}{2} b_2 \tan \alpha.$$

Using, then, equation (255) for flanges, we conclude that the angle of twist $\theta$ is obtained from equation (256) by substituting

---

[8] The deflection surface here is no longer cylindrical, but if $c$ is small in comparison with $r$, the curvature of the film in the tangential direction is small in comparison with that in the radial direction and can be neglected.

[9] The maximum stress occurs at the reentrant corners and will be discussed later (see art. 60, p. 329).

in it the quantity

$$\tfrac{1}{4}(c_2 + c_3)(c_2{}^2 + c_3{}^2)$$

instead of $c_2{}^3$.

The maximum stress usually occurs at the fillets and is of a localized character. Its magnitude will be discussed in art. 60. Considerable stress may also occur at the points $m$, Fig. 160 (b), at the middle of the outer surfaces of the flanges.
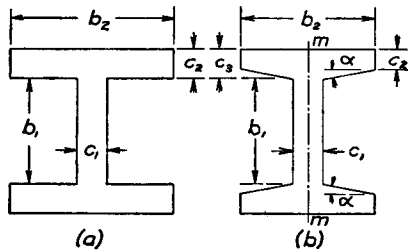


FIG. 160.

This latter stress is obtained, as before, by multiplying the angle of twist $\theta$ by $c_3G$, where $c_3$ is the maximum thickness of the flange.

It should be noted that in the derivation of equation (256) the formula for an infinitely narrow rectangle was used, and that the action of the narrow sides of the rectangle in Fig. 155 on the magnitude of the volume bounded by the soap film was entirely neglected. Owing to the presence of the narrow sides, the volume will evidently be somewhat diminished. At the same time at the corners of the channel section, Fig. 159 (c), where two rectangles come together, a larger deflection of the soap film should be expected than for a single rectangle, and this added deflection will cause some increase in the volume. Thus two factors, which were neglected in the derivation of equation (256), are acting in opposite directions and to some extent neutralize each other, so that equation (256) is sufficiently accurate—especially for thin-walled sections.[10]

---

[10] The experiments with torsion of thin-walled I beams were made

For the cases of torsion of rolled I beams and channels in which the thickness of the flanges is not small and is varying along the width of the flange, a more elaborate formula for torsional rigidity has been developed, which is in a very satisfactory agreement with experiments.[11]

### Problems

1. Find the ratio of the angles of twist of a seamless and of a split circular thin tube of equal geometrical dimensions (Fig. 161) under the action of equal torques.
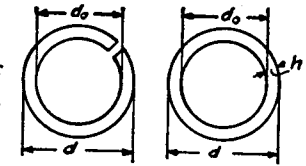


FIG. 161.

*Solution.* By using equations (151), Part I, and (253) we obtain for a seamless and for a split tube respectively

$$\theta = \frac{32M_t}{\pi d^4\left(1 - \dfrac{d_0{}^4}{d^4}\right)G};$$

$$\theta_1 = \frac{3M_t}{\pi\left(\dfrac{d + d_0}{2}\right)\left(\dfrac{d - d_0}{2}\right)^3 G}.$$

The ratio of the angles of twist is

$$\frac{\theta}{\theta_1} = \frac{2}{3}\frac{(d - d_0)^2}{d^2 + d_0{}^2}.$$

For very thin tubes $(d^2 + d_0{}^2) \approx 2d^2$ and the ratio of angles of twist is

$$\frac{4}{3}\left(\frac{h}{d}\right)^2.$$

---

by the writer, Bulletin of the Polytechnical Institute, St. Petersburg, Vol. 5, 1906. They showed a satisfactory agreement with equation (256). A very extensive series of torsional tests of rolled beams were made by A. Föppl, Sitz. Berichte d. Bayer. Akad. d. Wiss., 1921, p. 295, and "Der Bauingenieur," Vol. 3, 1922, p. 42. Some correction factors for equation (256) were suggested on a basis of these experiments.

[11] The experiments on a basis of which that formula was derived were made by Inge Lyse and B. G. Johnston, Lehigh University Publication, Vol. 9, 1935.

2. Determine the angle of twist per inch of a channel (Fig. 159, c) if $M_t = 20,000$ lbs. ins., $b_1 = 10$ in., $b_2 = 3.5$ in., $c_1 = 0.4$ in., $c_2 = 0.6$ in., $G = 12 \times 10^6$ lbs., per sq. in.

*Solution.*

$$\theta = \frac{3 \times 20,000}{(10 \times 0.4^3 + 7 \times 0.6^3)12 \times 10^6} = 0.00233 \text{ radians per in.}$$

3. Determine the ratio of the maximum shearing stresses of the tubes discussed in problem 1 if the torques are equal for both tubes.

4. Determine the torsional rigidity $C$ for the I beam considered on p. 275 if the sloping of the flanges is considered as explained on p. 276.

**52. Torsion of Thin Tubular Members.**—In discussing the torsion of thin tubular members the membrane analogy again can be used to advantage.[12]   In this case the outer and inner boundaries of the cross section are to be located in different horizontal planes with the membrane connecting the boundaries, as at $mn$ in Fig. 162.   If the thickness of the tube is small, the curvature of the membrane may be neglected,
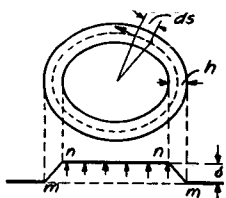


FIG. 162.

i.e., the lines $mn$ may be considered straight. The slope of the membrane surface is then constant over the thickness of the wall and is equal to $\delta/h$, where $\delta$ is the difference in the levels of the two boundaries and $h$ is the thickness of the tube, which may vary along the circumference of the cross section. The membrane analogy indicates that in this case the shearing stresses are uniformly distributed over the thickness of the wall and are given by the slope

$$\tau = \frac{\delta}{h}. \tag{a}$$

The stress along the circumference is therefore inversely proportional to the thickness of the wall. The volume included between the surfaces $mm$ and $nn$ is calculated by

---

[12] Torsion of tubular members was discussed by R. Bredt, V. D. I., Vol. 40, p. 815, 1896.   See also T. Prescott, Phil. Mag., Vol. 60, 1920.

using the center line of the ring cross section, indicated by the dotted curve in the figure.   If $A$ is the area bounded by this line, the volume $mmnn$ is $A\delta$ and, from the membrane analogy, we obtain

$$M_t = 2A\delta. \tag{b}$$

From eqs. (a) and (b) we then find

$$\tau = \frac{M_t}{2Ah}. \tag{258}$$

This equation may be used in calculating the stresses in tubular members under torsion if the thickness of the wall is small, variation in thickness is not abrupt, and there are no reëntrant corners.

The angle of twist $\theta$ per unit length of a tubular member may be calculated by considering the strain energy of torsion. The strain energy per unit length of the tubular member is

$$U = \int_0^s \frac{\tau^2 h\, ds}{2G},$$

where $s$ is the length of the center line of the ring cross section shown in Fig. 162 by the dotted line.   Substituting expression (258) for $\tau$ in this equation and equating the strain energy to the work done by the torque, we obtain

$$\frac{M_t^2}{8A^2G} \int_0^s \frac{ds}{h} = \frac{1}{2} M_t\theta, \tag{c}$$

from which

$$\theta = \frac{M_t}{4A^2G} \int_0^s \frac{ds}{h} = \frac{1}{2AG} \int_0^s \tau\, ds. \tag{259}$$

In the case of a tube of uniform thickness $\tau$ is constant and eq. 259 becomes

$$\theta = \frac{\tau s}{2AG}. \tag{260}$$

From this equation the angle of twist can be readily calculated as soon as the dimensions of the cross section are given, and $\tau$ is determined by using formula (258).

Equation (259), derived from a consideration of the strain energy of a twisted tubular member, can be obtained also from the membrane analogy. Considering the equilibrium of the plane $n$–$n$ in Fig. 162, we conclude that the pressure $pA$ [13] acting on this plane is balanced by the tensile forces $S$ acting in the membrane. The tensile force $Sds$, acting on an element $ds$ of the boundary, has a small slope equal to $\tau$; hence the vertical component of this force is $\tau Sds$, and the condition of equilibrium of the plane $n$–$n$ is

$$pA = \int_0^s \tau Sds. \tag{d}$$

Observing that the tension $S$ in the membrane is constant and that $p/S = 2G\theta$ (see eq. $a$, art. 50), we find from equation $(d)$:

$$\frac{p}{S} = \frac{1}{A}\int_0^s \tau ds = 2G\theta.$$

Solving this equation for $\theta$, we obtain formula (259), given above, for the angle of twist.

Sometimes the torsional stresses in a tubular member with intermediate walls, as in Fig. 163 $(a)$, must be calculated. The boundary of the cross section in this case is formed by the three closed curves. In applying the membrane analogy these curves are to be located in three different horizontal planes, $nn$, $pp$, and $mm$, as shown in Fig. 163 $(b)$. The soap film connecting these three curves forms a narrow surface, the cross sections of which are shown by the lines $mn$, $np$, and $pm$. Assuming again that the wall thicknesses—$h_1$, $h_2$, and $h_3$—are small, and neglecting the curvature of the membrane in the directions normal to the boundaries, we consider that the lines $mn$, $np$, and $pm$ are straight. In such a case
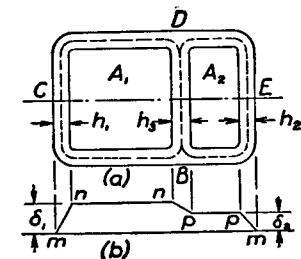


FIG. 163.

[13] In the case of thin-walled members the area $A$ bounded by the dotted line can be considered instead of the area of the plane $n$–$n$.

the slopes of the membrane, giving the stresses in the wall of the tubular member, are:

$$\tau_1 = \frac{\delta_1}{h_1}, \qquad \tau_2 = \frac{\delta_2}{h_2}, \tag{e}$$

$$\tau_3 = \frac{\delta_1 - \delta_2}{h_3} = \frac{h_1\tau_1 - h_2\tau_2}{h_3}. \tag{f}$$

The magnitude of the torque producing these stresses is obtained by doubling the volume of the space $mnppm$ in Fig. 163 $(b)$. If we denote the areas bounded by the dotted lines in Fig. 163 $(a)$ by $A_1$ and $A_2$ this torque is

$$M_t = 2(A_1\delta_1 + A_2\delta_2), \tag{g}$$

or, by using equations $(e)$, we obtain

$$M_t = 2A_1h_1\tau_1 + 2A_2h_2\tau_2. \tag{h}$$

Further equations for the solution of the problem are obtained by applying equation (259) to the two closed curves indicated by the dotted lines in Fig. 163 $(a)$. Assuming that the portion $BCD$ of the wall has a constant thickness $h_1$ and that the portions $DEB$ and $DB$ have the constant thicknesses $h_2$ and $h_3$, respectively, equation (259) becomes

$$\tau_1 s_1 + \tau_3 s_3 = 2G\theta A_1, \tag{i}$$

$$\tau_2 s_2 - \tau_3 s_3 = 2G\theta A_2. \tag{j}$$

Here $s_1$, $s_2$, and $s_3$ are the lengths measured along the dotted lines $BCD$, $DEB$ and $DB$, respectively. In applying the integral (259) to the closed curves $BCDB$ and $DEBD$, we are passing the portion $DB$ of the length $s_3$ in the two opposite directions. Hence the second terms on the left sides of equations $(i)$ and $(j)$ appear with opposite signs. The angle of twist $\theta$ on the right side of the equations $(i)$ and $(j)$ is evidently the same as the angle of twist of the entire tubular member. The four equations $(f)$, $(h)$, $(i)$ and $(j)$ contain the four unknown $\tau_1$, $\tau_2$, $\tau_3$ and $\theta$, which can be easily calculated. Eliminating $\theta$, we obtain for shearing stresses the following formulas:

$$\tau_1 = M_t \cdot \frac{h_3 s_2 A_1 + h_2 s_3 (A_1 + A_2)}{2[h_1 h_3 s_2 A_1^2 + h_2 h_3 s_1 A_2^2 + h_1 h_2 s_3 (A_1 + A_2)^2]}, \tag{k}$$

$$\tau_2 = M_t \cdot \frac{h_3 s_1 A_2 + h_1 s_3 (A_1 + A_2)}{2[h_1 h_3 s_2 A_1{}^2 + h_2 h_3 s_1 A_2{}^2 + h_1 h_2 s_3 (A_1 + A_2)^2]}, \quad (l)$$

$$\tau_3 = M_t \cdot \frac{h_1 s_2 A_1 - h_2 s_1 A_2}{2[h_1 h_3 s_2 A_1{}^2 + h_2 h_3 s_1 A_2{}^2 + h_1 h_2 s_3 (A_1 + A_2)^2]} \cdot \quad (m)$$

If the wall DB of the cross section in Fig. 163 (a) is the plane of symmetry of the cross section we have

$$s_1 = s_2, \qquad h_1 = h_2, \qquad \text{and} \qquad A_1 = A_2,$$

and equation (m) gives $\tau_3 = 0$. Thus in this case the torque is taken entirely by the outer wall of the tube, and the intermediate web remains unstressed.[14]

To obtain the angle of twist $\theta$ for the tubular member, we have to substitute the calculated values of stresses in equations (i) or (j). Thus the torsional problem for a tubular member, such as is shown in Fig. 163, can be readily solved with a sufficient accuracy provided the wall thickness is small in comparison with the general dimensions of the cross section.

### 53. Torsion of Thin-Walled Members in which Some Cross Sections are Prevented from Warping.

—In our previous discussion of the twist of I beams and channels (p. 275) it was assumed that the torque was applied at the ends of the bar and that all cross sections were completely free to warp. There are cases, however, where the conditions are such as to cause one or more cross sections to remain plane and the question arises as to how such prevention of warping affects the angle of twist and the distribution of stresses. For bars of solid cross sections, such as ellipses or rectangles such constraint produces only a negligible effect on the angle of twist [15] if the cross-sectional dimensions are small in comparison with the length of the bar. With I beams, channels and other thin-walled members the prevention of warping of the cross sections during twist is accompanied by a bending of the

---

[14] The small stresses corresponding to the change in slope of the membrane across the thickness of the web are neglected in this derivation.

[15] For the discussion of this question see "Theory of Elasticity," p. 273.

flanges and may have a considerable effect on the angle of twist, depending on the rigidity of the flanges. A simple case of this is an I beam which is twisted by a couple applied at the middle and supported [16] at the ends (Fig. 164). From
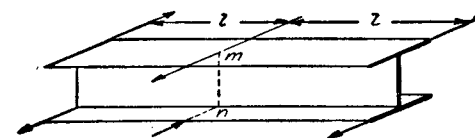


FIG. 164.

symmetry, the cross section mn must remain plane during twist and the consequent rotation of this cross section with respect to the end cross sections is accompanied by bending of the flanges. The end torque is balanced at any cross
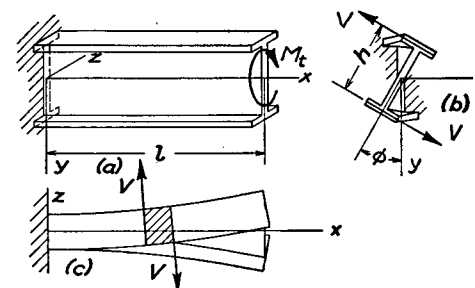


FIG. 165.

section partially by shearing stresses due to the twisting and partially by shearing stresses due to the bending of the flanges.[17] Figure 165 (a) represents half of the beam shown in Fig. 164. The middle section mn remains plane due to

---

[16] Supports are such that the ends of the beam can not rotate about a longitudinal axis but are free to warp.

[17] See paper by the author, Bull. Polyt. Inst. S. Petersburg, 1905–1906, and Ztschr. f. Math. u. Phys., Vol. 58, 1910, p. 361. See also K. Huber, Dissertation, München, 1922, and C. Weber, Ztschr. f. angew. Math. u. Mech., Vol. 6, 1926, p. 85. Further discussion of the problem for various shapes of thin-walled members is given by A. Ostenfeld,

symmetry and we may consider it as built in, with the torque applied at the other end of the beam. Let $\varphi$ be the angle of twist for any cross section of the beam. Then $d\varphi/dx = \theta$ is the angle of twist per unit length of the beam. That part of the torque $M_t'$ which is balanced by the shearing stresses due to torsion is determined from the equation:

$$M_t' = C\theta, \qquad (a)$$

in which $C$ is the *Torsional Rigidity* of the bar (see p. 270, Part I). In order to determine the portion $M_t''$ of the torque which is balanced by the shearing forces in the flanges due to bending, we must consider the bending of a flange (Fig. 165, $c$). Denoting by $h$ the distance between the centroids of the flanges (Fig. 165, $b$), the deflection at any cross section of the upper flange is

$$z = \frac{h\varphi}{2}, \qquad (b)$$

and by differentiation we obtain:

$$\frac{d^3z}{dx^3} = \frac{h}{2}\frac{d^3\varphi}{dx^3} = \frac{h}{2}\frac{d^2\theta}{dx^2}. \qquad (c)$$

Now, if we denote by $D$ the flexural rigidity of one flange in the plane $xz$ and observe that $z$ is positive as shown (Fig. 165, $c$), the expression for the shearing force in the flange due to bending becomes

$$V = \frac{dM}{dx} = D\frac{d^3z}{dx^3} = \frac{Dh}{2}\frac{d^2\theta}{dx^2}. \qquad (d)$$

Considering the positive direction of $V$ (as shown in Fig. 165, $c$), we therefore have

$$M_t'' = -Vh = -\frac{Dh^2}{2}\frac{d^2\theta}{dx^2} \qquad (e)$$

Laboratorium f. Baustatik d. techn. Hochschule, Kopenhagen, Mitteilung Nr. 6, 1931. The case of rectangular tubular members was discussed by H. Reissner, Zeitschr. f. Flugtechnik u. Motorluftschiffahit, Vol. 17, 1926, p. 385 and Vol. 18, 1927, p. 153.

and the total torque is

$$M_t = M_t' + M_t'' = C\theta - \frac{Dh^2}{2}\frac{d^2\theta}{dx^2}. \qquad (261)$$

In our case, $M_t$ is constant along the length $l$ of the beam, and the general solution of equation (261) is

$$\theta = \frac{M_t}{C}\left[ 1 - \frac{\cosh\left(\dfrac{l-x}{a}\right)}{\cosh\left(\dfrac{l}{a}\right)} \right], \qquad (f)$$

in which

$$a^2 = \frac{Dh^2}{2C}. \qquad (g)$$

Since the flexural rigidity $D$ and torsional rigidity $C$ are both measured in the same units (lbs. in.²), equation $(g)$ shows that $a$ has the dimension of length and depends upon the proportions of the beam.

If we know the portions $M_t'$ and $M_t''$ of the total torque $M_t$ may be calculated for any cross section from equations $(a)$ and $(e)$. For the built-in section $x = 0$, $\theta = 0$, and we obtain, from $(a)$, $M_t' = 0$. Hence at this point the whole torque is balanced by the moment of the shearing forces due to bending in the flanges, and we have $V = -M_t/h$. For the other end $x = l$, and from equation $(f)$

$$\theta = \frac{M_t}{C}\left( 1 - \frac{1}{\cosh\left(\dfrac{l}{a}\right)} \right). \qquad (h)$$

If the length of the beam is large in comparison with the cross sectional dimensions, $l$ is large in comparison with $a$, and the second term in the parenthesis of equation $(h)$ becomes negligible; hence $\theta$ approaches the value $M_t/C$.

Equation $(d)$ gives the shearing force in the flanges, and

from this the bending moment in the flange is

$$M = \frac{Dh}{2}\frac{d\theta}{dx}, \qquad (i)$$

or, substituting equation $(f)$ for $\theta$, and using notation $(g)$,

$$M = \frac{Dh}{2}\frac{M_t}{aC}\frac{\sinh\left(\dfrac{l-x}{a}\right)}{\cosh\left(\dfrac{l}{a}\right)} = \frac{a}{h}M_t\frac{\sinh\left(\dfrac{l-x}{a}\right)}{\cosh\left(\dfrac{l}{a}\right)}. \qquad (j)$$

For the bending moment at the built-in end we find

$$M_{\max} = \frac{a}{h}M_t \tanh\left(\frac{l}{a}\right). \qquad (k)$$

When $l$ is several times larger than $a$, $\tanh(l/a)$ approaches unity, and we can use

$$M_{\max} = \frac{aM_t}{h}, \qquad (l)$$

i.e., the maximum bending moment in the flange is the same as that in a cantilever of length $a$, loaded at the end by a force $M_t/h$. For a very short beam $l$ is small in comparison with $a$, $\tanh(l/a)$ approaches $l/a$, and we have, from equation $(k)$,

$$M_{\max} = \frac{M_t l}{h}. \qquad (m)$$

Take, as an example, a 12″ standard I beam with a cross-sectional area of 9.26 sq. in. Replacing the cross section by the equivalent cross section shown in Fig. 166 consisting of three rectangles having the same cross sectional areas of flanges and web [18] and using equation (256), we find

$$C = 1/3(10.91 \times 0.35^3 + 2 \times 5 \times 0.544^3)G = 0.692G. \qquad (n)$$

The magnitude of $D$ is obtained [19] by taking half of the moment of

---

[18] A somewhat better approximation for $C$ can be obtained by taking account of sloping of the flanges as explained on p. 276.

[19] The moment of inertia of the cross section of the web is neglected here.

inertia of the standard cross section about the vertical principal axis and multiplying it by $E$. Then $D = (9.5/2) \cdot E = 4.75E$, and we obtain from equation $(g)$

$$a = h\sqrt{\frac{D}{2C}} = h\sqrt{\frac{4.75 \times 2.6}{0.692 \times 2}} = 2.99h. \qquad (o)$$

Hence if the beam is loaded as in Fig. 164, the maximum bending moment in the flange, from equation $(l)$, is approximately three times the torque $M_t$, provided the beam is long enough to make $\tanh(l/a)$ approach 1. For instance, for $l/a = 2$, $l$ approaches $6h$, $\tanh(l/a) = 0.96$, and the error of the above calculation is 4 per cent.
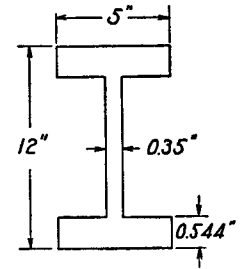


Fig. 166.

To calculate the angle of twist $\varphi$ we use equation $(f)$. Recalling that $\theta = d\varphi/dx$, integrating equation $(f)$ and adjusting the constant of integration to make $\varphi = 0$ when $x = 0$, we obtain

$$\varphi = \frac{M_t}{C}\left[x + \frac{a\sinh\left(\dfrac{l-x}{a}\right)}{\cosh\left(\dfrac{l}{a}\right)} - a\tanh\left(\frac{l}{a}\right)\right]. \qquad (p)$$

Substituting $x = l$ in this equation, the angle of twist at the end is

$$(\varphi)_{x=l} = \frac{M_t}{C}\left(l - a\tanh\left(\frac{l}{a}\right)\right). \qquad (q)$$

The second term in the parenthesis represents the effect of the bending of the flanges on the angle of twist. For long beams $\tanh(l/a) \approx 1$ and equation $(q)$ becomes

$$(\varphi)_{x=l} = \frac{M_t}{C}(l - a). \qquad (r)$$

The effect of the bending of the flanges on the angle of twist is therefore equivalent to diminishing the length $l$ by the quantity $a$.

The method developed above for a constant torque may

also be used when the torque varies along the length of the beam. It is only necessary to substitute in equation (261) in place of $M_t$ its expression as a function of $x$.
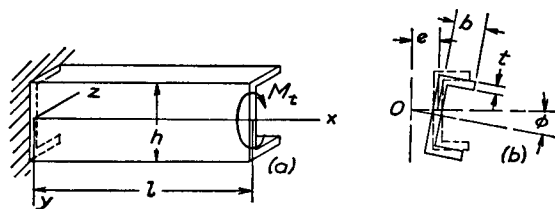


FIG. 167.

In the preceding discussion of torsion of an I beam, Fig. 165, it was concluded from symmetry that its cross sections are rotating with respect to the center axis of the beam. Hence only bending of the flanges has to be considered. It is seen also that this bending does not interfere with the simple torsion of the web since at the points of junction of the web and flanges the bending stresses in the flanges vanish. In the case of non-symmetrical cross sections or cross sections with only one axis of symmetry the problem becomes more complicated since not only bending of flanges but also that of the web will be produced during torsion. As an example of such a kind, let us consider the case of torsion of a channel, Fig. 167. It was already shown (see p. 51) that in this case each cross section rotates with respect to the center of twist $O$ which is on the horizontal axis of symmetry of the cross section at a distance (see p. 53)

$$e = b^2 h^2 t / 4 I_z \qquad (s)$$

from the middle plane of the web. From this it follows that the deflections of the flanges and of the web in their respective planes are

$$z = \pm \frac{h}{2} \varphi \qquad \text{and} \qquad y = e \varphi, \qquad (t)$$

where $\varphi$, as before, is the small angle of twist. It is assumed

that the thickness of the flanges and of the web are small so that the stresses due to bending of these parts in the directions perpendicular to their surfaces can be neglected. In such a
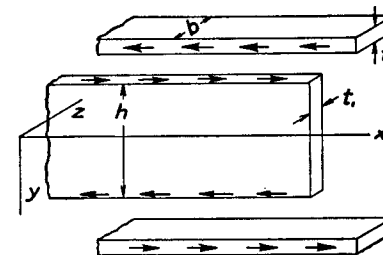


FIG. 168.

case the action between the upper flange and the web is represented only by shearing stresses $(\tau_{xz})_0$ shown in Fig. 168. These stresses produce bending and compression of the flange. If $S$ is the magnitude of the compressive force in the flange at a distance $x$ from the built-in end, we have

$$t(\tau_{xz})_0 = -\frac{dS}{dx} \qquad \text{and} \qquad S = t \int_x^l (\tau_{xz})_0 dx.$$

The magnitude of the force $S$ is now determined from the condition that the strain $\epsilon_x$ in a longitudinal direction at the junction of the web and the flange is the same for both these parts. Calculating the curvatures of the deflection curves from the expressions $(t)$, we find that this condition is represented by the equation

$$\epsilon_x = e \frac{d^2\varphi}{dx^2} \cdot \frac{h}{2} = \frac{h}{2} \frac{d^2\varphi}{dx^2} \cdot \frac{b}{2} - \frac{S}{btE}, \qquad (u)$$

from which, using expression $(s)$, and using notation $I_z = t_1 h^3/12 + bth^2/2$, we obtain

$$S = \frac{E b^2 h^4 t t_1}{48 I_z} \cdot \frac{d^2\varphi}{dx^2}. \qquad (v)$$

Having this expression for $S$ we can readily calculate the shearing stresses in the web and the flanges and also the portion $M_t''$ of the torque balanced by these stresses. Let us begin with the shearing stresses in the web. Taking two adjacent cross sections $mn$ and $m_1n_1$, Fig. 169 (a), and con-
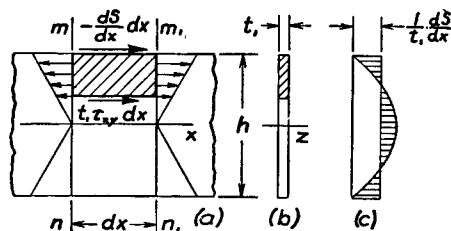


FIG. 169.

sidering in the usual way the equilibrium of the shaded element, we obtain the equation

$$\tau_{xy}t_1dx - \frac{dS}{dx}dx + \frac{dM}{dx}\cdot\frac{Q}{I_z'}dx = 0$$

in which $Q$ is the moment with respect to $z$ axis of the shaded portion of the cross section of the web, Fig. 169 (b), $I_z' = t_1h^3/12$ is the moment of inertia of the cross section of the web with respect to $z$ axis and $M$ is the bending moment in the web taken positive if producing tension at the upper edge and equal to

$$M = EI_z'e\frac{d^2\varphi}{dx^2} = Sh.$$

The expression for the stresses $\tau_{xy}$ then becomes

$$\tau_{xy} = \frac{dS}{t_1dx}\left(1 - \frac{Qh}{I_z'}\right).$$

Observing that the variation of $Q$ along the depth of the cross section follows the parabolic law, we find that the distribution of $\tau_{xy}$ is such as given by the shaded area in Fig. 169 (c) and that the resultant shearing force in the web vanishes. This

latter conclusion should be anticipated, since the shearing forces in the web and in the two flanges must balance the portion $M_t''$ of the torque and this is possible only if the shearing force in the web vanishes and the shearing forces in the two flanges form a couple.
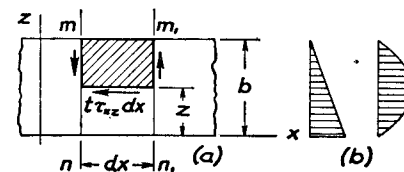


FIG. 170.

In calculating shearing stresses $\tau_{xz}$ in the flange, Fig. 170 (a), we observe that at a cross section $mn$ there are acting a compressive force $S$ and a bending moment [20]

$$M = D\frac{d^2\varphi}{dx^2}\cdot\frac{h}{2}.\tag{w}$$

Considering the equilibrium of the shaded element between the two adjacent cross sections we then obtain

$$t\tau_{xz}dx + \frac{dS}{dx}dx\cdot\frac{b-z}{b} + \frac{dM}{dx}dx\frac{Q_1}{I_1} = 0$$

where $Q_1$ and $I_1$ are to be calculated for the flange in the same manner as $Q$ and $I_z'$ for the web. Substituting for $M$ its expression $(w)$ we obtain

$$\tau_{xz} = -\frac{1}{t}\frac{dS}{dx}\frac{b-z}{b} - \frac{E}{t}\cdot\frac{d^3\varphi}{dx^3}\cdot\frac{hQ_1}{2}.$$

The two terms on the right-hand side of this equation are represented in Fig. 170 (b) by the shaded areas of the triangle and of the parabolic segment respectively. The sum of these two areas multiplied by $t$ gives the total shearing force in the

[20] $D = Etb^3/12$ denotes, as before, the flexural rigidity of the flange in its plane.

flange which is [21]

$$V = \frac{b}{2}\frac{dS}{dx} + E\frac{htb^3}{24}\frac{d^3\varphi}{dx^3}$$

or substituting for $S$ its expression $(v)$ and setting $\theta = d\varphi/dx$ we obtain

$$V = \frac{Eb^3ht}{24}\left(1 + \frac{t_1h^3}{4I_z}\right)\frac{d^2\theta}{dx^2}. \qquad (x)$$

Hence the torque balanced by the shearing forces in the flanges is

$$M_t'' = -Vh = -\frac{Dh^2}{2}\left(1 + \frac{t_1h^3}{4I_z}\right)\frac{d^2\theta}{dx^2}. \qquad (y)$$

This expression, instead of the expression $(e)$ obtained for the I beam, should be used in calculating the angle of twist of the channel shown in Fig. 167. Hence all the conclusions obtained for the I beam can be used also for the channel if the quantity $a^2$ given by expression $(g)$ is replaced by the quantity

$$a^2 = \frac{Dh^2}{2C}\left(1 + \frac{t_1h^3}{4I_z}\right).$$

The method used in discussing torsion of a symmetrical channel, Fig. 167, can be applied also in the more general case of a non-symmetrical channel section, Fig. 171. We begin with determination of the center of twist $O$. Assuming that the channel is built in at one end and loaded at the other end in such a way that the bending without twist occurs in the plane of the web, we find in the usual manner (see p. 53) the shearing forces $R_1$, $R_2$ and $V$ acting in the flanges and in the web of the channel. The resultant of these forces must pass through the center of twist $O$ (see art. 8). Another line passing through the same point is obtained, if we assume that the channel is bent in the horizontal plane and calculate again the
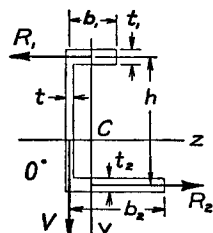


FIG. 171.

three corresponding shearing forces in the flanges and in the web. The point of intersection of the resultant of these latter forces and the previously determined resultant of the forces $R_1$, $R_2$ and $V$ is the required center of twist $O$ of the unsymmetrical cross section. Having this center and proceeding as before (see eqs. $(t)$), we express the deflection curves of the flanges and of the web by the angle of twist $\varphi$. The tension compression forces $S_1$ and $S_2$ in the flanges are now determined from the conditions that at the junctions the longitudinal strain $\epsilon_x$ is the same for the web as for the adjacent flange. When the forces $S_1$ and $S_2$ are calculated, the distribution of shearing stresses can be found as in the above discussed case of a symmetrical channel, and it can be shown [22] that the shearing force in the web vanishes and the shearing forces $R$ in the two flanges give a couple balancing the portion $M_t''$ of the torque.

### Problems

1. A cantilever of a ⌐ section, Fig. 172, built in at one end is twisted by a couple $M_t$ applied at the other end. Find the angle of twist and the maximum bending moment in the flanges.

*Solution.* In this case the center of twist coincides with the centroid $C$ of the cross section. There will be no bending of the web. The forces $S$ are



FIG. 172.

identical in this case for both flanges and the distribution of shearing stresses is such as shown in Fig. 172 $(b)$. The shearing force in the web vanishes and the equal and opposite shearing forces $V$ in the flanges equal

$$\pm\frac{Eb^3ht}{12}\left(2 - \frac{3bt}{2bt + ht_1}\right)\frac{d^3\varphi}{dx^3}$$

form a couple so that

$$M_t'' = -Vh = -Dh^2\left(2 - \frac{3bt}{2bt + ht_1}\right)\frac{d^3\varphi}{dx^3}$$
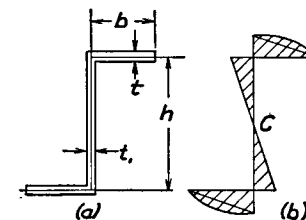
where $D$ is the flexural rigidity of one flange. The angle of twist and the maximum bending moment in the flanges are calculated from eqs. $(k)$ and $(l)$ in which, for this case,

$$a^2 = \frac{Dh^2}{C}\left(2 - \frac{3bt}{2bt + ht_1}\right).$$
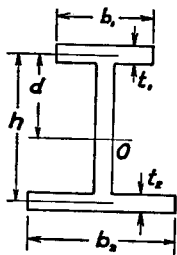
2. Solve the preceding problem assuming that the cross section is as shown in Fig. 173.

*Answer.* The shearing forces in the flanges are

$$V = \pm Dd\frac{d^3\varphi}{dx^3}$$

where

$$D = \frac{Et_1b_1^3}{12}, \qquad \frac{d}{h-d} = \frac{b_2^3t_2}{b_1^3t_1}.$$

FIG. 173.

The torque $M_t''$ taken by the bending of flanges is

$$M_t'' = -Ddh\frac{d^3\varphi}{dx^3}.$$

The value of $a$ to be substituted in eqs. $(k)$ and $(l)$ is obtained from the equation

$$a^2 = \frac{Ddh}{C}.$$

3. Solve the problem 1 for the cross sections shown in Fig. 174.

*Answer.* In both these cases the center of twist $O$ is at the junction of the flanges. Rotation with respect to this point does not produce any bending of flanges in their planes and the entire torque is transmitted by the torsional stresses alone.
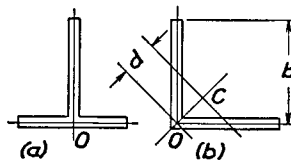
FIG. 174.

## 54. Torsional Buckling of Thin-Walled Compression Members.

—From the discussion of art. 51 it may be concluded that the torsional rigidity $C$ of thin-walled open sections decreases as the cube of the wall thickness while the flexural rigidities are decreasing in a smaller proportion. Hence a thin-walled member is more flexible in torsion than in flexure. If such

a member is submitted to the action of an axial compression a *torsional buckling* may occur [23] at a smaller load than the Euler load discussed in art. 35. The approximate magnitude of the load at which this torsional buckling occurs may be readily obtained by using in each particular case an equation, equivalent to equation (261) of the preceding article, defining the torsion of a thin-walled member one of the cross sections of which is prevented from warping. As an example let us consider here a column of a channel cross section, built-in at the bottom and centrally loaded at the top (Fig. 175, $a$). If the column buckles sidewise as indicated in the figure by the dotted lines, the vertical compressive force $P$ gives, in each cross section, a component $Pdy/dx$ acting in the plane of the cross section and passing through its centroid. The action of this force can be replaced by the bending action of an equal force passing through the shear center $O$, Fig. 175 $(b)$, and the torque
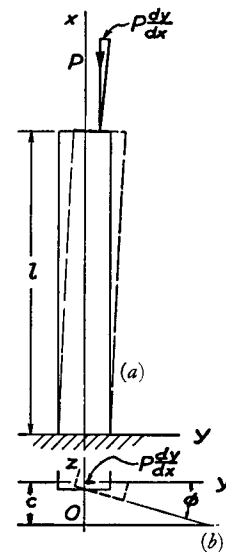
FIG. 175.

$$M_t = cP\frac{dy}{dx} = c^2P\frac{d\varphi}{dx} = c^2P\theta \qquad (a)$$

in which $c$ denotes the distance of the shear center $O$ from the centroid of the cross section and $\varphi$ is the angle of twist. If the compressive force $P$ is several times smaller than the Euler load for the buckling of the column in the $xy$ plane the above mentioned bending action may be neglected and only the

[23] The torsional buckling was discussed by H. Wagner, Technische Hochschule, Danzig, the 25th Anniversary Publication, 1904–1929. See also H. Wagner and W. Pretschner, Luftfahrtforschung, Vol. 11, 1934, p. 174; and R. Kappus, Luftfahrtforschung, Vol. 14, 1937, p. 444. English Translation of the later paper see in Tech. Mem. No. 851, 1938, Nat. Adv. Com. Aern. Regarding experiments with torsional buckling see paper by A. S. Niles, Tech. Notes No. 733, 1939, Nat. Adv. Com. Aern.

torsion considered.[24]   In such a case equation (261) can be used. Substituting for $M_t$ expression (a) and for $M_t''$ expression (y) derived for a channel section, we obtain

$$c^2 P\theta = C\theta - \frac{Dh^2}{2}\left(1 + \frac{t_1 h^3}{4I_z}\right)\frac{d^2\theta}{dx^2}$$

or

$$\frac{d^2\theta}{dx^2} + k^2\theta = 0 \qquad (b)$$

where

$$k^2 = \frac{c^2 P - C}{\dfrac{Dh^2}{2}\left(1 + \dfrac{t_1 h^3}{4I_z}\right)}. \qquad (c)$$

Since the lower end of the column is built in and there is no bending moment acting on the flanges at the top, the end conditions for $\theta$ are

$$(\theta)_{x=0} = 0, \qquad \left(\frac{d\theta}{dx}\right)_{x=l} = 0. \qquad (d)$$

To satisfy the first of these conditions we take the solution of the equation (b) in the following form:

$$\theta = A \sin kx. \qquad (e)$$

This solution will satisfy also the second of the conditions (d) if we put

$$kl = \frac{\pi}{2}, \qquad k = \frac{\pi}{2l}. \qquad (f)$$

Substituting for $k^2$ its expression (c) we obtain

$$P_{cr} = \frac{\pi^2}{4l^2} \cdot \frac{Dh^2}{2c^2}\left(1 + \frac{t_1 h^3}{4I_z}\right) + \frac{C}{c^2}. \qquad (262)$$

The first term on the right side of this equation is due to local bending resistance at the built-in end, and the second, independent of the length $l$, is due to torsional resistance.

If instead of a channel we have a thin-walled open section

---

[24] If this force is approaching the Euler load a more elaborate analysis is required as shown by R. Kappus, footnote 23.

of some other shape we have only properly to change the first member in expression (262) as explained in the preceding article.   In a particular case of a ⊥ section or of an angle, Fig. 174, the center of twist $O$ coincides with the point of junction of flanges, and there will be no bending of flanges in their respective planes during torsion.   Hence the first term in the expression (262) vanishes, and we obtain

$$P_{cr} = \frac{C}{c^2}. \qquad (263)$$

It should be noted that in the discussion of the preceding article the thickness of the flanges was assumed as very small and the flexural rigidity of the flanges in the direction perpendicular to the flange was neglected.   If that rigidity is taken into consideration, an additional term on the right side of the expression (263) appears, the magnitude of which for an angle with equal legs is $\pi^2 2bt^3 E/12(1 - \mu^2)4l^2$.   This is the sum of the Euler loads calculated for the two flanges.   It rapidly decreases as the length $l$ increases so that expression (263) has a satisfactory accuracy for long columns.[25]   Having the value of the torsional buckling load for a column with one end built-in and the other free, we readily obtain the buckling load for a member with hinged ends by substituting, as usual, $l/2$ for $l$.   In this way we obtain for a channel member with hinged ends, from expression (262)

$$P_{cr} = \frac{\pi^2}{l^2}\frac{Dh^2}{2c^2}\left(1 + \frac{t_1 h^3}{4I_z}\right) + \frac{C}{c^2}. \qquad (264)$$

---

[25] A more accurate formula for torsional buckling of an angle with equal legs was derived by the writer, considering each flange as a longitudinally compressed rectangular plate.   See Bull. of the Polyt. Inst. Kiev, 1907, and also Ztschr. f. Math. u. Phys., Vol. 58, 1910.   It seems that that problem was the first case in which the torsional buckling was discussed.   The fundamental equation (261) was given by the writer in 1905, loc. cit., p. 283.   The extension of this equation on channel sections was given by C. Weber, loc. cit., p. 283.   The application of the equation in studying torsional buckling is due to H. Wagner, Technische Hochschule, Danzig, the 25th Anniversary Publication, 1929.

It may be seen from the formula that the first term on the right side, dealing with bending of flanges, diminishes as the length $l$ increases so that for comparatively long members the stability is practically controlled by the second term in expression (264).

The formula was developed by assuming that the cross sections at the ends of the member are free to warp. Any constraint preventing free warping of the end cross sections will result in an increase of the first term in formula (264). If the ends are built-in the length $l/2$ instead of $l$ must be substituted in formula (264) and we obtain for this case

$$P_{cr} = \frac{4\pi^2}{l^2} \frac{Dh^2}{2c^2}\left(1 + \frac{t_1 h^3}{4 I_z}\right) + \frac{C}{c^2}. \qquad (265)$$

It is interesting to note that the formula

$$P_{cr} = \frac{C}{c^2}$$

which is obtained for the critical load if the bending resistance can be neglected follows at once from the energy consideration. Since during torsion the cross sections rotate with respect to their shear centers, the center line of the member becomes a helix, the tangent to which makes an angle $\theta c$ with the initially straight axis of the member. Due to this angle the compressive forces $P$ come together by an amount $\theta^2 c^2 l/2$. Equaling the corresponding work to the strain energy of torsion we obtain

$$P \frac{l}{2} \theta^2 c^2 = \frac{C\theta^2}{2} l$$

which gives

$$P_{cr} = \frac{C}{c^2}.$$

**55. Longitudinal Normal Stresses in Twisted Bars.**—In discussing torsion of circular shafts (art. 58, Part I), it is usually assumed that the distance between any two cross sections of a shaft remains unchanged during torsion. It will be shown now that this assump-

tion is very accurate for such material as steel in which the maximum shearing strain during torsion is very small. But for a material such as rubber the maximum shearing strain during torsion may be considerable. Then the change in distances between the cross sections of the shaft during torsion must be taken into account if we wish to get the correct values of stresses. The same conclusion holds also for steel torsional members of a narrow rectangular cross section or of thin-walled cross sections such as shown in Fig. 159.

Let us begin the discussion with the case of a solid circular shaft and assume first that the distance between the two consecutive cross sections, Fig. 176, remains unchanged during torsion. If $\gamma$ is the shearing strain at the surface of the shaft, the elongation of the longitudinal fiber $ac$ is obtained from the triangle $acc_1$ as follows:
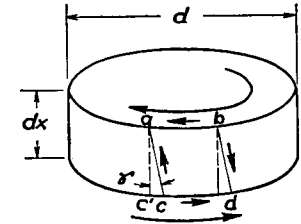


FIG. 176.

$$ac = \frac{ac_1}{\cos \gamma} = ac_1 \left(1 + \frac{1}{2}\gamma^2\right).$$

Expressing $\gamma$ by the angle of twist per unit length $\theta$, we obtain

$$ac = ac_1 \left[1 + \frac{1}{2}\left(\frac{\theta d}{2}\right)^2\right]$$

and the unit elongation of the fiber $ac$ is

$$\epsilon_{max} = \frac{ac - ac_1}{ac_1} = \frac{1}{2}\gamma^2 = \frac{1}{8}\theta^2 d^2 = \frac{1}{2}\frac{\tau^2_{max}}{G^2}. \qquad (a)$$

The corresponding tensile stress is

$$\sigma_{max} = \epsilon_{max} E = \frac{E}{2} \cdot \frac{\tau^2_{max}}{G^2}.$$

For any other fiber at a distance $r$ from the axis of the shaft, the unit shear is less than $\gamma$ in the ratio $r : d/2$ and the tensile stress is

$$\sigma = \sigma_{max}\left(\frac{2r}{d}\right)^2 = E \frac{2r^2}{d^2} \frac{\tau^2_{max}}{G^2}. \qquad (b)$$

The assumption made that the distance between the cross sections remains unchanged during twist brings us therefore to the conclusion that a longitudinal tensile force, producing tensile stresses (b), should be applied at the ends to keep its length unchanged. If no such

force is applied, but only a pure torque, the twist will be accompanied by some shortening of the shaft. Let $\epsilon_0$ be the corresponding unit shortening. Then instead of equation ($b$) we obtain

$$\sigma = \frac{2r^2}{d^2} \frac{E\tau_{max}^2}{G^2} - \epsilon_0 E. \qquad (c)$$

The quantity $\epsilon_0$ is determined from the condition that the longitudinal force corresponding to the stress distribution ($c$) should be equal to zero. Dividing the cross section into elemental rings and making a summation of forces corresponding to stresses ($c$), we obtain [26]

$$\int_0^{d/2} 2\pi r \sigma dr = 2\pi \int_0^{d/2} \left( \frac{2r^2}{d^2} \frac{E\tau_{max}^2}{G^2} - \epsilon_0 E \right) r dr$$
$$= \frac{\pi d^2 E}{4} \left( \frac{\tau_{max}^2}{4G^2} - \epsilon_0 \right) = 0,$$

from which

$$\epsilon_0 = \frac{\tau_{max}^2}{4G^2},$$

and the stress distribution, from equation ($c$), becomes

$$\sigma = \frac{E\tau_{max}^2}{4G^2} \left( \frac{8r^2}{d^2} - 1 \right). \qquad (266)$$

The maximum stress occurs at the outer surface, where $r = d/2$, and we obtain

$$\sigma_{max} = \frac{E\tau_{max}^2}{4G^2}. \qquad (267)$$

At the center of the cross section we obtain a compressive stress of the same amount.

It is interesting to note that the stress $\sigma$ is proportional to $\tau_{max}^2$; hence the importance of this stress increases with increasing $\tau_{max}$, i.e., with increasing angle of twist. For such material as steel $\tau_{max}$ is always very small in comparison with $G$ and the magnitude of $\sigma_{max}$ is therefore small in comparison with $\tau_{max}$, and can be neglected. But for such material as rubber $\tau_{max}$ may become of the same order as $G$ and $\sigma_{max}$ will no longer be small in comparison with $\tau_{max}$ and must be taken into consideration.

If, instead of a circular cross section, we have a narrow rec-

[26] It is assumed that the cosines of the angles between the fibers and the axis of the bar can be taken equal to unity.

tangular one, it can be shown [27] that even for such materials as steel the stresses $\sigma$ may become of the same order of magnitude as $\tau_{max}$. If the longer side of the cross section, $b$, is large in comparison with its shorter side, $c$, the maximum elongation of the most remote fiber due to twist alone is, from equation ($a$), with $b$ substituted for $d$,

$$\epsilon_{max} = \frac{b^2}{8} \theta^2.$$

For any fiber at distance $y$ from the axis, the elongation is less, in the ratio $(2y/b)^2$. Combining this elongation with the longitudinal unit contraction $\epsilon_0$, we obtain

$$\epsilon = \frac{b^2}{8} \theta^2 \left( \frac{2y}{b} \right)^2 - \epsilon_0 = \frac{\theta^2 y^2}{2} - \epsilon_0.$$

The corresponding tensile stress is

$$\sigma = E \left( \frac{\theta^2 y^2}{2} - \epsilon_0 \right). \qquad (d)$$

The constant $\epsilon_0$ is determined, as before, from the condition that the tensile longitudinal force is equal to zero; hence

$$\int_{-b/2}^{b/2} c\sigma dy = cE \int_{-b/2}^{b/2} \left( \frac{\theta^2}{2} y^2 - \epsilon_0 \right) dy = cE \left( \frac{\theta^2}{2} \cdot \frac{b^3}{12} - \epsilon_0 b \right) = 0,$$

from which

$$\epsilon_0 = \frac{\theta^2}{2} \cdot \frac{b^2}{12},$$

and we obtain, from ($d$),

$$\sigma = \frac{E\theta^2}{2} \left( y^2 - \frac{b^2}{12} \right). \qquad (e)$$

The maximum tensile stress for the most remote fiber ($y = b/2$) is

$$\sigma_{max} = \frac{E\theta^2 b^2}{12}. \qquad (f)$$

The maximum compressive stress at the center ($y = 0$) is

$$\sigma_{min} = - \frac{E\theta^2 b^2}{24}. \qquad (g)$$

[27] See paper by Buckley, Phil. Mag., 1914, p. 778. See also C. Weber, "Die Lehre der Verdrehungsfestigkeit," Berlin, 1921, and also his paper in A. Foeppl, Festschrift, Berlin, 1924.

To compare these stresses with $\tau_{max}$, equations (253) and (254) can be used. For a very narrow rectangular section we obtain

$$\theta = \frac{\tau_{max}}{cG}. \tag{h}$$

Substituting this in expressions ($f$) and ($g$), we obtain

$$\sigma_{max} = \frac{E\tau_{max}^2}{12G^2}\cdot\frac{b^2}{c^2}; \qquad \sigma_{min} = -\frac{E\tau_{max}^2}{24G^2}\cdot\frac{b^2}{c^2}. \tag{268}$$



Fig. 177.

It is seen that when $b/c$ is a large number the stresses $\sigma_{max}$ and $\sigma_{min}$ may not be small in comparison with $\tau_{max}$. The distribution of the stresses (see eq. $e$) is shown [28] in Fig. 177. These stresses have the direction of longitudinal fibers of the twisted strip, and are inclined to the axis of the strip at an angle $\theta y$. Their projections on the plane perpendicular to the axis of the bar are

$$\sigma\cdot\theta y = \frac{E\theta^3}{2}\left(y^3 - \frac{b^2y}{12}\right). \tag{k}$$

The component ($k$) of stress $\sigma$ per element $cdy$ of the cross section gives a moment, with respect to the axis of the bar equal to

$$\frac{E\theta^3}{2}\left(y^3 - \frac{b^2y}{12}\right)cydy.$$

Hence the torque resulting from the stresses $\sigma$ is

$$\int_{-b/2}^{b/2}\frac{E\theta^3}{2}\left(y^3 - \frac{b^2y}{12}\right)cydy = \frac{Ecb^5}{360}\theta^3.$$

Combining this torque with that due to the shearing stresses and determined from equation (253), we obtain the following expression for the total torque:

$$M_t = \frac{1}{3}bc^3G\cdot\theta + \frac{1}{360}Ecb^5\theta^3 = \frac{1}{3}bc^3G\theta\left(1 + \frac{1}{120}\frac{E}{G}\frac{b^4}{c^2}\theta^2\right). \tag{269}$$

[28] This stress distribution takes place at some distance from the ends. Near the ends a more complicated stress distribution, than that in expression ($e$), is produced and such as to make the ends entirely free from normal stresses. This kind of stress distribution is discussed in "Theory of Elasticity," p. 152.

It can be seen that in the case of a very narrow rectangular cross section and comparatively large angles of twist the stresses $\sigma$ may contribute an important portion of the torque since this portion, represented by the second term in equation (269), varies as $\theta^3$ while the portion due to the shearing stresses $\tau$ varies as $\theta$. When the magnitude of the torque is given, the corresponding angle of twist $\theta$ is found from equation (269). The maximum shearing stress $\tau_{max}$ is then calculated from equation ($h$) and $\sigma_{max}$, $\sigma_{min}$ from equations (268). Take, for example, $b = 4$ in., $c = 0.05$ in., $E/G = 2.6$, $G = 11.5 \times 10^6$ lbs. per sq. in. and $M_t = \frac{1}{3}bc^2 \times 15{,}000$ lbs. ins. $= 50$ lbs. ins. If the normal stresses $\sigma$ be neglected, equation (254) gives $\tau_{max} = 15{,}000$ lbs. per sq. in. and equation (253) gives

$$\theta = \frac{\tau_{max}}{cG} = 0.0261.$$

Taking into consideration the longitudinal stresses and using equation (269), we obtain

$$0.0261 = \theta(1 + 2{,}220\theta^2),$$

from which $\theta = 0.0164$;

$$\tau_{max} = \theta\cdot c\cdot G = 9{,}430 \text{ lbs. per sq. in.};$$

$$\sigma_{max} = \frac{E\tau_{max}^2}{12G^2}\frac{b^2}{c^2} = 10{,}700 \text{ lbs. per sq. in.}$$

It can be seen that for such a large angle of twist of a thin metallic strip the normal stresses $\sigma$ are of the same order as the shearing stresses $\tau$ and can not be neglected in calculating the angle of twist.

From the above given discussion it may be concluded that a uniform longitudinal tension will have some influence on the angle of twist of a thin rectangular strip. Assume, for example, that a uniform longitudinal tensile stress $\sigma_0$ is applied to the strip which was just considered. In such a case the equation for calculation $\epsilon_0$ is

$$cE\left(\frac{\theta^2}{2}\frac{b^3}{12} - \epsilon_0 b\right) = \sigma_0 bc,$$

and we obtain

$$\epsilon_0 = \frac{\theta^2}{2}\frac{b^2}{12} - \frac{\sigma_0}{E}.$$

The expression for longitudinal stress $\sigma$ then becomes

$$\sigma = \frac{E\theta^2}{2}\left(y^2 - \frac{b^2}{12}\right) + \sigma_0$$

and the corresponding torque is

$$\int_{-b/2}^{+b/2} \sigma\theta y \cdot cy\,dy = \frac{Ecb^5}{360}\theta^3 + \frac{\sigma_0\theta b^3 c}{12}.$$

For the total torque, instead of equation (269), we then obtain

$$M_t = \frac{1}{3}bc^3G\theta\left(1 + \frac{1}{120}\frac{E}{G}\frac{b^4}{c^2}\theta^2 + \frac{1}{4}\frac{\sigma_0}{G}\cdot\frac{b^2}{c^2}\right). \qquad (270)$$

It is seen that when $b/c$ is a large number, i.e., in the case of a thin strip, the tensile stress may reduce considerably the angle of twist $\theta$.



FIG. 178.

**56. Open Coiled Helical Spring.** —In the previous discussion of helical springs (see p. 271, Part I), it was assumed that the angle $\alpha$ between the coils and the plane perpendicular to the axis of the helix was very small. This angle neglected, the deformation is only a twisting of the wire. In open coiled springs the angle $\alpha$ is no longer small and the deformation produced by the axial loads $P$ consists of both twist and bending (Fig. 178). At any point $A$ the tangent to the helical center line of the spring is not perpendicular to the force $P$ and this force produces at the cross section $A$ of the wire the bending moment about the axis $n_1$ and torque. $P$ is resolved into two components: $P\cos\alpha$ and $P\sin\alpha$, respectively perpendicular to and parallel to the tangent at $A$. At this cross section the component $P\cos\alpha$ produces the torque

$$M_t = PR\cos\alpha, \qquad (a)$$

where $R$ is the radius of the helix, and the component $P\sin\alpha$

produces the bending moment

$$M = PR\sin\alpha. \qquad (b)$$

The maximum combined stress is (see p. 277, Part I):

$$\sigma_{max} = \frac{16}{\pi d^3}\left(M + \sqrt{M^2 + M_t^2}\right) = \frac{16PR}{\pi d^3}(1 + \sin\alpha), \qquad (271)$$

in which $d$ is the diameter of the wire. The maximum shearing stress is [29]

$$\tau_{max} = \frac{16}{\pi d^3}\sqrt{M^2 + M_t^2} = \frac{16PR}{\pi d^3}. \qquad (272)$$

Let us consider now the deflection of the spring on the assumption that it is fixed at the upper end and loaded by an axial load $P$ at the lower end. An element $ds$ between two adjacent cross sections at $A$ is twisted by the torque $M_t$ through the angle

$$d\varphi = \frac{PR\cos\alpha}{GI_p}ds. \qquad (c)$$

Due to this twist the lower portion of the spring rotates about the tangent at $A$ through the above angle $d\varphi$. This small rotation is represented in the figure by the vector $n$ along the tangent, which is taken in such a direction that between the direction of the vector and the direction of rotation there exists the same relation as between the displacement and the rotation of a right hand screw. The small rotation $n$ may be resolved into two components: (1) a rotation $n\cos\alpha$ about a horizontal axis, and (2) a rotation $n\sin\alpha$ about a vertical axis. The latter rotation does not produce any lowering of end $B$ of the spring and so need not be considered here. The discussion of the lowering of the end $B$ of the spring due to the rotation $n\cos\alpha$ follows the same form as that for a close coiled spring. Due to this rotation point $B$ is displaced to $B_1$ (Fig. 178, $c$) and we have $\overline{BB_1} = \overline{AB}\,n\cos\alpha$. The vertical component of this displacement is

$$\overline{BB_2} = \overline{BB_1}\cdot\frac{R}{\overline{AB}} = Rn\cos\alpha. \qquad (d)$$

---

[29] If the diameter $d$ of the wire is not very small in comparison with the diameter $2R$ of the helix this value must be multiplied by the correction factor, which, for $\alpha < 20°$, can be taken to be the same as for close coiled springs (p. 272, Part I). A further discussion of this subject is given by O. Göhner, V. D. I., Vol. 76, 1932, p. 269.

The total deflection of the end $B$ due to twist is the summation of elements such as given by eq. $(d)$, or

$$\delta_1 = \int_B^C Rn \cos \alpha, \qquad (e)$$

in which the summation is taken along the total length of the spring from the lower end $B$ to the upper fixed end $C$.

The deflection due to bending may be calculated in the same manner. The angular deflection due to the bending of the element $ds$ by the moment $M$ (eq. $b$) is

$$d\varphi_1 = \frac{PR \sin \alpha}{EI} ds. \qquad (f)$$

The corresponding rotation of the lower portion of the spring is shown in the figure by the vector $n_1$. In the same manner as above it may be shown that only its horizontal component $n_1 \sin \alpha$ contributes to the vertical displacement of the end $B$ and that the magnitude of this displacement is

$$\delta_2 = \int_B^C Rn_1 \sin \alpha. \qquad (g)$$

By adding $(e)$ and $(g)$, the total deflection of the end $B$ becomes

$$\delta = \delta_1 + \delta_2 = R \int_B^C (n \cos \alpha + n_1 \sin \alpha).$$

Substituting equation $(c)$ for $n$ and equation $(f)$ for $n_1$, we obtain

$$\delta = PR^2 \int_B^C \left( \frac{\cos^2 \alpha}{GI_p} + \frac{\sin^2 \alpha}{EI} \right) ds,$$

or, noting that the expression in the parenthesis is constant and denoting the length of the wire of the spring by $s$, we have

$$\delta = PR^2 s \left( \frac{\cos^2 \alpha}{GI_p} + \frac{\sin^2 \alpha}{EI} \right). \qquad (273)$$

If the diameter $d$ of the wire is not small in comparison with $2R$, the torsional rigidity $GI_p$ in equation $(273)$ must be multiplied by the correction factor

$$\beta = 1 + \frac{3 \left( \dfrac{d}{2R} \right)^2}{16 \left[ 1 - \left( \dfrac{d}{2R} \right)^2 \right]}.$$

The same factor can be used also for a spring with a square cross section.[30]

Equations $(271)$, $(272)$, and $(273)$ give us the complete solution to the problem of an open-coiled helical spring submitted to the action of an axial force.[31]

The *extension* of the spring is accompanied by *rotation* of the end $B$ with respect to the vertical axis of the helix. To determine this rotation, let us again consider the deformation of the element $ds$ in Fig. 178 $(a)$. Due to torsion of this element there will be rotation of the lower portion of the spring by an angle: [32]

$$n \sin \alpha = \frac{M_t ds}{GI_p} \sin \alpha.$$

Due to bending of the same element producing the angular change $n_1$, Fig. 178 $(a)$, the rotation of the lower portion of the spring with respect to the vertical axis is

$$- n_1 \cos \alpha = - \frac{M ds}{EI} \cos \alpha.$$

Hence the total rotation about the axis of the helix of the lower portion of the spring due to deformation of an element $ds$, is

$$ds \left( \frac{M_t \sin \alpha}{GI_p} - \frac{M \cos \alpha}{EI} \right). \qquad (h)$$

The sum of these elemental rotations equals the total angle of rotation $\varphi$ of the end $B$ with respect to the fixed end $C$ of the spring:

$$\varphi = s \left( \frac{M_t \sin \alpha}{GI_p} - \frac{M \cos \alpha}{EI} \right)$$
$$= sPR \sin \alpha \cos \alpha \left( \frac{1}{GI_p} - \frac{1}{EI} \right), \qquad (274)$$

where $s$ is the total length of the spring wire.

In the case of other forms of cross section of the wire, the corre-

---

[30] O. Göhner, loc. cit., p. 305.

[31] The theory of helical springs was developed by St. Venant; see C. R., Vol. 17, 1843, p. 1020. A series of particular cases was discussed by Thompson and Tait, Nat. Phil., 2d part, p. 139; I. Perry, Applied Mechanics, New York, 1907, p. 613; and G. W. Shearer, Engineering, Vol. 93, 1912, p. 206.

[32] A circular cross section of the wire is assumed.

sponding value of torsional rigidity $C$ instead of $GI_p$ must be substituted in equation (274).
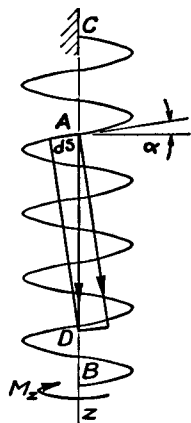
*Axial Torsion.*—Let the vector $\overline{AD}$ represent the torque $M_z$ applied at the end $B$ of the spring, Fig. 179. The bending and the twisting moments acting on the element $ds$ at $A$ are

$$M = M_z \cos \alpha, \qquad M_t = M_z \sin \alpha.$$

The rotation of the end $B$ of the spring around the $z$ axis due to deformation of the element $ds$ is

$$ds \left( \frac{M_t}{GI_p} \sin \alpha + \frac{M}{EI} \cos \alpha \right)$$

$$= ds\, M_z \left( \frac{\sin^2 \alpha}{GI_p} + \frac{\cos^2 \alpha}{EI} \right).$$

The total rotation of the end $B$ of the spring with respect to the $z$ axis produced by the torque $M_z$ is

FIG. 179.

$$\varphi_1 = s M_z \left( \frac{\sin^2 \alpha}{GI_p} + \frac{\cos^2 \alpha}{EI} \right). \tag{275}$$

Since the tensile force $P$ produces rotation $\varphi$ of the end $B$ of the spring, it can be concluded from the reciprocity theorem (p. 330, Part I) that the torque $M_z$ will produce the elongation of the spring. The magnitude $\delta$ of this elongation is obtained from the equation:

$$P\delta = M_z \varphi,$$

from which

$$\delta = \frac{M_z}{P} \varphi = M_z\, sR \sin \alpha \cos \alpha \left( \frac{1}{GI_p} - \frac{1}{EI} \right). \tag{276}$$

*Axial Bending.*—Sometimes we have to consider pure bending of a helical spring in its axial plane, Fig. 180. Let $M_b$, represented by vector $\overline{AB}$, Fig. 180 (b), be the magnitude of the bending couples in $yz$ plane. Considering an element $ds$ of the spring at a point $A$, defined by the angle $\theta$, we resolve the vector $\overline{AB}$ into two components: $\overline{AC} = M_b \cos \theta$, and $\overline{AD} = M_b \sin \theta$. The first component represents a couple in the plane tangent to the cylindrical surface of the radius $R$, which produces bending of the wire in that plane. The second component represents a couple acting in the axial plane of the spring, and can be resolved into torque, $M_b \sin \theta \cos \alpha$, and bending moment in the plane of the coil, $M_b \sin \theta \sin \alpha$. Hence the

element $ds$ undergoes bending by a combined bending moment equal to

$$\sqrt{M_b^2 \cos^2 \theta + M_b^2 \sin^2 \theta \sin^2 \alpha}, \tag{j}$$

and twist by a torque equal to $M_b \sin \theta \cos \alpha$. The strain energy of the element then, assuming a circular cross section, is

$$dU = ds \left[ \frac{M_b^2 (\cos^2 \theta + \sin^2 \theta \sin^2 \alpha)}{2EI} + \frac{M_b^2 \sin^2 \theta \cos^2 \alpha}{2GI_p} \right]. \tag{k}$$

Substituting $ds = Rd\theta / \cos \alpha$, and integrating from $\theta = 0$ to $\theta = 2\pi n$, where $n$ is the number of coils, we obtain

$$U = \frac{\pi n R}{\cos \alpha} \left[ \frac{M_b^2 (1 + \sin^2 \alpha)}{2EI} + \frac{M_b^2 \cos^2 \alpha}{2GI_p} \right]. \tag{l}$$

The angular deflection of one end of the spring with respect to the
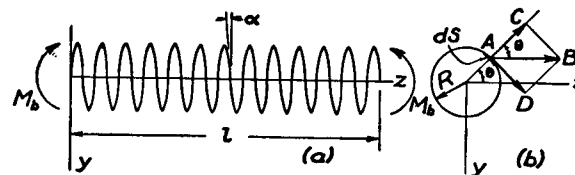
FIG. 180.

other is $l/\rho$, where $l$ is the length of the spring, Fig. 180 (a), determined from the expression

$$l = s \sin \alpha = \frac{2\pi R n}{\cos \alpha} \cdot \sin \alpha,$$

and $\rho$ is the radius of curvature of the deflection curve. Equating the work done by the bending couples $M_b$ to the strain energy $(l)$, we obtain

$$\frac{M_b}{2} \cdot \frac{l}{\rho} = U,$$

from which

$$\frac{1}{\rho} = M_b \cdot \frac{1}{\sin \alpha} \left[ \frac{1 + \sin^2 \alpha}{2EI} + \frac{\cos^2 \alpha}{2GI_p} \right]. \tag{277}$$

Hence the quantity

$$B = \frac{\sin \alpha}{\dfrac{1 + \sin^2 \alpha}{2EI} + \dfrac{\cos^2 \alpha}{2GI_p}} \tag{m}$$

must be taken as the flexural rigidity in the case of an axial bending of helical springs of circular cross section. If the angle $\alpha$ is small, we can assume with sufficient accuracy that $\sin^2 \alpha = 0$ and $\cos^2 \alpha = 1$.

Substituting also $\sin \alpha = l/s$, we represent the flexural rigidity of a helical spring by the formula:

FIG. 181.

$$B = \frac{2EIl}{s} \cdot \frac{1}{1 + \frac{E}{2G}} \cdot \quad (278)$$
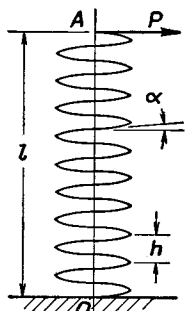
In considering bending of a helical spring by a lateral load, Fig. 181, we have to take into account not only deflections produced by bending moment but also deflections produced by shearing force. Assuming that the end $O$ of the spring is fixed and that $\alpha$ is small, we obtain the deflection $\delta_1$ of the upper end $A$ of the spring produced by the bending moment action from the usual cantilever formula by substituting the value (278) for flexural rigidity. Hence

$$\delta_1 = \frac{Pl^3}{3} \cdot \frac{s}{2EIl} \cdot \left(1 + \frac{E}{2G}\right). \quad (n)$$

In discussing the effect of shearing force on the deflections, let us consider the distortion of one coil in its plane [33] produced by the shearing force $V$, Fig. 182. The bending moment produced by $V$ at any point $A$ is $VR \sin \theta$, and the corresponding strain energy of one coil is

$$U = \int_0^{2\pi} \frac{M^2 R d\theta}{2EI} = \frac{V^2 R^3 \pi}{2EI}.$$

The relative displacement $e$ then is

$$e = \frac{\partial U}{\partial V} = \frac{\pi V R^3}{EI}.$$
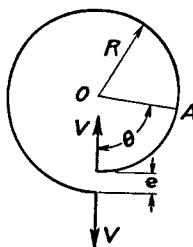
FIG. 182.

Dividing this displacement by the pitch $h$ of the helix, we obtain the additional slope $\gamma$ of the deflection curve produced by the shearing force action:

$$\gamma = \frac{e}{h} = \frac{\pi V R^3 n}{EIl}.$$

[33] The angle $\alpha$ is assumed small in this discussion.

This expression must be used instead of the expression $\alpha V/AG$ in the formulas for deflections produced by shear action in solid beams (see art. 39, Part I), if it is required to adapt these formulas to the calculation of lateral deflections of helical springs. In the case shown in Fig. 181 the shearing force is constant along the length $l$ and equal to $P$; hence the deflection due to shear is

$$\delta_2 = \gamma l = \frac{\pi n P R^3}{EI}. \quad (p)$$

Adding expressions $(n)$ and $(p)$ and assuming $s = 2\pi R n$, we obtain

$$\delta = \delta_1 + \delta_2 = \frac{\pi n P l^2 R}{3EI}\left(1 + \frac{E}{2G} + \frac{3R^2}{l^2}\right). \quad (279)$$

The last term in the parenthesis represents the effect of shear action. It is negligible if the radius $R$ of the helix is small in comparison with the length $l$.[34]

[34] Lateral buckling of helical springs under axial compression is discussed in "Theory of Elastic Stability," p. 165.

## CHAPTER VII

### STRESS CONCENTRATION

**57. Stress Concentration in Tension or Compression Members.**—In discussing simple tension and compression it was assumed that the bar has a prismatical form. Then for centrally applied forces the stress is uniformly distributed over the cross section. A uniform stress distribution was also assumed in the case of a bar of variable cross section (see Fig. 14, Part I), but this is an approximation which gives satisfactory results only when the variation in the cross section is gradual. Abrupt changes in cross section give rise to great irregularities in stress distribution. These irregularities are of particular importance in the design of machine parts subjected to variable external forces and to reversal of stresses. Irregularity of stress distribution at such places means that at certain points the stress is far above the average and under the action of reversal of stresses progressive cracks are likely to start from such points. The majority of fractures of machine parts in service can be attributed to such progressive cracks.

To illustrate the stress distribution in a bar of variable cross section under tension, let us consider a symmetrical wedge of a constant thickness $h$ loaded as shown in Fig. 183. An exact solution has been found for this case[1] which shows that there is a pure radial stress distribution. An element in the radial direction at a point $A$ is in a condition of simple radial tension. The magnitude of this radial tensile stress is given by the equation

$$\sigma_r = k\frac{P\cos\theta}{hr}, \tag{a}$$
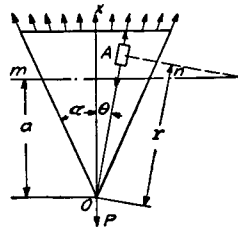


Fig. 183.

[1] See paper by A. Mesnager, Annales des Ponts et Chaussées, 1901. See also I. H. Michell, London Math. Soc. Proc., Vol. 32 (1900) and Vol. 34 (1902). The problem is discussed also in "Theory of Elasticity," p. 93, 1934.

---

in which $\theta$ is the angle between the $x$ axis and the radius $OA$, $r$ is the distance of the point $A$ from $O$ and $k = 1/(\alpha + \frac{1}{2}\sin 2\alpha)$ is a factor depending on the angle $2\alpha$ of the wedge.

The distribution of normal stresses $\sigma_x$ over any cross section $mn$ perpendicular to the axis of symmetry of the wedge is not uniform. Using eq. (17) (see p. 36, Part I) and substituting $r = a/\cos\theta$ in eq. (a) above, we find

$$\sigma_x = \sigma_r\cos^2\theta = \frac{kP\cos^4\theta}{ah}. \tag{b}$$

This shows that the normal stress is a maximum at the center of the cross section ($\theta = 0$) and a minimum at $\theta = \alpha$. The difference between the maximum and minimum stress increases with the angle $\alpha$. When $\alpha = 10°$, this difference is about 6 per cent of the average stress obtained by dividing the load $P$ by the area of the cross section $mn$. Analogous conclusions may be drawn for a conical bar. It may be shown that the distribution of normal stresses over a cross section approaches uniformity as the angle of the cone diminishes.

This discussion shows that the assumption of uniform distribution of normal stresses over a cross section of a non-prismatical bar gives satisfactory results if the variation in cross section along the bar is not rapid.

However the conditions are quite different when there are abrupt changes in the cross section. Then the distribution of stresses at the place of variation is very far from being uniform and results obtained on the assumption of uniform stress distribution are entirely misleading. Several examples of abrupt change in cross section are discussed in the subsequent two articles.

**58. Stresses in a Plate with a Circular Hole.**—If a small circular hole[2] is made in a plate submitted to a uniform tensile stress $\sigma$, a high stress concentration takes place at the points $nn$ (Fig. 184, a). The exact theory[3] shows that the tensile stress at these points is equal to $3\sigma$. It shows also that this stress concentration is of a very localized character and is confined to the immediate vicinity of the hole. If a circle be drawn concentric with the hole and of com-

[2] The diameter of the hole is less, say, than $\frac{1}{5}$ of the width of the plate.

[3] This theory was given by Kirsch, V. D. I., 1898. See also "Theory of Elasticity," p. 75, 1934.

paratively large radius $c$, as shown in Fig. 184 ($a$) by the dotted line, it can be assumed that the stress condition at the circumference of this circle is not materially affected by the presence of the hole. Let Fig. 184 ($b$) represent a circular ring cut out of the plate by a circular cylindrical surface of radius $c$. At each point of the outer surface of this ring we apply vertically directed stress of magnitude $\sigma \sin \varphi$, i.e., equal to the stress on the corresponding elemental area $A$ of the plate (see eq. 16, Part I); then the stresses in the ring will be approximately the same as in the portion of the plate bounded by the circle of radius $c$ (Fig. 184, $a$). In this manner the problem of the stress distribution near the hole in a plate is reduced to that of an annular ring of rectangular cross section subjected to known vertical forces of intensity $\sigma \sin \varphi$ continuously distributed along its outer boundary.[4] This latter problem may be solved by using the method discussed on p. 81. Considering one quadrant of the ring, the stresses acting across the cross section $mn$ are reduced to a longitudinal tensile force $N_0$ at the centroid of the cross section and a bending couple $M_0$. The longitudinal force can be determined from the equation of statics and is
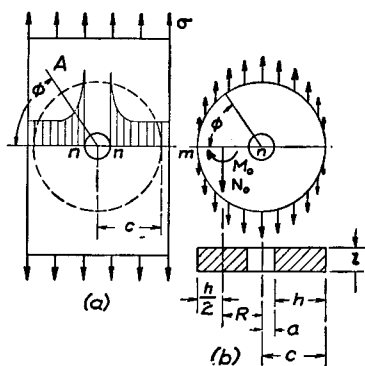


FIG. 184.

$$N_0 = \sigma c. \qquad (a)$$

The moment $M_0$ is statically indeterminate and is calculated by use of the theorem of least work. Equation (88), p. 84, is used for the potential energy, in which the longitudinal force and the bending moment at any cross section of the ring, determined by the angle $\varphi$ (Fig. 184, $b$), are

$$N = \sigma c \cos^2 \varphi \; ; \quad M = M_0 + \sigma c (1 - \cos \varphi)\left[ \frac{c}{2}(1 - \cos \varphi) + \frac{h}{2}\cos \varphi \right]$$
$$- \sigma c \left( c - \frac{h}{2} \right)(1 - \cos \varphi), \quad (b)$$

where $h$ is the depth of the rectangular cross section. Then

$$\frac{dU}{dM_0} = \int_0^{\pi/2} \frac{M d\varphi}{AEe} - \int_0^{\pi/2} \frac{N d\varphi}{AE} = 0,$$

[4] The thickness of the plate is assumed to be unity.

from which, after integration,

$$M_0 = \frac{2\sigma c^2}{\pi}\left[ 1 - \frac{3}{8}\pi - \frac{h}{2c}\left( 1 - \frac{1}{4}\pi \right) + \frac{e\pi}{4c} + \frac{R}{2c}(\pi - 2) \right]. \quad (c)$$

Here, as before, $R$ is the radius of the center line and $e$ the distance of the neutral axis from the centroid of the cross section.

The stress at the point $n$ of the cross section $mn$ of the ring consists of two parts: (1) the tensile stress produced by the longitudinal force $N_0$ and equal to

$$\sigma_1 = \frac{N_0}{h} = \frac{\sigma c}{h}, \qquad (d)$$

and (2) the bending stress produced by $M_0$ which is, from eq. (66),

$$\sigma_2 = \frac{M_0 h_1}{Aea} = \frac{M_0 \left( \frac{h}{2} - e \right)}{Aea} = \frac{M_0}{2ea}\left( 1 - \frac{2e}{h} \right), \qquad (e)$$

in which $a$ is the radius of the hole.

The distance $e$ is calculated by use of eq. (70) for various values of the ratio $c/a$ and then the quantities $\sigma_1$ and $\sigma_2$ are determined from eqs. ($d$) and ($e$). The maximum stress is

$$\sigma_{max} = \sigma_1 + \sigma_2.$$

The results of these calculations are given in the table 22 below.

TABLE 22

| $c/a =$ | 3 | 4 | 5 | 6 | 8 | 10 |
|---|---|---|---|---|---|---|
| $2e/h$............. | 0.1796 | 0.2238 | 0.2574 | 0.2838 | 0.3239 | 0.3536 |
| $\sigma_1/\sigma$............. | 1.50 | 1.33 | 1.25 | 1.20 | 1.14 | 1.11 |
| $\sigma_2/\sigma$............. | 2.33 | 1.93 | 1.83 | 1.83 | 1.95 | 2.19 |
| $\sigma_{max}/\sigma$............. | 3.83 | 3.26 | 3.08 | 3.03 | 3.09 | 3.30 |

Comparison of the figures of the last line of the above table with the exact solution $\sigma_{max} = 3\sigma$ for a small hole shows that for $5 < c/a < 8$ the results of approximate calculation agree closely with the exact solution. When $c/a < 5$, the hole cannot be considered as very small, but has a perceptible effect on the distribution of stresses along the circle of radius $c$ (Fig. 184, $a$), in which case our assumption regarding the distribution of forces along the outer boundary of the ring (Fig. 184, $b$) is not accurate enough. The

deviation from the exact theory for $c/a > 8$ is due to insufficient accuracy in the elementary theory of curved bars for the case where the inner radius is very small in comparison with the outer one.

Taking any point in the cross section $mn$, Fig. 184 (b), at a distance $r$ from the center of the hole the normal stress at that point is

$$\frac{\sigma}{2}\left( 2 + \frac{a^2}{r^2} + \frac{3a^4}{r^4} \right) \qquad (f)$$

where $\sigma$ is the uniform tensile stress applied at the ends of the plate. This stress distribution is shown in Fig. 184 (a) by the shaded areas. It is seen that the stress concentration is highly localized in this
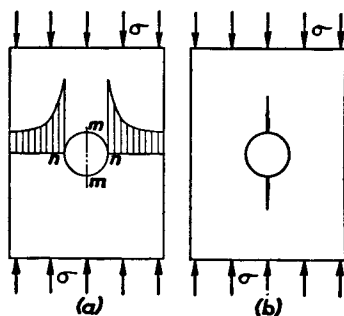


case. At points $n$, i.e., at $r = a$, we have $\sigma_{max} = 3\sigma$. The stresses decrease rapidly as the distance from this overstressed point increases; at a distance from the edge of the hole equal to the radius of the hole, i.e., for $r = 2a$, we obtain from expression $(f)$ the normal stress equal to $1\frac{7}{32}\sigma$. The stress decreases rapidly also with the increase of the angle $\varphi$, Fig. 184 (b), and for $\varphi = \pi/2$, i.e., for the cross section parallel to the applied tensile stresses $\sigma$ we find

FIG. 185.

at the edge of the hole a compressive stress in the tangential direction of the magnitude equal to the tensile stress $\sigma$ applied at the ends of the plate.

If, instead of tension, we have compression of the plate, Fig. 185 (a), we have only to change the sign of stresses obtained in our preceding discussion, and we conclude that there will be a compressive stress of the magnitude $3\sigma$ at points $n$ and a tensile stress of the magnitude $\sigma$ at points $m$. In the case of a brittle material such as glass which is very strong in compression and weak in tension the cracks usually start at points $m$ as shown in Fig. 185 (b).

Having the stresses for simple tension or compression and using the method of superposition, we readily obtain the stress concentration for the cases of *combined tension or compression* in two perpendicular directions. For example, in the case shown in Fig. 186(a) we find that the tangential stress at points $n$ is $3\sigma_y - \sigma_x$ and at points $m$ the stress is $3\sigma_x - \sigma_y$. In the particular case of *pure shear* we have

$$\sigma_x = -\sigma_y = \sigma$$

and we obtain for points $n$ the stress $-4\sigma$ and for the points $m$ the stress $+4\sigma$; thus in this case the maximum stress is four times larger than the stresses applied at the edges of the plate. Such a condition of high stress concentration we obtain in the torsion of a thin-walled circular tube with a small circular hole in it, Fig. 186 (b). If the
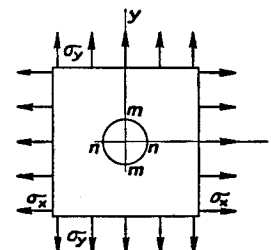


FIG. 186a.          FIG. 186b.

applied torque has the direction indicated in the figure, the maximum tensile stress, four times larger than the shearing stresses applied at the ends, is produced at the edge of the hole at the points marked by plus signs. At the points marked by the minus signs, there will be a compressive stress of the same magnitude.

The approximate method of calculation stresses at a circular hole described above can also be used for the case of a hole with a bead (Fig. 187). This calculation, worked out [5] for $b/t_1 = 11, t/2a = 0.01$, gave the following values of the ratio $\sigma_{max} : \sigma$ for various values of $c/a$:

| $c/a =$ | 4 | 5 | 6 |
|---|---|---|---|
| $\sigma_{max}/\sigma =$ | 2.56 | 2.53 | 2.56 |

In the range considered, the ratio $\sigma_{max}/\sigma$ varies but slightly with $c/a$, so further calculations are made for the case $c/a = 5$ only. The influence of the cross sectional area of the bead on the $\sigma_{max}$ can be studied by varying the dimension $b$ of the bead. If $A_1 = 2t_1a$ denotes the decrease in cross section of the plate due to the hole and $A_2 = (b - t_1)t$ the cross sectional area of the bead, the ratio $\sigma_{max}/\sigma$ for several values of the ratio $A_2/A_1$ is given below:



| $A_2/A_1 =$ | 0.10 | 0.20 | 0.30 | 0.40 | 0.50 |
|---|---|---|---|---|---|
| $\sigma_{max}/\sigma =$ | 2.53 | 2.17 | 1.90 | 1.69 | 1.53 |
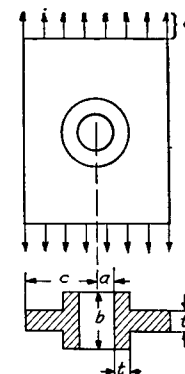
FIG. 187.

[5] Discussion of this problem is given in the author's paper, Journal of the Franklin Institute, Vol. 197, p. 505, 1924. It is assumed that the entire cross section of the bead is effective.

The above figures can be used also in the case of other shapes of bead cross section provided the dimension $t$ of the bead in the radial direction can be considered as small in comparison with the radius $a$ of the hole. Take, for instance, a wide plate in tension, $\frac{7}{16}$ in. thick, with a circular hole of 40 in. diameter. Let the edge of the hole be stiffened with two angle irons $4 \times 4 \times \frac{7}{16}$ in. In such a case $A_2/A_1 = 0.40$ and the above table gives $\sigma_{max} : \sigma = 1.69$.

### 59. Other Cases of Stress Concentration in Tension Members.

—There are only a few cases in which, as in the case of a circular hole, the problem on stress concentration is solved theoretically. In most cases our information regarding maximum stresses at points of sharp change in cross section is obtained from experiments.[6] In our further discussion we shall limit ourselves to the final results of some theoretical and experimental investigations, which may be of practical significance.
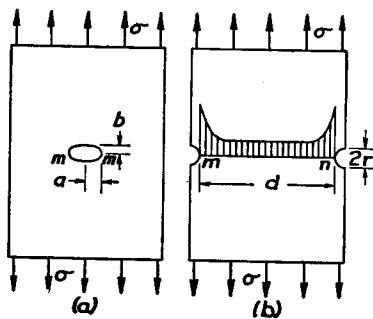


FIG. 188.

In the case of a small *elliptical hole* in a plate [7] (Fig. 188a) the maximum stress is at the ends of the horizontal axis of the hole, and is given by the equation:

$$\sigma_{max} = \sigma \left( 1 + 2\frac{a}{b} \right). \qquad (a)$$

where $\sigma$ is the tensile stress applied at the ends of the plate. This stress increases with the ratio $a/b$, so that a very narrow hole perpendicular to the direction of tension produces a very high stress concentration. This explains why cracks perpen-

[6] Various experimental methods of determining maximum stress are described in articles 63. See also E. Lehr, "Spannungsverteilung in Konstructionelementen," 1934.

[7] See G. Kolosoff, Dissertation, 1910, St. Petersburg; see also C. E. Inglis, Engineering, Vol. 95, 1913, p. 415, and Trans. Inst. of Naval Architects, 1913.

dicular to the direction of forces tend to spread. This spreading can be stopped by drilling holes at the ends of the crack to eliminate the sharp corners at the ends of the crack which produce high stress concentration.

Small *semi-circular grooves* in a plate subjected to tension (Fig. 188b) also produce high stress concentration. Experiments [8] show that at points $m$ and $n$ the stresses are about three times the stress applied at the ends of the plate, if the radius $r$ of the groove is very small in comparison with the width $d$ of the minimum section. In general the maximum
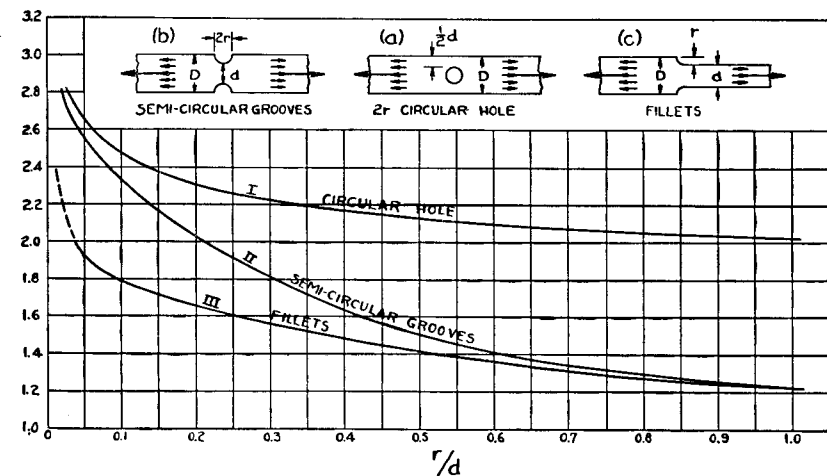


FIG. 189.

stress at points $m$ and $n$ is a function of the ratio $r/d$. The ratio of the maximum stress to the average stress in the minimum section such, as the cross section $mn$, is usually called the *factor of stress concentration* and denoted by $k$. The values of $k$ for various values of the ratio $r/d$ are given in Fig. 189 by the curve II.[9] In the same figure are given also the factors of stress concentration for the case of a circular hole (curve I)

[8] See M. M. Frocht, Journal of Applied Mechanics, Vol. 2, p. 67, 1935.
[9] The curves given in the following discussion are taken from the article by M. M. Frocht, Journal of Applied Mechanics, Vol. 2, 1935, p. 67.

and for the case of fillets (curve III). In Fig. 190 more information regarding stress concentration at fillets is given.

In Fig. 191 the factors $k$ are given for grooves of various depth having a circular shape at the bottom. It is seen that
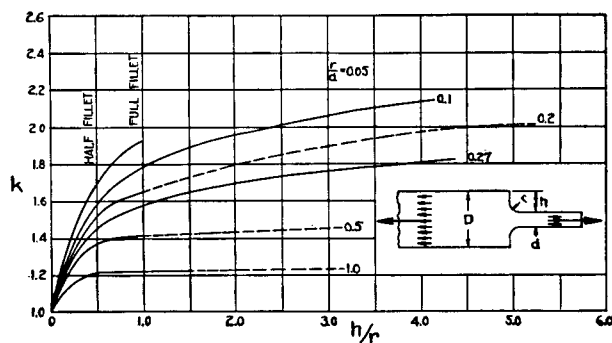


FIG. 190.
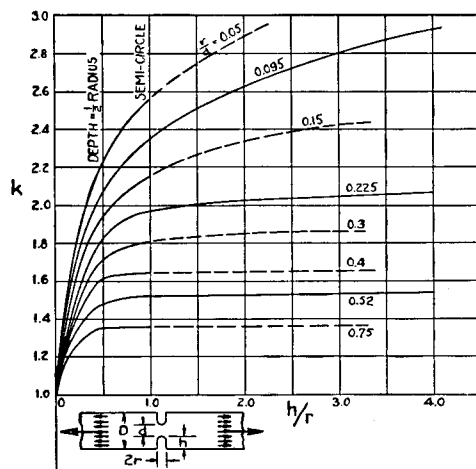


FIG. 191.

for deep grooves the factors of stress concentration are larger than those for semi-circular grooves with the same value of $r/d$.

The case of a plate of a very large width with hyperbolic grooves, Fig. 192, can be treated theoretically.[10] The solution shows that

[10] H. Neuber, Zeitsch. f. angew. Math. u. Mech., Vol. 13, 1933, p. 439.

the factor of stress concentration, i.e., the ratio of the maximum stress at the points $m$ and $n$ to the average tensile stress over the cross section $mn$, can be represented by the following approximate formula:[11]

$$k = \sqrt{0.8 \frac{d}{r} + 1.2} - 0.1 \qquad (b)$$

in which $d$ is the width of the minimum section and $r$ is the radius of curvature at the bottom of the groove. It is interesting to note the values of $k$ obtained from this formula are in very good agreement with experimental results obtained for deep grooves ($h/r = 4$) semi-circular at the bottom, Fig. 191.
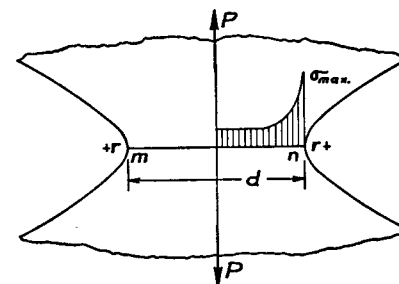


FIG. 192.

Assume now that Fig. 192 represents an axial section of a circular cylinder of a large diameter with deep grooves of a hyperbolic profile under an axial tension. The maximum tensile stress again occurs at the bottom of the groove and the value of the factor of stress concentration is [12]

$$k = \sqrt{0.5 \frac{d}{r} + 0.85} + 0.08. \qquad (c)$$

The comparison of this formula with formula (b) shows that in the case of a grooved cylinder the stress concentration is smaller than in the case of a grooved plate. A further discussion of this comparison is given later (see art. 62).

In the case of a cylinder in tension with an ellipsoidal cavity at the axis, for which Fig. 188 (a) can be considered as an axial

[11] The Poisson ratio is taken equal to 0.3 in formulas (b), (c) and (d).
[12] H. Neuber, loc. cit., p. 320.

section, the maximum tensile stress occurs at points $m$. Its value is given by the following approximate formula

$$\sigma_{\max} = \sigma \left( \sqrt{0.8 \frac{a}{r} + 0.05} + 0.78 \right) \qquad (d)$$

where $\sigma$ is a uniform tensile stress applied at the ends of the cylinder and $r$ is the radius of curvature of the ellipse at points $m$.

The standard tensile test specimen for concrete, Fig 193, is another example of a tension member with sharp variation in cross section. Experiments show[13] that the maximum stress occurs at points $m$ and $n$ and that this stress is about 1.75 times the average stress over the cross section $mn$.
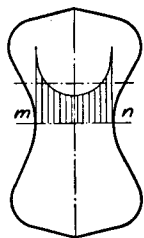
Figure 194 represents a *dovetail joint* which is often used in electric machines to hold the magnetic poles to the rim of the spider. The centrifugal force acting on the pole produces large tensile stresses over the cross section $mn$.

FIG. 193.

The distribution of these stresses is shown in Fig. 194 (b).[14] Due to the abrupt change in cross section a high stress concentration takes place at points $m$ and $n$. The tensile stresses $\sigma_x$ are accompanied by stresses $\sigma_y$ in a lateral direction. The distribution of these stresses along $mn$ is shown in Fig. 194 (b), and their distribution along the vertical plane of symmetry is shown in Fig. 194 (a).

All the conclusions regarding stress distribution made above assume that the maximum stresses are within the proportional limit of the material. Beyond the proportional limit stress distribution depends on the *ductility* of the material. A *ductile material* can be subjected to considerable

---

[13] See E. G. Coker, Proc. International Assoc. for Testing Materials, New York Congress, 1913.

[14] See paper by E. G. Coker, Journal of the Franklin Inst., Vol. 199 (1925), p. 289. T-heads which also have frequent application in machine design were tested by M. Hetényi, "Journal of Applied Mechanics," Vol. 6, 1939, p. 151.

stretching beyond the yield point without great increase in stress. Due to this fact, the stress distribution beyond the yield point becomes more and more uniform as the material stretches. This explains why, with ductile materials, holes and notches do not lower the *ultimate strength* when the notched piece is tested statically. Moreover, in testing mild steel specimens with deep grooves, a certain increase in the ultimate strength is usually obtained, due to the fact that the grooves prevent necking of the specimen at the cross section of fracture (see p. 421).
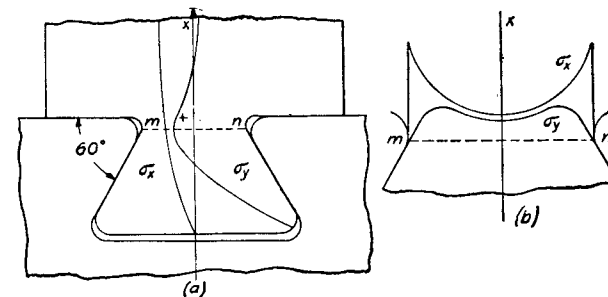


FIG. 194.

However in the case of a *brittle material*, such as glass, the high stress concentration remains right up to the point of breaking. This causes a substantial weakening effect, as demonstrated by the decrease in ultimate strength of any notched bar of brittle material. It is interesting to note that very fine scratches on the surface of a glass specimen do not produce a weakening effect, although stress concentration at the bottom of the scratch must be very high.[15] In explanation of this, it is assumed that common glass in its natural condition has many internal microscopic cracks, and small additional scratches on the surface do not change the strength of the specimen.

The above discussion shows, therefore, that the use of notches and reëntrant corners in design is a matter of judg-

---

[15] This phenomenon was investigated by A. A. Griffith, Phil. Trans. (A), Vol. 221 (1920), p. 163.

ment. In the case of ductile structural steel high stress concentration is not dangerous provided there is no alternating stress. For instance, in the construction shown in Fig. 194, the stresses are very often so high that yielding occurs at $m$ and $n$, but this yielding is not considered dangerous because the structure is subjected to the action of a constant force. In the case of brittle material, points of stress concentration may have a great weakening effect, and such places should be eliminated or the stress concentration reduced by using generous fillets.

In members subjected to reversal of stress the effect of stress concentration must always be considered, as progressive cracks are liable to start at such points even if the material is ductile (see art. 80).

## 60. Stress Concentration in Torsion Members.—In discussing the twisting of bars of various cross sections (see arts. 50 and 51) it was mentioned that reëntrant corners or other sharp irregularities in the boundary line of the cross section cause high stress concentration. Longitudinal holes have a similar effect.

As a first example let us consider the case of a *small circular hole* in a twisted circular shaft [16] (Fig. 195). In discussing this problem the *hydrodynamical analogy* is very useful. [17] The problem of the twisting of bars of uniform cross section is mathematically identical to that of the motion of a *frictionless fluid* moving with uniform angular velocity inside a cylindrical shell having the same cross section as the bar.
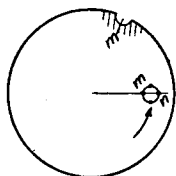
Fig. 195.

16 This case was investigated by J. Larmour, Phil. Mag., Vol. 33, 1892, p. 76.
17 This analogy was developed by Lord Kelvin and Tait, Natural Philosophy, Vol. 2; J. Boussinesq, Journal de Mathématique (Liouville), Vol. 16, 1871, and A. G. Greenhill, article "Hydromechanics," Encycl. Brit., 9th ed. Regarding the application of the analogy in experiments see the paper by J. P. Den Hartog and J. G. McGivern, "Journal of Appl. Mech.," Vol. 2, p. 46, 1935.

The velocity of the circulating fluid at any point is taken as representing the shearing stress at that point of the cross section of the bar when twisted. The effect of a small hole in a shaft of circular cross section is similar to that of introducing a stationary solid cylinder of the same size into the stream in the hydrodynamical model. Such a cylinder greatly changes the velocity of the fluid in its immediate neighborhood. The velocities at the front and rear points are reduced to zero, while those at the side points $m$ and $n$ are doubled. A hole of this kind therefore doubles the maximum stress in the portion of the shaft in which it is located. A small *semi-circular groove* on the surface parallel to the length of the shaft (Fig. 195) has the same effect. The shear in the neighborhood of the point $m$ will be nearly twice the shearing stress calculated for points on the surface of the shaft far away from the groove.

The same hydrodynamical analogy explains the effect of a *hole of elliptical cross section* or of a *groove of semi-elliptical cross section*. If one of the principal axes $a$ of the ellipse is in the radial direction and the other principal axis is $b$, the stresses at the edge of the hole at the ends of the $a$ axis are increased in the proportion $[1 + (a/b)] : 1$. The maximum stress produced in this case thus depends upon the magnitude of the ratio $a/b$. The effect of an elliptical hole on the stress is greater when the major axis of the ellipse is in the radial direction than when it runs circumferentially. This explains why a radial crack has such a weakening effect on the strength of a shaft. The above discussion applies also to the case of a semi-elliptical groove on the surface parallel to the axis of the shaft.

In the case of a *keyway* with sharp corners (Fig. 196), the hydrodynamical analogy indicates a zero velocity of the circulating fluid at the corners projecting outwards (points $m–m$); hence the shearing stress in the corresponding torsion problem is equal to zero at such corners. At points $n–n$, the vertices of the reëntrant angles, the velocity of the circulating fluid is theoretically infinite. In the corresponding torsion problem
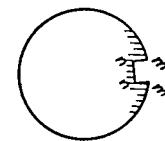
Fig. 196.

the shearing stress is also infinite at the points $n$–$n$, which means that even a small torque will produce permanent set at these points. Such stress concentration can be reduced by rounding the corners $n$–$n$.

Experiments made [18] on a hollow shaft of outer diameter 10 in., inner diameter 5.8 in., depth of keyway 1 in., width of keyway 2.5 in., and radius of fillet in corner of keyway $r$, showed that the maximum stress at the rounded corners is equal to the maximum stress in a similar shaft without a keyway multiplied by the factor $k$ given in the table below:

TABLE 23

| $r$ inches = | 0.1 | 0.2 | 0.3 | 0.4 | 0.5 | 0.6 | 0.7 |
|---|---|---|---|---|---|---|---|
| $k$ = | 5.4 | 3.4 | 2.7 | 2.3 | 2.1 | 2.0 | 1.9 |

This shows that the stress concentration can be greatly diminished by increasing the radius at the corners $n$.

The weakening effect of stress concentration in shafts due to holes and grooves depends on whether the material is ductile or not and the conclusions made in the previous article apply here as well.

If a tubular member has reëntrant corners, there is stress concentration at these corners and the magnitude of the maximum stress depends on the radius of the corners. The approximate value of this maximum stress can be obtained from the membrane analogy. Let us consider the simple case of a tube of constant thickness, and assume that the corner is bounded by two concentric circles (Fig. 197) with center at $O$ and radii $r_i$ and $r_a$. The surface of the membrane at the cross section $mn$ may be assumed to be a surface of revolution with axis perpendicular to the plane of the figure at $O$.[19] We have seen that the slope of the membrane surface at any point $M$ is numerically equal to the shearing stress $\tau$. Referring to
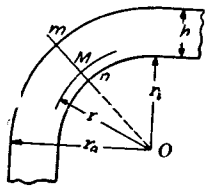
FIG. 197.

[18] See "The Mechanical Properties of Fluids," a collective work, p. 245, D. Van Nostrand Co., New York, 1924.

[19] This assumption is satisfactory provided $r_i$ is not small in comparison with $r_a$.

Fig. 198, which shows a meridional section through $mn$, the principal curvatures of the membrane at this point are

$$\frac{1}{R_1} = \frac{d\varphi}{ds} = \frac{d\tau}{dr}$$

for the meridian (taking an element $ds$ of the meridian equal to $dr$), and

$$\frac{1}{R_2} = \frac{\tau}{r}$$

for the section perpendicular to the meridian. The equation of equilibrium of the membrane, from eq. (157), is then

$$\frac{d\tau}{dr} + \frac{\tau}{r} = \frac{p}{S}$$

or, by using eq. ($a$), art. 50,

$$\frac{d\tau}{dr} + \frac{\tau}{r} = 2G\theta. \qquad (a)$$

FIG. 198.

Let $\tau_0$ denote the average shearing stress, obtained from eq. (258). From eq. (259) we then find

$$\frac{d\tau}{dr} + \frac{\tau}{r} = 2G\theta = \frac{\tau_0 s}{A}, \qquad (b)$$

in which $s$ is the length of the center line of the section of the tubular member. The general solution of eq. ($b$) is

$$\tau = \frac{C}{r} + \frac{\tau_0 s r}{2A}. \qquad (c)$$

The constant of integration $C$ is obtained from the condition: [20]

$$\int_{r_i}^{r_a} \tau\, dr = \tau_0 h.$$

[20] This condition follows from the hydrodynamical analogy (p. 324). If a fluid circulates in a channel having the shape of the cross section of the tubular member, the quantity of fluid passing each cross section of the channel must remain constant.
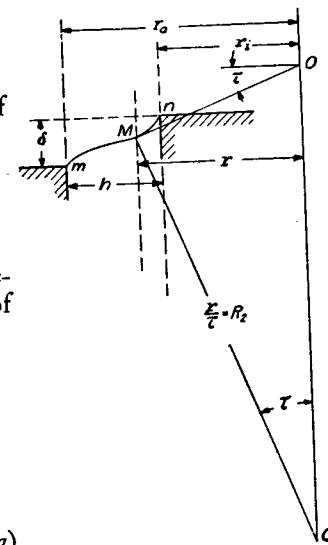
Substituting expression (c) for $\tau$, we find

$$C = \tau_0 h \frac{1 - \dfrac{s}{4A}(r_a + r_i)}{\log_n \dfrac{r_a}{r_i}},$$

and, from eq. (c),

$$\tau = \frac{\tau_0 h}{r} \cdot \frac{1 - \dfrac{s}{4A}(r_a + r_i)}{\log_n \dfrac{r_a}{r_i}} + \frac{\tau_0 s r}{2A}. \qquad (280)$$

At the reëntrant corners $r = r_i$, and substituting this in the above equation we can calculate the stress concentration at these corners.[21]
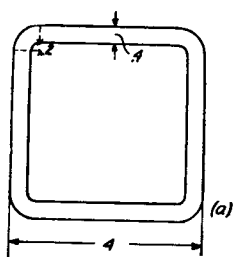


FIG. 199.
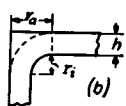
Take for example a square tube with outer dimensions $4 \times 4$ in., wall thickness $h = 0.4$ in. and radii at the corners $r_i = 0.2$ in.; $r_a = 0.6$ in. (Fig. 199). Then

$$A = 3.6 \times 3.6 - 0.4^2(4 - \pi)$$
$$= 12.82 \text{ sq. in.,}$$

$$s = 3.6 \times 4 - 0.4(8 - 2\pi) = 14.40$$
$$- 0.70 = 13.70 \text{ in.}$$

The average stress $\tau_0$ is given by eq. (258). The stress at the reëntrant corners, from eq. (280), is

$$\tau = 1.54\tau_0.$$

The factor of stress concentration in this case is 1.54. It may be seen that this factor increases with decrease in the inner radius $r_i$. Equation (280) can also be used for an approximate calculation of the stress concentration when only the reëntrant corner is rounded (Fig. 199, b). As the stresses are small at projecting corners we can take $r_a = h + r_i$, as indicated in the figure by the dotted line.

In the case of rolled profile sections such as shown in Fig. 159 (b) and 159 (c), (p. 274), the maximum stress occurs at the reëntrant corners. Its value is obtained by multiplying the stress calculated from formulas (254) or (257) (see p. 275) by the factor of stress concentration for which the following

[21] Such an equation was given by C. Weber in his paper, loc. cit., p. 301.

expression can be used [22]

$$k = 1.74 \sqrt[3]{\frac{c}{r}} \qquad (281)$$

in which $c$ is the thickness of the flange and $r$ the radius of the fillet.

**61. Circular Shaft of Variable Diameter.**[23]—If the diameter of a shaft varies gradually along its length, eq. (149) (see p. 264, Part I) derived for a cylindrical shaft gives the maximum stress with sufficient accuracy. But if the change in diameter is abrupt, as shown in Fig. 200, there is a high stress concentration at the points $m$–$m$ at the beginning of fillets. The magnitude of the maximum stress depends on the ratios $\rho/d$ and $D/d$, where $\rho$ is the radius of the fillet and $d$, $D$ are the diameters of the two cylindrical portions of the shaft. These high local stresses, although not dangerous for constant loading of a ductile material, may have a pronounced weakening effect when there are stress fluctuations, which is usually the case in such constructions as propeller shafts and crank shafts of Diesel engines. Many cases of fractures in service can be attributed to this cause. The theoretical calculation of the maximum stress at the fillet is too complicated [24] for engineering purposes and in the following an
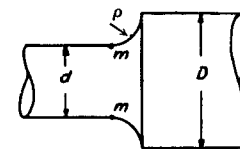


FIG. 200.

[22] E. Trefftz, Z. angew. Math. Mech., Vol. 2, 1922, p. 263. Equation (281) is derived for an angle, Fig. 159 (b), with equal thickness of flanges. In the case of two different thicknesses $c_1$ and $c_2$, as in Fig. 159 (c), the larger thickness must be used in equation (281). A further discussion of this question is given by H. M. Westergaard and R. D. Mindlin, Amer. Soc. C. E. Proceedings, 1935, p. 509.

[23] The general solution of this problem is due to J. H. Michell, Proc. London Math. Soc., Vol. 31 (1899), and A. Föppl, Sitzungsber. d. Bayer. Akad. d. Wissensch., Vol. 35 (1905), p. 249. The case shown in Fig. 200 was considered first by A. Föppl; see V. D. I., 1906, p. 1032. The literature on this subject is compiled in "Theory of Elasticity," p. 276, 1934.

[24] Such calculations were made by F. A. Willers by use of an approximate method of integration, Zeitschr. f. Math. u. Phys., Vol. 55 (1907), p. 225. See also R. Sonntag, Dissertation, München, 1926.

experimental method of measuring the maximum stress is given. This uses an analogy between the stress distribution in a twisted shaft and the distribution of electric current in a plate.[25]

Let us begin with a circular shaft of constant diameter. Imagine such a shaft divided into elemental tubes such that each tube takes an equal portion of the total torque $M_t$. In Fig. 201, for instance, the shaft is divided into five portions each carrying $\frac{1}{5}M_t$. These tubes will be called *equimomental tubes*, and the corresponding lines in a diametral



*Equimomental Tubes*　*Equiangular Surfaces*
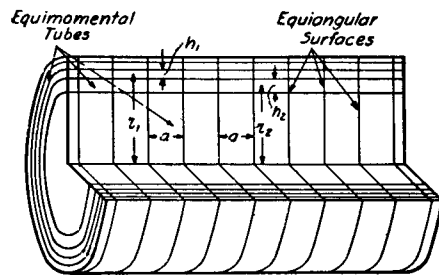
FIG. 201.

section of the shaft *equimomental lines*. Let $\Delta M_t$ denote the torque per tube, and assume the thickness of each tube to be small. The angle of twist per unit length is the same for all tubes, and is

$$\theta = \frac{\Delta M_t}{GI_p} = \frac{\Delta M_t}{G2\pi r^3 h},\qquad (a)$$

in which $r$ is the mean radius of the tube and $h$ its thickness. Since $\Delta M_t$ and $\theta$ [26] are the same for all tubes, the thickness of the tubes varies inversely as the cube of the mean radius. The average shearing stress in a tube is, from eq. (258),

$$\tau = \frac{\Delta M_t r}{I_p} = \frac{\Delta M_t}{2\pi r^2 h}.\qquad (b)$$

---

[25] This analogy was developed by L. S. Jacobsen; see Trans. Amer. Soc. Mech. Engrs., Vol. 47 (1926), p. 619.

[26] $\theta$ is the angle of twist for a solid shaft.

In Fig. 201 is shown a second system of lines in the diametral section. These lines are perpendicular to the equimomental lines and are called *equiangular lines*. They correspond to sections of the shaft which are called *equiangular surfaces* and which are so taken that the angle of twist between two consecutive equiangular surfaces is constant along the length of the shaft. Let $\Delta\varphi$ be this angle. In this case the equiangular surfaces are equidistant planes, and let $a$ be the distance between them. Then at any radius $r$ the shearing strain is

$$\gamma = \frac{\Delta\varphi r}{a}$$

and the corresponding stress is

$$\tau = \frac{G\Delta\varphi r}{a}.\qquad (c)$$

The two systems of perpendicular lines, equimomental and equiangular, divide the diametral section of the shaft into elemental rectangles, as indicated in the figure. The dimensions of these rectangles may be used to compare the shearing stresses at the corresponding points of the shaft. Using eq. (b) and comparing the shearing stresses $\tau_1$ and $\tau_2$ at radii $r_1$ and $r_2$ respectively, we find

$$\frac{\tau_1}{\tau_2} = \frac{r_2^2 h_2}{r_1^2 h_1}.\qquad (d)$$

From eq. (c) we find

$$\frac{\tau_1}{\tau_2} = \frac{r_1 a_2}{r_2 a_1}.\qquad (e)$$

In the case under consideration $a_1 = a_2 = a$, but eq. (e) will be used later for a more general case. It is evident that each system of lines may be used in calculating the shearing stresses. In one case (eq. d) the ratio of stresses depends on the ratio of the distances between equimomental lines $h_2/h_1$, while in the other case (eq. e) it depends on the ratio of the distances between equiangular lines $a_2/a_1$.

Let us consider a shaft of variable diameter as shown in Fig. 200. The irregularities in stress distribution produced at the fillets are of local character. At sufficient distance from the junction of the two diameters the stress distribution is practically the same as in a shaft of uniform cross section, and the two systems of lines described above can be constructed in the diametral section (Fig. 202). Near the cross section of discontinuity, the stress distribution is a more complicated one and the equimomental and equiangular lines become curved. Analysis of the problem shows [27] that, although curved, these lines remain mutually orthogonal and subdivide the diametral section into curvilinear rectangles as indicated by the shaded areas. Also eqs. ($d$) and ($e$), which were derived for a uniform shaft, are shown to hold here, if we take for $h$ and $a$ the dimensions measured at the middle of each curvilinear rectangle. Then the equimomental and equiangular lines give a complete picture of the stress distribution in the shaft. Considering, for instance, the equimomental lines and using eq. ($d$), we see that the stresses increase with decrease in the radius and thickness of the equimomental tubes. It is evident from the figure that the stress is a maximum at the fillets, where the thickness $h$ of the outer equimomental tube is the smallest. We come to the same conclusion also by considering the equiangular lines. It can be seen from the figure that at the fillets the distance $a$ between these lines is very small; hence, from eq. ($e$), the stress is large. From eq. ($d$) or ($e$) we can determine the ratio of the maximum stress at the fillet to the stress at any other point provided the equimomental or equiangular lines are known.
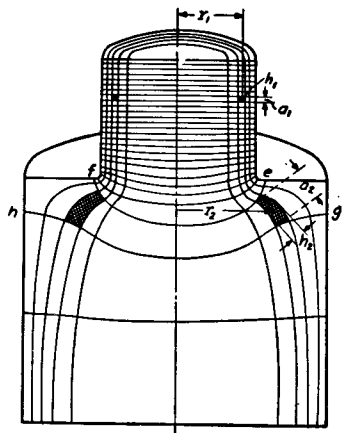


FIG. 202.

[27] See the paper by F. A. Willers, loc. cit., p. 329.

The electric analogy, mentioned above, provides a means for measuring the distances $a$ between the equiangular lines. These distances are measured at the surface of the shaft of smaller diameter $d$, first at a point remote from the cross section of discontinuity, and then at the fillet. The ratio of these two distances gives [see eq. ($e$)] the factor by which the stress, as calculated by the usual formula, must be multiplied to obtain the maximum stress at the fillet. In discussing the electric analogy, we begin with the case of a rectangular plate
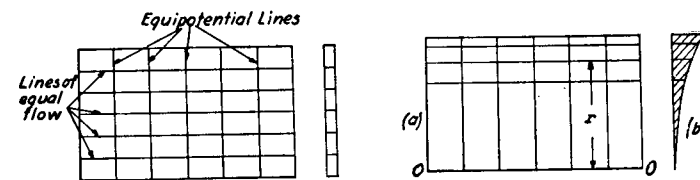


FIG. 203.                    FIG. 204.

of uniform thickness (Fig. 203). If the ends of the plate are maintained at a constant difference of potential, there will flow through the plate an electric current uniformly distributed over its cross section. By dividing the electric flow into equal parts we obtain a system of equidistant *stream lines*. The system of *equipotential lines* is perpendicular to these. With a homogeneous plate of uniform cross section the drop in potential will be uniform along the direction of the current and the equipotential lines are therefore equidistant vertical lines. In order to get two systems of lines analogous to those in Fig. 201, the thickness of the plate is varied as the cube of the distance $r$, as shown in Fig. 204 ($b$). Then the distance between the stream lines will be inversely proportional [28] to the cube of $r$, and the distance between the vertical equipotential lines remains constant as before. In this manner we can obtain the same system of mutually orthogonal lines as in Fig. 201. The edge O-O of the plate corresponds to the axis of the shaft. The equipotential lines correspond to the equiangular

[28] It is assumed that the flow per unit area of cross section is uniform over the cross section.

lines, and the stream lines to the equimomental lines of the torsional problem. Investigation shows [29] that this analogy also holds in the case of a plate of two different widths and of thickness varying as the cube of the distance $r$ (Fig. 205). This makes it possible to investigate the stress concentration at the fillet of a twisted shaft by an electric method. We maintain a constant difference in potential at the ends of the plate and measure the drop in potential along the edge $mnp$. The distances $a_1$ and $a_2$ between equipotential lines at a remote point $m$ and at the fillet $n$ respectively are thus obtained. The ratio $a_1/a_2$ of these distances gives the factor of stress concentration for the fillet at $n$.

Actual measurements were made on a steel model 24 in. long, 6 in. wide at the larger end and 1 in. maximum thickness at the edge $pq$. The drop of potential along the edge $mnpq$ of the model was investigated by using a very sensitive galvanometer, the terminals of which were connected to two
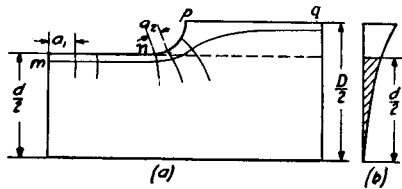


FIG. 205.
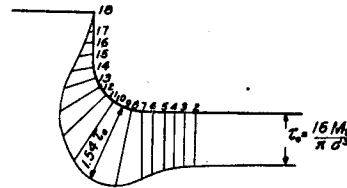
FIG. 206.

sharp needles fastened in a block at a distance 2 mm. apart. By touching the plate with the needles the drop in potential over the distance between the needle points was indicated by the galvanometer. By moving the needles along the fillet it is possible to find the place of maximum voltage gradient and to measure this maximum. The ratio of this maximum to the voltage gradient at a remote point $m$ (Fig. 205) gives the magnitude of the factor of stress concentration $k$ in the equation:

$$\tau_{max} = k \frac{16 M_t}{\pi d^3}. \qquad (282)$$

[29] See above-mentioned paper by L. S. Jacobsen, loc. cit., p. 330.

The results of such tests in one particular case are represented in Fig. 206, in which the potential drop measured at each point is indicated by the length on the normal to the edge of the plate at this point. From this figure the factor of stress concentration is found to be 1.54. The magnitudes of this factor obtained with various proportions of shafts are given in Fig. 207, in which the abscissas represent the ratios of the
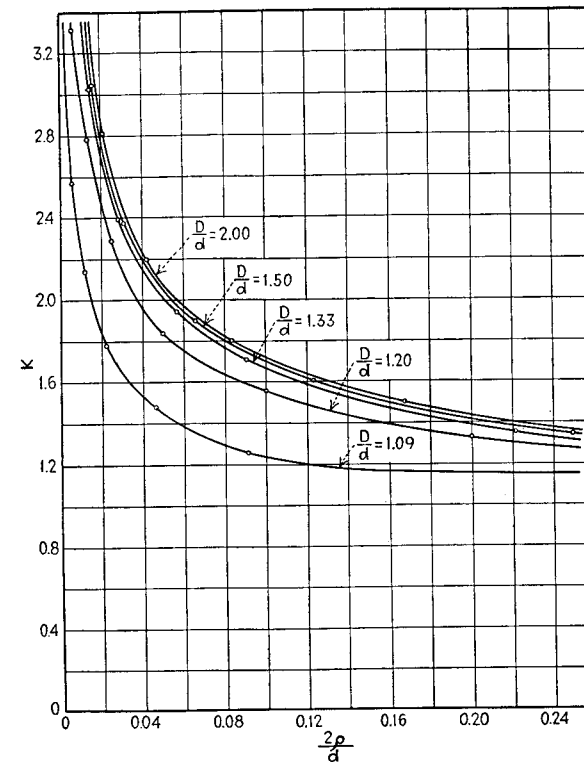


FIG. 207.

radius of the fillet to the smaller radius of the shaft, $2\rho/d$, and the ordinates the factor $k$ for various ratios of $D/d$.

**62. Stress Concentration in Bending.**—The formulas for bending and shearing stresses derived for prismatical beams are very often applied also to the cases of beams of variable

cross section. To give some idea of the accuracy of this method of calculation, the bending of a cantilever having the form of a wedge (Fig. 208) will be considered. The exact solution of this problem [30] shows that the stress at any point $A$ of the beam is a simple tension or compression in the radial direction $AO$, and has the magnitude
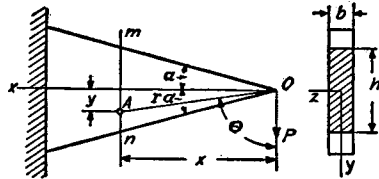


FIG. 208.

$$\sigma_r = k \frac{P \cos \theta}{rb}, \qquad (a)$$

where $r$ is the distance $OA$, $b$ is the thickness of the wedge, $\theta$ is the angle between the radius $AO$ and the direction of the force $P$, and

$$k = -\frac{2}{2\alpha - \sin 2\alpha},$$

is a constant depending upon the magnitude of the angle of the wedge. By using equations (17) and (18), Part I, p. 36, the normal and tangential components of the stress on a plane perpendicular to $x$ are found to be

$$\left.\begin{array}{l} \sigma_x = \sigma_r \sin^2 \theta = \dfrac{My}{I_z} \dfrac{4 \tan^3 \alpha \sin^4 \theta}{3(2\alpha - \sin 2\alpha)}; \\[3mm] \tau_{yx} = \dfrac{\sigma_r}{2} \sin 2\theta = \dfrac{P}{bh} \dfrac{16y^2}{h^2} \dfrac{\tan^3 \alpha \sin^4 \theta}{2\alpha - \sin 2\alpha}, \end{array}\right\} \qquad (b)$$

in which

$$I_z = \frac{bh^3}{12}; \qquad M = -Px.$$

For the neutral plane of the wedge $\theta = \pi/2$ and the normal and shearing stresses become zero. The maximum normal and shearing stresses occur at $\theta = (\pi/2) + \alpha$. They can be

[30] See I. H. Michell, Proceedings of the London Math. Soc., Vol. 32 (1900).

calculated from expressions (b) which give

$$(\sigma_x)_{\max} = -\beta \frac{Mh}{2I_z}; \qquad (\tau_{yx})_{\max} = 3\beta \frac{P}{bh}, \qquad (c)$$

where

$$\beta = \frac{4}{3} \cdot \frac{\tan^3 \alpha \cos^4 \alpha}{2\alpha - \sin 2\alpha}.$$

For $\alpha = 5°$, $10°$, $15°$ and $20°$, the factor $\beta$ has the magnitudes 1.00, 0.970, 0.947 and 0.906, respectively. It is seen that the maximum normal stress $\sigma_x$, from the first of the formulas (c), is approximately the same as that obtained from the usual beam formula provided the angle $\alpha$ be sufficiently small. For $\alpha = 20°$ the error of the simple beam formula, as it is seen from the value of the factor $\beta$, is about 10 per cent. The maximum shearing stress, given by the second of the formulas (c), is about three times the average shearing stress $P/bh$ and occurs at points most remote from the neutral axis. This latter fact is in direct opposition to the results obtained for prismatical bars (p. 109, Part I). In many cases the tangential stresses are of no great importance and only normal bending stresses are considered. Then the formula for maximum bending stress, derived for prismatical beams, can be used with a sufficient accuracy also for bars of variable cross section, provided the variation of the cross section is not too rapid.

If the change in cross section is abrupt there is a considerable disturbance in stress distribution at the section of discontinuity and the maximum stress is usually much greater than that given by the simple beam formula, and can be represented by formula

$$\sigma_{\max} = k\sigma \qquad (d)$$

in which $\sigma$ is the stress at the point under consideration as obtained from the prismatical beam formula and $k$ is the factor of stress concentration. In only a few cases is this factor obtained by the use of the equations of the theory of elasticity.[31]

[31] H. Neuber, Ingenieur-Archiv, Vol. 5, 1934, p. 238 and Vol. 6, 1935, p. 133.

The plate of large width with hyperbolic notches, Fig. 192, is one of the cases where we have a rigorous solution for stress distribution at the notches. This solution shows that in the case of pure bending of the plate by the couples acting in its middle plane the maximum stress occurs at points $m$ and $n$ and the factor of stress concentration in formula $(d)$ can be represented by the following approximate formula

$$k = \sqrt{0.355 \frac{d}{r} + 0.85} + 0.08 \qquad (e)$$

where $d$ is the minimum width of the plate and $r$ the radius of curvature at the bottom of the notch.

In the case of a circular shaft with a hyperbolic groove, for which Fig. 192 represents an axial section, the factor of stress concentration in the case of pure bending is

$$k = \frac{3}{4N}\left(\sqrt{\frac{d}{2r} + 1} + 1\right)\left[\frac{3d}{2r} - (1 - 2\mu)\sqrt{\frac{d}{2r} + 1} + 4 + \mu\right] \qquad (f)$$

where

$$N = 3\left(\frac{d}{2r} + 1\right) + (1 + 4\mu)\sqrt{\frac{d}{2r} + 1} + \frac{1 + \mu}{1 + \sqrt{\frac{d}{2r} + 1}}, \qquad (g)$$

$d$ is the diameter of the minimum cross section and $r$ the smallest radius of the curvature at the bottom of the groove. For large values of the ratio $d/2r$ the expression $(f)$ can be replaced with a sufficient accuracy by the approximate formula

$$k = \frac{3}{4}\sqrt{\frac{d}{2r}}. \qquad (h)$$

Most of the information regarding the magnitude of the factor $k$ in equation $(d)$ is obtained experimentally by the photoelastic method.[32] The factors of stress concentration for pure bending of plates with semi-circular grooves and with fillets in the form of a quarter of a circle and $D = d + 2r$ are given by the curves in Fig. 209. In Fig. 210 the factors of stress concentration for fillets with various values of the

---

[32] The curves given in the following discussion are taken from the article by M. M. Frocht, loc. cit., p. 319.

ratio $D/d$ are given. In Fig. 211 are given the factors of stress concentration for grooves of varying depth in pure bending.
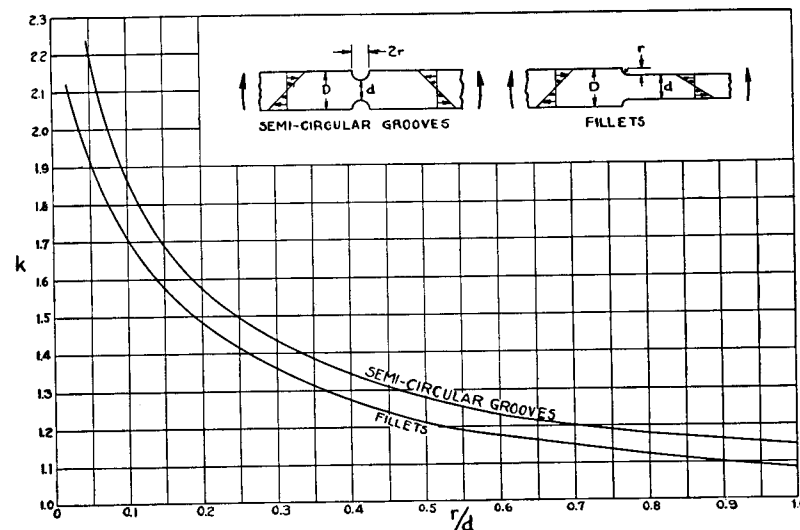


Fig. 209.
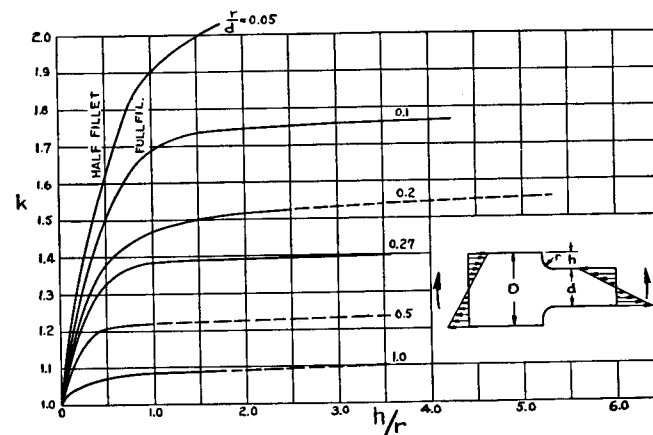


Fig. 210.

For comparison of factors of stress concentration in tension and in bending for plates and for circular shafts the curves
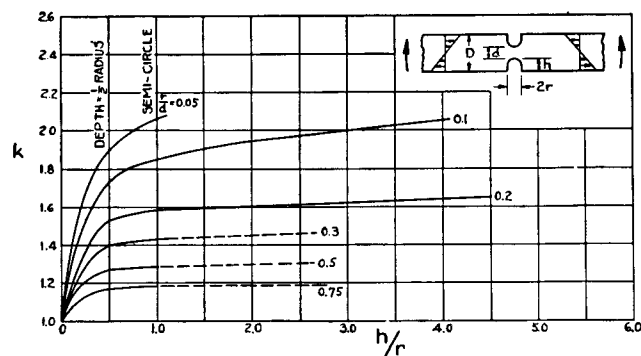
FIG. 211.
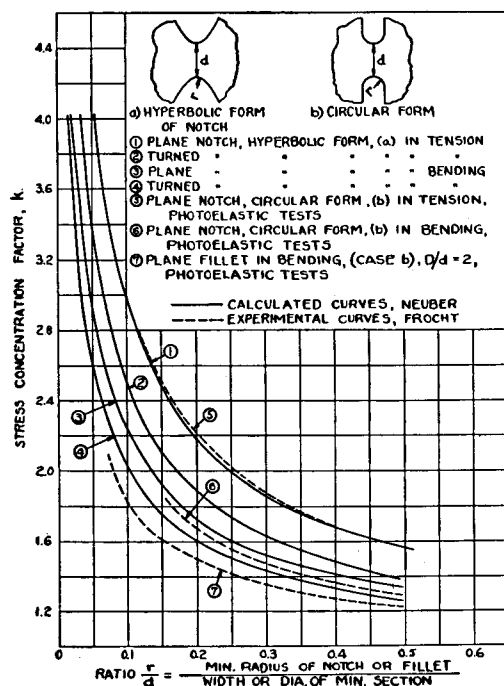


FIG. 212.

in Fig. 212 are given.[33] The curves 1 and 2 giving the factors of stress concentration for a hyperbolic notch in a plate and in a circular shaft in tension are calculated from formulas (b) and (c) in article 59. The curves 3 and 4 showing similar values for notches in pure bending are calculated from formulas (e) and (f), p. 338. It may be seen from these curves that the factors of stress concentration are higher for plates than for circular shafts, the difference being more pronounced in the case of tension. In the case of pure bending which is of greater practical importance, the difference between the two cases is small, around 6 to 8 per cent for notches of practical dimensions. The dashed curves (5) and (6) in Fig. 212 are obtained from the curves in Fig. 191 and 211 by extrapolating these curves to large values of the ratio $h/r$ which corresponds to a deep notch semi-circular at the bottom. It may be seen that the curves (5) and (6) agree satisfactorily with the curves (1) and (3) for hyperbolic notch for ratios $r/d$ between 0.15 and 0.50. This indicates that in the case of deep notches the magnitude of the factor of stress concentration depends principally on the magnitude of the ratio $r/d$ and not on the shape of the notch.

The dashed curve (7) is obtained from the curves in Fig. 210 and represents the factors of stress concentration at the fillets of a plate in pure bending with the ratio $D/d = 2$. It is seen that for fillets the factors of stress concentration are somewhat lower than for deep notches (curves 4 and 6) with the same ratio $r/d$.

To obtain the factors of stress concentration for fillets in circular shafts the direct test on large steel shafts with the diameter ratio $D/d = 1.5$ were made [34] at the Westinghouse research laboratories. The values of these factors obtained by the direct measurement of strain at the fillets are given by the points in Fig. 213. For comparison, the results of photo-

---

[33] This figure and the following are taken from the paper by R. E. Peterson and A. M. Wahl, Journal of Applied Mechanics, Vol. 3, 1936, p. 15.

[34] R. E. Peterson and A. M. Wahl, loc. cit., reference 33.

elastic experiments on flat models with $D/d = 2$ and $D/d = 1.5$ are given [35] in the same figure by the curves 1 and 2. From these experiments the very important conclusion can be made that the stress concentration factors for the circular shafts agree well with the values obtained photoelastically on flat specimens.
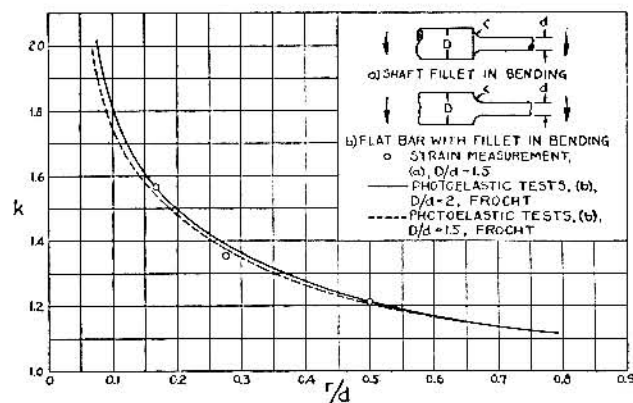


FIG. 213.

### 63. The Investigation of Stress Concentration with Models.
—It was already stated that a complete theoretical solution for the stress distribution at the section of discontinuity exists in only a few of the simplest cases, such as that of a circular or elliptical hole and hyperbolic notch. In the majority of cases, information regarding stress concentration is obtained by experiment. For this purpose strain measurements at the section of discontinuity may sometimes be made with sensitive extensometers. In this manner, for instance, the stress concentration at grooves in tension specimens has been investigated.[36] In using this method, difficulty arises from the highly localized character of the stress distribution at the place

[35] These curves were constructed from the data given in Fig. 210.

[36] See E. Preuss, V. D. I., Vol. 56, 1912, p. 1349, Vol. 57, 1913, p. 664, and Forschungsarbeiten, nr. 134, 1913. See also Th. Wyss, Proc. Intern. Congress for Applied Mechanics, Delft, 1924, p. 354, and his Dissertation, Zürich, 1923. See also F. Rötscher and J. Crumbiegel, V. D. I., Vol. 76, p. 508, 1932.

in question. A very small gauge length, and hence very high magnification, is necessary to obtain satisfactory results.[37]

A rough estimate of the factor of stress concentration may be obtained by loading the specimens or models of structures with increasing loads until yielding starts at the points of maximum stress. This yielding can be seen clearly in specimens of mild steel with polished surfaces. Figure 214
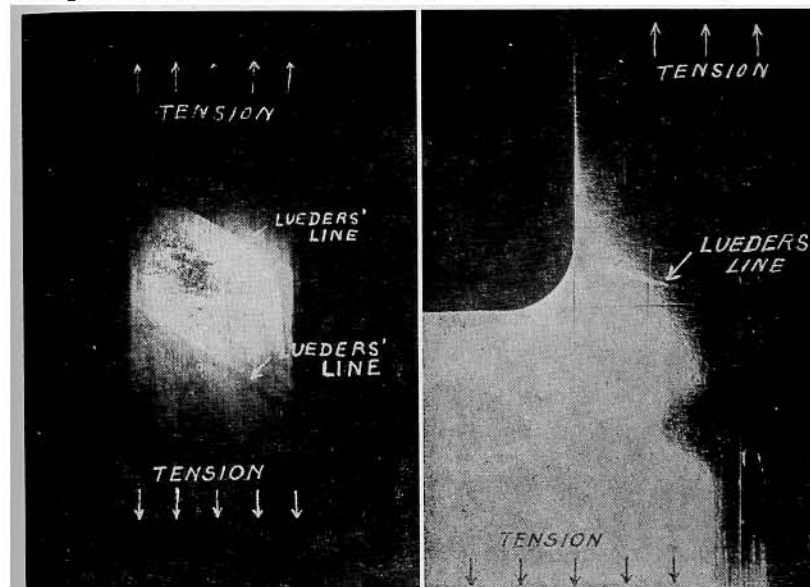


FIG. 214.                    FIG. 215.

is a photograph of the yield lines in a strip of mild steel. These yield lines (Lueders' lines, see p. 415) first appear at the places of maximum stress. The distribution of these lines gives valuable information regarding stresses at the places of discontinuity.[38]

[37] Rubber models to increase the deformations at the section of discontinuity have also been used in several cases; see paper by A. Stodola, V. D. I., Vol. 51, 1907, p. 1272; Hummel, Schweizerische Bauzeitung, 1924, p. 143. L. Chitty and A. J. S. Pippard, Proc. Roy. Soc., Vol. 156, 1936, p. 518.

[38] See paper by M. A. Voropaev, Bulletin of the Polytechnical Institute at Kiev, 1910, and writer's paper in Proc. Intern. Congress for Applied Mechanics, Zürich, 1926, p. 419.

Figure 215 shows a Lueders' line at the fillet on a mild steel model (Fig. 190), with the proportions $r/d = 0.157$ and $D/d = 2.5$. The line started from the point on the fillet where previous photoelastic experiments showed the maximum stress concentration was to be expected. The factor of stress concentration given by the curve in Fig. 190 is 1.85. According to this, yielding at the weakest part should start when the average tensile stress in the narrower portion of the model is only 1/1.85 of that necessary to produce Lueders' lines in
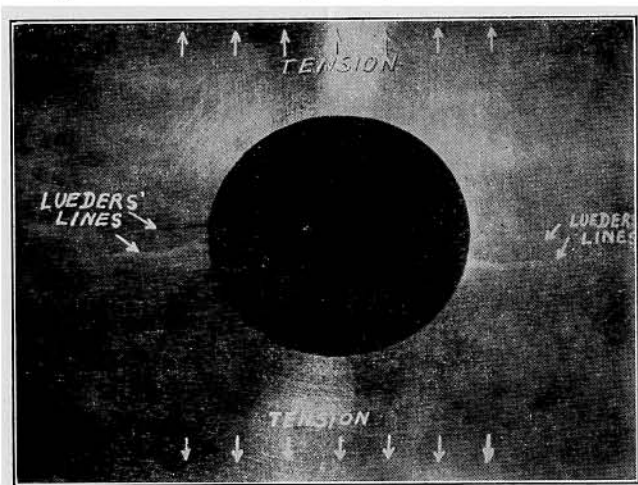


Fig. 216.

prismatical bars (Fig. 214) of the same material. Experiment showed that the load necessary to produce yielding at the fillet was 1/1.8 of that for the prismatical bar. Figure 216 represents the Lueders' lines at the edge of the circular hole in a strip of mild steel. Again these lines show accurately the points of maximum stress concentration. The average stress over the end cross section of the plate at which yielding occurred was 1/2.3 of that necessary to produce yielding in the prismatical bar.

In both cases the yielding at the place of maximum stress occurred at an average stress which is higher than indicated by the true factors of stress concentration. This can be explained as follows: The small region of overstressed material

is surrounded by portions where the stress does not exceed the proportional limit. This prevents the sort of sliding shown in Fig. 214, along surfaces perpendicular to the plane of the figure and inclined 45° to the direction of tension. In the cases shown in Fig. 215 and Fig. 216, the Lueders' lines started on the polished surfaces of the plates as thin lines perpendicular to the maximum tensile stress. This indicates that in these cases the sliding occurred along planes through these lines and inclined 45° to the plane of the plates. In such a case the thickness of the plate is an important factor. This thickness must be very small in comparison with the radii of the holes or fillets in order to have the surface of sliding totally within the region of highly overstressed material. The fact that the surface of sliding, beginning at the points of maximum stress, must cross a region with smaller stresses explains [39] the retardation in the appearance of Lueders' lines. In the case of the circular hole above, the width of the plate was 6 in. and the diameter of the hole 1 in., while the thickness of the plate was only 1/8 in. When testing models in which the thickness and the diameter of the hole are of the same order, it was impossible to detect any substantial effect due to stress concentration on the magnitude of the load producing Lueders' lines. Another reason for the Lueders' lines being retarded is the fact that a certain amount of permanent set may occur before Lueders' lines become visible.

The Lueders' lines method of testing the weak points of structures is not confined to any particular type of problem and has an advantage over the photoelastic method, described in the next article, in that it is applicable to three-dimensional problems. To make the yielding of metal visible on a rough surface the covering of the surface with a brittle paint has been successfully used in investigating stresses in boiler heads [40] and in built-up compression members.[41] By cutting

[39] This explanation was suggested to the writer by L. H. Donnell.
[40] See paper by F. Koerber u. E. Siebel, Mitteilungen K. W. Institute for Steel Research, Düsseldorf, Vol. 8, 1926, p. 63, and Vol. 9, 1927, p. 13.
[41] R. S. Johnston, Iron and Steel Institute, Vol. 112, 1925, p. 341.

specimens and models apart and using a special etching process on the cut surfaces it is possible to reveal the interior regions which have yielded and thus obtain information regarding the flow of metal at the points of stress concentration.[42]

### 64. Photoelastic Method of Stress Measurements.—

There are many stress analysis problems in which the deformation is essentially parallel to a plane. These are called *two-dimensional problems*. Illustrations are the bending of beams of a narrow rectangular cross section, bending of girders, arches, gear teeth, or, more generally, plates of any shape but of constant thickness acted on by forces or couples in the plane of the plate. Their shapes may be such that the stress distributions are very difficult to determine analytically and for such cases the *photoelastic* method has proved very
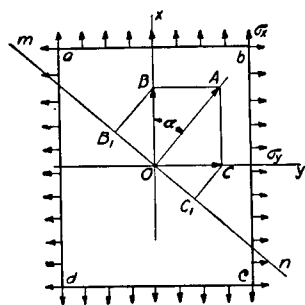


FIG. 217.

useful. In this method models cut out of a plate of an isotropic transparent material such as glass, celluloid or bakelite are used. It is well known that under the action of stresses these materials become *doubly refracting* and if a beam of *polarized light* is passed through a transparent model under stress, a colored picture may be obtained from which the stress distribution can be found.[43]

The application of the method in investigating stresses in machine parts was made by Dietrich and Lehr, V. D. I., Vol. 76, 1932. See also H. Kayser, "Bautechnik," 1936, and A. V. de Forest and Greer Ellis, Journal of the Aeronautical Sciences, Vol. 7, p. 205, 1940.

[42] See paper by A. Fry, Kruppsche Monatshefte, 1921; also Stahl u. Eisen, 1921.

[43] The phenomenon of double refraction due to stressing was discovered by D. Brewster, Phil. Trans. Roy. Soc., 1816. It was further studied by F. E. Neumann, Berlin Abh., 1841, and by J. C. Maxwell, Edinburgh Roy. Soc. Trans., Vol. 20, 1853, and his Scientific Papers, Vol. 1, p. 30. The application of this phenomenon to the solution of engineering problems was started by C. Wilson, Phil. Mag. (Ser. 5), Vol. 32 (1891), and further developed by A. Mesnager, Annales des Ponts et Chaussées, 1901 and 1913, and E. G. Coker, General Electric

In Fig. 217 *abcd* represents a transparent plate of uniform thickness and $O$ the point of intersection with the plate of a beam of polarized light perpendicular to the plate. Suppose that $OA$ represents the plane of vibration of the light and that the length $OA = a$ represents the amplitude of this vibration. If the vibration is considered to be simple harmonic, the displacements may be represented by the equation:

$$s = a \cos pt, \qquad (a)$$

where $p$ is proportional to the frequency of vibration, which depends on the color of the light.

Imagine now that the stresses $\sigma_x$ and $\sigma_y$, different in magnitude, are applied to the edges of the plate. Due to the difference in stresses the optical properties of the plate also become different in the two perpendicular directions. Let $v_x$ and $v_y$ denote the velocities of light in the planes $ox$ and $oy$ respectively. The simple vibration in the plane $OA$ is resolved into two components with amplitudes $\overline{OB} = a \cos \alpha$ and $\overline{OC} = a \sin \alpha$ in the planes $ox$ and $oy$ respectively, and the corresponding displacements are

$$x = a \cos \alpha \cos pt; \qquad y = a \sin \alpha \cos pt. \qquad (b)$$

If $h$ is the thickness of the plate, the intervals of time necessary for the two component vibrations to cross the plate are

$$t_1 = \frac{h}{v_x} \quad \text{and} \quad t_2 = \frac{h}{v_y}, \qquad (c)$$

and vibrations (b) after crossing the plate are given by the equations:

$$x_1 = a \cos \alpha \cos p(t - t_1); \qquad y_1 = a \sin \alpha \cos p(t - t_2). \qquad (d)$$

Co. Magazine, 1920, and Journal of Franklin Institute, 1925. For further development of the photoelastic method see the paper by Henry Favre, Schweizerische Bauzeitung, Vol. 20 (1927), p. 291; see also his dissertation: Sur une nouvelle methode optique de determination des tensions intérieures, Paris, 1929. The use of monochromatic light, so called "Fringe Method," was introduced by Z. Tuzi, "Inst. Phys. and Chem. Research," Vol. 8, p. 247, 1928.

These components have the phase difference $p(t_2 - t_1)$, due to the difference in velocities. Experiments show that the difference in the velocities of light is proportional to the difference in the stresses; hence

$$t_2 - t_1 = \frac{h}{v_y} - \frac{h}{v_x} = \frac{h(v_x - v_y)}{v_x v_y}$$

$$= \frac{h(v_x - v_y)}{v^2} \text{ (approximately)} = k(\sigma_x - \sigma_y), \quad (e)$$

where $v$ is the velocity of light when the stresses are zero, and $k$ is a numerical factor which depends on the physical properties of the material of the plate. We see that the difference of the two principal stresses can be found by measuring the difference in phase of the two vibrations. This can be done by bringing them into interference in the same plane. For this purpose a Nicol prism (called the *analyser*) is placed behind the plate in such a position as to permit the passage of vibrations in the plane $mn$ perpendicular to the plane $OA$ only. The components of the vibrations $(d)$, which pass through the prism, have the amplitudes $\overline{OB}_1 = \overline{OB} \sin \alpha = (a/2) \sin 2\alpha$ and $\overline{OC}_1 = \overline{OC} \cos \alpha = (a/2) \sin 2\alpha$. The resultant vibration in the plane $mn$ is therefore

$$\frac{a}{2} \sin 2\alpha \cos p(t - t_1) - \frac{a}{2} \sin 2\alpha \cos p(t - t_2)$$

$$= \left( a \sin 2\alpha \sin p \frac{t_1 - t_2}{2} \right) \sin p \left( t - \frac{t_1 + t_2}{2} \right). \quad (f)$$

This is a simple harmonic vibration, whose amplitude is proportional to $\sin p[(t_1 - t_2)/2]$; hence the intensity of the light is a function of the difference in phase $p(t_1 - t_2)$. If the stresses $\sigma_x$ and $\sigma_y$ are equal, $t_1$ and $t_2$ are also equal, the amplitude of the resultant vibration $(f)$ is zero and we have darkness. There will be darkness also whenever the difference in stresses is such that

$$p \frac{t_1 - t_2}{2} = n\pi, \quad (g)$$

where $n$ is an integer. The maximum intensity of light is obtained when the difference in stresses is such that

$$\sin p \frac{t_1 - t_2}{2} = \pm 1.$$

Imagine that instead of the element *abcd*, Fig. 217, we have a strip of a transparent material under simple tension. By gradually increasing the tensile stress we obtain a dark picture of the strip on the screen each time equation $(g)$ is fulfilled. In this manner we can establish experimentally for a given material of a given thickness the stress corresponding to the interval between two consecutive dark pictures of the specimen. For instance, for one kind of "phenolite" plate, 1 mm. thick, this stress was found [44] to be 1,620 lbs. per sq. in. Hence for a plate 1/4 in. thick, the corresponding stress will be $1,620/6.35 = 255$ lbs. per sq. in. With this information we can determine the stress in a strip under tension by counting the number of intervals between the consecutive dark images occurring during the gradual loading of the specimen. If we use a strip in pure bending, we obtain a picture such as is shown in Fig. 218. The parallel dark fringes indicate
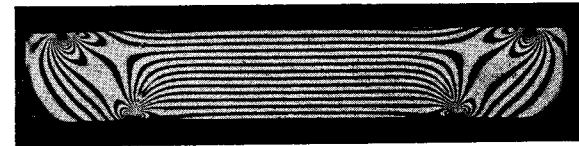


FIG. 218.

that in the portion of the strip at a considerable distance from the points of application of the loads the stress distribution is the same in all vertical cross sections. By counting the number of fringes we can determine the magnitudes of the stresses, as the stress difference between two consecutive fringes is the same as the stress difference between two con-

[44] Z. Tuzi, Sci. Papers, Inst. Phys. Chem. Research, Tokyo, Vol. 12, 1929, p. 247.

secutive dark images in simple tension. By watching the strip while the load is applied gradually, we may see how the number of dark fringes increases with increase of load. The new ones always appear at the top and the bottom of the strip and gradually move toward the neutral plane so that the fringes become more and more closely packed. The stress at any point is then obtained by counting the number of fringes which pass over the point.

The method of counting the number of dark fringes passing a chosen point can be used also for any plane stress distribution. As it is seen from our previous discussion, this number gives generally the difference between the two principal stresses at the point. For a complete determination of the stress at the point it remains then to find the directions of the principal stresses and their sum. Equation ($f$) shows that the intensity of the light passing through the analyzer is proportional to sin $2\alpha$, where $\alpha$ is the angle between the plane of polarization and the plane of one of the principal stresses, Fig. 217. If these two planes coincide, sin $2\alpha$ is zero and we obtain a dark spot on the screen. Hence in examining a stressed transparent model in polarized light we observe not merely the dark fringes discussed before but also dark lines connecting the points at which one of the principal stress directions coincides with the plane of polarization. By rotating both Nicol prisms, polarizer and analyzer, and marking dark lines on the image of the stressed plate for various directions of the plane of polarization, we obtain the system of so-called *isoclinic lines* which join together points with the same directions of principal stresses. Having these lines, we can draw the lines which are tangential at each point to the principal axes of stress. These latter lines are called the *trajectories* of the principal stresses, see p. 123, Part I. Thus the directions of the principal stresses at each point of the plate can be obtained experimentally.

The sum of the principal stresses can also be obtained experimentally by measuring the change $\Delta h$ in the thickness

$h$ of the plate due to the stresses $\sigma_x$ and $\sigma_y$ [45] and using the known relation

$$\Delta h = \frac{\mu h}{E}(\sigma_x + \sigma_y). \tag{h}$$

Having the difference of the two principal stresses from the photo-elastic test and their sum from expression ($h$), we can readily calculate the magnitude of the principal stresses. The fringes obtained in a plate with fillets submitted to the action of pure bending are shown as an illustration in Fig. 219.
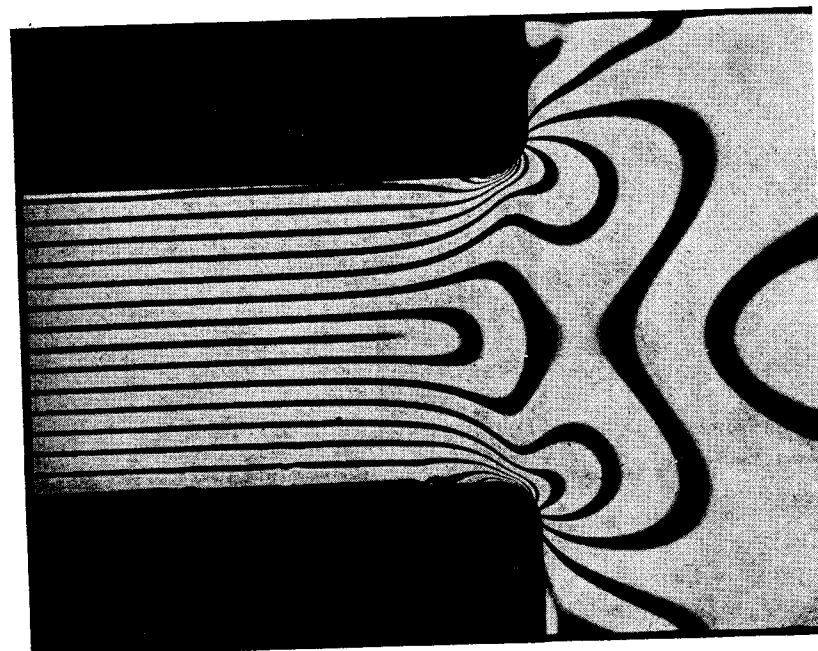


FIG. 219.

From the fact that the fringes are crowded at the fillets it may be concluded that a considerable stress concentration takes place at those points.

[45] This method was suggested by A. Mesnager, loc. cit., p. 346. The necessary lateral extensometer was developed and successfully used by A. M. Wahl, see paper by R. E. Peterson and A. M. Wahl, Journal of Appl. Mech., Vol. 2, 1935, p. 1.

In the previous discussion of the photo-elastic stress analysis it was always assumed that we were dealing with two-dimensional problems. More recently considerable efforts have been made to expand the photo-elastic method on three-dimensional problems and some promising results have already been obtained.[46]

**65. Stresses at the Point of Load Application.**—In discussing a symmetrical wedge under tension (see p. 312) it was indicated that in each point of that wedge there is only a simple tension in the radial direction. By making the angle $2\alpha$ of the wedge equal to $\pi$ and changing from tension to compression we obtain the case in which a concentrated force is pressing normally on a straight edge of a large plate, Fig. 220. An element such as shown at point $A$ undergoes a
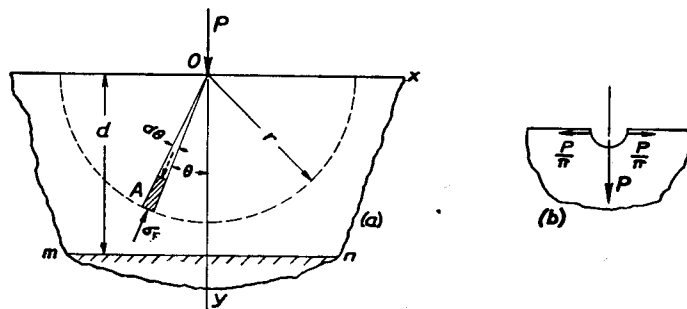


Fig. 220.

simple compression in the radial direction and the compressive stress, from equation $(a)$, p. 312, is

$$\sigma_r = k\, \frac{P \cos \theta}{hr} \qquad (a)$$

where $r$ is the radial distance from the point of application of the load and $h$ the thickness of the plate. The factor $k$ is

[46] See paper by M. Hetényi, Journal of Appl. Mech., Vol. 5, p. 149, 1938. See also R. Weller, Journal Applied Phys., Vol. 10, p. 266, 1939.

determined from the fact that the stresses $\sigma_r$ distributed along the length of the semi circle shown in the figure by the dotted line keep in equilibrium the load $P$. Hence

$$2h \int_0^{\pi/2} \sigma_r \cos \theta\, r d\theta = P.$$

Substituting for $\sigma_r$ its expression $(a)$ we obtain

$$k = \frac{2}{\pi}$$

and expression $(a)$ becomes

$$\sigma_r = \frac{2P}{\pi} \cdot \frac{\cos \theta}{hr}. \qquad (283)$$

If we consider a horizontal plane $mn$ at a distance $d$ from the edge of the plate, Fig. 220, the normal compressive stress acting on that plane is

$$\sigma_y = \sigma_r \cos^2 \theta = \frac{2P}{\pi} \frac{\cos^3 \theta}{hr} = \frac{2P}{\pi} \frac{\cos^4 \theta}{hd}. \qquad (284)$$

It is seen that the pressure rapidly diminishes as the angle $\theta$ increases. It is seen also that the stresses increase with a decrease of the distance $d$. Knowing the stresses produced by the action of one concentrated load $P$ and using the method of superposition we can readily discuss the cases in which several loads are acting.[47]

If a concentrated force is acting at the middle of a rectangular beam of a narrow cross section of a depth $d$ the highly concentrated stresses given by expression (283) are superposed on bending stresses in the beam and a complicated stress distribution results near the point of the load application. The photoelastic picture of this stress distribution is shown in Fig. 221. It is seen that the perturbation in stress distribution produced by the concentrated load is of a localized character and is of importance only in the close vicinity of

[47] See "Theory of Elasticity," p. 82.

the point of application of the load. If we consider a cross section of the beam at a distance from the load larger, say, than one half the depth of the beam, the stress distribution in that cross section is approximately that given by the simple beam formula. The number of fringes diminishes as the distance of the cross section from the load increases as it should be since the magnitude of the bending moment decreases as we approach the beam supports.

By making the resultant of the horizontal components of the radial pressures $h\sigma_r r d\theta$ for each half of the dashed semi-
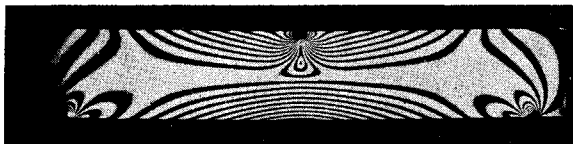


FIG. 221.

circle in Fig. 220 (a), it can be shown that the concentrated force $P$ produces a "wedging" action represented in Fig. 220 (b) by the two equal and opposite forces of the magnitude $P/\pi$. In the case of the beam of a depth $d$ and thickness $h$, Fig. 221, these forces acting at a distance $d/2$ from the axis of the beam produce in the middle cross section not only tensile stresses

$$\sigma_x' = \frac{P}{\pi dh} \qquad (b)$$

but also bending stresses given by the expression

$$\sigma_x'' = -\frac{Pd}{2\pi}\frac{y}{I_z}, \qquad (c)$$

in which $Pd/2\pi$ is the bending moment produced by the horizontal forces $P/\pi$, $y$ is the distance from the axis of the beam, taken positive downwards, and $I_z = hd^3/12$ is the moment of inertia of the cross section. Superposing the stresses (b) and (c) upon the bending stresses given by the ordinary beam formula, we find that the tensile stress in the most remote fiber

of the beam in the loaded cross section is

$$(\sigma_x)_{y=d/2} = \frac{Pl}{4}\cdot\frac{6}{hd^2} + \frac{P}{\pi dh} - \frac{3P}{\pi dh}$$

$$= \frac{Pl}{4}\cdot\frac{6}{hd^2}\left(1 - \frac{4}{3\pi}\frac{d}{l}\right). \qquad (d)$$

The second term in the parenthesis represents the "wedging action" of the load $P$. It is seen that in the case of short beams this action is of a considerable magnitude. The photoelastic experiments are in a very satisfactory agreement with expression $(d)$.[48]

The discussion of stress distribution at the point of application of a concentrated load can be expanded on the case in which instead of a plate, Fig. 220, we have a large body with a plane surface on which a concentrated load is acting. It can be shown that in this case the stresses are inversely proportional to the square of the distance from the point of application of the load.[49]

**66. Contact Stresses in Balls and Rollers.**—If two elastic bodies, say two balls, are pressing on each other, a small surface of contact is formed as a result of local deformation. The pressures distributed over this surface are called contact pressures. The magnitude of these pressures and the stresses produced in the bodies can be calculated by using equations of the theory of elasticity.[50] We will give here only the final results of such investigation. In the case of two balls compressed by forces $P$ (Fig. 222) the pressures are distributed over a small *circle of contact mn*, the radius of which
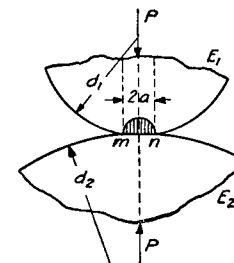


FIG. 222.

[48] See experiments by Carus Wilson, loc. cit., p. 346.

[49] This problem was discussed by J. Boussinesq, see his book, "Application des Potentiels," Paris, 1885. See also "Theory of Elasticity," p. 328, 1934.

[50] This problem was solved by H. Herz, Gesammelte Werke, Vol. 1, 1895. The discussion of the problem and the bibliography are given in "Theory of Elasticity," p. 339.

is given by the equation:

$$a = 0.88 \sqrt[3]{\frac{P \dfrac{1}{E_1} + \dfrac{1}{E_2}}{2 \dfrac{1}{d_1} + \dfrac{1}{d_2}}}. \qquad (285)$$

In this $E_1$ and $E_2$ are the moduli of the two balls and $d_1$ and $d_2$ the corresponding diameters. The maximum pressure occurs at the center of the *circle of contact* and is given by the equation:

$$p_{max} = 1.5 \frac{P}{\pi a^2}. \qquad (286)$$

Due to local deformation the centers of the balls approach one another by the distance

$$\lambda = 0.77 \sqrt[3]{2P^2 \left(\frac{1}{E_1} + \frac{1}{E_2}\right)^2 \left(\frac{1}{d_1} + \frac{1}{d_2}\right)}. \qquad (287)$$
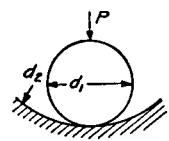
When the diameters of the balls and the moduli of elasticity are equal, the above equations become

$$a = 0.88 \sqrt[3]{\frac{Pd}{2E}}; \quad p_{max} = 0.62 \sqrt[3]{\frac{4PE^2}{d^2}}; \quad \lambda = 1.54 \sqrt[3]{\frac{2P^2}{E^2 d}}. \quad (288)$$

When a ball of diameter $d$ is forced against an elastic body having a plane surface, the required formulae are obtained by substituting $d_1 = d$, $d_2 = \infty$ in eqs. (285)–(287). Assuming $E_1 = E_2 = E$, we find for this case

$$a = 0.88 \sqrt[3]{\frac{Pd}{E}}; \quad p_{max} = 0.62 \sqrt[3]{\frac{PE^2}{d^2}}; \quad \lambda = 1.54 \sqrt[3]{\frac{P^2}{E^2 d}}. \quad (289)$$

In the case of a *ball in a spherical seat* (Fig. 223), the sign of $d_2$ in eqs. (285)–(287) must be changed. Then for the case $E_1 = E_2 = E$, we find



Fig. 223.

$$a = 0.88 \sqrt[3]{\frac{P}{E} \frac{d_1 d_2}{d_2 - d_1}};$$

$$p_{max} = 0.62 \sqrt[3]{PE^2 \left(\frac{d_2 - d_1}{d_2 d_1}\right)^2}. \qquad (290)$$

It is interesting to note that in the cases represented by eqs. (288) and (289) the maximum compressive stress at the center of the

surface of contact depends on the magnitude of the ratio $P/d^2$, i.e., the maximum stress remains constant if the above ratio is kept constant. This justifies the usual practice of determining the safe diameter of the ball by taking a definite magnitude of load per square inch of the diametral section of the ball. Since the material at the center of the surface of contact is prevented from lateral expansion, it is in a condition of compression from all sides and may sustain very high pressures (see art. 83). In experiments [51] with hardened crucible steel the allowable compressive force $P$ in the case of a ball pressed against a plane surface may be expressed by the equation:

$$P_{max} = 700d^2,$$

in which $d$ is in inches and $P$ in pounds. Substituting in the second of eqs. (289), we find $p_{max}$ equal to approximately 530,000 lbs. per sq. in.

In the general case of compression of two bodies having the same modulus $E$, let $1/r_1$ and $1/r_1'$ denote the principal curvatures at the point of contact of one of the bodies, and $1/r_2$ and $1/r_2'$ of the other,[52] $\varphi$ the angle between the normal planes containing curvatures $1/r_1$ and $1/r_2$. The *surface of contact* for the general case is an ellipse, the semi-axes of which are given by the equations

$$a = \alpha \sqrt[3]{\frac{Pm}{n}}; \qquad b = \beta \sqrt[3]{\frac{Pm}{n}}, \qquad (291)$$

in which $P$ is the compressive force and

$$m = \frac{4}{\dfrac{1}{r_1} + \dfrac{1}{r_1'} + \dfrac{1}{r_2} + \dfrac{1}{r_2'}}; \qquad n = \frac{4E}{3(1 - \mu^2)}.$$

The constants $\alpha$ and $\beta$ are taken from the table 24 below for each particular case. The angle $\theta$ in the first column of the table is calculated from the equation

$$\cos \theta = \frac{B}{A}, \qquad (a)$$

---

[51] See Stribeck, V. D. I., 1901, p. 73; Schwinning, V. D. I., 1901, p. 332, and A. Bauschlicher, V. D. I., 1908, p. 1185.

[52] The principal curvatures are the maximum and the minimum curvatures and these are in planes at right angles. The curvature of a body is considered as positive if the corresponding center of curvature is within the body.

in which

$$A = \frac{2}{m}; \quad B =$$

$$\frac{1}{2} \sqrt{\left(\frac{1}{r_1} - \frac{1}{r_1'}\right)^2 + \left(\frac{1}{r_2} - \frac{1}{r_2'}\right)^2 + 2\left(\frac{1}{r_1} - \frac{1}{r_1'}\right)\left(\frac{1}{r_2} - \frac{1}{r_2'}\right)\cos 2\varphi}. \quad (b)$$

TABLE 24.—CONSTANTS FOR CALCULATING THE SEMI-AXES OF THE ELLIPSE OF CONTACT

| $\theta$ degrees | $\alpha$ | $\beta$ | $\theta$ degrees | $\alpha$ | $\beta$ |
|---|---|---|---|---|---|
| 20 | 3.778 | 0.408 | 60 | 1.486 | 0.717 |
| 30 | 2.731 | 0.493 | 65 | 1.378 | 0.759 |
| 35 | 2.397 | 0.530 | 70 | 1.284 | 0.802 |
| 40 | 2.136 | 0.567 | 75 | 1.202 | 0.846 |
| 45 | 1.926 | 0.604 | 80 | 1.128 | 0.893 |
| 50 | 1.754 | 0.641 | 85 | 1.061 | 0.944 |
| 55 | 1.611 | 0.678 | 90 | 1.000 | 1.000 |

The expression for the maximum pressure at the center of the surface of contact is then

$$p_{max} = 1.5 \frac{P}{\pi ab}. \quad (292)$$

In the case of *rollers in compression*, Fig. 224, the contact area is a narrow rectangle whose width $b$ is given by the equation: [53]
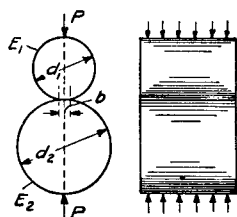


FIG. 224.

$$b = 2.15 \sqrt{\frac{P'}{2} \frac{d_1 d_2}{d_1 + d_2}\left(\frac{1}{E_1} + \frac{1}{E_2}\right)}, \quad (293)$$

in which $P'$ denotes the compressive force per unit length of the roller. The maximum unit pressure at the middle of the *rectangle of contact* is

$$p_{max} = 0.59 \sqrt{2P' \frac{d_1 + d_2}{d_1 d_2} \frac{1}{\frac{1}{E_1} + \frac{1}{E_2}}}. \quad (294)$$

[53] See A. Föppl, Technische Mechanik, Vol. 5, 1907, p. 351.

In the particular case in which the moduli for both rollers are equal

$$b = 2.15 \sqrt{\frac{P' d_1 d_2}{E(d_1 + d_2)}}; \quad p_{max} = 0.59 \sqrt{P'E \frac{d_1 + d_2}{d_1 d_2}}. \quad (295)$$

If one of the diameters be taken as infinitely large as in the case of a roller in contact with a plane surface, eqs. (293) and (294) reduce to

$$b = 2.15 \sqrt{\frac{P'd}{E}}; \quad p_{max} = 0.59 \sqrt{\frac{P'E}{d}}. \quad (296)$$

It will be seen that the maximum stress remains constant if $P'$ varies in the same proportion as $d$. This justifies the practice of determining the safe dimensions on the basis of the diametral cross sectional area of the roller. The allowable compressive force $P'$ in the case of ordinary steel rollers in bridges, for instance, is obtained from the equation:

$$P' = 700d.$$

Substituting this into eq. (296), we find the maximum pressure is about 85,000 lbs. per sq. in.[54]

### Problems

1. Determine the maximum pressure at the surface of contact $C$ in a single row ball bearing, shown in Fig. 225. The ball diameter is $d = 1.5$ in., the radius of the grooves 1 in., the diameter of the outer race 8 in. and the greatest compressive force on one ball $P = 5,000$ lbs.
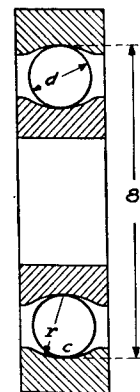


FIG. 225.

*Solution.* Using the notation of page 357,

$$r_1 = r_1' = \frac{1.5}{2} = \frac{3}{4} \text{ in.;} \quad r_2 = -1 \text{ in.;}$$

$$r_2' = -4 \text{ in.;}$$

$$m = \frac{4}{\frac{2}{1.5} + \frac{2}{1.5} - \frac{1}{1} - \frac{1}{4}} = 2.823;$$

$$n = \frac{4 \times 30 \times 10^6}{3 \times .91};$$

[54] For testing of steel rollers see W. M. Wilson, Univ. of Illinois, Engr. Exp. Sta. Bull. 162, 1927; 191, 1929; 263, 1934. See also V. P. Jensen, Iowa Engr. Exp. Sta., Bull. 138, 1937. Fatigue test of rollers discussed in art. 80.

$$2A = \frac{4}{m} = \frac{4}{2.823} = 1.417; \qquad 2B = \frac{1}{1} - \frac{1}{4} = 0.750.$$

Substituting in eq. (a) (p. 357),

$$\cos \theta = \frac{0.750}{1.417} = 0.529; \qquad \theta = 58°.$$

Then from the table, by interpolation,

$$\alpha = 1.536, \qquad \beta = 0.701.$$

The semi-axes of the ellipse of contact are, from eqs. (291),

$$a = 1.536 \sqrt[3]{\frac{5,000 \times 2.823 \times 3 \times 0.91}{4 \times 30 \times 10^6}} = 0.105 \text{ in.},$$

$$b = 0.701 \sqrt[3]{\frac{5,000 \times 2.823 \times 3 \times 0.91}{4 \times 30 \times 10^6}} = 0.048 \text{ in.}$$

Then, from eq. (292),

$$p_{max} = 1.5 \frac{5,000}{\pi ab} = 475,000 \text{ lbs. per sq. in.}$$

Such high stresses can be sustained by hardened steel due to the fact that at the center of the ellipse of contact the material is compressed not only in the direction of the force $P$ but also in the lateral directions.

2. Determine the surface of contact and the maximum pressure between two circular cylinders whose axes are mutually perpendicular. We have such a problem, for instance, in contact pressures at the point of contact of a wheel with cylindrical boundary and a rail.[55]

*Solution.* Denoting by $r_1$ and $r_2$ the radii of the cylinders and using the notation of page 357,

$$\frac{1}{r_1'} = 0; \quad \frac{1}{r_2'} = 0; \quad \varphi = \frac{\pi}{2}; \quad m = \frac{4}{\frac{1}{r_1} + \frac{1}{r_2}}; \quad n = \frac{4E}{3(1 - \mu^2)};$$

$$A = \frac{1}{2}\left(\frac{1}{r_1} + \frac{1}{r_2}\right); \qquad B = \frac{1}{2}\sqrt{\frac{1}{r_1^2} + \frac{1}{r_1^2} - \frac{2}{r_1 r_2}} = \pm\frac{1}{2}\left(\frac{1}{r_1} - \frac{1}{r_2}\right).$$

[55] The problem of contact pressures becomes more and more important as the axial load of modern locomotives is increased. For discussion of this problem, see the paper by H. Fromm, V. D. I., Vol. 73, 1929, p. 957.

The sign must be chosen so as to make $B$ positive. From eq. (a)

$$\cos \theta = \pm \frac{\frac{1}{r_1} - \frac{1}{r_2}}{\frac{1}{r_1} + \frac{1}{r_2}}$$

Knowing $\theta$, we get the semi-axes of the ellipse of contact from eqs. (291) and the maximum pressure from eq. (292).

In the particular case of two cylinders of equal radii, $\cos \theta = 0$, and from the table on p. 358 it can be concluded that the surface of contact has a circular boundary.

3. Find the maximum pressure between the wheel with a cylindrical rim of radius $r_1 = 15.8$ in. and the rail with the radius of the head $r_2 = 12$ in. if $P = 1000$ lbs. and Poisson's ratio $\mu = 0.25$.

*Answer.* The semi-axes of the ellipse of contact are

$$a = 0.0946 \text{ in.} \qquad \text{and} \qquad b = 0.0792 \text{ in.}$$

$$p_{max} = \frac{3}{2}\frac{P}{\pi ab} = 63,600 \text{ lbs. per sq. in.}$$

## CHAPTER VIII

### DEFORMATIONS BEYOND ELASTIC LIMIT

**67. Pure Bending of Beams the Material of Which Does Not Follow Hooke's Law.**—The experiments with beams the material of which does not follow Hooke's law indicate that during pure bending the cross sections of the beam remain plane; hence elongations and contractions of longitudinal fibers are proportional to their distances from the neutral surface. Taking this as a basis of our further discussion and assuming that during bending there exists the same relation between stress and strain as in the case of simple tension and compression, we can find without difficulty the stresses produced in the beam by a bending moment of a given magnitude.[1] Let us begin with a beam of rectangular cross section, Fig. 226, and assume that the radius of curvature of the neu-
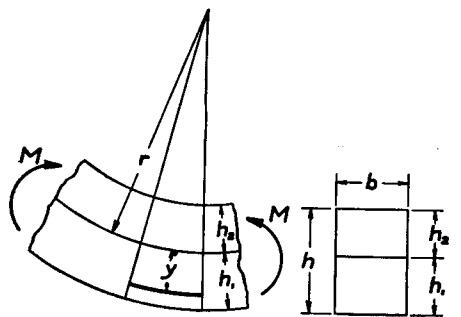


Fig. 226.

tral surface produced by the moments $M$ is equal to $r$. In such a case the unit elongation of a fiber a distance $y$ from the neutral surface is

$$\epsilon = \frac{y}{r}. \qquad (a)$$

---

[1] This theory has been developed by Saint Venant in his notes to the Navier's book: "Résumé des leçons. . . ." 3d ed., p. 173, 1864. See also paper by Eugen Mayer, Physik. Zeitsehr., 1907 and Dissertation by H. Herbert, Göttingen, 1909.

Denoting by $h_1$ and $h_2$ the distances from the lower and the upper surfaces of the beam respectively to the neutral axis, we find that the elongations in the utmost fibers are

$$\epsilon_1 = \frac{h_1}{r}, \qquad \epsilon_2 = -\frac{h_2}{r}. \qquad (b)$$

It is seen that the elongation or contraction of any fiber is readily obtained provided we know the position of the neutral axis, say ratio $h_1/h_2$, and the radius of curvature $r$. These two quantities can be found from the two equations of statics:

$$\int_A \sigma dA = b \int_{-h_2}^{h_1} \sigma dy = 0, \qquad (c)$$

$$\int_A \sigma y dA = b \int_{-h_2}^{h_1} \sigma y dy = M. \qquad (d)$$

The first of these equations states that the sum of normal forces acting on a cross section of the beam vanishes, since these forces represent a couple. The second equation states that the moment of the same forces with respect to the neutral axis is equal to the bending moment $M$.

Equation $(c)$ is now used for determining the position of the neutral axis. From equation $(a)$ we have

$$y = r\epsilon, \qquad dy = rd\epsilon. \qquad (e)$$

Substituting into equation $(c)$ we obtain

$$\int_{-h_2}^{h_1} \sigma dy = r \int_{\epsilon_2}^{\epsilon_1} \sigma d\epsilon = 0. \qquad (f)$$

Hence the position of the neutral axis is such that the integral $\int_{\epsilon_2}^{\epsilon_1} \sigma d\epsilon$ vanishes. To determine this position we use the curve $AOB$ in Fig. 227, which represents the tension-compression test diagram for the material of the beam, and we denote by $\Delta$ the sum of the absolute values of the maximum elonga-

tion and the maximum contraction, which is

$$\Delta = \epsilon_1 - \epsilon_2 = \frac{h_1}{r} + \frac{h_2}{r} = \frac{h}{r}. \qquad (g)$$

To solve equation $(f)$, we have only to mark the length $\Delta$ on the horizontal axis in Fig. 227 in such a way as to make equal the two areas shaded in the figure. In this manner we obtain the strain $\epsilon_1$ and $\epsilon_2$ in the utmost fibers; equations $(b)$ then give

FIG. 227.

$$\frac{h_1}{h_2} = \left| \frac{\epsilon_1}{\epsilon_2} \right|. \qquad (h)$$

This determines the position of the neutral axis. Observing that elongations $\epsilon$ are proportional to the distance from the neutral axis, we conclude that the curve $AOB$ also represents the distribution of bending stresses along the depth of the beam, if $h$ is substituted for $\Delta$. In calculating the radius $r$ we use equation $(d)$. Substituting for $y$ and $dy$ their expressions $(e)$, we represent equation $(d)$ in the following form:

$$br^2 \int_{\epsilon_2}^{\epsilon_1} \sigma\epsilon d\epsilon = M. \qquad (i)$$

By observing that $r = h/\Delta$ from equation $(g)$, the equation $(i)$, after a simple transformation, can be written as follows:

$$\frac{bh^3}{12} \cdot \frac{1}{r} \cdot \frac{12}{\Delta^3} \int_{\epsilon_2}^{\epsilon_1} \sigma\epsilon d\epsilon = M. \qquad (j)$$

Comparing this result with the known equation

$$\frac{EI}{r} = M \qquad (k)$$

for bending of beams following Hooke's law, we conclude that beyond the proportional limit the curvature produced by a
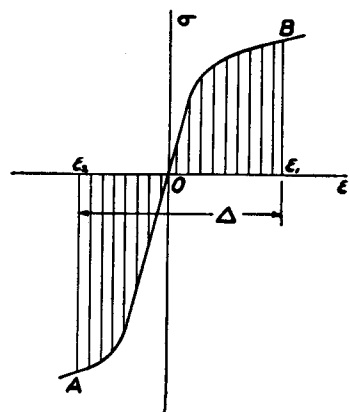
moment $M$ can be calculated from the equation:

$$\frac{E_r I}{r} = M, \qquad (297)$$

in which $E_r$ is the *reduced modulus* defined by the expression:

$$E_r = \frac{12}{\Delta^3} \int_{\epsilon_2}^{\epsilon_1} \sigma\epsilon d\epsilon. \qquad (298)$$

The integral in this expression represents the moment with respect to the vertical axis through the origin $O$ of the shaded area shown in Fig. 227. Since the ordinates of the curve in the figure represent stresses, and the abscissas, strain, the integral and also $E_r$ have the dimension of lb. in.$^{-2}$, i.e., the same dimension as the modulus $E$. The magnitude of $E_r$ for a given material, i.e., for a given curve in Fig. 227, is a function of $\Delta$ or of $h/r$. Taking several values of $\Delta$ and using each time the curve in Fig. 227 as was previously explained, we de-
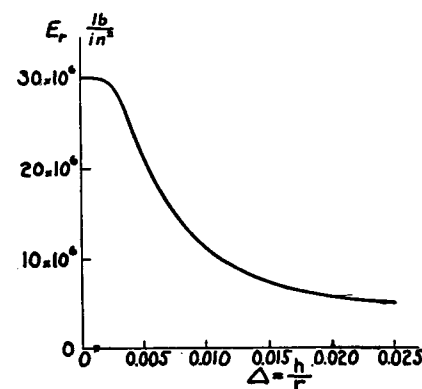
FIG. 228.

termine for each value of $\Delta$ the corresponding utmost elongations $\epsilon_1$ and $\epsilon_2$, and from expression (298) the corresponding value of $E_r$. In this way a curve representing $E_r$ as a function of $\Delta = h/r$ is obtained. In Fig. 228 such a curve is shown for structural steel with $E = 30.10^6$ lbs. per square inch and the proportional limit 30,000 lbs. per square inch. In such a case, for $\Delta < 0.002$, $E_r$ remains constant and equal to $E$.

With such a curve the moment corresponding to any assumed curvature can be readily calculated from equation (297), and we can plot a curve, Fig. 229, giving the moment $M$ as a function of $\Delta$. For small values of $\Delta$ the material follows Hooke's law, and the curvature is proportional to the bending moment $M$, as shown in the figure by the straight line $OC$. Beyond the proportional limit the rate of change of the curvature is always increasing as the moment increases.



FIG. 229.          FIG. 230.
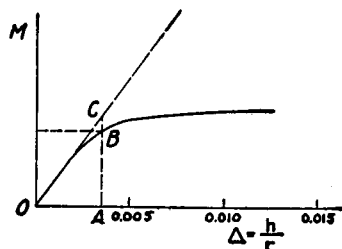
If instead of a rectangle we have any other symmetrical shape of the cross section, the width $b$ of the cross section is variable, and equations (c) and (d) must be written in the following form:

$$\int_{-h_2}^{h_1} b\sigma \, dy = r \int_{\epsilon_2}^{\epsilon_1} b\sigma \, d\epsilon = 0, \qquad (l)$$

$$\int_{-h_2}^{h_1} b\sigma y \, dy = r^2 \int_{\epsilon_2}^{\epsilon_1} b\sigma \epsilon \, d\epsilon = M. \qquad (m)$$

Take as an example the case of a $\perp$ section, Fig. 230. If we denote by $\epsilon'$ the longitudinal strain at the junction of the web and of the flange, the equations (l) and (m) can be written in the following form:

$$\int_{\epsilon_2}^{\epsilon'} \sigma \, d\epsilon + \int_{\epsilon'}^{\epsilon_1} \frac{b_1}{b} \sigma \, d\epsilon = 0, \qquad (n)$$

$$b r^2 \left( \int_{\epsilon_2}^{\epsilon'} \sigma \epsilon \, d\epsilon + \int_{\epsilon'}^{\epsilon_1} \frac{b_1}{b} \sigma \epsilon \, d\epsilon \right) = M. \qquad (o)$$
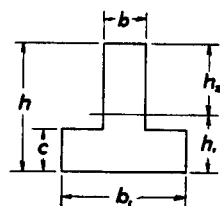
We see that in this case the ordinates of the tensile test curve in that portion corresponding to the flange of the cross section must be magnified in the ratio $b_1/b$. In determining the position of the neutral axis we proceed as in the preceding case: use the tension-compression test diagram, Fig. 231, and mark on the horizontal axis such a position of the assumed length $\Delta = h/r$ that the two shaded areas become numerically equal. In this manner the strains $\epsilon_1$ and $\epsilon_2$ in the utmost fibers are obtained. The strain $\epsilon'$ at the junction of the web and the flange is obtained from the equation

$$\frac{\epsilon_1 - \epsilon'}{\Delta} = \frac{c}{h},$$

in which $c$ is the thickness of the flange, Fig. 230. Having determined the position of the neutral axis and observing that the expression in the parentheses of equation (o) represents the moment of the shaded areas in Fig. 231 with respect to the vertical axis through the origin $O$, we can readily calculate from equation (o) the moment $M$, corresponding to the assumed value of $\Delta = h/r$. In this manner a curve similar to that shown in Fig. 229 can be constructed for a beam of $\perp$ section. An I beam can also be treated in a similar manner.
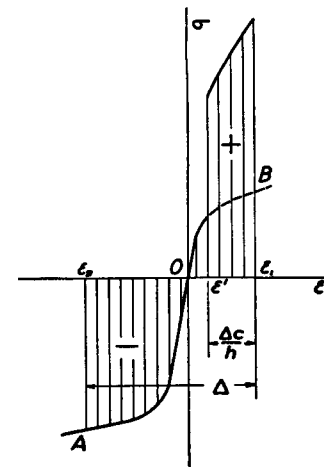


FIG. 231.

In the previous examples the tension-compression test diagram $AOB$ was used for determining the position of the neutral axis and the magnitude of the radius of curvature, $r$. If there exists an analytical expression for the curve $AOB$, the above quantities can be obtained by calculation alone without using the graphical method shown in Fig. 227 and Fig. 231. A very general equation for stress-strain curves was used by Saint Venant.[2] He assumed that for

[2] Loc. cit., p. 362.

bending beyond the proportional limit the distribution of tensile and compressive stresses along the depth of the beam can be represented by the following equations:

$$\left.\begin{aligned} \sigma &= \sigma_0\left[1 - \left(1 - \frac{y}{a}\right)^m\right], \\ \sigma' &= \sigma_0'\left[1 - \left(1 - \frac{y_1}{b}\right)^n\right], \end{aligned}\right\} \quad (p)$$

in which $\sigma_0$ and $\sigma_0'$ and also $a$ and $b$ are certain constants which, together with the exponents $m$ and $n$, define the stress distribution curves shown in Fig. 232. For very small distances $y$ and $y_1$ we can assume that

$$\left(1 - \frac{y}{a}\right)^m \approx 1 - \frac{my}{a}, \quad \text{and} \quad \left(1 - \frac{y_1}{b}\right)^n \approx 1 - \frac{ny_1}{b},$$

and equations (p) give

$$\sigma = \frac{\sigma_0 my}{a} = \frac{\sigma_0 mr\epsilon}{a}, \quad \text{and} \quad \sigma' = \frac{\sigma_0' ny_1}{b} = \frac{\sigma_0' nr\epsilon}{b}.$$

Hence

$$\frac{\sigma_0 mr}{a} = E_1, \quad \text{and} \quad \frac{\sigma_0' nr}{b} = E_2, \qquad (q)$$

where $E_1$ and $E_2$ are the moduli of the material for very small tension and compression respectively. If these two moduli of the material are equal, the two curves given by equations (p) have a common tangent at the neutral axis and we have

$$\frac{\sigma_0 m}{a} = \frac{\sigma_0' n}{b}. \qquad (r)$$

By using expressions (p) in equations of equilibrium (c) and (d), the position of the neutral axis and the radius of curvature can be calculated in each particular case. Taking, for example, $m = n = 1$ and using expressions (q) we obtain, from equations (p),



FIG. 232.

$$\sigma = \frac{E_1 y}{r}, \quad \sigma' = \frac{E_2 y_1}{r}. \qquad (s)$$

This is the case in which the material of the beam follows Hooke's
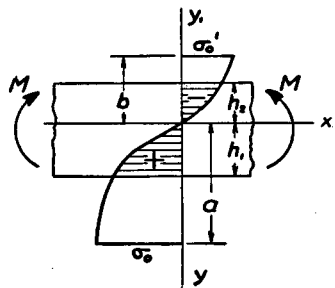
law but has a modulus in tension different from its modulus in compression. Substituting expressions (s) into equation (c) and assuming that the beam has a rectangular cross section, we obtain

$$E_1 h_1^2 = E_2 h_2^2,$$

which, together with the equation $h_1 + h_2 = h$, gives

$$h_1 = \frac{h\sqrt{E_2}}{\sqrt{E_1} + \sqrt{E_2}}, \quad \text{and} \quad h_2 = \frac{h\sqrt{E_1}}{\sqrt{E_1} + \sqrt{E_2}}$$

From equation (d) we then find

$$\frac{E_1 h_1}{r} \cdot \frac{bh_1}{2} \cdot \frac{2}{3} h = \frac{bh^3}{12} \cdot \frac{1}{r} \cdot \frac{4E_1 E_2}{(\sqrt{E_1} + \sqrt{E_2})^2}.$$

It is seen that in this case the curvature is obtained from equation (297) by using for the reduced modulus the value

$$E_r = \frac{4E_1 E_2}{(\sqrt{E_1} + \sqrt{E_2})^2}. \qquad (299)$$

This modulus is sometimes used in calculating the buckling load for a column compressed beyond the proportional limit of the material.[3]

As another example let us assume that the stress-strain curves in tension and compression are identical; then $m = n$, $a = b$ and $\sigma_0 = \sigma_0'$ in equations (p). Assuming also that $a = b = h/2$ we find, from equation (d), for a rectangular beam:



FIG. 233.

$$M = \sigma_{\max} \cdot \frac{bh^2}{6} \cdot \frac{3m(m + 3)}{2(m + 1)(m + 2)}. \qquad (300)$$

The neutral axis in this case goes through the centroid of the cross section. The curves giving the stress distribution for various values of the exponent $m$ are shown in Fig. 233. With increasing values of $m$ the moment approaches the value:

$$M = \frac{3}{2} \cdot \sigma_{\max} \cdot \frac{bh^2}{6}.$$
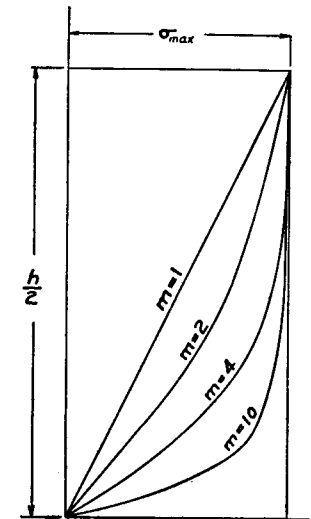
[3] "Theory of Elastic Stability," p. 156.

In the case of structural steel with a pronounced yield point the stretching of the material during yielding (the horizontal portion at $B$ in the tensile test diagram of Fig. 2$a$, p. 6, Part I) may be many times larger than the elastic elongation, say from 10 to 15 times larger. It may also be assumed for steel that the yield point stress is the same in tension and compression. Then the tension-compression test diagram can be represented with sufficient accuracy by the straight lines shown in Fig. 234. With a rectangular beam as an example, the strains $\epsilon_1$ and $\epsilon_2$ in the outermost fibers during bending beyond yield point are always equal, and equation ($i$) gives:
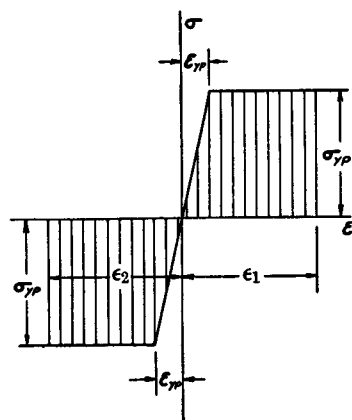


FIG. 234.

$$br^2\sigma_{Y.P.}(\epsilon_1^2 - \tfrac{1}{3}\epsilon_{Y.P.}^2) = M, \quad (t)$$

where $\epsilon_{Y.P.} = \sigma_{Y.P.}/E$ is the elastic elongation at the yield-point stress. If $\epsilon_{Y.P.}$ is small in comparison with $\epsilon_1$, the second term in the parentheses of equation ($t$) can be neglected, and we obtain

$$br^2\epsilon_1^2\sigma_{Y.P.} = M. \quad (u)$$

The distribution of stresses over the cross section of the beam is then represented by two rectangles, and the corresponding bending moment has the magnitude

$$M_{\mathrm{ult}} = \frac{bh^2}{4}\sigma_{Y.P.}, \quad (v)$$

which is obtained by substituting $\epsilon_1 = h/2r$ into equation ($u$). Denoting by $M_{Y.P.}$ the magnitude of bending moment at which the stress in the most remote fibers first arrives at the yield point, we have $\sigma_{Y.P.} = 6M_{Y.P.}/bh^2$ and equation ($v$) becomes

$$M_{\mathrm{ult}} = \tfrac{3}{2}M_{Y.P.}. \quad (301)$$

At the value $M_{\mathrm{ult}}$ of the bending moment all fibers of the

beam are in the condition of yielding and this yielding continues without increase in resisting moment as long as the stress-strain relation is as given by the diagram in Fig. 234. It will stop only when hardening of the material due to stretching becomes noticeable, but at that time the curvature of the beam due to plastic deformation becomes so large that it cannot be allowed in permanent structures; hence the value ($v$) of the bending moment must be considered as its *ultimate value*.



FIG. 235.

Applying the same reasoning in the case of an I-beam, Fig. 235, and assuming that at the ultimate values of the bending moment the stress in all fibers has the value $\sigma_{Y.P.}$, we obtain

$$M_{\mathrm{ult}} = \frac{\sigma_{Y.P.}}{4}\left[t_1h_1^2 + b(h^2 - h_1^2)\right]. \quad (302)$$

The moment at which yielding begins is obtained if we multiply $\sigma_{Y.P.}$ by the section modulus, which gives

$$M_{Y.P.} = \frac{\sigma_{Y.P.}}{4}\left[\frac{2t_1h_1^3}{3h} + \frac{b(h^2 - h_1^2)(h + h_1)}{2h}\right]. \quad (w)$$

Since in usual cases the difference between $h$ and $h_1$ is comparatively small, we see from expressions (302) and ($w$) that the ratio $M_{\mathrm{ult}} : M_{Y.P.}$ is much smaller for I-beams than for rectangular beams. Hence a comparatively small increase in the moment above the value $M_{Y.P.}$ may bring the beam to a critical condition.[4]

### 68. Bending of Beams by Transverse Loads Beyond Elastic Limit.

In the case of bending of beams by transverse loads we neglect the action of shear on deflection [5] and assume

---

[4] It was assumed in the above discussion that the beam is bent in the plane of its maximum rigidity and that lateral buckling of the compressed flange is prevented.

[5] The effect of shear has been discussed by A. Eichinger, Final Report, Second Congress International Assoc. Bridge and Structur. Engng., Berlin, 1938.
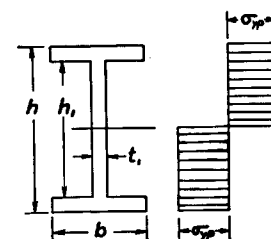
that the relation between the bending moment and the curvature is represented by equation (297) derived for pure bending. Then the area-moment method (see p. 144, Part I) can be applied in calculating deflections beyond the proportional limit. It is only necessary to observe that the flexural rigidity in this case is not constant but varies with the magnitude of the bending moment. To establish the relation between these two quantities for rectangular beams, we use the curve in Fig. 229. For any value of $\Delta = h/r$ the ordinate $\overline{AB}$ gives the corresponding value of the bending moment, and the ordinate $\overline{AC}$ represents the moment which we would have if the material followed Hooke's law. Hence
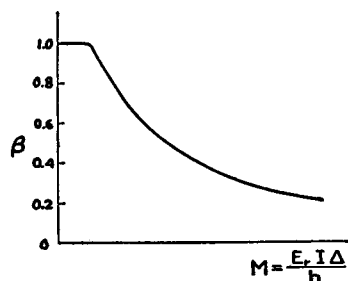


FIG. 236.

$$\overline{AB} : \overline{AC} = E_r : E.$$

In this way we obtain for each assumed value of the bending moment the ratio $E_r I/EI$ of the reduced flexural rigidity to the initial flexural rigidity of the beam. Denoting this ratio
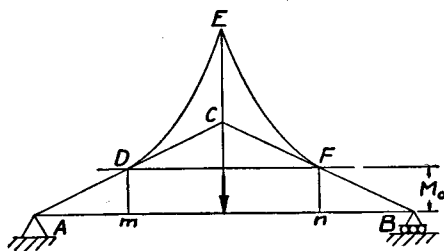


FIG. 237.

by $\beta$ we represent it as a function of the bending moment $M$ by the curve shown in Fig. 236. To illustrate how this curve can be used in the calculation of deflections, let us consider the case of a simply supported beam loaded at the middle, Fig. 237. The bending moment diagram in this case is the

triangle $ACB$. Let $M_0$ be the magnitude of that bending moment up to which the material follows Hooke's law. In such a case the portion $mn$ of the beam is stressed beyond its proportional limit and the reduced flexural rigidity, which varies along this portion of the beam, instead of the initial flexural rigidity, must be used in calculating deflections. Proceeding as in the case of beams of variable cross section (see p. 211, Part I), we divide the ordinates of the bending moment diagram by the corresponding values of $\beta$, taken from Fig. 236. In this manner the *modified* bending moment diagram $ADEFB$ is obtained. Considering the modified bending moment area as a fictitious load and proceeding in the usual way, we obtain the deflection at any cross section of the beam by dividing by $EI$ the bending moment produced at that cross section by the fictitious load.

We have discussed here only the case of a rectangular beam, but the same method is applicable in other cases provided the curve for the factor $\beta$, similar to that shown in Fig. 236, is obtained. Such a curve can be constructed by using the method illustrated in Fig. 231, or its ordinates can be calculated if the stress-strain relation beyond the proportional limit of the material is given analytically as by equations (p) in the preceding article.

In the case of a material such as steel, which has a pronounced yield point, Fig. 234, the bending of a rectangular beam beyond the yield point does not mean immediate failure of the beam. The yielding starts in the outermost fibers of the cross section with the maximum bending moment while the rest of the beam continues to work elastically. By plotting a load-deflection diagram for such a beam, we find that the shape of this diagram is quite different from the stress-strain diagram for the simple tension test of steel. When yielding of the material begins, we obtain in the load-deflection diagram only a slight deviation from a straight line, and a considerable flattening of the curve occurs only at a much higher load when yielding spreads over a large portion of the material of the beam. The amount of this flattening

of the load-deflection diagram and the magnitude of the corresponding permanent deflection of the beam depend upon the percentage of plastic flow at the yield point in the tension-compression test curve for the material. Assume, for example, that plastic flow at the yield point is $1\frac{1}{2}$ per cent, i.e., about fifteen times larger than the elastic elongation at the proportional limit of structural steel. If the outermost fibers of the beam undergo this much plastic flow, the stress distribution will approach that represented by two rectangles, and the corresponding bending moment is then seen (equation 301) to approach the value one and one-half times greater than the moment $M_{Y.P.}$ at which yielding first begins. ·The curvature in this case, from equation (g) of the preceding article, is

$$\frac{1}{r} = \frac{\Delta}{h} = \frac{0.03}{h} .$$

This large curvature will occur only in those portions of the beam where the bending moment approaches the above high value of $1\frac{1}{2}M_{Y.P.}$. This indicates that there will be a tendency for the bending to concentrate at the section of the maximum bending moment, and the deflection curve beyond the yield point will have a different shape from that below the elastic limit. In the case of bending of a beam by a force at the middle, Fig. 237, the yielding will occur principally at the middle, where a considerable curvature will result, while the remaining portions of the beam will be only slightly bent.

If, instead of a solid rectangular cross section, we take an I-section, the effect of plastic flow at the yield-point stress on the load-deflection diagram will be much more pronounced. This is obvious since most of the material is concentrated at the flanges of the beam, and consequently most of the fibers at the cross section of maximum bending moment begin to yield at about the same time. This yielding of material results finally in lateral buckling of the flanges.[6] Hence the maximum load that an I-beam may carry is only slightly

[6] "Theory of Elastic Stability," p. 273.

larger than the load that first produces yield-point stress in the flanges. From this discussion it may be seen that when we take the loading which first produces a yield-point stress as the basis for determining the allowable stress in a beam, the factor of safety for the loading which produces unpermissible damage depends on the shape of the cross section. In the case of a rectangular beam, this extra safety factor is considerably higher than in the case of an I-beam. In structural design this difference is usually disregarded, and beams of any cross section are designed on the basis of yield-point stress.[7] It is also usually assumed that up to this point our elementary formulas for calculating stresses, based on Hooke's law, are sufficiently accurate.

In our discussion of bending of beams by transverse loads it was assumed that the problem was statically determinate so that the construction of the bending moment diagram did not require any discussion of the deflection curve. In the statically indeterminate cases the problem becomes more involved, since beyond the proportional limit redundant forces and moments are no longer proportional to the acting loads, and the principle of superposition does not hold. Sometimes, however, the problem can be simplified by using a symmetry consideration. Assuming, for instance, that the ends of the beam in Fig. 237 are builtin, we conclude, from symmetry, that the bending moment vanishes at the quarter points, and the deflection curve consists of four identical portions which can be obtained in the same way as for a cantilever loaded at the end. In the case of a uniformly loaded beam with built-in ends we conclude from symmetry that the moments at the ends are equal. The magnitude of these moments can be obtained by trial and error method. It is necessary to assume some value for these moments and construct the modified bending moment diagram, as explained for the case shown in Fig. 237. The correct value of the moments is evidently that value at which the total fictitious load, represented by the modified bending moment area, vanishes.

[7] Another way of beam design is discussed on p. 376.

It may be seen from the above discussion that in the case of bending beyond the proportional limit the calculation of redundant forces and redundant moments requires usually a complicated investigation. In the case of such materials, however, as structural steel, which has a pronounced yield point, the analysis of statically indeterminate structures can be simplified very much if we limit our consideration to that stage of loading at which the structure reaches the *critical* condition and begins to yield without a further increase in the load. Take again, as an example, the uniformly loaded beam with built-in ends, and assume that the intensity of the load is gradually increasing. At a certain magnitude of this load the redundant moments at the ends reach the value $M_{Y.P.}$, and the material begins to yield. The corresponding bending moment diagram, calculated on the assumption that Hooke's law holds up to the yield point, is shown in Fig. 238, *a*. Proceeding further with the increasing load, we observe that a stage will be reached at which the redundant moments become equal to $M_{ult}$. This loading condition is not yet critical for our beam, since the moment at the middle remains smaller than the $M_{ult}$ value, and the beam can withstand the load action. With a further increase in load, owing to yielding of the material, the moments at the ends do not change their magnitude, and further deflection occurs as in the case of a simply supported beam.[8] The critical condition is finally reached when the bending moment at the middle becomes equal to $M_{ult}$. The corresponding bending moment diagram is shown in Fig. 238, *b*. At this load the local bending at the ends and at the center proceeds without any further increase in load, and a considerable plastic deformation will be produced before the hardening of material begins to counteract the yielding.

It was already shown (see p. 371) how the magnitude of $M_{ult}$ can be calculated for a beam of a given cross section. Knowing $M_{ult}$, we can readily construct the bending moment

[8] Any hardening of material is entirely neglected in this discussion.

diagram for the critical condition, and determine the *critical value* of the load. For instance, in the case of a uniform load, Fig. 238, *b*, we find the critical value of load intensity from the equation:

$$\frac{q_{cr}l^2}{8} = 2M_{ult}.$$

At the same time, the load intensity at which yielding begins, Fig. 238, *a*, is defined by the equation:

$$\frac{q_{Y.P.}l^2}{8} = 1\tfrac{1}{2}M_{Y.P.}.$$

Hence

$$\frac{q_{cr}}{q_{Y.P.}} = \frac{4}{3}\frac{M_{ult}}{M_{Y.P.}}.$$

It is seen that the ratio $q_{cr}/q_{Y.P.}$ depends on the shape of the cross section of the beam. For rectangular beams this ratio is equal to 2.
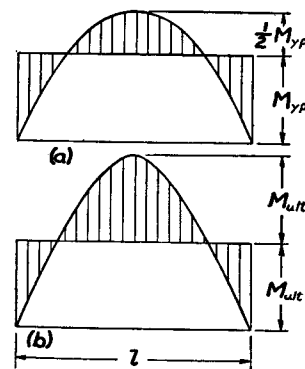


FIG. 238.
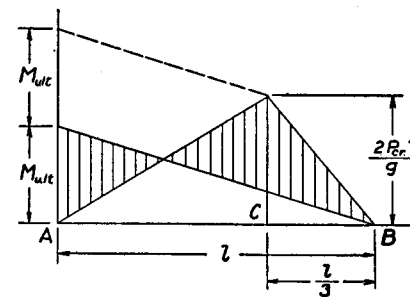


FIG. 239.

A similar discussion can be repeated for any other kind of loading of a beam with built-in ends and also for beams with other end conditions or for continuous beams; in each case the magnitude of the critical load can be readily established. For example, in Fig. 239 the bending moment diagram is shown for the critical condition of the beam built-in at the

left end, simply supported at the right end, and loaded at the third point $C$. This diagram is readily constructed if we observe that at the critical condition the bending moments at $A$ and $C$ are equal to $M_{ult}$. The critical value of the load at which yielding at $A$ and $C$ proceeds without a further increase in the load is given by the equation:

$$\frac{2}{9} P_{cr} l = 1\tfrac{1}{3} M_{ult}.$$

In Fig. 240 the bending moment diagram for the critical condition of a uniformly loaded continuous beam is shown. The
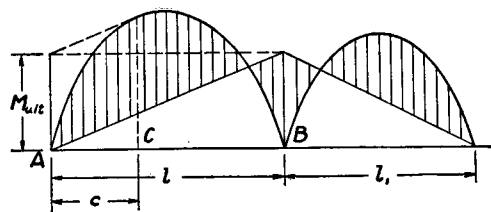


FIG. 240.

magnitude of $q_{cr}$ and the distance $c$ defining the position of the critical cross section $C$ are obtained from the two conditions: 1) the bending moment at $C$ is a maximum, and 2) its magnitude, as also the magnitude of the moment at $B$, is equal to $M_{ult}$, which give

$$\frac{q_{cr}l}{2} - \frac{M_{ult}}{l} - q_{cr}c = 0,$$

$$\frac{q_{cr}l}{2} c - \frac{q_{cr}c^2}{2} - \frac{M_{ult}c}{l} = M_{ult}.$$

From these equations we find

$$c = l(\sqrt{2} - 1), \qquad q_{cr} = \frac{2M_{ult}}{l^2(3 - 2\sqrt{2})}.$$

From these examples it can be appreciated that the calculation of the critical loads can be readily made in various particular cases of statically indeterminate beams. This

calculation is usually simpler than that required in determining the values of the loads at which yielding begins, since we do not need to go into analysis of the statically indeterminate systems.[9]

It was already indicated that under the action of the critical loads the steel structures undergo considerable deformation which is not permissible under normal service conditions; hence it is important to consider those critical loads in the design and to determine the safe load on the structure dividing the magnitude of the critical load by a proper factor of safety. Such a procedure appears logical in the cases of steel structures submitted to the action of stationary loads, since in such cases a failure owing to the fatigue of metal is excluded, and only failure due to yielding of metal has to be considered.[10]

**69. Residual Stresses Produced by Inelastic Bending.**— If a beam is bent beyond the elastic limit, some permanent set is produced, and the deformation does not vanish after the load is removed. The fibers which suffered a permanent set prevent the elastically stressed fibers from recovering their initial length after unloading, and in this way some *residual stresses* are produced. To determine the distribution of these stresses over the cross section, let us begin with the simplest case of a rectangular beam in which the stress distribution in bending beyond the yield point can be represented by two rectangles, *oklm* and *oprn*, shown in Fig. 241, *a*. We assume also that the material, if stretched beyond the yield point and

[9] M. Grüning, Handbuch f. Bauing. Bd. IV, Der Eisenbau, 1929, Grüning-Kulka, "Die Bautechnik," 1928, p. 274.

[10] Such a method of determining safe dimensions of steel structures was proposed by N. C. Kist, "Der Eisenbau," vol. 11, 1920. The experiments for determining critical loads were made by Maier-Leibnitz, "Die Bautechnik," 1928, and by K. Girkmann, "Die Bautechnik," 1932. A theoretical discussion of the bending of beams beyond the yield point was given by J. Fritsche, Bauingenieur, 1930 and 1931. The combination of bending with compression was discussed by K. Girkmann, Sitzungsber. Akad. Wiss. Wien, Abt. IIa, vol. 140, 1931. In this country the question of design on basis of the critical loading has been discussed by J. A. Van den Broek, Trans. A. S. C. E. Vol. 105, 1940, p. 638.

then unloaded, follows Hooke's law during unloading, as shown in Fig. 241, $b$ by the dotted line. As a result of this assumption it can be concluded tha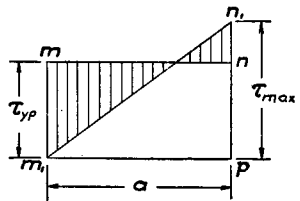t the bending stresses which are subtracted while unloading the beam follow the linear law indicated in Fig. 241, $a$ by the line $m_1 n_1$. The difference between the two stress distributions, rectangular while loading and triangular while unloading, shown by the shaded areas in Fig. 241, $a$, represents the stresses which remain in the beam after unloading. These are the residual stresses produced in the beam by plastic deformation.
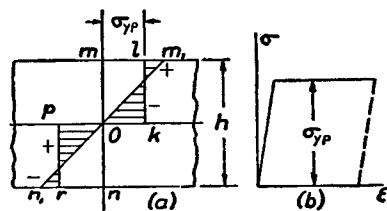


FIG. 241.

The signs of these stresses, shown in the figure, are obtained by assuming that the initial bending produced the curvature convex downward. Since the rectangular and the triangular stress distributions both represent the bending moment of the same magnitude, it can be concluded that the moment with respect to the axis $pok$ of the triangle $omm_1$ is equal to the moment of the rectangle $oklm$ about the same axis. Hence the stress represented in the figure by the length $mm_1$ must be equal to $1\frac{1}{2}\sigma_{Y.P.}$, and the maximum tension and compression which remain in the most remote fibers after unloading the beam is equal to $\frac{1}{2}\sigma_{Y.P.}$. The residual stresses in the fibers near the neutral surface are as high as $\sigma_{Y.P.}$. It may be seen that the stress distribution represented in the figure by the shaded areas reduces to two equal and opposite couples, with the value $\sigma_{Y.P.}bh^2/27$, which are in equilibrium. The existence of these residual stresses can be shown experimentally by sawing the beam along the neutral plane. Then each half of the beam obtains a certain curvature. If a beam with such residual stresses as indicated in Fig. 241, $a$ is bent again by moments of the same magnitude and in the same direction as in the previous experiment, the stresses produced by these moments and represented by the straight line $m_1 n_1$, will be superposed on

the residual stresses, given by the shaded areas, so that the resultant stress distribution will be that represented by the rectangles $oklm$ and $onrp$. The maximum resultant stress is $\sigma_{Y.P.}$, and no yielding will occur during this second bending. Hence the residual stresses produced by the first bending are of such a nature as to increase the bending moment which can be sustained by the bar elastically provided the direction of bending is unchanged. This phenomenon of improving the elastic capacity of a structure by a preliminary loading and creation of suitable residual stresses is sometimes used in practice. Some particular cases will be discussed later (see art. 74).

In a more general case of inelastic bending of a rectangular beam the stress distribution is given by a curve such as the curve $n_1 o m_1$ in Fig. 242, $a$. Assuming again that during
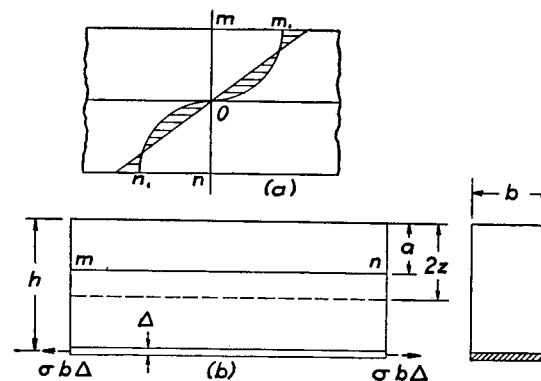


FIG. 242.

unloading the material of the beam follows Hooke's law, we find that the residual stresses produced by plastic flow are distributed as shown in the figure by the shaded areas. If the curve $n_1 o m_1$ is determined as explained in article 67, the magnitude of the residual stress can be readily obtained for each fiber. If the curve $n_1 o m_1$ is unknown, the residual stress distribution can be investigated experimentally by taking off from the beam, one after the other, thin layers parallel to the

neutral plane and by measuring after each cut the elastic deformation which ensues in the beam.

Assume that the residual stress at the lower side of the beam is tension of a magnitude $\sigma$. Then the removal of a thin layer of a thickness $\Delta$, indicated in Fig. 242, $b$, evidently produces the same deformation in the rest of the beam as would be produced by the application of the two equal and opposite forces $\sigma b \Delta$, shown in the figure by the dotted arrows. We shall find that after cutting off the thin layer the axis of the beam acquires an elongation and a curvature given by the formulas:

$$d(\epsilon) = \frac{\sigma b \Delta}{Ebh}, \qquad d\left(\frac{1}{r}\right) = \frac{\sigma b \Delta (h - \Delta) 12}{2Eb(h - \Delta)^3} \approx \frac{\sigma b \Delta h}{2EI}. \qquad (a)$$

It is seen that if the curvature $d(1/r)$ is measured, $\sigma$, the magnitude of the residual tensile stress in the most remote fiber, is readily calculated from the equation $(a)$. The determination of the residual stress $\sigma_a$ in a fiber $mn$ at a distance $a$ from the upper side of the beam, Fig. 242, $b$, is more involved. By taking off one layer after the other we finally reach the layer $mn$, and we can determine the stress in it by using an equation similar to equation $(a)$. This stress, however, will have a magnitude $\sigma_a'$ different from the residual stress $\sigma_a$, since the cutting off layer after layer produces changes of stresses in the remaining portion of the beam. It is evident that only after investigation of these changes will the determination of the required residual stress $\sigma_a$ be possible. Let us assume that by taking off layer after layer we reached the fibers indicated by the dotted line in Fig. 242, $b$, at a distance $2z$ from the upper side of the beam. If a new thin layer of thickness $\Delta$ is now taken off, the stress $\sigma_z'$ in this layer is obtained from the equation:

$$d\left(\frac{1}{r}\right) = \frac{\sigma_z' bz \Delta}{EI_z}, \qquad \text{where} \qquad I_z = \frac{b(2z)^3}{12}$$

from which

$$\sigma_z' = \frac{d(1/r) EI_z}{bz\Delta}. \qquad (b)$$

The removing of this layer will produce in the fiber $mn$ a direct stress of the magnitude

$$\frac{\sigma_z' b \Delta}{2bz}, \qquad (c)$$

and a bending stress of the magnitude

$$\frac{\sigma_z' bz \Delta (a - z)}{I_z}. \qquad (d)$$

Formulas $(c)$ and $(d)$ give us the changes in the stress of the fiber $mn$ owing to the removal of one layer. Taking now into consideration all thin layers by varying $2z$ from $h$ to $a$, we obtain the total change in the stress of the fiber $mn$ as follows:

$$\Sigma \frac{\sigma_z' \Delta}{2z} + \Sigma \frac{\sigma_z' bz \Delta (a - z)}{I_z}, \qquad (e)$$

where $\sigma_z'$ for each step is calculated from formula $(b)$ by using in it the measured values of $d(1/r)$. The required residual stress $\sigma_a$ in the fiber $mn$ is now obtained by subtracting the quantity $(e)$ from the stress $\sigma_a'$, which is found by substituting $a$ for $2z$ in formula $(b)$. Hence

$$\sigma_a = \sigma_a' - \Sigma \frac{\sigma_z' \Delta}{2z} - \Sigma \frac{\sigma_z' bz \Delta (a - z)}{I_z}. \qquad (f)$$

This method of experimental determination of longitudinal residual stresses can be applied not only in the case of bending but also in other cases of prismatical bars submitted to longitudinal plastic deformation (see art. 71). It was, for example, successfully applied in measuring residual stresses in cold drawn brass tubes.[11] To take off thin layers of metal a special chemical solution was used in that work. The changes in curvature were measured optically. In this way complete information regarding residual stresses in cold drawn tubes can be obtained. Such information is of great practical importance in developing the proper technique in manufacturing tubes.

**70. Torsion Beyond the Elastic Limit.**—Let us begin with the torsion of circular shafts and assume that beyond the elastic limit the cross sections of the twisted shaft continue to

---

[11] This method was developed by N. N. Dawidenkow, Journal of Techn. Phys., Vol. 1, 1931, Leningrad, and Zeitschrift für Metallkunde, Vol. 24, 1932, p. 25. See also the doctor's thesis by C. G. Anderson, University of Michigan, 1935. Another method suitable for measuring residual stresses in rolled sections such as I-beams and channels was developed by J. Mathar, Archiv für das Eisenhüttenwesen, Vol. 6, 1932–33, p. 277.

remain plane and their radii remain straight.[12]  In such a case the shearing strain $\gamma$ at a distance $r$ from the axis of the shaft is determined by the same formula as in the case of torsion within the elastic limit (see p. 261, Part I):

$$\gamma = r\theta, \qquad (a)$$

where $\theta$ is the angle of twist per unit length of the shaft.  To determine the magnitude of the torque which is required for producing the twist $\theta$, it is necessary to know the relation between shearing strain $\gamma$ and shearing stress $\tau$ beyond the proportional limit.  Assume that the diagram in Fig. 243 gives the required relation.[13]  If $a$ is the outer radius of the shaft, the maximum shearing strain is $a\theta$ and the corresponding maximum shearing stress is given by the ordinate $mn$ in the diagram of Fig. 243.  In the same way the shearing stress at any distance $r$ from the axis can be readily obtained from the diagram.  The torque $M_t$ which must be applied to produce the assumed magnitude $\theta$ of the twist is now obtained from the equation of statics:
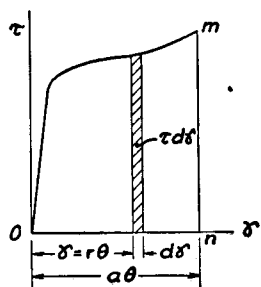
$$\int_0^a 2\pi r^2 dr\tau = M_t. \qquad (b)$$

Substituting in this equation from equation $(a)$

$$r = \frac{\gamma}{\theta}, \qquad dr = \frac{d\gamma}{\theta},$$



FIG. 243.

---

[12] This theory was developed by Saint Venant, Journal de Mathematiques, Vol. 16, 1871, p. 373.  See also I. Todhunter and K. Pearson, History of the Theory of Elasticity, Vol. 2, Part I, p. 170.  For a further discussion of this subject see A. Nadai, "Plasticity," 1931, p. 126.

[13] Such a diagram can be obtained experimentally by making a torsion test on thin tubes.  To eliminate the possibility of buckling, the wall thickness can be only locally reduced to a small value by making a circumferential groove of a rectangular shape in a thicker tube.

we obtain

$$\frac{2\pi}{\theta^3} \int_0^{a\theta} \gamma^2\tau d\gamma = M_t. \qquad (c)$$

The integral on the left side of this equation has a simple geometrical meaning; namely, it represents the moment of inertia with respect to the vertical axis $o\tau$ of the area $omno$ in Fig. 243.  After calculating this moment of inertia for any assumed value of $a\theta$, the corresponding torque is readily obtained from the equation $(c)$.  Hence a curve representing the relation between $M_t$ and $\theta$ can be plotted if the diagram in Fig. 243 is given.  Since the abscissas in Fig. 243 are proportional to the radial distances, the curve $om$ also represents to a certain scale the shearing stress distribution along a radius of the shaft.  If during the twist the material follows Hooke's law at all times, we have $\tau = \gamma G = r\theta G$, and equation $(b)$ gives

$$2\pi\theta G \int_0^a r^3 dr = \theta G I_p = M_t, \qquad (d)$$

which is the known equation for torsion within the elastic limit.

If the material of the shaft has a very pronounced yield point, the curvilinear portion of the diagram in Fig. 243 can be replaced by the horizontal line with the abscissa $\tau_{Y.P.}$.  Hence, for a considerable angle of twist the distribution of shearing stresses along a radius of the shaft approaches uniform distribution.  The corresponding magnitude of torque we call by $(M_t)_{ult}$.  Its value is obtained by substituting $\tau_{Y.P.}$ for $\tau$ in equation $(b)$, which gives

$$(M_t)_{ult} = \frac{2\pi a^3}{3} \tau_{Y.P.}. \qquad (e)$$

When the torque reaches this value, a further twist of the shaft proceeds without a further increase in torque up to the point at which the hardening of the material becomes noticeable.  For comparison we calculate also the value of the torque $(M_t)_{Y.P.}$ at which yielding begins.  For this purpose we

use equation $(d)$ and substitute in it the value of $\theta$ at which yielding begins. This latter value is obtained from equation $(a)$ by taking $r = a$ and $\gamma = \gamma_{Y.P.}$, which gives

$$\theta_{Y.P.} = \frac{\gamma_{Y.P.}}{a} = \frac{\tau_{Y.P.}}{aG}.$$

Hence, from equation $(d)$,

$$(M_t)_{Y.P.} = \theta_{Y.P.}I_p = \frac{\pi a^3}{2}\tau_{Y.P.}. \qquad (f)$$

It is seen, from equations $(e)$ and $(f)$, that

$$(M_t)_{\text{ult}} : (M_t)_{Y.P.} = \frac{4}{3}.$$

If, after applying the torque $(M_t)_{\text{ult}}$, we unload the shaft, some residual stresses will remain in it. The magnitude of these stresses can be obtained by repeating the same reasoning which was applied in the case of bending (p. 379). Let the ordinates of the horizontal line $mn$ in Fig. 244 represent the shearing stress $\tau_{Y.P.}$ produced by the moment $M_{\text{ult}}$ and uniformly distributed along the radius of the shaft. During unloading of the shaft the material follows Hooke's law, and the torsional stresses which are to be subtracted while unloading the shaft follow the linear law indicated in Fig. 244 by the line $m_1n_1$. The difference between the two stress distributions, rectangular while loading and triangular while unloading, represents the stresses which remain in the shaft after unloading. The distribution of these stresses along a radius of the shaft is shown in Fig. 244 by the shaded areas. The magnitude of the ordinate $n_1p$, denoted by $\tau_{\max}$, is found from the fact that the rectangular and the triangular stress distributions both represent a torque of the same magnitude $M_{\text{ult}}$. For the rectangular stress distribution this torque is



FIG. 244.

given by the formula $(e)$. The formula for the same torque and for the triangular stress distribution is obtained by substituting $\tau_{\max}$ for $\tau_{Y.P.}$ in the formula $(f)$:

$$\frac{2\pi a^3}{3}\tau_{Y.P.} = \frac{\pi a^3}{2}\tau_{\max},$$

$$\tau_{\max} = 1\tfrac{1}{3}\tau_{Y.P.}.$$

It is seen that the residual torsional stress at the surface of the shaft is equal to $\tfrac{1}{3}\tau_{Y.P.}$. Near the center that stress is equal to $\tau_{Y.P.}$.

The distribution of residual torsional stresses can be investigated experimentally. For this purpose it is necessary to machine off successive thin layers of metal from the shaft and measure, after removing each layer, the change in the angle of twist of the shaft.[14]

If the material of the shaft has a pronounced yield point, the membrane analogy (see p. 267) can be used to advantage in studying torsion beyond the yield point. When the magnitude of the torque is somewhat larger than $(M_t)_{Y.P.}$, the outer portion of the shaft is in the condition of yielding while the inner portion continues to deform elastically. To extend the membrane analogy to this case, it is necessary to use, together with the membrane, a rigid cone $ACB$, Fig. 245, the slope of which represents the yield point stress $\tau_{Y.P.}$ to the proper scale. If a small pressure $p$ is acting on the membrane, the deflections are also small, and the conical surface does not interfere with the free deflection of the membrane. Hence its surface defines the stress distribution for the case of an elastic torsion, such as was previously discussed (see p. 268). With an increase in pressure the deflections of the membrane also increase, and finally the outer portion of the membrane comes into contact with the rigid cone as shown in Fig. 245. This condition represents torsion
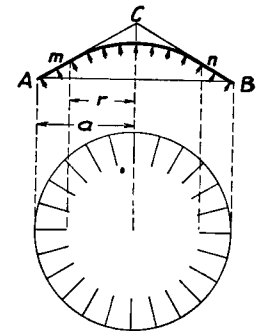


FIG. 245.

[14] A further discussion of this subject can be found in A. Nadai's "Plasticity," 1931, p. 266.

beyond the yield point. The outer portion of the membrane, coinciding with the cone, has the constant slope corresponding to the yield point stress $\tau_{Y.P.}$. The inner portion $mn$ of the membrane corresponds to the inner portion of the shaft, which is in an elastic condition. The double volume between the membrane and the plane of the boundary $AB$ continues to represent the torque. From this we conclude that the double volume of the cone must give us the value of $M_{ult}$. Since the slope of the cone is $\tau_{Y.P.}$, its height is equal to $a\tau_{Y.P.}$, and its double volume is $\frac{2}{3}\pi a^2 a\tau_{Y.P.}$ which coincides with the expression $(e)$.

The same method can also be used in the case of non-circular cross sections of shafts, and is very useful in determining these portions of the shaft in which yielding begins. Consider as an example a rectangular shaft. In investigating torsion of this shaft beyond its yield point the membrane must be used together with a rigid roof surface, Fig. 246, which has a constant slope at all points representing to a certain scale the yield point stress $\tau_{Y.P.}$. It is
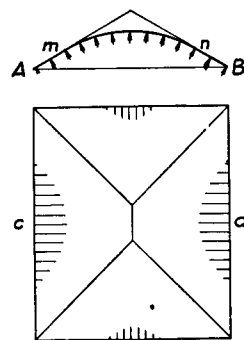


FIG. 246.

evident that the membrane, deflecting under increasing uniform pressure, touches the roof first at points $c$ and $d$, the middle points of the longer sides of the rectangle. At these points the yielding begins and at a higher pressure some portions of the membrane will coincide with the roof as indicated in the figure by the shaded areas. These areas define the regions where the material yields. In the rest of the shaft we have only elastic deformation. A further increase in pressure on the membrane increases the portions of contact with the roof, as well as the regions of plastic deformation. The double volume between the roof and the plane $AB$ evidently gives the magnitude of $M_{ult}$ for the rectangular shaft.

If a rectangular bar of wrought iron is twisted beyond the yield point, the regions of plastic flow can be revealed by a proper etching of the cross section. After etching, there appears in plastic regions of the cross section dark parallel lines of such directions as shown in Fig. 246. These lines indicate the layers parallel to the axis of the shaft along which the sliding of the metal, produced by the yield point stress, occurs.[15]

[15] Interesting photographs of these lines, obtained for various shapes of twisted bars, are shown in the paper by A. Nadai, Trans. A. S. M. E., Vol. 53, p. 29, 1931.

**71. Plastic Deformation of Thick Cylinders under the Action of Internal Pressure.**[16]—Discussing an elastic deformation of a thick-walled cylinder under the action of internal pressure $p$, we found (see p. 239) that the radial and the tangential stresses at a radial distance $r$ from the axis of the cylinder are represented by the formulas:

$$\sigma_r = \frac{a^2 p}{b^2 - a^2}\left(1 - \frac{b^2}{r^2}\right), \qquad \sigma_t = \frac{a^2 p}{b^2 - a^2}\left(1 + \frac{b^2}{r^2}\right), \quad (a)$$

where $a$ and $b$ are the inner and the outer radii of the cylinder respectively. The maximum tangential tension and the maximum radial compression occur at the inner surface of the cylinder. At that surface also the maximum shearing stress acts. The magnitude of it is

$$\tau_{max} = \left(\frac{\sigma_t - \sigma_r}{2}\right)_{r=a} = \frac{pb^2}{b^2 - a^2}. \quad (b)$$

By gradually increasing the internal pressure, we finally reach a point when the material at the inner surface begins to yield. This occurs when the maximum shearing stress $(b)$ becomes equal to the yield point stress $\tau_{Y.P.}$.[17] Substituting this value into formula $(b)$, we find that the pressure at which yielding begins is

$$p_{Y.P.} = \tau_{Y.P.}\frac{b^2 - a^2}{b^2}. \quad (c)$$

Assuming, for example, $b = 2a$, we find that in this particular case $p_{Y.P.} = 0.750\tau_{Y.P.}$. With a further increase in pressure the plastic deformation penetrates deeper and deeper into the wall of the cylinder and finally at a certain pressure, which we

[16] An investigation of plastic flow in thick cylinders submitted to inner pressure was made by Saint-Venant; see C. R., Vol. 74, 1872, p. 1009; see also Todhunter and Pearson, History of the Theory of Elasticity, Vol. 2, part I, p. 172, and the paper by L. B. Turner, Cambridge Phil. Soc. Trans., Vol. 21, 1913, p. 377.

[17] The question of yielding of a material under various stress conditions is discussed in article 83. We assume here that $\tau_{Y.P.}$ has the same value as in the case of torsion (see p. 385).

shall call $p_{ult}$, the entire wall of the cylinder is brought into the state of yielding. The distribution of stresses in the wall at this yielding condition can be investigated without much difficulty if we assume that the material has a very pronounced yield point, which means that the yielding proceeds under the action of a constant shearing stress equal to $\tau_{Y.P.}$. This gives us for every point in the region of plastic deformation the equation:

$$\frac{\sigma_t - \sigma_r}{2} = \tau_{Y.P.}. \qquad (d)$$

Another equation for determining the principal stresses $\sigma_r$ and $\sigma_t$ is obtained by considering the equilibrium of an element of the wall, shown in Fig. 142. From our previous discussion (see p. 236) the equation of equilibrium is

$$\sigma_t - \sigma_r - r\frac{d\sigma_r}{dr} = 0. \qquad (e)$$

Substituting for the difference of the principal stresses its value from equation $(d)$, we obtain

$$\frac{d\sigma_r}{dr} = \frac{2\tau_{Y.P.}}{r}. \qquad (f)$$

The integration of this equation gives

$$\sigma_r = 2\tau_{Y.P.}\log r + C. \qquad (g)$$

The constant of integration $C$ is obtained from the condition that at the outer surface of the cylinder, i.e., at $r = b$, the radial stress $\sigma_r$ vanishes. This gives

$$0 = 2\tau_{Y.P.}\log b + C, \qquad C = -2\tau_{Y.P.}\log b.$$

Substituting this value of the constant of integration $C$ into equation $(g)$, we obtain

$$\sigma_r = 2\tau_{Y.P.}\log \frac{r}{b}. \qquad (303)$$

This gives for the inner surface of the cylinder

$$(\sigma_r)_{r=a} = 2\tau_{Y.P.}\log \frac{a}{b}, \qquad (304)$$

and the pressure which is required to bring the entire wall of the cylinder into the state of plastic flow is

$$p_{ult} = -(\sigma_r)_{r=a} = -2\tau_{Y.P.}\log \frac{a}{b}.$$

Taking again $b = 2a$, we find $p_{ult} = 2\tau_{Y.P.}\log 2 = 0.693(2\tau_{Y.P.})$.

Having expression (303) for radial stresses, we obtain tangential stresses from equation $(d)$, which gives

$$\sigma_t = 2\tau_{Y.P.}\left(1 + \log \frac{r}{b}\right). \qquad (305)$$

If $b = 2a$, this expression becomes

$$(\sigma_t)_{r=a} = 2\tau_{Y.P.}\left(1 + \log \frac{a}{b}\right) = 0.307(2\tau_{Y.P.}),$$

$$(\sigma_t)_{r=b} = 2\tau_{Y.P.}.$$
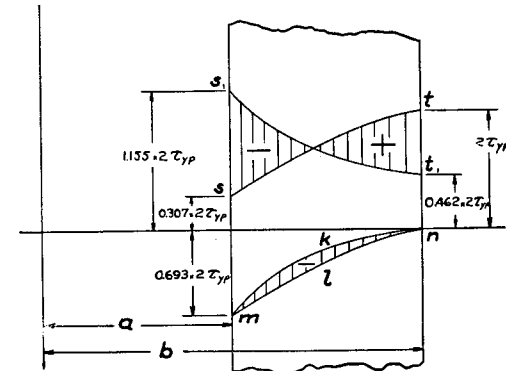


Fig. 247.

The distribution of stresses $\sigma_r$ and $\sigma_t$ along the thickness of the wall for the particular case $b = 2a$ is shown in Fig. 247 by the curves $mln$ and $st$ respectively. If, after bringing the material of the cylinder to the condition of yielding, we remove

the internal pressure, some residual stresses remain in the wall of the cylinder. These stresses can be readily calculated if we assume that during unloading the material of the cylinder follows Hooke's law. In such a case the stresses which are to be subtracted while unloading the cylinder are given by the expressions (a) if we substitute in these expressions $p_{ult}$ instead of $p$. These stresses for the particular case $b = 2a$ are shown in Fig. 247 by the curves $s_1 t_1$ and $mkn$. The shaded areas then give us the residual stresses in the wall of the cylinder. It is seen that owing to the plastic deformation, considerable compressive tangential stresses are produced in the portion of the cylinder wall.[18] If a cylinder with such residual stresses is again loaded by the internal pressure equal to $p_{ult}$ the tangential stresses produced by this pressure and given by the curve $s_1 t_1$ will be superposed on the residual stresses, given by the shaded areas, so that the resultant stress distribution will be that represented by the curve $st$. The maximum resultant stress is $2\tau_{Y.P.}$, and no yielding will occur during this second application of the internal pressure. Hence the residual stresses produced by the plastic expansion of the cylinder are of such a nature as to increase the pressure which can be sustained by the cylinder elastically. This fact is sometimes used in manufacturing guns which must withstand high internal gas pressures.[19]

It was assumed in our discussion that the applied inner pressure is such as to bring the entire cylinder to the condition of yielding, but the method can also be applied without any difficulty to cases in which only the inner portion of the cylinder wall is in the state of yielding while the outer portion is in the elastic state. Assume that a pressure $p'$, larger than $p_{Y.P.}$ but smaller than $p_{ult}$, is applied, and let $c$ be the radius of the

---

[18] It is assumed that this compressive stress is less than yield point stress and that no yielding occurs during unloading. The case of yielding during unloading was studied by L. B. Turner, loc. cit., p. 389.

[19] The description of this use of the initial plastic deformation can be found in the book by L. Jacob, "Résistance et Construction des Bouches à Feu. Autofretage," Paris. See also S. J. Brown, United States Naval Institute Proceedings, Vol. 46, 1920, p. 1941.

cylindrical surface separating the plastic region of the wall from the elastic. There will be a radial pressure acting between these two regions which we shall call $X$. The magnitude of this pressure can be found from a consideration of the outer, elastic, portion of the wall. The maximum shearing stress $\tau_{max}$ in this portion is found from equation (b) by substituting $c$ instead of $a$ and $X$ instead of $p$ in that equation which gives

$$\tau_{max} = \frac{Xb^2}{b^2 - c^2}.$$

Since the cylindrical surface $r = c$ separates the elastic and the plastic zones, the material at that surface just reaches the yield point. Hence $\tau_{max} = \tau_{Y.P.}$. The equation for determining the pressure $X$ is then

$$\tau_{Y.P.} = \frac{Xb^2}{b^2 - c^2}, \tag{h}$$

and we obtain

$$X = \frac{\tau_{Y.P.}(b^2 - c^2)}{b^2}. \tag{i}$$

Having this pressure, we can readily calculate the stresses at any point in the elastic region of the wall by using equations similar to equations (a).[20]

For calculating stresses in the plastic region of the wall we use equation (g). The constant of integration $C$ is found from the condition that for $r = c$, $\sigma_r = -X$, which gives

$$-X = 2\tau_{Y.P.} \log c + C, \qquad C = -X - 2\tau_{Y.P.} \log c.$$

Substituting this value of $C$ in equation (g) and using expression (i) we obtain

$$\sigma_r = 2\tau_{Y.P.} \log \frac{r}{c} - \frac{\tau_{Y.P.}(b^2 - c^2)}{b^2}. \tag{306}$$

Taking $r$ equal to the inner radius $a$ of the cylinder, we obtain

---

[20] The radius $c$ instead of $a$ and $X$ instead of $p$ must be used in these equations.

the magnitude $p'$ of the pressure which must be used to produce the plastic flow in the wall up to the depth corresponding to the radius $r = c$. This pressure is

$$p' = - 2\tau_{Y.P.} \log \frac{a}{c} + \frac{\tau_{Y.P.}(b^2 - c^2)}{b^2}. \qquad (307)$$

Taking our previous example where $b = 2a$ and assuming $c = 1.5a$, we find from equation (307) that $p' = 0.624(2\tau_{Y.P.})$.

The distribution of tangential stresses $\sigma_t$ is obtained from equation $(d)$, which gives

$$\sigma_t = 2\tau_{Y.P.} + \sigma_r = 2\tau_{Y.P.} \log \frac{r}{c} + \tau_{Y.P.} \frac{b^2 + c^2}{b^2}. \qquad (308)$$

For $r = c$ the first term on the right side vanishes and the value of $\sigma_t$ becomes equal to the value of the tangential stress produced by pressure $X$ in the adjacent elastic zone of the wall. Equations (307) and (308) give us the stresses produced in the inner portion of the cylinder wall, which undergoes plastic deformation. For the outer portion, which remains elastic, equations similar to equations $(a)$ must be used. In this way the problem of stress distribution for the case of a cylinder which undergoes only a partial plastic deformation is completely solved.

If, after partial yielding of the cylinder wall, the inner pressure $p'$ is removed, some residual stresses will remain in the wall of the cylinder. The inner portion of the wall, in which plastic deformation occurred, does not return to its initial diameter and undergoes a pressure from the side of the outer elastic portion of the wall. The stress distribution produced in this way is similar to that produced by shrink-fit pressures in built-up cylinders (see art. 45). To calculate these stresses we proceed in exactly the same way as was explained before and illustrated in Fig. 247.

All these calculations are based on the assumption that beyond the yield point the material yields without an increase in stress. If this is not the case, the residual stresses cannot be calculated as explained above, and recourse must be made

to an experimental determination of residual stresses. In such cases a method similar to that used in determining residual bending stresses can be applied. We machine off thin layers of the metal one after the other beginning from the inner surface of the cylinder, and after each cut measure the strain produced in the axial and the circumferential directions at the outer surface of the cylinder. Such measurements furnish sufficient information for calculating residual stresses.

Residual stresses in cylinders can be produced not only by the plastic deformation described above, but also by non-uniform cooling and by volume changes of metals during recrystalization in various processes of heat treatment. Sometimes these stresses become of primary importance as, for instance, in big forgings, and several methods of their determination have been developed.[21]

[21] The first investigation of this kind was made by N. Kalakoutzky, St. Petersburg, 1887. See also N. Kalakoutzky, Investigation into the Internal Stress in Cast Iron and Steel, London, 1888. The complete solution of the problem was given by G. Sachs, Zeitschr. f. Metallkunde, Vol. 19, 1927, p. 352 and Zeitschr. Ver. Deutsch. Ing., Vol. 71, 1927, p. 1511. These two papers contain a complete bibliography of the subject. Further improvements in the methods of measuring residual stresses in tubes were made by N. N. Dawidenkow, Journal of Technical Physics, Vol. 1, 1931, S. Petersburg. See also G. Sachs, Trans. of the A. S. M. E., 1939, p. 821. The bibliography on plastic deformation of metals and on residual stresses is given in "Handbuch der Metallphysik," Vol. 3, part I, by G. Sachs, Leipzig, 1937.

# CHAPTER IX

## MECHANICAL PROPERTIES OF MATERIALS

**72. Tension Test.**—The most common method of investigating mechanical properties of metals is by the tension test.[1] For this test circular cylindrical specimens and sometimes specimens of rectangular cross section are used. To make the results of test comparable, certain proportions for tensile test specimens have been established, which are recognized as *standard proportions*. In this country, for instance, the standard tensile test specimen is circular, with $\frac{1}{2}$ in. diameter and 2 in. gage length, so that

$$\frac{l}{d} = 4 \quad \text{or} \quad l = 4.51 \sqrt{A},$$

where $A = \pi d^2/4$ is the cross sectional area of the specimen. In central Europe two different proportions of circular specimens are in use: (1) a long specimen for which $l = 10d = 11.3\sqrt{A}$ and (2) a short specimen for which $l = 5d = 5.65\sqrt{A}$. In the case of rectangular specimens it is preferable to take the same relation between the length and the cross sectional area as for circular specimens.[2] The length of the cylindrical portion of the specimen is always somewhat greater than the gage length and is usually at least $l + d$. The ends of the specimen are generally made of heavier section to prevent the specimen from breaking in the grips of the testing machine, where the stress conditions are more severe, due to local irregularities in stress distribution. The long type of cylin-

drical specimen is represented in Fig. 248 (*a*), which shows also the spherical seats in the grips of the machine, used to insure central application of the load. Figure 248 (*b*) shows a flat
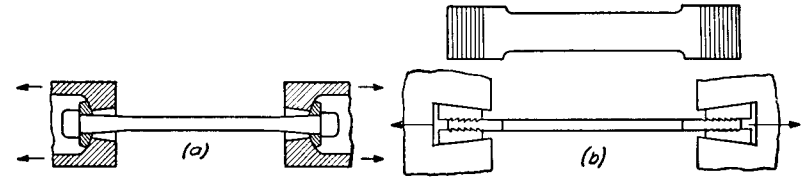


FIG. 248.

rectangular specimen. Tensile test machines are usually provided with a device which automatically draws a tensile test diagram representing the relation between the load $P$ and the elongation $\delta$ of the specimen. Such a diagram exhibits very important characteristics of the material. Figure 249, for instance, shows a series of diagrams for carbon steel with various contents of carbon. These indicate that as the carbon content increases the strength of the steel increases but at the same time the elongation before fracture decreases, i.e., the material loses ductility.

The *strength* and the *ductility* are the two important characteristics usually obtained from the tensile test.[3] For defining the strength of a material the *proportional limit*, the *yield point* and the *ultimate strength* are usually determined (see p. 6, Part I).



FIG. 249.

In determining the proportional limit sensitive extensometers are necessary to detect the slightest deviation from

[1] A description of the procedure of testing and of testing machines can be found in the book by Batson and Hyde, Mechanical Testing, 1922. See also O. Wawrziniok, Handbuch d. Materialprüfungswesens, Berlin, 1923, K. Memmler, Das Materialprüfungswesen, Stuttgart, 1924, and "Handbuch d. Werkstoffprüfung," E. Siebel, 1940.

[2] The British Engineering Standards Assn. recommends 8-in. gage length for rectangular specimens of plate material for boilers.

[3] A complete bibliography on tensile tests is given in the books by G. Sachs, "Der Zugversuch," Leipzig, 1926, and "Mechanische Technologie der Metalle," Leipzig, 1925. These books present modern developments in investigating mechanical properties of materials. See also C. W. MacGregor's paper presented at the Annual Meeting of Am. Soc. Test. Mat. 1940.

proportionality in the tensile test diagram. Obviously the position found for this limit depends a good deal on the sensitivity of the instruments. In order to get a greater uniformity in results, a certain amount of permanent set or a certain deviation from proportionality is often taken as the basis for determining the proportional limit. The International Congress for Testing Materials at Brussels (1906) defined the proportional limit, which experiments show to be the same as the elastic limit for steel, as that tensile stress at which the permanent set is 0.001 per cent. Recently there has been a tendency to increase this limiting magnitude of permanent set to 0.01 per cent.[4]

The *yield point* is a very important characteristic for such a material as structural steel. At this stress the specimen elongates a considerable amount (in the case of mild steel sometimes more than 1 per cent) without increase in load. Sometimes the yielding is accompanied by an abrupt decrease in load and the tensile test diagram has a shape such as is represented in Fig. 250. In such a case the upper and lower limits of the load at *a* and *b*, divided by the initial cross sectional area, are called the *upper* and *lower yield points* respectively. The position of the upper yield point is affected very much by the speed of testing, the form of the specimen and by the shape of the cross section.[5] The lower yield point is usually considered as a true characteristic of the material, which can be used as a basis for determining working stresses.[6]
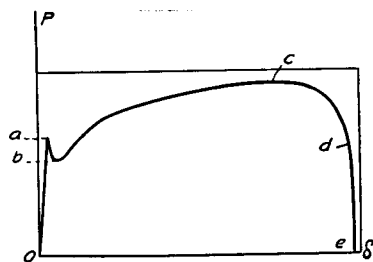


FIG. 250.

---

[4] See paper by P. Ludwik, "Bruchgefahr und Materialprüfung," Schweiz. Verband für die Materialprüfungen der Technik, Bericht, nr. 13, 1928, Zürich.

[5] See paper by Kühnel, V. D. I., Vol. 72, 1928, p. 1226, and paper by M. Moser, Forschungsarbeiten, nr. 295, Berlin, 1927. See also C. W. MacGregor, Trans. A. S. M. E., Vol. 53, 1931, p. 187.

[6] C. Bach first indicated the importance of determining the lower

Due to the relatively large stretching of the material at the yield point it is not necessary to use sensitive extensometers to determine this point. It can be determined with the simplest instruments or can be taken directly from the tensile test diagram. For structural carbon steel the stress at yield point is about 55–60 per cent of the ultimate strength. Structural steel with about 1 per cent Si has a stress at yield point about 70–80 per cent of the ultimate which may be the same as for carbon steel. Such a high value for the yield point justifies the usual practice of taking higher working stresses for this kind of steel.

There are materials which do not have a pronounced yield point; in such cases the stress at which the permanent set (plastic elongation) reaches the value 0.2 per cent is sometimes considered as the yield point. It must be kept in mind that the yield point defined in this manner does not represent a definite physical characteristic of the material and its position depends upon the arbitrarily chosen permanent set. In the case of structural steel with a pronounced yield point the amount of stretching at yield point is usually greater than 0.2 per cent and the actual yield point coincides with that defined by the above 0.2 per cent permanent set limit.

The *ultimate strength* is usually defined as the stress obtained by dividing the maximum load reached before breaking the specimen, point *c* in Fig. 250, by the *initial* cross sectional area. This quantity is very often taken as a basis for determining working stresses.

The area under the tensile test diagram *Oacde* (Fig. 250) represents the work required to produce fracture. This quantity is also sometimes used as a characteristic property of the material. It depends on not only the strength but also the ductility of the material.

The *ductility of metals* is usually considered to be characterized by the *elongation* of the gage length of the specimen during a tensile test and by the *reduction in area* of the cross section at the fracture.

---

yield point. See V. D. I., Vol. 58, 1904, p. 1040, and V. D. I., Vol. 59, 1905, p. 615.

In the first stage of plastic elongation, from $a$ to $c$ in the diagram, Fig. 250, the specimen elongates uniformly along its length and this uniform elongation is accompanied by a uniform lateral contraction so that the volume of the specimen remains practically constant.[7]   At the point $c$ the tensile force reaches a maximum; further extension of the specimen is accompanied by diminishing of the load.   At this stage of plastic elongation the deformation becomes localized, *necking* begins, and the specimen takes the shape shown in Fig. 251.



FIG. 251.

It is difficult to determine with accuracy the moment when necking begins and to establish separately the magnitude of the uniform stretching and the magnitude of the elongations due to necking. It is customary, therefore, to measure the total increase in the gage length when the specimen is fractured.   The *elongation* is then defined as the ratio of this total elongation of the gage length to its initial length.   In practice the elongation at fracture is usually given in per cent.   If $l$ is the original gage length and $\delta$ the total elongation, the elongation at failure in per cent is

$$\epsilon = \frac{\delta}{l} \cdot 100. \qquad (a)$$

This elongation is usually taken as the measure of the ductility of a material.   *Elongation* obtained in this manner depends on the proportions of the specimen.   The increase in the gage length, due to necking, is a large part of the total increase and is practically the same for a short gage length as it is for a long one.   Hence the *elongation* as defined by eq. (*a*) becomes larger the shorter the gage length.   For steel the elongation obtained for specimens with $l = 5d$ is usually 1.22 as large as obtained for a specimen of the same material with $l = 10d$. Experiments show also that local deformation at the neck depends very much on the shape of the cross section; hence

[7] The small elastic deformation in which the volume does change can be neglected in comparison with the comparatively large plastic deformation.

this shape affects the elongation of the specimen.   This shows that comparable results with respect to elongation can be obtained only by using geometrically similar specimens.

The *reduction in area* at the cross section of fracture is usually expressed in per cent of the original cross sectional area as follows:

$$q = \frac{A_0 - A_1}{A_0} \cdot 100, \qquad (b)$$

in which $A_0$ is the initial cross sectional area and $A_1$ the final cross sectional area at the fracture.

If we assume that longitudinal strain is uniformly distributed over the cross section of fracture and that the volume of the material is constant, the unit elongation $\epsilon_1$ at this cross section is determined by the equation

$$A_1(1 + \epsilon_1) = A_0,$$

from which

$$\epsilon_1 = \frac{A_0}{A_1} - 1$$

or, using eq. (*b*),

$$\epsilon_1 = \frac{q}{100 - q}. \qquad (c)$$

This quantity is sometimes called [8] the *effective elongation*. It is usually much larger than the elongation $\epsilon = \delta/l$ determined from the total elongation $\delta$ of the gage length.   Some results in static tests of certain steels are given in the table on pp. 497–498.
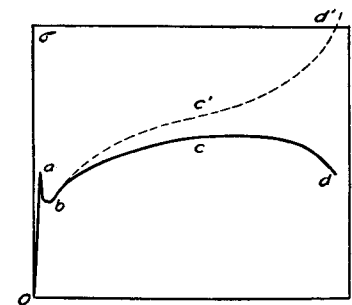


FIG. 252.

In defining the yield point and the ultimate strength the area used in calculating the stress was taken as the original cross sectional area. The curve *Oabcd* in Fig. 250 and Fig. 252 was obtained in this manner.   This curve represents the *true stress* only so long as

[8] See P. Ludwik, Elemente der Technologischen Mechanik, Berlin, 1909.

the elongation is small. For larger elongations the reduction in cross sectional area must be considered in order to get the true stress. The curve $bc'd'$ in Fig. 252 was obtained by multiplying the ordinates of the $Oabcd$ curve by the ratio $A_0/A$ of the original cross-sectional area to the varying cross sectional area $A$ as it was at each instant during the tensile test. From this curve it is evident that, although the load decreases from the point $c$ on, the true stress continues to increase and has its maximum value at the moment of fracture.

The relation between $\sigma$ and $\epsilon$ represented by a *true tensile test curve*, such as curve $bc'd'$, has a definite physical meaning so long as the bar continues to stretch uniformly. After the beginning of necking the elongation is not uniformly distributed along the length of the bar and the quantity $\epsilon = \delta/l$ no longer has a simple physical meaning. In investigating this portion of a tensile test it has proved very useful to construct curves in which the true stress $\sigma$ is plotted against the reduction in area $q$ (eq. $b$).[9] A curve of this kind
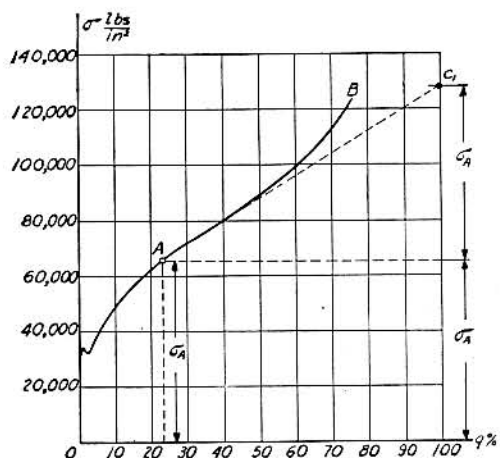


Fig. 253.

obtained with mild steel (0.05% carbon) is shown in Fig. 253.[10] The

[9] See paper by F. Körber and W. Rohland, Mitteilungen K. W. Institut, Vol. 5, 1924, p. 37.

[10] See paper by P. Ludwik, "Bruchgefahr und Materialprüfung" Diskussions, Bericht nr. 35 der Eidg. Materialprüfungsanstalt, Zürich, 1928.

point $A$ of this curve corresponds to the beginning of necking,[11] and the portion $AB$ of the curve represents the process of necking. It can be seen that the true stress increases up to the moment of fracture. Some applications of this type of curve are given later.[12]

**73. Compression Test.—** The compression test is principally used for testing brittle materials such as stone, concrete and cast iron. In testing stone and concrete, cubic specimens are



Fig. 254.

often used. In compressing them between the plane surfaces of the testing machine it is usually assumed that the compressive force is uniformly distributed over the cross section. The actual stress distribution is much more complicated, even if the surfaces are in perfect contact. Due to friction on the surfaces of contact between the specimen and the compressing head of the machine, the lateral expansion which accompanies compression is prevented at these surfaces and the material in this region is in a more favorable stress condition. As a result of this the type of fracture obtained in a compression test of cubic specimens of concrete is of the sort shown in the photograph, Fig. 254. The material in contact with the machine remains unaffected while the material at the sides is crushed out. In order to obtain the true resistance to compression of a material such as concrete, the influence of friction at the surfaces of contact must be eliminated or minimized. For this purpose A. Föppl covered the surfaces of contact with paraffin.[13] The ultimate strength obtained in such a manner was greatly reduced and the type of failure
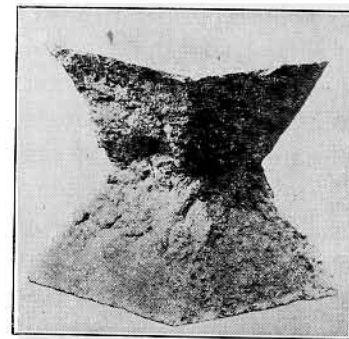
[11] It can be shown that in such diagrams as $OAB$ the tangent $AC$, at the point $A$, representing the beginning of necking, cuts the ordinate at $q = 100$ per cent at a height of $2\sigma_A$.

[12] The Bibliography related to the analysis of tensile test diagrams is given in the paper by C. W. MacGregor, The Annual Meeting, A. S. T. M., 1940.

[13] A. Föppl, Mitteilungen aus dem Mech. Techn. Laboratorium in München, nr. 27, 1900.

was completely different; a cubic specimen fails by subdividing into plates parallel to one of the lateral sides. Another method of eliminating the effect of friction forces is to use specimens in the form of prisms having the height in the direction of compression several times larger than the lateral dimensions. The middle portion of the prism then approaches a condition of uniform compression.[14] A very interesting method of producing a uniform compression on cylindrical specimens used in Kaiser Wilhelm Institute [15] is shown in Fig. 255. The portions of the testing machine in contact with the cylindrical
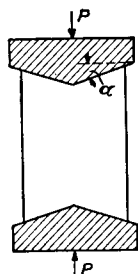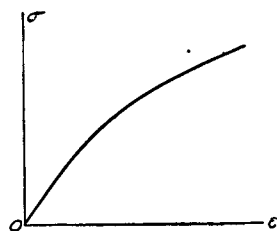


FIG. 255.          FIG. 256.

specimen and the ends of the specimen are machined to conical surfaces with the angle $\alpha$ equal to the angle of friction. Thus the effect of friction is compensated for by the wedge action and uniform compression results.

Compression tests of materials such as concrete, stone and cast iron show that these materials have a very low proportional limit.[16] Beyond the proportional limit the deformation increases at a faster rate relative to the load and the compression test diagram has a shape such as shown in Fig. 256. Sometimes it is desirable to have an analytical expression for such a diagram. For these cases C. Bach proposed [17]

[14] See L. Prandtl and Rinne, Neues Jahrbuch für Mineralogie, 1907. See also W. Gehler, Der Bauingenieur, Vol. 9, 1928, p. 21. Cylindrical specimens with height twice the diameter are sometimes used in testing concrete.

[15] Mitteilungen K. W. Institut, Düsseldorf, Vol. 9, 1927, p. 157.

[16] The proportional limit for cast iron in tension was determined by Grüneisen, Berichte d. Deutschen Phys. Gesellschaft, 1906.

[17] See C. Bach, Elasticität u. Festigkeit, V ed. 1905, Berlin, p. 67.

the exponential law given by the equation:

$$\epsilon = \frac{\sigma^n}{E}, \qquad (a)$$

in which $n$ is a number depending on the properties of the material. Bach found the values $n = 1.09$ for pure cement and $n = 1.13$ for granite.

Compression tests of ductile materials show that the shape of the diagram depends very much on the proportions of the specimen. As the dimension in the direction of the compression decreases, the effect of friction at the ends becomes more and more pronounced and the compression test diagram becomes steeper. For instance Fig. 257 shows the results of
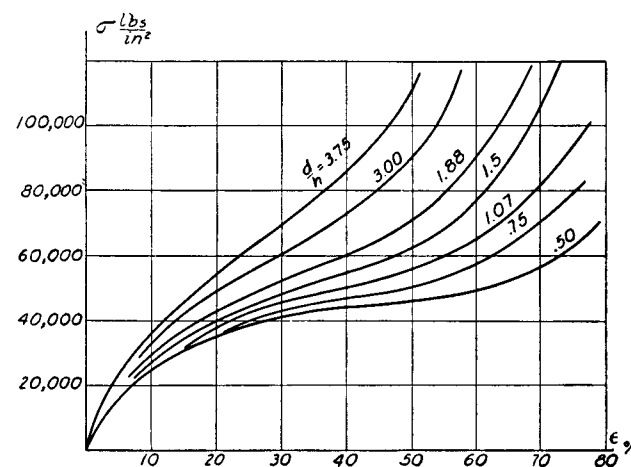


FIG. 257.

compression tests [18] on copper cylinders with various ratios $d/h$ of the diameter to the height of the specimen. In compression tests of such ductile materials as copper, fracture is seldom obtained. Compression is accompanied by lateral expansion and a compressed cylinder ultimately assumes the shape of a flat disc.

[18] See G. Sachs, Grundbegriffe der Mechanischen Technologie der Metalle, Leipzig, 1925, p. 36.

**74. Strain Hardening.**—It is well known that plastic deformation causes ductile materials such as mild steel, copper, and aluminum to become harder. Their strength increases and at the same time their ductility, as given by elongation or lateral contraction in the simple tensile test, decreases. This hardening effect of plastic deformation is also shown by the phenomenon of the *increase of the yield point* of the ductile material when subjected to stretching beyond the initial yield point. Figure 258 shows a tensile test diagram for mild steel.[19] After stretching the bar to the point $C$ it was unloaded. During this unloading the material followed an approximately
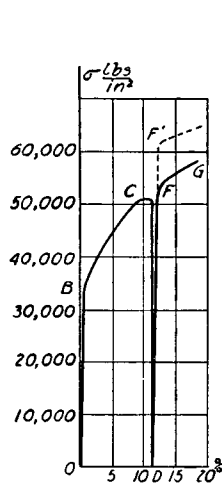


FIG. 258.



FIG. 259.

straight line law as shown by the line $CD$ on the diagram. Repeating the loading of the bar, the line $DF$ was obtained along which the material approximately followed Hooke's law. At the point $F$, which corresponds to the previous loading at $C$, the curve abruptly changed character and traced the portion $FG$, which can be considered as a prolongation of the curve $BC$. This is the *raising of the yield point* produced by stretching the material. If an interval of time, say several

---

[19] See Ewing, "Strength of Materials," 1914, p. 35.
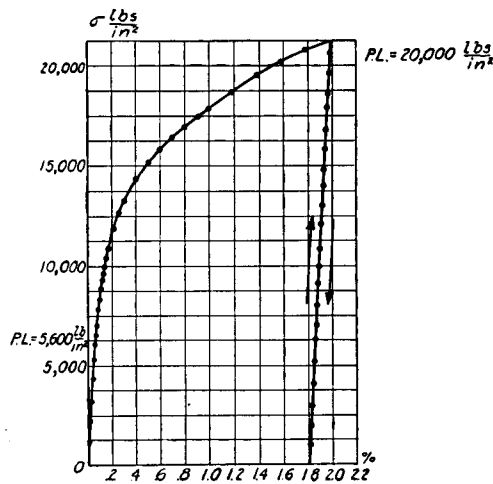
days, is allowed to elapse after unloading, then upon reloading a still higher yield point may be obtained, as indicated by the dotted line at $F'$. In Fig. 259 are shown the results of a tensile test of die cast aluminum.[20] The initial proportional limit of the material was 5,600 lbs. per sq. in. After stretching the specimen 2 per cent, the proportional limit upon reloading was found to be 20,000 lbs. per sq. in.

More complete investigations show that the time which elapses between unloading and reloading is of great influence on the stress strain curve during reloading. If reloading begins immediately after unloading, accurate measurements show that there are deviations from the straight line law at very low stress, and the proportional limit is greatly lowered. But if a considerable interval of time elapses between unloading and reloading, the material recovers its elastic properties completely. Figure 260 shows the curves obtained by Ewing with mild steel which show that, if reloading follows in ten minutes after overstrain, the material does not follow Hooke's law, but after 5 days it has partially recovered its elasticity and after 21 days it has almost completely recovered it.
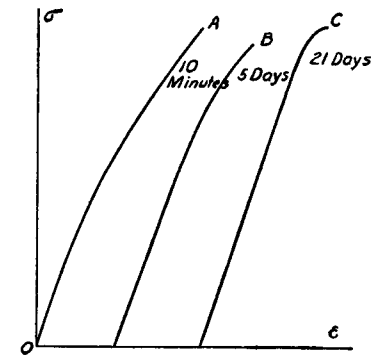
The experiments show that if the material is submitted to mild heat treatment after unloading, say in a bath of 100° Centigrade, the recovery of elastic properties occurs in a much shorter interval of time. Figure 261 shows the results of such a test made on a steel bar by I. Muir.[21] The initial tensile test is represented by the curve $A$. Curve $B$ represents the reloading of the same bar ten minutes after unloading. A considerable deviation from Hooke's law is noticeable. Curve $C$ is the diagram obtained with the same bar after a second



FIG. 260.

---

[20] Westinghouse Elec. Mfg. Co. Research Laboratory.
[21] I. Muir, Phil. Trans. Roy. Soc., 1899.

unloading and after keeping it at a temperature of 100° Centigrade for 4 minutes. It may be seen that after this treatment the material completely recovered its elastic properties.

The phenomenon of hardening due to plastic deformation is encountered in many technological processes such as rolling
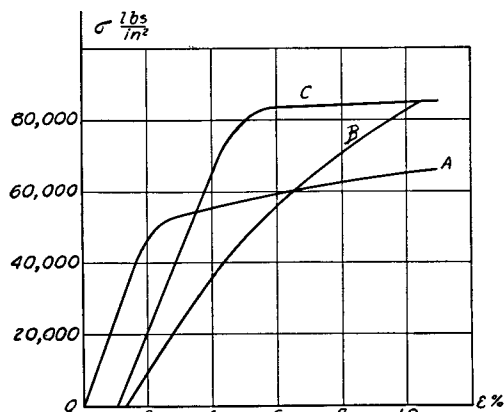


FIG. 261.

of bars or drawing tubes and wires at low temperature, cutting sheet metals by shears, and drawing and punching holes. In all these cases the part of the material which undergoes plastic deformation becomes harder and its ductility is greatly reduced.[22] To eliminate this undesirable effect of strain hardening it is customary to anneal the material, which reestablishes the initial ductility.[23]

Sometimes the strain hardening of ductile materials finds a practical application in manufacturing. It is common practice to submit the chains and cables of hoisting machines to a certain amount of overstrain to eliminate undesirable stretching of these parts in service. The cylinders of hydraulic

[22] For a general discussion of the properties of cold worked metals see the paper by Z. Jeffries and R. S. Archer, Chemical and Metallurgical Eng., Vol. 27, 1922, p. 747. See also G. Masing and M. Polanyi, Kaltreckung und Verfestigung, Springer, Berlin, 1923.

[23] See paper by Rees, Iron and Steel Inst. Journal, 1923.

presses are sometimes submitted to an initial internal pressure sufficient to produce a permanent deformation in the walls. The strain hardening and the residual stresses produced by this prevent any permanent set in service. The overstraining of metal is sometimes used in the manufacture of guns (see p. 243). By stretching the metal in the wall of a gun beyond the initial yield point and afterwards submitting it to a mild heat treatment, the elastic properties of the material are improved; at the same time initial stresses are produced which combine with the stresses produced by the explosion to give a more favorable stress distribution. Turbine discs and rotors are sometimes given an analogous treatment. By running these parts at overspeed, a permanent set is obtained around the central hole, which raises the yield point of the material there and produces initial stresses, which are in a favorable direction.[24] Die cast aluminum fans are sometimes submitted to overstrain at the bore to prevent any possibility of their loosening on the shaft in service. A considerable plastic flow of metal is sometimes produced in pressing the hub of locomotive wheels onto their axles and this has proved to have a favorable effect. Copper bars in the commutators of electric machinery are submitted to considerable cold work by drawing to give them the required strength.

In using overstrain in this manner to raise the yield point and improve the elastic properties of a structure, it is necessary to keep in mind (1) that the hardening disappears if the structure is submitted to annealing temperatures and (2) that the stretching of metal in a certain direction, while making it stronger with respect to tension in this direction, does not proportionately improve the mechanical properties with respect to compression in the same direction.[25] This phenomenon is clearly shown in Fig. 262, which represents tests

[24] See A. Nadai and L. H. Donnell, Trans. A. S. M. E., Vol. 51, 1929, p. 173.

[25] This phenomenon was discovered by J. Bauschinger, Mitteilungen aus dem Mech. Techn. Laboratorium in München, 1886. See also Dinglers, Polytech. Journal, Vol. 266, 1886.

made with electrolytic copper.[26] Curve (a) shows the mechanical properties of the copper in the annealed condition. The proportional limit and yield point [27] in this condition are very low. Such material cannot be used in structures which



FIG. 262.

are submitted to the action of appreciable stresses. Curve (b) represents tensile and compression tests of the same material after giving the bar an elongation of 15 per cent. The proportional limit and yield point have been raised considerably, especially in tension. Curves (c) and (d) show the results of tests after a stretching of 20 per cent and 25 per cent. The additional stretching produces still further improvement of the mechanical properties, especially in tension. At the same time the proportional limit in compression is somewhat lowered. Curve (e) represents tensile and compressive tests on a bar, which had been drawn through a die,

[26] Westinghouse Elec. Mfg. Co. Research Laboratory.
[27] The yield point is defined as the point where unit elongation or unit compression is 0.2 per cent.

reducing the cross sectional area of the bar by 15 per cent. In the drawing process the material is submitted not only to longitudinal tension but also to lateral compression. To this fact must be attributed the difference between curves (b) and (e). Although in both cases the bar received about the same reduction in cross sectional area, the material drawn through a die showed better mechanical properties with respect to compression than the material which was subjected to a uniform longitudinal stretching in a testing machine.

This fact that stretching a metal in a certain direction does not improve the mechanical properties in compression in the same proportion as it does in tension must not be overlooked in cases in which the material is submitted to reversal of stresses (see article 78).

It must also be kept in mind that strain hardening, while raising the yield point of a material, does not affect the ultimate
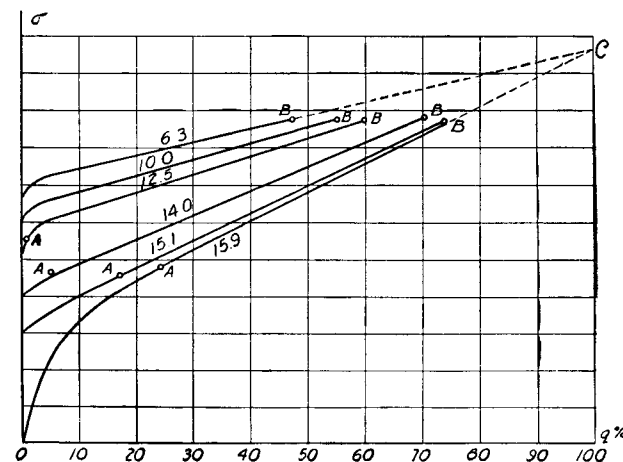


FIG. 263.

strength of the material in the same proportion, and the true stress at fracture is probably unchanged. At the same time the elongation and reduction in area at fracture are considerably reduced due to strain hardening. Curves representing the true stress as a function

of the reduction in area $q$ (p. 402) are especially useful in investigating the effect of strain hardening. Several curves of this kind obtained with drawn copper [28] are shown in Fig. 263. The lowest line represents a tensile test of the copper wire in its initial condition. The other curves represent tensile tests of the same copper wire after various degrees of drawing. The amount of cold work is indicated by the reduction in the diameter, the magnitude of which is given on each curve in millimeters. Points $A$ indicate the beginning of necking and points $B$ the moment of fracture. Between $A$ and $B$ the diagrams are straight lines which intersect, when prolonged, at a common point $C$. These curves indicate that cold work does not affect the true stress at fracture and affects only slightly the true stress at the beginning of necking. At the same time it affects considerably the elongations and the lateral contraction of the materials.

In concluding this discussion it should be mentioned that there are indications [29] that material which has suffered yielding at a certain place is more sensitive at this place to chemical actions and there is a tendency for corrosion to enter the metal along the surfaces of sliding. This phenomenon is of particular importance in the case of boilers and other containers submitted simultaneously to stresses and to chemical action.

**75. Strain Hardening and Residual Stresses.**—In discussing the causes of strain hardening of metals it is necessary to consider the crystalline structure of the metals. A metallic test specimen is a conglomerate of crystals so small in size that a cubic inch usually contains millions of them. In studying the plastic deformation of such crystalline materials it has proved very useful to investigate the mechanical properties of a single crystal. Methods of preparing large single crystals have been developed in recent years so that it is now possible to have tensile test specimens of considerable size consisting

[28] See paper by W. Müller, Forschungsarbeiten, nr. 211 (1918). See also G. Sachs, loc. cit., p. 397.

[29] See paper by F. Körber and A. Pomp, Mitteilungen K. W. Institut, Vol. 8, 1926, p. 135. See also S. W. Parr and F. G. Straub, Engineering, Vol. 124, 1927, p. 216.

of a single crystal.[30] Tensile tests of such specimens show that the mechanical properties of crystals depend greatly on the direction of the tension with respect to the directions of the axes of the crystal. In the case of copper, for instance, the ratio of the maximum tensile strength to its minimum value is $3 : 1$.[31] The plastic deformation of these specimens consists in sliding in certain direction along certain crystallographic
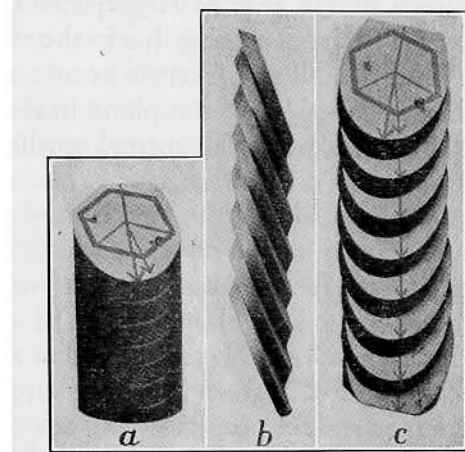


Fig. 264.

planes, as schematically indicated in Fig. 264.[32] The beginning of sliding depends upon the magnitude of the shearing stress along these planes in the direction of sliding and is independent of the normal stress acting on the same plane. As the elongation of the specimen is continued the number of planes along which the sliding occurs increases and likewise

[30] The development of methods for producing large crystals of metals is due to the work of H. C. Carpenter and C. F. Elam, Proc. Roy. Soc., Vol. 100A, 1921, p. 329; P. W. Bridgman, Proc. Amer. Acad. Sc., Vol. 60, 1925, p. 306; C. A. Edwards and Pfeil, Jour. Iron and Steel Inst., Vol. 109, 1924, p. 129. The first large crystals of copper were obtained by J. Czochralski, V. D. I., 1923, p. 536.

[31] See J. Czochralski, "Moderne Metallkunde," Berlin, 1924, p. 206.

[32] See H. Mark, M. Polanyi and E. Schmid, Zeitschrift f. Phys., Vol. 12, 1922, p. 58; see also G. I. Taylor and C. F. Elam, Proc. Roy. Soc., Vol. 102A, 1923, p. 643, Vol. 108A, 1925, p. 28. G. I. Taylor, Proc. Roy. Soc., A, Vol. 145, p. 362, 1934.

the magnitude of the shearing stress acting on these planes. This increase in stress necessary to continue the stretching of the specimen represents the *strain hardening* of a single crystal. Due to the type of sliding indicated in Fig. 264 (*b*) an originally circular, single crystal specimen of ductile material becomes elliptical in cross section and, if stretched to destruction, becomes wedge-shaped instead of cone-shaped at the cross section of fracture. In the case of single crystals of brittle materials, such as rock salt, stretching due to the sliding action described above is very small and fracture occurs as the result of the overcoming of cohesion over a plane having a certain crystallographic direction, when the normal tensile stresses on this plane reach a certain critical limit.

Crystalline materials, such as the metals used in industry, are conglomerates of very small crystals, which can be seen only with a special microscope on a plane surface, finely polished and etched in a special manner. In an ordinary tensile test specimen these crystals are located at random, and the mechanical characteristics given by a tensile test represent an average of the mechanical properties in various directions of an individual crystal.[33] Due to the small size and large number of crystals these average values are usually independent of the direction in which a specimen is cut from a block of material,[34] and such a material can be considered as isotropic in calculating stresses and deflections in large structures.

Observations with a microscope of the deformation of the small individual crystals in a specimen during a tensile test show that the deformation of these crystals in conglomerate is

---

[33] Intercrystalline material is neglected in this discussion. Experiments show that planes of slidings and fractures always go through the crystals and not between them.

[34] Cold work may produce some differentiation in the orientation of crystals along certain directions. The mechanical properties of a tensile test specimen will then depend on the orientation of the specimen with respect to the direction of the cold working. Bibliography on this subject can be found in the paper by G. Sachs, O. Bauer and F. Göler, Zeitschr. f. Metallkunde, Vol. 20, 1928, p. 202. See also paper by W. Köster, Bericht nr. 23, d. Eidg. Materialprüfungsanstalt, 1927, Zürich.

of the same nature as in the case of a single crystal specimen. In each individual crystal sliding of the sort shown in Fig. 264 begins when the tensile stress in the specimen reaches a certain value, depending upon the orientation of that crystal with respect to the direction of the tension. On the polished surface this sliding is indicated by microscopic lines, called *slip bands*. This sliding stops at the boundary of the crystal; in the neighboring crystals the planes of sliding may have another direction and sliding may start when the stress in the specimen reaches a different value. It is generally believed that such slidings in individual small crystals unfavorably situated with respect to the tensile stress in the specimen are the cause of small deviations from Hooke's law and a small permanent sets at a comparatively low tensile stress in materials which, in general, follow Hooke's law.

When the material has a pronounced yield point and the tensile stress in the specimen reaches this point, a large plastic deformation takes place, which consists in the sliding of considerable portions of the specimen along planes inclined about 45° to the axis of the specimen, i.e., along the planes in which the shearing stress is a maximum. These planes of sliding usually begin at points of stress concentration, for instance, near the fillets at the ends of the specimen, and gradually spread over the length of the specimen.[35] If the surface of a specimen has been polished, these planes of sliding are revealed on the surface by easily discernible lines (see Fig. 214). These lines were first noticed by Lueders and are called *Lueders' lines*.[36] Due to the described deformation the individual crystals become strain hardened and if the specimen is unloaded and loaded again it will be found that the yield point is raised.

There is another point of importance. Since some individual crystals may receive a permanent set during a tensile test, while neighboring crystals, more favorably orientated,

---

[35] See paper by C. W. MacGregor, loc. cit., p. 398.

[36] An investigation of these lines in various cases was made by Hartman; see his book, "Phénomènes qui accompagnent la déformation permanente," 1900.

may only deform elastically, it follows that after unloading there may remain in the stretched specimen some *residual stresses* in the individual crystals. The crystals which received a permanent set do not return completely to their initial shape, and as a result of this there will be some "wedging effect" on the neighboring crystals. The possibility of such stresses can be demonstrated by the system of three bars shown in Fig. 265. Assume that all three bars are of the same material and the same cross-sectional area. We know that under the action of the load $P$ the stress in the middle bar is larger than in the inclined bars (see p. 19, Part I); i.e., like the crystals mentioned above, this element of the system is less favorably situated than the others. If the load is gradually increased, this bar will reach the yield point first. Let the straight line $OA$ (Fig. 265, $b$) represent the load deflection diagram for this sys-
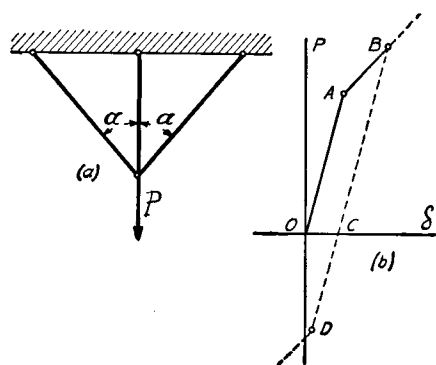


FIG. 265.

tem under elastic conditions. At $A$ the vertical bar begins to yield and any further increase in the load will be taken by the inclined bars only.[37] Hence beyond the point $A$ an increase in the load produces a greater increase in the deflection than when all three bars were in the elastic state, and the load deflection diagram follows some such line as $AB$. If, on reaching $B$, the system is gradually unloaded, the deformation in the reverse direction, due to the elastic behavior of all

[37] It is assumed that the material has a pronounced yield point and that after yielding a considerable stretching can occur without increase in stress.

three bars, follows the linear law represented by the straight line $BC$, parallel to $OA$. When the load is entirely removed the deflection $OC$ still remains and there will therefore be tensile stresses in the inclined bars and a compressive stress in the vertical bar, even after unloading. These are *residual stresses* due to the plastic deformation of the middle bar. If the system is reloaded, the load deflection diagram will be the same straight line $CB$ as during unloading and the yield point of the system will have been raised to the point $B$, corresponding to the initial loading. If, after unloading, the system is reloaded with a vertical force in the upward direction, compressive stresses will be produced in the bars, which superpose on the residual stresses. Since the vertical bar already has an initial compression, a force at $D$ (Fig. 265, $b$) smaller than that corresponding to the point $A$ will be sufficient to bring the middle bar to the yield point, if we assume that the yield point of the material in compression is the same as in tension. Hence the original loading raised the yield point of the system in the direction of this loading but lowered the yield point in the opposite direction. This discussion shows that the presence of residual stresses may explain why a bar strain hardened by stretching has a higher yield point in tension than in compression (see p. 410).

The residual stresses produced by uniform stretching of a bar of a crystaline material are of an extremely localized type. They are confined to microscopical regions around the crystals which suffered plastic deformation at a comparatively low average stress in the specimen. In the process of drawing or rolling, residual stresses of a less localized type are sometimes produced. In drawing a bar through a die, for instance, the metal at the outside is stretched more than the metal at the middle. Hence drawn bars have considerable residual stresses in tension at the surface and in compression at the middle. In drawn copper bars of narrow rectangular cross section the distribution of these stresses at a distance from the ends is approximately as shown in Fig. 266 (*a*). If the bar is cut lengthwise, there will be bending such as shown in Fig. 266 (*b*).

Measurement of this bending shows that the maximum residual stresses produced in drawing the copper bars are of the same order as the yield point of the material.[38]  These stresses
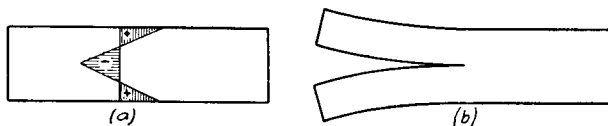


FIG. 266.

are of great practical importance.  They cause undesirable warping in the process of machining [39] and to them must be attributed also *season cracking* in various copper alloys which have been cold worked and not properly annealed afterwards.[40]

**76. Types of Failures.**[41]—In the previous article two kinds of fracture of a single crystal specimen were mentioned. In a crystal of a ductile material there is a plastic deformation preceding fracture which consists of sliding along certain planes and there is a considerable reduction in cross-sectional area before fracture occurs.  In this case the strength depends principally upon *the resistance to sliding*.  In the case of a crystal of brittle material fracture occurs without appreciable reduction in the cross section and is due to overcoming the cohesive forces on a certain crystallographic plane.  Here the strength depends principally upon *the resistance to separation*. These two types of failure, *sliding failure* and *separation failure*,

[38] Direct measurements made on commutator bar copper in the research laboratory of the Westinghouse Elec. and Mfg. Co. showed stresses of 22,000 lbs. per sq. in. in bars which were reduced 15 per cent in area by drawing.

[39] The first systematic investigation of these stresses was made by E. Heun.  See Zeitschr. f. Metallographie, Vol. 1, 1910, p. 16; Stahl u. Eisen, Vol. 31, 1911, p. 760; Mitteilungen Materialprüf. Amt, Vol. 35, 1917, p. 1; Naturwiss., Vol. 9, 1921, p. 321.  For further discussion see art. 69, p. 379.

[40] See "The Failure of Metals under Internal and Prolonged Stress," published by Faraday Soc., London, 1921.  See also G. Masing, Zeitschr. f. Metallkunde, 1924, p. 257.

[41] A complete bibliography on this subject is given in the paper by P. Ludwik, "Bruchgefahr und Materialprüfung," Diskussionsbericht nr. 35, der Eidg. Materialprüfungsanstalt, Zürich, 1928.  See also P. Ludwik, Forschungsarbeiten, nr. 295, 1927, Berlin.

are encountered also in crystalline materials which consist of an aggregate of small crystals.   In the case of brittle materials such as cast iron, fracture occurs without appreciable plastic deformation and on a cross section perpendicular to the direction of tension.  This is a *separation failure*.  A specimen of a ductile material such as mild steel undergoes considerable plastic deformation and reduction in cross sectional area due to sliding along planes inclined $45°$ to the axis of the specimen before fracture occurs.  This is *sliding failure*.  In studying these two distinct kinds of fracture the theory has been forwarded [42] that the strength of a material can be described by two characteristics, the resistance of the material to *separation* and the resistance to *sliding*.  If the resistance to sliding is greater than the resistance to separation, we have a brittle material and fracture will occur as a result of overcoming cohesive forces without appreciable deformation.   If the resistance to separation is larger than resistance to sliding, we have a ductile material.  The sliding over inclined planes begins first and fracture occurs only after a considerable reduction in the cross sectional area, after which, due to strain hardening, the resistance to sliding may become larger than the resistance to separation.

The relation between the resistance to separation and the resistance to sliding does not remain constant for the same material.  It depends very much upon the velocity of deformation and upon the temperature at which a test is made. There are evidences that the resistance to sliding increases as the velocity of deformation increases and as the temperature is lowered.   At the same time the resistance to separation is not affected to the same degree by these two factors.  This would explain why a bar of a metal such as zinc can be bent like a ductile material under slow loading while the same bar fractures without plastic deformation if the loading is applied suddenly.[43]   Another example of this is asphalt.  It may flow under the action of its own weight if the forces act a long

[42] See P. Ludwik, loc. cit., p. 418.
[43] P. Ludwik, Stahl u. Eisen, Vol. 43 (1923), p. 1427.

time, but it proves to be brittle under the action of suddenly applied forces. In both of these cases the resistance to sliding was less than the resistance to separation under slow deformation and the materials behaved in a ductile manner. At high speed the ratio between the two kinds of resistance was reversed and they behaved like brittle materials.

The type of fracture depends also on the manner of testing. If the loading is of such a nature that fracture due to separation is prevented, a considerable plastic deformation may be obtained in a material usually considered brittle. This phenomenon is illustrated by the plastic deformation of rocks submitted to large pressures on all sides.[44] Likewise a ductile material may have a fracture of the brittle type if the form of the specimen or the type of stress distribution is such that plastic deformations, due to sliding, are prevented. This latter case is of great practical importance and it is worth while to examine in more detail the conditions under which such a brittle fracture may occur. Experience shows that these fractures sometimes occur under the action of residual stresses due to cold work or under the action of thermal stresses, and that they can be attributed to one of the following two causes: (1) a three-dimensional stress condition; (2) a form preventing sliding.

The ductility of materials such as structural steel is usually determined from a simple tensile test. In such a test there is a constant ratio between the maximum tensile stress and the maximum shearing stress equal to two. Under such conditions the resistance to sliding is overcome first and the sliding type of failure results. Imagine now a three-dimensional stress condition such as that represented in Fig. 51, Part I, by Mohr's circles. The maximum shearing stress in this case is equal to $(\sigma_x - \sigma_z)/2$ and if $\sigma_z$ is nearly the same as $\sigma_x$ the maximum tensile stress may be many times larger than the maximum shearing stress. In this case fracture due to overcoming the cohesive forces on the plane on which the maximum tensile stress is acting may occur before there can

[44] See Th. v. Kármán, Forschungsarbeiten, nr. 118, 1912, Berlin.

be any sliding. Such a fracture is not accompanied by appreciable plastic deformation and has the type of a brittle failure, although the material may be very ductile under a simple tensile test. Figure 267 represents the beginning of fracture at the neck of a tensile test specimen of a ductile material.[45] In the middle portion of the cross section at the neck there is a three-dimensional stress condition. Due to the necking, elements here undergo tension in not only the axial direction, but also in the radial direction. This causes a crack of a brittle type at the center of the cross section, as shown in



FIG. 267.

the figure. At the same time material near the surface continues to yield by sliding, and a sliding fracture finally takes place near the boundary.
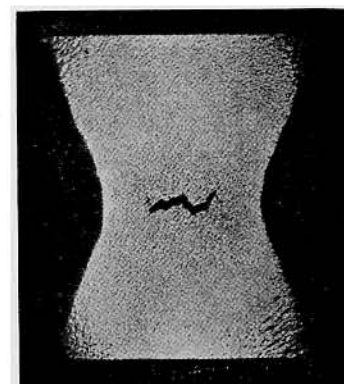
The effect of the form on the type of fracture may be shown by making tensile tests on grooved specimens of the shape shown in Fig. 268. Due to the presence of the portions of larger diameter $D$, sliding along 45° planes at the groove is inhibited, and reduction of the cross-sectional area at the groove during a tensile test is partially prevented. It is natural that this action should increase as the width $\delta$ of the groove decreases. In the following table are given some results of such tests obtained with two different materials:[46] (1) *carbon steel* with a proportional limit 56,000 lbs. per sq. in., yield point 64,500 lbs. per sq. in., ultimate strength 102,000,
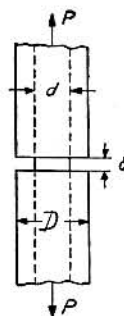


FIG. 268.

[45] In this case the material was aluminum; see P. Ludwik, V. D. I., Vol. 71, 1927.

[46] These tests were made at the Westinghouse Elec. and Mfg. Co. Research Laboratory; see also the tests by P. Ludwik u. R. Scheu, Stahl u. Eisen, Vol. 43, 1923, p. 999.

lbs. per sq. in., elongation $26\frac{1}{2}$ per cent, reduction in area 55 per cent; (2) *nickel chrome steel* with a proportional limit 80,000 lbs. per sq. in., yield point 85,000 lbs. per sq. in., ultimate strength 108,000 lbs. per sq. in., elongation 27 per cent, reduction in area 69 per cent. These figures were obtained from ordinary tensile tests on normal cylindrical specimens $\frac{1}{2}$ in. in diameter and with 2-in. gage length; the original cross-sectional area was used in calculating the stresses. The specimens of the type shown in Fig. 268 had $d = \frac{1}{2}$ in., $D = 1\frac{1}{2}$ in. and $\delta = \frac{1}{8}$ in., $\frac{1}{16}$ in., $\frac{1}{32}$ in.

TABLE 25.—ULTIMATE STRENGTH OF CYLINDRICAL AND GROOVED SPECIMENS

| Carbon Steel | $\delta$ | Ultimate Strength | | NiCr Steel | $\delta$ | Ultimate Strength | |
|---|---|---|---|---|---|---|---|
| | | Orig. Area | Red. Area | | | Orig. Area | Red. Area |
| | $\frac{1}{32}$ in. | 163,000 | 176,000 | | $\frac{1}{32}$ in. | 193,000 | 237,000 |
| | $\frac{1}{16}$ " | 164,000 | 177,000 | | $\frac{1}{16}$ " | 184,000 | 232,000 |
| | $\frac{1}{8}$ " | 143,000 | 158,000 | | $\frac{1}{8}$ " | 154,000 | 199,000 |
| Norm. spec. | | 102,000 | 227,000 | Norm. spec. | | 108,000 | 348,000 |

The table shows that in all cases the breaking load for the grooved specimens was larger than for cylindrical specimens. With the grooved specimens only a small reduction in area took place and the appearance of the fracture was like that of brittle materials. The true ultimate strength of the cylindrical specimens was larger than that of the grooved specimens, because the fracture of the cylindrical specimens occurred after considerable plastic flow; this caused strain hardening and increased not only the resistance to sliding but also the resistance to separation.

An effect analogous to that of the narrow groove in Fig. 268 may be produced by internal cavities in forgings and castings. Thermal stresses and residual stresses may combine with the effect of stress concentration at the cavity to produce a crack and the resulting fracture will have the characteristics of a brittle failure without appreciable plastic flow, although the material may prove ductile in simple tensile tests.

The combination of a grooved or notched form of specimen with great velocity of application of the load may produce a still more pronounced "groove effect." These conditions are realized in impact tests of notched bars. Another type of fracture of ductile materials without appreciable plastic deformation is that caused by reversal of stresses. This is of great practical importance and will be discussed in the article on fatigue of metals (see p. 428).

**77. Time Effect and Hysteresis.**—Observation shows that when a tensile load is applied to a bar it does not produce the complete elongation immediately. There is a certain *creep*, that is, the bar continues to elongate slowly for a considerable length of time. This *time effect* depends on the material of the bar and on the magnitude of the stresses involved. In the case of a single crystal specimen, loaded within the proportional limit, the time effect is very small and can be explained by considering thermodynamical and electrical effects. Assume that the bar is loaded quickly as represented by the portion $OA$ of the tensile test diagram (Fig. 269). This process of elongation may be considered to be *adiabatic*; it is accompanied by a lowering of the temperature of the bar due to increase in its volume. The bar gradually warms up to the initial temperature and thereby elongates an additional amount $AB$ without change of load. Then a quick unloading gives the straight line $BC$ on the diagram. At $C$, due to the decrease in the volume, in the process of unloading the bar has a temperature higher than the initial; after a time, cooling causes it to shorten the amount $CO$. Although the deformations $AB$ and $CO$ are very small, this discussion shows how there may be a certain time effect due to thermal causes in the case of an ideal elastic substance within the proportional limit.[47] An analogous effect due to electrical causes may also be observed under certain conditions.[48] In the case of non-homogeneous materials, such as
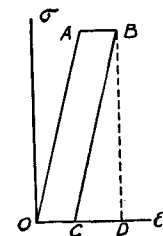


FIG. 269.

---

[47] W. Thomson, Quarterly Journal of Math., 1855.
[48] See A. F. Joffe, "The Physics of Crystals," New York, 1928.

commercial metals, the time effect is much larger. It cannot be explained by thermal causes alone and is usually attributed to the continuation of sliding deformation within unfavorably orientated crystals after the load has been applied. The time effect after unloading is explained by residual stresses, which continue to produce sliding within unfavorably orientated crystals and thus cause creep in the material for some time after the removal of the load.

In discussing the time effect on tensile and compressive test diagrams, we must distinguish between metals having a comparatively low melting point such as lead or zinc and metals having much higher melting temperatures such as steel or copper.[49] Experiments show that tensile and compressive test diagrams of metals of the first group depend very much upon the speed with which the experiments are made. Figure 270, for instance, represents compression test diagrams for lead
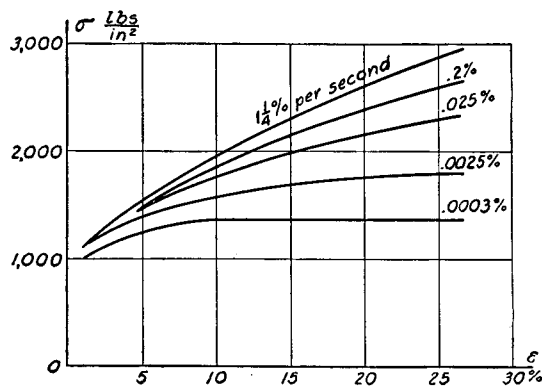


FIG. 270.

at different speeds of loading.[50] In these diagrams the true compressive stress is used, plotted against compressive strain. The speeds of shortening in per cent per second are indicated

[49] These metals when at temperatures nearer their own melting points show the characteristics of the first class of metals at room temperature (see p. 462).

[50] See paper by E. Siebel and A. Pomp, Mitteilungen K. W. Institut, Vol. 10, 1928, p. 63.

on the curves. If the speed of unit compression is 0.0003 per cent per second, the load remains practically constant after reaching a unit compression of 10 per cent. This large effect of speed with such metals is explained by the fact that they recrystallize at room temperature. Hence the hardening effect of plastic deformation may be removed by recrystallization if the loading process goes slowly enough.

In the case of metals with a high melting point the speed has much less effect. Figure 271 represents compression test
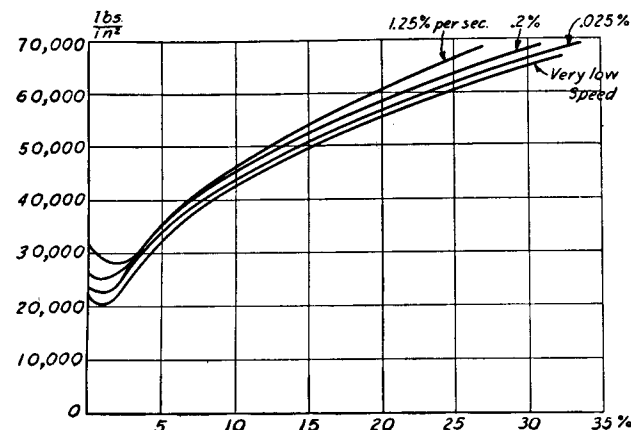


FIG. 271.

diagrams at different speeds of loading for steel. Again the true compressive stresses are plotted against unit compression in per cent. It will be seen that the most important effect of speed is that on the position of the lower yield point. At a high speed of loading the yield point of mild steel is about 30 per cent higher than its value with a low speed of testing. This phenomenon is important in the impact testing of metals and explains why fracture in dynamical tests requires more work than in static tests on specimens of the same material.

This discussion of the time effect shows that even under the most ideal conditions, when the specimen is a single crystal (Fig. 269), there may be some difference between the curve which represents loading of the specimen and the curve which

represents unloading. This means that a certain amount of energy is dissipated during a loading-unloading cycle. In Fig. 269 the area $OABD$ represents the work done during the process of loading (see p. 281, Part I), the area $BCD$, the work restored during unloading, and hence the area $OABC$ represents the energy dissipated per cycle. This quantity is very small and can be eliminated if the process of loading and unloading is carried out so quickly that no appreciable exchange in heat takes place. We have such conditions, for instance, in high-frequency vibrations produced in a single crystal specimen. The dissipation of energy, due to electrical causes, as in a quartz crystal, can be eliminated by choosing a certain crystal-lographic direction for the tension and compression.[51] This property has found wide application in the generation of sustained electric vibrations. Due to very small energy losses, quartz oscillators show a very sharp resonance effect at high frequencies.

If a single crystal specimen is stretched beyond the proportional limit until sliding takes place in the crystal, and it is then unloaded and loaded again, a stress-strain diagram like that in Fig. 272 will be obtained. After repeated loading and unloading we may arrive[52] at a condition in which there is no noticeable change in the permanent set at $C$. The cycle $ABCD$ will then be "elastic." The energy dissipated during each cycle represented by the area $ABCD$ is usually larger than that discussed in connection with Fig. 269 and cannot be entirely explained by the thermal or electrical causes mentioned. Such *looping* may also be obtained with multi-crystalline materials, such as the commercial metals, and with amorphous materials such as glass. This phenomenon is called *elastic hysteresis*. In multicrystalline materials it can be partially explained as described before (see p. 424), but the complete explanation is still unknown.[53]

---

[51] See the book by A. Joffe, loc. cit., p. 423.

[52] It is assumed that the stress is not very large, so that a large number of loadings and unloadings will not produce a fatigue fracture.

[53] See the theory of hysteresis by Bennewitz, Physikal. Zeitschr., Vol. 21, 1920, p. 703, and Vol. 25, 1924, p. 417. A very interesting

The areas of these *hysteresis loops*, representing the energy dissipated per cycle, are of practical interest, as the amount of this energy determines the *damping properties of the material*. Measurements made by Rowett[54] with steel showed that this energy increases as the cube of the maximum stress during each cycle. This subject has also been studied by B. Hopkinson[55] and more recently by O. Föppl.[56] Hysteresis loops may be demonstrated by using the model shown in Fig. 273.[57] It consists of a fixed base $A$ and two movable wooden blocks $B$ and $C$, which can slide along the steel rod fixed in $A$. The block $B$ can slide freely while the block $C$, attached to $B$ by the helical spring, moves against an adjustable friction. Figure 273 (*b*) represents the relation between the force $P$ applied to block $B$ and the displacement of this block. At $m$ the friction of the block $C$ is overcome and sliding continues without increase in the load. Figure 273 (*c*) shows the cycle obtained by applying a load first in one direction and then in the other. Other phenomena in tension and compression, such as deviation from the straight line law at the proportional limit, sudden yielding at the yield point, hysteresis loops, residual stresses, etc., may be demonstrated with a model consisting of several units similar to that in Fig. 273, put side by side with all the blocks $B$ clamped together. Each unit represents a crystal in a multicrystalline specimen. The
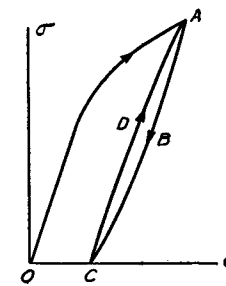
FIG. 272.

---

mechanical model illustrating time effect and hysteresis was developed by L. Prandtl; see Zeitschr. f. Angew. Math. u. Mechanik, Vol. 8, 1928, p. 85.

[54] Rowett, Proc. Roy. Soc., Vol. 89, 1913, p. 528.

[55] B. Hopkinson and G. T. Williams, Proc. Roy. Soc. (A), Vol. 87, 1912.

[56] O. Föppl und E. Becker, Forschungsarbeiten, nr. 304, 1928. See also Reports of the International Congress of Applied Mechanics, Zürich, 1926, and Mitteilungen des Wöhler-Instituts, Braunschweig, Heft 30, 1937. For bibliography on hysteresis see H. Fromm, Handbuch Phys. and Techn. Mech., Vol. 4, 1, p. 436, 1931.

[57] Such a model was used for demonstrations by C. F. Jenkin. See Engineering, Vol. 114, 1922, p. 603.

beginning of sliding of the individual blocks $C$ represents yielding in individual crystals. By adjusting the friction in the blocks $C$, diagrams of various types can be obtained. When the friction of the individual blocks differs greatly, there will be a large difference between the proportional limit
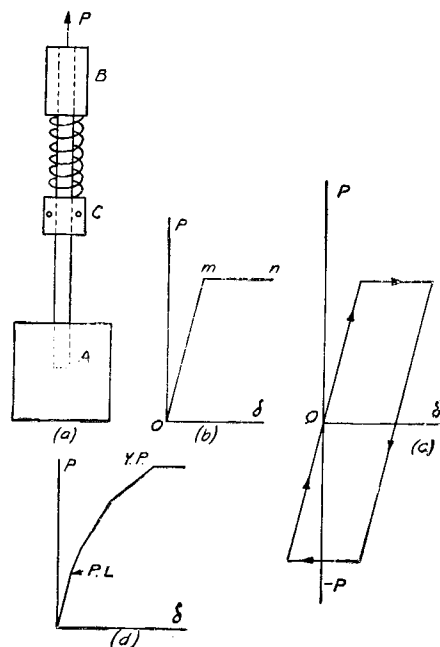


FIG. 273.

and the yield point, as in Fig. 273 $(d)$. By making the frictions equal, a diagram such as in Fig. 273 $(b)$ is obtained representing a well-defined yield point. If the friction of individual blocks $C$ differs, then they will begin to slide at different positions of $B$ and, after unloading, certain forces will remain in the springs, representing residual stresses produced by stretching multicrystalline specimens.

## 78. The Fatigue of Metals.[58]—Machine parts are very often subjected to varying stresses and it is very important to

[58] This subject is very completely discussed in the two recent books: "The Fatigue of Metals," by H. J. Gough, 1924, London; "The Fatigue

know the strength of materials under such conditions.[59] It is well known that, under repeated loading and unloading or reversed stresses, failure can be produced by stresses smaller than the ultimate strength of the material obtained in the static test and that the magnitude of these stresses required to produce failure decreases as the number of *cycles* of stresses increases. This phenomenon of the decreased resistance of a material to varying stresses is called *fatigue*, and the testing of a material by such stresses is called an *endurance test*.

If $\sigma_{max}$ and $\sigma_{min}$ are respectively the maximum and minimum values of the varying stress, then the algebraic difference

$$R = \sigma_{max} - \sigma_{min} \qquad (a)$$

is called the *range of stress*. The cycle is completely defined if the range and the maximum stress are given. The average stress is

$$\sigma_m = \tfrac{1}{2}(\sigma_{max} + \sigma_{min}). \qquad (b)$$

In the particular case of *reversed stress* $\sigma_{min} = -\sigma_{max}$, $R = 2\sigma_{max}$, $\sigma_m = 0$. Any cycle of varying stresses can be obtained by superposing a cycle of *reversed stress* on the steady average stress. The maximum and minimum values of the varying stress are then given by the following formulas:

$$\sigma_{max} = \sigma_m + \frac{R}{2}; \qquad \sigma_{min} = \sigma_m - \frac{R}{2}. \qquad (c)$$

There are various methods of applying the load in an endurance test. The specimen can be subjected to direct tension and compression, to bending, to torsion or to some combi-

of Metal," by H. F. Moore and J. B. Kommers, 1927, New York. Both these books contain a very complete bibliography on the subject. For additional information see the mimeographed lectures of H. J. Gough given at Mass. Inst. of Techn. during summer school, June 21 to July 16, 1937.

[59] J. O. Roos found from examination of a large number of fractures of machine parts that 80 per cent could be attributed to fatigue, Proc. Intern. Assoc. Testing Mat., 1912.

nation of these. The simplest way is by reversed bending.[60] A common cantilever form of fatigue test bar [61] is shown in Fig. 274. The cross section of the specimen is varied along the length in such a manner that the maximum stress occurs between cross sections $mn$ and $m_1n_1$ and is practically constant within that region. The effect of stress concentration is
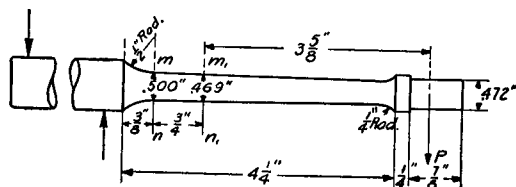


FIG. 274.

eliminated by using a large fillet radius and by increasing the diameter of the bar near the fillet. The load $P$ is always downward, while the specimen rotates. The stress therefore changes sign every half revolution and the number of cycles of stress is equal to the number of revolutions of the machine. The stress is a completely *reversed stress*, the average stress being zero and the range of stress twice $\sigma_{max}$. By taking several specimens and testing them at various loads $P$, a curve such as shown in Fig. 275 can be obtained. Here $\sigma_{max}$ is represented as a function of the number of cycles $n$ necessary to produce fracture. The curve shown was obtained with mild steel. At the beginning $\sigma_{max}$ decreases rapidly as $n$ increases but after 4–5 millions of cycles there is no longer any appreciable change in $\sigma_{max}$ and the curve approaches asymptotically the horizontal line $\sigma_{max} = 27,000$ lbs. per sq. in. The stress corresponding to such an asymptote is called the *endurance limit* of the material tested for *reversed stresses*. It

[60] There are evidences that the endurance limit obtained from bending tests coincides with that obtained by testing under direct stress. See paper by P. L. Irwin, Proc. Amer. Soc. Test. Mat., Vol. 25, 1925, and Vol. 26, 1926. A further discussion of this subject is given by R. D. France, Proc. Amer. Soc. Test. Mat., Vol. 31, 1931.

[61] See McAdam, Chemical and Met. Engr., 1921. The same type of specimen is used also by the Research Laboratory of the Westinghouse Elec. and Mfg. Co.

is now a usual practice in endurance tests to plot the curve $\sigma$ against $\log n$. In this manner a definite mark of discontinuity in the curve, defining the magnitude of the endurance limit, has been disclosed.

There is a great difference between the fractures of mild steel specimens tested statically and those tested by alternating
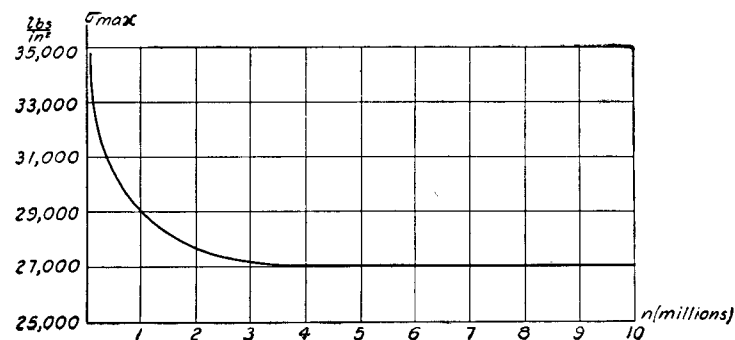


FIG. 275.

stresses. In the first case a considerable plastic flow precedes fracture, and the surfaces at the ruptured section show a silky, fibrous structure due to the great stretching of the crystals. A fatigue crack, however, looks entirely different. A crack starts at a certain place, due to a local defect in the material, or due to stress concentration produced by an abrupt change in the cross section. Once formed, it spreads due to stress concentration at its ends under the action of alternating stresses, and this spreading progresses until the cross section becomes so reduced that the remaining portion fractures suddenly under the load. Two zones can usually be distinguished in a fatigue fracture, one due to the gradual development of a crack and the other due to sudden fracture. The latter resembles the fracture of a tensile test specimen with a narrow deep groove (see p. 421) in which the form prevents sliding and fracture occurs as a result of overcoming the cohesive forces; this fracture is of the *brittle* type, such as occurs in cast iron, even if the material is ductile. In the case of cantilever test specimens

(Fig. 274)· the maximum stresses are at the outer fibers; the fatigue crack is usually started at the circumference and spreads towards the center. Where there is stress concentration due to fillets, grooves or holes, the crack usually starts at the most highly stressed portion and spreads from this point as a center; in such cases fracture reveals concentric rings with respect to this starting point. This is a very familiar type of fracture in machine parts which have been submitted to alternating stresses. It is thus evident that the "brittle" type of a fatigue fracture is due to the peculiar mechanism of fracture and not to "crystallization."

W. Fairbairn was the first to state, on the basis of experiments on a full size, wrought iron girder,[62] that there is a *limiting stress*, which can be applied safely an infinite number of times. Although it cannot be proved by direct test, all experimental evidence [63] supports the statement, now generally accepted, that for most metals there is a definite limiting range of stress which can be withstood for an infinite number of cycles without fracture.

It is of great practical importance to know how quickly the $\sigma$–$n$ curve approaches the asymptote as the number of cycles necessary to establish the endurance limit depends upon this. Experiments show that for ferrous metals the endurance limit can be established with sufficient accuracy on the basis of from 6 to 10 millions of cycles. In the case of non-ferrous metals a much larger number of cycles is needed.[64]

It is evident from the above discussion that the determination of the endurance limit for a definite material requires a considerable number of tests and considerable time; hence it would be of practical interest to establish relations between the endurance limit and other mechanical properties which can be determined by static tests. The large amount of experi-

[62] See W. Fairbairn, Phil. Trans. Roy. Soc., 1864.

[63] A large number of endurance test curves were analyzed by O. H. Basquin, Proc. Amer. Soc. for Test. Mat., Vol. 10, 1910.

[64] See H. F. Moore and J. B. Kommers, Bulletin No. 124, Eng. Expt. Stat., University of Illinois, U. S. A.

mental data accumulated has not made it possible to establish such a correlation.[65] As a rough estimate in the case of ferrous metals the endurance limit for reversal of stresses can be taken equal to from 0.40 to 0.55 ultimate strength obtained in the usual way from tensile tests. When we are working with materials belonging to a group, such as carbon steels, whose mechanical characteristics are very well known, such estimates can be considered reliable. Otherwise estimates of this type are likely to be misleading and recourse must be made to direct endurance test. Some results in endurance tests of certain steels are given in the table on pp. 497, 498.

In the majority of cases the arrangement of endurance tests is such that only the endurance limit for reversed stresses ($\sigma_{max} = -\sigma_{min}$) is determined, while in many cases in machine design we have varying stresses which are not completely reversed. It is necessary to know the endurance limits under these varying stresses. A. Wöhler was the first experimenter who studied the phenomenon of fatigue systematically.[66] He showed that the range of stresses $R$, necessary to produce fracture, decreases as the mean stress $\sigma_m$ increases. On the basis of these tests and of Bauschinger's work [67] W. Gerber proposed [68] a parabolic law relating the range of stress $R$ with the mean stress $\sigma_m$. This is illustrated by several parabolic curves in Fig. 276, in which the mean stress and the range of stress are expressed as fractions of the ultimate strength. The range is a maximum when the stress is completely reversed ($\sigma_m = 0$) and it approaches zero when the mean stress approaches the ultimate strength. If the endur-

[65] See book by H. J. Gough, loc. cit., p. 428. See also his lectures, loc. cit., p. 429.

[66] A. Wöhler, Zeitschrift für Bauwesen, Vols. 8, 10, 13, 16 and 20, 1860/70. An account of this work in English is given in Engineering, Vol. 11, 1871; see also Unwin's book, "The Testing of Materials of Construction," 3d ed., 1910.

[67] J. Bauschinger, Mitteilungen d. Mechanischtechnischen Laboratoriums in München, nr. 13 und 25.

[68] W. Gerber, Zeitschr. d. Bayerischen Arch.- und Ing.-Vereins, 1874. See also Unwin's book, "Elements of Machine Design," Vol. 1, Chap. 2.

ance limit for reversed stress and the ultimate strength are known, the endurance limit for any varying stress can be obtained from such curves. More recent investigations show that there is no fixed general law connecting the mean stress and the range of stress.[69]  For instance, there are materials[70] for which the straight lines indicated in dots in Fig. 276 represent the actual relation between $R$ and $\sigma_m$ better than parabolas. The straight lines $OA$ and $OB$ shown in Fig. 276 and having
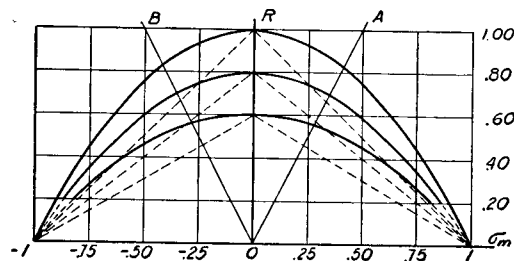


FIG. 276.

slope equal to 2 determine the region $AOB$ in which the stress changes sign during a cycle.  Outside of this region the stress always remains tension or compression.  Experimental results in the region $AOB$ usually lie between the parabolas and the corresponding straight lines.[71]  When the stress is always tension or always compression, the ranges $R$, obtained by tests, are sometimes not only below Gerber's parabolas but also below the corresponding straight lines.

All the results discussed up to now were obtained from tension-compression or from bending tests, in which cases we have a uniaxial stress condition.  In practical problems we very often encounter a combined stress condition, and it is important to know the endurance limit for such conditions.  The simplest

[69] An extensive discussion of this question is to be found in the book by H. J. Gough, loc. cit., p. 428.  See also his lectures, loc. cit., p. 429.

[70] See paper by B. P. Haigh, Journal Inst. Metals, Vol. 18, 1927.

[71] Some recent experiments with mild steel do not show that there is any appreciable influence of mean stress $\sigma_m$ on the magnitude of the range $R$.  See H. J. Gough lectures, loc. cit., p. 429.

case of this kind is pure shear, which we encounter in shafts under torsion.  A good many torsion fatigue tests have been made from which the endurance limit can be determined. These tests show that the ratio between the endurance limit in shear and that in tension-compression is not far from 0.50, being usually somewhat above this value.[72]

By combining reversed torsion with constant axial tension it was found[73] that the endurance limit in shear $\tau$ is obtained from the equation:

$$\frac{\tau^2}{\tau_e{}^2} + \frac{\sigma^2}{\sigma_{\mathrm{ult}}{}^2} = 1 \qquad (a)$$

in which $\tau_e$ is the endurance limit for the reversed torsion without axial tension, $\sigma$ is the applied axial tensile stress, and $\sigma_{\mathrm{ult}}$ is the ultimate strength of the material in tension.

The combination of reversed bending and reversed torsion acting in phase was investigated by H. J. Gough and H. V. Pollard.[74]  By varying the ratio of the maximum bending moment to the maximum torsion moment, it was found that in the case of mild carbon steel and of nickel-chromium steel the limiting values of the bending stress $\sigma$ and of the shearing stress are found from the equation:

$$\frac{\sigma^2}{\sigma_e{}^2} + \frac{\tau^2}{\tau_e{}^2} = 1, \qquad (b)$$

in which $\sigma_e$ is the endurance limit for bending and $\tau_e$ is the endurance limit for torsion.

In the case of brittle materials, such as cast iron, the same experiments showed that the fatigue action depends only on

[72] In the case of mild steel, W. Mason found this ratio equal to 0.50, Proc. Inst. Mech. Engrs., London, 1917, p. 121.  H. F. Moore and T. M. Jasper found the average value of this ratio equal to 0.56, Bulletin No. 136, Eng. Expt. Sta., University of Illinois.  McAdam found this ratio to vary between 0.55 and 0.68 over a wide range of materials, Proc. Amer. Soc. Test. Mat., Vol. 23, 1923.

[73] K. Hohenemser and W. Prager, "Metallwirtschaft," Vol. 12, p. 342, 1933; for the description of the machine used for this experiment see paper by E. Lehr and W. Prager in "Forschung," Vol. 4, 1933.

[74] The Institution of Mechanical Engineers, 1935 and 1936.

the magnitude of the maximum principal stress, and that the failure occurs when this maximum approaches the value of the endurance limit found from the usual rotating cantilever tests.

**79. Various Factors Affecting Endurance Limit.**—After a general discussion of the preceding article let us consider various factors which may affect the results obtained by endurance tests.

*Effect of cold work on the endurance limit.* In discussing stretching, drawing, and rolling of ductile metals at room temperature it was pointed out (see art. 74) that due to such cold work the material becomes stronger, the yield point is raised and the ultimate strength is somewhat increased. Hence we must expect that cold work will also affect the endurance limit of the material. The experiments made with steel specimens submitted to cold stretching [75] showed that a moderate degree of stretching produces some increase in the endurance limit. With a further increase in cold working a point may be reached at which some drop in the endurance limit may occur due to overworking.[76] A further improvement of a cold worked material can be obtained by submitting it, after cold work, to a mild heat treatment—say by leaving the material in boiling water for some time.

*Overstressing and understressing.* Experiments have been made in which cycles of stress above the endurance limit were applied a number of times before starting a normal endurance test. Such *overstressing* of specimens showed that there is a *limiting number* of cycles of overstress, depending on the magnitude of overstress, below which the endurance limit is

[75] H. F. Moore and J. B. Kommers, Bull. No. 124, Univ. of Illinois, Eng. Exper. Sta., 1921 and O. J. Horger, Trans. A. S. M. E., Vol. 57A, p. 128, 1935. In Moore's experiments carbon steel, 0.18 per cent C, and the stretching 8 per cent and 18 per cent were used. In Horger's experiments with carbon steel, 0.48 per cent C, the same 8 per cent and 18 per cent stretching were used.

[76] See H. F. Moore and T. M. Jasper, Bull. No. 136, Eng. Expt. Sta., Univ. of Illinois, and R. M. Brown, Trans. Inst. Engrs., Shipbuilders Scot., 1928.

not affected by overstress, but above which number of cycles the endurance limit was observed to decrease. By plotting the maximum stresses of the cycles of overstress against the limiting numbers of these cycles, a *damage curve* [77] for the tested material is obtained. The area below this curve defines all those degree- of overstressing which do not cause damage. The damage curve is of practical importance when we are dealing with a machine part normally working at cycles of stress below the endurance limit, but subjected from time to time to the cycles of overstress. If the magnitude of overstress is known, the safe number of cycles of overstress is readily obtained from the damage curve.[78]

By running an endurance test at a load just below the endurance limit and then increasing the load by small increments the endurance limit can be raised. This phenomenon is called the *understressing* effect. The amount by which the endurance limit can be raised in this way depends on the material.[79] For mild steel this amount is sometimes as high as 30 per cent of the original endurance limit, while Armco iron and copper remain practically unaffected by understressing.

*Frequency effect.* The effect of the frequency of the cycles in endurance tests has also been studied, but no appreciable effect was observed up to a frequency of 5,000 per minute. For higher frequencies some increase in the observed endurance limit with the frequency, was found. Very interesting experiments of this kind have been made by C. F. Jenkin.[80] Increasing the frequency up to over 1,000,000 cycles per minute he found at that high frequency an increase in the

[77] H. J. French, Trans. A. S. S. T., Vol. 21, p. 899, 1933, and H. W. Russell and W. A. Welcker, Proc. A. S. T. M., Vol. 36, 1936.

[78] B. F. Langer suggested a formula for calculating the number of cycles of overstress of various intensities which a machine part can withstand before failure. See "Journal of Applied Mechanics," Vol. 4, p. A-160, 1937.

[79] H. F. Moore and T. M. Jasper, Bull. No. 142, Univ. of Illinois, Eng. Expt. Sta., 1924; J. B. Kommers, Eng. News Record, 1932.

[80] C. F. Jenkin, Proc. Roy. Soc., Vol. 109A, 1925, p. 119 and C. F. Jenkin and G. D. Lehmann, Proc. Roy. Soc., Vol. 125A, 1929.

endurance limit of more than 30 per cent for such materials as Armco iron and aluminum. To obtain such high frequencies Jenkin used forced vibrations of small specimens. A rotating beam machine was used by G. N. Krouse [81] for high speed tests 30,000 cycles per minute. For aluminum and brass he found 8 per cent increase in endurance limit at this speed.

*Temperature effect.* In the previous discussion we were dealing with endurance tests made at room temperature; there are, however, cases when engineering structures and machine parts are submitted to the action of cycles of stresses at low temperature, as, for instance, in the case of aeroplanes, or at high temperature, as in steam turbines and internal combustion engines. Hence, endurance tests at low and at high temperatures are of practical importance. The comparative endurance tests made [82] at $+ 20°$ C. and $- 40°$ C. with Monel metal, stainless steel, nickel steel and chromium-molybdenum steel showed in all cases some increase in endurance limit with the decrease of temperature. Similar conclusions were also obtained for other materials.[83]

The endurance tests at *high temperatures* made with various kinds of steels on rotating beam machines [84] and also on reversed direct stress machines [85] all indicate that up to $300°$ C.–$400°$ C. there is no great effect of temperature on the endurance limit. The maximum endurance limit is usually obtained at $300°$ C.–$400°$ C., while at $100°$ C.–$200°$ C. the endurance limit is usually somewhat less than at room temperature. The experiments show also that the $\sigma$–$n$ curves do not approach their asymptotes so rapidly as at room temperature, and that more than $10^7$ cycles are required for determining the magnitude of the endurance limit.

[81] G. N. Krouse, Proc. A. S. T. M., Vol. 34, 1934.
[82] H. W. Russell and W. A. Welcker, Proc. A. S. T. M., Vol. 31, p. 122, 1931.
[83] W. D. Boone and H. B. Wishart, Proc. A. S. T. M., Vol. 35, 1935.
[84] H. F. Moore and T. M. Jasper, Bull. No. 152, Univ. of Illinois, Engr. Expt. Sta., 1925 and H. F. Moore, S. W. Lyon and N. P. Inglis, Bull. No. 164, Univ. of Illinois, Engr. Expt. Sta., 1927.
[85] H. J. Tapsell and J. Bradley, Journal Inst. Met., Vol. 35, 1926.

The phenomenon called *corrosion fatigue* is also of practical importance. This term is used to designate the simultaneous action of corrosion and fatigue. In 1917 Haigh [86] published the results of some very interesting endurance tests on brasses, in which he found some lowering of the endurance limit when the specimen under alternating stress was subjected to the action of salt water, ammonia, or hydrochloric acid. He pointed out also that the damaging effect of ammonia on brass was not produced unless the corrosive substance and the alternating stresses were applied simultaneously. Further progress in the investigation of *corrosion fatigue* was made by McAdam,[87] who investigated the combined effect of corrosion and fatigue on various metals and alloys. These tests proved that in most cases a severe corrosion prior to an endurance test is much less damaging than a slight corrosion which takes place simultaneously. Tests with carbon steels with various carbon contents and having endurance limits [88] in reversed stress varying from 20,000 lbs. per sq. in. to 40,000 lbs. per sq. in. showed that, if the specimens are subjected to the action of fresh water during the endurance tests, the endurance limits are greatly diminished and vary from 16,000 lbs. per sq. in. to 20,000 lbs. per sq. in. These lowered endurance limits are called *corrosion fatigue limits*. The tests showed that while for testing in air the endurance limit increases approximately in the same proportion as the ultimate strength of the steel the results obtained when testing in fresh water are quite different. The corrosion fatigue limit of steel having more than about 0.25 per cent carbon cannot be increased and may be decreased by heat treatment.[89] It was shown also that by adding enough chromium to increase the ordinary corrosion resistance of

[86] B. P. Haigh, Journal Institute of Metals, Vol. 18, 1917.
[87] D. J. McAdam, Proc. Amer. Soc. Test. Matls., Vol. 26, 1926; Trans. Amer. Soc. Steel Treating, Vol. 2, 1927; Proc. Amer. Soc. Test. Matls., Vol. 27, 1927; Proc. International Congress for Testing Materials, Vol. 1, 1928, p. 305, Amsterdam.
[88] Determined by tests in air.
[89] McAdam, Proc. International Congress at Amsterdam, Vol. 1, p. 308, 1928.

steel, the corrosion fatigue limit can be raised considerably above that for carbon or nickel steels.[90]

The endurance tests in an atmosphere of steam [91] showed that dry steam does not affect the endurance limit, but in the case of steam containing air or water a lowering of the endurance limit was observed. The experiments in vacuum [92] showed that the endurance limit of steel is about the same as that obtained from the tests in air, while experiments with copper and brass demonstrated an increase of endurance limit of no less than 14 per cent and 16 per cent respectively.

There are many known cases of failures in service which must be attributed to corrosion fatigue; they include failures of such parts as marine propeller shafts, water-cooled piston rods of marine oil engines, turbine blades, locomotive springs, pump rods in oil wells, boilers and super-heater tubes, and so on. In many cases corrosion-fatigue failures were eliminated by introducing corrosion-resisting materials. The McAdam experiments with corrosion-resisting steels showed that such steels give very satisfactory results in corrosion-fatigue tests. Recent experiments with special bronzes [93] showed that phosphor bronze and aluminum bronze, tested under extremely corrosive conditions, have a remarkable corrosion-fatigue resistance, which compares favorably with that of the best stainless steels.

Protective coatings [94] of parts subjected to corrosion-fatigue and surface cold work [95] were also successfully used in eliminating corrosion-fatigue failures.

[90] See McAdam, Trans. Am. Soc. Mech. Engrs., Applied Mech. Divis., 1928.

[91] See T. S. Fuller, Trans. Amer. Soc. Steel Treat., Vol. 19, 1931, p. 97.

[92] H. J. Gough and D. G. Sopwith, "Journal Inst. Metals," Vol. 49, p. 93, 1932.

[93] H. J. Gough and D. G. Sopwith, "Journal Inst. Met.," Vol. 60, p. 143, 1937.

[94] D. G. Sopwith and H. J. Gough, "Journal of the Iron and Steel Inst.," 1937.

[95] O. Föppl, O. Behrens und Th. Dusold, "Zeitschr. f. Metallkunde," Vol. 25, 1933.

*Effect of residual stresses.* During heat treatment of machine parts and during welding of structures, considerable residual stresses are usually produced, and the question arises what effect these stresses may have on the endurance limit. The experiments with quenched steel specimens tested in the rotating beam fatigue testing machine showed [96] that, due to application of cycles of reversed stresses, the initial residual stresses are reduced to less than one quarter of their initial value and that the effect of these stresses on the endurance limit is negligible. Similar conclusions were obtained also from fatigue tests of welded I-beams.[97]

The effect of *surface finish* on the endurance limit has also been studied. Tests were made on 0.49 per cent carbon steel with an ultimate strength of 95,000 lbs. per sq. in. and an ordinary endurance limit of 48,000 lbs. per sq. in. By taking 100 as the endurance limit for highly polished specimens, the following results were obtained for various finishes: [98] *ground finish* 89, *smooth-turned finish* 84, *rough-turned finish* 81. Tests with 0.02 per cent C steel (Armco iron) gave for the last two types of finish 92 and 88 respectively. Similar experiments were made with 0.33 per cent C steel by W. N. Thomas,[99] who measured the magnitude of the scratches in various finishes with a microscope; other experiments have been made by W. Zander.[100]

The tables on pages 497 and 498 give the results obtained in static and endurance tests of certain steels often used in engineering.

[96] See H. Bühler und H. Buchholtz, "Stahl u. Eisen," Vol. 53, p. 1330, 1933, and Mitteil. Forsch. Inst., Verein. Stahlwerke, Dortmund, Vol. 3, p. 235, 1933.

[97] E. H. Schulz und H. Buchholtz, "Stahl u. Eisen," Vol. 53, p. 545, 1933.

[98] See H. F. Moore and J. B. Kommers, Bulletin No. 124, loc. cit., p. 683.

[99] W. N. Thomas, Engineering, Vol. 116, 1923, p. 483. Recent development in investigating surface roughness is discussed in the paper by S. Way, see reference 111, p. 455.

[100] W. Zander, Dissertation, Technische Hochschule Braunschweig, 1928.

**80. Fatigue and Stress Concentration.**—In discussing stress concentration produced by sharp variation in the cross sections of bars or shafts (see Chapter VII), it was indicated that such stress concentration is especially damaging in the case of varying stresses.   In machines stress concentration is always present owing to fillets, grooves, holes, keyways, etc., in their parts, and experience shows that most of fatigue cracks start at points of stress concentration.   Several examples of such failures will now be briefly discussed.   Figure 277 repre-
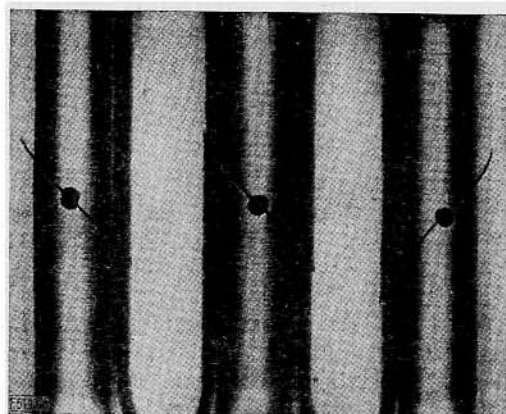


Fig. 277.

sents [101] fatigue failures of circular shafts with transverse circular holes subjected to the action of reversed torsion. The maximum stress in such a case occurs at the ends of the diameters of the hole inclined 45 degrees to the axis of the shaft (see p. 317).   At these points the cracks start and gradually develop along a helical path following the direction of one of the principal stresses.   Figure 278 represents the torsional fatigue failure of a shaft of a large motor-generator set which unfortunately operated near resonance.[102]   The

---

[101] See paper by A. Thum, "Forschung," Vol. 9, p. 57, 1938.

[102] This figure and the following three are taken from the paper by R. E. Peterson presented at a conference on "Strength of Materials Problems in Industry," Mass. Inst. Techn., July, 1937.   The mechanism of cracks growth is discussed in the paper by R. E. Peterson, Journal of Appl. Mech., Vol. 1, p. 157, 1933.

crack started at the keyway, where a high stress concentration takes place, and gradually developed along the helical path.
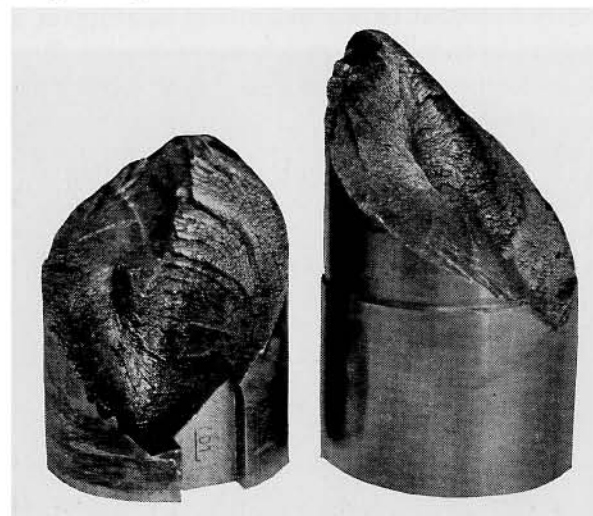


Fig. 278.

The helical crack corresponding to the direction of the second principal stress can also be seen on the photograph.   Figure 279 represents torsion failure of a shaft of a Diesel driven generator.   A high stress concentration at the small radius
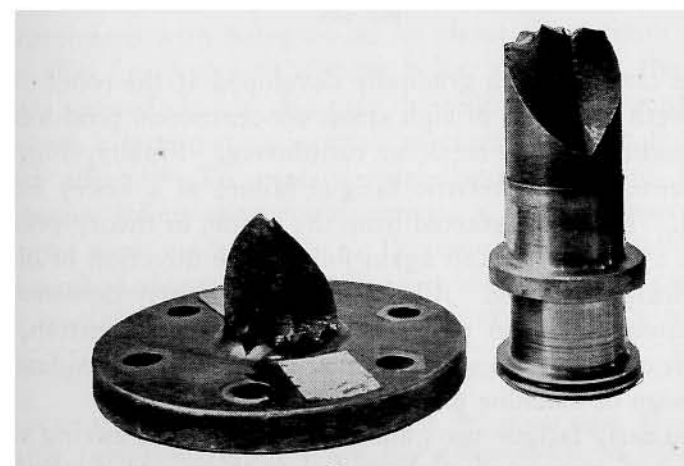


Fig. 279.

fillet resulted in several helical cracks, which, joined together, produce a saw-tooth appearance. In Fig. 280 are shown the
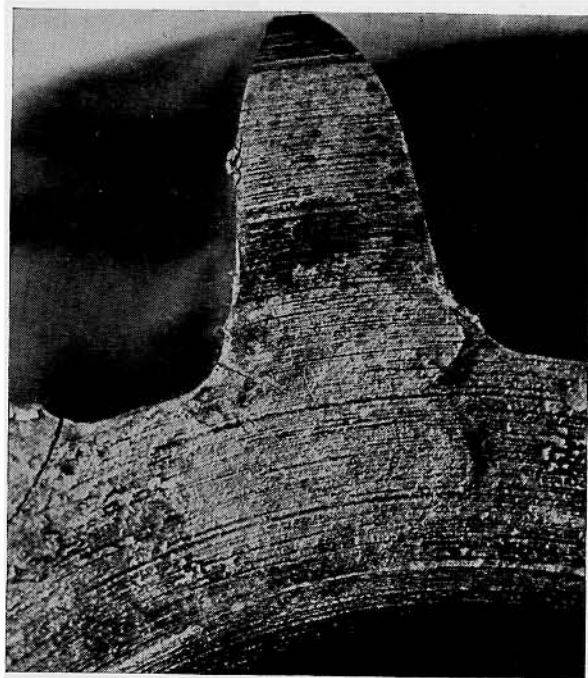


FIG. 280.

fatigue cracks, which gradually developed at the roots of the gear teeth at points of high stress concentration produced by the bending of the teeth as cantilevers. Finally, Fig. 281 represents a characteristic fatigue failure of a heavy helical spring. The crack started from the inside, as theory predicts (see p. 272, Part I), and again follows the direction of one of the principal stresses. All these pictures clearly demonstrate the damaging action produced by stress concentration, and make it clear that this factor must be seriously considered in the design of machine parts.

The early fatigue tests made with specimens having sharp changes of cross section showed that there was a reduction

in strength due to stress concentration, but this reduction was usually found to be much smaller than would be expected from the magnitude of the calculated factor of stress concentration. For instance, in the case of flat steel specimens with small circular holes subjected to direct stress the theoretical factor of stress concentration is equal to three (see p. 313),
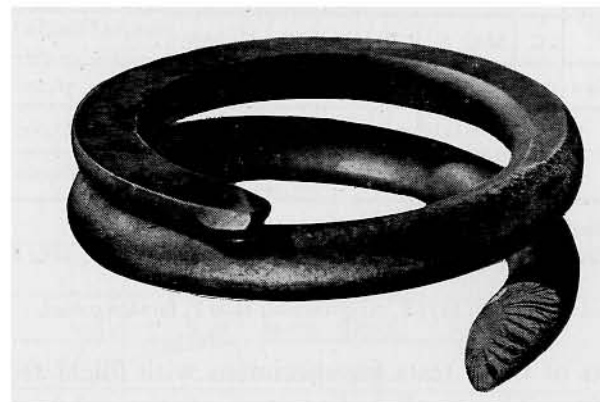


FIG. 281.

and if the magnitude of the peak stress is the controlling factor in endurance tests, it would be expected that the tension-compression load required to produce fatigue failure of specimens with holes would be about three times smaller than that for specimens without holes. However, the experiments showed that in this case the reduction in strength due to stress concentration is small as compared with the calculated effect.[103] To explain this discrepancy and to give necessary information for designers, a very extensive series of tests were made by R. E. Peterson at the Westinghouse Research Laboratories.[104] Geometrically similar cantilever test specimens varying in diameter from 0.1 in. to 3 in. with a

[103] B. P. Haigh and J. S. Wilson, "Engineering," Vol. 115, p. 446, 1923.
[104] R. E. Peterson, Trans. A. S. M. E., "Journal Appl. Mech.," Vol. I, p. 79, 1933, Vol. 1, p. 157, and R. E. Peterson and A. M. Wahl, Trans. A. S. M. E., Journal Appl. Mech., Vol. 3, p. 15, 1936.

fillet or with a transverse circular hole and of different materials, as given in the table below, were tested in special fatigue testing machines.[105]

TABLE OF MATERIALS USED IN TESTS

| Steel | Chemical Composition | | | | | | | | Y.P. lbs./in.² | Ult. lbs./in.² | Elong. per cent |
|---|---|---|---|---|---|---|---|---|---|---|---|
| | C | Mn | Si | S | P | Ni | Cr | Mo | | | |
| Medium[1] carbon | 0.45 | 0.79 | 0.18 | 0.03 | 0.013 | — | — | — | 32,500 | 76,000 | 32 |
| Ni-Mo[2] | 0.52 | 0.68 | 0.19 | — | 0.014 | 2.96 | — | 0.38 | 45,500 | 97,000 | 26 |
| Ni-Cr[3] | 0.54 | 0.65 | — | — | — | 1.38 | 0.64 | — | 91,000 | 120,000 | 24 |

[1] Normalized: 1560 F, air cooled.

[2] Normalized and drawn: 1750 F, air cooled; 1460 F, air cooled; 1160 F, furnace cooled.

[3] Quenched and drawn: 1475 F, oil quenched; 1200 F, furnace cooled.

The results of these tests for specimens with fillets are given in Fig. 282. The smaller diameters of the specimens are taken as abscissae while the ordinates represent the ratios $k_f$ of the endurance test loads for plain specimens to the endurance test loads found for the corresponding test specimens with stress concentration. Similar results were also obtained for specimens with transverse holes. The horizontal lines in Fig. 282 give the values of the factors of stress concentration obtained for each proportion of the fillet by a direct measurement of strain at the points of maximum stress concentration (see p. 341). These values are designated by $k_t$ and are called *theoretical values* of stress concentration in the following discussion. If the fatigue strength of the specimens depends only on the peak stress, $k_t$ must evidently be equal to $k_f$.

On a basis of his tests, R. E. Peterson came to the following conclusions:

(a) *In some cases fatigue results are quite close to theoretical stress concentration values.* This conclusion is of great prac-

---

[105] The description of these machines is given in the paper by R. E. Peterson, Proc. Am. Soc. Test. Mat., Vol. 29, p. 371, 1929.

tical importance, since a general idea seems to exist, based on some early experiments, that fatigue data for stress-concentration cases are always well below theoretical values, i.e., on the safe side for design purposes.
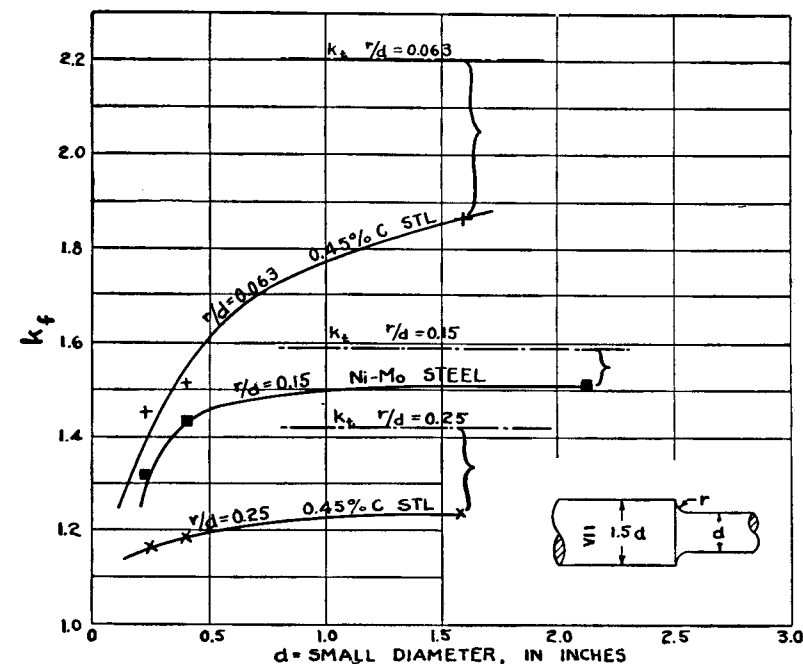


FIG. 282.

(b) *Fatigue results for alloy steels and quenched carbon steels are usually closer to theoretical values than are the corresponding fatigue results for carbon steels not quenched.* It was expected in these tests that theoretical values $k_t$ would be reached for all steels provided specimens were made large enough, but Fig. 282 shows that the fatigue-data curves for normalized 0.45 per cent carbon steel are apparently asymptotic to values considerably below the theoretical.

(c) *With a decrease in the size of specimen the reduction in fatigue strength due to a fillet or hole becomes somewhat less; and for very small fillets or holes the reduction in fatigue strength is*

*comparatively small.* This can be clearly seen from the curves in Fig. 282.

Another way of presenting fatigue test results showing the extent to which theoretical values $k_t$ of stress concentration are reached, is obtained by introducing the quantity

$$q = \frac{k_f - 1}{k_t - 1}, \qquad (a)$$

which is sometimes called the *sensitivity index*. As $k_f$ approaches the value $k_t$, the value of $q$ approaches unity, and when the stress concentration has only a small effect on fatigue strength, $k_f$ is close to unity, and $q$ approaches zero. By using the experimental data given in Fig. 282 and by plotting the values of $q$ against the diameter magnitudes $d$, the curves shown in Fig. 283 are obtained. It is seen that the sensitivity
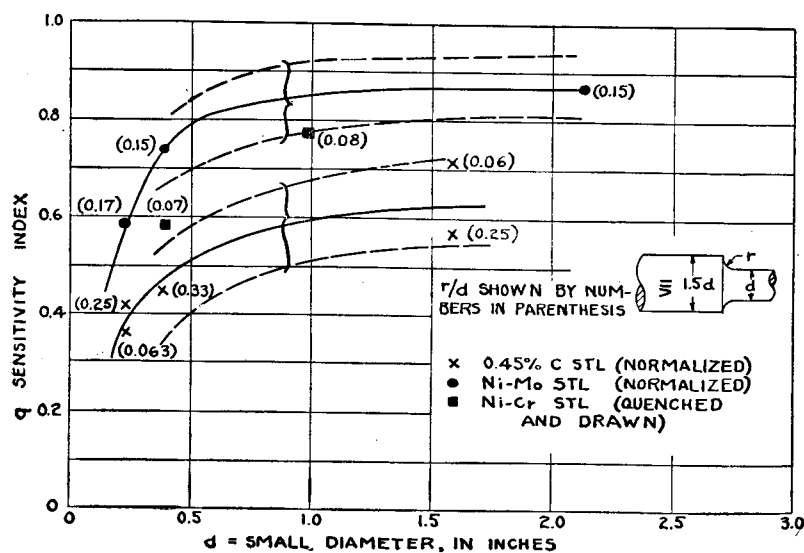


FIG. 283.

index is not a constant. It depends not only on the kind of material but also on the size of specimens. In the case of alloy steels and for larger specimens $q$ approaches the value

of unity, while for a coarser material, 0.45 per cent carbon steel, it approximates a somewhat lower value.[106] Similar curves were also obtained for the specimens with transverse holes.

On the basis of the above discussion the use of the theoretical value $k_t$ of stress concentration can be recommended in the design of larger size machine parts and in the case of the finer-grained steels, such as alloy steels and heat-treated carbon steels. In the cases of smaller dimensions and coarser materials the reduced values of the stress concentration factor which, from equation $(a)$, are

$$k_f = q(k_t - 1) + 1$$

can be used. The values of $q$, obtained experimentally for fillets and holes and represented for the case of fillets by the full lines in Fig. 283, can be used as a guide in selecting the proper values of $k_f$ in other cases of stress concentration.

To explain the "size effect" in fatigue tests it is necessary to consider grain size of crystalline materials. When we speak of geometrically similar specimens of the same material, their metallographical structure obviously is not geometrically similar, and that fact may affect the fatigue tests. If we consider a region of peak stress, a different result would be expected when only few grains are contained in that region than if many thousands are contained in the same region. The relationship between the sensitivity index $q$ obtained from fatigue tests and the grain size of the materials used is discussed in a recent paper by R. E. Peterson.[107]

It can be appreciated that the problem of reducing the damaging effect of stress concentration is of primary importance to designers. Some lowering of stress concentration can be obtained by a proper change in design. For instance,

[106] Tests of cast iron have shown very small effect of stress concentration on fatigue tests results. A. Thum and H. Ude, Zeitschr. V. D. I., Vol. 74, p. 257, 1930.

[107] See Stephen Timoshenko Anniversary Volume, p. 179, 1938.

the design can be considerably improved by eliminating sharp reentrant corners and introducing fillets of a generous radius, by designing fillets of a proper shape, by introducing relieving grooves, etc. But all these measures are sometimes not sufficient to eliminate fatigue failures. As an important example of this kind let us consider the typical failures which occur at the wheel seat of locomotive and railroad-car axles, at the wheel or bearing seats of automobile axles, at the pressed or fitted bits of long drill rods in oil-well operations, etc. All these cases of fitted members subjected to the action of variable stresses have been a constant source of fatigue failures. Considering, for example, the case of a wheel-hub pressed on the axle, Fig. 284, $a$, we can see that a high stress
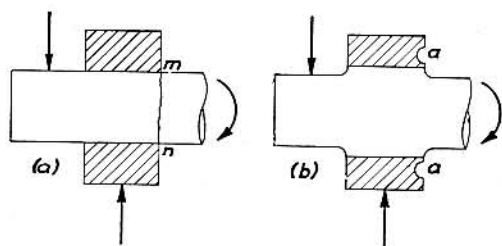


FIG. 284.

concentration is produced at the reentrant corners $m$ and $n$. During rolling of the axle the reversal of stress at points $m$ and $n$ takes place, and finally a fatigue failure over the cross section $mn$, such as shown in Fig. 285, may occur. Stress concentration can be somewhat reduced by introducing raised seats and fillets as shown in Fig. 284, $b$. A further improvement is obtained by introducing the relief groove $a$, Fig. 284, $b$. Although such changes are in the right direction, they are not sufficient in this case. Experience shows that the mere press-fit of a hub on an axle, Fig. 284, $a$, reduces the fatigue strength of the axle to less than half of its initial strength, while the changes shown in Fig. 284, $b$, raise the fatigue strength of the axle perhaps no more than 20 per cent.

To improve the condition and eliminate fatigue failures, the surface cold-rolling of the axle in the region of stress concentration has been successfully applied. The early experiments [108] with surface cold work were made on small
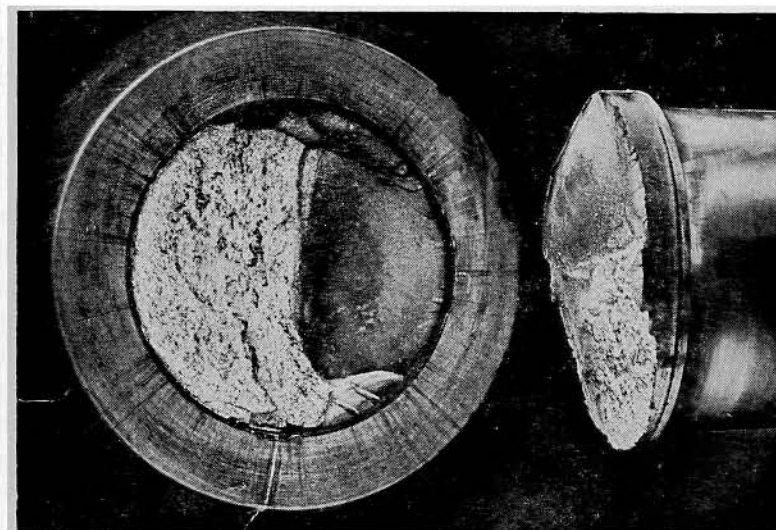


FIG. 285.

specimens, and to get sufficient information for practical application, an extensive series of laboratory tests with larger specimens were made. Three types of fatigue tests made by O. J. Horger at the laboratory of the University of Michigan [109]

[108] The improvement of fatigue strength by surface cold-working was introduced by O. Föppl, "Stahl u. Eisen," Vol. 49, p. 575, 1929. It was applied in various fatigue tests at the Wöhler-Institut. See Mitteilungen d. Wöhler-Instituts, Vol. 1 to Vol. 37, 1929–1940. See also A. Thum und F. Wunderlich, Mitteilungen d. Materialprüfungsanstalt, Techn. Hochsch. Darmstadt, Vol. 5, 1934, and R. Kühnel, "Stahl u. Eisen," Vol. 110, p. 39, 1932.
[109] The description of these experiments is given in the papers by O. J. Horger, Journal of Appl. Mech., Vol. 2, p. 128A, 1935; and O. J. Horger and J. L. Maulbetsch, Journal of Appl. Mech., Vol. 3, p. 91A, 1936. The work done at the Westinghouse Research Laboratories is described in the paper by R. E. Peterson and A. M. Wahl, Journal of Appl. Mech., Vol. 2, 1935, p. 1A.
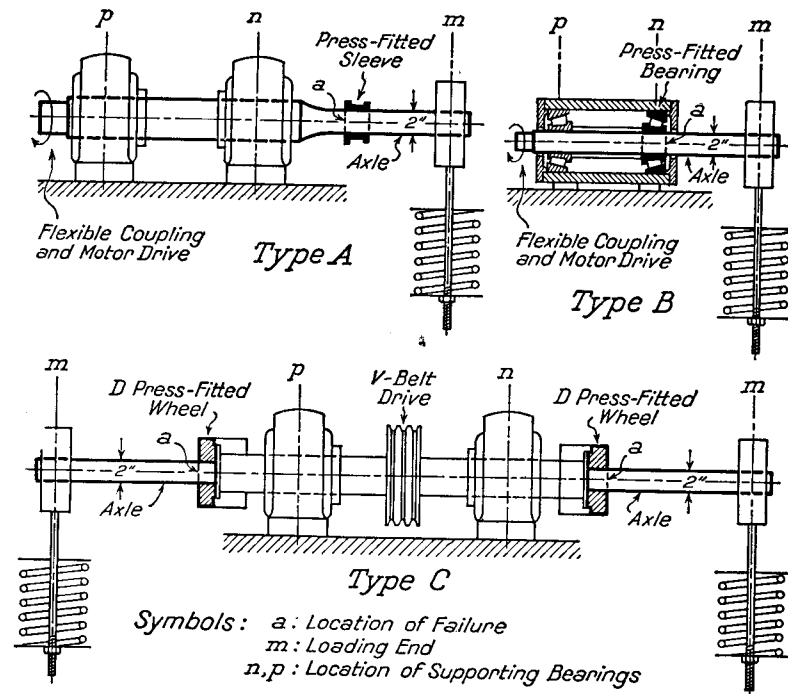
FIG. 286.

are shown in Fig. 286. The properties of the materials used in these tests are listed in the table below.

MATERIALS USED FOR TESTS IN FIG. 286

| Steel | Chemical Composition | | | | | | | Y.P. | Ult. | Elong. per cent |
|---|---|---|---|---|---|---|---|---|---|---|
| | C | Mn | P | S | Si | Cr | Ni | lbs./in.² | lbs./in.² | |
| S.A.E.[1] 1045 | 0.47 | 0.72 | 0.015 | 0.034 | 0.23 | 0.03 | 0.05 | 47,800 | 88,800 | 32 |
| 2.75 per cent[2] Nickel | 0.24 | 0.86 | 0.034 | 0.021 | 0.24 | — | 2.79 | 86,300 | 111,000 | 23 |

[1] Normalized 1620 F and Drawn 1115 F.
[2] Quenched 1475 F and Tempered 1150 F.

The endurance limits obtained for S.A.E. and for Ni steel from the usual cantilever beam fatigue tests are 34,000 lbs.

per sq. in. and 48,000 lbs. per sq. in. respectively. After pressing on the sleeve, as in tests type A, Fig. 286, the endurance limit of S.A.E. steel was reduced to 15,000 lbs. per sq. in. In tests of types B and C the endurance limits were found to be 12,000 lbs. per sq. in. and 14,000 lbs. per sq. in. respectively. This indicates that owing to press-fit the fatigue strength of specimens was diminished to less than one-half of its initial value. Similar results were also obtained for Ni steel specimens. To improve the fatigue strength the surface
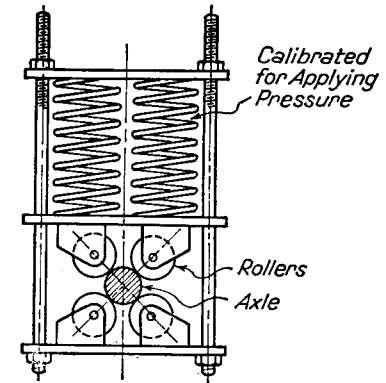


FIG. 287.

of the rest of the specimens was cold-rolled before pressing on the sleeves or hubs by using the device shown in Fig. 287. A lathe was adapted for this rolling operation by supporting the specimen in lathe centers and the rolling device in a transverse slide fixed to the lathe carriage. To secure a
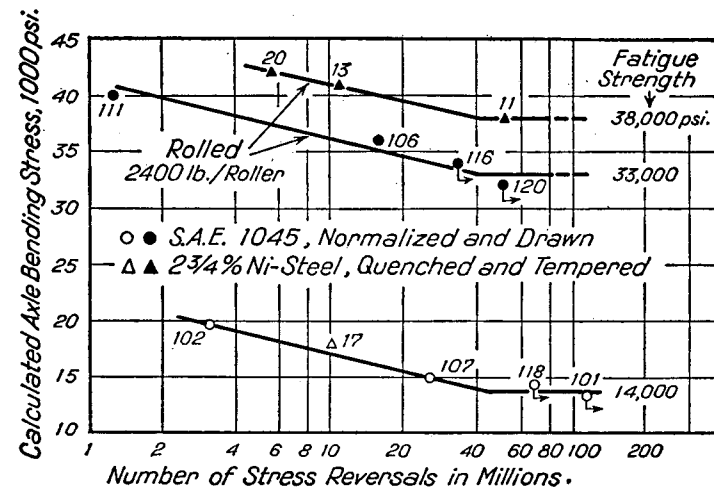


FIG. 288.

sufficiently smooth surface after rolling, the feeds giving more than 40 threads per inch were used.

The results of fatigue tests of Type $C$, Fig. 286, made with cold-rolled specimens, are shown in Fig. 288. It is seen from these tests that the fatigue strength of S.A.E. steel specimens increased, due to cold rolling, to a value more than twice their initial strength. Similar results were also obtained with Ni steel specimens.
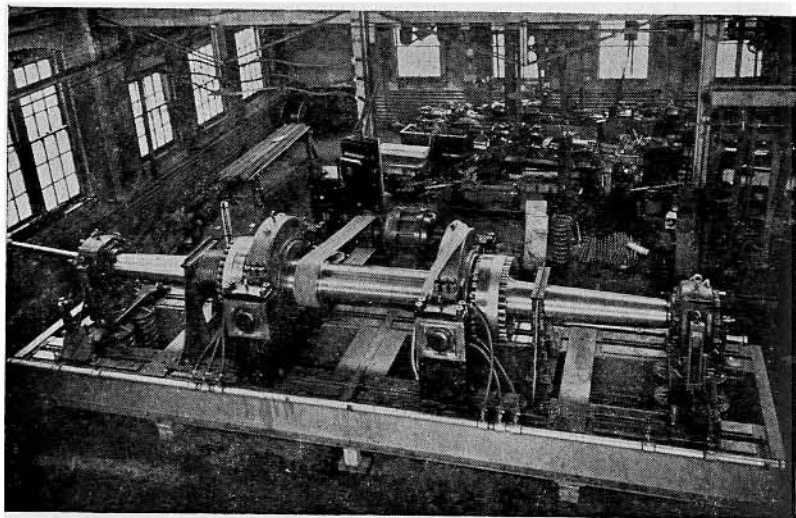


FIG. 289.

A further step in the investigation of the effect of cold-rolling on fatigue strength was made by building special large fatigue-testing machines, in which full size locomotive axles can be tested. Figure 289 represents one of these machines.[110] The arrangement is similar to that used in type $C$ tests in Fig. 286, and is the same as was used by Wöhler in his famous fatigue tests of axles.

Another case of fatigue failure under the action of highly concentrated stresses is represented by the *surface failure* of

[110] Three machines of this kind are working at present in the research laboratory of the Timken Roller Bearing Company, Canton, Ohio. Figure 285 is taken from these tests.

rollers and gears under the repeated action of contact pressures during rotation. Considering two rotating rollers pressed together by the forces $P$, Fig. 290, we can calculate the maximum compressive stress at the surface of contact by using the formulas of art. 66. In the case of an ideally smooth surface this calculated stress is the true stress, and the surface fatigue strength of rollers of a given material will depend only on the magnitude of this stress. In actual cases the roller surface has various kinds of unevenness, the magnitudes of which depend on the kind of surface finish. Several examples of surface finish are shown [111] in magnified form in Fig. 291. Naturally the surface roughness will affect the pressure distribution at the surface of contact of the rollers in Fig. 290,



FIG. 290.
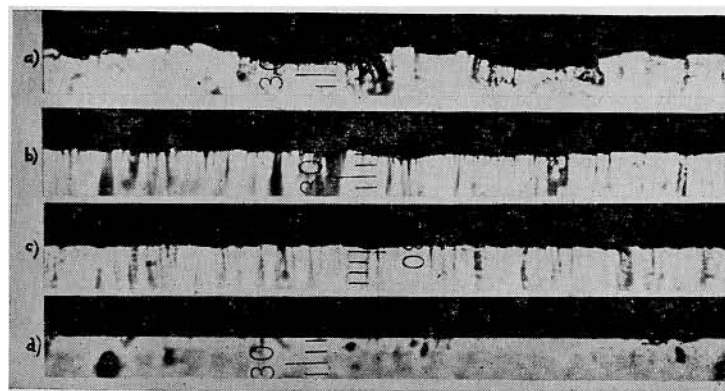


FIG. 291.

and as a result of local overstressing at the points of the most unfavorable irregularities fatigue cracks will start earlier than

[111] This picture and the two following are taken from the paper by S. Way presented at the meeting of the American Gear Manufacturers Association, May, 1940. Various methods of investigation of surface finish are described in the S. Way paper published in the "Proceedings of the Special Summer Conferences on Friction and Surface Finish," Mass. Inst. Techn., June 1940. In this paper a complete bibliography of the subject is given.

in the case of smooth rollers. This indicates that the fatigue strength of rollers depends on the degree of roughness of their surface.

Experiments show that if the surface fatigue tests are made with lubricated rollers, surface fatigue cracks grow to *pits*. *Pitting cracks*, which sometimes develop in rollers and gears under service conditions, are very undesirable, and



Fig. 292.

considerable efforts were extended in studying the causes of pitting.[112] These investigations showed that the causes of growth of pitting cracks are of a hydrodynamical nature. The pitting cracks assume a direction that slopes obliquely into the metal; they are roughly in the form of a conical surface

[112] Such investigations were made at Westinghouse Research Laboratories by S. Way; see his paper in Journal of Applied Mech., Vol. 2, 1935.

so that they meet the surface in a curve in the form of a parabola, or $V$, with the vertex of the $V$ being the part that during rotation is run over first. In Fig. 292, representing the magnified photograph of a roller surface, the starting point of a pit crack is shown by an arrow. It is seen that any oil that enters such a crack will tend to be trapped as the crack passes under the loaded region. A high oil pressure in a crack will produce high tensile stresses at the end of the crack and the crack may be driven further into the metal. This theory explains why oil is necessary for pitting crack growth and why changing the direction of rotation or relief of oil pressure in the crack stops crack growth.

To obtain comparative values of pitting resistance of various materials, the fatigue tests were made [113] with pairs of rollers, Fig. 290, one of each pair being 1.576 in. in diameter, the other being 1.500 in. in diameter, and the width of the test surface being 0.500 in. All rollers had a finely ground surface on which the maximum depth of irregularities was between 0.0001 in. and 0.00018 in. The speed of rotation was between 300 and 500 r.p.m., with lubrication by an oil bath of a machine oil of viscosity 700–900 seconds Saybolt at the operating temperature. The maximum compressive stress, given by equation (295), p. 359, and calculated for compressive load just sufficient to cause at least one pit per square inch of test surface in 10 million cycles was defined as the *pitting limit* of the material. The results of these tests for the case of 0.45 per cent carbon steel and for various heat treatments are represented in Fig. 293 by the curve $B$. The hardness numbers [114] of the tested rollers are taken as the abscissas, and the corresponding pitting limits make up the ordinates. For comparison, a straight line giving for the pitting limit the values 324 times the hardness number is also shown. Since pitting is a fatigue failure, we would expect the pitting strength to increase proportionally to hardness.

[113] See S. Way paper, reference 103.
[114] The hardness numbers can be considered proportional to the ultimate strength of the surface layer of the roller's material.

The experiments showed that the assumption of a linear relationship between pitting strength and hardness is on the side of conservatism.

The curve $A$ in Fig. 293 gives the values of the pitting limits found from the experiments with gears made of the

**COMPARISON OF APPROXIMATE PITTING RESISTANCE OF GEARS AND ROLLERS**

CURVE A – COMPRESSIVE STRESS ON GEAR TEETH JUST BELOW PITCH POINT (CALCULATED ASSUMING SMOOTH TEETH WITH NO PROFILE ERRORS BUT TAKING ACCOUNT OF LEAD ERRORS AND MISALLIGNMENT) SUFFICIENT TO CAUSE ABOUT SIX PITS, OR ONE PIT PER SQ. IN. OF AREA BETWEEN PITCH LINE AND END OF ONE TOOTH CONTACT.- GROUND TEETH -$10^7$ GEAR REVS.

CURVE B – COMPRESSIVE STRESS ON TEST ROLLERS (1.500" 1.576" DIAMS.) WITH GROUND SURFACES SUFFICIENT TO CAUSE ONE PIT PER UNIT AREA IN $10^7$ CYCLES.



FIG. 293.

same material as the previously discussed rollers. The conditions at the surface of contact of gear teeth are somewhat different from those we had in rollers, the principal difference being the fact that rolling is associated with sliding. This difference of conditions results, as we see, in some increase of the pitting limit.

**81. Causes of Fatigue.**—Although a great amount of data concerning strength in fatigue has been accumulated, up to now no fundamental theory has been established to explain the cause and the mechanism of the phenomena. A fatigue fracture was formerly attributed to "crystallization" of the metal, making it brittle. Such a theory was advanced on the basis of the appearance of the fracture (see p. 432).

We now know that the individual crystals remain unchanged during an endurance test except that there may be some "slipping" within these crystals.

Bauschinger was the first to start investigation of cycles of stress. He loaded and unloaded the specimens slowly and used sensitive extensometers to establish the stress-strain relation under these conditions.[115] In this manner he showed that the *proportional limits* in tension and compression are not fixed points for a given material and that they may be displaced by submitting a specimen to cycles of stress. To explain the fact that the endurance limit for steel under reversed stress is sometimes lower than the proportional limit obtained from static tests, Bauschinger advanced the theory that the material as received from the manufacturer may have its proportional limits in tension and compression raised by cold work and that the true or *natural proportional limits* are those which are established after submitting the material to cycles of stress; these natural proportional limits are supposed to define the *safe range* in fatigue tests.

This idea of Bauschinger was developed further by Bairstow.[116] Using a slow loading and unloading machine (2 cycles per minute), with a Martens mirror extensometer fixed on the specimen, he obtained the stress-strain relation for cycles with various ranges of stresses. Figure 294 represents some of Bairstow's results obtained with axle steel (yield point 50,000 lbs. per sq. in. and ultimate strength 84,000 lbs. per sq. in.) under reversed stress (mean stress equal to zero). The line $A$ represents the initial tension-compression test with

[115] J. Bauschinger, loc. cit., p. 409.
[116] L. Bairstow, Phil. Trans. Roy. Soc., Vol. 210A, p. 35, 1911, London.

the range 31,400 lbs. per sq. in.; within these limits the stress-strain relation evidently follows accurately the straight line law.[117]   After this the specimen was subjected to cycles of reversed stresses of 31,400 and it was observed that the initial straight line *A* develops gradually into a loop of definite shape.   This loop as obtained after 18,750 cycles is repre-
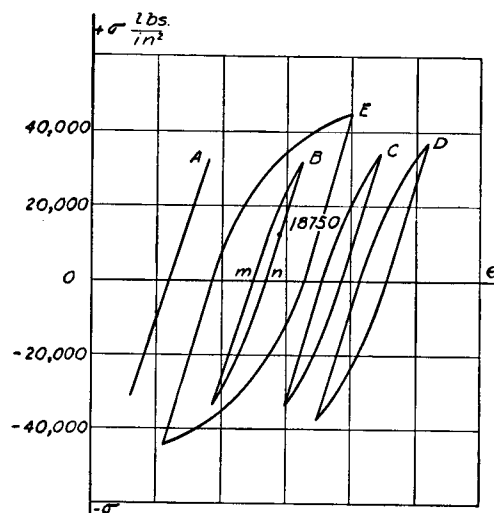


FIG. 294.

sented by the curve *B*.   It can be seen that in this case the *initial* proportional limits were higher than the so-called *natural* proportional limits shown after many cycles of reversed stress.   Since these limits are below the 31,400 lbs. per sq. in., a *cyclical permanent set* equal to the width *mn* was produced.   The loops *C*, *D*, and *E* were obtained after a number of cycles of reversed stress equal to 33,500, 37,500 and 47,000 lbs. per sq. in. respectively sufficient apparently to stabilize the size of the loops.   When the width of these loops was plotted against the corresponding maximum stress, Bairstow found that the results of his experiments gave

---

[117] The gage length in these tests was only 0.5 in. and the small "elastic hysteresis" could not be detected by Martens extensometers.

approximately a straight line.   The intersection of this line with the stress axis determines the range of stress at which there is no looping effect.   The range of stress defined in this manner was assumed by Bairstow to be the *safe range of stress*, and subsequent endurance tests have verified this assumption with sufficient accuracy.   Since then various methods for the rapid determination of fatigue ranges on this basis have been developed.[118]

This measurement of hysteresis loops suggested by Bairstow to determine the safe range of stresses can be replaced by calorimetric measurements.   The area of the loop represents the energy dissipated per cycle.   It is transformed into heat, and the quantity of this can be measured.   The first experiments of this kind were made by Hopkinson and Williams,[119] who showed that the areas of the loops as determined by calorimetric methods agree within 6 per cent with the area determined by extensometer measurements.   In these tests it was shown also that it is possible to have a certain amount of hysteresis which will never cause destruction, and this can be considered as the true "elastic hysteresis."   Some short-time methods for determining endurance limits have also been developed on the basis of these calorimetric measurements.

The first attempt to explain the mechanism of fracture in endurance tests was made by Ewing and Humfrey.[120]   They used a rotating specimen of Swedish iron with a polished surface and examined this surface with a metallurgical microscope after applying cycles of reversed stress.   They found that, if stresses above a certain limit were applied, *slip bands* appeared on the surface of some of the crystals after a number of cycles.   As the cycles were repeated the number of slip bands increased and some of the previous slip bands

---

[118] See book by H. J. Gough, Chapter 10, loc. cit., p. 428.  See also E. Lehr, Die Abkürzungsverfahren, Dissertation, Stuttgart, 1925.

[119] B. Hopkinson and G. T. Williams, Proc. Roy. Soc. (A), Vol. 87, 1912.

[120] J. A. Ewing and J. C. W. Humfrey, Phil. Trans. Roy. Soc. (A), Vol. 200, 1903, p. 241.

seemed to broaden out. This broadening process continued till finally cracking occurred, the crack following the marking of the broadened slip bands. They found that a reversed stress of 11,800 lbs. per sq. in. could be applied millions of times without producing any slip bands. A stress of 15,400 lbs. per sq. in. produced only one isolated slip band in the region examined after three million cycles and this line was confined to the middle portion of the crystal. From these tests it was concluded that 15,400 lbs. per sq. in. was the endurance limit for Swedish iron. On the basis of such investigations the theory was advanced that cycles of stress, which are above the safe range, produce slip bands in individual crystals; if we continue to apply such cycles of stress there is a continual sliding along the surfaces accompanied by friction, similar to that between sliding surfaces of rigid bodies. As a result of this friction, according to the theory the material gradually wears along the surfaces of sliding and a crack results.

Further investigation in this direction [121] showed that slip bands may occur at stresses which are much lower than the endurance limit of the material. They may develop and broaden, as was observed by Ewing and Humfrey, without leading to the formation of a crack. This shows that the appearance of slip bands cannot be taken as a basis for determining the endurance limit and cannot explain the mechanism of fatigue cracks. It seems probable that more light will be brought on the causes of fatigue by testing single crystal specimens and by going into the study of the molecular structure of crystals.[122]

## 82. Mechanical Properties of Metals at High Temperatures.

There are many cases in which parts of engineering structures are submitted simultaneously to the action of stresses and of high temperatures. Such conditions are found for instance in power plants and chemical industries. Due to the modern tendency to increase the initial temperature of

---

[121] H. J. Gough and D. Hanson, Proc. Roy. Soc. (A), Vol. 104, 1923.
[122] See H. J. Gough, Phil. Trans. Roy. Soc., Vol. 226, 1926.

steam [123] in power plants, the question of the strength of materials at high temperature has become of practical importance, and a considerable amount of research work has
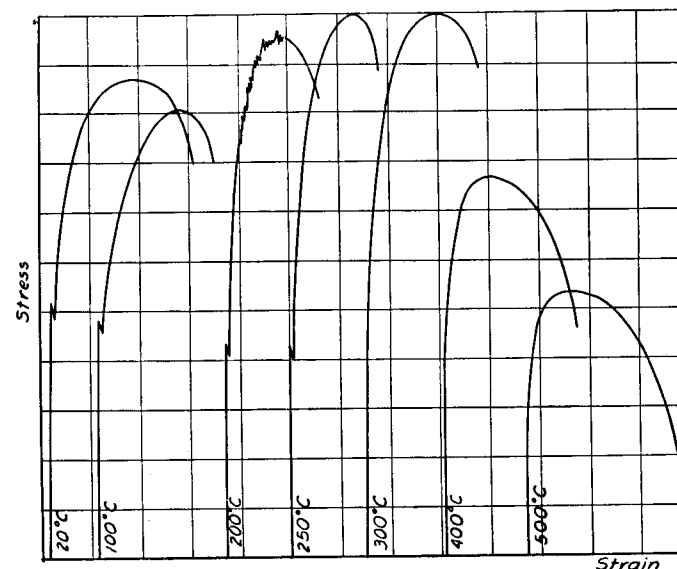


Fig. 295.

been done in this field.[124] Experiments show that the yield point and ultimate strength of metals in tension depend very much on the temperature. Several tensile test diagrams for medium carbon steel at different temperatures are shown in Fig. 295.[125] Up to about 250° Centigrade the ultimate

---

[123] Mellanby and Kerr, Proc. Inst. Mech. Engr., London, 1927; Guy, H. L., Proc. Inst. Mech. Engr., 1929, and The Engineer, Vol. 147, 1929, p. 136.

[124] A bibliography on this research work can be found in the "Symposium on effect of temperature on the properties of metals," Proc. Amer. Soc. Test. Matls., Vol. 24, 1924. See also paper by H. J. French, H. C. Cross and A. A. Peterson, Technologic Papers of the Bureau of Standards, No. 362, 1928.

[125] See report of work done at the Westinghouse Research Laboratory by R. B. Wilhelm, Proc. Amer. Soc. Test. Matls., Vol. 24, part 2, 1924, p. 151.

strength of the steel increases, but with further increase in temperature it drops off rapidly. Also the yield point becomes less pronounced as the temperature increases and at 300° C. it cannot be distinguished on the diagram. In Fig. 296 the first portions of the same diagrams are shown to a larger scale. These show that the proportional limit of the
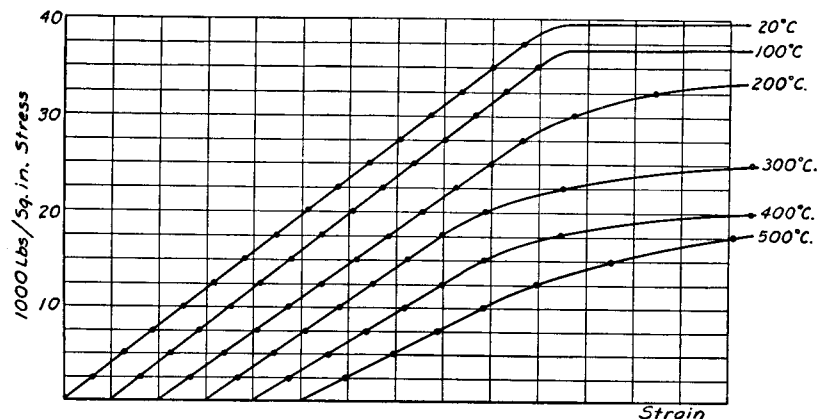


FIG. 296.

steel diminishes as the temperature increases. At the same time there is a decrease in the slope of the straight portions of the diagrams, and hence in the modulus of elasticity. All the results obtained in the above tests are summarized in Fig. 297, which shows that, while the strength of the material decreases as the temperature increases, its ductility, as characterized by elongation and reduction in area, increases.

Experiments at high temperatures show that the results of tensile tests depend very much on the duration of the test. As the duration of the tensile test increases, the load necessary to produce fracture becomes smaller and smaller. In Fig. 298 are shown the tensile test diagrams for the same steel as above at 500° C. and for test durations of 6 minutes, 70 minutes and 240 minutes respectively. It is evident from this that tensile test data obtained from the usual short duration tests (lasting

say 15 or 20 minutes), as given in Fig. 297, are useful only for cases in which the loads act but a short time.[126]

For loads acting over a long period of time and at high
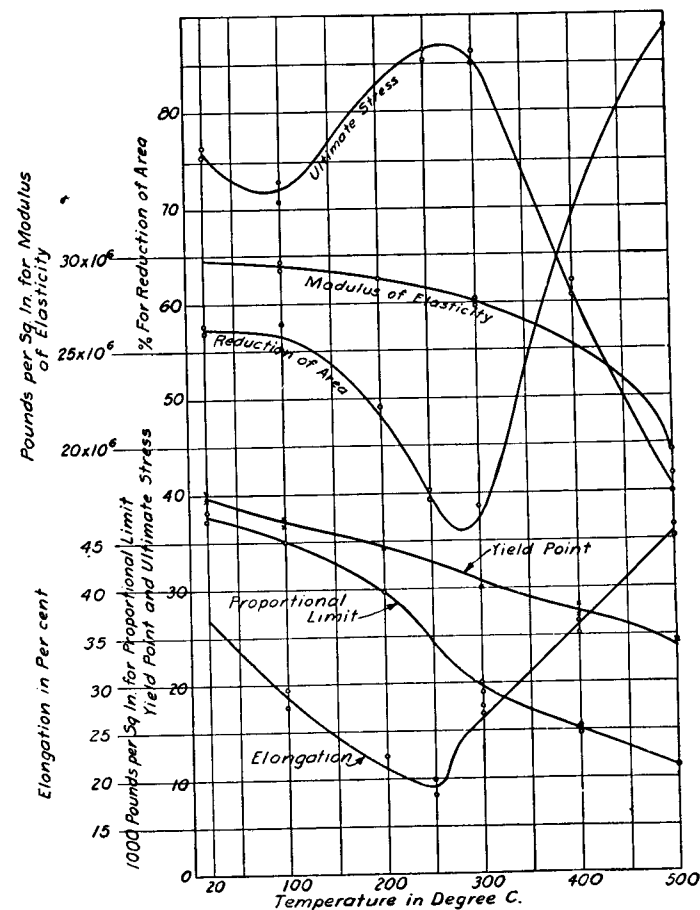


FIG. 297.

temperature, as for instance the weight of a structure or steam pressure in power plants, we need additional information regarding the *time effect*. Experience shows that under such

---

[126] To eliminate time effect, vibration tests have been used in determining modulus of elasticity. See paper by G. Versé, Journal of Appl. Mech., Vol. 2, 1935.

conditions a continuous deformation, "creep," may take place, which is the most important factor to be considered in design. Although a considerable amount of research work in this direction has been done [127] and much more is now in progress, the question of the behavior of metals under high temperature and prolonged loading cannot be considered completely cleared.
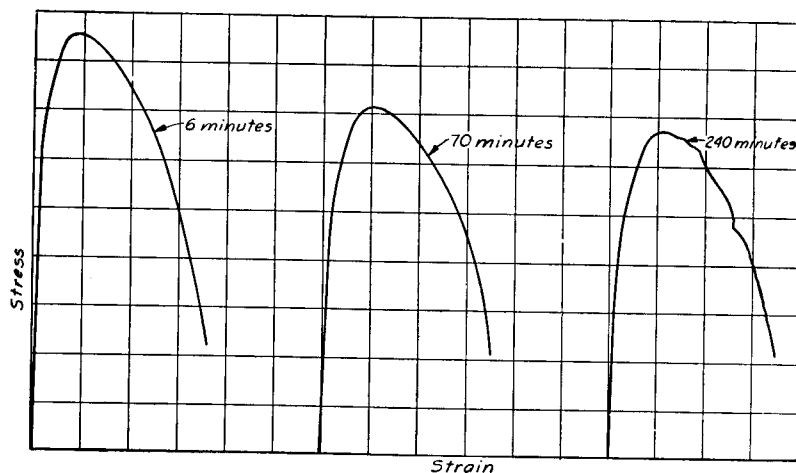


FIG. 298.

In most experiments of this kind the gradual elongation of materials under prolonged tension is studied. Tensile test specimens at high temperature are submitted to a certain

[127] See papers: J. H. S. Dickenson, Journal of Iron and Steel Inst., Vol. 106, 1922, p. 103; H. J. French and W. A. Tucker, Technologic Papers, Bureau of Standards, No. 296, 1925; T. D. Lynch, N. L. Mochel and P. G. McVetty, Proc. Amer. Soc. Test. Matls., Vol. 25, part 2, 1925; H. J. Tapsel and J. Bradley, Engineering, Vol. 120, 1925, pp. 614 and 746, and Journal Inst. of Metals, Vol. 35, 1926, p. 75; P. G. McVetty and N. L. Mochel, Trans. Amer. Soc. Steel Treating, Vol. 11, 1926, p. 73; A. E. White and C. L. Clark, Trans. Amer. Soc. Mech. Eng., Vol. 48, 1926, p. 1075; H. J. Tapsell and W. J. Clenshaw, Dept. of Scientific and Industrial Research, Eng. Research, Report No. 1, 1927. Information regarding more recent publications see in the book by H. J. Tapsell, "Creep of Metals," 1931; see also Symposium, A. S. T. M., Chicago, 1931; E. L. Robinson, Journal Appl. Mech., Vol. 1, p. 145, 1933 and P. G. McVetty, Proc. Am. Soc. Test. Math., Vol. 37, 1937.

constant load and temperature, and the *progressive creep* under this load is investigated.

The results of such experiments made for a given temperature and for various values of the load can be represented by time-extension curves, such as is shown in Fig. 299.[128] Curve *A* represents a typical *creep curve* for a relatively high stress. After application of the load *creep* proceeds at a gradually diminishing *rate*. At point *a* an inflection occurs and the creep rate begins to increase until the test specimen breaks. The curve *B*, corresponding to a somewhat smaller load, has a similar shape. Owing to lower *creep rates* it takes a longer time to produce fracture. As the load is further reduced, similar tests on different specimens give curves *C*, *D*, *E*, *F* and *G*. As the stress diminishes, a longer and longer time is required to obtain the inflection point on the creep curve. To determine the inflection points for such curves as *F* and *G*, tests of extremely long duration would be required. It is seen that, as the stress decreases, the creep curve is essentially a straight line for a progressively longer period of time as it approaches its inflection point. The working stresses encountered in practice are usually below that corresponding to the curve *G*; hence the assumption that the creep curve approaches a straight line is sufficiently accurate for practical purposes. The slope of this line gives us the *minimum creep rate* for a given stress and a given temperature.
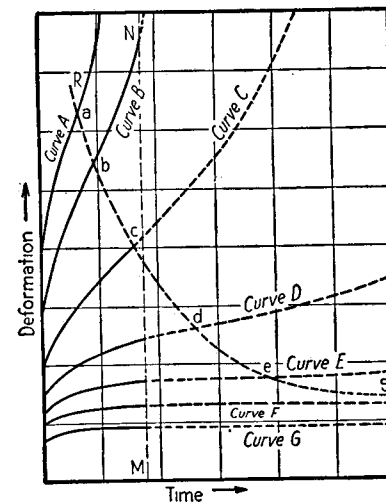


FIG. 299.

[128] This figure and the three following are taken from McVetty's papers; see Mechanical Engineering, 1934, p. 149 and Proc. Am. Soc. Test. Mat., Vol. 34, 1938.

The magnitude of this creep rate diminishes as the stress decreases, but there is no conclusive evidence that it will ever vanish—that is, that there is a *limiting stress* at which the specimen can indefinitely resist the stress and high temperature.

In studying the *progressive creep* of tensile test specimens under constant load and high temperature, two phenomena must be kept in mind: (1) hardening of the material due to plastic strain, and (2) removal of this hardening or "*softening*" of the material due to the prolonged action of the high temperature. The mechanism of plastic flow at high temperature is the same as at room temperature. The plastic deformation is due to sliding of the metal. This sliding is accompanied by an increase in the resistance to sliding, which represents the strain hardening (p. 412).

The rate at which the effect of strain hardening is removed depends on the temperature. It was mentioned before (p. 409) that the effect of strain hardening can be eliminated in a short time by *annealing* metal at a certain high temperature which depends on the kind of metal. But the same effect can be obtained at much lower temperatures acting over a longer period of time. It has been shown,[129] for instance, in investigating the softening of cold worked copper, that the softening produced in 12 minutes at 300° C. would take 10.4 days at 200° C. and that apparently it would take about 300 years to produce the same softening at 100° C.

The time-extension curves, Fig. 299, show that during the initial extension the rate of extension gradually diminishes. This is due to strain hardening. At the inflection point a certain constant rate of extension is established at which the hardening and softening counteract each other; that is, the strain hardening produced by creep is continuously destroyed by the softening effect of the high temperature, and creep continues at a constant rate depending on the magnitudes of stress and temperature.

[129] See Pilling and Halliwell, Proc. Amer. Soc. Test. Matls., Vol. 25, 1925. See also R. W. Bailey, Journal Inst. of Metals, Vol. 35, 1926.

Since we always have to consider progressive creep in members subjected to the simultaneous action of high temperature and stress, the design must be based on the assumption of a certain duration of service of the structure and of a certain amount of permanent deformation which can be considered as permissible. The working stresses must be chosen in each particular case so that the permanent deformation of the structure during its lifetime will not exceed a definite limit depending on the type of structure. The purpose of long-duration high-temperature tests is to furnish the designer with sufficient information for a satisfactory calculation of the above mentioned permanent deformations due to creep.

The duration of the laboratory tests usually does not exceed a few thousand hours, and for the prediction of the creep deformation during the lifetime of a structure some extrapolation of the laboratory test results becomes necessary. The experiments with various steels show that in the first portion of the creep curves, Fig. 299, the excess of creep rate above the minimum creep rate decreases geometrically as time increases arithmetically. Hence, denoting by $\epsilon$ the total inelastic elongation at a certain time $t$, by $v$ the corresponding creep rate, and by $v_0$ the minimum creep rate, we can take for the creep rate the expression [130]

$$v = \frac{d\epsilon}{dt} = v_0 + ce^{-\alpha t}, \qquad (a)$$

in which $c$, $v_0$ and $\alpha$ are certain constants which must be determined from the creep curves. Take, for example, a metal, the creep curves of which for several values of stress and for a constant temperature 850° F. are given in Fig. 300. Measuring the slope in five points of each of these curves, we obtain the five values of the creep rate for each stress at five different values of $t$, and the curves shown in Fig. 301 are constructed. The horizontal asymptotes to these curves evidently give us the values of $v_0$ for the applied values of stress.

[130] See reference 128. For comparison methods of extrapolation of test data see J. Marin, Proc. Am. Soc. Test. Mat., Vol. 37, p. 258, 1937.

Plotting now the values of log $(v - v_0)$ against time, we obtain the system of inclined parallel lines which indicate that the assumed expression (a) is satisfactorily chosen. From these lines the values of constants $c$ and $\alpha$ in expression (a) are
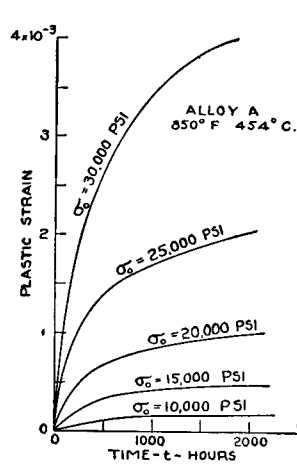


FIG. 300.
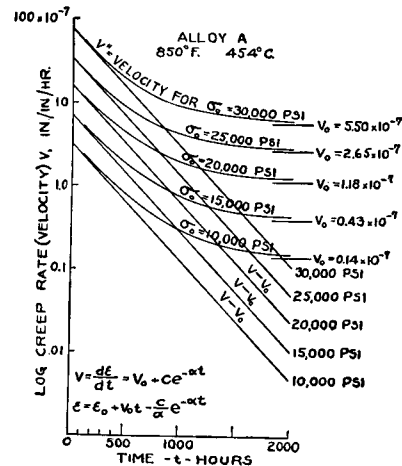


FIG. 301.

obtained by measuring the ordinates of the lines at $t = 0$ and their slope. The plastic elongation is now obtained by the integration of equation (a) which gives

$$\epsilon = \epsilon_0 + v_0 t - \frac{c}{\alpha} e^{-\alpha t}, \qquad (b)$$

where $\epsilon_0$ is a constant.

Applying this equation to some specific value of $t$, for which the plastic elongation is known from Fig. 300, the value of $\epsilon_0$ can be calculated. Hence all the constants entering in the equation (b) are determined by using the curves of Figs. 300 and 301, and we can now apply this equation for calculating $\epsilon$ for any given interval of time. In this way the curves shown in Fig. 302 are obtained. Having such a system of curves for a definite material and a definite temperature, a designer can readily select the proper value of working stress if the lifetime of the structure and the permissible plastic deformation are given.

In our previous discussion it has been assumed that plastic flow is accompanied by strain hardening. Experiments show that with increase in temperature the strain hardening becomes less and less pronounced. The maximum temperature at which strain hardening is observed varies with the material, and in the case of steels it varies with the composition of the steel. For instance, with mild carbon steel (0.17 C) at a stress of 2,200 lbs. per sq. in. no strain hardening was observed [131] at a temperature of 647° C. Under such conditions the time extension curve has a shape such as shown in Fig. 303; i.e., the rate of creep increases continuously with the time. It is interesting to note that the two kinds of time-extension curves shown in Figs. 299 and 303 are associated with different
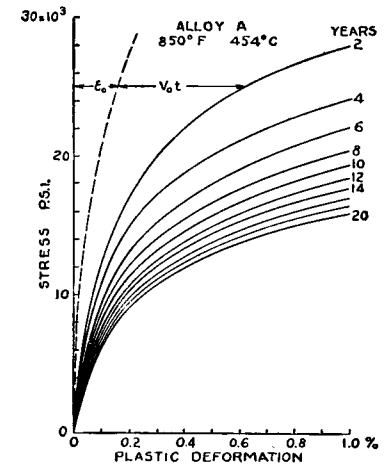


FIG. 302.



FIG. 303.

types of fracture. When strain hardening is present, yielding at a certain point in the specimen increases the resistance at this point and the next sliding occurs at some other cross section. As a result of this a uniform elongation takes place and the specimen remains cylindrical up to the beginning of "necking." When strain hardening is absent, the local yielding which begins at the weakest cross section spreads at a decreasing rate towards the ends of the specimen. As a result of this the two parts of a broken specimen are tapered from the ends to the cross section of fracture.
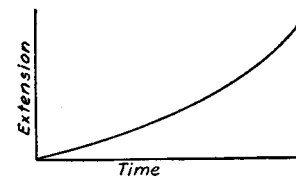
[131] Book by H. J. Tapsell, loc. cit., p. 466.

Under the prolonged action of high temperature a metallographic transformation in metal takes place of such a nature that the resistance of the steel to creep is reduced. This effect is more pronounced in the case of high carbon steels. To reduce this structural transformation it is necessary to apply a suitable heat treatment assuring the metallographical stability.[132]

Most of the data regarding the strength of metals at high temperatures has been obtained from simple tension tests and the strength of metals under combined stress remains an unexplored field. In order to get some information about the creep of steel under such conditions Mr. Bailey made some interesting tests with lead.[133] This metal has a low melting point and creep phenomena occur at room temperature. Experiments with combined stresses are much simpler at this temperature and may throw some light on the behavior of steel under combined stresses at high temperature.

The long-duration high-temperature torsion tests with thin tubular steel specimens were made at the University of Michigan by F. L. Everett.[134] This kind of test has some advantages as compared with usual tensile tests, since the plastic torsional deformation does not affect the cross-sectional dimensions of specimens and since small volume changes owing to temperature fluctuation and to metallographical transformation do not affect the measured angle of twist.

Before concluding this discussion it should be noted that progressive creep may produce a redistribution of stresses in parts submitted to the simultaneous action of stresses and high temperatures. At points of high stress concentration the rate of creep is larger and hence creep will result in a more favorable stress distribution. This fact must be considered in

[132] See F. R. Hensel and E. I. Larsen, Trans. Am. Inst. Min. Metalg. Engrs., Vol. 99, p. 55, 1932.

[133] See paper presented at the World Power Conference, Tokyo, 1929.

[134] Trans. Am. Soc. Mech. Engrs., Vol. 53, p. 117, 1931.

design. Several examples of this kind have been discussed by Mr. Bailey.[135]

**83. Various Strength Theories.**[136]—The mechanical properties of structural materials have chiefly been investigated with testing machines which subject specimens to the simplest sort of stress conditions. Most of our information regarding the strength of metals is obtained from simple tensile tests, while the strength of brittle materials such as stone or concrete has mostly been studied by compression tests; we also have a certain amount of information regarding the strength of materials in shear. The strength of materials under more complicated stress conditions than these has only been investigated in exceptional cases. In order to have some basis for determining working stresses for the conditions of combined stress which are often encountered in design, various strength theories have been advanced. The purpose of these theories is to establish laws by which we can, from the behavior of a material in simple tension or compression tests, predict the condition of failure under any kind of combined stress; here failure signifies either *yielding* or *actual rupture* whichever may occur first.
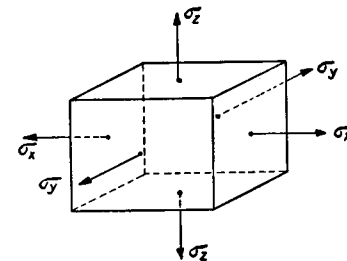


FIG. 304.

In the most general case the stress condition of an element of a stressed body is defined by the magnitude of the three principal stresses, $\sigma_x$, $\sigma_y$ and $\sigma_z$, Fig.

[135] R. W. Bailey, Inst. Mech. Eng., 1927. Engineering, Vol. 124, 1927, p. 44. Vol. 129, 1930; Inst. Mech. Engrs., 1935. See also C. R. Soderberg, Journal Appl. Mech., Vol. 1, p. 131, 1933; G. H. MacCullough, Journal Appl. Mech., Vol. 1, p. 87, 1933. J. Marin, Journal Franklin Inst., Vol. 226, p. 645, 1938.

[136] A description of these theories can be found in papers by H. M. Westergaard, Jour. Franklin Inst., 1920; A. J. Becker, Bull., nr. 85, Eng. Expt. Stat., University of Illinois; F. Schleicher, Zeitschr. f. Angew. Math. u. Mech., Vol. 5, 1925, p. 199. A. Nadai, Journal Appl. Mech., Vol. 1, p. 111, 1933.

304. The following relation between the algebraic values of principal stresses is assumed:

$$\sigma_x > \sigma_y > \sigma_z, \qquad (a)$$

in which tension is taken positive and compression negative. The oldest theory, the so-called *maximum stress theory*,[137] takes the maximum stress as the criterion for strength and assumes that, in the case of ductile materials, yielding starts in an element such as shown in Fig. 304 when the maximum stress becomes equal to the yield point stress of the material in simple tension or the minimum stress becomes equal to the yield point stress of the material in simple compression. This makes the conditions for yielding

$$\text{or} \qquad \left.\begin{aligned} \sigma_x &= \sigma_{Y.P.} \\ \sigma_z &= \sigma_{Y.P.}', \end{aligned}\right\} \qquad (309)$$

in which $\sigma_{Y.P.}$ is the yield point in tension and $\sigma_{Y.P.}'$ the yield point in compression. There are many evidences contradicting this theory. We have seen, for instance (Fig. 214), that in the case of simple tension sliding occurs along planes inclined to the axis of the specimen, i.e., on planes where the tensile stress is not a maximum. It is known also that a homogeneous and isotropic material, although weak in simple compression, may sustain very large hydrostatic pressures without yielding. This indicates that the magnitude of the maximum tensile or compressive stress alone does not define the condition for yielding.

Another strength theory, attributed usually to Saint Venant, is the so-called *maximum strain theory*. In this theory it is assumed that yielding of a ductile material starts either when the maximum strain (elongation) becomes equal to the strain at which yielding occurs in simple tension or when the minimum strain (compressive strain) becomes equal to the

[137] Sometimes called *Rankin's Theory*.

unit strain in simple compression. That is, from eqs. (43, Part I), either

$$\text{or} \qquad \left.\begin{aligned} \frac{\sigma_x}{E} - \frac{\mu}{E}(\sigma_y + \sigma_z) &= \frac{\sigma_{Y.P.}}{E} \\ \frac{\sigma_z}{E} - \frac{\mu}{E}(\sigma_x + \sigma_y) &= \frac{\sigma_{Y.P.}'}{E}. \end{aligned}\right\} \qquad (310)$$

There are evidences against this theory also. For instance, when a plate is subjected to tension in two perpendicular directions, the maximum strain theory indicates that the yield point must be higher than in the case of simple tension, because the elongation in each of the two directions is somewhat decreased by the tension in the perpendicular direction. This conclusion is not supported by experiments.[138] Experiments with specimens under uniform hydrostatic pressure also contradict this theory.

Much better agreement with experiment, at least with ductile materials having $\sigma_{Y.P.} = \sigma_{Y.P.}'$, is given by the *maximum shear theory*, which assumes that yielding starts when the maximum shearing stress becomes equal to the maximum shearing stress at yield point in a simple tensile test. Since the maximum shearing stress is equal to half the difference between the maximum and the minimum principal stresses, the condition for yielding is[139]

$$\tfrac{1}{2}(\sigma_x - \sigma_z) = \tfrac{1}{2}\sigma_{Y.P.}. \qquad (311)$$

In machine design the maximum shear theory is now generally used for ductile materials. This theory is in good agreement with experiment and is very simple to apply.[140]

[138] See Wehage, Mitteilungen d. Techn. Versuchsanstalten, p. 89, 1888, Berlin.

[139] This theory is supported by the experiments of J. J. Guest, Phil. Mag., Vol. 50, 1900, p. 69. See also L. B. Turner, Engineering, Vol. 86, p. 169; W. A. Scoble, Phil. Mag., 1906, December, and 1910, January; C. A. Smith, Engineering, Vol. 88, p. 238.

[140] The comparison of various strength theories as applied in machine design is given by J. Marin, "Product Engineering," May, 1937.

The *quantity of strain energy* stored per unit volume of the material has also been proposed as a basis for determining starting of yielding.[141]   By using the general eq. (192) (p. 307, Part I) and equating the energy for the case shown in Fig. 304 to the energy at yield point in simple tension, the condition of yielding is found to be

$$w = \frac{1}{2E}\left(\sigma_x^2 + \sigma_y^2 + \sigma_z^2\right)$$

$$- \frac{\mu}{E}\left(\sigma_x\sigma_y + \sigma_y\sigma_z + \sigma_x\sigma_z\right) = \frac{\sigma_{Y.P.}^2}{2E}. \quad (312)$$

To compare the various strength theories let us consider the case of pure shear.   In this case the maximum tensile stress is equal to the maximum compressive stress and to maximum shearing stress (article 16, Part I).   Then

$$\sigma_x = -\sigma_z = \tau; \qquad \sigma_y = 0.$$

Assuming that the material has the same yield point in tension and compression, the conditions for yielding according to the various theories are

$$\tau = \sigma_{Y.P.} \qquad \text{from eqs. (309),}$$

$$\tau = \frac{1}{1 + \mu}\sigma_{Y.P.} \qquad \text{from eqs. (310),}$$

$$\tau = \tfrac{1}{2}\sigma_{Y.P.} \qquad \text{from eq. (311).}$$

Equation (312) for this case gives

$$w = \frac{\sigma_x^2(1 + \mu)}{E} = \frac{\sigma_{Y.P.}^2}{2E},$$

from which

$$\tau = \frac{\sigma_{Y.P.}}{\sqrt{2(1 + \mu)}}.$$

[141] This proposal was first made by Beltrami, Rendiconti, p. 704, 1885; Math. Annalen, p. 94, 1903; see also Girtler, Sitzungsberichte d. Wiener Akad., Vol. 116, IIa, 1907, p. 509, and B. P. Haigh, Engineering, Vol. 109, 1920, p. 158, and Brit. Assoc. for the Adv. of Science, Reports, Edinburgh, 1921.

Taking $\mu = 0.3$, as for steel, we find:

| | |
|---|---|
| $\tau = \sigma_{Y.P.}$ | from the maximum stress theory, |
| $\tau = 0.77\sigma_{Y.P.}$ | from the maximum strain theory, |
| $\tau = 0.50\sigma_{Y.P.}$ | from the maximum shear theory, |
| $\tau = 0.62\sigma_{Y.P.}$ | from the maximum strain energy theory. |

It may be seen that the difference between the various theories in this particular case [142] is a considerable one.   If we have a circular shaft in torsion, for instance, and assume a certain value for $\tau_{max} = \tau_{Y.P.}/n$, we will find from eq. (149), Part I, for the various strength theories, the following ratios of diameters:

$$1 : \sqrt[3]{\frac{1}{0.77}} : \sqrt[3]{\frac{1}{0.50}} : \sqrt[3]{\frac{1}{0.62}}, \qquad \text{or} \qquad 1 : 1.09 : 1.26 : 1.17.$$
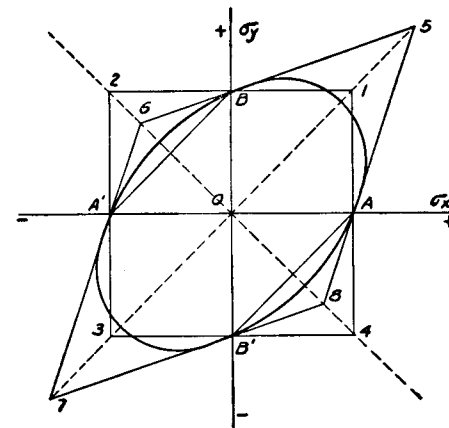


FIG. 305.

Figure 305 compares graphically the four theories presented above for the case when there are only two principal stresses ($\sigma_z = 0$) [143] and $\sigma_{Y.P.} = \sigma_{Y.P.}'$.   The lines in the figure repre-

[142] Comparisons of various strength theories in application to various design problems are given in the paper by Roth; see Zeitschr. f. Math. u. Phys., Vol. 48, 1902.

[143] See papers by A. J. Becker, loc. cit., p. 473, and B. P. Haigh, loc. cit., p. 476.

sent the values of $\sigma_x$ and $\sigma_y$ at which yielding starts, according to the various theories. The maximum stress theory is represented by the square 1234. The lengths $OA$ and $OB$ represent the yield points in simple tension in the $x$ and $y$ directions respectively. In the same manner $A'$ and $B'$ correspond to simple compression. Point 1 represents equal tensions in two perpendicular directions, each equal to the yield point in simple tension. The maximum stress theory states that there is no yielding at any point inside of the square 1234. The maximum strain theory is represented by the rhombus 5678. Since a tension in one direction reduces the strain in the perpendicular direction, two equal tensions, according to the maximum strain theory, can have much higher values at yielding (as represented by point 5) than with the maximum stress theory (point 1). If the two principal stresses are equal and opposite in sign, the maximum strain theory (points 6 and 8) indicates that yielding starts at lower values than the maximum stress theory would indicate. The maximum shear theory is represented by the irregular hexagon $A1BA'3B'A$. It coincides with the maximum stress theory when both principal stresses are of the same sign, but there is considerable difference between the two theories when the principal stresses have opposite signs. Equation (312) for the maximum strain energy theory reduces, for two-dimensional problems, to

$$\sigma_x{}^2 + \sigma_y{}^2 - 2\mu\sigma_x\sigma_y = \sigma_{Y.P.}{}^2.$$

By plotting this we obtain the ellipse shown in Fig. 305, enclosing all the points at which no yielding takes place, according to the maximum strain energy theory.

The maximum strain energy theory was further developed by Huber.[144] In order to bring the theory into agreement with the

[144] M. T. Huber, Czasopismo techniczne, 1904, Lwov (Lemberg). See also R. v. Mises, Göttinger Nachrichten, Math. Phys. Kl., 1913, p. 582; H. Hencky, Zeitschr. f. Angew. Math. u. Mech., Vol. 5 1925, p. 115;

fact that materials can sustain very large hydrostatic pressures without yielding, Huber proposed, when the average stress $\frac{1}{3}(\sigma_x + \sigma_y + \sigma_z)$ is compression, to split the strain energy into two parts, one due to the change in volume and the other due to the distortion, and consider only the second part. Using the notation

$$\tfrac{1}{3}(\sigma_x + \sigma_y + \sigma_z) = p$$

and eq. (45) (Part I) for the unit change in volume $\Delta$, the strain energy due to the change in volume is

$$w_1 = \frac{p\Delta}{2} = \frac{3(1 - 2\mu)}{2E}\, p^2 = \frac{1 - 2\mu}{6E}\,(\sigma_x + \sigma_y + \sigma_z)^2.$$

Subtracting this from the total energy $w$ (eq. 312), we find for the energy of distortion

$$w_2 = w - w_1 = \frac{1 + \mu}{6E}\left[(\sigma_x - \sigma_y)^2 + (\sigma_x - \sigma_z)^2 + (\sigma_y - \sigma_z)^2\right]. \quad (313)$$

In case $p < 0$ it was proposed to use $w_2$ instead of the total energy $w$ as the condition of yielding.

Applying this also to pure shear and to simple tension we find, from eq. 313, for shear ($\sigma_x = -\sigma_z = \tau$; $\sigma_y = 0$)

$$w_2 = \frac{(1 + \mu)\tau^2}{E}$$

and for tension ($\sigma_x = \sigma$; $\sigma_y = \sigma_z = 0$)

$$w_2 = \frac{(1 + \mu)\sigma^2}{3E}.$$

The condition of yielding in shear is

$$\frac{(1 + \mu)\tau^2}{E} = \frac{(1 + \mu)\sigma_{Y.P.}{}^2}{3E}$$

from which [145]

$$\tau = \frac{1}{\sqrt{3}}\,\sigma_{Y.P.} = 0.557\sigma_{Y.P.}. \quad (314)$$

[145] F. Schleicher, loc. cit., p. 473, and M. Roś and A. Eichinger, Proc. Intern. Congress for Applied Mechanics, 1926, Zürich.

[145] Recent experiments by W. Lode, Zeitschrift f. Physik, Vol. 36, 1926, p. 913, Forschungsarbeiten, nr. 303, 1928, and of M. Roś and A. Eichinger, Materialprüfungsanstalt an d. E. T. H., Zürich, 1926, Diskussion, Berichte, nr. 28, 1928, and nr. 34, 1929, agree better with this maximum strain energy theory than with maximum shear theory,

The maximum shear theory was given a further development by O. Mohr.[146] In this development he made use of the representation of stress conditions on an element of a stressed body by circles, as explained in article 18, Part I. In this representation the normal and shearing components of the stress acting on any plane are given by the coordinates of a certain point in the shaded areas (Fig. 306). Points lying on the same vertical line such as $MN$ represent the stresses on planes with the same normal stress $\sigma$ and with various shearing stresses. It is natural to assume that the weakest of all these planes is the plane with the maximum shearing stress, whose stress condition is represented by the point $N$ lying on the outer circle. Repeating the same reasoning with points lying on any other vertical line, we finally arrive at the conclusion that the
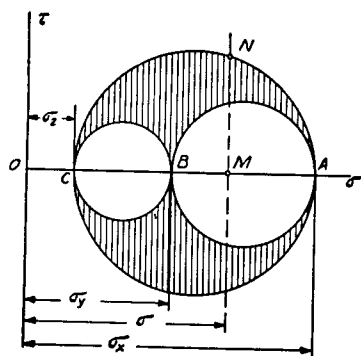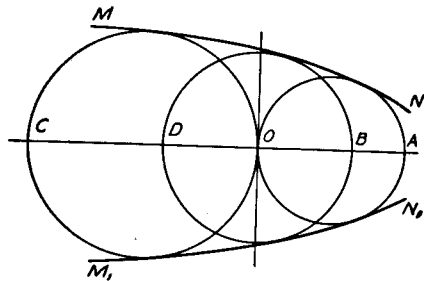
FIG. 306.

FIG. 307.

weakest plane must be one of the planes whose stress conditions are represented by points on the outer circle $ANC$. Hence the outer circle alone is sufficient to determine the *limiting stress condition*, i.e., the stress condition at which yielding begins. In Fig. 307 the

but in most cases the difference between these two theories is not so large as to make it of practical importance to introduce the maximum energy theory in machine design. For further development of this theory see the paper by F. Schleicher, loc. cit., p. 473. See also W. v. Burzyński, Sweiz. Bauz., Vol. 94, 1929.

[146] O. Mohr, V. D. I., Vol. 44, 1900, p. 1524. See also his "Abhandlungen aus dem Gebiet d. technischen Mechanik," sec. ed., p. 192, 1914, Berlin.

length $OA$ represents the yield point in simple tension and the circle with the diameter $OA$ represents the condition for yielding in simple tension. In the same manner the circle with the diameter $OC$ represents the condition for yielding in simple compression, and the circle with the diameter $DB$ represents the condition for yielding in pure shear. If several circles of this kind are obtained for a given material by experiments, the envelopes of these circles, in this case $MN$ and $M_1N_1$, can be constructed. Then Mohr assumed that any stress condition at which yielding would start is represented by a circle tangent to these envelopes. Assume, for instance, that the envelopes $MN$ and $M_1N_1$ can be replaced by straight lines
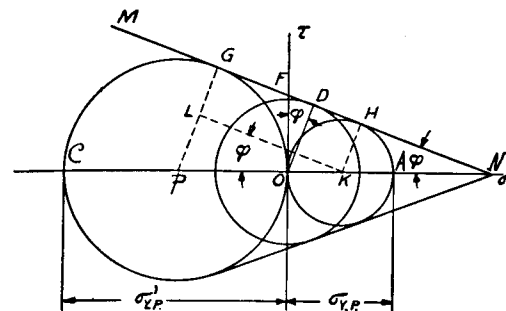
FIG. 308.

(Fig. 308). Then, knowing the limiting condition in simple tension $(\sigma_x = \sigma_{Y.P.})$ and in simple compression $(\sigma_z = \sigma_{Y.P.}')$, the conditions for yielding in pure shear can easily be obtained. From the figure,

$$\overline{OF} = \overline{FG} = \overline{FH} = \tfrac{1}{2}\overline{GH} = \tfrac{1}{2}\overline{LK} = \tfrac{1}{2}\frac{\sigma_{Y.P.} - \sigma_{Y.P.}'}{2}\cos\varphi.$$

Then the stress producing yielding in pure shear, represented by the radius $OD$ of the circle with center at $O$ and tangent to $MN$, is

$$\tau_{Y.P.} = \overline{OD} = \overline{OF}\cos\varphi = \tfrac{1}{4}(\sigma_{Y.P.} - \sigma_{Y.P.}')\cos^2\varphi. \qquad (a)$$

The angle $\varphi$ may be calculated from the triangle $KLP$, from which

$$\cos\varphi = \frac{\sqrt{\overline{PK^2} - \overline{PL^2}}}{PK} = \frac{\sqrt{-\sigma_{Y.P.}\sigma_{Y.P.}'}}{\tfrac{1}{2}(\sigma_{Y.P.} - \sigma_{Y.P.}')}. \qquad (b)$$

Substituting in $(a)$

$$\tau_{Y.P.} = -\frac{\sigma_{Y.P.}\sigma_{Y.P.}'}{\sigma_{Y.P.} - \sigma_{Y.P.}'}, \qquad (c)$$

when $\sigma_{Y.P.} = -\sigma_{Y.P.}'$, eq. (c) coincides with the maximum shear theory. If we apply eq. (c) to cast iron [147] and assume that the ultimate stress in compression is four times the ultimate stress in tension, we find for the ultimate stress in shear, from (c),

$$\tau_{ult} = \frac{4\sigma_{ult}^2}{5\sigma_{ult}} = 0.8\sigma_{ult} = 0.8 \text{ ult. str. in tension.}$$

This is in satisfactory agreement with experiments made by C. Bach with hollow cast iron cylinders.[148] Very extensive experiments with marble and sandstone have been made by Th. v. Kármán [149] and R. Böker.[150]

**84. Working Stresses.**—The problem of choosing an adequate factor of safety in design of structures and machine parts is of the utmost practical importance. If this factor is taken too low, making the working stresses too high, the structure may prove weak in service. On the other hand if the working stresses are too low the structure becomes unnecessarily heavy and uneconomical. In discussing the various factors to be considered in choosing working stresses let us take a simple example of tension of a prismatical bar. We assume that the yield point of the material is taken as the basis for determining the working stress; then the safe cross sectional area $A$ is obtained from the equation:

$$\frac{\sigma_{Y.P.}}{n} = \frac{P}{A}. \tag{a}$$

We see that the cross-sectional area depends on the magnitude of the external load $P$, on the yield point of the material, $\sigma_{Y.P.}$, and on the factor of safety $n$. Obviously the magnitude of this factor, which is sometimes called the *factor of ignorance*, depends on the accuracy with which we know the quantities in eq. (a), namely, the external load and the mechanical prop-

---

[147] In the case of brittle materials the above theory applies to the ultimate stresses, instead of yield point stresses.

[148] C. Bach, Elastizität und Festigkeit, 7th ed., p. 362.

[149] Th. v. Kármán, Forschungsarþeiten, nr. 118; see also V. D. I., Vol. 55, 1911.

[150] R. Böker, Forschungsarbeiten, nr. 175/176.

---

erties of the material, and on the accuracy with which this equation represents the maximum stress.

There are cases where the external forces are known with good accuracy. We know exactly, for instance, the hydrostatic pressure acting on a dam if the depth of the water is known. We know accurately the centrifugal forces acting in a rotor having a definite angular velocity. But in the majority of cases the forces are known only approximately and the most unfavorable loading condition for a structure can be estimated only on the basis of long experience. Consider, for instance, the design of a bridge. The weight of the bridge itself and the weight of the train moving across the bridge may be known with satisfactory accuracy. But in designing the bridge dynamic effects must be taken into account. Due to the balance weights the pressure of a locomotive wheel on the rail is not constant and the maximum pressure is larger than the static pressure. Under the action of the moving and varying loads the bridge will be brought into vibration and under such conditions the problem of determining the forces in individual members of the bridge becomes extremely involved. Another type of forces acting on the bridge, which we do not know accurately, is wind pressure. The magnitude of such forces is usually estimated on the basis of experience with existing structures. From this discussion it is obvious that if eq. (a) represents the condition of safety for a member of a bridge, the force $P$ is not known to us exactly and can be estimated only with some approximation. The accuracy with which the estimate can be made will affect the magnitude of the factor of safety.

The magnitude of $\sigma_{Y.P.}$ is also not an exactly known quantity. It may vary to a certain extent for the same material, and this variation depends on the homogeneity of the material. It is quite natural therefore that in the case of such homogeneous materials as steel the factor of safety may be taken lower than in the case of such materials as wood or stone.

The accuracy of the formula itself must also be con-

sidered in choosing the factor of safety. Equation (*a*) can be considered very accurate for calculating the stresses in a tensile test specimen (see Fig. 248) because special precautions are taken to apply the load centrally and to distribute it uniformly over the weakest cross section. But again taking as an illustration the design of a member of a bridge, it can be appreciated that eq. (*a*) is only a rough approximation depending usually on the assumption that there are ideal hinges at the joints. The actual stress condition in such a member is very far from simple tension. Due to rigid joints the members of a bridge truss undergo not only direct stress, but also bending. The corresponding bending stresses are sometimes of a considerable magnitude and if they are not taken into account and the simple eq. (*a*) is used in determining the cross sectional area of the member, then the inaccuracy of eq. (*a*) in this case is usually compensated for by increasing the factor of safety.

From this discussion it can be seen how difficult it would be to give any definite recommendations regarding the magnitude of the factor of safety and how much this factor depends and always will depend upon the experience and judgment of the designer.

In the following discussion it is assumed that the forces are established on the basis of experience with past practice and that the mechanical properties of the material are known. Methods are then considered for determining the effect of various kinds of stress conditions on the choice of working stresses. Knowledge of this enables us to design a structure in such a manner as to have the same factor of safety in all parts of the structure. It is obvious that this latter requirement must always be fulfilled if the design is to be economical, because the ultimate strength of a structure is determined by the strength at the weakest place.

Let us begin the discussion with the cases in which the *stresses remain constant*, as, for instance, in structures submitted only to static loads or in rotors of machines running continuously at the same speed. The first question to be

considered is whether to take the yield point or the ultimate strength as the limiting stress in determining the working stress. In the case of *ductile materials*, such as structural steel, it seems logical to take the yield point as the basis for determining working stresses, because the considerable deformations, which take place at yield point, are seldom permissible in engineering structures. In the case of brittle materials, such as cast iron or concrete, the working stresses are usually taken as some part of the ultimate strength.

Knowing the yield point $\sigma_{Y.P.}$ of a ductile material,[151] the working stress in tension or compression is

$$\sigma_w = \frac{\sigma_{Y.P.}}{n}, \qquad (b)$$

where $n$ is the factor of safety. In structural engineering this factor is often taken equal to 2. If the most unfavorable loading condition is taken, the factor of safety is sometimes lowered to 1.5.[152] It must be noted that when the loading is static and the material is ductile the stress concentration due to holes or reëntrant corners is usually disregarded, and the maximum stress is calculated from simple equations such as eq. (*a*) for direct stress, eq. (149), Part I, for twist and eqs. (58), Part I, for bending.

After having established the working stress for simple tension and compression, the working stress for any other stress condition is usually determined on the basis of the *maximum shear*[153] *theory* (p. 475), from which we find for pure shear

$$\tau_w = \frac{\sigma_w}{2} = \frac{1}{2} \frac{\sigma_{Y.P.}}{n}. \qquad (c)$$

This magnitude of working stress for shear must be used in all

[151] It is assumed that the yield point in tension and compression is the same.

[152] Sometimes the calculations are made for two different conditions: (1) the usual service loading condition and (2) emergency condition, when the most unfavorable loading condition possible is assumed. A lower factor of safety is used for this second condition.

[153] Application in design of other theories has been discussed by J. Marin, "Product Engineering," May, 1937.

cases of combined stresses; that is, the structure is designed so as to make

$$\frac{\sigma_x - \sigma_z}{2} = \tau_w = \frac{1}{2}\frac{\sigma_{Y.P.}}{n}, \qquad (d)$$

in which $\sigma_x$ and $\sigma_z$ are the maximum and the minimum principal stresses respectively, so that the left side of eq. (d) represents the maximum shearing stress. In the particular case of combined bending and twist of a circular shaft (art. 62), Part I, we have, for example,

$$\frac{\sigma_x - \sigma_z}{2} = \tau_w = \frac{16}{\pi d^3}\sqrt{M^2 + M_t^2},$$

from which

$$d = \sqrt[3]{\frac{16}{\pi \tau_w}\sqrt{M^2 + M_t^2}}.$$

In the case of *brittle materials* the working stresses in tension and compression are

$$\sigma_w = \frac{\sigma_{ult}}{n_1}; \qquad \sigma_w' = \frac{\sigma_{ult}'}{n_1}, \qquad (e)$$

in which $\sigma_{ult}$ is the ultimate strength in tension, $\sigma_{ult}'$ the ultimate strength in compression and $n_1$ is the factor of safety. For such materials as concrete or cast iron this factor is usually taken comparatively high, varying in various cases from 4 to 8.

Once we have the working stresses for tension and compression, the working stress for any other stress condition can be obtained by using Mohr's theory as explained on p. 480. In practice the *maximum stress theory* (p. 474) is often used in the case of brittle materials; that is, the dimensions are determined so as to have the maximum tensile stress not larger than the working stress in simple tension and the maximum compressive stress not larger than the working stress in compression. It must be noted that for brittle materials the stress concentration must be taken into account (see Chapter VII) in calculating these maximum tensile and compressive stresses.

It was assumed in the above discussion that the principle of superposition holds, which means that the maximum stress is proportional to the load. Hence the factor of safety $n$, which we use in determining the working stress, applies also to the external loads, and we can state that the yielding in the structure begins under the load which is $n$ times the actual safe load. If the principle of superposition does not hold, the maximum stress is no longer proportional to the load, and it is necessary to apply the factor of safety to the load and determine the dimensions of the structure in such a manner that the yielding will begin only if the acting loads are increased $n$ times. The application of this method to the case of combined bending and direct stress is discussed in art. 4 (see p. 32). This method is recommended also in the design of columns on a basis of the assumed inaccuracies (see p. 255, Part I).

In discussing plastic deformations in structures, it was pointed out that instead of applying the factor of safety to the load at which yielding begins, we can apply the factor of safety to the load at which a complete failure of the structure occurs. Some applications of this latter method of design are discussed in article 68. Sometimes, as, for example, in aeroplane design, both methods are applied and the two different factors of safety are used—one with respect to the load up to which no yielding occurs, and the other with respect to the load sufficient to produce the complete collapse of the structure.

In the case of *variable stresses* the problem of selection of working stresses becomes more complicated, since the stresses produced by dynamic causes, such as vibrations and impact, are usually known with much less accuracy than the statically produced stresses, and also the properties of materials under the action of variable stresses have not yet been completely studied. As a basis for determining working stresses the fatigue tests are usually taken in this case. If for a given material there are sufficient test data to construct an empirical curve, such as Gerber's parabolas, or straight lines such

as are shown in Fig. 276, the working stress can be selected on a basis of such curves. In most cases, however, we do not have such complete information, and a decision regarding working stresses must be taken on a basis of the known endurance limit $\sigma_e$ for reversed stresses ($\sigma_{max} = - \sigma_{min}$) and the yield point stress in tension $\sigma_{Y.P.}$.

A method sometimes successfully applied in the design of machine parts will now be discussed.[154] We shall begin with a direct variable stress and solve it in two parts, constant mean stress and reversed stress, given by the formulas:

$$\sigma_m = \frac{\sigma_{max} + \sigma_{min}}{2}; \qquad \sigma_r = \frac{\sigma_{max} - \sigma_{min}}{2}.$$

Taking $\sigma_m$ as abscissa and $\sigma_r$ as ordinate, we can represent any variable stress by a point in the $\sigma_m$, $\sigma_r$ plane shown in Fig. 309. In this figure, let $A$ represent the yield point in a static
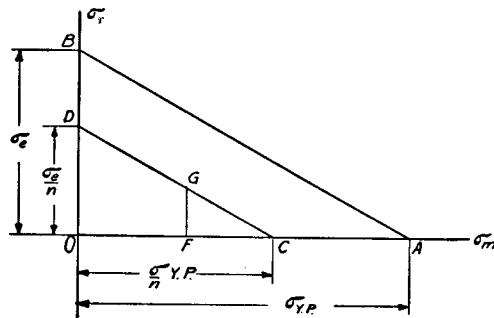


FIG. 309.

tension test ($\sigma_r = 0$), and $B$ the endurance limit for reversed stress ($\sigma_m = 0$). Having these two limiting stresses, let us assume that the limiting stress conditions [155] for other cases are represented by points on the straight line $AB$. From the

---

[154] This method is used in machine design of the Westinghouse Electric and Manufacturing Co.; see papers by C. R. Soderberg, Trans. A. S. M. E., Vol. 52, p. 52, 1930; Journal of Appl. Mech. Vol. 1, p. 131, 1933. See also A. M. Wahl, "Machine Design," 1938.

[155] The limiting stress condition is defined as that which produces a failure; that is, fatigue fracture or stretching beyond the permissible limit.

discussion given on page 434 it is evident that such an assumption is on the safe side as compared with Gerber's parabolas and the straight lines of Fig. 276. If we divide $\overline{OA}$ and $\overline{OB}$ by the factor of safety $n$, we obtain points determining the straight line $CD$, parallel to $AB$, which represents *safe stress conditions*. From this line we can determine the safe value of $\sigma_m$ and $\sigma_r$ for any value of the ratio $\sigma_r/\sigma_m$. For example, for the stress condition represented by the point $G$, $\sigma_m = \overline{OF}$, $\sigma_r = \overline{FG}$, and from the similar triangles $GFC$ and $DOC$ we find

$$\frac{\sigma_r}{\frac{\sigma_{Y.P.}}{n} - \sigma_m} = \frac{\sigma_e}{\sigma_{Y.P.}}, \tag{f}$$

from which

$$\frac{1}{n} = \frac{\sigma_r}{\sigma_e} + \frac{\sigma_m}{\sigma_{Y.P.}} \tag{315}$$

and

$$\sigma_r = \frac{\sigma_e}{n} \frac{1}{1 + \frac{\sigma_e}{\sigma_{Y.P.}} \frac{\sigma_m}{\sigma_r}}; \qquad \sigma_m = \frac{\sigma_{Y.P.}}{n} \frac{1}{1 + \frac{\sigma_{Y.P.}}{\sigma_e} \frac{\sigma_r}{\sigma_m}}. \tag{316}$$

It is seen that for any given value of the ratio $\sigma_r/\sigma_m$ the allowable values of $\sigma_r$ and $\sigma_m$ are obtained from equations (316) if the values of $\sigma_e$ and $\sigma_{Y.P.}$ are known from tests, and the magnitude of the factor of safety $n$ is selected. As an illustration of the application of these equations let us assume that a prismatical bar of steel having $\sigma_{Y.P.} = 42,000$ lbs. per sq. in. and $\sigma_e = 30,000$ lbs. per sq. in. is submitted to repeated stresses, varying between the limits 0 and $\sigma_{max}$. Then

$$\sigma_r = \sigma_m = \frac{\sigma_{max}}{2}, \qquad \frac{\sigma_m}{\sigma_r} = 1,$$

and for $n = 2$ we find, from eqs. 316,

$$\sigma_r = \frac{30,000}{2} \frac{1}{1 + \frac{1}{1.4}} = 8,750 \text{ lbs. per sq. in.};$$

$$\sigma_m = \frac{42,000}{2} \frac{1}{1 + 1.4} = 8,750 \text{ lbs. per sq. in.}$$

Hence

$$\sigma_{max} = \sigma_m + \sigma_r = 17,500 \text{ lbs. per sq. in.}$$

In the above discussion it is assumed that we are dealing with a prismatical bar and that the direct stress is obtained by dividing the axial force by the cross-sectional area of the bar. If the form of the bar is such that there is stress concentration at certain points, as, for example, in a bar with fillets or in a bar with a hole, this stress concentration must be considered in selecting allowable stresses. Experience shows that a satisfactory design is obtained if the stress concentration is considered only in dealing with the variable portion of the stress and disregarded when calculating the constant mean stress. Some justification of this procedure is obtained if we consider the case in which the acting forces increase above the allowable limit and some yielding of a ductile material, such as steel, occurs at the points of high stress concentration. As a result of such yielding, cycles of stress finally will be established for which $\sigma_{max} = \sigma_{Y.P.}$. Since for cycles in which $\sigma_{max} \lessgtr \sigma_{Y.P.}$ the range of stress is practically independent of the magnitude of the mean stress,[156] the omitting of the factor of stress concentration in the calculation of mean stress does not effect the conclusion regarding the fatigue strength. Using the symbols $\sigma_m$ and $\sigma_r$ for the nominal values of stresses (neglecting stress concentration) and the symbol $k$ for the factor of stress concentration, which is applied only to variable stress, we obtain the allowable values of $\sigma_m$ and $\sigma_r$ by substituting $k\sigma_r$ instead of $\sigma_r$ in equations (315) and (316), which gives

$$\frac{1}{n} = \frac{k\sigma_r}{\sigma_e} + \frac{\sigma_m}{\sigma_{Y.P.}}, \qquad (317)$$

$$\sigma_r = \frac{\sigma_e}{kn} \frac{1}{1 + \frac{\sigma_e}{\sigma_{Y.P.}} \frac{\sigma_m}{k\sigma_r}}, \qquad \sigma_m = \frac{\sigma_{Y.P.}}{n} \frac{1}{1 + \frac{\sigma_{Y.P.}}{\sigma_e} \frac{k\sigma_r}{\sigma_m}}. \qquad (318)$$

[156] See R. E. Peterson's discussion in Proceedings Am. Soc. Test. Mat., Vol. 37, 1937.

Considering again the bar of the previous example and assuming, for example, that the local stress concentration is such that $k = 2$, we obtain from equations (318)

$$\sigma_r = \frac{30,000}{2 \times 2} \frac{1}{1 + \frac{1}{1.4} \cdot \frac{1}{2}} = 5,530 \text{ lbs. per sq. in.;}$$

$$\sigma_m = \frac{42,000}{2} \frac{1}{1 + 1.4 \times 2} = 5,530 \text{ lbs. per sq. in.;}$$

$$\sigma_{max} = \sigma_r + \sigma_m = 11,060 \text{ lbs. per sq. in.}$$

Equations (318) can also be used in bending. Suppose, for instance, that a shaft of steel with $\sigma_{Y.P.} = 42,000$ lbs. per sq. in. and $\sigma_e = 30,000$ lbs. per sq. in. is bent by its own weight while rotating. Then $\sigma_m = 0$ and, assuming, for example, $n = 2$ and $k = 1.7$, we would have

$$\sigma_r = \frac{\sigma_e}{kn} = \frac{30,000}{1.7 \times 2} = 8,800 \text{ lbs. per sq. in.,}$$

which represents the maximum nominal bending stress allowable in this case.

Since the endurance limit in shear is usually not far from half the endurance limit in reversed direct stress (see p. 435) we can assume that the maximum shear theory, which was originally proposed for constant stresses, applies also in cases where fracture occurs due to fatigue.[157] Hence for pure shear, using the notations $\tau_r$ and $\tau_m$ for the reversed and constant parts of the stress, and $k$ for the factor of stress concentration, we find, from eqs. (318),

$$\tau_r = \frac{\sigma_e}{2kn} \frac{1}{1 + \frac{\sigma_e}{\sigma_{Y.P.}} \frac{\tau_m}{k\tau_r}}; \qquad \tau_m = \frac{\sigma_{Y.P.}}{2n} \frac{1}{1 + \frac{\sigma_{Y.P.}}{\sigma_e} \frac{k\tau_r}{\tau_m}}. \qquad (319)$$

[157] Application of various strength theories to fluctuating stresses is discussed by J. Marin, Journal Appl. Mech., Vol. 4, p. 55, 1937.

Assume, for example, that a shaft of the same material as above is submitted to a pulsating torque such that $\tau_{min} = \frac{1}{2}\tau_{max}$ and that the dimensions are such that the factor of stress concentration at the fillets (see p. 335 is $k = 1.7$. Then

$$\tau_m = \frac{\tau_{max} + \tau_{min}}{2} = \frac{3}{4}\tau_{max}; \quad \tau_r = \frac{\tau_{max} - \tau_{min}}{2} = \frac{1}{4}\tau_{max}.$$

Assuming a factor of safety $n = 2$, we find, from eq. (319),

$$\tau_r = \frac{30,000}{2 \times 1.7 \times 2}\frac{1}{1 + \frac{1}{1.4} \times \frac{3}{1.7}} = 1,950 \text{ lbs. per sq. in.;}$$

$$\tau_m = \frac{42,000}{4}\frac{1}{1 + 1.4 \times \frac{1.7}{3}} = 5,860 \text{ lbs. per sq. in.;}$$

$$\tau_{max} = \tau_m + \tau_r = 7,810 \text{ lbs. per sq. in.}$$

Equation (319) can also be used for the general case of stress condition represented in Fig. 304, provided the plane of maximum shear remains immovable in the material, while the principal stresses vary.[158]  In this case

$$\tau_{max} = \left(\frac{\sigma_x - \sigma_z}{2}\right)_{max}, \quad \tau_{min} = \left(\frac{\sigma_x - \sigma_z}{2}\right)_{min}$$

and the quantities

$$\tau_m = \frac{\tau_{max} + \tau_{min}}{2} \quad \text{and} \quad \tau_r = \frac{\tau_{max} - \tau_{min}}{2}$$

are determined from eqs. (319).

There are sometimes more complicated cases, when not only the magnitude of the maximum shearing stress but also the position in the body of the plane in which it occurs changes. The simplest case of this kind is that of combined bending and torsion. For this case the nominal value of the maximum shearing stress is (see eq. 161, p. 278, Part I)

---

[158] Such a condition we have, for example, in the case of combined reversed bending and reversed torsion if the bending and the torsion moments are in phase.

$$\tau_{max} = \frac{16}{\pi d^3}\sqrt{M^2 + M_t^2}, \tag{g}$$

where $M$ and $M_t$ are the maximum values of the bending and of the twisting moments respectively. In calculating the diameter $d$ from this equation we substitute $\sigma_{Y.P.}/2n$ for $\tau_{max}$, as for static conditions, and take care of fluctuation of stresses by multiplying $M$ and $M_t$ by certain numerical factors $m$ and $m_1$, so that the equation for determining $d$ becomes

$$\frac{\sigma_{Y.P.}}{2n} = \frac{16}{\pi d^3}\sqrt{(mM)^2 + (m_1 M_t)^2}. \tag{320}$$

The values of $m$ and $m_1$ depend on the relative values of the moments $M$ and $M_t$ and on their fluctuation. A satisfactory working formula will be obtained if the values $m$ and $m_1$ are chosen so as to satisfy the two extreme conditions: (1) when $M_t = 0$, and we have a fluctuating bending and (2) when $M = 0$, and we have a fluctuating torque. For these two extreme conditions equation (320) gives

$$\frac{\sigma_{Y.P.}}{2n} = \frac{16}{\pi d^3}mM, \tag{h}$$

$$\frac{\sigma_{Y.P.}}{2n} = \frac{16}{\pi d^3}m_1 M_t. \tag{i}$$

The first of these equations corresponds to the fluctuating bending and the second to the fluctuating torsion. Both these cases were already discussed, and we have only to adjust the factors $m$ and $m_1$ so as to bring equations (h) and (i) into coincidence with the previous equations (318) and (319). Let us begin with the case of fluctuating bending and use the symbols $M_m$ and $M_r$ for the mean value and the variable value of the fluctuating bending moment $M$, so that

$$M = M_m + M_r. \tag{j}$$

The corresponding nominal values of stresses are

$$\sigma_m = \frac{32 M_m}{\pi d^3} \quad \text{and} \quad \sigma_r = \frac{32 M_r}{\pi d^3}, \tag{k}$$

and

$$M = M_m + M_r = \frac{\pi d^3}{32}(\sigma_m + \sigma_r).$$

Substituting this value of $M$ in the equation $(h)$, we obtain

$$\frac{\sigma_{Y.P.}}{n} = m(\sigma_m + \sigma_r). \qquad (l)$$

If there is no stress concentration, this equation must coincide with equation (315). Hence

$$\frac{m(\sigma_m + \sigma_r)}{\sigma_{Y.P.}} = \frac{\sigma_r}{\sigma_e} + \frac{\sigma_m}{\sigma_{Y.P.}}, \qquad (m)$$

and

$$m = \frac{1 + \dfrac{\sigma_r}{\sigma_m}\dfrac{\sigma_{Y.P.}}{\sigma_e}}{1 + \dfrac{\sigma_r}{\sigma_m}}. \qquad (n)$$

Since $\sigma_{Y.P.}$, $\sigma_e$ and the ratio $\sigma_r/\sigma_m$ are known, the factor $m$ is readily calculated from the equation $(n)$. If there is stress concentration, the equation $(l)$ must coincide with equation (317) and we obtain

$$m = \frac{1 + k\dfrac{\sigma_{Y.P.}}{\sigma_e}\dfrac{\sigma_r}{\sigma_m}}{1 + \dfrac{\sigma_r}{\sigma_m}}. \qquad (o)$$

Considering in the same manner the fluctuating torque given by equation $(i)$, we obtain

$$m_1 = \frac{1 + k_1\dfrac{\sigma_{Y.P.}}{\sigma_e}\dfrac{\tau_r}{\tau_m}}{1 + \dfrac{\tau_r}{\tau_m}}, \qquad (p)$$

in which $k_1$ is the factor of stress concentration in torsion, which is generally different from $k$, the factor for bending.

It is seen that for given values of the fluctuating bending and torsion moments the values of the factors $m$ and $m_1$ can

be calculated from equations $(o)$ and $(p)$. The necessary diameter is then obtained from equation (320).

As an example take a shaft of the same material as considered before and assume that the bending moment $M$ is completely reversed [159] and the torque fluctuates in such a way that $M_t = (M_t)_m(1 \pm 0.1)$. If the proportions of fillets are such that the factor of stress concentration in bending [160] $k = 1.7$ and the factor of stress concentration in twist $k_1 = 1.7$,[161] then by substituting $\sigma_m = 0$ and $\tau_r = 0.1\tau_m$, we obtain from eqs. $(o)$ and $(p)$

$$m = k\frac{\sigma_{Y.P.}}{\sigma_e} = 1.7 \times 1.4 = 2.38; \quad m_1 = \frac{1 + 1.7 \times 1.4 \times 0.1}{1 + 0.1} = 1.13.$$

The diameter of the shaft can be obtained by substituting these in eq. (320).

In the previous discussion it was assumed that the dimensions are determined by strength considerations only. There are sometimes additional requirements which must be considered in design. There are cases in which a limiting deflection is prescribed and must be taken as a basis for calculating the dimensions. The deflection is of great importance in cases in which vibration of the system is to be considered. Sometimes there are requirements regarding the maximum deflection of beams or girders. Shafts must sometimes satisfy requirements regarding the angle of twist per unit length.

In the case of structures submitted to the action of high temperature the design must be based on the assumption of a certain duration of service of the structure and of a certain amount of distortion which can be considered as permissible. The working stresses are chosen so that the distortion of the structure during its life time will not exceed a definite limit depending on the type of structure (see art. 82).

---

[159] This is always the case when the rotating shaft is under the action of loads fixed in space.

[160] If we determine $k$ from the same table as used for the two-dimensional problem shown in Fig. 210, we shall always be on the safe side.

[161] It is assumed that the stress concentrations in bending and twist are at the same point. This is approximately true at the fillets of shafts of variable diameter.

From all this discussion it may be seen that the choice of working stresses is a very important and at the same time a very complicated problem. In establishing the factor of safety $n$ the designer must always be guided by past experience. The above discussion giving a comparison of the working stresses for various stress conditions is not intended to replace the use of past experience but may be helpful in interpreting this experience and in arriving at a design which is equally strong in all parts. It may be useful also in making comparisons of different designs and in comparing the strengths of existing structures. The study of actual failures and the investigation of the causes of these failures in the light of the above theoretical discussion form a very useful method for acquiring a deeper knowledge of the strength of our structures.[162] Combining such an analysis of failures with theoretical investigations of the stress distribution in various cases and with laboratory investigations of the strength of materials under various stress conditions will enable us to accumulate a more reliable knowledge, of the actual strength of structures. When we have such knowledge, the present specifications for working stresses in various branches of engineering can be considerably improved. This will without doubt result in an economy of material and in greater reliability for structures and machines.

---

[162] In this respect such publications as Technical Reports, British Engine, Boiler, El. Insurance Co. are of great practical importance.

*Mechanical Properties of Steels*

| Number | Material | State | Proport. Limit lbs./in.² | Yield Point lbs./in.² | Ultim. Strength lbs./in.² | Elong. on 2 ins. % | Reduction Area % | Endurance Limit lbs./in.² | Remarks |
|---|---|---|---|---|---|---|---|---|---|
| 1¹ | .37 C, .55 Mn | Annealed at 850° C. | 36,500 | 37,800 | 70,000 | 32 | 49 | ± 29,000 | Bar 2¼ in. diam. |
| 2¹ | " | Normalized at 850° C. | 38,000 | 41,500 | 79,200 | 29 | 46 | ± 29,300 | " " |
| 3¹ | " | Heat-treated, Water at 850° C., Temp. at 550° C. | 65,000 | 69,000 | 105,000 | 22 | 56 | ± 51,000 | " " |
| 4² | .49 C, .46 Mn | Normalized at 910° C. | 44,700 | 47,100 | 91,500 | 27 | 40 | ± 33,000 | Bar 15/16 in. square |
| 5² | " | Heat-treated, Oil at 790° C., Temp. at 430° C. | 75,800 | 78,800 | 121,800 | 11.3 | 51 | ± 64,000 | " |
| 6¹ | .35 C, .45 Mn, 3.4 Ni | Rolled | 47,000 | 60,000 | 105,000 | 21 | 42 | ± 41,000 | Plate 3½ ft. x 2 ft. x 2 in. |
| 7¹ | " | Annealed at 840° C. | 52,000 | 60,000 | 104,000 | 22 | 49 | ± 44,000 | " " |
| 8¹ | " | Normalized at 840° C., Temp. at 730° C. | 52,000 | 56,000 | 94,000 | 25 | 48 | ± 47,500 | " " |
| 9¹ | " | Heat-treated, Water at 800° C., Temp. at 600° C. | 72,000 | 77,000 | 107,000 | 23 | 56 | ± 52,000 | " |

*Mechanical Properties of Steels (Continued)*

| Number | Material | State | Propart. Limit lbs./in.² | Yield Point lbs./in.² | Ultim. Strength lbs./in.² | Elong. on 2 ins. % | Reduction Area % | Endurance Limit lbs./in.² | Remarks |
|---|---|---|---|---|---|---|---|---|---|
| 10[2] | .24 C, .37 Mn, 3.3 Ni, .87 Cr | Annealed at 780° C. | 56,700 | 60,000 | 87,000 | 33 | 67 | ±49,000 | Bar 2 in. x 1 in. |
| 11[2] | " | Heat-treated, Oil 830° C. | 115,000 | 128,000 | 138,000 | 18 | 62 | ±68,000 | " |
| 12[3] | .30 C, .56 Mn, 4.3 Ni, 1.4 Cr | Air-hardened from 800° C. | 45,000 | 177,000 | 244,000 | 10.8 | 37 | ±102,000 | Bar 1⅛ in diam. |
| 13[3] | " | Air-hardened from 800° C., Temp. 600° C. | 92,000 | 142,000 | 157,000 | 17.5 | 55 | ±80,000 | " |
| 14[1] | .32 C, .74 Mn, .32 Si | Cast | 20,000 | 33,500 | 76,000 | 26 | 34 | ±30,500 | Bar 2¼ in. x 1¼ in. |
| 15[1] | " | Annealed at 925° C. | 37,000 | 41,000 | 80,000 | 27 | 40 | ±35,000 | " |
| 16[1] | " | Normalized at 925° C. | 40,500 | 46,000 | 85,000 | 28 | 46 | ±35,000 | " |

[1] Research Laboratory, Westinghouse El. & Mfg. Co. See Applied Elasticity, S. Timoshenko and J. M. Lessells, 1924, p. 522.
[2] Bulletin of Univ. of Illinois, nr. 136, p. 33, H. F. Moore and T. Jasper.
[3] Engineedring Steels, p. 209, L. Aitchison, 1921.

# AUTHOR INDEX

# SUBJECT INDEX

*Numbers refer to pages*